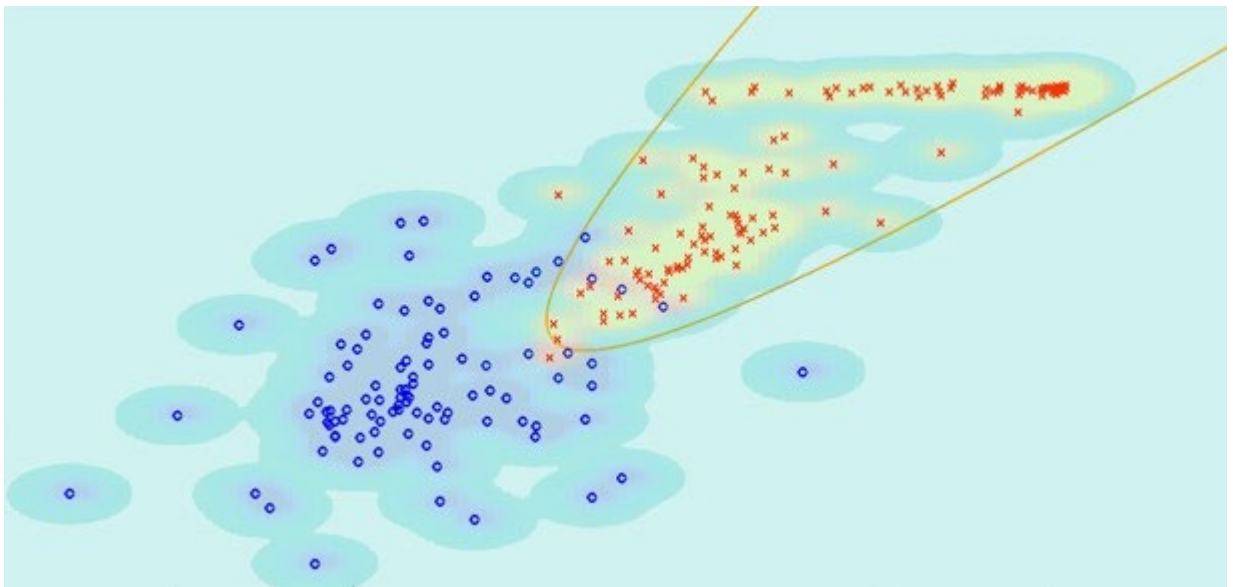




NIST Internal Report
NIST IR 8518

Applied and Computational Mathematics Division

Summary of Activities for Fiscal Year 2023



This publication is available free of charge from:
<https://doi.org/10.6028/NIST.IR.8518>

**NIST Internal Report
NIST IR 8518**

Applied and Computational Mathematics Division

Summary of Activities for Fiscal Year 2023

Ronald F. Boisvert, Editor
*Applied and Computational Mathematics Division
Information Technology Laboratory*

This publication is available free of charge from:
<https://doi.org/10.6028/NIST.IR.8518>

April 2024



U.S. Department of Commerce
Gina M. Raimondo, Secretary

National Institute of Standards and Technology
Laurie E. Locascio, NIST Director and Under Secretary of Commerce for Standards and Technology

Certain equipment, instruments, software, or materials, commercial or non-commercial, are identified in this paper in order to specify the experimental procedure adequately. Such identification does not imply recommendation or endorsement of any product or service by NIST, nor does it imply that the materials or equipment identified are necessarily the best available for the purpose.

NIST Technical Series Policies

[Copyright, Use, and Licensing Statements](#)

[NIST Technical Series Publication Identifier Syntax](#)

Publication History

Approved by the NIST Editorial Review Board on 2024-03-27

How to Cite this NIST Technical Series Publication

Ronald F. Boisvert (2024) Applied and Computational Mathematics Division: Summary of Activities for Fiscal Year 2023. (National Institute of Standards and Technology, Gaithersburg, MD), NIST Internal Report (IR) NIST IR 8518. <https://doi.org/10.6028/NIST.IR.8518>

NIST Author ORCID iD

Ronald F. Boisvert: 0000-0002-4445-1044

Contact Information

Ronald F. Boisvert, 100 Bureau Drive, Mail Stop 8910, NIST, Gaithersburg, MD 20899-8910, phone 301-975-3812, email boisvert@nist.gov, or see the Division's Web site at <https://www.nist.gov/itl/math/>.

Abstract

This report summarizes recent technical work of the Applied and Computational Mathematics Division of the Information Technology Laboratory at the National Institute of Standards and Technology (NIST). Part I (Overview) provides a high-level overview of the Division's activities, including highlights of technical accomplishments during the previous year. Part II (Features) provides further details on projects of particular note this year. This is followed in Part III (Project Summaries) by brief synopses of all technical projects active during the past year. Part IV (Activity Data) provides listings of publications, technical talks, and other professional activities in which Division staff members have participated. The reporting period covered by this document is October 2022 through December 2023.

Keywords

applied mathematics; computational science and engineering; high-performance computing; materials modeling and simulation; mathematical knowledge management; mathematical modeling; mathematics of biotechnology; mathematics of metrology; scientific visualization; quantum information science.

Cover Visualization

Example of a homotopy optimization method applied to classification of COVID-19 serology data. Blue o and red x correspond to blood samples that are known to belong to individuals that are naive to and previously infected by SARS-CoV-2, respectively. The horizontal and vertical axes correspond to measurements of antibodies that bind to different parts of the SARS-CoV-2 virus. The objective function being minimized here is the empirical mis-classification rate. However, finding the boundary that minimizes this objective function is an ill-posed mathematical problem. Thus, the homotopy method "blurs out" the data (indicated by the color map) to make the optimization problem well posed. The blurring is sequentially decreased to recover the original objective function, as well as a boundary that approximates the true minimizer. See page 17.

Acknowledgements

Thanks to Lochi Orr who compiled Part IV. Thanks also to Brian Cloteaux and Aliza Reisberg who read the manuscript and offered corrections and suggestions for improvement. The "word cloud," which is found at the start of each Part of this document was created using the Wordle word cloud app, with the text of this document as input.

Table of Contents

PART I: OVERVIEW	1
Introduction	3
Highlights	5
<i>Recent Technical Highlights</i>	<i>5</i>
<i>Technology Transfer and Community Engagement</i>	<i>7</i>
Staff News.....	9
<i>Arrivals</i>	<i>9</i>
<i>Departures</i>	<i>11</i>
<i>Recognition.....</i>	<i>12</i>
PART II: FEATURES	15
Accidental Insights on Classification, Uncertainty Quantification, and their Unification with Artificial Intelligence	17
Restoration of Noisy Orientation Maps from Electron Backscatter Diffraction Imaging	25
Explainable Boosting Machines for Scientific Image Data	30
ASTRA: Studying and Controlling Electronic Motion in Atoms and Molecules	33
Curvelet Uncertainty Principles, and the Infeasibility of Quantum Algorithms for Finding Short Lattice Vectors.....	37
Coexistence for Node Synchronization in Quantum Network Entanglement Distribution	41
PART III: PROJECT SUMMARIES.....	45
Mathematics of Metrology.....	47
<i>ITVOLT: An Iterative Solver for the Time-Dependent Schrödinger Equation.....</i>	<i>47</i>
<i>Riesz Capacity and Related Topics</i>	<i>48</i>
<i>True Becquerel: A New Paradigm for 21st Century Radioactivity Measurements.....</i>	<i>48</i>
<i>TOMCAT: X-ray Imaging of Nanoscale Integrated Circuits for Tomographic Reconstruction.....</i>	<i>49</i>
<i>Computing Ill-Posed Time-Reversed Evolution Equations Using Stabilized Explicit Schemes Run Backward in Time</i>	<i>50</i>
<i>A Science Gateway for Atomic, Molecular and Optical Physics</i>	<i>53</i>
<i>Computational Tools for Image and Shape Analysis</i>	<i>55</i>
<i>Topological Shape and Data Analysis</i>	<i>57</i>
<i>Elastic Shape Registration of Surfaces in 3-dimensional Space</i>	<i>59</i>
<i>Machine Learning Models to Predict the Infrared Spectra of Chemical Compounds</i>	<i>60</i>
<i>Improved Discrimination of Mass Spectral Isomers.....</i>	<i>61</i>
<i>AI4Wind.....</i>	<i>62</i>
Mathematics of Biotechnology	64
<i>Mechanics of Fluid Interfaces.....</i>	<i>64</i>

<i>Mathematical Modeling and Optimization for Cryobiology</i>	65
<i>Spatial-Temporal Dynamics of Photoreceptors in the Eye</i>	66
<i>Discriminating Drug Compounds Using Novel Probability-Based Similarity Scores of Their Electron-Ionization Mass Spectra</i>	68
<i>Application of Novel Algorithms for Improved Certainty in Identification of Complex Chemical Mixtures</i>	69
<i>Metrology for Cytometry and Microfluidics</i>	71
<i>Distinguishing Population and Instrument Induced Uncertainties in Flow Cytometry Using a Cell Sorter</i>	72
<i>Artificial Intelligence for Low-Field Magnetic Resonance Imaging</i>	73
<i>Time-dependent Multiclass Antibody Kinetics</i>	76
<i>Topological Data Analysis of the NIST Monoclonal Antibody (NISTmAb)</i>	77
<i>Impact of the Exposure Time and Distance Thresholds on the Performance of Automatic Contact Tracing</i> ...	78
<i>Wireless Channel Characterization for UWB Communication in Capsule Endoscopy</i>	80
<i>A Preliminary Study on Propagation Channels for Brain Telemetry Using a Flexible Wearable Antenna</i>	81
<i>Adaptive Maximization of the Harvested Power for Wearable or Implantable Sensors</i>	82
<i>A Low Complexity Power Maximization Strategy for Coulomb Force Parametric Generators</i>	84
<i>Modeling for Biological Field Effect Transistor Experiments</i>	85
Materials Modeling	87
<i>OOF: Finite Element Analysis of Material Microstructures</i>	87
<i>Mathematics of Uncertainty in Engineering Reliability</i>	88
<i>Micromagnetic Modeling</i>	90
High Performance Computing and Visualization	91
<i>High Precision Calculations of Fundamental Properties of Few- Electron Atomic Systems</i>	91
<i>Simulation of Dense Suspensions: Cementitious Materials</i>	93
<i>Immersive Visualization for the Design of a Wearable Wireless Monitoring System</i>	95
<i>Visualization of Greenhouse Gas Emissions</i>	95
<i>Transition to Open Source Visualization Software</i>	96
<i>Development of Visualization Infrastructure to Support Future Collaborations in a Hybrid Data Analysis Environment</i>	97
<i>Standards in Visualization</i>	98
<i>WebXR Graphics and Standards</i>	99
<i>Towards Robust Autotuning of Noisy Quantum Dot Devices</i>	100
<i>Tuning Arrays with Rays: Physics-informed Tuning of Quantum Dot Charge States</i>	102
<i>Principled State Identification for Quantum Dot Data</i>	104
<i>Optimizing High-Fidelity Readout Using Reinforcement Learning Methods</i>	106
<i>Data Generation for Machine-Learning Classification of Quantum Dot Devices</i>	108
<i>Towards Robust Bootstrapping of Quantum Dot Devices</i>	110
<i>FrEQuENT: A Framework Encoding for Quantum Dot Electronically Navigated Tuning</i>	111
<i>Machine Learning Applications in Laser Cooling and Trapping Atoms</i>	112
<i>Predicting the Temperature of an Atomic Cloud Using Machine Learning</i>	113
Quantum Information	115
<i>Quantum Information Science</i>	115
<i>Quantum Characterization Theory and Applications</i>	116
<i>Tests of Quantum Computational Advantage</i>	118

<i>Time-energy Uncertainty Relation for Noisy Quantum Metrology</i>	119
<i>Taxonomy of Classical and Quantum Error-correcting Codes</i>	120
<i>Bounds on Autonomous Quantum Error Correction</i>	120
<i>Realizing Phases of Quantum Matter with a Generalized Stabilizer Formalism</i>	121
<i>New Frontiers in Molecular Quantum Information Processing</i>	121
<i>Quantum Algorithms and the Power of Forgetting</i>	123
<i>Quantum Depth in the Random Oracle Model</i>	124
<i>Local Hamiltonians with No Low-Energy Stabilizer States</i>	125
<i>Post-Quantum Cryptography</i>	127
<i>Modern Quantum Tools for Bosonic Systems</i>	128
<i>Single Photon Sources and Detectors Dictionary</i>	129
<i>Network Synchronized Source of Indistinguishable Photons for Quantum Networking</i>	130
<i>Polarization Stabilization for Quantum Networks</i>	131
<i>Deployed Metropolitan-Scale Precision Time Synchronization for Quantum Networking</i>	132
<i>Quantum Network and Component Metrology</i>	133
<i>Thin-film Lithium Niobate Integrated Photonics for Quantum Information Processing</i>	136
<i>Frequency Translation for Quantum Networking</i>	136
<i>SiC-based Integrated Quantum Device Efforts</i>	137
<i>Joint Center for Quantum Information and Computer Science</i>	139
Foundations of Measurement Science for Information Systems	140
<i>Algorithms for Identifying Important Network Nodes for Communication and Spread</i>	140
<i>Towards Risk Evaluation and Mitigation in Networked Systems</i>	141
<i>Measurements of the Effects of Homophily on Epidemic Processes</i>	142
<i>Determination and Measurements of Interference Between Network Slices in 5G/6G Networks</i>	144
<i>Towards Developing Carbon Aware Algorithms</i>	145
<i>Combinatorial Testing for Software Based Systems</i>	146
<i>Measurements of the Benefits of Incremental Server Learning in Federated Learning with Heterogeneous Datasets</i>	150
<i>Topological Analysis of Detector Ensembles for Cybersecurity Applications</i>	151
Mathematical Knowledge Management	152
<i>Digital Library of Mathematical Functions</i>	152
<i>Visualization of Complex Functions Data</i>	154
<i>DLMF Standard Reference Tables on Demand</i>	155
<i>NIST Digital Repository of Mathematical Formulae</i>	156
<i>Accessible Scientific Document Corpora</i>	158
<i>Linear and Nonlinear Exploration of Rotating Self-Gravitating Inviscid Incompressible Fluid Ellipsoids</i>	159
<i>Fundamental Solutions and Formulas for Special Functions and Orthogonal Polynomials</i>	162
Outreach and Diversity	165
<i>Student Internships in ACMD</i>	165
<i>Network Analysis to Investigate Physics Programmatic Survey Results</i>	165
<i>A Modular Analysis of Ego-driven Institutional Networks</i>	167
<i>Aspects of Postdoctoral Researcher Experience Scale Survey</i>	168
<i>An Evaluation of the NIST Scientific Integrity Program</i>	169

PART IV: ACTIVITY DATA	173
Publications	175
<i>Appeared</i>	175
Refereed Journals	175
In Conference Proceedings.....	178
Technical Reports.....	180
Other Publications	180
Blog Posts.....	180
<i>Accepted</i>	181
<i>In Review</i>	181
<i>Patents</i>	183
<i>ACMD in the News</i>	183
Presentations	183
<i>Invited Talks</i>	183
<i>Conference Presentations</i>	187
<i>Poster Presentations</i>	190
<i>Multimedia</i>	193
Web Services	193
Software Released	193
Data Released	194
Conferences, Minisymposia, Lecture Series, Courses	194
<i>ACMD Seminar Series</i>	194
<i>Shortcourses</i>	195
<i>Conference Organization</i>	195
Leadership	195
Committee Membership	195
Session Organization	196
Other Professional Activities	197
<i>Internal</i>	197
<i>External</i>	197
Editorial	197
Boards and Committees.....	197
Adjunct Academic Appointments.....	198
Thesis Direction.....	199
Community Outreach	199
Awards and Recognition	200
External.....	200
Internal.....	200
Funding Received	200
External.....	200
Internal.....	200

Grants Funded..... 201

External Contacts..... 202

 Industrial Labs 202

 Government/Non-profit Organizations 202

 Universities 202

PART V: APPENDIX..... 205

Staff..... 207

Glossary of Acronyms 210

Introduction

Founded in 1901, the National Institute of Standards and Technology (NIST) is a non-regulatory federal agency within the U.S. Department of Commerce. Its mission is to promote U.S. innovation and industrial competitiveness by advancing measurement science, standards, and technology in ways that enhance economic security and improve our quality of life. The technical disciplines represented in the NIST Laboratories include physics, electrical engineering, nanotechnology, materials science, chemistry, biotechnology, manufacturing and construction engineering, fire research, information technology, mathematics, and statistics. The NIST Labs operate in two locations: Gaithersburg, MD, (headquarters—234 hectare/578-acre campus) and Boulder, CO (84 hectare/208-acre campus). NIST employs about 3400 scientists, engineers, technicians, and support personnel, and also hosts about 3500 associates from academia, industry, and other government agencies, who collaborate with NIST staff and access its facilities.

The Information Technology Laboratory (ITL) is one of six major organizational units that make up the NIST Labs. ITL's singular purpose is to cultivate trust in information technology and metrology. This is done through the development of measurements, standards, tests, and guidance to support innovation in and deployment of information technology by industry and government, as well as through the application of advanced mathematics, statistics, and computer science to help ensure the quality of measurement science.

The Applied and Computational Mathematics Division (ACMD) is one of six technical Divisions in ITL. At its core, ACMD's purpose is to nurture trust in metrology and scientific computing. To do so, ACMD provides leadership within NIST in the use of applied and computational mathematics to solve technical problems arising in measurement science and related applications. In that role staff members

- perform research in applied mathematics and computational science and engineering, including analytical and numerical methods, high-performance computing, and visualization,
- perform applied research in computer science and engineering for future computing and communications technologies,
- engage in peer-to-peer collaborations to apply mathematical and computational techniques and tools to NIST problems,
- develop and disseminate mathematical reference data, software, and related tools, and
- work with internal and external groups to develop standards, tests, reference implementations, and other measurement technologies for current and future scientific computing systems.

Division staff is organized into four groups:

- Mathematical Analysis and Modeling Group (*Timothy Burns, Leader*). Performs research and maintains expertise in applied mathematics, mathematical modeling, and numerical analysis for application to measurement science.
- Mathematical Software Group (*Bonita Saunders, Leader*). Performs research and maintains expertise in the methodology and application of mathematical algorithms and software in support of computational science within NIST as well as in industry and academia.
- High Performance Computing and Visualization Group (*Judith Terrill, Leader*). Performs research and maintains expertise in the methodologies and tools of high-performance scientific computing and visualization for use in measurement science.
- Computing and Communications Theory Group (*Ronald Boisvert, Acting Leader; Oliver Slattery, Project Leader*). Performs research and maintains expertise in the fundamental mathematics, physics, computer science, and measurement science necessary to enable the development and analysis of current and future computing and communications systems.

The technical work of the Division is organized into seven thematic areas; these are described in the sidebar. Project descriptions in Part III of this document are organized according to these broad themes.

Division Thematic Areas

Broad Areas

Mathematics of Metrology. Mathematics plays an important role in measurement science. Mathematical models are needed to understand how to design effective measurement systems and to analyze the results they produce. Mathematical techniques are used to develop and analyze idealized models of physical phenomena to be measured, and mathematical algorithms are necessary to find optimal system parameters. Mathematical and statistical techniques are needed to transform measured data into useful information. We develop fundamental mathematical methods and tools necessary for NIST to remain a world-class metrology institute, and to apply these to measurement science problems.

High Performance Computing and Visualization. Computational capability continues to advance rapidly, enabling modeling and simulation to be done with greatly increased fidelity. Doing so often requires computing resources well beyond what is available on the desktop. Developing software that makes effective use of such high-performance computing platforms remains very challenging, requiring expertise that application scientists rarely have. We maintain such expertise for application to NIST problems. Such computations, as well as modern experiments, typically produce large volumes of data, which cannot be readily comprehended. We are developing the infrastructure necessary for advanced interactive, quantitative visualization and analysis of scientific data, including the use of 3D immersive environments, and applying the resulting tools to NIST problems.

Current Focus Areas

Mathematics of Biotechnology. As proof-of-concept academic work in engineering biology meets the market realities of bringing lab science to product initiation, there are needs to compare biological products, measure whether desired outcomes are realized, and optimize biological systems for desired behaviors. NIST is working to deliver tools and standards to measure such biological technologies, outputs, and processes from healthcare to manufacturing and beyond. We support this effort with the development and deployment of innovative mathematical modeling and data analysis techniques and tools.

Materials Modeling. Mathematical modeling, computational simulation, and data analytics are key enablers of emerging manufacturing technologies. The Materials Genome Initiative (MGI), an interagency program with the goal of significantly reducing the time from discovery to commercial deployment of new materials using modeling, simulation, and informatics, is a case in point. To support the NIST role in the MGI, we develop and assess modeling and simulation techniques and tools, with emphasis on uncertainty quantification, and collaborate with other NIST Laboratories in their efforts to develop the measurement science infrastructure needed by the materials science and engineering community.

Quantum Information Science. An emerging discipline at the intersection of physics and computer science, quantum information science is likely to revolutionize 21st century science and technology in the same way that lasers, electronics, and computers did in the 20th century. By encoding information into quantum states of matter, one can, in theory, enable phenomenal increases in information storage and processing capability. At the same time, such computers would threaten the public-key infrastructure that secures all of electronic commerce. Although many of the necessary physical manipulations of quantum states have been demonstrated experimentally, scaling these up to enable fully capable quantum computers and networks remains a grand challenge. We engage in (a) theoretical studies to understand the power of quantum computing, (b) collaborative efforts with the multi-laboratory experimental quantum science program at NIST to characterize and benchmark specific physical realizations of quantum information processing, and (c) demonstration and assessment of technologies for quantum networking.

Foundations of Measurement Science for Information Systems. ITL assumes primary responsibility within NIST for the development of measurement science infrastructure and related standards for IT and its applications. ACMD develops the mathematical foundations for such work. This can be very challenging. For example, many large-scale information-centric systems can be characterized as an interconnection of many independently operating components (e.g., software systems, communication networks, the power grid, transportation systems, financial systems). Exactly how the structure of such large-scale interconnected systems and the local dynamics of its components leads to system-level behavior is only weakly understood. This inability to predict the systemic risk inherent in system design leaves us open to unrealized potential to improve systems or to avoid potentially devastating failures. A looming new example of importance to NIST is the Internet of Things. We are developing models to aid in the development of applications from individualized health IT devices to large-scale sensor networks.

Mathematical Knowledge Management. We work with researchers in academia and industry to develop technologies, tools, and standards for representation, exchange, and use of mathematical data. Of particular concern are semantic-based representations which can provide the basis for interoperability of mathematical information processing systems. We apply these representations to the development and dissemination of reference data for applied mathematics. The centerpiece of this effort is the Digital Library of Mathematical Functions, a freely available interactive and richly linked online resource, providing essential information on the properties of the special functions of applied mathematics, the foundation of mathematical modeling in all of science and engineering.

Highlights

In this section we identify some of the major accomplishments of the Division during the past year. We also provide news related to ACMD staff.

Recent Technical Highlights

ACMD has made significant technical progress on many fronts during the past year. Here we highlight a few notable technical accomplishments.

- The arXiv preprint repository¹ is now using ACMD's LaTeXML tool² to create HTML/MathML versions of submitted manuscripts. The main reason that arXiv cites as the need for HTML is accessibility, which is much more challenging for PDF documents, especially those with lots of technical content such as equations. LaTeXML was judged to be the most capable open source tool available for their use. LaTeXML was originally developed by Bruce Miller for use in the Digital Library of Mathematical Functions (DLMF) project³. See page 158.
- Paul Patrone and Anthony Kearsley of ACMD have been leading a high-profile NIST Innovations in Measurement Science (IMS) project with the goal of developing greatly improved techniques for flow cytometry, a technique that uses microfluidic techniques to measure characteristics of cells for cancer detection, drug development, and biomedical research. Working with colleagues in NIST PML, the team has developed a new cytometer that can make multiple measurements of the same cell in sequence, enabling self-validating, time-dependent measurements of cell behavior. For their device, cell classification accuracy is 99.5 % and tracking errors are fewer than 1 in 10,000 at a throughput of 1 million cells per hour, a revolutionary improvement over existing techniques. Following these successes, the team participated in a FedTech incubator program whose goal is to start companies based on NIST inventions. As a result of this effort, a company (Lumos NanoLabs) was created to commercialize the NIST microfluidic flowmeter. See page 71.
- Barry Schneider of ACMD, working with guest researchers Ryan Schneider (no relation) and Heman Gharibnejad have developed a novel approach for solving the time-dependent Schrödinger equation. The method converts the differential equation to an equivalent Volterra integral equation, which is discretized using a global Lagrange interpolation of the integrand to obtain a linear system, which is then solved iteratively. In tests on two quantum systems, a two-level atom exposed to a laser and a linearly driven harmonic oscillator, the method compares quite well to existing methods. Software embodying the method, named INTVOLT, has been included in the *Computer Physics Communications* software library. See page 47.
- In contrast to some other communities, the atomic, molecular, and optical physics community has lagged behind in developing community supported software packages that are robust and widely used outside the group that was responsible for developing the software. With the goal of promoting increased software reuse in this community, Barry Schneider of ACMD has led a team of researchers from 10 institutions, both academic and national labs, to develop the Atomic, Molecular, and Optical Science (AMOS) Gateway,⁴ which provides the community with the ability to exercise codes modeling static and dynamic properties of multi-electron and molecular systems without having to install software locally. This year the team received a \$2.46M five-year award from the NSF to help sustain and enhance the project. See page 53.

¹ <https://arxiv.org/>

² <https://math.nist.gov/~BMiller/LaTeXML/>

³ <https://dlmf.nist.gov/>

⁴ <https://amosgateway.org/>

- The black-box nature of most machine learning (ML) models makes them unsuitable for applications like medicine, finance, and metrology, that require human users to understand why a model provides the output it does. Explainable Boosting Machines (EBMs) are models designed to simultaneously be highly explainable while achieving accuracy comparable to state-of-the-art ML methods. However, to date EBMs have only been used with tabular data. Justyna Zwolak of ACMD and Craig Greenberg of ITL's Information Access Division, in collaboration with Rich Caruana (one of the developers of EBMs), have investigated the use of EBMs to classify image data. Using a novel Gabor wavelet transform-based method to extract and tabularize visual features from images, they have demonstrated that EBMs can effectively reveal physically meaningful patterns. The proposed approach provides better explanations than other state-of-the-art machine learning explainability methods for images. See page 30.
- Electron backscatter diffraction (EBSD) is a scanning electron microscope technique which can be used to probe material's grain structure and orientations at the microscale. Unfortunately, such scans may be noisy, resulting in errors and missing data. Günay Doğan of ACMD, working with colleagues at Clarkson University, has developed postprocessing techniques that greatly improves the quality of such imagery, allowing it to be effectively used in quantitative studies of material microstructure. See page 17.
- Roldan Pozo of ACMD has completed a major comparative survey of algorithms for the k-median problem, which requires identifying a subset of k vertices that minimize the total distance to all other vertices in a graph. While known to be computationally challenging (NP-hard) several approximation algorithms have been proposed. Pozo has compared eight algorithms specifically designed for complex real-world networks (i.e., those with heavy-tailed degree distributions), evaluating their performance for a variety of application problems, some very large (e.g., 4M vertices and 42M edges). With some 16 000 computational experiments this effort has yielded insights on best practices for providing efficient solution techniques to this challenging problem. See page 140.
- Public-key cryptosystems, like RSA, are built upon the hardness of certain computational problems. However, an adversary with a quantum computer could easily break them. Problems involving high-dimensional lattices, such as the approximate Shortest Vector Problem and Bounded Distance Decoding, are considered candidates for the development of cryptosystems which may be resistant to quantum attack. However, little can be proven about the practical hardness of these problems for a quantum computer. Yi-Kai Liu of ACMD has taken an important step in this direction by proving that a class of potential algorithms based on the quantum curvelet transform cannot succeed in creating the necessary lattice superposition needed as a preliminary step. See page 37.
- There are quantum algorithms that can find the way out of a particular type of maze exponentially faster than the best classical algorithm, but only if the path taken is not recorded. Matthew Coudron of ACMD, working with colleagues at the University of Maryland recently proved this counterintuitive result about the power of forgetting.⁵ See page 123.
- Victor Albert of ACMD and colleagues continue to grow the Error Correction Zoo, a website that catalogs and classifies classical and quantum error correction codes. Some 641 such codes have been classified so far. Community engagement has been robust, with contributions from 92 researchers. The Zoo hosts an average of about 500 users per day. See page 120.
- Distributing quantum entanglement over long distances in optical fibers is a challenging but essential requirement for quantum networks. The tight timing tolerances needed for certain quantum processes and applications becomes very difficult to satisfy at distribution distances of over 100 km, which are needed to realize regional and metropolitan scale quantum networks. As part of a collaboration between ITL, PML and CTL, ACMD staff have successfully implemented high-fidelity entanglement distribution over 100 km in fiber coexisting with a classical signal for the first time. See page 41.

⁵ <https://www.quantamagazine.org/to-move-fast-quantum-maze-solvers-must-forget-the-past-20230720/>

- Division staff members Thomas Gerrits, Paulina Kuo, and Oliver Slattery have worked with colleagues in NIST PML to create a dictionary that defines terms and metrics relevant to the characterization of single-photon detectors and sources, with the goal of promoting better understanding and communication, and providing a useful reference for the quantum and single-photon communities. The need for such a dictionary was cited by the Quantum Economic Development Consortium (QED-C), and standards development organizations have already shown interest in adoption. See page 129.
- Quantum dots are semiconductor particles with unique properties that allow them to act as artificial atoms. Their compatibility with industrial semiconductor fabrication makes them ideal candidates as the basis for quantum computers. But QD devices suffer from material issues that makes them difficult to harness for use as quantum bits (qubits). This can be overcome by adjusting control parameters to bring the device into an operational regime. However, tuning even a double dot device is nontrivial, requiring days of a technician's time. Manually tuning a device with hundreds or thousands of dots is simply intractable. Beginning in 2018, Justyna Zwolak of ACMD pioneered the use of machine learning techniques for automated tuning of quantum dots, having designed and led the first ever *in situ* experimental validation of automated control procedures that combine AI, computer vision, and physics-based models. This groundbreaking research initiated a whole new field within the semiconductor community that now involves research groups around the world. As a result of their leadership in this field, Zwolak, along with colleague Jacob Taylor of PML were invited to write a major survey of this new field for Reviews of Modern Physics, the American Physical Society's premier physics review journal. See, for example, page 102.

Technology Transfer and Community Engagement

The volume of technical output of ACMD remains high. During the last 15 months, Division staff members were (co-)authors of 61 articles appearing in peer-reviewed journals, 39 papers in conference proceedings, and six published in other venues. Seventeen additional papers were accepted for publication, while 40 others are undergoing review. Division staff gave 79 invited technical talks and presented 74 others in conferences and workshops. Staff members were co-inventors on six patents undergoing review.

ACMD continues to maintain an active website with a variety of information and services, most notably the Digital Library of Mathematical Functions, though legacy services that are no longer actively developed, like the Guide to Available Mathematical Software, the Matrix Market, and the SciMark Java benchmark still see significant use. During calendar year (CY) 2023, the division web server satisfied more than 14.3 million requests for pages during more than 940 000 user visits. Another indication of the successful transfer of our technology is references to our software in refereed journal articles. For example, our software system for nano-magnetic modeling (OOMMF) was cited in 202 such papers published in CY 2023 alone.

Members of the Division are also active in professional circles. Staff members hold a total of 12 editorial positions in peer-reviewed journals. For example, Barry Schneider is an Associate Editor-in-Chief for IEEE's *Computing in Science and Engineering*. Staff members are also active in conference organization, serving on 29 organizing/steering/program committees. Of note, ACMD played an important role as sponsor or (co-)organizer of several significant events this year, including the following:

- *5th International Workshop on IoT Enabling Technologies in Healthcare, Co-located with IEEE International Conference on Communications (IEEE ICC), Rome, Italy, June 1, 2023.* (K. Sayrafian, Co-Organizer)

The Internet of Things (IoT) has numerous applications in healthcare, from smart wearable or implantable sensors to remote monitoring of elderly, medical device networking, and in general creating a healthcare network infrastructure. Wearable sensors have received a remarkable growth in recent years; however, a pervasive IoT-Health infrastructure is still long way from commercialization. The end-to-end health data connectivity involves the development of many technologies

that should enable reliable, secure, and location-agnostic communication between a patient and a healthcare provider. This workshop focused on the design, development, performance evaluation and experimentation of IoT enabling technologies in healthcare applications. Ten papers were presented in this half-day event.

- *Advances in the Automation of Quantum Dot Devices Control*,⁶ National Cybersecurity Center of Excellence, Rockville, MD, July 19-20, 2023. (J. Zwolak and J. Taylor, Organizers)

This workshop convened stakeholders from industry, academia, and the government interested in the research and development of semiconductor quantum computing technologies. Topics discussed included opportunities for research and development of tuning, characterization, and control methods for semiconductor quantum dot devices, the need

for facilitating interaction and collaboration between the stakeholders to build a large open-access database of experimental and simulated data for benchmarking new machine learning algorithms, determining key performance metrics for the various aspects of the tuning, characterizing, and controlling of quantum dot devices, and identifying barriers to near-term and future applications of the auto-tuning methods. Furthermore, this workshop provided a discussion place to consider methods of collaboration and future roadmap development for methods for tuning large-scale devices. Researchers representing 16 different research institutes from six countries participated. A workshop report has been submitted for publication.

- *13th Annual Conference on Quantum Cryptography (QCrypt)*,⁷ University of Maryland, College Park, MD, August 14-18, 2023. (O. Slattery, Co-General Chair)

The Annual conference on quantum cryptography (QCrypt) is a conference for students and researchers working on all aspects of quantum cryptography. This includes theoretical and experimental research on the possibilities and limitations of secure communication and computation with quantum mechanical devices or in the presence of quantum mechanical devices. (The conference includes but is not limited to research on quantum key distribution.) This event brought together 220 researchers from 28 countries and featured opening remarks by UMD President Darryll Pines and NIST Associate Director for Laboratory Programs Charles Romine.

- *The 14th International Conference on Post-Quantum Cryptography (PQCrypto)*,⁸ University of Maryland, College Park, MD, August 16-18, 2023. (Y.-K. Liu, General Chair)

The aim of this event is to serve as a forum for researchers to present results and exchange ideas on the topic of cryptography in an era with large-scale quantum computers. 140 attendees were present for the 29 invited and contributed talks.

Service within professional societies is also prevalent among our staff. For example, Bonita Saunders is a member of the Board of Trustees of the Society for Industrial and Applied Mathematics (SIAM). Staff



Figure 1. University of Maryland President Darryll J. Pines (center) and NIST Associate Director for Laboratory Programs Charles H. Romine (right) greet ACMD associate Yicheng Shi at the QCrypt 2023 conference in College Park, MD. Oliver Slattery, a co-organizer of the event looks on. (Photo courtesy of the University of Maryland.)

⁶ <https://www.nist.gov/news-events/events/2023/07/advances-automation-quantum-dot-devices-control>

⁷ <https://2023.qcrypt.net/>

⁸ <https://pqcrypto2023.umiacs.io/>

members are also active in a variety of working groups. Ronald Boisvert and Andrew Dienstfrey serve as members of the International Federation for Information Processing (IFIP) Working Group 2.5 on Numerical Software, Donald Porter is a member of the Tcl Core Team, Bruce Miller is a member of W3C's Math Working Group, and Sandy Ressler is a member of the W3C Advisory Committee. Barry Schneider represents NIST on the High-End Computing (HEC) Interagency Working Group of the Federal Networking and Information Technology Research and Development (NITRD) Program. Further details can be found in Part IV of this report.

Staff News

With NIST providing increased options for telework and remote work in the post-pandemic era, we are now experiencing a more truly hybrid working environment. While this provides staff with greater opportunities to balance work life with home life, it continues to pose challenges for the types of seamless interactions needed for state-of-the-art research. We are compensating for this in a number of ways. All of our Division seminars are now hybrid affairs to allow participation by both local and remote staff. The Division Chief holds weekly open online office hours in which remote staff can drop in to ask questions and discuss concerns. Most recently, NIST management has asked teleworkers to include Tuesdays and Thursdays as on-campus days to help restore a sense of community through face-to-face interaction. The situation continues to evolve.

Once again, ACMD experienced an unusually large number of staffing changes during this period. We welcomed four new permanent staff members and four new NRC Postdoctoral Associates, while bidding farewell to four postdocs and one long-term Federal employee. We continue to host a large number of guest researchers, 43 at last count (which includes both postdocs and senior researchers), half of whom primarily work on one of the NIST campuses with the rest being off-site collaborators. We provided internship opportunities to 40 students, including 19 graduate students, 17 undergraduate students, and 4 high school students. See Table 6 and Table 7 on page 172 for a list of our interns.

Further details on our staff changes and awards are provided below.

Arrivals

Leroy Jia joined ACMD in August 2023. He received a dual B.S. in Physics and Mathematics at the Georgia Institute of Technology in 2012 and a Ph.D. in Applied Mathematics from Brown University in 2018. His dissertation was entitled *Geometry and mechanics of self-assembled colloidal membranes*. Leroy's research interests are in applied analysis and geometry of soft, fluid, and active matter systems. Before coming to NIST he was a Research Fellow in the Flatiron Institute's Center for Computational Biology. At NIST Leroy will apply his expertise in partial differential equation modeling of soft materials to applications in biometrology.

Shawn Geller became a permanent member of ACMD's Boulder Quantum Theory Project in March 2023. He received a B.A. in Physics from Reed College in 2015 and an M.S. in Physics from the University of Colorado, where he continues as a Ph.D. candidate. From 2019 until 2023 Shawn was a PREP research assistant in ACMD working with Manny Knill and Scott Glancy. His research interests are in quantum information theory, especially in mathematical techniques and protocols for quantum characterization, verification, and validation.

Alex Kwiatkowski, a Ph.D. candidate in physics at the University of Colorado, also joined NIST in March 2023. He received a B.S. and M.S. in Physics from Stanford in 2017 and was a PREP research assistant with Manny Knill and Scott Glancy before becoming a permanent NIST staff member. Alex also has some experience as a community college physics instructor as well as a software engineer at several small companies. His interests include quantum optics, Gaussian quantum information, protocols to establish distant

entanglement, measurement theory of continuous-variable systems, randomized benchmarking, and other methods of characterizing quantum states, operations, and measurements.

In May 2023 **Lakshmi Venkataramanan** joined NIST to provide administrative support for the ACMD Mathematical Software Group and the High Performance Computing and Communications Group. She has B.S. in Healthcare Administration from George Mason University and an M.S. in Cybersecurity Management and Policy from the University of Maryland. She has held previous Federal administrative positions at HHS, DHS, DOD, and the NSF.

In December 2022, **William Earwood** began a two-year NRC Postdoctoral Associateship in ACMD. He received a Ph.D. in Chemistry from the University of Mississippi, where he developed new theoretical methods and resulting computer software for calculating term energies and dipole polarizabilities of lithiumlike ions. At NIST, William is working with Barry Schneider on numerical methods for the time-dependent Schrodinger equation needed to study atomic and molecular systems exposed to short pulse, intense electromagnetic radiation. The methods and software will be used to calculate polyatomic excitation and ionization cross-sections, but these new methods are quite general and have applications to other areas of chemistry and physics.

Stephen Sorokanich joined ACMD as an NRC Postdoctoral Associate in December 2022. Stephen received a Ph.D. in Applied Mathematics and Mathematical Physics from the University of Maryland College Park in May of 2022. For his thesis he carried out a mathematical analysis of several models for the dilute interacting Bose gas and the phenomenon of Bose-Einstein condensation (BEC). In that work he developed the spectral theory for a family of approximate Hamiltonians via their transformation by a non-Hermitian pair excitation operator. At NIST he is working with Howard Cohl to study the nonlinear evolution of rotating self-gravitating incompressible inviscid bodies, an application of ellipsoidal harmonics.

Melinda Kleczynski began her tenure as a NIST/NRC Postdoctoral Associate in August 2023. She received a B.S. in Mathematics from the University of Michigan in 2006, an M.S. in Mathematics from Michigan Tech in 2016, and a Ph.D. in Applied Mathematics from the University of Delaware in 2023. In her dissertation, which was entitled *The Shape of Ecological Communities: From Pollinators to Purple Martins*, she applied topological data analysis to extract information from complex data sets. At NIST she is working with her advisor Anthony Kearsley and other collaborators on chemometric data analysis as well as applications of optimization in computer security.

Anne Talkington joined ACMD as a NIST/NRC Postdoctoral Associate in December 2023. She received a B.S. in mathematics and a B.A. in biology from Duke in 2016, an M.S. in applied mathematics from the University of North Carolina in 2019, and a Ph.D. in bioinformatics and



Figure 2. Four new permanent staff members joined ACMD in 2023. From top to bottom) Leroy Jia, Shawn Geller, Alex Kwiatkowski, and Lakshmi Venkataramanan. (Photos provided by the subjects.)



Figure 3. New NIST/NRC postdoctoral associates this year included (l to r) William Earwood, Stephen Sorokanich, Melinda Kleczynski, and Anne Talkington. (Photos of Earwood, Sorokanich, and Talkington provided by the subjects. Photo of Kleczynski by Riley Wilson of NIST.)

computational biology from UNC in 2021. Her Ph.D. dissertation was entitled *A Physiologically Based, Pharmacokinetic Model for the Clearance of PEGylated Nanomedicines*. Before joining NIST she was a postdoctoral researcher at the University of Virginia where she worked on modeling of intercellular communication in melanoma tumors. In ACMD she plans to work with adviser Tony Kearsley on optimization of immunotherapeutic strategies in tumor microenvironments.

At NIST, all staff who are not Federal employees are termed guest researchers. These can include student interns, postdocs, and senior researchers. Many guests work on one of the NIST campuses, and others are remote collaborators. ACMD hosts many such guest researchers. During the current 15-month period, for example, we brought on, or renewed the appointments of, 45 different guest researchers. The senior researchers who began working full-time on the Gaithersburg campus during this period include the following:

- Amudhan Krishnaswamy-Usha. Amudhan received a Ph.D. in mathematics from Texas A&M in 2020 with a dissertation on spectral operators in finite Von Neumann algebras. Before joining ACMD in 2023 he was a postdoctoral researcher at the Technical University of Delft. Here he is working with Paul Patrone on methods to quantify the total uncertainty induced by a cytometer when making measurements of cell properties, e.g., to inform whether they are cancer.
- Stephen Tennyson. Stephen received B.S. degrees in biology (neurobiology and physiology specialization) and nutrition from the University of Maryland in 2016. In 2021 he also received a B.S. degree in computer science from Maryland. He has had seven years of experience in software development for scientific applications. In ACMD Stephen is working with Paul Patrone to develop software that allows end-users to use ACMD's newly developed methods for optimal diagnostic classification and prevalence estimation (e.g., of a medical condition).

Departures

Lisa Ritter, an NRC Postdoctoral Associate in ACMD, departed NIST in July 2023 to take a position with STR in Arlington, VA. STR works on problems in cybersecurity, distributed sensing, and AI. At NIST Lisa worked with Howard Cohl on orthogonal polynomials and special functions, and with Justyna Zwolak on the use of AI to process imagery from Bose-Einstein condensate experiments.

Rayanne Luke, an NRC Postdoctoral Associate in ACMD, accepted a tenure-track faculty position in the Mathematics Department at George Mason University beginning in September 2023. At NIST Rayanne worked with Paul Patrone and Tony Kearsley on improving diagnostic testing accuracy with applications to saliva-based SARS-CoV-2 assays, and on accurate multiclass classification strategies for interpreting antibody tests. Rayanne will continue her association with ACMD as a guest researcher.

Robert DeJaco was an NRC Postdoctoral Associate in ACMD from 2020 to 2022 and continued as a PREP postdoc until departing NIST in June 2023 to take a position with Compact Membrane Systems in Newport, Delaware. At NIST he worked with Tony Kearsley on a variety of projects from breakthrough curve analysis for carbon capture to uncertainty quantification in fluorescence in PCR measurements. Rob continues his association with ACMD as a guest researcher.

In July 2020, **Danielle Middlebrooks** began her tenure at NIST as a NIST Fellow's Postdoc working with Geoffrey McFadden. She also worked with Paul Patrone on the analysis of cytometry systems, and with Justyna Zwolak on the use of AI for the tuning of quantum dots. In December 2023 she began an appointment at the National Security Agency.

Timothy Burns, Leader of the Mathematical Analysis and Modeling Group, retired from NIST in December 2023 after 37 years of service. Tim began his tenure at NIST in 1986 as a staff member of the Scientific Computing Division in the Computing and Applied Mathematics Laboratory. Tim's expertise is in nonlinear dynamics, which he has applied to the mathematical modeling of the mechanical properties of materials. Over the years he has had extensive collaborations with the Engineering Lab modeling aspects of high-speed machine tools as well as pulse-heated Kolsky bar measurements of high strain rate flow stress. The NIST publications database lists 45 technical papers on these and other topics. In 2004, Tim was a member of a multi-OU team which won the prestigious Allen Astin Measurement Science Award. The team was cited for outstanding advancements in measurement science for dynamic material properties, leading to the first ever measurement of the stress-strain relationship of a material under high strain-rate and heating-rate conditions prior to temperature-induced transformation.



Figure 4. Timothy Burns (left) working with Richard Rhorer on the Kolsky bar. (Photo credit: NIST)

Recognition

ACMD staff members were recognized with a variety of awards this year, including the following.

Scott Glancy and **Emanuel Knill** of ACMD, along with four colleagues from NIST's Physical Measurement Laboratory were recipients of the 2022 Department of Commerce Gold Medal. They were honored "for pioneering experimental techniques to generate and precisely measure the quantum entanglement of two macroscopic mechanical resonators." The highest honorary award granted by the Secretary of Commerce, the Gold Medal is awarded for distinguished performance characterized by extraordinary, notable, or prestigious contributions that impact the mission of the Department. The medals were conferred at ceremonies held at DOC headquarters in January 2023. Notably, ACMD postdoc **Ezad Shojaee** and PREP graduate students **Alex Kwiatkowski** and **Shawn Geller**, who helped develop the theory and wrote, analyzed, and tested the data analysis code that enabled this accomplishment were not cited because they were ineligible for DOC awards since, at that time, they were not Federal employees. Instead, they were honored with a 2023 ITL Associate Reflection Award for their contributions to that effort.

Thomas Gerrits of ACMD, along with colleagues in PML and MML, was recognized with a 2023 Department of Commerce Bronze Medal for developing precision measurement techniques for molecular



Figure 5. Department of Commerce Medal winners from ACMD: Left to right: Emanuel Knill (Gold), Scott Glancy (Gold), Thomas Gerrits (Bronze), Anthony Kearsley (Gold), Paul Patrone (Gold). (Photo credits: NIST)

absorption of photon pairs that resulted in the refutation of controversial published claims about quantum-enhanced microscopy.

It was announced in early 2024 that **Anthony Kearsley** and **Paul Patrone** of ACMD, along with colleagues Gregory Cooksey and Matthew DiSalvo of NIST PML will receive a 2023 Department of Commerce Gold Medal for the invention of serial cytometry, which will enable early cancer identification and tracking of residual disease via rare-cell detection. Their achievements enable rigorous, single-cell measurements in cytometry, removing a longstanding hindrance to robust medical diagnostics and providing the first ever real-time dynamic measurements of cellular functions. The advance is the result of a NIST Innovations in Measurement Science project led by ACMD.

In 2023, ACMD captured two of the 11 awards given out in the annual ITL Awards program. The ACMD winners were:

- **Barry Schneider**
Outstanding Collaboration
For leading a collaborative, NIST-wide effort to develop and document a coherent vision for research computing at NIST. (Joint with Walid Keyrouz of ITL’s Software and Systems Division.)
- **Anouar Rahmouni**
Outstanding Associate
For support in experimental research on quantum devices and systems aligned to the NIST quantum program and metrology mission.

ACMD’s **Bonita Saunders** was re-elected to a second term on the Society for Industrial and Applied Mathematics (SIAM) Board of Trustees in the fall of 2022. The Board of Trustees is the group responsible for the management of SIAM.

In late 2022 ACMD mathematician **Danielle Middlebrooks** was selected to receive an MGB-SIAM Early Career (MSEC) Fellowship⁹ for the 2023-2025 term. The MGB-SIAM Early Career Fellowship reflects a joint commitment by Mathematically Gifted & Black (MGB) and the Society for Industrial and Applied Mathematics to promote long-term engagement of researchers within SIAM and continued success within the wider applied mathematics and computational sciences community. The fellowship will provide multiple opportunities to network with and contribute to the SIAM community, such as special events, professional development workshops, committee shadowing, cohort-specific activities, as well as formal and informal mentoring by and with other members of the SIAM community.

⁹ <https://www.siam.org/students-education/programs-initiatives/mgb-siam-early-career-fellowship>

Raghu Kacker of ACMD, along with D. Richard Kuhn of ITL and collaborators from the University of Texas at Arlington, were selected for a Most Influential Paper Award (MIP) of the Decade award in the category of MIP Practical for a paper they presented 10 years ago at the 2013 IEEE International Conference on Software Testing, Verification and Validation (ICST). The paper, entitled “ACTS: A Combinatorial Test Generation Tool,” described a new software tool for automatically generating inputs for testing software based on an analysis of combinations of input parameters most likely to identify faults. The award was conferred at the 2023 ICST conference held in Dublin in April 2023.



Figure 6. Raghu Kacker of ACMD (second from left) and colleagues received the Most Influential Paper Award for a paper presented 10 years ago at the IEEE International Conference on Software Testing. (Photo credit: NIST)

Deborah McGlynn, a NIST/NRC Postdoctoral Associate in ACMD, won a Best Poster Award at the 2023 International Applied Mathematics, Modeling and Computational Science Conference held in Waterloo, Canada in August 2023. Her poster was entitled “Using the High Dimensional Consensus Mass Spectral Similarity Algorithm for Improved Identification of Isomers.” Co-authors on the work were Jason Eveleth and Anthony Kearsley of ACMD and Nirina Rabe Andriamaharavo of the NIST Mass Spectrometry Data Center.

Sesha Challa, a NIST Associate in ACMD was selected for the American Vacuum Society (AVS) Nanoscale Science and Technology Division Early Career Award. The award, which highlights and celebrates exceptional researchers working on the frontiers of nanoscience, was presented at the AVS 69th International Symposium and Exhibition held in Portland, OR in November 2023. He was cited for his work on process development for fabrication of low-loss thin-film lithium niobate waveguides.

The Washington Metropolitan Quantum Network Research Consortium (DC-QNet) recognized ACMD staff with two awards at its interagency program review in September 2023. **Oliver Slattery** received the Exceptional Leadership Award for serving as DC-QNet Execution Manager of a DARPA seed study on a proposed Quantum Augmented Classical Testbed. In addition, **Oliver Slattery, Thomas Gerrits, and Paulina Kuo** of ACMD were presented with an Outstanding Contribution Award for implementing the DARPA QuANET Feasibility Study (joint with NIST staff in ITL, PML, and CTL).

Geoffrey McFadden, an ACMD mathematician and NIST Fellow, who retired in 2021, was inducted into the NIST Portrait Gallery of Distinguished Scientists, Engineers and Administrators in ceremonies held in October 2022. He was cited for fundamental contributions to the theory of phase transitions, hydrodynamic and morphological stability, and thermo-solutal transport in materials. NIST Portrait Gallery honors NIST alumni for outstanding career contributions to the work of NIST. Portraits and biographies of those selected are displayed in the corridor of the NIST cafeteria at Gaithersburg, and in the Digital Portrait Gallery at NIST Gaithersburg and NIST Boulder sites. At most 10 new alumni are inducted each year.



Figure 7. Geoffrey McFadden was named a Distinguished NIST Alumnus. (Photo credit: NIST)

Accidental Insights on Classification, Uncertainty Quantification, and their Unification with Artificial Intelligence

In September of 2020, a collaborator asked us to answer a pair of seemingly simple questions: what was the best assay for detecting SARS-CoV-2 antibodies, and how should the resulting measurements be used to classify samples? Little did we know that this would launch us on a more than three-year journey in search of answers. Driven increasingly by the needs of the pandemic, we came to understand that the shortcomings in data analysis for diagnostics arise from a lack of a theoretical foundation to describe the associated measurements. Yet hiding in plain sight, the biologists' own intuition pointed us towards probability and measure theory to resolve this problem. Here we discovered a rich tapestry of ideas that not only reinterpret classification as an exercise in uncertainty quantification, but also resolve longstanding paradoxes in epidemiology. Ultimately this analysis led us to a fundamentally new perspective on the relationships between uncertainty quantification, optimization, and surprisingly, artificial intelligence.

Anthony Kearsley
Paul Patrone

One could be forgiven for believing that the analytical theory of classification contains few surprises anymore. In some sense, the modern perspective on this field is already old, tracing back nearly 100 years to the seminal work of Fisher [1, 2]. By the time computers became widespread in the late 20th century, much of the scientific community appeared to have already moved on, focusing their efforts on developing computational tools for data analysis algorithms [3]. More recently, this trend has accelerated with the increased adoption of machine-learning (ML) based classification. Nowadays, one could easily conclude that all of the interesting problems can be reduced to construction of an appropriate neural network or generative classifier.

Surprisingly, large pockets of the scientific community still remain unaware of the theoretical developments of the last 100 years. In diagnostics, for example, classification problems are still routinely solved using techniques that date back to bomber detection algorithms from WWII [4]. In fact, the community long ago identified, but did not fully resolve, a significant number of issues associated with construction of unbiased estimates of prevalence (i.e., the fraction of a population in a class) and minimum error classifiers [5]. More notably, canonical approaches to diagnostic classification often rely on arguments that violate basic principles of logic.

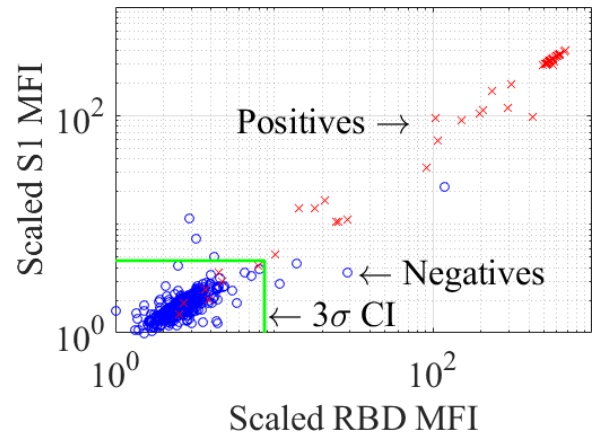


Figure 8. Example of serology data. The axes correspond to fluorescence measurements of SARS-CoV-2 receptor binding domain (RBD) and spike (SI) antibodies. The green box indicates the 3σ confidence interval associated with the algorithm described in the main text.

With this backdrop, a collaborator came to us in late 2020 with two seemingly simple questions: (1) among the available SARS-CoV-2 diagnostic tests at her disposal, which was the best; and (2) what was the best way to identify SARS-CoV-2 seropositive individuals from that test? Little did we know that it would take us more than three years and nine manuscripts to answer these questions. And we are still grappling with their broader implications for ML and artificial intelligence (AI).

Back to Basics. It almost goes without saying that the COVID-19 pandemic was a time of intense emotional strain. For those of us in applied math working at the outer periphery biology, this state-of-being was further twisted by an inability to find useful outlets for our skills to help end the public-health crisis. This situation can lead to a type of “autoregression” wherein seasoned researchers embrace a state of near-total ignorance in order to learn a completely new field. This is akin to starting graduate school over, with only the benefit of being hardened by years of experience in another field.

Such was the state in which we found ourselves in September 2020, learning the fundamentals of diagnostics and epidemiology as applied to COVID-19 blood testing. Initially, we were convinced that the mathematical and metrological aspects of these fields are straightforward. Most diagnostic systems are variations on three basic components: an *assay* or “testing platform,” a collection of samples drawn at random from a population, and a strategy for analyzing measurement outputs associated with each sample [4]. Each sample is assumed to belong to a unique class, e.g., COVID-19

positive or negative in the case of a binary setting. Applying the assay to a sample amounts to measuring some property of it, such as a fluorescence value that correlates with antibody levels of some type, and ideally, the class. In practice, one may think of this output as a random variable $\mathbf{r}(\omega) \in \mathbb{R}^n$, where ω denotes the sample in question and n is a positive integer that can range from 1 to $\mathcal{O}(10)$. See Figure 8.

Given this basic setup, diagnosticians typically seek to answer two questions: (I) which samples are associated with a given medical condition, and (II) how many people in the original population have the condition? Beyond this, there appears to be little agreement or uniformity on how to answer these questions, either in practice or theory.

A surprisingly common example illustrates this problem in the context of diagnostic classification (question I). One canonical approach for identifying “positive” samples in a binary setting involves two steps. First, the assay is used to measure samples in a *training population* of confirmed negative individuals. Then, one computes the mean measurement outcome μ_i and standard deviation σ_i for each dimension of \mathbf{r} separately. The positive samples are taken to be those for which $\mathbf{r}_i > \mu_i + 3\sigma_i$ for any component \mathbf{r}_i of \mathbf{r} . In other words, a sample at random is assigned to the positive class if it has a low probability of being negative [4]. While this approach nominally seems sound, it suffers notable performance issues with increasing prevalence. Perhaps motivated by this, a host of other methods also appear in the literature. Receiver operating characteristics (ROC) are a common tool for defining classification cutoffs that invoke both positive and negative training data. But such techniques are limited to one-dimensional (1D) data and, as we would later show, can be interpreted as implicitly assuming a fixed disease prevalence; thus, they also suffer decreased accuracy as prevalence changes [4]. Other approaches rely on ML algorithms, dimension-reduction, clustering, etc. In the early days of the pandemic, we even saw assays wherein diagnosticians simply added degrees-of-freedom together in ad-hoc linear combinations until the rates of false-positives and false-negatives fell in some desirable range.

To better understand why this heterogeneity has become the norm, it may be useful to take a broader perspective. In our experience, diagnostics is a multi-billion dollar industry in which innovation is largely driven by instrumentation and biochemistry. Data analysis is often relegated to lowest priority, if even acknowledged at all. In part, this may be due to a degree of “stove-piping.” Collaboration outside of biology, especially with mathematicians and physicists, is, as far as we can tell, rare. A close collaborator and disease ecologist once summarized it this way: “Before we met you, we had never heard anyone speak [mathematically] the way you do.”

As we found, this disengagement with mathematics can lead to severe problems in analytical reasoning, which likely explains many of the issues we were uncovering. Consider the 3σ classification approach, for example. *In a strict sense, it is a logically invalid interpretation of data.* For a value of \mathbf{r} falling outside the confidence interval, the probability of being positive could still be zero. Or measurements near the mean of the negatives could have an exponentially higher probability of being positive. At heart, the issue with such an analysis is that it makes no use of information about the positive samples: low probability of being negative does not imply high probability of being positive. More subtle but just as important, this perspective does not correctly account for correlations in data. Each dimension is treated independently, and not even this is done self-consistently; the 3σ level-set should be an n -dimensional ellipse, not a rectangle. As we would later discover, other techniques in use suffer from similar problems.

Having come in contact with these issues first-hand, by the end of 2020 it was becoming clear to us that the key problem plaguing diagnostic data analysis was a lack of a rigorous mathematical framework to ground and unify the existing methods. One hallmark of this problem was an inability in the community to distinguish what can be proved about classification from what must be modeled or assumed; we were now identifying assumptions that could neither be justified nor even articulated by those making them. Absent this, it was not clear to us *how* uncertainty quantification (UQ) could be realized to provide actionable information on the quality and usefulness of diagnostic tests. And looming in the background was the question of to what extent these problems reflected unresolved issues in the theory of classification itself, not to mention machine learning.

A Simple Foundation and a Surprising Find. Despite its shortcomings, the 3σ classification method is rooted in a way of thinking that merits further exploration. In diagnostic settings, one often hears that 3σ corresponds to a 99% confidence interval. We distinguish two facets of this claim. First, Chebyshev tells us that this confidence interval does not hold in general, and thus it is likely that the speaker is thinking of normal distributions [4]. Second, the concept of a confidence interval suggests a probabilistic interpretation of the data. The first observation concerns a *model* (i.e., a choice), which is not fundamental to classification theory *per-se*. We return to this later. The second observation, however, is related to a perspective that can be grounded in measure theory and probability, a foundation from which we can understand classification more generally.

In this light, we began in a binary setting, postulating the existence of functions $P(\mathbf{r})$ and $N(\mathbf{r})$, which are the probability density functions (PDFs) of measurement outcomes conditioned on the underlying sample

being positive or negative [4]. The law of total probability relates these PDFs to the probability density $Q(\mathbf{r})$ of a measurement outcome for an individual at random. Importantly, this definition introduces the prevalence q via the expression

$$Q(\mathbf{r}) = qP(\mathbf{r}) + (1 - q)N(\mathbf{r}).$$

With this information alone, a surprisingly simple (but heretofore unknown) result suggested itself to us. We can safely assume that \mathbf{r} must fall in some set $\Gamma \in \mathbb{R}^n$, and one is always free to choose some subset $D \subset \Gamma$. Letting

$$P_D = \int_D P(\mathbf{r}) d\mathbf{r}$$

$$N_D = \int_D N(\mathbf{r}) d\mathbf{r}$$

and similarly for Q_D , integrating the above gives the linear equation

$$Q_D = qP_D + (1 - q)N_D. \quad (1)$$

At first blush, this does not appear useful. However, recognize that Q_D is the fraction of samples from a *test* population whose measurement values \mathbf{r} fall in D . As such, this quantity can be computed in terms of the Monte Carlo estimate

$$Q_D \approx \tilde{Q}_D = \frac{1}{s} \sum_{j=1}^s \mathbb{I}(\mathbf{r}_j \in D)$$

where s is the number of samples \mathbf{r}_j in the test population. This expectation converges in mean-square to Q_D , and as such, Eq. (1) can be inverted to yield an unbiased and converging estimate of prevalence of the form

$$q \approx \tilde{q} = \frac{\tilde{Q}_D - N_D}{P_D - N_D} \quad (2)$$

provided $P_D \neq N_D$.

To the best of our knowledge, Eq. (2) in its full generality was unknown the diagnostics community until the appearance of Ref. [4]. The implications of this estimator are profound, pointing to a Pandora's box of new questions. Perhaps most obvious, the set D has nothing to do with classification. This fact alone is counter to traditional thinking in epidemiology. The status quo is to first classify samples, and then count the number of positive samples to estimate prevalence, possibly with a bias-correction factor. In fact, in our experience it is a commonly held belief that prevalence *cannot* be estimated without classifying samples. But to convince yourself otherwise, compare the following questions: (a) how many samples are positive; and (b) which samples are positive. The first question is more general and quantifies a property of a population; thus, intuitively it stands to reason that it can be answered without answering question (b). In fact, we eventually took this

argument further, using a tool from measure theory to prove that the D minimizing uncertainty in the prevalence is divorced from an optimal classifier [5].

Equation (2) also has surprising implications for classification. To assign a class to a measurement, diagnosticians often partition the measurement space Γ in one-to-one correspondence with the class labels. A point \mathbf{r} is then assigned to a class according to the domain into which it falls. Momentarily assuming knowledge of $P(\mathbf{r})$ and $N(\mathbf{r})$, it is well-known that the minimum-error classifier corresponds to the domains

$$D_p^* = \{\mathbf{r}: qP(\mathbf{r}) > (1 - q)N(\mathbf{r})\} \quad (3)$$

$$D_n^* = \{\mathbf{r}: qP(\mathbf{r}) < (1 - q)N(\mathbf{r})\} \quad (4)$$

where the p and n subscripts denote the “positive” and “negative” classification domains. Any point for which $qP(\mathbf{r}) = (1 - q)N(\mathbf{r})$ can be assigned to either class (although this set has a special significance that only became apparent to us much later.)

To see the connection to Eq. (2), note that the partition depends on the q . *In other words, the natural order of tasks is to first estimate prevalence and then classify.* For decades the diagnostics community had been doing the opposite, and moreover, they believed that what we proposed was impossible. Perhaps more surprising to us, these observations arose simply by grounding classification in probability and measure theory.

Unpacking Pandora's Box: The Role of Modeling. A key benefit of mathematical analysis is its ability to distinguish between what can be known and what must be inferred from data. Here the situation is no different. Eq. (1) and all that follows is exact under the assumption that $P(\mathbf{r})$ and $N(\mathbf{r})$ exist. But in real-world classification problems, we rarely, if ever have exact knowledge of the true distributions. Typically, one is just given training data from which to construct them. In practice, the task of modeling $P(\mathbf{r})$ and $N(\mathbf{r})$ therefore comes down to the creativity and skill of individual data analysts [4, 6, 7].

In this light, it is ironic that without explicitly stating so, canonical approaches such as the 3σ classifier assume that the conditional PDFs correspond to normal random variables. However, in the context of serology, we have never seen data that can plausibly be quantified in terms of this distribution. In contrast, our initial approaches relied on other parameterized distributions, typically formulated by hand, and trained via regression techniques such as maximum likelihood analysis [4, 6, 7]. In typical serology settings, this approach is slow but works reasonably well in one dimension (1D) or two dimensions (2D), since one often has $\mathcal{O}(100)$ datapoints; see, e.g., Figure 9. In higher dimensions, however, one typically lacks sufficient data to effectively model correlations, and it can be difficult to validate models in such cases.

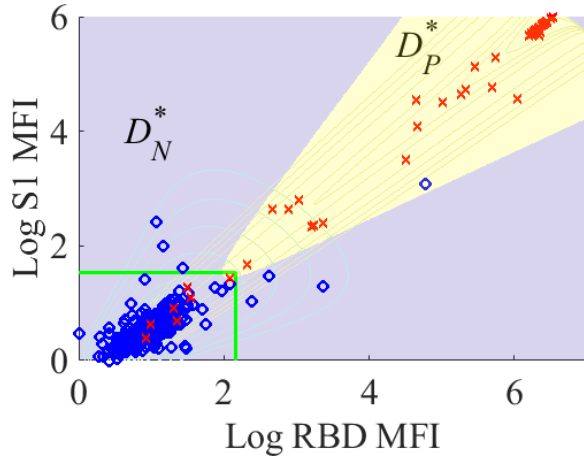


Figure 9. Examples of conditional probability models (contour lines) and Bayes optimal classification domains (yellow and pink). The data is the same as in Figure 8.

Before addressing the problem of dimensionality, however, details of the COVID-19 pandemic forced us to confront other pressing issues, many of which again revolved around modeling. It is well known, for example, that antibodies developed in response to an infection can last for years; this is why they are often used to track the spread of diseases. However, over time the concentration in blood begins to wane. By the star of 2021, it was becoming apparent that those infected by SARS-CoV-2 in 2020 were losing their protection on the time-scale of months [8]. Not only did this impact personal safety considerations, it also stymied public health officials’ ability to track the seroprevalence of the disease.

These issues were compounded by the widespread arrival of vaccines in mid-2021 [9]. There was growing awareness that vaccination *and* a history of infection conferred the best protection. But the vaccines were designed to elicit an immune response that included the production of anti-SARS-CoV-2 antibodies. This made it difficult to distinguish individuals having a history of infection from those that were infected and vaccinated or only vaccinated. Moreover, it changed the course of seroprevalence studies: less emphasis was placed on tracking COVID, and more was given to distinguishing classes and estimating “correlates of protection” [12].

Solving the analytical aspects of these problems entailed relatively straightforward generalizations of Eqs. (1)-(4). The optimal prevalence estimator can be recast as a matrix inversion problem [9], and it is easy to see that the corresponding multiclass classifiers amount to assigning \mathbf{r} to the class that has the highest prevalence-weighted probability of generating the data [9]. Accounting for time-dependent behavior is more challenging. In such situations, the law of total probability becomes a convolution that intertwines an individual’s antibody kinetics with the *incidence* or rate of new infections. It is still possible to construct optimal

classifiers and prevalence estimates, but doing so requires numerically solving difference equations that account for the entire history of a pandemic [8].

In both cases, however, the modeling becomes more challenging. The multi-class problem benefits from increasing dimensionality in order to better distinguish classes. In the context of SARS-CoV-2, for example, this arises from the fact that vaccinated individuals do not have a response to so-called “nucleocapsid” antibody assays, whereas previously infected individuals typically do. In the time-dependent problem, distributions of time-dependent antibody levels must be modeled, which also increases dimensionality of the associated inference problem. Even more challenging is the task of quantifying the effects of reinfection and boosted vaccination.

Ultimately each success pointed to the looming issue that model construction is the bottleneck in realizing practical, adaptable diagnostic classifiers. Yet, if the PDFs are not given *a priori*, how could one avoid the need for inference?

Deeper Connections to Probability, Measure Theory, and ML.

In retrospect, our first breakthrough in solving the dimensionality problem came early and from an unexpected place. In mid-2021 we were asked to develop an algorithm for minimizing the number of samples labeled as “indeterminate” in an assay developed at Johns Hopkins University (JHU) [6]. In some diagnostic settings, there are regions of the measurement space where the overlap between positive and negative samples is sufficiently great that the classifier is essentially a coin toss. In such cases, it can be desirable to *not* classify the sample, since the odds are relatively high that a patient will be given an incorrect result. Better to repeat the test, or simply not report the result at all. At the same time, holding out too many samples equates to a waste of resources and time. Thus, it is important to only hold out samples that have a high misclassification rate.

It turns out that the solution to this problem can be framed in terms of an odd-sounding result called a *bath-tub-type principle* [5, 6]. In the context of diagnostics, this principle can be understood by first formulating a *local accuracy* $Z(\mathbf{r})$, which we defined via

$$Z(\mathbf{r}) = \frac{qP(\mathbf{r})\mathbb{I}(\mathbf{r} \in D_p^*) + (1 - q)N(\mathbf{r})\mathbb{I}(\mathbf{r} \in D_n^*)}{Q(\mathbf{r})}$$

The function $Z(\mathbf{r})$ satisfies the inequalities $1/2 < Z(\mathbf{r}) < 1$ and can be interpreted as the probability that an optimally classified sample is assigned to the correct class. Interestingly, it is straightforward to show that the expected value $E[Z(\mathbf{r})]$ with respect to $Q(\mathbf{r})$ is the average classification accuracy, which justifies calling $Z(\mathbf{r})$ a local quantity. In this context, a strategy that simultaneously minimizes the classification error and the size of the holdout domain is to label as indeterminate those points \mathbf{r} for which $Z(\mathbf{r}) < X$ for some user-defined

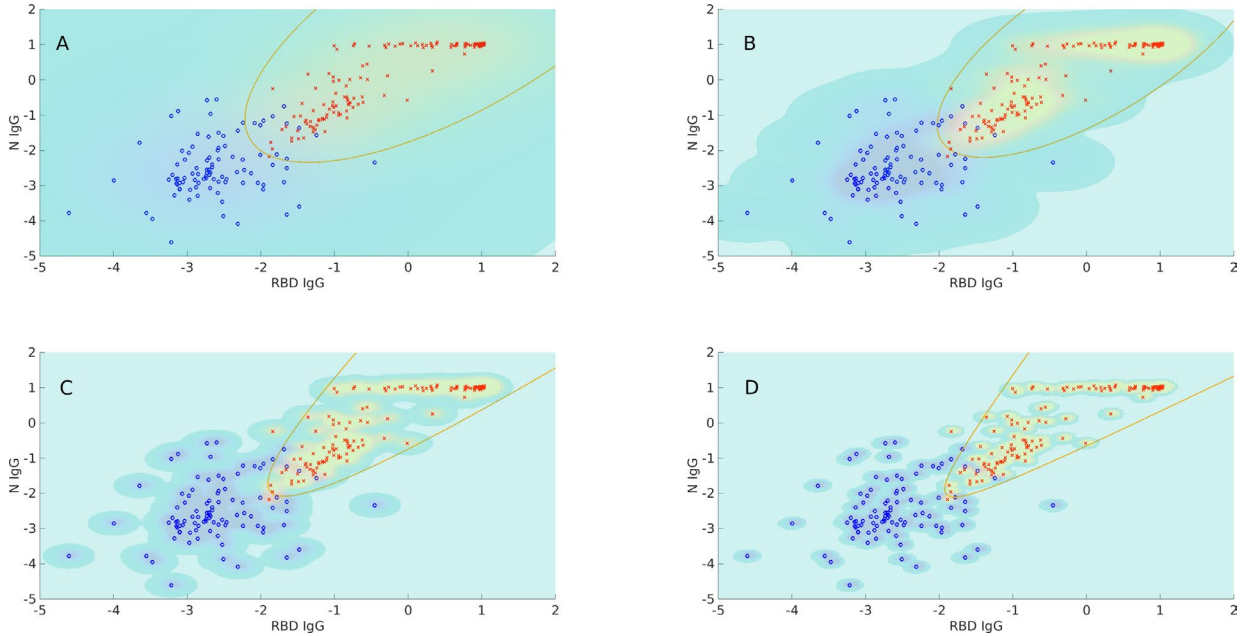


Figure 10. Conceptual illustration of the homotopy method. The goal is to draw a boundary that minimizes the empirical classification error. To do so, the individual datapoints are first blurred out and the corresponding minimizing problem solved. The solution to this is used as the initial boundary in a new optimization problem with less regularization (blurring). We proceed in this way until all of the regularization is removed. Panels A-D indicate decreasing levels of blurring and show the resulting classification boundaries.

threshold X . This last quantity controls the expected accuracy associated with the data that is classified, and it is easy to see that taking $X \rightarrow 1/2$ corresponds to a vanishing holdout domain.

While $Z(\mathbf{r})$ nominally solves the classification problem with holdouts, it is also an object of inherent interest. For one, it suggests a reinterpretation of how to count without classifying: the prevalence is the expected number of positives, i.e., $E[qP(\mathbf{r})/Q(\mathbf{r})]$. More importantly, it recasts classification as a task of computing the *relative probability* of belonging to a class. To see this, note that we may express $Z(\mathbf{r})$ in the form

$$Z(\mathbf{r}) = \frac{q\mathbb{I}(\mathbf{r} \in D_p^*) + (1 - q)R(\mathbf{r})\mathbb{I}(\mathbf{r} \in D_n^*)}{Q(\mathbf{r})}$$

where $R(\mathbf{r}) = N(\mathbf{r})/P(\mathbf{r})$. For a given test population, the data itself is an empirical representation of $Q(\mathbf{r})$, and we can use this data to approximate expectation values, *provided we have* $R(\mathbf{r})$. Thus, classification does not actually require the full conditional PDFs.

In hindsight, this fact was actually apparent from the beginning. The optimal classification domains D_p^* and D_n^* can also be expressed uniquely in terms of $R(\mathbf{r})$. In fact, the set

$$B^* = \left\{ \mathbf{r}: \frac{q}{1 - q} = R(\mathbf{r}) \right\}$$

can be interpreted *both* as a relative probability level set *and* a boundary that partitions the measurement space into the classification domains (ignoring issue with sets of measure zero). This result is surprisingly powerful.

The set B^* can be interpreted as a discriminative classifier: nominally it only partitions the data into two classes. Yet it contains information about the relative probability of belonging to a class.

In fact, we were able to take this observation further. It is a theorem that the classifier associated with D_p^* and D_n^* minimizes the error

$$\mathcal{E}(q) = \int_{D_p} (1 - q)N(\mathbf{r})d\mathbf{r} + \int_{D_n} qP(\mathbf{r})d\mathbf{r}$$

given the conditional PDFs and a choice of negative and positive classification domains D_n and D_p . For this reason, Eqs. (3) and (4) are often called the *Bayes optimal classifier*, with q acting as a prior distribution (although we can estimate it without assuming a prior) [4]. But we also proved the converse: given a classifier that minimizes $\mathcal{E}(q)$, the corresponding sets have the same inequality structure as the Bayes optimal classifier [10]. Thus, if it stands to reason that we can identify a boundary that minimizes, e.g., the empirical error associated with training data, that boundary should approximate B^* as defined above.

To see the usefulness of this, note that B^* is easier to generalize to arbitrary dimension as compared to $P(\mathbf{r})$ and $N(\mathbf{r})$. In practice, boundary sets are $n - 1$ dimensional manifolds, whereas P and N are n dimensional functions. More importantly, the boundary sets typically have low-order structure. In many cases, we found that quadratic approximations work exceptionally well. Moreover, in such situations, B can be defined in terms

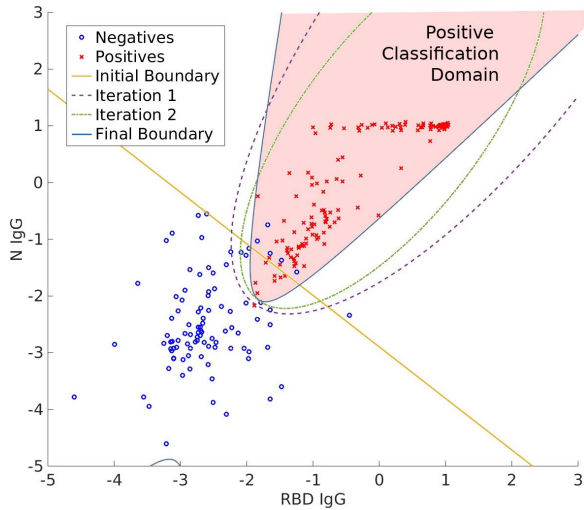


Figure 11. Illustration of the homotopy method applied to SARS-CoV-2 immunoglobulin G (IgG) data. The vertical axis corresponds to nucleocapsid (N) antibodies, which are often used to distinguish previous infections from vaccination.

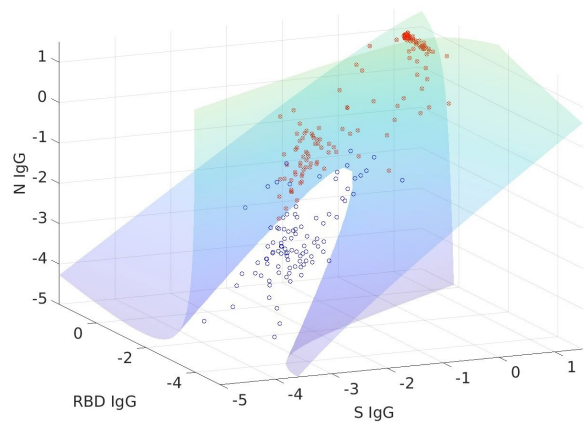


Figure 12. An example illustrating the ability of the homotopy method to classify data in higher dimensions. Very few datapoints are classified incorrectly (although this is difficult to capture in a single perspective).

of a quadratic form, which is easy to express in terms of matrix computations. This choice is also surprisingly general; in [10] we showed that such boundaries can arise from a class of probability models that greatly extend beyond normal distributions.

A more subtle but equally important observation is as follows. Consider that one can, in principle, solve a collection of optimization problems, each of which minimizes the prevalence-weighted empirical error rate for a different q . This yields a family of boundary sets B_q^* . Each such set corresponds to a level set for which $R(\mathbf{r}) = q/(1 - q)$. Thus, in this way, the minimizers trace out a contour plot of relative probabilities. In other words, a family of discriminative classifiers contains the same information as the full Bayes optimal classifier while only modeling a single function, $R(\mathbf{r})$, instead of

$P(\mathbf{r})$ and $N(\mathbf{r})$. This also yields uncertainty quantification for free: we automatically know the relative probability that a sample with \mathbf{r} belongs to a given class. Stated differently, generative (i.e., Bayes optimal) and discriminative classifiers that minimize classification error are true converses of another [10].

Realizing these ideas in practice is more complicated than first appears, however. Two main problems arise. First, threading an $n - 1$ dimensional manifold through a finite amount of n dimensional data in a way that minimizes the error is not a well-posed problem. The empirical error has a gradient that is everywhere zero or undefined. This can be solved by regularization, e.g., by using a homotopy-type algorithm to smooth the objective function and solve the corresponding optimization problem. One then sequentially takes the limit that the smoothing goes to zero; see Figure 10, Figure 11, and Figure 12 as well as [10]. A more difficult issue arises from the fact that the level-sets so constructed can cross, which yields contradictions in the resulting definition of relative probability. To overcome this issue, we have found that is necessary to simultaneously determine all of the B_q^* , subject to the constraint that the distance from the boundary of each data-point be a monotone function of prevalence [10].

Returning to the Beginning: A Surprise in Plain Sight. By the time these last projects began taking shape, it was early 2023. Up to this point, we still had not answered the question of how to *select* an optimal assay. In part, this was due to the fact that the practical requirements informing optimality had constantly changed. At the beginning of the pandemic, prevalence estimation and accuracy were at the forefront of everyone’s minds. In 2021, when vaccines started appearing, there was an increasing demand to solve multi-class problems. And by 2022, with herd immunity strongly building, the primary goal was to use assays to quantify immunity [12]. Thus, how to define a “best” assay when the definition of “best” keeps changing?

Analysis has a surprisingly powerful answer to this question hidden in the concept of *uniform* bounds. A canonical example of this is the notion of uniform convergence, wherein the difference between one function trending to another is bounded by some constant that does not depend on the independent variables. Taking inspiration from this idea, we proposed that a “best” assay is one with the smallest least-upper bound optimal uncertainty associated with all of the potential information extracted from the assay. Here a key challenge is to relate the least upper bound to both classification accuracy and uncertainty in prevalence estimation.

It turns out that one solution arises by analyzing the confusion matrix \mathbf{P} whose elements \mathbf{P}_{jk} are the measure of the j th conditional probability density function on domain D_k , assuming now a multiclass setting. The diagonal entries of \mathbf{P} can be interpreted as the rate of

classifying samples in the j th class correctly, with the off-diagonal elements corresponding to false classifications. A viable assay turns out to be one for which there exists a confusion matrix \mathbf{P} that is diagonally dominant. Given that, and the observation that \mathbf{P} is also a stochastic matrix, it is possible to prove that the largest Gershgorin radius¹⁰

$$\rho_{\max} = \max_j \{1 - P_{jj}\}$$

provides the needed uniform bounds [11]. In the case of prevalence estimation, for example, this leads to an unusual looking variance bound of the form

$$\sigma_q^2 \leq \frac{2c\rho_{\max} - \frac{c^2}{c-1}\rho_{\max}^2}{s(1-2\rho_{\max})^2} + \sum_{j=1}^c \frac{q_j(1-q_j)}{s},$$

where s is the number of samples, c is the number of classes, and q_j are the relative fractions of individuals in each class. Thus, ρ_{\max} can be treated as an objective function whose minimum corresponds to the best assay [11].

It is worth noting at this point that the off-diagonal elements of \mathbf{P} are often referred to as the assay sensitivity and specificity when working in a binary setting. These quantities are objects of intense interest in diagnostics and epidemiology, but primarily for regulatory purposes [4, 6]. Rarely are they considered in and of themselves. Yet, in returning to these simple concepts we had discovered that they were the key to the first question ever posed to us. *And no one had seen it before now, hiding in plain sight.*

Looking Outwards. While our investigations into diagnostics, and ultimately classification, led to surprising discoveries, they also point to a host of new and unresolved questions that are still active areas of research. Among them are problems related to generalization of our level-set methods to more classes, as well as proofs of convergence of the underlying algorithms.

The issues of modeling also highlight deeper methodological problems in serology. A key issue that has largely remained unresolved is the task of comparing measurements on different instruments. Fundamentally the measurement of antibody concentrations is actually a quantification of the binding affinity between an antibody and a substrate, i.e., one is measuring the properties of a chemical reaction, not the reactants per se. This has led to confusion in the community as to how to properly harmonize measurements. Recently we showed that such issues can be resolved by adopting a thermodynamic perspective of serology [12], but such work is on-going.

More interesting, however, are the deeper connections to machine learning. Bayes optimal classifiers and

the level-set classifiers we considered are prototypical examples of generative and discriminative algorithms. It has long been held that these are fundamentally distinct [10], yet we showed that they are essentially the same, provided we are willing to train the algorithms by minimizing a special objective function. But this begs the question: to what extent should we revisit the theory of ML to understand the connection between the objective function and an AI's connection to UQ? The need for this is perhaps presaged by the perception ML is a "black box," and that we could one day pay a heavy price for failing to understand how such algorithms represent information. Thus, perhaps it is time to go back to basics and ask simpler questions about the foundations of ML. If our experience has showed anything, there is value in returning to the basics. Sometimes important discoveries are still hiding in plain sight.

References

- [1] R.A. Fisher. The Use of Multiple Measurements in Taxonomic Problems. *Annals of Eugenics* 7:2 (1936), 179–188. DOI: [10.1111/j.1469-1809.1936.tb02137.x.hdl:2440/15227](https://doi.org/10.1111/j.1469-1809.1936.tb02137.x.hdl:2440/15227)
- [2] R. A. Fisher. (1938). The Statistical Utilization of Multiple Measurements. *Annals of Eugenics* 8:4 (1938), 376–386. DOI: [10.1111/j.1469-1809.1938.tb02189.x.hdl:2440/15232](https://doi.org/10.1111/j.1469-1809.1938.tb02189.x.hdl:2440/15232)
- [3] G. M. Martin, D. T. Frazier, and C. P. Robert. Computing Bayes: Bayesian Computation from 1763 to the 21st Century. Preprint, arXiv:2004.06425. DOI: [10.48550/arXiv.2004.06425](https://doi.org/10.48550/arXiv.2004.06425)
- [4] P. N. Patrone and A. J. Kearsley. Classification Under Uncertainty: Data Analysis for Diagnostic Antibody Testing. *Mathematical Medicine and Biology: A Journal of the IMA* 38:3 (2021), 396–416. DOI: [10.1093/imammb/dqab007](https://doi.org/10.1093/imammb/dqab007)
- [5] P. N. Patrone and A. J. Kearsley. Minimizing Uncertainty in Prevalence Estimates. *Statistics and Probability Letters* 205 (2024) 109946. DOI: [10.1016/j.spl.2023.109946](https://doi.org/10.1016/j.spl.2023.109946)
- [6] P. N. Patrone, P. Bedekar, N. Pisanic, Y. C. Manabe, D. L. Thomas, C. D. Heaney, and A. J. Kearsley. Optimal Decision Theory for Diagnostic Testing: Minimizing Indeterminate Classes with Applications to Saliva-based SARS-CoV-2 Antibody Assays. *Mathematical Biosciences* 351 (2022), 108858. DOI: [10.1016/j.mbs.2022.108858](https://doi.org/10.1016/j.mbs.2022.108858)
- [7] R. A. Luke, A. J. Kearsley, N. Pisanic, Y. C. Manabe, D. L. Thomas, C. D. Heaney, and P. N. Patrone. Modeling in Higher Dimensions to Improve Diagnostic Testing Accuracy: Theory and Examples for Multiplex Saliva-Based SARS-Cov-2 Antibody Assays. *PLOS One* 18:3 (2023), e0280823. DOI: [10.1371/journal.pone.0280823](https://doi.org/10.1371/journal.pone.0280823)
- [8] P. Bedekar, A. J. Kearsley, and P. N. Patrone. Prevalence Estimation and Optimal Classification Methods to Account for Time Dependence in Antibody Levels.

¹⁰ Because the matrix \mathbf{P} is a (column-wise) stochastic matrix, the diagonal entries of $\mathbf{I}-\mathbf{P}$ are in fact the Gershgorin radii.

- Journal of Theoretical Biology* **559** (2023), 111375.
DOI: [10.1016/j.mbs.2022.108858](https://doi.org/10.1016/j.mbs.2022.108858)
- [9] R. A. Luke, A. J. Kearsley, and P. N. Patrone. Optimal Classification and Generalized Prevalence Estimates for Diagnostic Settings with More Than Two Classes. *Mathematical Biosciences* **358** (2023), 108982. DOI: [10.1016/j.mbs.2023.108982](https://doi.org/10.1016/j.mbs.2023.108982)
- [10] P. N. Patrone, R. A. Binder, C. S. Forconi, A. M. Moormann, and A. J. Kearsley. Minimal Assumptions for Optimal Serology Classification: Theory and Implications for Multidimensional Settings and Impure Training Data. In review.
- [11] P. N. Patrone and A. J. Kearsley. Inequalities for Optimization of Diagnostic Assays. In review.
- [12] P. N. Patrone, L. Wang, S. Lin-Gibson, and A. J. Kearsley. Uncertainty Quantification of Antibody Measurements: Physical Principles and Implications for Standardization. In review.

Participants

Prajakta Bedekar, Anthony Kearsley, Rayanne Luke, Amudhan Krishnaswamy-Usha, Paul Patrone (ACMD); Lily Wang, Sheng Lin-Gibson (NIST MML); Nora Pisanic, Yukari C. Manabe, David L. Thomas, Christopher Heaney (Johns Hopkins University); Raquel Binder, Ann Moormann, Catherine Forconi (UMass Chan Medical School)

Restoration of Noisy Orientation Maps from Electron Backscatter Diffraction Imaging

The macroscale behavior of a solid material, e.g., its strength, flexibility, conductivity, is determined not only by its composition, but also fundamentally by its microstructure, that is the geometric layout or organization of its constituents at the microscopic level. Thus, measurements and quantitative characterization of the microstructure are also key to designing and manufacturing new materials that will perform as intended in various scientific and engineering applications. In this project, we developed computational algorithms to improve the quality of a certain class of microscopy imagery obtained to understand and characterize microstructures of solid materials.

Günay Doğan

Many common and useful materials, such as metals, ceramics, rocks, are polycrystals, which are composed of many crystallites or grains [1]. A grain is a region of a material that is highly ordered, i.e., the constituents are organized in a lattice. Hence, a grain and the locations in a grain have an orientation with respect to a lab frame, and the orientation can be measured to aid in characterizing the microstructure of a material. As the union of the grains compose the polycrystalline material, the orientations of the grains constitute the texture of the material.

To analyze the microstructure of a polycrystalline material sample, material scientists study the sizes, shapes and locations of the grains and their boundaries, and also the statistics of the orientations and texture [2]. For this, they can use a map of the grains in the form of an image, which can be obtained with scanning electron microscopy (SEM). In many cases of the interest, the image is acquired such that each pixel location in the image contains the orientation information, usually in the form of three Euler angles (as opposed to RGB values for color images), encoding the 3D orientation of the corresponding physical location. This produces an orientation map of the material sample, which is very helpful for quantitative analysis and characterization.

The orientation map can also be loaded into simulation software, such as NIST's Object Oriented Finite Element (OOF) system, to perform virtual experiments on the physical sample [3]. For this, OOF generates a finite element mesh matching the grains and their boundaries in the orientation map; the user can then solve physics equations, to model such properties as elasticity and heat transfer, on the mesh representing the material sample (see the project summary *OOF: Finite Element Analysis of Material Microstructures* on page

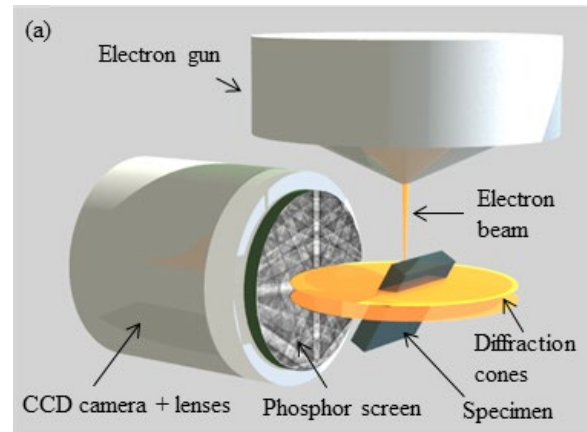


Figure 13. Illustration of a typical EBSD imaging hardware configuration. (Image by Stefano Vespucci et al. licensed as CC BY-SA 3.0, <https://commons.wikimedia.org/w/index.php?curid=129474938>)

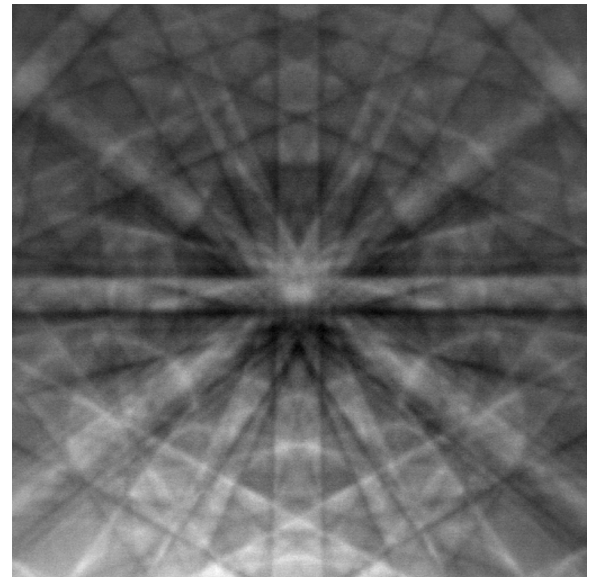


Figure 14. An example of the Kikuchi pattern produced by the scattered electrons from one probed location on the material sample during EBSD imaging. (Image by BenBritton, CC BY-SA 3.0, <https://commons.wikimedia.org/w/index.php?curid=5316267>)

87 for more information). Such analyses require an accurate orientation map.

Electron backscatter diffraction (EBSD) is a SEM technique that can generate a map of the grains and their orientations. It is a technique that utilizes a focused electron beam to probe a material sample one point at a time. To obtain a complete map, either the electron gun or the sample is moved in a systematic pattern so that each location on the sample can be probed. The sample is at a tilted angle with respect to the electron beam (see Figure



Figure 15. This figure shows the Euler angles in multiple grains of an example EBSD map as an RGB image. The image on the left shows the ground truth orientations. The image on the right shows the noisy map with up to 15° error in the Euler angles. The green pixels show the jumps due to the angle discontinuity at 0° - 360° .

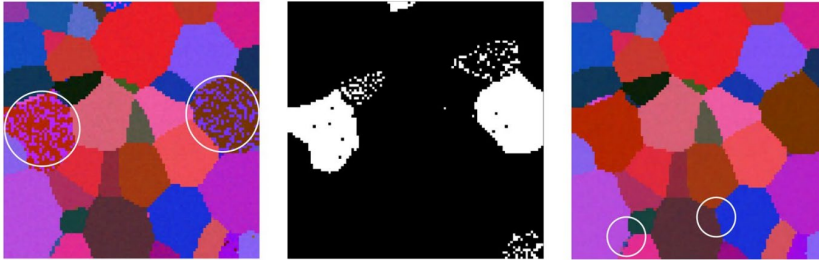


Figure 16. Illustration of the preprocessing applied to remove artifacts due to angle jump discontinuity at 0° - 360° . Two grains with very noisy appearances due to the jump discontinuity are circled in the left-most image. These are detected and marked on a binary mask (middle image) by the preprocessing algorithm. The algorithm then corrects for these artifacts and also replaces small outlier spots, circled in the rightmost image.

13 for an illustration of a typical EBSD setup). When the electron beam hits the sample, the electrons are backscattered from the lattice layers, and as the backscattered electrons interact with the atoms of the sample, they are diffracted and lose energy. The scattered electrons leave the sample at different angles and hit a phosphor screen, where they form the so-called Kikuchi patterns (see Figure 14). In principle, a Kikuchi pattern can be indexed to infer the orientation at the probed location, but in practice, errors and ambiguities can creep in due to various factors in the physical setup and in the indexing algorithm. The quality of the orientation thus acquired may sometimes not be at the level desired. The orientation map might have a noisy look because of the errors, including some impulse noise due to large errors at isolated points. Additionally, the orientation information at some locations of the map might be missing when the indexing algorithm fails to estimate the orientation from the corresponding Kikuchi pattern. In this project, we developed a denoising algorithm to restore high quality EBSD orientation maps by removing the noise from the acquired orientation maps.

Many image denoising algorithms are available in the image processing literature, and some of these have been applied to EBSD maps. Those commonly used for this purpose are mean filter, median filter, spline filter, Kuwahara filter, and half-quadratic filter. These algorithms work by replacing the orientation value at a given pixel with a weighted (and in some versions, also thresholded) average of the values from the neighboring pixels.

This filtering procedure can also be viewed as a finite difference discretization of a diffusive partial differential equation (PDE). When a rough or noisy function is used as the initial condition of a diffusive PDE, the initial function will gradually evolve into a smoother function as the PDE is evolved in time. In the discrete setting, the initial function is replaced by an image to be smoothed, and the discrete analog of the smooth PDE solution, namely the smoothed image, is computed with iterative updates to the image by a filtering scheme obtained from the discretization of the PDE. A key consideration is how much to iterate on the input image. Too many smoothing iterations not only remove noise, but also smooths out and destroys informative variations and features in the image. Thus, the smoothing algorithm should iterate and update the noisy image only as

many times as needed, but not much more.

Over-smoothing or blurring is a common problem that can be observed in some of the results in Figure 17 and Figure 18. There the grain boundaries are blurred by some of the denoising algorithms. It is however important to maintain sharp grain boundaries, and also to avoid moving the boundaries, which can be a side effect of some denoising algorithms. These effects can be alleviated or worsened by different settings of an algorithm's parameters. Obtaining the best looking denoised image can sometimes require a tedious tuning of algorithm parameters, such as the number of filtering iterations or the threshold values in the algorithm. The user needs to re-run the algorithm for different settings of the parameters. This has a computational cost and a time cost to the user.

There are additional issues that come up in denoising EBSD maps, in which each pixel value is a triplet of Euler angles (different from RGB images, which also have three channels, but each with values in the range 0 to 255 or 0.0 to 1.0). One issue is the apparent jump in value from angle 0° to angle 360° , both of which are clearly equivalent angles, denoting the same orientation. In the presence of noise, a grain with an average orientation angle close to 0° can have a mixture of angles close to 0° and 360° resulting in a very noisy appearance (see Figure 15 as an example). For example, if three neighboring pixels have angle values 3° , 359° , 1° , the numerical difference between the middle value and the first and third values are 354° and 358° respectively. These values are misleading, because the true

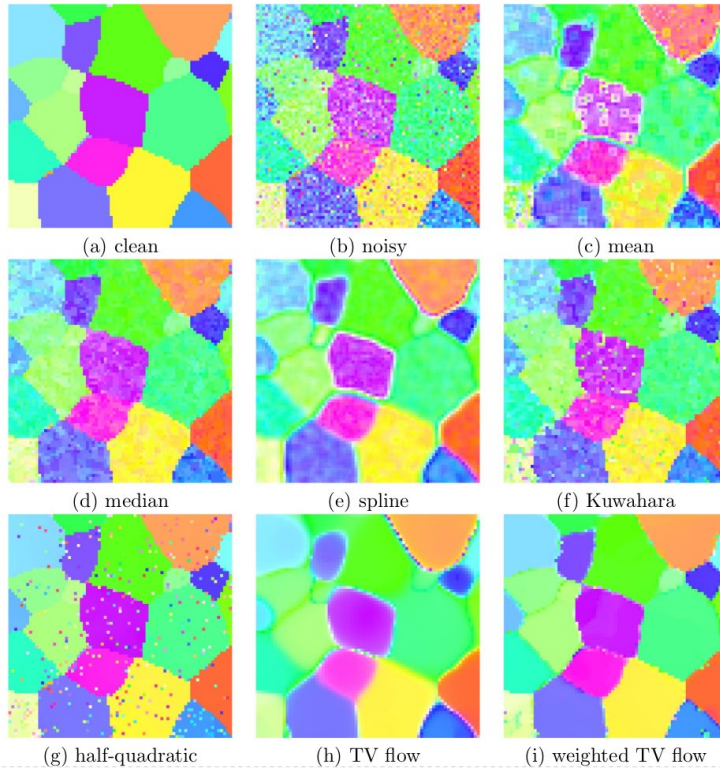


Figure 17. Denoised EBSD maps (shown using IPF-z color scheme) obtained with various denoising algorithms. The input to the algorithms was a synthetic EBSD map corrupted with de la Vallée Poussin noise with half-width $b = 8$ and 5% impulse noise.

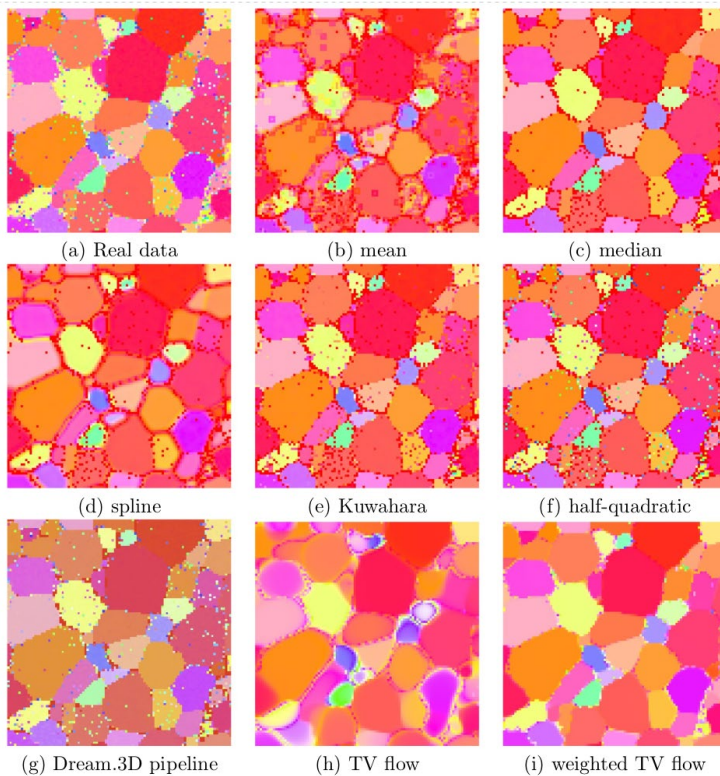


Figure 18. Details of a selected region of the real EBSD map and the denoised maps from Figure 19.

angle differences are only 4° and 2° as $359^\circ \equiv -1^\circ$. Thus, a filtering scheme using weighted averaging might attempt to compute and use the averages by $181^\circ = (3^\circ + 359^\circ)/2$ and $180^\circ = (359^\circ + 1^\circ)/2$ which are wrong. The denoising scheme should recognize that correct averages would be obtained with $1^\circ = (3^\circ - 1^\circ)/2$ and $0^\circ = (-1^\circ + 1^\circ)/2$. A similar, but more complicated issue arises from crystal symmetry. Multiple orientations of the same crystal configuration can look the same, and result in the same Kikuchi pattern. For example, a cubic layout with atoms placed at its corners looks the same from six different orientations when viewed across its faces. This leads to an ambiguity in EBSD imaging, when there might be multiple distinct orientations to assign to a probed location based on its Kikuchi pattern.

As pointed out earlier, some of the discrete filters for image denoising have a connection to and can be derived from a corresponding diffusion PDE. Realization of this connection has led to the derivation of a variety of diffusion PDEs for denoising in the mathematical image processing community. A well-studied diffusion PDE proposed for image denoising is the total variation (TV) equation [4, 5]. An important property of the TV equation is that it tends to preserve edges and boundaries during the diffusion, and initial functions (or images) tend to evolve to piecewise constant functions (or images). This makes the TV equation a good option for EBSD maps as the orientation values (Euler angles) are usually homogeneous and close to constant within a grain but may differ sharply across grain boundaries.

Thus, in denoising EBSD maps, it is desirable to smooth the orientation values within each grain, but also to avoid smoothing or blurring across grain boundaries. To denoise a given EBSD map, Dr. Doğan and his collaborators viewed it as three-channel image $f(k)$, $k = 1, 2, 3$, and used it as initial function $u(k)(\cdot, 0) = f(k)$ for the TV partial differential equation

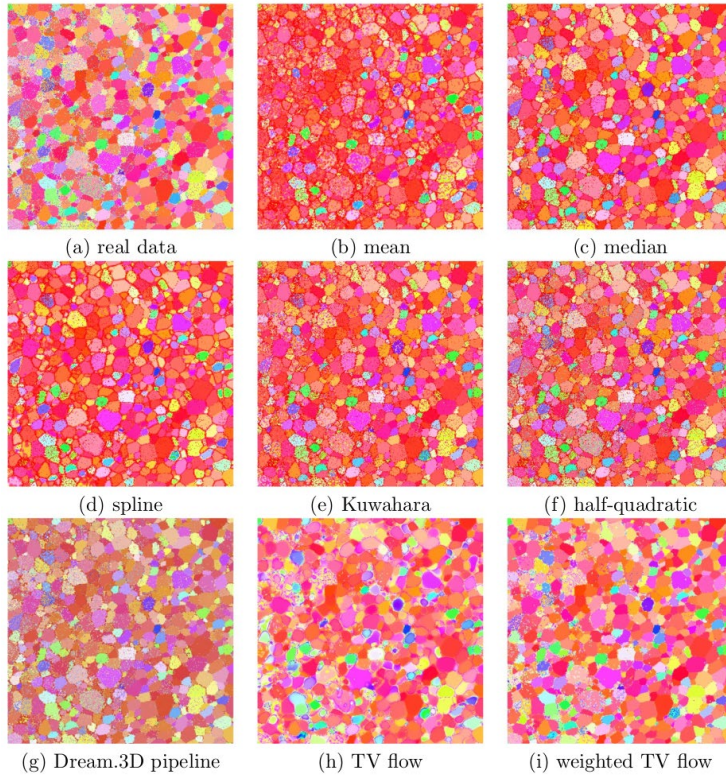


Figure 19. Denoised EBSD maps (shown using IPF-z color scheme) obtained with various denoising algorithms. The input in this experiment was a real EBSD map provided by Dr. Adam Creuziger from NIST MML.

$$\frac{\partial \mathbf{u}^{(k)}}{\partial t} = \frac{\|\mathbf{u}^{(k)}\|_{TV}}{\|\mathbf{u}\|_{TV}} \operatorname{div} \left(\frac{\nabla \mathbf{u}^{(k)}}{|\nabla \mathbf{u}^{(k)}|} \right), \text{ for } k = 1, 2, 3$$

where $\mathbf{u} = (u(1), u(2), u(3))$ is the image function that is solved for. To compute the solution, the TV equation is discretized using finite differences, and the initial function $\mathbf{u}^{(k)}(\cdot, 0)$ is iteratively updated by integrating the PDE forward in time. The final solution $\mathbf{u}(\cdot, T)$ at time $t = T$ is the denoised EBSD image [6].

The TV equation is the backbone of the denoising algorithm we have proposed for EBSD maps, but it is not enough on its own in the presence of the commonly encountered issues in EBSD denoising algorithms mentioned above. In order to obtain the best denoising results, we addressed each of these issues, and devised modifications and enhancements to their approach. Specifically,

1. To prevent blurring of grain boundaries, we added a spatially varying weight function in the divergence term of the TV equation to act as a switch. The weight function turns off the diffusion/smoothing on grain boundaries (detected by an edge detector filter) but allows diffusion/smoothing in the interiors of the grains.
2. To help users to determine the optimal stopping time T , we implemented a noise estimation

algorithm, and used it to find T automatically based on the noise, as opposed to having the user run repeated experiments to compute the cleanest-looking image. This is a key feature that makes the denoising algorithm practically parameter-free and easy to use.

3. To overcome the angle jump discontinuity issue at 0° to 360° , we developed a preprocessing algorithm that detects the grains where this issue arises. The preprocessing algorithm then offsets the angles in these grains to have them all close to either 0° or 360° . This procedure is illustrated in Figure 16.

4. To resolve orientation ambiguities due to crystal symmetries, we normalized the orientations in the given EBSD maps by projecting them into the fundamental zone of orientations, which acted as a unique default option in the existence of multiple equivalent orientations.

The effectiveness of the new denoising algorithm was demonstrated in detailed experiments with synthetic and real data [6]. The synthetic EBSD maps were generated using the DREAM.3D software [7]. The real EBSD maps were acquired and provided by Dr. Adam Creuziger at

MML/NIST [8]. In these experiments, the denoising algorithm using weighted TV equation was compared with mean, median, spline, Kuwahara, half-quadratic filtering and unweighted TV denoising. For real data, a DREAM.3D pipeline of thresholding, neighborhood correlation, and mask dilation was also used as a denoising algorithm in the comparisons. Better restoration from noisy EBSD maps can be seen in denoised images in Figure 17, Figure 18, and Figure 19 when weighted TV denoising used.

The synthetic EBSD maps were used for a more rigorous quantitative evaluation of the denoising performance. De la Vallée Poussin noise was added to clean ground truth images generated with DREAM.3D at increasing levels by increasing the half-width parameter b . At each noise level, ten synthetic images were generated and denoised. Availability of the ground truth images made it possible to compute per pixel errors in the denoised images; in other words, to quantify how close the denoised images were to the original clean images. The statistical significance of the comparisons and conclusions were also computed. The error values and the resulting conclusions (with their statistical significance) are reported in Table 1 for varying de la Vallée Poussin noise and 5 % impulse noise. Weighted TV denoising can be seen to outperform the competing denoising algorithm in Figure 17, Figure 18, and Figure

Table 1. Per pixel denoising errors (in degrees) for various denoising algorithms processing synthetic EBSD maps corrupted with noise with half-width parameters: 4, 8, 12, and 16, as well as 5 % impulse noise. The empirically best denoising error is in bold, while the error with the empirically second-best method is in italics. The stars indicate the p -value for the statistically best performance compared with the empirically second-best method. The p -values reported are for the paired t -test between the best methods and its closest competitor. * $p < .1$, ** $p < .01$, *** $p < .001$.

Half-width (b)	Mean	Median	Spline	Kuwahara	Half-quadratic	Weighted TV flow	p -values
4	.600°	.370°	.478°	.414°	.392°	.365°	.21007
8	.784°	.669°	.702°	.699°	.700°	.629°*	.01308
12	.812°	.674°	.725°	.726°	.868°	.595°*	.02166
16	.898°	.821°	.839°	.836°	1.06°	.690°***	.00019

19. For high noise levels, the improvement is much more pronounced. For low noise levels, weighted TV denoising and half-quadratic filtering have comparable denoising performance by looking at the error numbers in Table 1. On visual inspection, weighted TV denoising produced better looking restorations on most of the synthetic and real examples.

References

- [1] S. Zaefferer. A Critical Review of Orientation Microscopy in SEM and TEM. *Crystal Research and Technology* **46**:6 (2011), 607–628. DOI: [10.1002/crat.201100125](https://doi.org/10.1002/crat.201100125)
- [2] A. Creuziger and M. Vaudin. Report on VAMAS Round Robin of ISO 13067: Microbeam Analysis - Electron Backscatter Diffraction - Measurement of Average Grain Size. NISTIR 7814, National Institute of Standards and Technology, 2011. DOI: [10.6028/NIST.IR.7814](https://doi.org/10.6028/NIST.IR.7814)
- [3] S. A. Langer, E. R. Fuller, W. C. Carter. OOF: An Image-Based Finite-Element Analysis of Material Microstructures. *Computing in Science and Engineering* **3**:3 (2001), 15–23, 2001. DOI: <https://doi.org/10.1109/5992.919261>
- [4] L. I. Rudin, S. Osher, and E. Fatemi. Nonlinear Total Variation Based Noise Removal Algorithms. *Physica D Nonlinear Phenomena* **60**:1–4 (1992), 259–268. DOI: [10.1016/0167-2789\(92\)90242-f](https://doi.org/10.1016/0167-2789(92)90242-f)
- [5] P. Athavale, R. Xu, P. Radau, A. Nachman, and G. A. Wright. Multiscale Properties of Weighted Total Variation Flow with Applications to Denoising and Registration. *Medical Image Analysis* **23**:1 (2015), 28–42. DOI: [10.1016/j.media.2015.04.013](https://doi.org/10.1016/j.media.2015.04.013)
- [6] E. Atindama, P. Lef, G. Doğan, and P. Athavale. Restoration of Noisy Orientation Maps from Electron Backscatter Diffraction Imaging. *Integrated Material Manufacturing Innovation* **12** (2023), 251–266. DOI: [10.1007/s40192-023-00304-8](https://doi.org/10.1007/s40192-023-00304-8)
- [7] Dream.3D. <http://dream3d.bluequartz.net/>. Online, accessed September 9, 2020.
- [8] A. Creuziger and M. Vaudin, Data Publication: Data from NIST IR “Report on VAMAS Round Robin of ISO 13067: Microbeam Analysis - Electron Backscatter Diffraction - Measurement of Average Grain Size.” National Institute of Standards and Technology, 2023. DOI: [10.18434/mds2-2951](https://doi.org/10.18434/mds2-2951) (Accessed 2024-01-12)

Participants

Günay Doğan (ACMD); Prashant Athavale, Emmanuel Atindama, Peter Lef (Clarkson University)

Explainable Boosting Machines for Scientific Image Data

As the deployment of computer vision technology becomes increasingly common in science, the need for explanations of the system and its output has become a focus of great concern. Driven by the pressing need for interpretable models in science, we propose using Explainable Boosting Machines (EBMs) for scientific image data. Inspired by an important application underpinning the development of quantum technologies, we apply EBMs to cold-atom soliton image data vectorized using Gabor Wavelet Transform-based techniques that preserve the spatial structure of the data. In doing so, we demonstrate the use of EBMs for image data for the first time and show that our approach provides explanations consistent with human intuition about the data.

Justyna P. Zwolak

Given the widespread application of machine learning (ML), there is a growing need for explainable ML, allowing human users to understand why a model provides the output it does. While glass-box models, such as decision trees, linear regression, or classification rules, are relatively easy for humans to interpret, they tend to underperform compared to the state-of-the-art black-box models, such as deep neural networks (DNN). Moreover, glass-box models are not always easily adaptable to image data. At the same time, many experiments in the sciences produce data in the form of images, the nuanced analysis of which is limited by our preconceptions of the patterns and anomalies that could be present in the data. While some analysis tasks, such as data pre-processing, classification, and feature detection, have been automated using black-box ML techniques, the complex relationship between inputs and outputs in such models makes them difficult to interpret. This limits their application in areas where human-user understanding of the model output or the correlations between features implicitly utilized by the model are strictly necessary.

Prior work has demonstrated that some saliency methods, such as SmoothGrad or Gradient-weighted Class Activation Mapping (Grad-CAM), are independent of the model being explained as well as the data-generating process [1]. This fundamental shortcoming calls into question whether these methods provide explanatory information or are more akin to edge detectors.

We tackle the problem of ML explainability for image data using Explainable Boosting Machines (EBMs). EBMs are generalized additive models (GAMs) that account for pairwise interactions, i.e.,

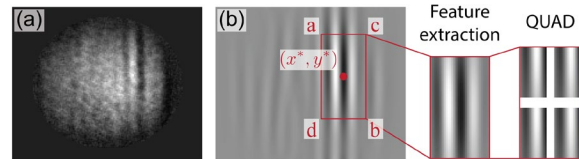


Figure 20. (a) Sample image of Bose-Einstein condensate from the reduced soliton dataset. (b) The optimized Gabor filter for the image shown in (a). Reproduced from [5].

$$g(E[y]) = \beta + \sum_i f_i(x_i) + \sum_{i \neq j} f_{ij}(x_i, x_j),$$

where g is the link function. The contribution of each feature to a final prediction can be visualized and understood either through a plot of $f_i(x_i)$ vs. x_i for the univariate terms or through heatmaps of the $f_{ij}(x_i, x_j)$ in the two-dimensional x_i, x_j -plane. This ability to analyze features either independently or, for the strongly interacting ones, as pairs is what makes EBMs highly intelligible. Moreover, since EBMs are additive models, they are modular in the sense that it is easy to reason about the contribution of each feature to the prediction [2].

EBMs are models designed to be highly intelligible and explainable, while also achieving comparable accuracy against state-of-the-art ML methods [3]. However, to date, EBMs have only been used with tabular data and have not been adapted to any other data type. To use EBMs with image data, we need to be able to automatically and in an interpretable way translate the primary visual features captured in images into a vectorized representation. We achieve this using a Gabor wavelet transform (GWT)-based method combined with parameter space optimization. The GWT is a multi-scale multi-directional wavelet initially formulated for signal detection in computer vision and image processing. It relies on convolving the Gabor kernel with an input image across a range of parameters to extract the characteristic features in the image. The 2D GWT kernel is defined by the product of a Gaussian and a plane wave, i.e.,

$$G_p(x, y) = \frac{e^{-\frac{1}{2} \left(\frac{x^2}{\sigma_x^2} + \frac{y^2}{\sigma_y^2} \right)}}{\sqrt{2\pi}\sigma_x\sigma_y} e^{i\lambda(x \sin(\theta) + y \cos(\theta))},$$

where σ_x and σ_y represent scale in x and y , and θ and λ are the wave direction and wavelength. By optimizing the parameters defining the Gabor kernel on a per-image basis, we can determine the locations and the size (scale) of the regions of interest (ROI).

Table 2. The results of 6-fold cross-validation for the reduced soliton dataset. The results are sorted by method (columns) and by data class (rows). Reproduced from [5].

Class	Metric	PF	GF	GF+PF	DNN	CNN	CAE+NN	EGF	EGF+PF
		+EBM						+EBM	
All	Accuracy	87.4(4)	84.8(6)	91.4(4)	82.3(8)	86.9(9)	91.9(5)	88.0(4)	92.8(5)
Longitud.	Precision	89.4(2)	87.4(6)	92.7(6)	88.2(1.3)	88.8(7)	95.4(8)	90.4(3)	94.0(4)
	Recall	95.7(4)	93.9(7)	96.9(4)	93.0(1.3)	95.8(1.4)	94.3(5)	95.1(5)	97.4(2)
Partial	Precision	81.0(1.2)	76.3(1.8)	87.5(1.1)	83.0(3.5)	84.6(2.5)	85.4(1.9)	87.7(7)	89.1(1.2)
	Recall	71.4(7)	66.2(2.1)	81.0(2.0)	64.6(3.2)	67.9(3.6)	84.5(2.7)	73.3(8)	83.7(1.4)
Vortex	Precision	22.6(20.9)	16.7(11.5)	83.9(4.4)	17.7(10.1)	26.8(8.8)	62.3(12.4)	67.3(4.6)	87.5(2.9)
	Recall	1.8(1.8)	1.5(1.0)	31.8(3.3)	50.7(9.4)	43.8(6.4)	96.6(2.8)	22.4(8.5)	44.5(3.1)

An example of an image dataset in which understanding the relative importance of and correlations between visual features characterizing the physical systems allows one to differentiate between different states of the system is the *Dark solitons in Bose-Einstein condensates (BECs) dataset v.2.0* [4]. We focus on the subset of the soliton dataset consisting of data containing exactly one excitation [class-1 data, see Figure 20(a)]. Each image in class-1 of the soliton dataset is tagged with a physically motivated subcategory label and associated physics-based fits of an inverted and skewed Mexican-hat function to one-dimensional (1D) background-subtracted projections of solitonic excitations candidates obtained using a least-squares fit [6]. We simplify the class-1 data into a 3-class dataset by combining data from the physically symmetric *top* and *bottom* partial soliton classes into a single category *partial* and the *clockwise* and *counterclockwise* solitonic vortices into a single category *vortex*. The data from the bottom partial and counterclockwise solitonic vortex classes are augmented via horizontal flipping to be consistent with the top partial and clockwise solitonic vortex classes, respectively. We call the final dataset used in the experiments the *reduced soliton dataset*. It includes 2229 images in the *longitudinal* class, 796 in the *partial* class, and 66 in the *vortex* class.

For the reduced solitonic excitation dataset, there is a single dominant ROI (at a single orientation) that corresponds to the primary excitation and its shoulders. Due to the unique expressiveness of the GWT, we can locate this region with a single filter, see Figure 20(b). This process consists of optimizing over the space of GWT parameters σ_x , σ_y , and λ with $\theta = 0$. Specifically, σ_x^* and σ_y^* correspond to the optimized width and height of the excitation while λ^* determines its optimized scale.

Given the role of symmetry in distinguishing different classes of excitations, our algorithm extracts the magnitudes in each quadrant of the region obtained by the optimized parameters. These subregions are found by describing the region around

$$(x^*, y^*) = \operatorname{argmax} \left(\left(G_{\sigma_x^*, \sigma_y^*, \lambda^*} * u \right) (x, y) \right)$$

bounded by $(\pm\sigma_x^*, \pm\sigma_y^*)$. Each subregion is then measured in terms of its L^2 -norm to acquire a single numerical description of the response.

To assess the classification performance of various methods using accuracy, precision, and recall, we carry out five 6-fold stratified cross-validations and report averaged results, with precision and recall analyzed at the class level. The experiments involve benchmarking EBMs on the physics-based fits (PF+EBM) and testing new methods using tabularized features from GWT (GF) and EBMs (GF+EBM). We also use EBMs on data representing GWT features and the physics-based fits (GF+PF+EBM). All tests using EBMs are performed in the one-versus-rest fashion. For comparison with more advanced classification techniques, we also test several NN-based classification methods. We train a DNN with just fully connected layers, a fine-tuned convolutional autoencoder (CAE+NN), and a simple convolutional neural network (CNN).

The results from all experiments, presented in Table 2, show that the GF+PF+EBM method is on par with the CAE+NN method in terms of accuracy, with 91.4(4) % and 91.9(5) %, respectively. On a per-class level, we observe that the GF+PF+EBM method has comparable precision and recall to the CAE+NN method for the longitudinal and partial classes. For the vortex class, the GF+PF+EBM method has significantly better precision, whereas CAE+NN method has a better recall.

To determine interpretability, we test the EBM on the raw GF the intensity of the GWT filter response in each quadrant of the extracted ROI consisting of top left (TL), top right (TR), bottom left (BL), and bottom right (BR) measures as well as the optimized excitation center (x^*, y^*) , see Figure 20(b). EBMs provide a global explanation for all the predictions by graphically depicting the contribution of individual features and pairwise correlations to the model. For example, Figure 21(a) and Figure 21(b) show feature importance for class partial and vortex, respectively. For the partial class, we observe that the offset in the y direction (y^*) emerged as one of the most significant features, aligning with human intuition due to the nature of partial excitations occurring in the upper half of the BEC. In contrast, for the vortex class, the expected asymmetry with respect to

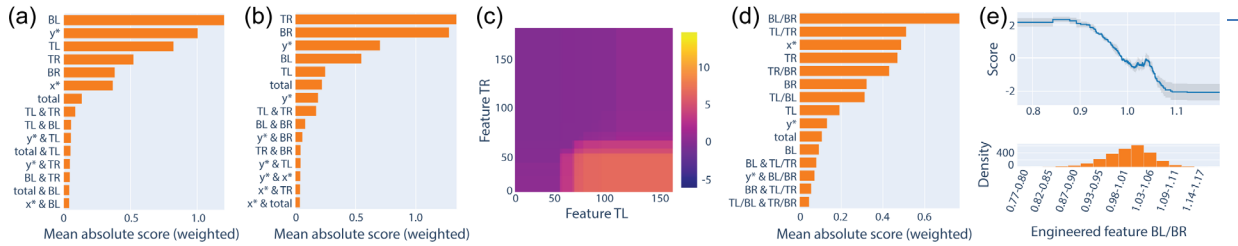


Figure 21. Interpretability results for the EBMs: feature importance for the (a) partial and (b) vortex classes, (c) pairwise interaction for TL and TR features for the vortex class, (d) engineered features importance for vortex class, and (e) the BL/BR engineered feature dependence plot. Reproduced from [5].

the x -axis is confirmed by EBMs consistently ranking the TR and BR quadrants as the most important. The pairwise interaction map for these two features shown in Figure 21(c) further confirms this intuitive dependence. Such correlations can guide the creation of new features capturing such interactions, potentially enhancing model performance.

Indeed, adding engineered GF (EGF) features representing primary pairs (TL/BL, TR/BR, TL/TR, and BL/BR) resulted in substantial performance improvements, particularly for the underrepresented vortex class as seen in Table 2. Figure 21(d) further confirms the importance of EGF features, with all four included in the list of top seven features, which indicates that they indeed provide additional predictive value. Figure 21(e) shows that $BL/BR < 1$ (i.e., stronger response in BR than in BL quadrant) indicates a vortex characteristic, which, again, agrees with the intuition. Similar analysis can be carried out for the remaining features and for all classes further validating the interpretability of the FGs and EFGs.

While our experiments focus on soliton in BEC data, our methods can readily adapt to other image-based scientific datasets with underlying visual structures. For more complex data requiring considerations of feature orientation or scale, the design of a tailored GWT-based filter bank may be necessary. Future research directions include applying these techniques to diverse scientific datasets, such as additional cold atoms datasets [6], quantum dot data [7], and medical datasets. We also plan to investigate their utility in clustering unlabeled data with unknown class counts.

References

- [1] B. Letham, et al. Interpretable Classifiers Using Rules and Bayesian Analysis: Building a Better Stroke Prediction Model. *Annals of Applied Statistics* **9** (2015), 1350–1371.
- [2] R. Caruana, et al. Intelligent Models for HealthCare: Predicting Pneumonia Risk and Hospital 30-Day Readmission. In *Proceedings of the 21th ACM SIGKDD International Conference on Knowledge Discovery and Data Mining*. Sydney, Australia, 2015, 1721–1730.
- [3] Y. Lou et al. Accurate Interpretable Models with Pairwise Interactions. In: *Proceedings of the 19th ACM SIGKDD International Conference on Knowledge Discovery and Data Mining*. Chicago, IL, 2013, 623–631.
- [4] Dark solitons in BECs dataset (2022). Database: data.nist.gov. DOI: [10.18434/mds2-2363](https://doi.org/10.18434/mds2-2363)
- [5] D. Schug, S. Yerramreddy, R. Caruana, C. Greenberg, and J. P. Zwolak. Extending Explainable Boosting Machines to Scientific Image Data. Preprint arXiv:2305.16526, 2023.
- [6] D. Schug, S. Yerramreddy, B. Egleston, R. Caruana, I. B. Spielman, C. Greenberg, and J. P. Zwolak. Explainable Machine Learning for Ultracold Atoms Image Data. In preparation.
- [7] D. Schug, T. J. Kovach, M. A. Wolfe, J. Benson, S. Park, J. P. Dodson, J. Corrigan, M. A. Eriksson, and J. P. Zwolak. Explainable Classification Techniques for Quantum Dot Device Measurements. In preparation.

Participants

Justyna P. Zwolak (ACMD); Craig Greenberg (NIST ITL); Daniel Schug, Sai Yerramreddy (University of Maryland); Rich Caruana (Microsoft)

ASTRA: Studying and Controlling Electronic Motion in Atoms and Molecules

Thirty five years after the discovery of above threshold ionization (ATI) and high-harmonic generation (HHG), we are in the midst of a revolution in the application of strong-field physics. The importance of these discoveries led to the 2023 Nobel Prize in Physics being awarded to Anne L’Huillier, Ferenc Krausz, and Pierre Agostini for the pioneering research which led to the birth of the field of attosecond science. Attosecond metrology has since emerged, enabling the study of several hitherto immeasurably fast electron phenomena in atoms, molecules, and solids. The importance of electron processes for the physical and life sciences, technology and medicine has rendered the young field of attosecond science one of the most dynamically expanding research fields of the new millennium. This article describes theoretical and computational work, undertaken by NIST researchers in collaboration with scientists at the University of Central Florida, which enhances the ability of attosecond science to help understand and control the electron dynamics in atoms and molecules.

Barry Schneider
William Earwood

The advent of attosecond spectroscopy has made it possible to produce electromagnetic radiation on sufficiently short timescales so that it is possible to study electron dynamics on its natural sub-femtosecond (10^{-18} sec) timescale. Attosecond technology followed decades of work by a number of researchers, in particular Anne L’Huillier, Ferenc Krausz and Pierre Agostini [1] who were awarded the 2023 Nobel prize in physics. This work included the discovery of both above-threshold ionization (ATI) and high-harmonic generation (HHG). Both of these phenomena were surprising but were eventually explained by a simple three-step model, involving: 1) tunneling of the electrons out of the atom due to the lowering of the Coulomb barrier by the electromagnetic field; 2) acceleration of the electrons in the electromagnetic field once liberated; and 3) when the field reverses its phase, re-collision of the electron with the atom. Some of the electrons escape and produce the ATI peaks, others recombine or slam back into the atom producing the HHG. After the discovery of ATI and HHG, much attention turned to using the radiation to explore new physical processes. Over time, it has become possible to produce well characterized pulses and to use these pulses to study the correlated motion of electrons in atoms, and perhaps even more critically, to control that motion and explore new physics. The work of our

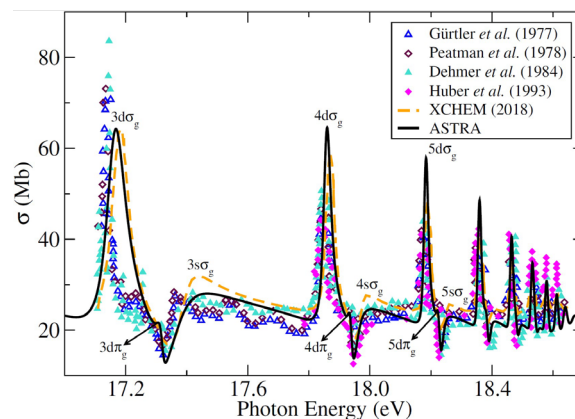


Figure 22. Total photoionization cross section of N_2 in the Hopfield resonances region. The spectrum computed with *astra* (solid black line) is compared with four independent measurements (triangles and diamonds) [8–11] and another theoretical spectrum obtained with *XCHEM* (dashed line) [12].

group is devoted to examining these processes in molecular systems where the many-body problem plays a critical role.

At a very fundamental level, the theoretical and computational study of atomic and molecular attosecond processes requires solving the time-dependent Schrödinger equation (TDSE),

$$\left(i \frac{\partial}{\partial t} - \hat{H}_M - \hat{E}_{int}\right) \Psi = 0 \quad (1)$$

where \hat{H}_M is the molecular Hamiltonian and \hat{E}_{int} the interaction of the molecular electrons with the electromagnetic field. The TDSE in general has high dimensionality, and its solution requires elaborate computational and numerical methods so that one can arrive at observables of interest, for example the probability that the system is in some state of the bare atom/molecule/ion with one or more electrons residing in either a bound or free state. It is often necessary to rely on powerful, high-performance computing machines within this context.

ASTRA (AttoSecond TRANSitions), a state-of-the-art molecular ionization code, has recently been introduced in the literature [2]. ASTRA employs a transition-density-matrix, close-coupling (TDMCC) formalism, uses overlapping Gaussian-type orbitals (GTOs) and numerical orbitals within the molecular charge density region, and can incorporate electron-electron exchange and correlation interactions in a systematically improvable fashion. It is capable of treating single and multiple ionization events and can be used to study HHG and ATI. The features that distinguish ASTRA from other existing molecular ionization codes

are its abilities to study a variety of ionization processes (in particular those induced by attosecond laser technology) for comparatively large target molecules. This flexibility arises from two sources; 1) by relying on the TDMs to describe the target ionic states, electronic correlation effects in the target are described in a compact fashion and 2) the use of numerical functions that extend over the entire molecular complex gives enormous flexibility in describing ionization.

Description of ASTRA. ASTRA's TDMCC formalism uses a close coupling (CC) approach as its starting point. Matrix elements between ionic states that are needed to compute the molecular bound and scattering states, and also the external electromagnetic field induced electron dynamics, are expressed in terms of transition density matrices (TDMs). The second quantized form of quantum mechanics and use of Wick's theorem helps to arrive at the final TDMCC equations.

ASTRA is a standalone code with its own implementation of modules and algorithms that are used to solve atomic and molecular scattering/ionization problems. Part of ASTRA's configuration involves interfacing with a few external codes that perform specific numerical tasks. These tasks include: 1) generating and optimizing an initial set of GTOs and computing the integrals between them; 2) building correlated ionic CC states and calculating the required TDMs between them; and 3) calculating one- and two-body electronic integrals between GTOs and hybrid numerical orbitals. The initial set of GTOs are generated from a quantum chemistry (QC) program. While many general QC codes are suitable for this job, ASTRA has relied on DALTON [3] thus far. LUCIA [4] is a second QC code, developed by one of our collaborators, that optimizes the initial set of GTOs, determines the correlated ionic states, and calculates the required TDMs. Like Dalton, Lucia involves only GTOs. Integrals involving GTOs and hybrid numerical orbitals are necessary if one elects to augment the GTOs with numerical functions, and if the GTOs are allowed to overlap the augmenting functions. To its advantage, ASTRA does both, affording considerable flexibility to its CC space. The hybrid orbitals are constructed from radial B-splines (typically of order 7 or greater) multiplied by real spherical harmonics placed at the molecular center of mass. The B-splines extend as far out in space from their origin as is needed for a particular problem, and are separated into internal and external regions, the former being those that overlap with the GTOs.

The number of integrals involving hybrid orbitals can in many applications reach the billions, so it is important to have an efficient numerical quadrature scheme to solve this problem. Thus far, GBTOLib [5] has been used for this purpose. Discussed in more detail below, we are in the process of deploying a new quadrature scheme suitable for problems involving more extended molecules.

Following its configuration, ASTRA can assemble the Hamiltonian matrix from the integrals and TDMs and solve the coupled-channel scattering problem for an electron in the field of the ion. While a complete description of how to solve this problem and the TDSE is beyond the scope of this discussion, a few remarks are in order. One avenue is to employ the solutions to the time-independent CC Schrödinger equation as a basis for the expansion of the TDSE. Once these are available it is possible to form wavepackets of these states at $t = 0$ and to couple them via the electron-field interaction and then propagate in time using split-operator or other techniques. To extend the solution of the time-independent Schrödinger to very large distances it is necessary to allow the wavefunction to behave correctly at long-range. This can be accomplished by adding a single, non-zero basis function, at the boundary of the computational region and then matching that to the proper outgoing wave. For problems involving only a single free electron at infinity, this may be done exactly. For problems involving multiple ionization, approximations need to be invoked.

For a localized wavepacket, one may actually sidestep the computation of the coupled-channel scattering states and employ a *discrete* set of Siegert states computed using an absorbing potential inside a large (i.e., a few hundred Bohr radii) box. These states exponentially decay and cannot be directly used to obtain observables depending on the wavefunction at very large distances, but nonetheless work quite well for predicting total photoionization cross sections or the energies of autoionizing states which "live" inside a confined space.

In our work to date, we have concentrated on the calculation of properties that do not depend on representing the asymptotic form of the exact wavefunction at very large distances very precisely. Hence, we have been able to use Siegert states to compute quantities like total photoabsorption cross sections and/or the position of localized resonance states by diagonalizing the Hamiltonian plus a complex absorbing potential (CAP) which turns on at long range. Siegert states are regular eigenfunctions of the Hamiltonian and satisfy outgoing wave boundary conditions at large distances. This can only happen if the energy and wave vector of the solution to the Schrödinger equation is complex. Using a complex absorbing potential at long range, if properly formulated, is equivalent to other approaches to computing Siegert eigenstates of the Schrödinger equation.

Development of a New Hybrid Integral Library. The GTOs extracted from Dalton and Lucia are, in general, linear combinations of ordinary Gaussian functions multiplied by a fixed real regular solid harmonic and are therefore non-zero in disjoint regions of space. Fortunately, there are well-known analytical formulas for evaluating the one- and two-electron integrals between GTOs. If, however, one needs an integral between a GTO and a hybrid orbital involving B-splines, one must

rely on numerical integration. There are at least two ways one could calculate these integrals. The first involves a spherical harmonic expansion about an arbitrary reference frame. This approach can be very efficient but is slowly converging when either 1) the disjoint GTO regions are well-separated or 2) the GTOs rapidly decay at more than one point in space. With increasing molecular size, condition 1) inevitably occurs. In practice, condition 2) occurs if one's study involves non-hydrogenic atoms.

The approach we are implementing is a type of *integral partitioning scheme*, which circumvents the problem described above. For any of the *hybrid* integrals involving both GTOs and numerical orbitals, a solution is to decompose a multi-centered integral into a sum over localized single-centered pieces [6]. This technique relies on the construction of a set of weight functions, $\{w_n(\vec{r})\}$ which form a partition of unity over all space,

$$\sum_n w_n(\vec{r}) = 1 \quad (2)$$

Using this partition, any integral involving a 3D function $F(\vec{r})$ can be localized about a fixed number of centers. For molecules, these centers are naturally the nuclear positions from which the multi-center character of each $F(\vec{r})$ originates, i.e.,

$$I = \int F(\vec{r}) d\vec{r} = \sum_n \int w_n(\vec{r}) F(\vec{r}) d\vec{r} \quad (3)$$

In practice, following the ideas detailed in our previous work [7], it is useful to modify each weight function so that it vanishes outside some finite radius R . To restore the partition of unity, a complementary weight function is introduced. This feature is particularly important when generating a large list $\{I_{ijkl}\}$ of two-electron, six-dimensional integrals,

$$I_{ijkl} = \int \frac{\phi_i(\vec{r}_1)\phi_j(\vec{r}_1)\phi_k(\vec{r}_2)\phi_l(\vec{r}_2)}{|\vec{r}_1 - \vec{r}_2|} d\vec{r}_1 d\vec{r}_2 \quad (4)$$

Essential to the operation of ASTRA, a big problem is the sheer size of this integral list, considering that in general $\sim N^4$ integrals that have to be computed for an orbital set of length N . For the problems we wish to solve, $N \sim 10^3$ is anticipated, and we have had to carefully consider how memory is managed and how our algorithms scale with increasingly large N . Along these lines, we have built in both molecular and permutational integral symmetry to reduce the size of these integral lists as much as possible. In addition, we are working towards *ad hoc* integral screening methods so that numerically insignificant floating point operations are avoided at various stages of the calculations.

Examples: N₂, H₂CO. Figure 22 compares the photoionization cross section in N₂ computed with ASTRA

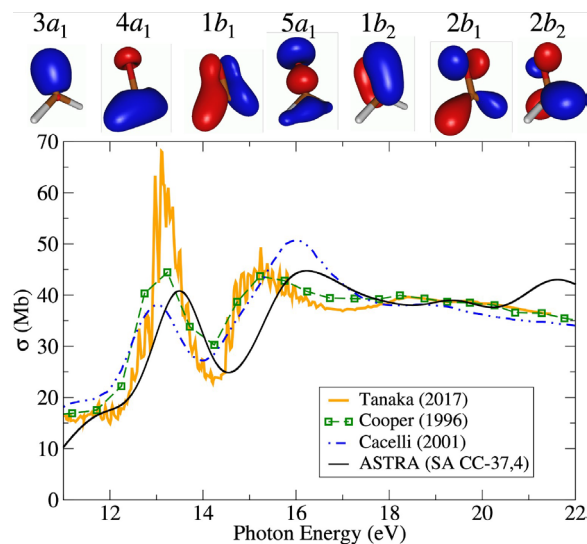


Figure 23. Formaldehyde total photoionization cross section above the ionization threshold. The ASTRA result (black-solid line) is obtained by including 37 ions in the CC expansion with $\ell \leq 4$. The ions were obtained through a CASCI using the orbitals coming from a SA-MCSCF calculation (see text for details). The ASTRA spectrum is compared with the RPA calculation in [13] (dotted-dash line) and two measurements, with lower resolution (dashed line and squares) and higher spectral resolution (orange-solid line) [14, 15]. The top of the figure shows the first seven molecular orbitals included in the ASTRA active space, in ascending energy order, up to the LUMO ($2b_2$) [16, 17].

to previous experimental work and an additional theoretical (XCHEM) computation. The theoretical signals have been convoluted with a 0.015 eV width normalized Gaussian to account for the experimental resolution. The ASTRA result is in very good agreement with both the XCHEM calculation and with the experimental spectra. For the first resonant feature corresponding to $3d\sigma_g$, both theoretical results show a broader peak than the measured value, which is likely due to residual electronic correlation missing in the lower lying members of the Rydberg series.

Figure 23 compares the photoionization cross-section of formaldehyde computed with ASTRA between 11 eV and 22 eV, with Cacelli *et al.*, an RPA calculation [13], and with two measurements: one from a lower-resolution 1996 experiment by Cooper *et al.* [14] and the other from a higher resolution 2017 experiment by Tanaka *et al.* [15]. The CC calculation included 10 open and 27 closed channels but no short-range correlation terms.

The spectrum exhibits two prominent shape resonances, a narrower one near 13 eV, and a broader less pronounced one at 15 eV. In the higher-resolution experiment by Tanaka, the first peak has smaller width and larger height. Considering the different resolutions, however, the results of the two experiments are compatible with each other. The RPA calculation [13] predicts the position of the first peak quite accurately but overestimates the position of the second peak by about 1 eV.

The heights of the first (second) peak are significantly under (over) estimated. These results suggest that both resonances are highly sensitive to correlation. ASTRA overestimates the position of the first peak by about 0.2 eV, but its magnitude is in better agreement with the experiment by Cooper. As is the case with Cacelli's result, the position of the second peak predicted by ASTRA is about 1 eV above the experimental value. The peak height, however, is almost coincident with one observed in the experiment. The results obtained with ASTRA are arguably the ones in best agreement with the experiment, to date. However, they also suggest that the theoretical model used here is still incomplete. Two possible causes for the discrepancy with the experiment are the residual dynamic correlation not captured by the CC expansion, and the fixed-nuclei approximation, which prevents us from accounting for the effects of nuclear motion and rearrangement in the molecular ion. We plan to tackle both of these challenges in the future.

References

- [1] Nobel Prize in Physics, 2023. URL: <https://www.nobelprize.org/prizes/physics/2023/press-release/>
- [2] J. Randazzo, C. Marante, S. Chattopadhyay, B. Schneider, J. Olsen, and L. Argenti. ASTRA: Transition-density-matrix Approach to Molecular Ionization. *Physical Review Research* **5** (2023), 043115. DOI: [10.1103/PhysRevResearch.5.043115](https://doi.org/10.1103/PhysRevResearch.5.043115)
- [3] K. Aidas, C. Angeli, K. Bak, V. Bakken, R. Bast, L. Boman, O. Christiansen, R. Cimraglia, S. Coriani, P. Dahle, et al. The Dalton Quantum Chemistry Program System. *Wiley Interdisciplinary Reviews: Computational Molecular Science* **4** (2014), 269. DOI: [10.1002/wcms.1172](https://doi.org/10.1002/wcms.1172)
- [4] J. Olsen, B. O. Roos, P. Jørgensen, and H. J. A. Jensen. Determinant Based Configuration Interaction Algorithms for Complete and Restricted Configuration Interaction Spaces. *The Journal of Chemical Physics* **89** (1988), 2185. DOI: [10.1063/1.455063](https://doi.org/10.1063/1.455063)
- [5] Z. Mašin, J. Benda, J. D. Gorfinkiel, A. G. Harvey, and J. Tennyson. UKRmol+: A Suite for Modelling Electronic Processes in Molecules Interacting with Electrons, Positrons and Photons using the R-matrix Method. *Computer Physics Communications* **249** (2020), 107092. DOI: [10.1016/j.cpc.2019.107092](https://doi.org/10.1016/j.cpc.2019.107092)
- [6] A. D. Becke. A Multicenter Numerical Integration Scheme for Polyatomic Molecules. *The Journal of Chemical Physics* **88** (1988), 2547. DOI: [10.1063/1.454033](https://doi.org/10.1063/1.454033)
- [7] H. Gharibnejad, N. Douguet, B. Schneider, J. Olsen, and L. Argenti. A Multi-center Quadrature Scheme for the Molecular Continuum. *Computer Physics Communications* **263** (2021), 107889. DOI: [10.1016/j.cpc.2021.107889](https://doi.org/10.1016/j.cpc.2021.107889)
- [8] P. Gürtler, V. Saile, and E. Koch. High Resolution Absorption Spectrum of Nitrogen in the Vacuum Ultraviolet. *Chemical Physics Letters* **48** (1977), 245. DOI: [10.1016/0009-2614\(77\)80308-4](https://doi.org/10.1016/0009-2614(77)80308-4)
- [9] W. B. Peatman, B. Gotchev, P. Gürtler, E. E. Koch, and V. Saile. Transition Probabilities at Threshold for the Photoionization of Molecular Nitrogen. *The Journal of Chemical Physics* **69** (1978), 2089 (1978). DOI: [10.1063/1.436808](https://doi.org/10.1063/1.436808)
- [10] P. M. Dehmer, P. J. Miller, and W. A. Chupka. Photoionization of $N_2 X^1\Sigma_g^+$, $v''=0$ and 1 Near Threshold. Preionization of the Worley–Jenkins Rydberg Series. *The Journal of Chemical Physics* **80** (1984), 1030. DOI: [10.1063/1.446829](https://doi.org/10.1063/1.446829)
- [11] K. P. Huber, G. Stark, and K. Ito. Rotational Structure in the Hopfield Series of N_2 . *The Journal of Chemical Physics* **98** (1993), 4471. DOI: [10.1063/1.465006](https://doi.org/10.1063/1.465006)
- [12] M. Klinker, C. Marante, L. Argenti, J. González-Vázquez, and F. Martín. Electron Correlation in the Ionization Continuum of Molecules: Photoionization of N_2 in the Vicinity of the Hopfield Series of Autoionizing States. *Journal of Physical Chemistry Letters* **9** (2018), 756. DOI: [10.1021/acs.jpcclett.7b03220](https://doi.org/10.1021/acs.jpcclett.7b03220)
- [13] I. Cacelli, R. Moccia, and R. Montuoro. Calculation of the Differential Photoionization Cross-Section of Formaldehyde. *Chemical Physics Letters* **347** (2001), 261. DOI: [10.1016/S0009-2614\(01\)01006-5](https://doi.org/10.1016/S0009-2614(01)01006-5)
- [14] G. Cooper, J. E. Anderson, and C. Brion. Absolute Photoabsorption and Photoionization of Formaldehyde in the VUV and Soft X-ray Regions (3–200 eV). *Chemical Physics* **209** (1996), 61-77. DOI: [10.1016/0301-0104\(96\)00079-1](https://doi.org/10.1016/0301-0104(96)00079-1)
- [15] H. K. Tanaka, F. V. Prudente, A. Medina, R. R. T. Marinho, M. G. P. Homem, L. E. Machado, and M. M. Fujimoto. Photoabsorption and Photoionization Cross Sections for Formaldehyde in the Vacuum-ultraviolet Energy Range. *The Journal of Chemical Physics* **146** (2017), 094310. DOI: [10.1063/1.4938054](https://doi.org/10.1063/1.4938054)
- [16] G. Schaftenaar and J. H. Noordik. Molden: A Pre- and Post-processing Program for Molecular and Electronic Structures. *Journal of Computer-Aided Molecular Design* **14** (2000), 123-134. DOI: [10.1023/A:1008193805436](https://doi.org/10.1023/A:1008193805436)
- [17] G. Schaftenaar, E. Vlieg, and G. Vriend. Molden 2.0: Quantum Chemistry Meets Proteins. *Journal of Computer-Aided Molecular Design* **31** (2017), 789-800. DOI: [10.1007/s10822-017-0042-5](https://doi.org/10.1007/s10822-017-0042-5)

Participants

Barry I. Schneider, William Earwood (ACMD); Heman Gharibnejad (Computational Physics Inc.); Luca Argenti, Carlos Marante, Siddhartha Chattopadhyay (U. of Central Florida); Juan Martin Randazzo (Consejo Nacional de Investigaciones Científicas y Técnicas, Argentina), and Jeppe Olsen (Aarhus University, Denmark)

Curvelet Uncertainty Principles, and the Infeasibility of Quantum Algorithms for Finding Short Lattice Vectors

If large-scale fault-tolerant quantum computers are ever constructed, they will be able to break essentially all of the public key encryption schemes and digital signatures that are currently used to protect communications on the internet. This threat has motivated the development of post-quantum cryptosystems that could perform these critical functions, and whose security is derived from computational problems that are hard for quantum computers to solve.

Among many cryptosystems that have been proposed, lattice-based cryptosystems are considered to be especially promising. These cryptosystems are based on problems involving high-dimensional lattices, such as the approximate Shortest Vector Problem (approximate SVP), and Bounded Distance Decoding (BDD). These problems are conjectured to be hard for quantum computers. Testing this conjecture requires developing the theory of quantum algorithms and computational complexity. In this work, we take a step in this direction.

We study a class of quantum algorithms that use the quantum curvelet transform to prepare lattice superposition states, which are potentially useful for solving approximate SVP and BDD. Previously, these techniques have been used to prove upper bounds on the computational complexity of approximate SVP and BDD. But this line of research has not resulted in an efficient quantum algorithm. Here, we prove that no quantum algorithm of this type can succeed in solving approximate SVP and BDD. Our proof uses an uncertainty principle for quantum measurements in the curvelet basis, which is also new.

Yi-Kai Liu

One of the most spectacular developments in the study of quantum computation was Peter Shor's discovery, in 1994, of a fast quantum algorithm for factoring large numbers and computing discrete logarithms. This theoretical result showed that, if large fault-tolerant quantum computers are ever built, they will be able to break essentially all of the public-key encryption schemes and digital signatures that are currently used to protect communications on the Internet (such as the RSA cryptosystem, Diffie-Hellman key exchange, and cryptosystems based on elliptic curve discrete logarithms).

This has motivated the development, standardization and deployment of so-called "post-quantum" cryptosystems, which could be used in place of existing public-key encryption schemes and digital signatures and would be secure against adversaries with large fault-

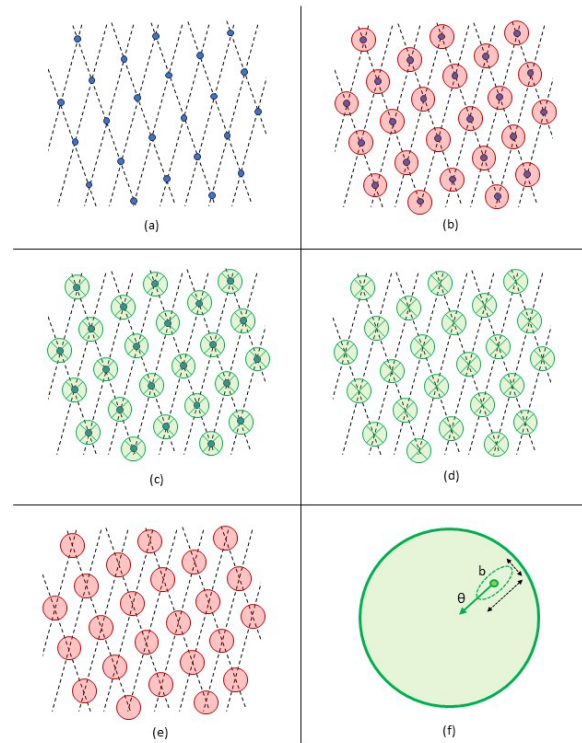


Figure 24. Stages in a potential quantum algorithm to solve the Bounded Distance Decoding problem.

tolerant quantum computers. (See *Post-Quantum Cryptography*, page 127).

But how does one gain confidence that these post-quantum cryptosystems really cannot be broken by quantum computers? This question leads to the very foundations of quantum mechanics, cryptography, and computational complexity theory.

On one hand, the power of quantum computers relies on phenomena such as quantum superposition, entanglement, and uncertainty (when measuring a quantum superposition state). But these phenomena are subtle. For instance, a quantum superposition $|0\rangle + e^{i\phi}|1\rangle$ is "coherent," meaning that it contains some additional information (namely the complex phase factor $e^{i\phi}$) that is not present in a classical probability distribution. But the information in a quantum superposition can only be accessed by performing measurements, which collapse the superposition. This imposes strong constraints (such as uncertainty principles) on the kinds of information that can be extracted from a quantum superposition.

Furthermore, whenever two or more quantum systems are present, they can be prepared in entangled states (for instance, the state $|01\rangle - |10\rangle$), which exhibit

correlations that cannot be reproduced by any classical physical theory (more precisely, any “local realistic” theory). But these correlations are not arbitrarily powerful. For instance, they cannot be used to communicate faster than the speed of light or violate other well-established physical laws.

In the context of quantum algorithms, researchers have come to a similar conclusion: the power of quantum computers is subtle. There is evidence that quantum computers cannot solve generic NP-complete problems in polynomial time, and thus cannot achieve an exponential speedup over classical computers for most of the hard computational problems that occur in the real world. But there are notable examples of computational problems—particularly problems with the right kind of algebraic structure, and problems that involve simulating the time evolution of many-body quantum systems—that really are easy for quantum computers and seem hard for classical computers. This highlights the importance of studying quantum cryptanalysis, as a generalization of classical cryptanalysis.

When considering the design of post-quantum cryptosystems, one encounters an additional complication. There are two broad classes of cryptosystems: symmetric cryptosystems (such as block ciphers and hash functions), and public key cryptosystems (such as public key encryption schemes and digital signatures). Quantum algorithms (in particular, Shor’s algorithm) are primarily a threat to public key cryptosystems, not symmetric cryptosystems. Unfortunately, public key cryptosystems are a more recent innovation, compared to symmetric cryptosystems, and the scientific understanding of how to design public key cryptosystems is continuing to evolve. For some of these cryptosystems (e.g., those based on elliptic curve isogenies), the state of the art has changed substantially in recent years [1].

Among the post-quantum cryptosystems that have been proposed, lattice-based cryptosystems are one of the leading candidates for deployment on the Internet. These cryptosystems are based on the computational hardness of certain problems involving high-dimensional lattices, in particular, the approximate Shortest Vector Problem (approximate SVP), and the Bounded Distance Decoding problem (BDD), in certain parameter regimes (specifically, when the SVP approximation ratio is polynomial in the lattice dimension, and when the BDD decoding radius is inverse polynomial in the lattice dimension).

There is some evidence that these problems are hard for quantum computers. Most of this evidence is circumstantial: it comes from developing the theory of quantum algorithms and investigating different approaches to designing quantum algorithms for these problems. There has been progress along these lines [2, 3], and it is perhaps reassuring that this progress seems to fall short of the specific kinds of lattices and the specific parameter regimes that are relevant to post-quantum cryptography.

These works can be viewed as examples of a broader research program, where one identifies classes of quantum algorithms, and analyzes their capabilities and limitations.

Here, we investigate an approach to designing quantum algorithms for approximate SVP and BDD, by preparing certain lattice superposition states using the quantum curvelet transform. These techniques have an interesting history. Lattice superposition states have been used to show upper-bounds on the complexity of approximate SVP and BDD [4], and worst-case-to-average-case reductions from approximate SVP and BDD to a problem called “Learning with Errors” (LWE), which is widely used in lattice-based cryptography [5]. The curvelet transform has been used in classical algorithms for solving wave equations [6], and quantum algorithms for certain oracle problems [7].

The idea of using the quantum curvelet transform to prepare lattice superposition states is quite natural, and it has been tried before, without success [8]. But the reasons for this failure were not immediately apparent. In this work, we provide the first proof that a large class of quantum algorithms using this idea cannot succeed in solving approximate SVP and BDD [9]. This proof relies on an uncertainty principle for quantum measurements in the curvelet basis, which is also new.

We now describe these ideas in more detail. Given a set of basis vectors $b_1, \dots, b_n \in R^n$, let $L = L(b_1, \dots, b_n)$ be the lattice consisting of all integer linear combinations of b_1, \dots, b_n . The Bounded Distance Decoding problem (BDD), with decoding radius $0 < r < 1/2$, is defined as follows:

Given basis vectors b_1, \dots, b_n , and a vector $t \in R^n$ that is promised to be “close” to the lattice $L = L(b_1, \dots, b_n)$, find the lattice point $x \in L$ that is closest to t (with respect to the l_2 norm).

Here, t is called the “target vector,” and we are promised that the distance from t to the closest lattice point x is at most $r\lambda_1(L)$, where $\lambda_1(L)$ is the length of the shortest vector in L . In the following discussion, it is natural to work with the BDD problem. However, these ideas can also be applied to approximate-SVP, by switching to the dual lattice and using the techniques developed in [5].

We will make use of a particular class of quantum states, which are often called lattice superposition states. For simplicity, we describe these states using unnormalized wavefunctions over R^n . (This calculation can be made rigorous, by restricting the wavefunctions to a finite subset of the lattice, so that they can be normalized, and by sampling the wavefunctions on a discrete grid in R^n , so that they can be represented on a quantum computer using a polynomial number of qubits [9].)

These lattice superposition states have the form

$$|\psi\rangle \propto \sum_{x \in L} |G_x\rangle$$

where the state $|G_0\rangle$ is an isotropic wavefunction (i.e., a wavefunction that is symmetric with respect to rotations), which is supported (up to a negligible error) within a ball of radius $\lambda_1(L)/2$ around the origin; and each state $|G_x\rangle$ is a copy of $|G_0\rangle$ that is centered at the point x . There are many possible choices for the isotropic wavefunction that defines $|G_0\rangle$. Perhaps the simplest choice is an n -dimensional Gaussian.

We will also make use of the quantum curvelet transform. This is an efficiently computable quantum operation, which is related to the classical curvelet transform in the same way that the quantum Fourier transform is related to the classical Fourier transform. The classical curvelet transform, in turn, is a special kind of wavelet transform, whose basis functions resemble wave packets in R^n .

Each curvelet basis function is identified by a triple (a, b, θ) , where $b \in R^n$ is the “position” of the wavepacket, $\theta \in S^{n-1}$ is the “direction” in which the wavepacket oscillates, and $0 < a < 1$ is the “scale” of the wavepacket, which specifies its spatial extent and frequency. The quantum curvelet transform, then, maps a wavefunction $|f\rangle$ on R^n to a wavefunction $|\Gamma_f\rangle$ that is a superposition over these triples (a, b, θ) :

$$|f\rangle = \sum_{x \in R^n} f(x)|x\rangle \mapsto |\Gamma_f\rangle = \sum_{0 < a < 1} \sum_{b \in R^n} \sum_{\theta \in S^{n-1}} \Gamma_f(a, b, \theta) |a, b, \theta\rangle$$

We are interested in the possibility of a quantum algorithm that uses the quantum curvelet transform to prepare lattice superposition states, and then uses these states to solve BDD. Such an algorithm would work as follows:

1. Prepare a uniform superposition over all lattice points, $\sum_{x \in L} |x\rangle$ (Figure 24, panel (a))
2. Initialize a second quantum register. Conditioned on the state $|x\rangle$ in the first register, prepare the state $|G_x\rangle$ in the second register. This produces the state $\sum_{x \in L} |x\rangle |G_x\rangle$ (see panel (b))
3. Apply the quantum curvelet transform on the second register. This produces the state $\sum_{x \in L} |x\rangle |\Gamma_{G,x}\rangle$, where $|\Gamma_{G,x}\rangle$ is a superposition over “lines” that pass near the point x (see panel (c)). (More precisely, $|\Gamma_{G,x}\rangle$ is a superposition over triples (a, b, θ) , where the line $\{b + \lambda\theta \mid \lambda \in R\}$ passes near the point x .)
4. Conditioned on the second register, compute x , and transform the state of first register from $|x\rangle$ to $|0\rangle$. This produces the state $\sum_{x \in L} |0\rangle |\Gamma_{G,x}\rangle$ (see panel (d)).

5. Discard the first register and apply the inverse quantum curvelet transform on the second register. This produces the desired lattice superposition state: $|\psi\rangle \propto \sum_{x \in L} |G_x\rangle$ (see panel (e)).
6. Define a potential function $V(\cdot)$ on R^n , by setting $V(y) = \langle \psi | S_y | \psi \rangle$, where S_y is the “shift by y ” operator, $S_y: |x\rangle \mapsto |x + y\rangle$. Use $|\psi\rangle$ to evaluate $V(\cdot)$ (up to a small additive error) and use $V(\cdot)$ to solve BDD. (These steps can be done efficiently, using an iterative sampling procedure [5].)

When does this algorithm succeed? This depends critically on the choice of the isotropic wavefunction $|G_0\rangle$. This determines (1) whether the lattice superposition state $|\psi\rangle$ can be prepared using the quantum curvelet transform, and (2) whether the resulting potential function $V(\cdot)$ can be used to solve approximate SVP and BDD. Taken individually, each of the conditions (1) and (2) is not difficult to satisfy. But it is much harder to construct a wavefunction $|G_0\rangle$ that satisfies both (1) and (2) simultaneously.

We show that it is impossible for a wavefunction to satisfy both of the above requirements simultaneously. To do this, we prove a novel uncertainty principle for quantum measurements in the curvelet basis. This shows that, in step 3 of the quantum algorithm, any measurement or computation that involves the vector b projected onto the subspace orthogonal to θ , always suffers from a certain amount of statistical uncertainty (Figure 24, panel (f)). This implies strong constraints on the kinds of wavefunctions $|G_0\rangle$ that can satisfy requirement (1) above.

We then give a precise characterization of requirement (2), by approximating the autocorrelation function of the wavefunction $|G_0\rangle$ as a mixture of Gaussians. By combining these two results, we conclude that no quantum algorithm of the kind described above can succeed in solving BDD or approximate SVP.

References

- [1] W. Castryck and T. Decru. An Efficient Key Recovery Attack on SIDH. In *Advances in Cryptology – EUROCRYPT 2023*, Lecture Notes in Computer Science **14008** (2023). DOI: [10.1007/978-3-031-30589-4_15](https://doi.org/10.1007/978-3-031-30589-4_15)
- [2] R. Cramer, L. Ducas, and B. Wesolowski. Short Stickelberger Class Relations and Application to Ideal-SVP. In *Advances in Cryptology – EUROCRYPT 2017*, Lecture Notes in Computer Science **10210** (2017). DOI: [10.1007/978-3-319-56620-7_12](https://doi.org/10.1007/978-3-319-56620-7_12)
- [3] L. Eldar and S. Hallgren. An Efficient Quantum Algorithm for Lattice Problems Achieving Subexponential Approximation Factor. Preprint, 2022. URL: <https://arxiv.org/abs/2201.13450>
- [4] D. Aharonov and O. Regev. A Lattice Problem in Quantum NP. In *44th Annual IEEE Symposium on*

- Foundations of Computer Science (FOCS)*, 2003, 210–219. DOI: [10.1109/SFCS.2003.1238195](https://doi.org/10.1109/SFCS.2003.1238195)
- [5] O. Regev. On Lattices, Learning with Errors, Random Linear Codes, and Cryptography. *Journal of the ACM* **56**:6 (2009), 1–40. DOI: [10.1145/1568318.1568324](https://doi.org/10.1145/1568318.1568324)
- [6] E. J. Candes and D. L. Donoho. Continuous Curvelet Transform: I. Resolution of the Wavefront Set. *Applied and Computational Harmonic Analysis* **19**:2 (2005), 162–197. DOI: [10.1016/j.acha.2005.02.003](https://doi.org/10.1016/j.acha.2005.02.003)
- [7] Y.-K. Liu. Quantum Algorithms Using the Curvelet Transform. In *Proceedings of the 41st Annual ACM Symposium on Theory of Computing (STOC)*, 2009, 391–400. DOI: [10.1145/1536414.1536469](https://doi.org/10.1145/1536414.1536469)
- [8] Y.-K. Liu. “Preparing Lattice Superpositions on a Quantum Computer.” Workshop on Post-Quantum Information Security. Joint Quantum Institute, University of Maryland, College Park, MD, USA. October 2010.
- [9] Y.-K. Liu. An Uncertainty Principle for the Curvelet Transform, and the Infeasibility of Quantum Algorithms for Finding Short Lattice Vectors. Preprint, 2023). URL: <https://arxiv.org/abs/2310.03735>
-

Participants

Yi-Kai Liu

Coexistence for Node Synchronization in Quantum Network Entanglement Distribution

Distributing quantum entanglement over long distances in optical fibers is a challenging but essential requirement for quantum networks. The tight timing tolerances needed for certain quantum processes and applications becomes very difficult to satisfy at distribution distances of over 100 km, which are needed to realize regional and metropolitan scale quantum networks. One option is to use high-accuracy precision time protocol (HA-PTP) signals for picosecond level synchronization of distant nodes in the same optical fiber as the single photon level quantum signal – a technique known as coexistence. While long proposed, this had never been attempted at such distances. As part of a multi-NIST organizational unit collaboration between ITL, the Physical Measurement Laboratory (PML) and the Communications Technology Laboratory (CTL), we have studied the feasibility and limits of coexistence and have successfully implemented high-fidelity entanglement distribution over 100 km in fiber coexisting with a classical HA-PTP signal for the first time.

Anouar Rahmouni
Thomas Gerrits
Oliver Slattery

The fundamental resource for quantum communications is the entanglement of quantum bits (called qubits), enabling their quantum states to maintain a strong correlation across time and distance such that an action (e.g., a measurement) on one of the qubits will impact the other qubits despite their physical separation. This

amazing property can enable seemingly magical applications such as the teleportation of quantum information, the realization of secure communications, and the sharing of quantum computing resources and quantum sensing processes across multiple separated quantum devices.

The essence of a quantum communication network is to distribute the entanglement to the nodes of the network where these actions and processes can be implemented. A longstanding challenge for the development of quantum networks is to ensure that the entangled qubits – distributed using carrier optical photons – arrive at and are processed at the network nodes within extremely tight timing tolerances. As the quantum network expands to metropolitan and regional scales and the distance between nodes increases to several tens or over 100 kms, the synchronization of the processes at these nodes becomes very challenging. This is particularly true when transmitting carrier photons over long-distance optical fibers since path length changes due to environmental conditions become more dominant and need to be tracked in near real-time.

For many quantum networking applications, one approach is to use classical synchronization signals through the same fiber strand as the quantum signal in a technique known as coexistence. In this way, the classical signal will encounter the same conditions as the quantum signal and can be analyzed and processed to ensure high precision node fiber-length estimation and therefore time synchronization between the nodes for the quantum applications. There are other benefits to using coexistence such as for the distribution of verification signals, for classical header information, for the compensation for drifts in polarization and phase,

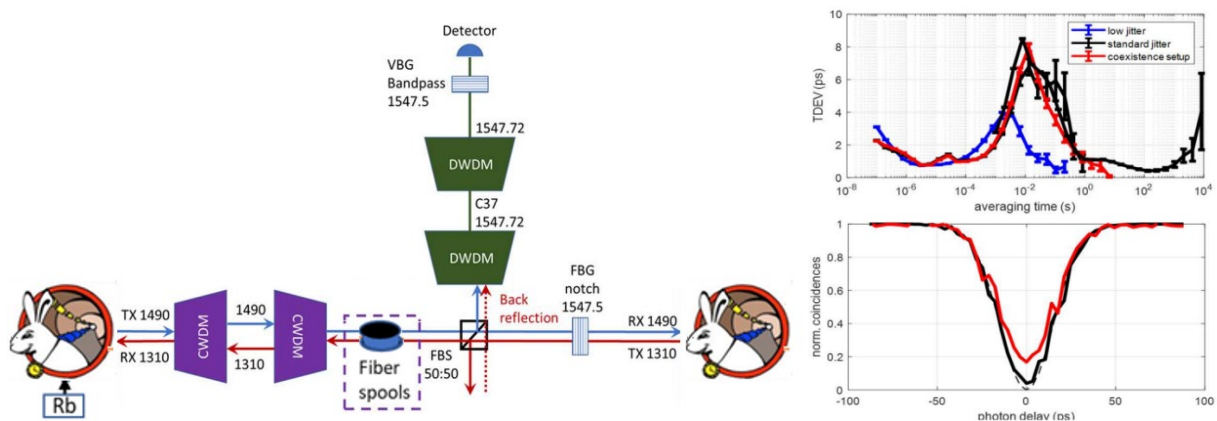


Figure 25. Experimental configuration to assess and verify feasibility of using WR-PTP in coexistence with quantum channel signals for compatibility with quantum networks. For details, see reference [3]. The upper graph on the right shows the time deviation between the two WR synchronized nodes. The lower graph shows a simulated interference dip using this level of synchronization with typical single-photon source and detector characteristics.

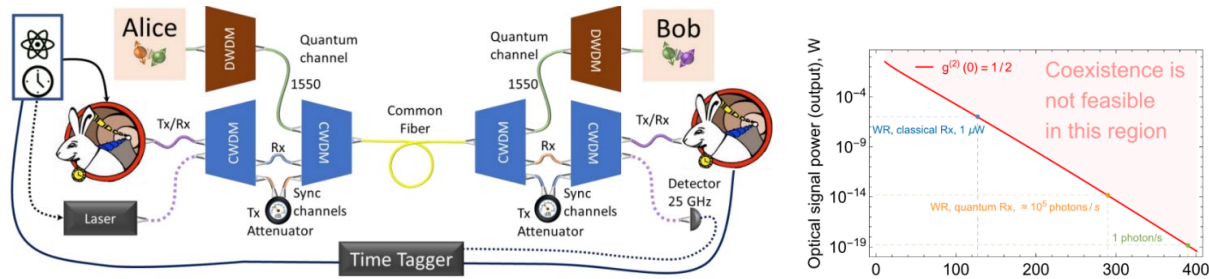


Figure 26. The Time-Synchronized Quantum Network Testbed. For details, see reference [4]. The yellow loop shows the common optical fiber spool used for the investigating the limits of coexistence of quantum and classical signals. The commercial classical timing solution used for synchronization of the nodes is the White Rabbit Precision Time Protocol (WR-PTP). The graph on the right shows the coexistence limit as a function of fiber link length. The limit is defined as when the HOM interference visibility $g^{(2)}(0) = 0.5$ (red line).

and for reducing deployment costs by enabling the use of existing classical fiber network infrastructure. However, having an intense classical light signal, or more specifically the noise it generates, in the same fiber as the fragile single-photon quantum signal has prevented the practical implementation of coexistence in very long-distance quantum networks.

With the support of funding from the internal NIST Quantum Networking Grand Challenge (QNGC), researchers from ITL, PML and CTL have faced this challenge head-on: verifying the feasibility for using commercial classical synchronization systems in quantum network configurations, defining the limits of practical coexistence with existing commercial classical timing solutions and, for the first time, reporting high-fidelity entanglement distribution through more than 100 km of optical fiber in coexistence with classical timing signals.

Assessment of Coexistence and Quantum Node Synchronization with Classical White Rabbit Signals.

Developed at CERN, White Rabbit (WR) Precision Time Protocol (WR-PTP) is an Ethernet-based protocol for optical two-way time transfer (O-TWTFT), which has now evolved to become an IEEE standard for precision synchronization [1]. Current state-of-the-art commercial WR systems have timing precision (timing jitter) of a few ps [2] and synchronization accuracy of less than 1 ns. To assess WR for use in quantum links, we were interested in looking at the short-term (1 s) variability between two separated WR systems, in this case configured as a leader and a follower. Also, to assess compatibility with quantum network configurations, we studied the WR-PTP on the same actual fiber as a desired quantum channel and observed the effect in the quantum channel.

Figure 25 shows the measurement setup used to verify the feasibility of coexistence of the classical two-way WR synchronization signals (at the wavelengths of 1310 nm and 1490 nm) and to study the impact on a quantum channel near 1550 nm. With the two WR synchronization nodes separated by fiber spools of various distances, we observed that that number of noise photons increased

proportionally with the length of the fiber. We experimentally verified that the noise photons are due to Raman scattering of the WR signals at the wavelength closest to the quantum channel. This told us that the level of detuning between the classical WR synchronization signal and the quantum channel is critical for compatibility with quantum networks.

The time-deviation between the two WR nodes, a measure of the synchronization between them, was studied for a standard version and a higher performance “low-jitter” version of the WR system. Unsurprisingly, the low-jitter version resulted in less time-deviation between the nodes. In both systems however, the feasibility of coexistence was verified with a simulated measurement of the single photon interference possible for a typical entangled photon pair source and single photon detection system characteristics. The simulated Hong-Ou-Mandel dip shows viable single-photon interference even in the presence of measured background noise. This study verified that coexistence of classical WR and quantum signals is viable and provided clues on how to optimize the configuration of the quantum network for implementing it.

Limits of Coexistence. There are practical limits to the implementation of coexistence with commercial off-the-shelf classical signal transmitters and receivers. At issue is the 10^{10} difference in optical power between the classical and quantum channel signals. To establish the limits of coexistence for off-the-shelf classical timing solutions, we built a Time-Synchronized Quantum Network Testbed (TSQNT) consisting of two nodes (Alice and Bob) implementing the WR-PTP as shown in Figure 26. To allow for coexistence, the classical signal needs to be sufficiently detuned from the quantum signal and its power kept as minimal as needed for the synchronization protocol to operate. We used the theoretical model of classical signal induced background noise generation in long fiber links that was derived and experimentally verified by characterizing fiber patches of different lengths [5]. We have shown (see the graph in Figure 26) that these limits enable the distribution of entanglement over metropolitan distances (up to 100

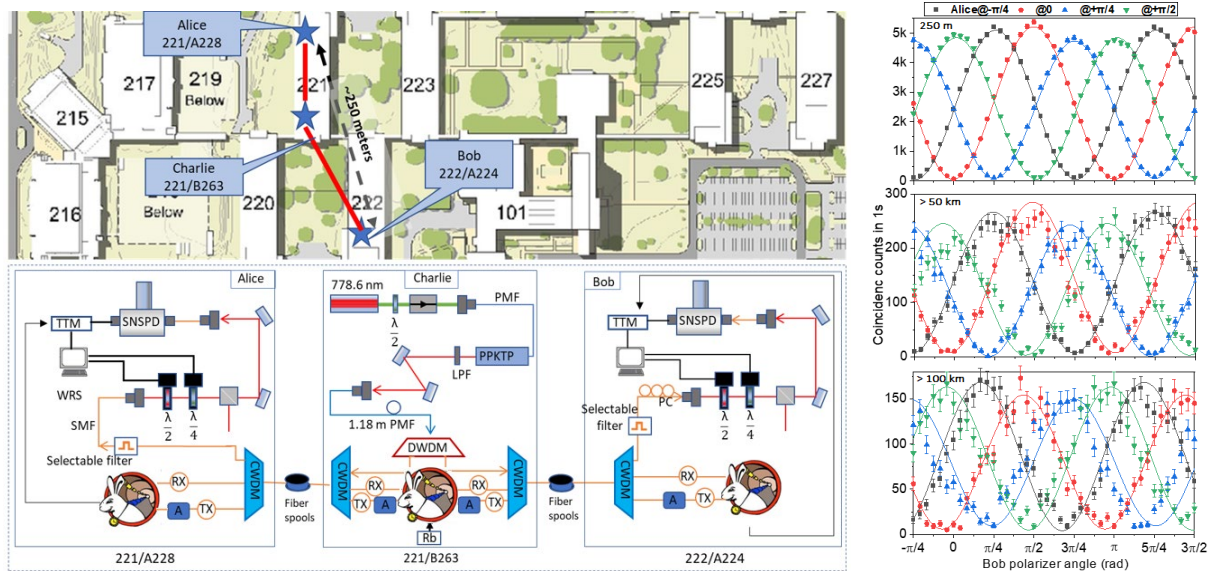


Figure 27. Experimental configuration for long distance entanglement distribution with coexistence with classical synchronization signals. For details, see reference [4]. The upper part of the figure shows a map of the NIST Gaithersburg campus indicating where the experiment was implemented, and the lower part of the figure shows the schematic of the experimental setup. The graphs on the right show the polarization entanglement measurement fringes for three separation distances between the receiver nodes of Alice and Bob including 250 m (top), over 50 km (middle) and over 100 km (bottom).

km) in optical fibers (with microwatt-level classical signals) if the coexistence network is carefully designed and cleverly implemented using standard two-way transmitters and receivers. Further, we have been able to extend that limit with more sensitive customized commercial classical signal receivers (beyond 100 km) and have identified the limit for state-of-the-art “quantum” receivers (up to 300 km) and for ultimate sensitivity ‘one-photon level’ receivers (up to 400 km) [4]. The extension of coexisting links beyond 400 km is unfeasible, because the classical power of 1 photon per second at the receiver sets the practical limit for any useful synchronization protocol (green dashed lines).

High Fidelity Entanglement Distribution over 100 km with Coexistence. Based on previous results, we customized the setup and chose optimal WR-PTP system transmitter and receiver signal wavelengths (1270 nm for one direction and 1290 nm in the other direction, both far inside the o-band and further detuned from the desired quantum channel) and implemented the synchronization coexisting in a single fiber with a quantum signal at 1550 nm [6]. This enabled the use of a much more sensitive WR receiver of -41 dB, greatly reducing the power requirement for the classical signal. The increased detuning from the quantum channel resulted in less classical signal induced noise mixing with the quantum signal.

The experiment was performed between three nodes (Alice, Bob and Charlie) across two buildings on the NIST Gaithersburg campus, as shown in Figure 27. Alice’s node is located at the end of building 221, Charlie’s node is located at the other end of the same

building, and Bob’s node is located in the adjacent building 222. There were three receiver node separation distances including 250 m, > 50 km, and > 100 km.

A high-quality, yet compact and movable, polarization entangled photon source (EPS) was implemented (at Charlie) using a non-linear process called Spontaneous Parametric Down Conversion (SPDC), a well-established mechanism for generating entangled pairs of photonic qubits. This EPS system and the corresponding entangled photon analyzers (EPA) (one each located at Alice and Bob) were designed and built in-house. The analyzers included in-house built and well-characterized superconducting nanowire single photon detectors (SNSPDs) for optimal detection of the single photon entanglement carriers.

The graphs in Figure 27 show the results for the distribution of entanglement from the source at Charlie to the receivers at Alice and Bob. The sinusoidal fringes from the coincidence counts are analyzed to provide the entanglement visibility. While the visibility of the entanglement over longer distances is reduced due to losses, noise and decoherence in the transmission channels, the longest distance (over 100 km of fiber between Alice and Bob) retains a visibility of greater than 81 %, well above the theoretical threshold ($\frac{1}{\sqrt{2}} \approx 71\%$) needed to verify that quantum entanglement is preserved.

The study of the fundamental limits of coexistence will be a valuable and useful guide for designing and implementing real-life coexisting quantum/classical links for quantum networks. The implementation of high-fidelity entanglement distribution over very long fiber distances represents a significant step towards the

practical implementation of robust and efficient metropolitan-scale quantum networks.

References

- [1] M. Lipiński, T. Włostowski, J. Serrano, and P. Alvarez. White Rabbit: A PTP Application for Robust Sub-Nanosecond Synchronization. In *2011 IEEE International Symposium on Precision Clock Synchronization for Measurement, Control and Communication*, September 2011, 25-30.
 - [2] M. Rizzi, M. Lipinski, P. Ferrari, S. Rinaldi, and A. Flammini. White Rabbit Clock Synchronization: Ultimate Limits on Close-in Phase Noise and Short-Term Stability Due to FPGA Implementation. *IEEE Transactions on Ultrasonics, Ferroelectrics, and Frequency Control* **65:9** (2018), 1726-1737.
 - [3] T. Gerrits, I. A. Burenkov, Y.S. Li-Baboud, A. Rahmouni, D.J. Anand, O. Slattery, A. Battou, and S. V. Polyakov. White Rabbit-assisted Quantum Network Node Synchronization with Quantum Channel Coexistence. In *CLEO: QELS Fundamental Science, 2022*, FM1C-2.
 - [4] I. A. Burenkov, A. Semionov, Hala, T. Gerrits, A. Rahmouni, D.J. Anand, Y. S. Li-Baboud, O. Slattery, A. Battou, and S.V. Polyakov. Fundamental Coexistence Limit of Quantum Stages with White Rabbit Synchronization in Quantum Networks. In *CLEO: Technical Digest Series 2023*, FM1A.4.
 - [5] I. A. Burenkov, A. Semionov, T. Gerrits, A. Rahmouni, D.J. Anand, Y. S. Li-Baboud, O. Slattery, A. Battou, and S. V. Polyakov. Synchronization and Coexistence in Quantum Networks. *Optics Express* **31:7** (2023), 11431-11446.
 - [6] A. Rahmouni, P. Kuo, Y. S. Li-Baboud, I. A. Burenkov, Y. Shi, M.V. Jabir, N. Lal, D. Reddy, M. Merzouki, L. Ma, A. Battou, S.V. Polyakov, O. Slattery, and T. Gerrits. Metropolitan-Scale Entanglement Distribution with Coexisting Quantum and Classical Signals in a Single Fiber. In review.
-

Participants

Thomas Gerrits, Oliver Slattery, Anouar Rahmouni, Paulina Kuo, Yicheng Shi, Nijil Lal, Lijun Ma (ACMD); Ya-Shian Li-Baboud (ITL); Sergey Polyakov, Ivan Burenkov, Hala, Alexandra Semionov, M.V. Jabir, Dileep Reddy, Josh Bienfang (PML); Abdella Battou, Mheni Merzouki, DJ Anand (CTL).

Mathematics of Metrology

Mathematics plays an important role in measurement science. Mathematical models are needed to understand how to design effective measurement systems and to analyze the results they produce. Mathematical techniques are used to develop and analyze idealized models of physical phenomena to be measured, and mathematical algorithms are necessary to find optimal system parameters. Mathematical and statistical techniques are needed to transform measured data into useful information. We develop fundamental mathematical methods and tools necessary for NIST to remain a world-class metrology institute, and to apply these to measurement science problems

ITVOLT: An Iterative Solver for the Time-Dependent Schrödinger Equation

Barry I. Schneider
Heman Gharibnejad (Computational Physics Inc.)
Ryan Schneider (UC San Diego)

In atomic units, the time-dependent Schrödinger equation (TDSE) takes the form

$$\left[i \frac{\partial}{\partial t} - H(\mathbf{r}, t) \right] \psi(\mathbf{r}, t) = 0$$

for a Hamiltonian $H(\mathbf{r}, t)$ and a corresponding wavefunction $\psi(\mathbf{r}, t)$, where \mathbf{r} denotes the spatial variables of the system. Solutions to the TDSE are central to a variety of research efforts in physics and quantum chemistry [1-3]. Numerical methods for the problem attempt to balance the need for highly accurate solutions with the computational constraints associated with problems in quantum mechanics.

As an extension of recent work [4], and specifically motivated by research of Ndong et al. [5], we devised a new method that propagates a solution to the TDSE by solving an equivalent Volterra integral equation. Referred to as Iterative Volterra Propagator or ITVOLT, our method solves the TDSE on successive intervals $[\tau_j, \tau_{j+1}]$ by first converting it to the Volterra integral equation

$$\begin{aligned} \psi(\mathbf{r}, t) &= e^{-iH_j(\mathbf{r})(t-\tau_j)}\psi(\mathbf{r}, \tau_j) \\ &\quad - i \int_{\tau_j}^t e^{-iH_j(\mathbf{r})(t-t')}V_j(\mathbf{r}, t')\psi(\mathbf{r}, t')dt' \end{aligned}$$

which holds for $\tau_j \leq t \leq \tau_{j+1}$. Here, $H_j(\mathbf{r})$ is the value of H at the midpoint time $\frac{\tau_j+\tau_{j+1}}{2}$ while $V_j(\mathbf{r}, t)$ is the time-dependent part of H minus its value at the same point.

Choosing a set of quadrature points $\{t_p\}_{p=1}^n$ in $[\tau_j, \tau_{j+1}]$ and computing a corresponding set of weights $\{w_{p,l}\}$ via Lagrange interpolation, we can replace the

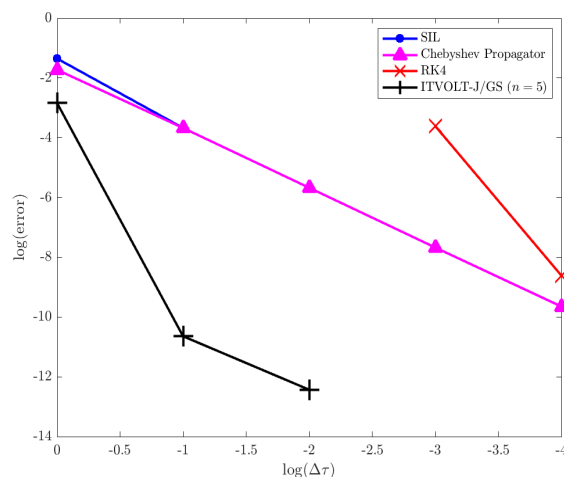


Figure 28. Accuracy vs. propagation step size $\Delta\tau$ for various methods of solving the driven harmonic oscillator TDSE. For ITVOLT, n is the number of quadrature points used on each propagation interval. Accuracy is measured as worst-case population probability error in the first 300 states. Plot taken from [6].

Volterra integral equation with a linear system, where at each quadrature point t_p

$$\begin{aligned} \psi(\mathbf{r}, t_p) &\approx e^{-iH_j(\mathbf{r})(t_p-\tau_j)}\psi(\mathbf{r}, \tau_j) \\ &\quad - i \sum_{l=1}^n w_{p,l} e^{-iH_j(\mathbf{r})(t_p-t_l)}V_j(\mathbf{r}, t_l)\psi(\mathbf{r}, t_l). \end{aligned}$$

ITVOLT proceeds by solving this linear system iteratively. The numerical details are flexible, allowing for a variety of choices of quadrature points and iteration techniques. Throughout, the use of easily accessible Lagrange interpolations promotes efficiency. As shown in Figure 28, ITVOLT is capable of outperforming existing, standard techniques, including both fourth order Runge-Kutta and second order, short-time propagators.

These results were published, alongside a Fortran implementation, in a special issue of Computer Physics Communications on software for attosecond chemistry [6]. Current work explores the scalability of ITVOLT to larger, resource-constrained problems, in particular the TDSE for the 3D hydrogen atom.

- [1] I. Gainullin. High-performance GPU Parallel Solver for 3D Modeling of Electron Transfer During Ion-Surface Interaction. *Computer Physics Communications* **210** (2017), 72-78.
- [2] E. Paquet and H. L. Viktor. Computational Methods for Ab Initio Molecular Dynamics. *Advances in Chemistry* (2018), 9839641.
- [3] M. Abu-samha and L. B. Madsen. Multielectron Effect in the Strong-Field Ionization of Aligned Nonpolar Molecules. *Physics Review A* **38** (2022), 013117.
- [4] H. Gharibnejad, B. I. Schneider, M. Leadingham, and H. J. Schmale. A Comparison of Numerical Approaches to the Solution of the Time-Dependent Schrödinger Equation in One Dimension. *Computer Physics Communications* **252** (2020), 106808.
- [5] M. Ndong, H. Tal-Ezer, R. Kosloff, and C. P. Koch. A Chebyshev Propagator with Iterative Time Ordering for Explicitly Time-Dependent Hamiltonians. *The Journal of Chemical Physics* **132** (2010), 064105.
- [6] R. Schneider, H. Gharibnejad, and B. I. Schneider. ITVOLT: An Iterative Solver for the Time-Dependent Schrödinger Equation. *Computer Physics Communications* **291** (2023), 108780.

Riesz Capacity and Related Topics

John P. Nolan

Debra J. Audus (NIST MML)

Jack F. Douglas (NIST MML)

Capacity is used to understand the properties of general shape. The Newtonian capacity of a molecule is related to many physical properties of an object, e.g., the electrostatic capacity of charged objects, and understanding how particles diffuse in liquids, how heat flows to/from an object, etc. Riesz α -capacity is a generalization of the standard capacity. We developed an algorithm to compute α -capacity for general shapes in \mathbb{R}^d using stable random walks to approximate the equilibrium measure of an object. The Walk-In-Out-Balls (WIOB) generalizes the Walk-On-Spheres method. This work has resulted in two publications; see [1] and [2].

Ongoing work is to extend the method to compute logarithmic capacity, computing swept volumes of objects, proving results about α -capacity, and developing stable random walks on half-spaces.

- [1] J. P. Nolan, D. J. Audus, and J. F. Douglas. Computation of Riesz α -capacity C_α of General Sets in \mathbb{R}^d using Stable Random Walks. *SIAM Journal on Applied Mathematics* (2024), to appear.
- [2] L. Devroye and J. P. Nolan. Random Variate Generation for the First Hit of the Symmetric Stable Process in \mathbb{R}^d . *Journal of Statistical Theory and Practice* (2024), to appear.

True Becquerel: A New Paradigm for 21st Century Radioactivity Measurements

Bradley Alpert

Ryan Fitzgerald (NIST PML)

Denis Bergeron (NIST PML)

Richard Essex (NIST PML)

Svetlana Nour (NIST PML)

Galen O'Neil (NIST PML)

Daniel Schmidt (NIST PML)

Gordon Shaw (NIST PML)

Mike Verkouteren (NIST MML)

Kelsey Morgan, Daniel Swetz, Joel Ullom, et al. (NIST PML)

Expanding applications of radioactivity in medicine, energy, and security demand quantification of complex mixtures at uncertainty levels that are currently unachievable. This project is enabling measurement of absolute activity (Bq) of radionuclide mixtures, avoiding chemical separation, by analysis of the decay heat signature of gravimetric samples embedded within microcalorimeter detectors. This capability consolidates multiple measurements into one, reducing cost and uncertainty. Success is creating a primary realization of the Bq for direct assay of real-world samples at NIST and beyond, resulting in faster clinical trials of new radiopharmaceuticals and a faster, expanded nuclear forensics “fingerprinting” method for improved decision making.

The project enters its fourth year of NIST Innovations in Measurement Science funding with establishment of a new transition-edge-sensor (TES) spectrometry laboratory in Gaithersburg as well as procedures and initial practice with dispensing, weighing, and TES-embedding of mg-quantity radioactive nuclides. This work has involved integration of detectors and low-temperature electronics fabricated in Boulder with commercial room-temperature electronics and a He dilution refrigerator in a new laboratory, in pursuit of the goal of quantitative determination of sample constituents at the level of 0.1 % uncertainty. Initial spectrometry of Am-241 decays have been validated with standard methods involving liquid scintillation. Mixtures with additional radionuclides are next.

The analysis challenges include (1) characterization of detector dynamics, to enable determination of decay energies of events with poor temporal separation, limiting detector dead time, at an accuracy that reflects the exquisite precision of the TES detector, (2) characterization of the partial energy losses due to transport out of the absorber material of alpha, beta, and gamma rays, and (3) disambiguation of the spectrum into constituents, based on a library of radionuclide decays, with full quantification. Two new tools for detector dynamics

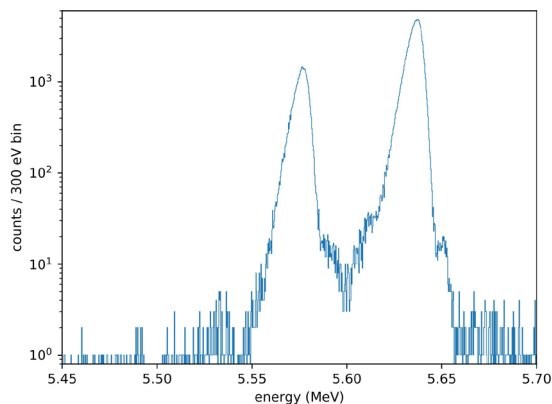


Figure 29. Americium-241 can decay, losing energy of 5.638 MeV by emission of an alpha particle and gamma ray. The latter is most commonly of energy approximately 60 keV, which is the energy difference of the two peaks here, due to escape of some gamma rays from the energy absorber. This decay energy spectrometry (DES) measurement, from the new laboratory in Gaithersburg equipped with transition-edge-sensor (TES) microcalorimeters designed and fabricated in Boulder, enables comparison with standard liquid scintillation counting.

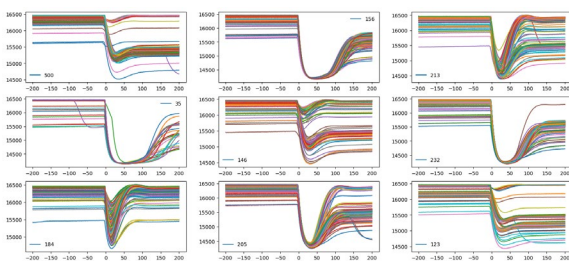


Figure 30. A small fraction of the Am-241 decays produced pulses of unexpected shape in the newly designed and fabricated energy absorber and TES microcalorimeter. The unusual pulses were gathered into clusters to help understand the underlying physical mechanism—absorption of the alpha particles and gamma rays sometimes at unexpected locations—and a revised absorber design is being fabricated. Here the horizontal axis is time from pulse arrival in (9.998543 μ s) samples and the vertical axis is TES current (raw readout units).

characterization are (a) fabricated capability for electronic excitation of the detector with known energy depositions, and (b) algorithms for ODE parameter sensitivity, of much recent attention, to determine an ODE system from its input/output behavior. This machine learning (ML) technique will be combined with more conventional supervised ML for library-based disambiguation of spectra. The uncertainty, and risk, for both techniques is whether the stringent accuracy requirements of the project can be achieved.

- [1] R. P. Fitzgerald, B. K. Alpert, D. T. Becker, D. E. Bergeron, R. M. Essex, K. Morgan, S. Nour, G. O’Neil, D. R. Schmidt, G. E. Shaw, D. Swetz, R. M. Verkouteren, and D. Yan. Toward a New Primary Standardization of Radionuclide Massic Activity Using Microcalorimetry and Quantitative Milligram-Scale Samples. *Journal of Research of the National Institute of Standards and Technology* **126** (2021), 126048. DOI: [10.6028/jres.126.048](https://doi.org/10.6028/jres.126.048)

TOMCAT: X-ray Imaging of Nanoscale Integrated Circuits for Tomographic Reconstruction

Bradley Alpert

Nathan Nakamura (NIST PML)

Zachary Levine (NIST PML)

Dan Swetz, Joel Ullom, et al. (NIST PML)

Edward Jimenez, Amber Dagel, et al. (Sandia National Laboratory)

George Barbastathis et al. (MIT)

As the leading semiconductor manufacturing techniques progress through 7 nm, 5 nm, and now 3 nm technology nodes, the ability to fabricate these chips has outrun the ability to image them. This limitation makes a variety of diagnostic needs much more difficult to satisfy. The NIST Quantum Sensors Group (PML), in collaboration with researchers at Sandia National Laboratory, has led a project for IARPA’s RAVEN (Rapid Analysis of Various Emerging Nanoelectronics) program to develop a small-laboratory capability to image integrated circuits by x-ray tomography. In distinction from other RAVEN projects, TOMCAT exploits a scanning electron microscope (SEM) rather than a synchrotron beamline and does not destroy the chip under test. This is enabled by the exquisite energy resolution of NIST-developed cryogenic microcalorimeter spectrometers, comprised of transition-edge sensors (TES), which are being extended to larger arrays (now to 3000 detectors), as well as with better individual-detector throughput (up to 1000 counts/s) and energy resolution (< 10 eV FWHM). The detectors measure fluorescent photons produced when SEM electrons strike a target following their differential attenuation by different materials in the chip.

A principal analysis challenge of the project, enabling tomographic structure recovery in this limited exposure angle, limited-photon regime, is the development of physics-assisted machine learning (PAML) customized for the details of photon fluorescence, absorption, and scattering in this instrument configuration. George Barbastathis, who has had considerable success in PAML for optics, has led this ML work. A significant advantage in photon efficiency from ML was achieved on x-ray measurements of chip facsimiles generated from a simple model of the layered interconnect structure found in semiconductor circuitry.

An integrated circuit (IC) with 130 nm features was imaged from x-ray measurements using customized tomography software that exploited (1) PENELOPE particle transport modeling code to determine x-ray fluorescence spot size from the SEM spot size, (2) corresponding diffuse source in the tomography for the x-ray forward model, (3) analytic modeling of motion blur, and (4) region of interest modeling to account for

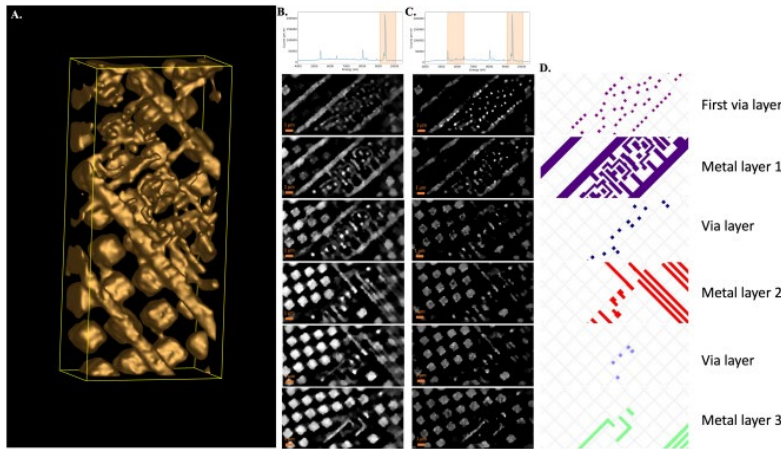


Figure 31. (A) 3-dimensional reconstruction of an IC fabricated at the 130 nm node, using X-rays in the 9.1-10.1 keV energy band. This band includes all Pt L α photons. (B) Spectrum from the TES detector with the 9.1-10.1 keV energy band used for reconstruction highlighted in orange (top). Reconstruction results, separated by IC layer, are shown under the spectrum. These slices were taken from the reconstruction shown in A. (C) Multi-energy reconstruction results, using the 9.1-10.1 keV and the 5.4-6.4 keV band, shown under the TES spectrum with the X-ray energies used highlighted in orange. Here, only the first via layer is resolved more clearly than when only using 9.1-10.1 keV photons, indicating a material other than Cu may be present. (D) GDS ground truth for each of the metal via and wiring layers, for comparison with reconstruction results.

lower photon flux at the edges than the center of the imaged region. Comparisons with the GDS specification file of the IC were made. In addition, nano-patterned varied-material targets were developed to enable higher spatial resolution for subsequent measurements.

Due to the limited set of IC measurements by SEM source with TES detectors available to date for training a neural network for machine learning, additional samples according to simple IC simulation specifications (dubbed CircuitFaker) were fabricated by additive manufacturing. Full-angle x-ray measurements were taken to obtain ground truth and were sparsely selected for training a neural network. Comparisons of reconstructions between simulated and actual measurements, and among various algorithms, were evaluated, with the machine learning enabling a measurement reduction factor of between 2.5 and 8 and a notable improvement in resilience to measurement noise.

A follow-on project for a 10,000-TES spectrometer in combination with a high-resolution CCD panel is being pursued within NIST PML using CHIPS Act funding.

- [1] J. W. Fowler, B. K. Alpert, G. C. O’Neil, D. S. Swetz, and J. N. Ullom. Energy Calibration of Nonlinear Microcalorimeters with Uncertainty Estimates from Gaussian Process Regression. *Journal of Low Temperature Physics* **209** (2022), 1047-1054. DOI: [10.1007/s10909-022-02740-w](https://doi.org/10.1007/s10909-022-02740-w)
- [2] Z. Guo, J. Ki Song, G. Barbastathis, M. E. Glinsky, C. T. Vaughan, K. W. Larson, B. K. Alpert, and Z. H. Levine. Physics-assisted Generative Adversarial Network for X-Ray Tomography. *Optics Express* **30**:13 (2022), 23238-23259. DOI: [10.1364/OE.460208](https://doi.org/10.1364/OE.460208)

[3] Z. Guo, J. Ki Song, G. Barbastathis, M. E. Glinsky, C. T. Vaughan, K. W. Larson, B. K. Alpert, and Z. H. Levine. Advantage of Machine Learning over Maximum Likelihood in Limited-Angle Low-Photon X-Ray Tomography. In *Machine Learning for Scientific Imaging 2022 Conference*, IS&T Electronic Imaging 2022.

[4] N. Nakamura, P. Szypryt, A. L. Dagele, B. K. Alpert, D. A. Bennett, W. B. Doriese, M. Durkin, J. W. Fowler, D. T. Fox, J. D. Gard, R. N. Goodner, J. Z. Harris, G. C. Hilton, E. S. Jimenez, B. L. Kern, K. W. Larson, Z. H. Levine, D. McArthur, K. M. Morgan, G. C. O’Neil, N. J. Ortiz, C. G. Pappas, C. D. Reintsema, D. R. Schmidt, P. A. Schulz, K. R. Thompson, J. N. Ullom, L. Vale, C. T. Vaughan, C. Walker, J. C. Weber, J. W. Wheeler, and D. S. Swetz. A Tabletop X-Ray Tomography Instrument for Nanometer-Scale Imaging: Integration of a Scanning Electron Microscope with a Transition-Edge Sensor Spectrometer. In review. Preprint: [arxiv:2212.10591](https://arxiv.org/abs/2212.10591)

[5] Z. H. Levine, B. K. Alpert, A. L. Dagele, J. W. Fowler, E. S. Jimenez, N. Nakamura, D. S. Swetz, P. Szypryt, K. R. Thompson, and J. N. Ullom. A Tabletop X-Ray Tomography Instrument for Nanometer-Scale Imaging: Reconstructions. *Microsystems & Nanoengineering* **9** (2023), article 47. DOI: [10.1038/s41378-023-00510-6](https://doi.org/10.1038/s41378-023-00510-6)

[6] Z. Guo, Z. Liu, G. Barbastathis, Q. Zhang, M. E. Glinsky, B. K. Alpert, and Z. H. Levine. Noise-Resilient Deep Learning for Integrated Circuit Tomography. *Optics Express* **31** (10) (2023), 15355. DOI: [10.1364/OE.486213](https://doi.org/10.1364/OE.486213)

Computing Ill-Posed Time-Reversed Evolution Equations Using Stabilized Explicit Schemes Run Backward in Time

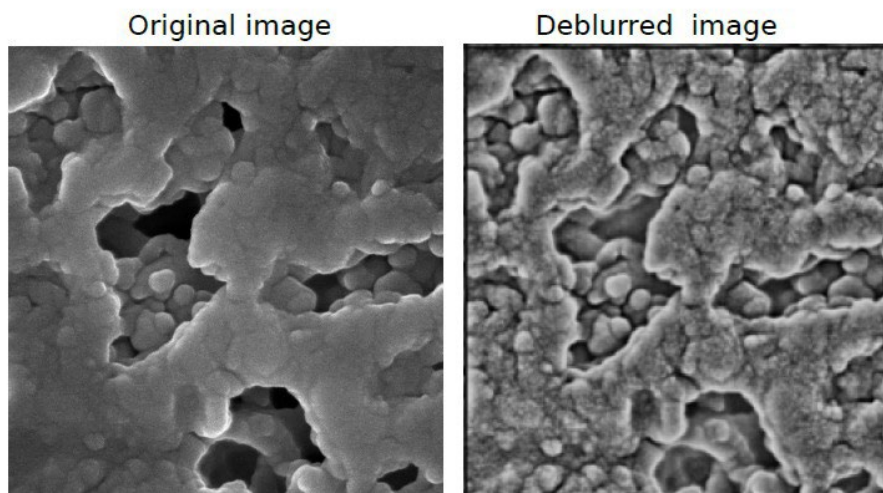
Alfred S. Carasso

As will be seen in the examples in Figure 32 and Figure 33 below, important developments have taken place in this ongoing research project during the past year. The blind deconvolution approaches discussed in [1-3] have been strengthened and can now produce exceptional deblurring in NIST nanoscale electron microscope imagery. The data assimilation procedures discussed in [4-6] have now been successfully applied to challenging 2D incompressible Navier-Stokes examples, as well as 2D coupled sound and heat flow problems. As noted in [6], the non-iterative direct mathematical procedures

used in the present work, invite valuable scientific debate and comparisons with the numerous artificial intelligence iterative methods listed in the bibliography of [6], and generally involving neural networks coupled with machine learning.

Ill-posed deconvolution problems and related time-reversed dissipative evolution equations, pervade measurement science. In numerous scientific measurements, the instrument point spread function is a bell-shaped distribution that may be well-approximated by a Gaussian, or by a heavy-tailed infinitely divisible probability density, often with parameters that are only tentatively known. This is the case in important NIST work on engineered nanostructures, involving scanning electron microscopes (SEM), Helium ion microscopes (HIM), and transmission electron microscopes (TEM). The latter are also frequently used in nanoscale biomedical and plant biology imaging. Reformulating the integral equation deconvolution problem into an equivalent time-reversed generalized diffusion equation, provides significant advantages. Marching backward in time stepwise, from a positive time T to time $t = 0$, allows the deconvolution to unfold in slow motion, provides the ability to monitor that process, and the possibility of terminating it prior to time $t = 0$, to prevent serious noise contamination and/or development of ringing artifacts. Such an approach, involving time-reversed fractional or logarithmic diffusion equations, was previously successfully applied in deblurring MRI and PET brain scans, nanoscale electron micrographs, and galactic scale Hubble Space Telescope imagery [1-3]. However, most recently, a significant improvement was discovered. Preconditioning electron microscope imagery by using adaptive histogram equalization, often reveals hidden structures, while noticeably increasing noise. Smoothing that image by convolution with a heavy-

NEW DEBLURRING PROCEDURE IN SEM IMAGERY



NEW DEBLURRING PROCEDURE IN HIM IMAGERY

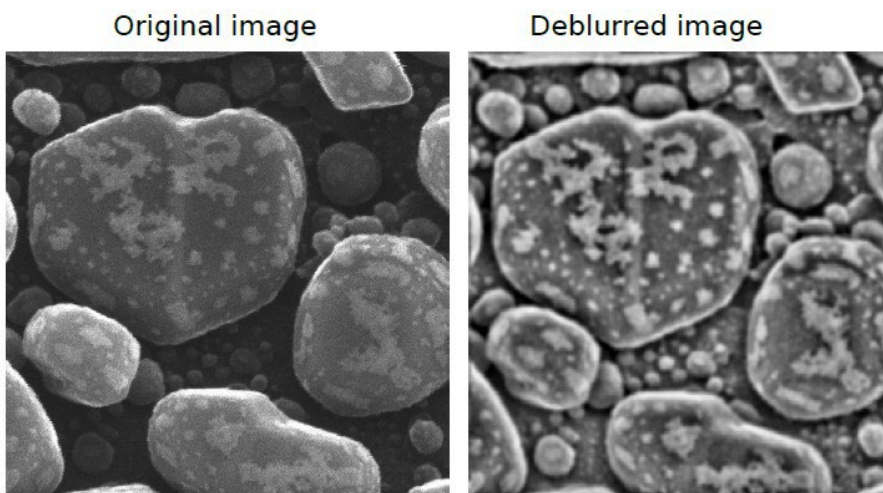


Figure 32. Improved blind deconvolution in scanning electron micrographs (SEM), and Helium ion micrographs (HIM). (Original images courtesy of NIST Microsystems and Nanotechnology Division)

tailed, low exponent Lévy stable density, can remove some of that noise. Subsequent application of logarithmic diffusion blind deconvolution to the preconditioned image often produces noticeably sharper images, together with unexpected detail. These improvements require interactive adjustments of parameters, by experienced analysts familiar with the algorithms and with the imagery being studied. Further exploration of preconditioned logarithmic diffusion deconvolution of NIST electron micrographs is contemplated.

Direct Stabilized Backward Marching Explicit Schemes. Time-reversed dissipative equations also occur in contexts unrelated to measurement science. In environmental forensics, much success has been achieved by solving advection diffusion equations backward in time to locate sources of groundwater

DATA ASSIMILATION IN 2D NAVIER-STOKES EQUATIONS
AT REYNOLDS NUMBER $RE=11,500$

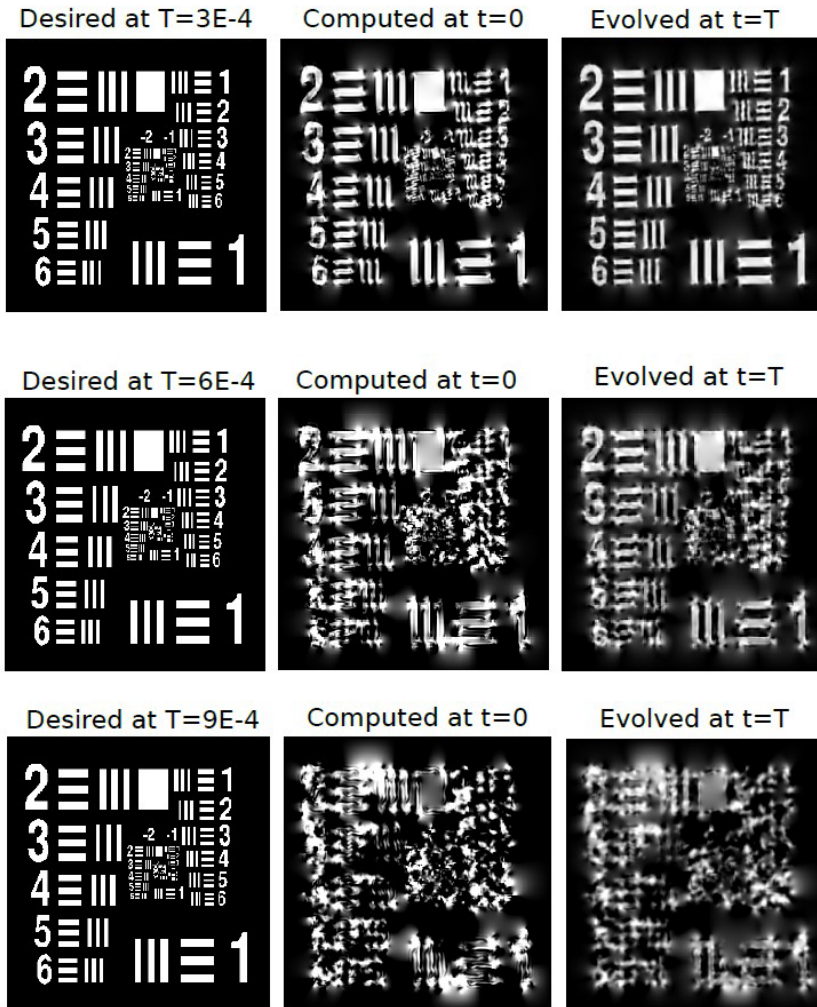


Figure 33. Data assimilation is successful if the rightmost image is a useful approximation to the desired leftmost image. Here, this requires $T \leq 5.0 \times 10^{-4}$. At the present Reynolds number, such a T value is significantly larger than expected, based on the best-known Navier-Stokes uncertainty estimates given in Reference [18].

contamination [7]. In numerical weather prediction and other geophysical computations, data assimilation involving time-reversed dissipative equations plays a major role in initializing prediction models [8-11]. While iterative methods are often used to solve ill-posed evolution equations, such methods are time-consuming and often develop stagnation points. Recently, a powerful non-iterative direct approach has been developed for time-reversed multidimensional nonlinear dissipative equations, based on stabilizing explicit backward marching finite difference schemes. An appropriate easily synthesized compensating smoothing operator is applied at every time step to quench the instability. The stabilized scheme now becomes unconditionally stable, but slightly inconsistent, and eventually leads to a distortion away from the true solution. This is the

stabilization penalty. However, in many problems of interest, the cumulative error is sufficiently small to allow for useful results. In a series of papers [12-17], such stabilized schemes have been successfully applied to interesting classes of time-reversed nonlinear initial value problems for parabolic equations, viscous wave equations, coupled sound and heat flow, thermoelastic vibrations, 2D viscous Burgers equations, and 2D incompressible Navier-Stokes equations. Such computations had not previously been considered possible.

Data Assimilation in 2D Dissipative Equations. Stabilized backward marching explicit schemes offer significant computational advantages in the growing field of geophysical data assimilation. Current research aims to demonstrate this point by focusing on computational examples involving 8 bit, 256×256 pixel gray-scale images, defined by highly nonsmooth intensity data. Such data are difficult to synthesize mathematically and pose significant challenges in ill-posed reconstruction. Here, images provide an invaluable exploratory tool in time-reversed dissipative equations. The data assimilation problem is fundamentally different, and more challenging, than the backward recovery problem discussed in [12-17]. In the above backward recovery papers, the

given data at time $T > 0$, is a relatively smooth noisy function, that differs from an actual solution at time T by a known small $\delta > 0$, in a given L^p norm. In the data assimilation problem, hypothetical nonsmooth data may be given at time $T > 0$, that may not correspond to an actual solution, or that may differ from an actual solution by an unknown, possibly large $\delta > 0$, in that same L^p norm. It may not be possible to find initial values at $t = 0$, that can evolve into a useful approximation to the desired data at time $T > 0$. This is exemplified in Figure 33, dealing with time-reversed 2D incompressible Navier-Stokes equations applied to hypothetical data at time $T > 0$, consisting of the nonsmooth USAF Resolution Chart, with Reynolds number $RE = 11\,500$. Data assimilation is successful when $T = 3.0 \times 10^{-4}$,

as shown in the first row of Figure 33, but becomes increasingly more difficult with increasing T , as shown in the second and third rows in Figure 33. However, successful data assimilation at the T values shown is quite significant. As noted in [16], at such high Reynolds numbers, useful backward Navier-Stokes reconstructions would seem to require considerably smaller T , based on the best-known uncertainty estimates given in [18].

- [1] A. S. Carasso. The APEX Method in Image Sharpening and the Use of Low Exponent Lévy Stable Laws. *SIAM Journal on Applied Mathematics* **63** (2002), 593-618.
- [2] A. S. Carasso, D. S. Bright, and A. E. Vldar. APEX Method and Real-Time Blind Deconvolution of Scanning Electron Microscope Imagery. *Optical Engineering* **41** (2002), 2499-2514.
- [3] A. S. Carasso. Bochner Subordination, Logarithmic Diffusion Equations, and Blind Deconvolution of Hubble Space Telescope Imagery and Other Scientific Data. *SIAM Journal on Imaging Sciences* **3** (2010), 954-980.
- [4] A. S. Carasso. Data Assimilation in 2D Viscous Burgers Equation Using a Stabilized Explicit Finite Difference Scheme Run Backward in Time. *Inverse Problems in Science and Engineering* **29**:13 (2021), 3475-3489. DOI: [10.1080/17415977.2021.2009476](https://doi.org/10.1080/17415977.2021.2009476)
- [5] A. S. Carasso. Data Assimilation in 2D Nonlinear Advection Diffusion Equations, using an Explicit Stabilized Leapfrog Scheme Run Backward in Time. NIST Technical Note, NIST TN 2227. DOI: [10.6028/NIST.TN.2227](https://doi.org/10.6028/NIST.TN.2227)
- [6] A. S. Carasso. Data Assimilation in 2D Hyperbolic/Parabolic Systems using a Stabilized Explicit Finite Difference Scheme Run Backward in Time. *Applied Mathematics in Science and Engineering* **32**:1 (2024). DOI: [10.1080/27690911.2023.2282641](https://doi.org/10.1080/27690911.2023.2282641)
- [7] J. Atmadja and A. C. Bagtzoglou. State of the Art Report on Mathematical Methods for Groundwater Pollution Source Identification. *Environmental Forensics* **2** (2001), 205-214.
- [8] J. Lundvall, V. Kozlov, and P. Weinerfelt. Iterative Methods for Data Assimilation for Burgers' Equation. *Journal of Inverse and Ill-Posed Problems* **14** (2006), 505-535.
- [9] D. Auroux and J. Blum. A Nudging-Based Data Assimilation Method for Oceanographic Problems: The Back and Forth Nudging (BFN) Algorithm. *Nonlinear Processes in Geophysics* **15** (2008), 305-319.
- [10] D. Auroux, P. Bansart, and J. Blum. An Evolution of the Back and Forth Nudging for Geophysical Data Assimilation: Application to Burgers Equation and Comparison. *Inverse Problems in Science and Engineering* **21** (2013), 399-419.
- [11] H. F. de Campos Velho, V. C. Barbosa, and S. Cocke. Special Issue on Inverse Problems in Geosciences. *Inverse Problems in Science and Engineering* **21** (2013), 355-356.
- [12] A. S. Carasso. Stable Explicit Marching Scheme in Ill-Posed Time-Reversed Viscous Wave Equations. *Inverse Problems in Science and Engineering* **24** (2016), 1454-1474.
- [13] A. S. Carasso. Stabilized Richardson Leapfrog Scheme in Explicit Stepwise Computation of Forward or Backward Nonlinear Parabolic Equations. *Inverse Problems in Science and Engineering* **25** (2017), 1719-1742.
- [14] A. S. Carasso. Stabilized Backward in Time Explicit Marching Schemes in the Numerical Computation of Ill-Posed Time-Reversed Hyperbolic/Parabolic Systems. *Inverse Problems in Science and Engineering* **27** (2019), 134-165.
- [15] A. S. Carasso. Stable Explicit Stepwise Marching Scheme in Ill-Posed Time-Reversed 2D Burgers' Equation. *Inverse Problems in Science and Engineering* **27** (2019), 1672-1688.
- [16] A. S. Carasso. Computing Ill-Posed Time-Reversed 2D Navier-Stokes Equations, using a Stabilized Explicit Finite Difference Scheme Marching Backward in Time. *Inverse Problems in Science and Engineering* **28**:7 (2019), 988-1010. DOI: [10.1080/17415977.2019.1698564](https://doi.org/10.1080/17415977.2019.1698564)
- [17] A. S. Carasso. Stabilized Leapfrog Scheme Run Backward in Time, and the Explicit $O(\Delta t)^2$ Stepwise Computation of Ill-Posed Time-Reversed 2D Navier-Stokes Equations. *Inverse Problems in Science and Engineering* **29**:13 (2021), 3062-3085. DOI: [10.1080/17415977.2021.1972997](https://doi.org/10.1080/17415977.2021.1972997)
- [18] R. J. Knops and L. E. Payne. On the Stability of Solutions of the Navier-Stokes Equations Backward in Time. *Archives of Rational Mechanics and Analysis* **29** (1968), 331-335.

A Science Gateway for Atomic, Molecular and Optical Physics

Barry I. Schneider

Klaus Bartschat (Drake University)

Kathryn Hamilton (University of Colorado, Denver)

Igor Bray (Curtin University, Australia)

Armin Scrinzi (Ludwig-Maximilians U., Germany)

Fernando Martín (U. Autónoma de Madrid, Spain)

Jesus Gonzalez Vasquez (U. Autónoma de Madrid)

Jimena Gorfinkiel (Open University, UK)

Robert Lucchese (Lawrence Berkeley National Laboratory)

Sudhakar Pamidighantam (Indiana University)

Andrew Brown (University of Belfast, UK)

Nicholas Douquet (Kennesaw State University)

<https://amosgateway.org/>

An international effort has been underway since early 2019 to develop and maintain a Science Gateway for Atomic Molecular and Optical Science (AMOS) [1, 2, 3]. The gateway was renamed from a Science Gateway for Atomic, and Molecular Physics, to a Science Gateway for Atomic Molecular and Optical Science to reflect the broader nature of the ongoing activity. The purposes of the gateway are to 1) collect and make available to the community a set of advanced computational tools

The AMOS Gateway hosts state-of-the-art atomic, molecular, and optical science (AMOS) software suites and provides the community with an easy-to-use platform for calculations involving the static and dynamic properties of multi electron atoms and molecules.

Codes are available for computing spectra, lifetimes and transition rates between bound states, cross sections for electron scattering, photoionization and solutions of the time-dependent Schrödinger equation in the presence of strong and ultrafast electromagnetic fields. While use of the gateway is free, you must [create an account](#).

Featured Codes:

- BSR - B spline R-matrix
- CCC - Convergent Close Coupling
- DBSR HF - B-spline Dirac-Hartree-Fock Program
- ePolyScat - MESA
- GRASP - General Relativistic Atomic Structure Package
- RMT - R-Matrix with time
- SPHF - Spline Hartree-Fock Program
- tRecX - time-dependent Recursive index
- UKRmol+ - UK Molecular R-matrix
- Xchem

Calculations performed using the gateway will be archived here. Links to other useful data bases are also posted.

Gateway Publications

- Gateway for Atomic, Molecular and Optical Physics.
- Atomic, Molecular and Optical Scattering Applications in an Apache Airavata Science Gateway.

Gateway Workshops

- NIST AMOP Gateway Workshop Dec 11-13 2019 Agenda (with links to slides)
- Harvard Workshop May 14-16, 2018

Topics of Interest

Attosecond Chemistry COST Action February 2021 virtual workshop YouTube link | Schedule, invited speakers, etc.

Figure 34. The AMOS Gateway home page.

that are actively being used to study atomic and molecular collisions and the interaction of radiation with atoms and molecules, 2) provide educational materials for beginning and advanced users desiring to learn the ideas and concepts of AMOS, both theoretical and computational, and 3) make available to the broad community atomic and molecular data needed for many applications. The availability of collision data is critical to many areas of physics including astrophysics, fusion energy, the study of lighting and microelectronics, and is an activity consistent with the mission of NIST.

Codes for modeling and simulation of such phenomena have been developed in specific groups by graduate students and postdocs but are often poorly documented, and unavailable outside the group developing the software. This leads to “reinventing the wheel” in too many instances. Maintaining these computational tools, as well as enhancing their capabilities, is one of the major goals of the project and is critical to ensure continued scientific progress in AMOS.

Another important goal is to enable the code developers themselves to compare the calculations of specific well-defined problems using different methodologies. This enables the verification of results of different codes and encourages comparison with experiment, where available. It has already been demonstrated that a few of these codes are often more accurate than experiment and thus provide a predictive capability when experimental results are unavailable.

At the outset, the group acknowledged that, in contrast to some other communities, the AMOS community has lagged behind in developing community supported software packages that are robust and widely used outside the group that was responsible for developing the software. Our group was convinced the time had arrived to change existing practices and make these tools available to and easily used by future generations of AMOS scientists as well as the developers themselves.

The group wrote a proposal to the NSF XSEDE program (now ACCESS) to fund some initial development of the gateway. The proposal was successful and, importantly, provided the developers with some hands-on assistance from the Extended Collaborative Support Services arm of XSEDE. This was vital to the success of the effort. In particular, we acknowledged the important contribution of Sudhakar Pamidighantam and his colleagues at Indiana University in making our efforts a success.

There have been some important advances since the first instantiation of the gateway: 1) the original web pages for the gateway have been completely revamped and new material has been added, 2) the original six major codes chosen for initial deployment have been expanded to eleven codes and many have already been ported to at least three ACCESS supercomputers, as well as the leadership class Frontera computer at the Texas Advanced Computing Center, and 3) there is a new version of an API available to enable users to perform calculations with at least one of the codes, tRecX, and this is serving as a model for the other applications. A contract that NIST awarded to Indiana University in 2021 was used to further develop the needed GUI interfaces expired.

However, the need for longer term support for the project was recognized as an essential ingredient to its ultimate success. The single most important development this year was the funding by the NSF of a \$2.46M, five-year award for a project entitled *Frameworks: An Advanced Cyberinfrastructure for Atomic, Molecular, and Optical Science (AMOS): Democratizing AMOS for Research and Education*,¹¹ with Professor Kathryn Hamilton of the University of Colorado/Denver as the PI. Co-PI's include Sudhakar Pamidighantam from IU,

¹¹ https://www.nsf.gov/awardsearch/showAward?AWD_ID=2311928

Klaus Bartschat from Drake University and Nicholas Douquet from Central Florida. Barry Schneider from NIST, and Robert Lucchese from LBNL have the role of Senior Investigators.

The current portal contains a good description of the codes, the people involved, links to documentation, a bibliography, a preliminary data repository and some nice graphical material illustrating a few of the calculations that have been done with the codes.

- [1] B. I. Schneider, K. Bartschat, O. Zatarinny I. Bray, A. Scrinzi, F. Martin, M. Klinker, J. Tennyson, J. Gorfinkiel, and S. Pamidighanta. A Science Gateway for Atomic and Molecular Physics. Preprint: [arXiv:2001.02286](https://arxiv.org/abs/2001.02286)
- [2] B. I. Schneider, K. Bartschat, O. Zatsarinny, K. Hamilton, I. Bray, A. Scrinzi, F. Martin, J. G. Vasquez, J. Tennyson, J. Gorfinkiel, R. Lucchese, and S. Pamidighantam. Atomic and Molecular Scattering Applications in an Apache Airavata Science Gateway. In *PEARC '20: Practice and Experience in Advanced Research Computing*, July 2020, 270-277. DOI: [10.1145/3311790.3397342](https://doi.org/10.1145/3311790.3397342)
- [3] B. I. Schneider. AMO for All: How Online Portals Are Democratizing the Field of Atomic, Molecular and Optical Physics. Taking Measure Blog, NIST, November 2, 2022. URL: <https://www.nist.gov/blogs/taking-measure/amo-all-how-online-portals-are-democratizing-field-atomic-molecular-and-optical>

Computational Tools for Image and Shape Analysis

Günay Doğan

Prashant Athavale (Clarkson University)

Emmanuel Atindama (Clarkson University)

Peter Lef (Clarkson University)

Selin Aslan (Koç University, Turkey)

Doğa Gürsoy (Argonne National Laboratory)

Jiyoung Park (Texas A&M University)

The main goal of this project is to develop efficient and reliable computational tools to detect geometric structures, such as curves, regions and boundaries, from given direct and indirect measurements, e.g., microscope images or tomographic measurements, as well as to evaluate and compare these geometric structures or shapes in a quantitative manner. This is important in many areas of science and engineering, where practitioners obtain their data as images, and would like to detect and analyze the objects in the data. Examples are microscopy images for cell biology or micro-CT (computed tomography) images of microstructures in material science, and shoeprint images in crime scenes for footwear forensics.

In FY 2023, advances were made in the various fronts of this project. Python implementations of solutions for problems in these areas were implemented, and documentation and examples were provided. In the following, we provide more details on the specific work carried out.

Image segmentation is the problem of finding distinct regions and their boundaries in given images. It is a necessary data analysis step for many problems in cell biology, forensics, and material science, as well as other fields in science and engineering. In FY 2023, G. Doğan and his collaborators continued to work on multiple strategies for image segmentation. This included preprocessing algorithms to improve segmentation and image analysis performance. The new algorithms were implemented and released as part of scikit-shape Python package.¹²

Images obtained in different domains can have very different characteristics and can vary substantially in quality. Thus, domain-specific solutions are often required. An application domain of interest at NIST is the analysis of material microstructures. Various imaging modalities enable imaging of material microstructures with the goal of quantitatively characterizing them and relating the microstructure geometry to the material's macroscopic behavior. Electron backscatter diffraction imaging (EBSD) is one such modality used to obtain orientation images of a material's crystal structure. EBSD images can sometimes be noisy and can include various artifacts, which makes it hard to segment and analyze them. Doğan, Athavale, Atindama and Lef developed a novel image restoration algorithm for EBSD images [1]. This algorithm built on the denoising properties of the total variation equation and showed state-of-the-art restoration performance on benchmark tests with real and synthetic EBSD data, compared with other commonly used algorithms. More details on this work given in the feature article in this report by Doğan and his collaborators on page 17.

In the image segmentation literature, many algorithms have been developed using a model-based approach, and more recently a learning-based approach. The advantages of the model-based approaches are their efficiency, interpretability and the fact that they require no training data. On the other hand, the advantage of learning-based approaches are their flexibility and superior performance if sufficiently large training datasets are available. In FY2023, Doğan continued his work on model-based segmentation algorithms from the previous years, but also explored learning-based segmentation solutions. One model-based algorithm he developed previously is a phase-field segmentation method, in which a candidate segmentation is represented implicitly by a phase field function defined on the image grid. The criteria for a correct segmentation are encoded in a

¹² <http://scikit-shape.org>

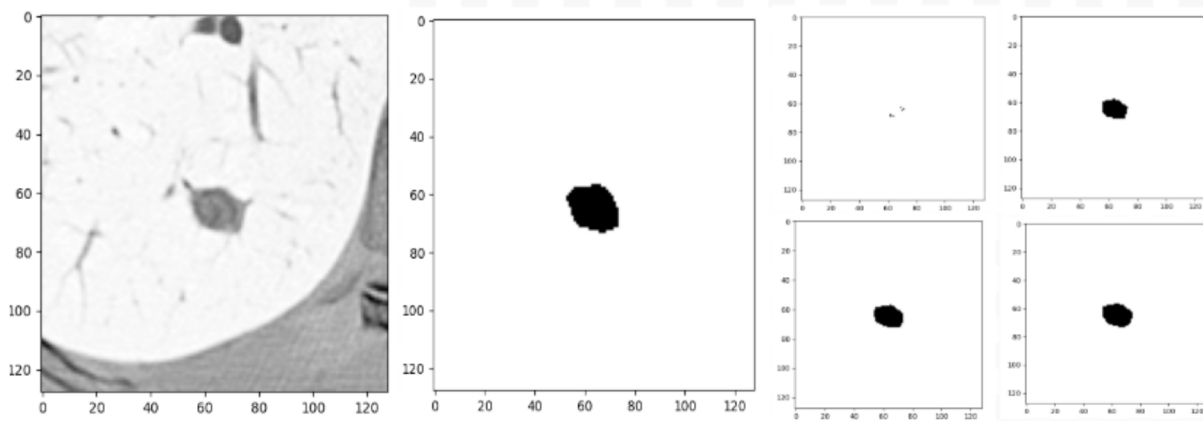


Figure 35. Comparing the input image (left) and known ground-truth segmentation (middle), with computed results from probabilistic U-Net algorithm (right top two) and results from modified U-Net algorithm (right bottom two) inducing spatial coherency of the target.

segmentation energy for the phase field function, and its minimum needs to be computed to obtain the segmentation. Doğan made improvements to the optimization algorithm used to compute the minimum, as well as changes to the regularization term of the energy to obtain better-defined regions in the segmentation.

Doğan, Aslan and Gürsoy investigated segmentation problems related to computed tomography. Computed tomography is a versatile technology used in medical imaging, material science and non-destructive testing for engineering. Typically, an image of a medium or component is reconstructed as a result of computed tomography. Then regions or objects of interest are segmented out for further analysis. Doğan et al. formulated a new model to compute the segmentation directly from tomographic measurements bypassing the need for image reconstruction. Their preliminary analysis and experimentation show that the model has promise. They aim to implement and test the final algorithm in FY 2024.

Doğan worked on learning-based algorithms as well in FY 2023. Previously he had implemented a class of segmentation algorithms that clusters and classifies image pixels based on bags of features. In this approach, each pixel is supplemented with additional image features, such as image gradients, local patches, etc., to better inform classification algorithms to improve the region assignments of pixels for segmentation. In FY 2023, Doğan added more image features to those previously available to the algorithm and increased the options for the learning algorithms as well. He tested these in various scenarios to see which features and algorithms were better fits for these scenarios.

An alternative to using pre-selected bags of image features is for the segmentation algorithm to learn the informative image features (in addition to learning a classifier to partition the pixels into regions). This is where recent deep learning algorithms excel. They learn both the right informative image features and an effective classifier, producing impressive segmentation

results. However, this performance is contingent upon the availability of large representative training data sets. Unlike typical computer vision applications, creating large, annotated data sets for scientific applications can be difficult and sometimes impractical. This can be a barrier to using deep learning algorithms. Doğan has been investigating hybrid approaches that can incorporate partial model information, such as regularity and invariances, to obtain more economical deep learning models. In FY 2023, Doğan worked with J. Park, a Ph.D. student from Texas A&M University to research and test possible hybrid algorithms. One such algorithm was a modified version of the probabilistic U-Net algorithm [3, 4], in which modules were incorporated that induced spatial coherence of segmented objects (see Figure 35). In preliminary experiments, the modified algorithm outperformed the probabilistic U-Net algorithm. Doğan and Park will continue to further develop the hybrid algorithm in FY 2024.

Most data analysis and machine learning algorithms rely on dissimilarity metrics or distances that quantify how dissimilar or far the data components (e.g., image, shape, text) in the analyzed data set are. The choice of dissimilarity metric is central to achieving data analysis and machine learning goals successfully. On the other hand, using different data representations or different versions of the algorithms lead to different dissimilarity metrics, and this brings the question of which metric would perform best. In the previous years, Doğan and Fleisig (UC Berkeley) developed a Python program, VEMOS (Visual Explorer for Metrics Of Similarity) that can be used to evaluate and compare multiple competing similarity/dissimilarity metrics. VEMOS can be used in a versatile manner to evaluate multiple alternative dissimilarity metrics for heterogeneous data sets, including images, shapes, point clouds and other data types. In FY 2023, Doğan continued to develop VEMOS, made bug fixes, and added new features. A report describing capabilities of VEMOS is available as a

NIST technical note [5], and the software is available for download.¹³

- [1] E. Atindama, P. Lef, G. Doğan, and P. Athavale. Restoration of Noisy Orientation Maps from Electron Backscatter Diffraction Imaging. *Integrating Materials and Manufacturing Innovations* **12** (2023), 251–266. DOI: [10.1007/s40192-023-00304-8](https://doi.org/10.1007/s40192-023-00304-8)
- [2] H. Antil, S. Bartels, and G. Doğan. A Region-based Segmentation Model with Fractional Diffusion for Improved Boundary Regularization. In process.
- [3] O. Ronneberger, P. Fischer, and T. Brox. U-net: Convolutional Networks for Biomedical Image Segmentation. In *Proceedings of Medical Image Computing and Computer-Assisted Intervention—MICCAI*, Munich, Germany, October 5-9, 2015.
- [4] S. Kohl, B. Romera-Paredes, C. Meyer, J. De Fauw, J.R. Ledsam, K. Maier-Hein, S.M. Eslami, D. Jimenez Rezende, and O. Ronneberger. A Probabilistic U-net for Segmentation of Ambiguous Images. *Advances in Neural Information Processing Systems* **31** (2018).
- [5] E. Fleisig and G. Doğan. VEMOS: GUI for Evaluation of Similarity Metrics of Complex Data Sets. NIST Technical Note 2160, June 2021, 34 pages. DOI: [10.6028/NIST.TN.2160](https://doi.org/10.6028/NIST.TN.2160).

Topological Shape and Data Analysis

Zachary J. Grey

Jeanie Schreiber (George Mason University)

Olga Doronina (National Renewable Energy Lab)

Andrew Glaws (National Renewable Energy Lab)

Günay Doğan

Adam Kreuziger (NIST MML)

Efficient representations and statistics of shapes are important facets of computational tasks in artificial intelligence, design, and manufacturing. The challenge is to define a prudent treatment of data with an intrinsic notion of shape. Example applications include: (i) wind turbine airfoils which must be designed, manufactured, and measured more precisely than ever for next generation offshore wind energy applications, (ii) investigation and statistical hypothesis testing of material microstructures in a manufacturing process, (iii) inference involving the evolution of protein structures, (iv) quantifying distributions of persistent structures in general image classification, and (v) change point detection in the ecology of animal population responses to climate change.

The notion of “shape” is typically induced by identifying shape preserving transformations and “dividing out” these transformations to explore what remains in a so-called quotient topology. These topologies can vary

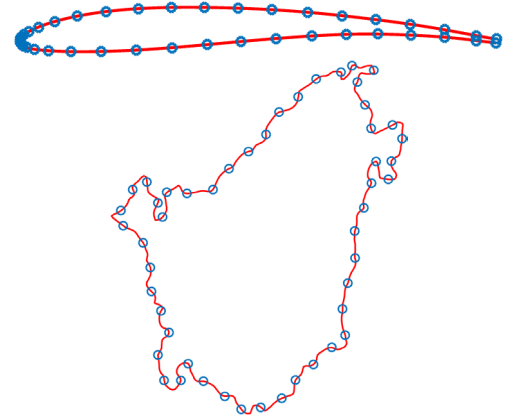


Figure 36. (top) a discretized airfoil shape with arbitrary ordering of landmarks as blue circles depicted along a red boundary. (bottom) a discretized grain boundary with arbitrary ordering of landmarks depicted along a red boundary.

from one application to the next but are useful in studying and understanding persistent characteristics and “modes” of shape as data. Moreover, these prudent treatments of shape induce improved metric spaces offering better notions of “distance” between paired shapes in a framework which is inherently non-linear. Thus, with this formalism for defining notions of shape, we can offer improved coordinate systems for domain definition, interpolation, and inferential statistics.

In our analysis, a shape can be represented as a boundary defined by a curve, $c: [0,1] \rightarrow \mathbb{R}^2$. However, in a computational setting, we represent airfoil shapes or grain boundaries as a discrete ordered sequence of landmarks $(x_i) \in \mathbb{R}^2$ for $i = 1, \dots, n$. That is, we view a shape through an identification with some unknown curve $c(s)$ and compute with reparametrized landmarks $x_i = c(s_i)$ for $0 \leq s_1 < s_2 < \dots < s_n \leq 1$. Moving along the curve, this sequence of planar vectors along a shape boundary can be represented as a matrix $X = [x_1, \dots, x_n]^T \in \mathbb{R}_*^{n \times 2}$ constituting a discrete representation of the shape.

We introduce a scaling of landmark data to parametrize new shape deformations over the Grassmannian, $\mathcal{G}(n, 2)$. The nature of this revised representation “divides out” the effect of matrix scaling operations, XM , thus separating affine characteristics of shape—when combined with translations—and offering a novel non-linear (non-Euclidean) domain of discrete shapes.

Computationally, these separable shape tensors are

$$X_0(t, l) = \tilde{X}(t)M(l)$$

where $\tilde{X}(t)$ are representative elements parametrized over coordinates t of a Grassmannian submanifold and $M(l)$ are the separated elements of scale variations over subgroups of the general linear group, GL_2 , giving rise to product submanifold definitions of discrete-shape

¹³ <https://github.com/usnistgov/VEMOS>

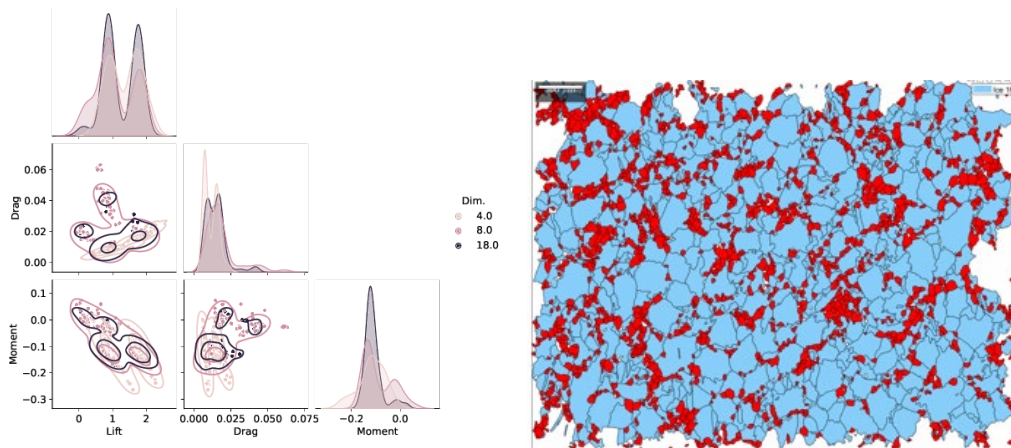


Figure 37. (left) Aerodynamic moments for variable dimensions of regularized airfoil shapes indicating, via maximum mean discrepancy, the ability to significantly reduce dimensionality for optimization and inverse problems. (right) A distribution of thousands of grain boundaries with a red-highlighted persistent structure extracted by computing a bi-filtration over Euclidean spatial distances and shape distances over a product submanifold of separable shape tensors.

spaces. This defines a pair of *independent coordinate vectors* (t, l) describing any shape up to translations. This separability is a desirable characteristic for aerospace/wind-turbine designers who regularly prescribe or fix $M(l) \in GL_2$ but seek undulations $[\tilde{X}](t) \in \mathcal{G}(n, 2)$ in the shape to explore deformations resulting from blade soiling or manufacturing variations. Moreover, this separability enables a more precise investigation for studying how grain shapes within a material microstructure may be deformed through a manufacturing process or loading condition.

Continuously, a recent interpretation has motivated interest in a related form as a homogeneous Fredholm integral equation of the second kind,

$$\int k(s, u)v_j(u)d\mu(u) = \lambda_j v_j(s).$$

The hope is to motivate novel interpretations of a reproducing kernel Hilbert space of curves for further study and regularization of shape.

In aerodynamic applications, reduced-dimension data-driven domains of transformed separable representations offer improved regularization of deformations and novel methods of interpolation for both 2D and 3D design. In materials science applications, distributions of shapes as grain boundaries measured with electron back-scatter diffraction (EBSD) can be transformed into separable representations for hypothesis testing, indicating which features of shape are statistically significant from one measurement of a set of grains to the next.

These highly scalable non-Euclidean treatments of discrete shapes leverage implementations over matrix manifolds to achieve efficiencies necessary for computations involving tens of thousands of shapes. In one instance, we have successfully explored and deployed data-driven approaches to build wind turbine airfoil shape domains with more than 16 000+ shapes represented by refinements of 1 000+ landmarks per shape.

Alternatively, given scans of microstructures, we can compute statistical moments of thousands of grain boundaries in a matter of seconds on a common laptop.

These innovations have enabled significantly more tractable inverse designs with machine learning for next generation wind-turbine blades, transforming the classical problem of designing with hundreds of blade design parameters into one involving as few as four parameters. The study [4] employed the representations of the regularized shapes to recognize improved designs for reducing the life-cycle cost of wind energy. Additionally, these representations are showing promise with two-sample hypothesis testing of segmented grain boundaries subjected to different environmental conditions. This facilitates a novel set of tools for materials scientists to quantify specific structural differences in distributions of grain boundaries from one EBSD scan to another. This interpretation on separable shape tensors was originally presented at the AI for Design and Manufacturing Conference [1] and subsequently published in the Oxford University Press, *Journal of Computational Design and Engineering* [2]. A codebase and summary in the *Journal of Open Source Software* details a GitHub code repository for applications relevant to aerodynamic design [3].

- [1] O. A. Doronina, Z. J. Grey, and A. Glaws. Grassmannian Shape Representations for Aerodynamic Applications. In *Workshop on AI for Design and Manufacturing (ADAM)*, 36th AAAI Conference on Artificial Intelligence, (2022). URL: <https://arxiv.org/abs/2201.04649>
- [2] Z. J. Grey, O. A. Doronina, and A. Glaws. Separable Shape Tensors for Aerodynamic Design. *Journal of Computational Design and Engineering*, to appear. DOI: [10.1093/jcde/qwac140](https://doi.org/10.1093/jcde/qwac140)
- [3] O. A. Doronina, Z. Grey, A. Glaws. G2aero: A Python Package for Separable Shape Tensors. *Journal of Open Source Software* **8**:89 (2023), 5408. DOI: [10.11578/dc.20220422.1](https://doi.org/10.11578/dc.20220422.1)

- [4] J. Jasa, A. Glaws, P. Bortolotti, G. Vijayakumar, and G. Barter. Wind Turbine Blade Design with Airfoil Shape Control Using Invertible Neural Networks. *Journal of Physics: Conference Series* **2265** (2022), 042052.

Elastic Shape Registration of Surfaces in 3-dimensional Space

Javier Bernal
James Lawrence

A fundamental problem in shape analysis [3, 7] is to determine the similarity of two objects. Applications include human biometrics, proteomics, and search in image or object databases. In elastic shape analysis, similarity measures are sought which are invariant with respect to translation, rotation, scaling, and reparametrization. An important primitive is elastic shape registration, which seeks to find a mapping that assigns each point on an object with a unique point on another object. Such a mapping can be used to obtain a metric for the distance between two objects, which can then be used as a similarity measure.

In this work, we develop methods for computation of the elastic shape registration of two simple surfaces in 3-dimensional space, and therefore of the elastic shape distance between them. Similar work has been carried out by Kurtek, Jermyn, et al. [4, 6]. As presented in [1], our work starts with the careful development, as in [4, 6], of the mathematical framework necessary for the elastic shape analysis of 3-dimensional surfaces, which culminates with the definition and justification of a distance measure between two such surfaces. This distance, and therefore the registration, is the result of minimizing a distance function in terms of rotations of one surface and reparametrizations of the other one. With a simple surface defined as a parametrized surface in 3-d space, that is, the range of a one-to-one function from an elementary region in the plane into 3-d space, we have defined a shape function of a parametrized surface in 3-dimensional space, different from the one in [6] but similar to the one in [4] and have established some fundamental results about this function. A similar definition and similar results have been presented in [2, 3, 5, 7, 8] in the context of the shape function of a parametrized curve in d -dimensional space, d any positive integer. Based on this definition of the shape function of a parametrized surface, we have defined the elastic shape distance between two parametrized surfaces. This is done by alternating computations of rotations of one of the surfaces through the minimization of a certain double integral in terms of rotations of the surface, and computations of reparametrizations of the other surface through the minimization of the same double integral in terms of homeomorphisms from the elementary region

that is part of the definition of the parametrized surfaces, onto itself, the homeomorphisms having Jacobians of positive determinant.

We demonstrated in [1] that this distance is well defined using arguments similar to those used for justifying the definition of the distance between curves in d -dimensional space found in [3, 7]. We then developed an algorithm that minimizes the distance function in terms of rotations and a special subset of the set of reparametrizations, with the optimization over reparametrizations based on dynamic programming. We have implemented the proposed algorithm and results obtained with it have been presented in [1].

Of course, this approach does not necessarily produce an optimal solution of the registration and distance problem, but perhaps a solution closer to optimal than the local minimum provided by a gradient descent algorithm for optimizing over the entire set of reparametrizations, such as those proposed in [4, 6]. In fact, we have proposed that when computing the elastic shape registration of two simple surfaces and the elastic shape distance between them with a gradient descent algorithm, that our proposed algorithm be used to obtain an initial starting point for the search. We are currently in the process of implementing this idea, using the conjugate gradient algorithm for the follow-on search.

- [1] J. Bernal and J. Lawrence. Partial Elastic Shape Registration of 3D Surfaces using Dynamic Programming. NIST Technical Note 2274 (2023). DOI: [10.6028/NIST.TN.2274](https://doi.org/10.6028/NIST.TN.2274)
- [2] J. Bernal, J. Lawrence, G. Dogan, and C. R. Hagwood. On Computing Elastic Shape Distances between Curves in d -dimensional Space. NIST Technical Note 2164 (2021). DOI: [10.6028/NIST.TN.2164](https://doi.org/10.6028/NIST.TN.2164)
- [3] J. Bernal. Shape Analysis, Lebesgue Integration and Absolute Continuity Connections. NISTIR 8217 (2018). DOI: [10.6028/NIST.IR.8217](https://doi.org/10.6028/NIST.IR.8217)
- [4] I. H. Jermyn, S. Kurtek, E. Klassen, and A. Srivastava, A. Elastic Shape Matching of Parameterized Surfaces Using Square Root Normal Fields. In *Proceedings of the 12th European Conference on Computer Vision (ECCV'12)*, Volume V, Springer, Berlin (2012), 804-817.
- [5] S. H. Joshi, E. Klassen, A. Srivastava, and I. H. Jermyn. A Novel Representation for Riemannian Analysis of Elastic Curves in R^n . In *Proceedings of the IEEE Conference on Computer Vision and Pattern Recognition (CVPR)*, Minneapolis, MN, June 2007.
- [6] S. Kurtek, E. Klassen, Z. Ding, and A. Srivastava. A Novel Riemannian Framework for Shape Analysis of 3D Objects. In *Proceedings of the IEEE Conference on Computer Vision and Pattern Recognition (CVPR)*, San Francisco, CA, June 2010.
- [7] A. Srivastava and E. P. Klassen, *Functional and Shape Data Analysis*. Springer, New York, 2016.
- [8] A. Srivastava, E. P. Klassen, S. H. Joshi, and I. H. Jermyn. Shape Analysis of Elastic Curves in Euclidean Spaces. *IEEE Transactions on Pattern Analysis and Machine Intelligence* **33:7** (2011), 1415-1428.

Machine Learning Models to Predict the Infrared Spectra of Chemical Compounds

Chen Qu

Barry I. Schneider

Thomas Allison (NIST MML)

Walid Keyrouz (NIST ITL)

Anthony Kearsley

Joel Bowman

Tyler Martin (NIST MML)

Bradley Sutliff (NIST MML)

Recently, neural network (NN) based machine learning (ML) methodologies have become practical due to the availability of high-speed algorithms implemented on graphics processing units, resulting in an explosion of application of these methodologies to a wide range of problems. We have applied a graph neural network (GNN) [1] to predict various molecular properties, including Kovats retention index [2], boiling point [3], and mass spectrum [4]. In this fiscal year, we focused on the infrared (IR) spectra of molecules.

The infrared spectrum results from the absorption of IR radiation due to molecular vibrations. The frequency and the intensity of the absorption depend on the functional groups and their environments. Therefore, it can be used to identify substances. For example, it is routinely used in recycling facilities to identify different (sub)types of polyolefins. Thus, a model that can accurately and simply predict the IR spectrum when given the molecular structure is extremely valuable to experimentalists such as collaborators Tyler Martin and Bradley Sutliff from NIST MML. Most first-principle approaches to predict the IR spectra are based on harmonic approximations, which leads to large errors in frequencies. More sophisticated theories can predict the spectrum with high accuracy, but they are computationally extremely intensive. We aim to train a ML model to predict the IR spectrum of a molecule with high fidelity and low cost. However, experimental IR spectra are scarce, so our first step is to train models that can accurately reproduce theoretical IR spectra.

Two different ML models have been trained, each with their advantages and limitations. The first model uses the same GNN architecture we applied previously for molecular property prediction. In this model, the IR spectrum is represented as a histogram, with each bin representing one frequency of the radiation (in cm^{-1}), and the height of that bin representing the spectral intensity at that frequency. The model is trained using computed IR spectra of approximately 80 000 compounds from the NIST Chemistry Webbook,¹⁴ with

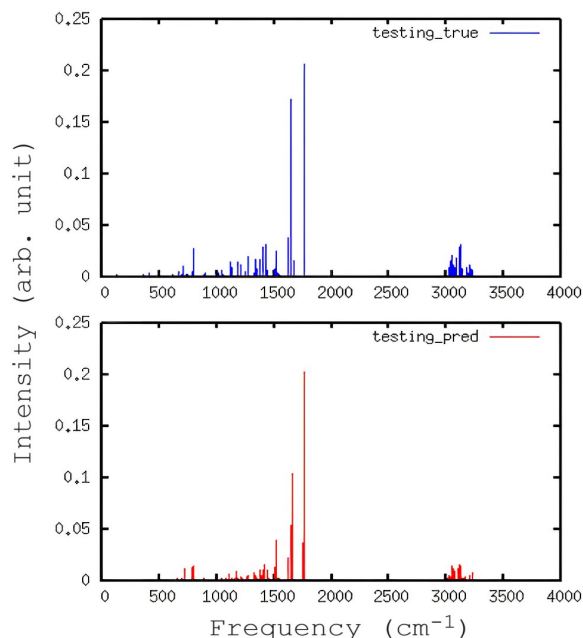


Figure 38. Comparison between the IR spectrum computed using B3LYP (above, blue, used as true spectrum in this work) and the predicted spectrum using the GNN model (below, red).

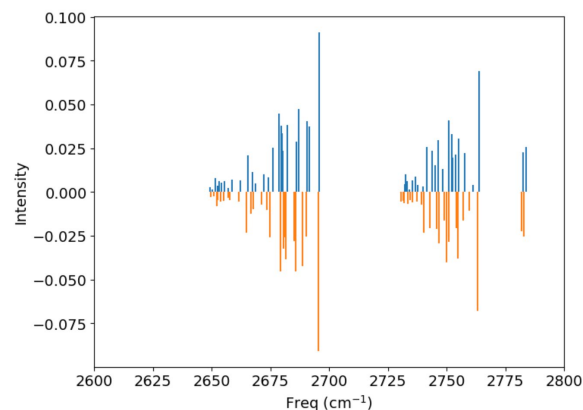


Figure 39. Comparison between the IR spectrum computed using PM7 (above, blue, used as true spectrum in this work) and the predicted spectrum using the machine learning model (below, orange).

density functional B3LYP. The symmetrized Kullback-Leibler divergence between two spectra \mathbf{u} and \mathbf{v} [5]

$$\sum_i \left(u_i \ln \frac{u_i}{v_i} + v_i \ln \frac{v_i}{u_i} \right)$$

is used as the loss function and the metric for spectral similarity. Figure 38 shows a prediction of this model and the comparison to the ground truth (in this case, the theoretically computed spectrum). The agreement is quite satisfying, but one issue is that this model produces spurious lines in the prediction.

¹⁴ <https://webbook.nist.gov/chemistry/>

For the second model, we focus on the C-H stretches in small hydrocarbons (up to 60 carbons, to model vibrations in polyolefins). The IR spectra of these hydrocarbons were computed using the semiempirical PM7 method [6]. We applied the multilayer perceptron model, and the outputs are N vibrational frequencies and corresponding intensities, where N is the number of C-H bonds in the molecule. The input to this model is the molecular representation implemented in the package chemreps [7], such as a Coulomb matrix or bag of bonds, computed from the Cartesian coordinates of carbon atoms. This model achieved an accurate prediction of the IR spectra, as shown in Figure 39. However, this model is restricted to a specific N and thus not a generic model.

One potential solution that can overcome the above limitations (spurious peaks in the first model and fixed N in the second model) is to predict the molecular Hessian matrix (force-constant matrix) instead of the spectrum directly. Diagonalization of the predicted Hessian matrix leads to vibrational frequencies. In this way, the model would work for molecules of arbitrary size and with the correct number of vibrational frequencies. This approach will be investigated in the next fiscal year.

- [1] C. Chen, W. Ye, Y. Zuo, C. Zheng, and S. P. Ong. Graph Networks as a Universal Machine Learning Framework for Molecules and Crystals. *Chemistry of Materials* **31** (2019), 3564–3572.
- [2] C. Qu, B. I. Schneider, A. J. Kearsley, W. Keyrouz, and T. C. Allison. Predicting Kováts Retention Indices Using Graph Neural Networks. *Journal of Chromatography A* **1646** (2021), 462100.
- [3] C. Qu, A. J. Kearsley, B. I. Schneider, W. Keyrouz, and T. C. Allison. Graph Convolutional Neural Network Applied to the Prediction of Normal Boiling Point. *Journal of Molecular Graphics and Modelling* **112** (2022), 108149.
- [4] C. Qu, B. I. Schneider, A. J. Kearsley, W. Keyrouz, and T. C. Allison. Applying Graph Neural Network Models to Molecular Property Prediction Using High-quality Experimental Data. In review.
- [5] C. McGill, M. Forsuelo, Y. Guan, W. H. Green. Predicting Infrared Spectra with Message Passing Neural Networks. *Journal of Chemical Information and Modeling* **61** (2021), 2594–2609.
- [6] J. J. P. Stewart. Optimization of Parameters for Semiempirical Methods VI: More Modifications to the NDDO Approximations and Re-optimization of Parameters. *Journal of Molecular Modeling* **19** (2013), 1–32.
- [7] D. Folmsbee, S. Upadhyay, A. Dumi, D. Hiener, and D. Mulvey. chemreps/chemreps: Molecular Machine Learning Representations. Zenodo, (2019). URL: <https://zenodo.org/records/3333856>

Improved Discrimination of Mass Spectral Isomers

Deborah F. McGlynn

Nirina Rabe Andriamaharavo (NIST MML)

Anthony J. Kearsley

Isomers are known to have varying physical properties, making their unique identification an important task. However, discrimination of electron ionization mass spectra of isomers remains a challenge due to their similar fragmentation patterns and close retention indices. This study employs a new high-dimensional consensus (HDC) mass spectral (HDCMS) similarity scoring technique to discriminate isomers collected using an electron ionization mass spectrometer [1]. The HDCMS method calculates the mean and standard deviation of compound mass spectral peaks to construct high dimensional consensus mass spectra. Using this method, spectral variability is used as a signature by which to discriminate spectra [1].

In this study, the HDCMS method was employed in the discrimination of three cymene positional isomers ($C_{10}H_{14}$) collected on an Electron Ionization-Mass Spectrometer (EI-MS). The close experimental retention indices and indistinguishable fragmentation patterns (Figure 40) make these compounds a perfect test case for the HDCMS method. Fifteen replicate measurements of *p*-cymene, *o*-cymene, and *m*-cymene were collected and divided into query and library sets (3 and 12 replicates, respectively). The mass spectra of these three isomers are given in Figure 40. High dimensional consensus mass spectra were calculated from the query and library sets; each query was compared to each library HDCMS to yield a match factor (Table 3). For every query, the top rank match for each positional isomer was the library compound.

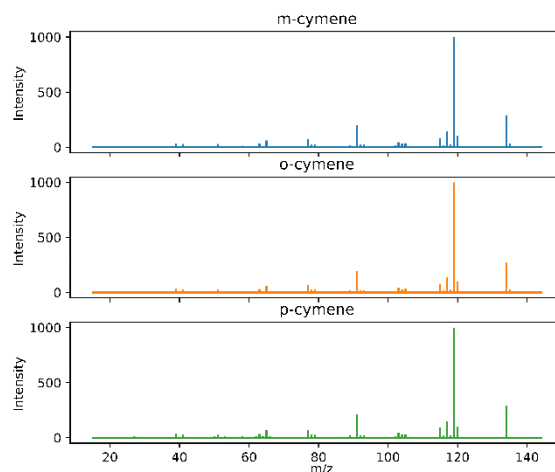


Figure 40. Mass spectra of *m*-cymene, *o*-cymene, and *p*-cymene and their associated structures.

Table 3. The top three match scores from searching for each compound query HDCMS against each compound library HDCMS. The match score ranges between 0 and 1.

Query is m-Cymene		Query is o-Cymene		Query is p-Cymene	
Match Result	Match Score	Match Result	Match Score	Match Result	Match Score
m-Cymene	0.968	o-Cymene	0.989	p-Cymene	0.977
o-Cymene	0.873	m-Cymene	0.890	m-Cymene	0.880
p-Cymene	0.862	p-Cymene	0.858	o-Cymene	0.857

The high dimensional consensus mass spectral similarity algorithm distinguished these positional isomers, which are not distinguishable with established methods. This suggests that these isomers yield a measurement variability signature by which they can be distinguished. However, many questions remain in the application of this method to mass spectral compound discrimination. For example, it is still unclear if the number of replicates needed for discrimination changes with the number of ion fragments or if the method can be employed on compounds with very little fragmentation. This work is part of an ongoing and larger effort in which these questions are being addressed but is expected to be published in the coming months.

- [1] M. J. Roberts, A. S. Moorthy, E. Sisco, and A. J. Kearsley. Incorporating Measurement Variability When Comparing Sets of High-resolution Mass Spectra. *Analytica Chimica Acta* **1230** (2022), 340247. DOI: [10.1016/j.aca.2022.340247](https://doi.org/10.1016/j.aca.2022.340247)

AI4Wind

Zachary J. Grey

Ryan King (National Renewable Energy Lab)

Alireza Doostan (University of Colorado Boulder)

Gianluca Geraci (Sandia National Labs)

AI has recently (re)-emerged as a compelling universal computational framework for addressing several scientific, commercial, and economic challenges. Based on initiatives outlined by Executive Order (EO) 14110 Safe, Secure, and Trustworthy Development and Use of Artificial Intelligence, the call for leveraging AI to overcome economic and scientific challenges has never been more transparent. Our basic thesis is to explore the use of AI for creating a cleaner and more secure energy future for the nation by utilizing the novel physical infrastructure of offshore wind turbines. This funded initiative by the Department of Energy Wind Energy Technology Office seeks to: (i) rigorously evaluate a use-case for trustworthy AI implementations to deliver on the goals set forth by the administration, (ii) promote the application of AI to deliver on U.S. energy economy security as well as global climate initiatives, and (iii)

demonstrate the efficacy of inter-agency and academic collaborations to these ends.

Offshore wind energy technology has been identified as an excellent compromise towards renewable, clean energy co-located with areas of high population density. However, assessing the viability of offshore wind deployment, designing next generation floating offshore wind turbines, and monitoring/securing these difficult-to-access power plants introduces several technological challenges. Each of these challenges present tremendous opportunity for coupled design and measurement science.

Offshore wind turbine designs are relatively immature and offshore sites are significantly more difficult to access and maintain. Our challenge is to supplement and facilitate tools for resilient commercial deployments considering interactions of (i) a complex ocean system ecology, (ii) local economies, and (iii) an incredibly volatile ocean environment fraught with uncertainty and extreme events. An extensive modeling, analysis, and measurement of these interactions must be trustworthy given inherent difficulties and expenses of accessing offshore sites. Overcoming these high-risk challenges will require technical innovations in offshore design and measurement from modeling to manufacturing to monitoring.

In contrast to conventional AI/ML applications, which have enormous training data sets, wind energy observational data are characteristically sparse, noisy, and multimodal. Further, they are often non-Euclidean (e.g., conical lidar slices, airfoil shapes), which prohibits the straightforward application of existing AI/ML techniques developed for image processing. Domain-specific data representations, such as knowledge graph structures and improved shape representations, can reduce problem complexity and improve AI/ML predictive performance and interpretability. Finally, a rich modeling hierarchy exists for many wind energy applications, but new multifidelity approaches to AI/ML model training and evaluation are necessary to make the best use of these model hierarchies to reduce computational burdens, address data limitations, and characterize AI/ML uncertainty.

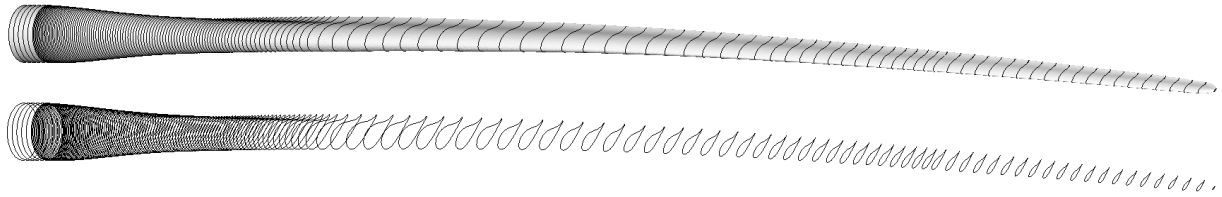


Figure 41. An example of a nominal wind turbine blade configuration using a geometric generative model developed in collaboration between NREL and NIST/ACMD presented at the AI for Wind Energy Workshop in Boulder, CO, June 27th-28th, 2023.

Specifically, this work will improve the measurement and subsequent generation of inflow conditions (wind and wave states) that lead to extreme turbine responses and discover new representations for latent spaces that are better informed of extreme events. We will produce a multifidelity latent diffusion model that learns to efficiently generate coupled wind-wave inflows by making use of multiple fidelity training datasets and measurements. This will dramatically reduce the computational barriers to performing floating offshore wind energy simulations and studying extreme loading conditions. We will also develop physics-informed AI/ML techniques that enforce correct boundary layer properties in the high-fidelity simulations and the generated inflows, addressing key inaccuracies in current large eddy simulation wall modeling for offshore conditions.

Finally, this effort will maximize explainable insights from AI/ML workflows by representing data with wind-specific parameterizations that improve representations of underlying abstract geometries. This improves explainability of limited observations and simulations by reducing dimensionality to enable efficient exploration of the parameter space, more explicit constraint definitions, improved statistical descriptions, and unfolding disparate data modalities that commonly characterize the multi-physical processes in offshore wind problems. The enhanced interpretability and explainability will address concerns about AI/ML being a “black box” and increase the confidence in and adoption of AI/ML models across the wind energy community.

Mathematics of Biotechnology

As proof-of-concept academic work in engineering biology meets the market realities of bringing lab science to product initiation, there are questions in how to compare biological products, measure whether desired outcomes are realized, and optimize biological systems for desired behaviors. NIST is working to deliver tools and standards to measure such biological technologies, outputs, and processes from healthcare to manufacturing and beyond. We support this effort with the development and deployment of innovative mathematical modeling and data analysis techniques and tools.

Mechanics of Fluid Interfaces

Leroy Jia

William Irvine (University of Chicago)

Michael Shelley (Flatiron Institute and NYU)

Cell membranes, biological tissues, and thin films are all examples of fluid interfaces that are necessary for the miracle of life. Mathematically speaking, instabilities and singularities are common in such systems, and they have historically defied the suite of mathematical techniques that has proven “unreasonably effective” at modeling macroscopic phenomena. Below, we outline progress over the last year in developing robust analytical and computational methods for these complex systems.

For ordinary fluids, viscosity has a damping effect that discourages velocity gradients. So-called Newtonian materials are described by a stress tensor $\boldsymbol{\sigma}$ of the form

$$\boldsymbol{\sigma} = \eta(\nabla\mathbf{u} + \nabla\mathbf{u}^T)$$

where \mathbf{u} is the fluid velocity field, ∇ is the gradient operator, T is the matrix transpose operator, and η is the viscosity coefficient. However, this need not be the case for materials that break time-reversal symmetry, such as fluids composed of active particles that convert energy into motion. In two dimensions, active fluids can exhibit an anomalous non-dissipative odd viscosity, through which constituent particles can interact with each other transversely, leading to some highly unusual flow patterns. The odd viscous stress tensor describing forces in a 2D chiral fluid is given by

$$\boldsymbol{\sigma}_{odd} = \eta_o(\nabla^\perp\mathbf{u} + \nabla\mathbf{u}^\perp)$$

where η_o is the odd viscosity coefficient and $(\cdot)^\perp$ indicates rotation of a 2D vector by $\pi/2$; here, the perp operators have the effect of coupling the normal and tangential components of the flow. In the spirit of classical mixed boundary value problems in potential theory, the resulting dynamics can be written in terms of a complicated singular integral equation, the analysis of which was published in the *Journal of Fluid Mechanics* [1] last year. In this paper, we showed that odd viscosity is responsible for manifestly non-Newtonian phenomena

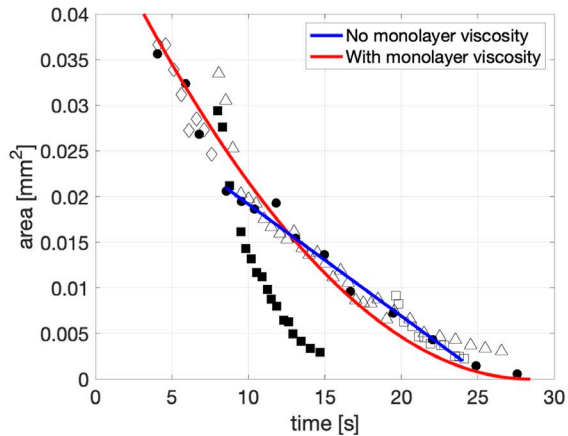


Figure 42. The area of a hole in a punctured Langmuir film that closes over time due to line tension. The straight blue line is the prediction of the original paper [2], which assumed that monolayer viscosity was negligible. Accounting for monolayer viscosity yields the curved red line, which provides a better fit over a broader range of data. Image taken from [3].

such as unidirectional edge currents in fluid domains and inwardly directed radial motion in certain active fluids, even in the absence of edge tension.

Interestingly, a simplified version of this integral equation governs a seemingly unrelated classical fluid interfacial system: the Langmuir monolayer, which is used in coating and deposition processes, as well as in experiments with biological membranes. In reviewing the literature for Langmuir monolayers, we discovered that the simplifying, but unphysical, assumption of vanishing monolayer viscosity had been taken in a series of highly cited papers. This assumption has profound consequences in measurement science: for example, one of these papers describes a method in which a circular cavity was punctured in a Langmuir monolayer, and the rate at which this cavity closed was used to measure the line tension of the monolayer [2]. If the monolayer viscosity vanishes, the area of the cavity simply decreases linearly with time. We reformulated this model and explained the nontrivial corrections that arise by considering a regularizing monolayer viscosity (Figure 42). Our findings suggest that measurements of the line tension of fluid interfaces using this method may have been systematically underestimated by a factor of approximately six

due to this unphysical assumption. Our work appeared in the *Journal of Fluid Mechanics* [3] and was presented at the 76th Annual Meeting of the American Physical Society Division of Fluid Dynamics in November of 2023.

The controllable self-healing and self-annihilating properties of soft and fluid interfaces have the potential to find applications in materials science, biology, and metrology, and our work will provide a framework for understanding and harnessing these properties. Ongoing computational work includes the development of a highly accurate boundary integral formulation describing the dynamics of a 2D odd viscous fluid layer of arbitrary shape. A related analytical question is the mechanical stability of an odd viscous disk or cavity; the analysis of these configurations is complicated by the appearance of singularities of the flow field at the boundary. Finally, work is ongoing to generalize these methods to curved active interfaces such as cell membranes.

- [1] L. L. Jia, W. T. M. Irvine, and M. J. Shelley. Incompressible Active Phases at an Interface. Part 1. Formulation and Axisymmetric Odd Flows. *Journal of Fluid Mechanics* **951** (2022), A36. DOI: [10.1017/jfm.2022.856](https://doi.org/10.1017/jfm.2022.856)
- [2] J. C. Alexander, A. J. Bernoff, E. K. Mann, J. A. Mann, Jr., and L. Zou. Hole Dynamics in Polymer Langmuir Films. *Physics of Fluids* **18** (2006), 062103. DOI: [10.1063/1.2212887](https://doi.org/10.1063/1.2212887)
- [3] L. L. Jia and M. J. Shelley. The Role of Monolayer Viscosity in Langmuir Film Hole Closure Dynamics. *Journal of Fluid Mechanics* **948** (2022), A1. DOI: [10.1017/jfm.2022.550](https://doi.org/10.1017/jfm.2022.550)

Mathematical Modeling and Optimization for Cryobiology

Daniel Anderson

Anthony Kearsley

James Benson (University of Saskatchewan, Canada)

Jessica Masterson (George Mason University)

Cryobiology, the study of biological specimens at cryogenic temperatures, plays an enormous role in a wide range of fields. In the field of medicine, cryobiology is the basis for cryopreservation in assisted reproduction, organ transplantation, biobanking and personalized medicine. Cryo-banking is used in the agriculture industry as well as for initiatives aimed at preserving rare and endangered plant and animal species and in the development of more productive agricultural yields. Applications in forensics arise in the processing and preservation of frozen biological samples that are often important and fragile evidence in criminal investigations. The breadth and depth of these applications reflect the complexity of the biological, chemical, and physical aspects required to describe and model these problems.

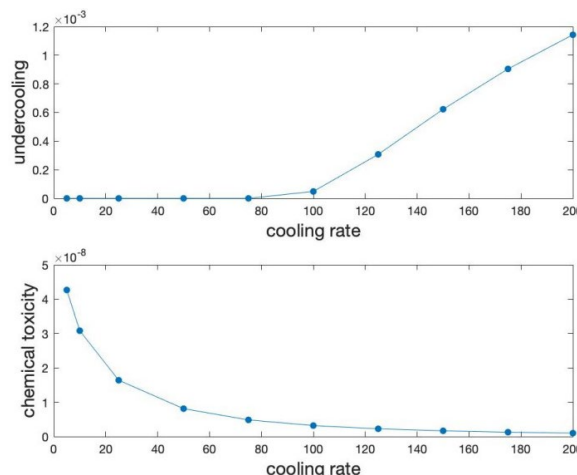


Figure 43. Computed damage function proxies as a function of cooling rate.

Mathematical and computational models can be used to probe these complex systems and in conjunction with sophisticated control and optimization schemes, can establish more effective protocols for cryopreservation.

Cryopreservation of a human cell is a form of biomimicry that attempts to do in the laboratory, or in silica, what some frog and amphibian species can do naturally. A cryoprotectant, effectively an antifreeze, aims to play the role that substances like glucose play in the winter preservation of frozen frogs. These cryoprotectants, which are added to the extra-cellular environment, help to remove water from a cell before cooling, thus reducing the likelihood of intracellular ice formation. This, however, comes at a price due to the cell's limited ability to withstand the elevated levels of chemicals, including the naturally occurring salts in the cell, possibly damaging the cell, or causing death by chemical toxicity. Thus, the maintenance of a viable cell during cryopreservation is complicated by two primary factors. Cooling the cell too quickly increases the undercooling and the likelihood of intracellular ice formation and cell damage or death while cooling the cell too slowly can overexpose the cell to high solution concentrations and lead to chemical toxicity. This amounts to a high-stakes goldilocks problem from the cell's perspective.

Mathematical modeling in cryobiology thus requires a detailed understanding of thermal and chemical transport in bulk phases as well as across a semipermeable cell membrane. Additionally, phase transformation of these multicomponent solutions – phenomena that link cryobiology to a wide range of other fields, from geophysics to industrial materials processing [6], must also be included. Cryopreserving a cell requires a delicate balance between two competing damage mechanisms, and thus a delicate optimization problem. We are exploring foundational aspects of biochemical and physical modeling in cryobiology, computational

methods for the solution of these models, and applications of these ideas to cryopreservation of cells.

The focus of [1] was to establish the foundations of the chemical thermodynamics necessary to describe transport processes during cryopreservation. This work formulated chemical potentials and related thermodynamics quantities for non-dilute and non-ideal multicomponent solutions of experimental and theoretical interest to cryobiologists. Next, the multiphase, multi-species transport equations were developed along with a consistent characterization of cell membrane dynamics and solid-liquid phase transitions [2]. A critical aspect of our work was to obtain, from first principles, mathematical models that address both spatial and temporal dynamics of chemical species and heat transport. Various aspects of the freezing of a spherical biological cell were addressed in [3] and [4]. Based on a numerical algorithm outlined in [4], we explored in [3] the evolution of the thermal fields in the solid, liquid, and intracellular regions along with the concentration of cryoprotectant and the intra- and extracellular salts. These studies incorporated the effects of confinement and partial solute rejection, which had not previously been examined in cryobiology. These observations led to the development of objective functions in [4], which provide a measure of both intracellular undercooling and chemical toxicity. These objective functions appear more suited to help establish cooling protocols than previously employed toxicity functions [5].

The mathematical models and computational algorithms established in this foundational series of papers [1-4] form the basis for our current work towards optimal control of these systems. Our current work underway with J. Masterson has first involved the identification of proxies for cell/tissue damage that can be used in optimal control settings (see Figure 43). These are objective functions whose state variables are solutions of a coupled nonlinear moving free-boundary problem and, as such, fit the mathematical framework of PDE-constrained optimization. That is, the bio/chemical/physical model constrains variables such as thermal and solute fields, that help define objective functions such as those measuring tissue undercooling and chemical toxicity. Controls for these systems typically involve, at least, specification of a boundary temperature as a function of time. The framework of adjoint model formulation in optimal control theory provides a highly efficient means to compute gradients of the objective function necessary for mathematical and computational minimization schemes. Our work with J. Masterson is underway to obtain these adjoint problem formulations and implement them computationally. Our first objective is to address optimal protocols in the freezing/cooling stage. A second goal is to extend this framework to explore strategies that can optimize protocols for cryo-recovery where warming and/or melting occur. The central role played by phase transformation

and transport in multicomponent systems links these cryobiological processes and their mathematical descriptions to related ones that occur under vastly different conditions in geophysics and industrial materials processing [6].

- [1] D. M. Anderson, J. D. Benson, and A. J. Kearsley. Foundations of Modeling in Cryobiology I: Concentration, Gibbs Energy, and Chemical Potential Relationships. *Cryobiology* **69** (2014), 349-360. DOI: [10.1016/j.cryobiol.2014.09.004](https://doi.org/10.1016/j.cryobiol.2014.09.004)
- [2] D. M. Anderson, J. D. Benson, and A. J. Kearsley. Foundations of Modeling in Cryobiology II: Heat and Mass Transport in Bulk and at Cell Membrane and Ice-liquid Interfaces. *Cryobiology* **91** (2019), 3-17. DOI: [10.1016/j.cryobiol.2019.09.014](https://doi.org/10.1016/j.cryobiol.2019.09.014)
- [3] D. M. Anderson, J. D. Benson, and A. J. Kearsley. Foundations of Modeling in Cryobiology III: Heat and Mass Transport in a Ternary System. *Cryobiology* **92** (2020), 34-46. DOI: [10.1016/j.cryobiol.2019.09.013](https://doi.org/10.1016/j.cryobiol.2019.09.013)
- [4] D. M. Anderson, J. D. Benson, and A. J. Kearsley. Numerical Solution of Inward Solidification of a Dilute Ternary Solution Towards a Semi-permeable Spherical Cell. *Mathematical Biosciences* **316** (2019), 108240. DOI: [10.1016/j.mbs.2019.108240](https://doi.org/10.1016/j.mbs.2019.108240)
- [5] J. D. Benson, A. J. Kearsley, and A. Z. Higgins. Mathematical Optimization of Procedures for Cryoprotectant Equilibration using a Toxicity Cost Function. *Cryobiology* **64** (2012), 144-151. DOI: [10.1016/j.cryobiol.2012.01.001](https://doi.org/10.1016/j.cryobiol.2012.01.001)
- [6] D. M. Anderson, P. Guba, and A. J. Wells. Mushy Layer Convection. *Physics Today* **75** (2022) 34-39. DOI: [10.1063/PT.3.4940](https://doi.org/10.1063/PT.3.4940)

Spatial-Temporal Dynamics of Photoreceptors in the Eye

Danielle C. Brager
Anthony J. Kearsley
Daniel M. Anderson

The light reflected into your eyes from the colorful, sunlit plumage of a scarlet macaw, or from a fast-moving car in your peripheral view, or from a dimly lit obstacle in your path on a dark, moonless night is processed by your brain in a figurative “blink of an eye.” The light’s path through this complex optical system—the outermost tear film, cornea, anterior chamber, pupil, lens, and vitreous chamber—results in focused light into the retina, which is the thin, light-sensitive tissue at the back of the eye that converts light into electrochemical signals sent on to the brain via the optic nerve resulting in, for healthy eyes, visual recognition (see Figure 44).

The retina itself has a multitude of components and functions; we explore specifically the photoreceptors, of which there are two types, rods and cones, and an underlying retinal pigment epithelium (RPE). Rods are

concentrated in the outer regions of the retina while the cones are concentrated near the fovea, which is in the center, macular, region of the retina. Figure 45 shows this rod and cone spatial distribution for humans and for Rhesus Monkeys. Rods are known to be responsible for visual function in low-light (night vision) and peripheral vision. Cones are responsible for day vision, color vision, and visual acuity. A photoreceptor includes an inner segment (IS) and an outer segment (OS). The photoreceptor IS, as the main site of the mitochondria, is the photoreceptor's metabolic center. The photoreceptor's OS is made up of disc-like lamellae and contains photopigments that absorb incident photons and undergo structural alteration in the process of creating electrochemical signals. The outer segments, whose lengths are on the order of tens of microns in human photoreceptors, undergo continuous shedding and periodic renewal facilitated by the RPE which acts to recycle the shed parts of the OS and serves as an effective nutrient source sustaining the function of the rods and cones.

Retinal degenerations include a group of disorders that lead to photoreceptor loss. This photoreceptor cell loss is common to degenerative eye disorders such as retinitis pigmentosa, age-related macular degeneration, and cone-rod dystrophy. Research in this field is focused on developing strategies to delay or prevent the onset of photoreceptor degeneration [4, 5]. However, there is currently no cure for diseases linked to photoreceptor degeneration.

Mathematical modeling plays an important role in this research effort [3]. There exist mathematical and computational models of various regions of the retina in retinal development, health, and disease. Many of these are based on ordinary differential equations, such as the one by Camacho and Wirkus [6], which has been compared with retinal OS regrowth data by Guerin et al. [8, 9]. Other work has explored spatial dependence in photoreceptor dynamics (e.g., Roberts et al. [10]) to investigate mechanisms associated with retinitis pigmentosa. However, to our knowledge, our work [2] is the first mathematical model of the physiology of photoreceptors in a healthy eye that incorporates the interplay between the spatial photoreceptor density distribution, OS length, and a nutrient source. Predictions from our model compare well with the Guerin et al. [8,9] spatial-temporal Rhesus monkey OS regrowth data and are the first to account for the spatial dependence of this retinal detachment data (Figure 46). Our model also compares well with spatial measurements of human photoreceptor OS length from Wilk et al. [10] (Figure 47). While our efforts have focused on healthy eye conditions, the model we have developed establishes a framework in which future studies of retinal pathologies may be undertaken.

- [1] C. K. Adams, J. M. Perez, and M. N. Hawthorne. Rod and Cone Densities in the Rhesus. *Investigations in Ophthalmology* **13** (1974), 885-888.

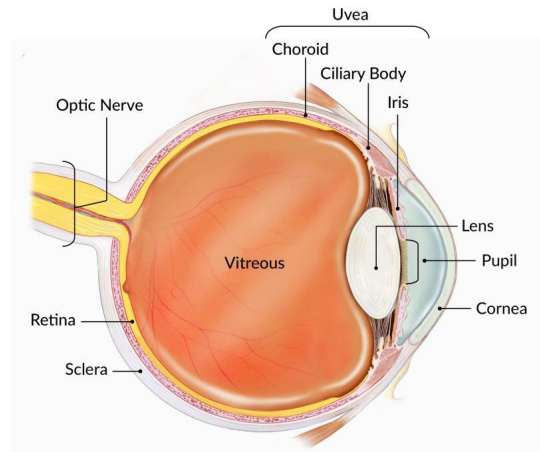


Figure 44. Components of the eye. (Image source: [How the Eyes Work | National Eye Institute, nih.gov](https://www.nia.nih.gov/eye/how-the-eyes-work))

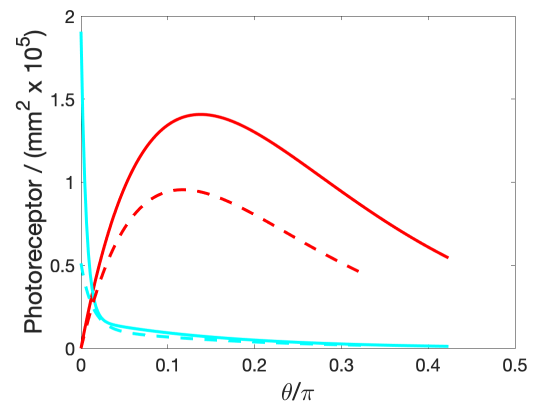


Figure 45. Spatial dependence of Rod Outer Segment (red curves) and Cone Outer Segment (cyan curves) for humans (solid curves – data from Curcio et al. [7]) and Rhesus Monkeys (dashed curves – data from Adams et al. [1]). The angle is measured in radians from the fovea (functional center of the retina).

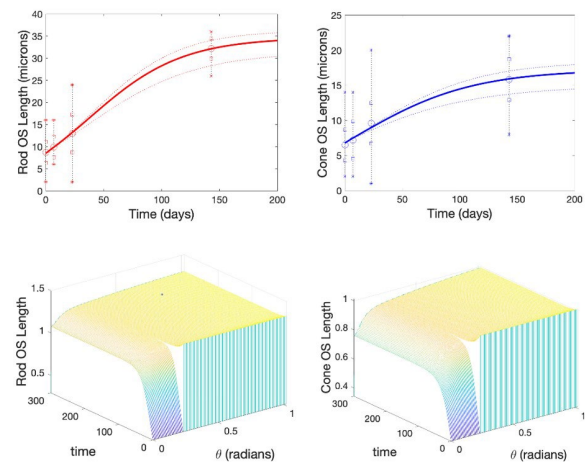


Figure 46. Averaged Rod and Cone OS lengths in the macular region during regrowth along with Rhesus monkey data from Guerin et al. (upper plots). Rod and Cone OS length dynamics as a function of position on the retina for macular region OS regrowth.

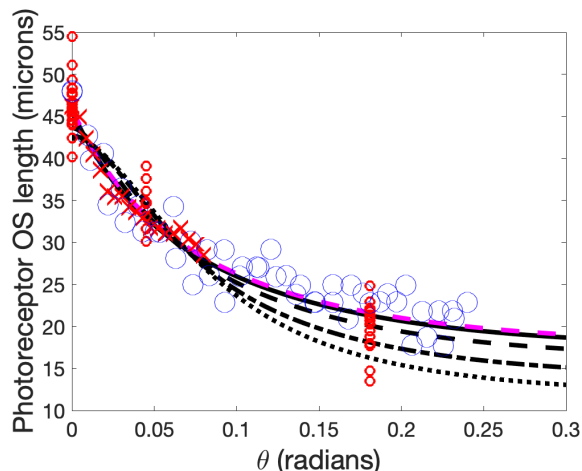


Figure 47. Rod OS and Cone OS length predictions (solid and dashed curves) in comparison with Wilk et al. [11] data (various symbols) of human photoreceptor lengths in radians measured from the fovea.

- [2] D. M. Anderson, D. C. Brager, and A. J. Kearsley. Spatially Dependent Model for Rods and Cones in the Retina. *Journal of Theoretical Biology*, to appear.
- [3] D. C. Brager. Modeling and Analyzing the Progression of Retinitis Pigmentosa. Doctoral dissertation, Arizona State University, 2020.
- [4] E. T. Camacho, L. A. Melara, M. C. Villalobos, and S. Wirkus. Optimal Control in the Treatment of Retinitis Pigmentosa. *Bulletin of Mathematical Biology* **76**:2 (2014), 292-313.
- [5] E. T. Camacho, S. Lenhart, L. A. Melara, M. C. Villalobos, and S. Wirkus. Optimal Control with MANF Treatment of Photoreceptor Degeneration. *Mathematical Medicine and Biology: A Journal of the IMA* **37**:1 (2020), 1-21.
- [6] E. T. Camacho and S. Wirkus. Tracing the Progression of Retinitis Pigmentosa Via Photoreceptor Interactions. *Journal of Theoretical Biology* **317** (2013), 105-118.
- [7] C. A. Curcio, K. R. Sloan, R. E. Kalina, and A. E. Hendrickson. Human Photoreceptor Topography. *Journal of Computational Neurology* **292** (1990), 497-523.
- [8] C. J. Guerin, D. H. Anderson, R. N. Fariss, and S. K. Fisher. Retinal Reattachment of the Primate Macula. *Investigations in Ophthalmology and Visual Science* **30** (1989), 1708-1725.
- [9] C. J. Guerin, G. P. Lewis, S. K. Fisher, and D. H. Anderson. Recovery of Photoreceptor Outer Segment Length and Analysis of Membrane Assembly Rates in Regenerating Primate Photoreceptor Outer Segments. *Investigations in Ophthalmology and Visual Science* **34** (1993), 175-183.
- [10] P. A. Roberts, E. A. Gaffney, P. J. Luthert, A. J. E. Foss, and H. M. Byrne. Mathematical models of retinitis pigmentosa: The oxygen toxicity hypothesis. *Journal of Theoretical Biology* **425** (2017), 53-71.

- [11] M. A. Wilk, B. M. Wilk, C. S. Lango, R. F. Cooper, and J. Carroll. Evaluating Outer Segment Length as a Surrogate Measure of Peak Foveal Cone Density. *Visual Research* **130** (2017), 57-66.

Discriminating Drug Compounds Using Novel Probability-Based Similarity Scores of Their Electron-Ionization Mass Spectra

Amudhan Krishnaswamy Usha
 Briana Capistran (NIST MML)
 Edward Sisco (NIST MML)
 Anthony Kearsley

A mass spectroscope, at its most basic, operates by breaking a compound into charged ions, which are then separated based on their mass-to-charge (m/z) ratio. The mass spectrum of a compound is the set of resulting m/z ratios and the corresponding intensities of its ion fragments. M/z values obtained from gas chromatography coupled electron-ionization mass spectroscopy (GC-EIMS) are typically stored as integers. A mass spectrum can therefore be viewed as a vector in some d -dimensional Euclidean space, where d is the number of m/z values with non-zero intensity.

Classical approaches to discriminate between compounds based on their mass spectra rely on similarity functions which act on two spectra and returns a value between 0 and 1. Given an unknown compound, one computes its similarity score against a library of mass spectra, which are then used to generate a list of most probable matches. The simplest of these is the cosine similarity score, which computes the cosine of the angle between the two mass spectra vectors.

There are several compounds of forensic interest which are structurally and functionally different but generate very similar mass spectra which are difficult to distinguish using conventional methods. Recent work involving some of the authors in the current project has explored the use of replicate mass spectra to account for variability in the measured m/z and intensity values [1]. Using a set of replicate mass spectra, they construct a “high dimensional consensus” (HDC) spectrum for each compound. In essence, this involves representing a compound’s mass spectrum as a set of 2-D Gaussian probability distributions, where the mean of each Gaussian corresponds to the averaged peaks of the traditional mass spectrum. The authors use this HDC spectrum to compute a “HDC similarity score,” which possesses better discriminatory power compared to classical similarity scores.

The HDC approach to mass spectra involves a modeling choice: the intensity and m/z values are assumed

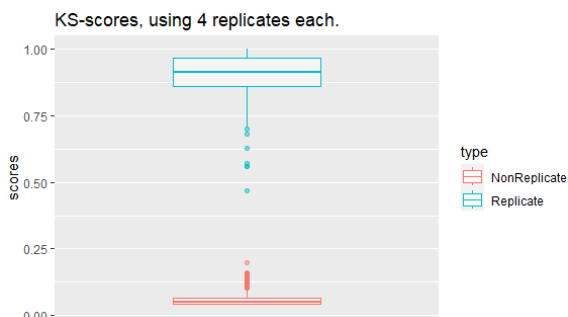


Figure 48. KS-scores computed by sampling 4 replicates each from a set of replicate mass spectra of 16 drug compounds. “Replicate” indicates that both sets of spectra used to compute the score came from the same compound.

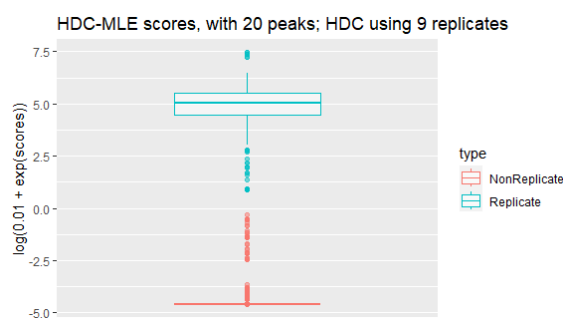


Figure 49. HDC-MLE scores computed using samples of 9 replicates for the library compound.

to be normally distributed. Due to binning and truncation, this may not be true in all cases, and could lead to sub-optimal results.

In this project, we investigate similarity scores based on non-parametric statistical comparison tests as an alternative to the HDC score. Given two sets of replicate mass spectra, we may apply the Kolmogorov-Smirnoff (KS) test to determine if the corresponding sets of intensities at each m/z value arise from the same distribution. The resulting vector of p-values may be suitably averaged to produce a composite p-value, which we call the KS similarity score. Tests on a class of compounds of interest to forensic chemists indicate that this is an improvement on the HDC similarity score (See Figure 48.)

It often may not be possible to obtain multiple replicate mass spectra of the compound of interest, especially in forensic settings where only trace samples might be present. The HDC and KS scores described above require both the analyte and the library compounds to have replicate mass spectra, and therefore cannot be used in this case. A second component of this project involves identifying similarity scores which reduce or eliminate this requirement, while still accounting for measurement variability. By viewing the compound identification problem as a discrete maximum likelihood estimation problem, we compute what we call the HDC maximum likelihood (HDC-MLE)

score, which takes one analyte spectra and multiple library spectra as input and returns a real number. The HDC-MLE score performs just as well as the HDC score and has the added advantage of a natural threshold: tests with a set of replicate drug spectra indicate that negative HDC-MLE scores almost always imply that the spectra arise from different compounds. (See Figure 49.)

Future work in this direction will explore the incorporation of the compounds’ chromatograms and retention times into these similarity scores, and the relationship of the KS-scores to a true p-value.

- [1] M. J. Roberts, A. S. Moorthy, E. Sisco, and A. J. Kearsley. (2022). Incorporating Measurement Variability When Comparing Sets of High-Resolution Mass Spectra. *Analytica Chimica Acta* **1230** (2022), 340247.

Application of Novel Algorithms for Improved Certainty in Identification of Complex Chemical Mixtures

Deborah F. McGlynn

Lindsay D. Yee (University of California at Berkeley)

Lewis Y. Geer (NIST MML)

Yuri A. Mirokhin (NIST MML)

Dmitrii V. Tchekhovskoi (NIST MML)

Coty N. Jen (University of California at Berkeley)

Allen H. Goldstein (University of California at Berkeley)

Anthony J. Kearsley

Stephen E. Stein (NIST MML)

Environmental sampling allows for improved understanding of baseline conditions and identification of contaminants. A common analytical method employed in atmospheric environmental sampling is gas chromatography electron ionization mass spectrometry or GC-EI-MS. Whole air sampling yields chromatograms containing a complex mixture made up of tens to hundreds of chemical compounds which are typically identified using EI-MS libraries. The NIST EI-MS library contains $\approx 400,000$ spectra. However, low identification percentages are common when applying identifications to complex mixtures sampled from the environment. Despite significant additions to mass spectral libraries over the last three decades, identifications of compounds from complex mixtures have not kept pace (Stein, 2012). Additionally, it is common for mass spectral compounds with similar structures to be incorrectly identified [3]. This suggests that improvements in spectral identification methods are needed.

In this work, two identification methods have been tested on a complex chemical mixture dataset collected from wildfire emissions by UC Berkeley. The first method involved the automated consideration of retention indices which is typically done in a manual fashion

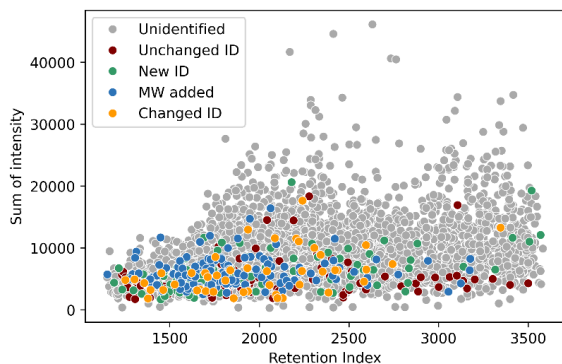


Figure 50. Identities in the FIREX dataset using various new identification methods. Unchanged IDs are in red, New IDs are green, Changed IDs are yellow, and spectra with added molecular weight (MW) which allows for the use of the HSS are in blue. Unidentified spectra are grey.

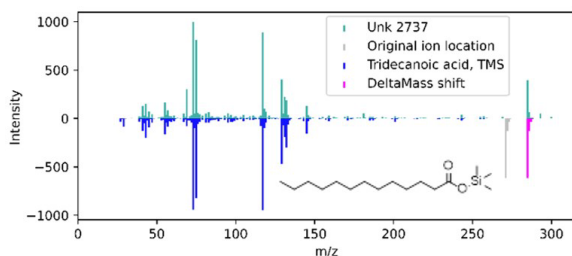


Figure 51. Head-to-tail plot of hybrid similarity search match between unknown 2737 and tridecanoic acid, TMS derivative. The HSS match factor is 933 out of 999. The chemical structure of the library match is overlaid with the spectral library match.

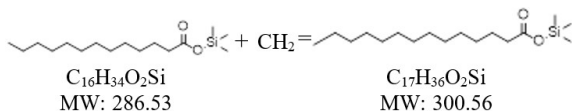


Figure 52. The structure of the library match added to the chemical structure associated with the DeltaMass calculated from the HSS.

when applying identifications to a spectrum. The other method is an extension of the well-established and utilized method for compound identification, cosine similarity (Stein et al., 1994). The method is the Hybrid Similarity Search [2]. The Hybrid Similarity Search calculates mass spectral similarity after calculation of the mass difference between the unknown and library (“DeltaMass”) and a shift in library ions by that amount. The utilization of these two methods was employed to improve the certainty of the applied match by excluding erroneous matches and increasing identities by extending the use of existing mass spectral libraries [2].

An EI-MS dataset containing $\approx 3,000$ unique atmospherically collected wildfire emissions collected by UC Berkeley [1] serves as a test case for developing methods to improve mass spectra identifications. Previously 148 compounds were identified in this dataset. The dataset contains experimental retention indices, making it

an easy test case for automated retention index consideration in spectral matching. The dataset was run against the NIST 2023 EI-MS dataset using the identity search method. The RI window was set to ± 15 . Spectral matches that fell outside of this RI window were penalized by 200 match factor units. This analysis resulted in 46 of the original 148 identified compounds to have a change in identity (Figure 50). Additionally, 98 new identities were added while 102 identities were unchanged (Figure 50).

We then determined the molecular weight of ≈ 130 mass spectra with a high signal to noise ratio in the dataset. Then using the HSS for matching, the NIST EI-MS database was searched for appropriate matches to these unknowns. When searching for a match using HSS, we pulled a library spectrum with a high match factor to the unknown, a similar retention index, and a DeltaMass corresponding to a reasonable and identifiable chemical structure. Then, the library structure was adjusted based on the DeltaMass to create a new structure for the unknown spectra. This method is also being combined with automated retention index thresholding between unknown and library spectra. The application of the HSS and adjustment of the structure by the DeltaMass, added an additional ≈ 130 identities. This method is depicted in Figure 51 and Figure 52. The head-to-tail plot in Figure 51 shows one unknown with a molecular weight of 300 matched against a library spectrum with a molecular weight of 286 shifted by the DeltaMass of 14. Figure 52 shows the structure of the library spectra added to the DeltaMass. This gives a new structure that is a better match to the unknown spectra.

Applying the hybrid similarity search algorithm to large sets of unknown spectra increases the use of spectral databases and increases the number of identities in complex mixtures. Additionally, this method, in combination with automated retention index thresholding between unknown and library spectra, increases the certainty in applying identities to unknowns. This work is currently in progress but, future avenues of this work include developing an automated pipeline by which to calculate chemical formulas from a DeltaMass and applying this formula to the library spectra. This work is applicable to fields that work with complex mixtures such as medical, forensic, pharmaceutical, industrial formulations to name a few. Furthermore, this methodology could be employed in identification of emerging contaminants.

- [1] C. N. Jen, L. E. Hatch, V. Selimovic, R. J. Yokelson, R. Weber, A. E. Fernandez, N. M. Kreisberg, K. C. Barsanti, and A. H. Goldstein. Speciated and Total Emission Factors of Particulate Organics from Burning Western US Wildland Fuels and Their Dependence on Combustion Efficiency. *Atmospheric Chemistry and Physics* 19:2 (2019), 1013–1026. DOI: [10.5194/acp-19-1013-2019](https://doi.org/10.5194/acp-19-1013-2019)
- [2] A. S. Moorthy, W. E. Wallace, A. J. Kearsley, D. V. Tchekhovskoi, and S. E. Stein, S. E. (2017). Combining

Fragment-Ion and Neutral-Loss Matching during Mass Spectral Library Searching: A New General Purpose Algorithm Applicable to Illicit Drug Identification. *Analytical Chemistry* **89**:24 (2017), 13261–13268. DOI: [10.1021/acs.analchem.7b03320](https://doi.org/10.1021/acs.analchem.7b03320)

- [3] S. Stein, S. (2012). Mass Spectral Reference Libraries: An Ever-Expanding Resource for Chemical Identification. *Analytical Chemistry* **84**:17 (2012), 7274–7282. DOI: [10.1021/ac301205z](https://doi.org/10.1021/ac301205z)

Metrology for Cytometry and Microfluidics

Paul Patrone

Anthony Kearsley

Prajakta Bedekar

Amudhan Krishnaswamy-Usha

Matthew DiSalvo (NIST PML)

Nicholas Drachman (Brown University)

Graylen Chickering (Brown University)

Megan Catterton (NIST PML)

Gregory Cooksey (NIST PML)

For more than 30 years, flow cytometry, a technique used to measure characteristics of cells, has been a mainstay for cancer detection, drug development, and biomedical research. It has remained a primarily qualitative metrology platform, however, because measurement uncertainties associated with this technique are so large. While exact economic figures are difficult to estimate, this has clearly had a significant impact on the roughly \$200 billion of waste in the healthcare industry and contributed to the broader reproducibility crisis in biomedical research [1]. The challenge of making cytometry an accurate and precise metrological tool arises from the competing requirement that it have high throughput. Typical biological samples can have up to hundreds of millions of cells, which must be analyzed over a few hours.

To achieve this throughput, cytometers direct cells through a microfluidic channel at high-speed, past an optical interrogation region that collects fluorescence light from antibodies attached to surface proteins. The total fluorescence collected from each cell should then, in principle, be proportional to the total number of markers on its surface. But in practice, this idealized picture is complicated by the cumulative effects of the physical phenomena involved: fluid-dynamic forces cause cells to move across streamlines and/or have unpredictable trajectories; optical geometric collection efficiencies depend on position in the interrogation region; and signal acquisition and processing tools introduce non-linear effects and measurement uncertainties through discrete sampling. These challenges, in addition to the complexity of exactly replicating the necessary measurement infrastructure at the micron scale, have made it virtually

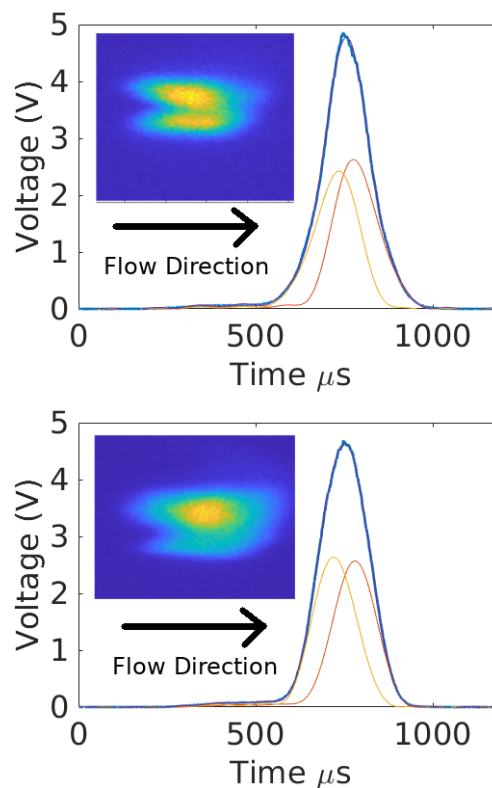


Figure 53. Two examples of doublet deconvolution. The solid blue curve is a measured signal, whereas the two smaller yellow and orange curves are the singlets extracted from the signal. The inset shows visual verification that these events are indeed doublets.

impossible to reproduce measurements on a single cell, a necessary first step towards fully assessing and controlling uncertainties in cytometry.

ACMD, PML, and MML staff were awarded a NIST Innovations in Measurement Science (IMS) award to develop a microfluidic-based cytometer, whose design explicitly allows control and study of repeat measurements of cells. Following on work from FY 2021 and FY 2022, we are continuing a series of research projects on uncertainty quantification (UQ) for cytometry. In FY 2022, we derived a key result indicating that all cytometry events (e.g., for a fixed cell-marker type) are identical up to a set of straightforward linear transformations that depend on physical parameters such as the cell size, speed, and number of biomarkers. Using optimization, we can determine these unknown parameters by mapping different signals onto one another. Critically, this also yields multiple, model-based but distinct realizations of what a measurement would look like if it could be reproduced on the same measurand. When applied to large collections of signals, residuals not accounted for by the data collapse quantify uncertainty in the shape of the time-series associated with each event [2].

In FY 2023, we pursued this line of reasoning further by showing that UQ resulting from this analysis induces a new set of data analyses that solve outstanding

problems in cytometry. In particular, one of the greatest challenges in analyzing raw cytometry data is identifying multiplets, i.e., events wherein multiple cells or particles travel through the same time through the laser interrogation region. In such cases, the time-series appears by eye to have the same shape as a “singlet,” although the amplitude is larger. Thus, it is often impossible to distinguish bright singlets from dim doublets using subjective techniques alone. To address this problem, we developed a novel homotopy-based optimization algorithm that determines the most probable number of singlets in a signal given the aforementioned uncertainty in the singlet shape. As a byproduct, the analysis also yields estimates of the signals themselves; see Figure 53. A manuscript on this work is in preparation.

We are also pursuing a new set of projects that aim to identify and potentially measure the elasticity of deformable particles in a cytometer. Here the key idea is to recognize that as a particle traverses the interrogation region, its shape is convolved with the laser profile. Thus, a deformable particle should have a signal whose shape is distinguishable from a sphere, for example. Preliminary analysis using our data collapse algorithms indicate that the corresponding residuals for deformable particles cannot be explained by the UQ for rigid spheres, indicating that our instrument is likely sensitive enough to detect shape change. As a prototypical case, we have also performed this “shapes analysis” on cells undergoing growth and division, showing that we can in fact distinguish between normal cells and those whose DNA has doubled in anticipation of mitotic division. A manuscript on this latter work is in preparation. In the arena of cytometry, we also continue efforts to define and quantify concepts such as limits of quantification and limit of detection, issues that have yet to be fully addressed.

Work in cytometry has also led to new efforts in the broader field of microfluidics. Following on successes from FY 2018 – FY 2022, we participated in a FedTech incubator program whose goal is to start companies based on NIST inventions. As a result of this effort, a company (Lumos NanoLabs) was created to commercialize our microfluidic flowmeter. En route to realizing this technology in the field, we also recently solved the problem of quantifying the relaxation kinetics of our flowmeter in response to time-varying flow rates [3].

- [1] W. H. Shrank, T. L. Rogstad, and N. Parekh. Waste in the US Health Care System: Estimated Costs and Potential for Savings. *JAMA* **322**:15 (2019), 1501-1509.
- [2] P. N. Patrone, M. DiSalvo, A. J. Kearsley, G. B. McFadden, and G. A. Cooksey. Reproducibility in Cytometry: Signals Analysis and its Connection to Uncertainty Quantification. *PLoS One* **18** (2023), e0295502.
- [3] N. Drachman, P. N. Patrone, and G. Cooksey. Dynamics of optofluidic flow measurements. *Physics of Fluids*, to appear.

Distinguishing Population and Instrument Induced Uncertainties in Flow Cytometry Using a Cell Sorter

*Amudhan Krishnaswamy Usha
Gregory Cooksey (NIST MML)
Paul Patrone*

Flow cytometry and flow cytometry-based cell sorting are valuable tools in biotechnology, biomedical research, and clinical diagnostics. In a typical flow cytometer, a stream of beads or cells is suspended in a fluid medium and tagged with fluorophores, and then sent through a laser interrogation region. A photodetector of some kind then measures the intensity of the fluorescence emitted by the bead/cell. A common application might involve tagging a cell sample with fluorophores that only bind to specific antibodies, and using the measured fluorescence intensities to infer the fraction of cells which possess said antibodies. The measured intensity differs from the fluorescence emitted by the bead due to the presence of noise from various sources, such as laser focusing issues or photon noise in the photodetector. Previous work on uncertainty quantification in a cytometer has therefore largely focused on modeling particular sources of noise. In this project, we investigate a simple model which allows us to estimate the total (instrument and parameter specific) noise present in a flow cytometry measurement.

Note that if one had the ability to take repeated measurements of a single bead with the same laser profile, it would be easy to account for the underlying noise (assuming it is homoscedastic across the bead population). Although this is not currently feasible, it is possible to take repeated aggregate measurements of selected subpopulations by utilizing a cell sorter. A fluorescence-activated cell sorter applies a small electric charge to sort particles based on their measured fluorescence intensities. These particles can be collected and re-measured in the cytometer. Consider a scenario where a set of beads is run through a cytometer, and the beads whose intensities lie below a certain threshold are collected and remeasured. If there was no noise present in the instrument, the second set of measurements would also lie entirely below the threshold. The presence of noise leads to some amount of ‘spillover’ above the threshold (see Figure 54). Assuming that the noise as well as the true population distribution are normally distributed, we derive the probability density function of the post-sort distribution, and show how this allows us to estimate the variance of the underlying noise distribution. We then show how an affine translation model allows us to leverage these estimates to obtain noise estimates for cytometers which are not equipped with a cell sorter. We use these estimates to quantify how instrumental parameters such as the flow rate of the sheath

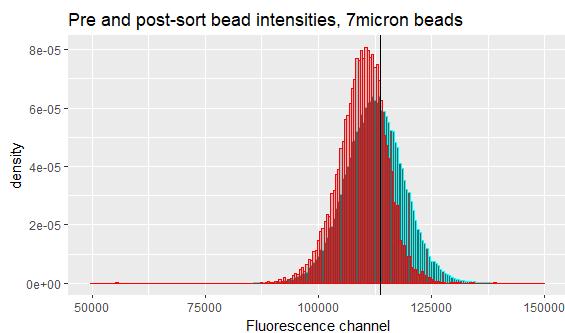


Figure 54. Probability density functions of the pre (in blue) and post (in red) sort fluorescence intensities for a set of 7 micron beads. The black vertical line is the sorting threshold, or “gate.”

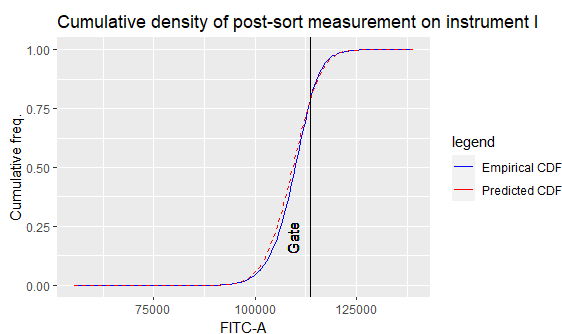


Figure 55. Empirical vs predicted (based on estimated noise) cumulative distribution functions of the post-sort measurement shown above. The predicted curve has a less than 2 % discrepancy with the empirical curve.

fluid affect the noise, as well as to derive various quantities of practical interest, such as the minimal separation required to optimally separate two populations. Future work in this direction includes models to incorporate non-Gaussian signals and noise and the incorporation of uncertainty coming from the sorter. Additionally, our analysis indicates that many of our assumptions hold only locally (i.e., over suitably small intervals, and not over the entire range of intensities). Further work is therefore required to transform such local noise estimates into a global estimate of the instrument noise.

Artificial Intelligence for Low-Field Magnetic Resonance Imaging

Andrew Dienstfrey
 Zydrunas Gimbutas
 Adele Peskin (NIST ITL)
 Joe Chalfoun (NIST ITL)
 Kathryn Keenan (NIST PML)
 Kalina Jordanova (NIST PML)
 Stephen Ogier (NIST PML)

Emerging 64 mT magnetic resonance imaging (MRI) systems offer the promise of low-cost, point-of-care imaging that could be conducted in, for example, developing countries, rural locations, and eventually even in an ambulance. However, present such low-field MRI results in images with low spatial resolution and high noise. These poor qualities complicate quantitative analyses necessary for advanced diagnostics. Recent research suggests that machine learning (ML) methods can potentially restore image quality and furthermore may enable quantitative mapping of tissue parameters [1]. Such claims must be validated via rigorous comparisons to existing measurement standards for high-field (1.5 T or 3.0 T) MRI. For background, scope, and motivations for the NIST Use-Inspired AI Program on Low-Field MRI see previous summaries [2]. In FY 2023 we continued our investigation of ML-based analysis in low-field MRI measurement contexts. Additionally, we made preliminary investigations analyzing geometric distortions induced by the 64 mT scanners most commonly used at this time. Updates for both projects are presented below.

Dual-Field MRI Brain Scan Database. We are continuing toward our goal of developing a machine learning workflow for MRI-based measurement of the apparent diffusion coefficient of water (ADC). ADC is a measure of water mobility generally reported in units of $\mu\text{m}^2/\text{s}$. This mobility is related to structural characteristics of tissue and thereby can serve as a biomarker for several medical conditions including stroke, traumatic brain injury, and Alzheimer’s disease. [3]

Previous work focused attention on MRI measurements of the NIST Diffusion Phantom, a standard reference object developed with consortium partners from the Radiological Society of North America and the National Institutes of Health [4, 5]. This phantom is used to assess the quality of ADC measurements obtained by MRI scanners. The phantom consists of thirteen vials containing one of six polymer solutions (5 duplicates and 1 triplicate). The diffusivities of these solutions range from (128 to 1127) $\mu\text{m}^2/\text{s}$ at 0°C , and their values are determined by precision measurements traceable to the International System of Units (SI) [6].

As a preliminary study, we trained several machine-learning models to infer ADC. The training data for

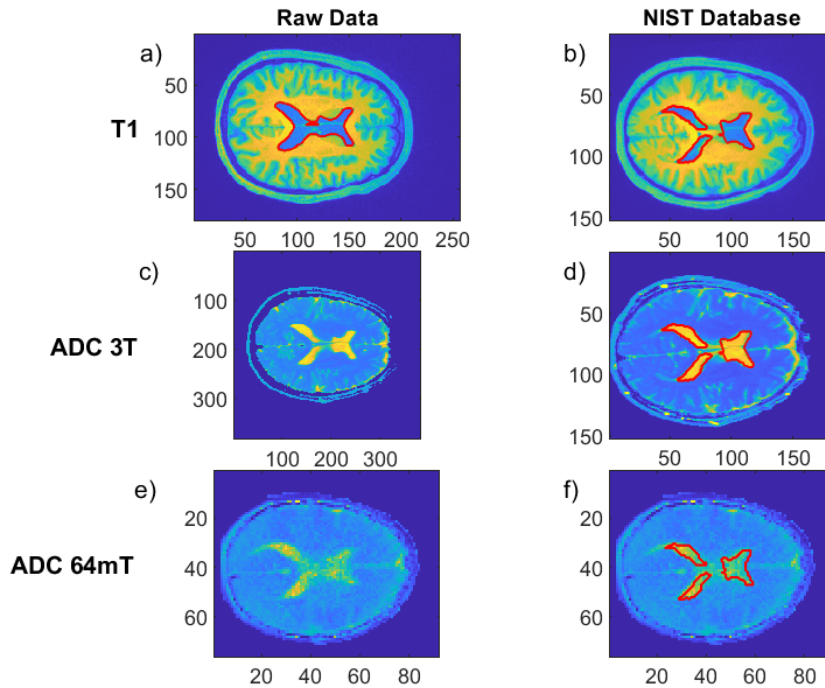


Figure 56. Example data from the new NIST Dual Field Database. Original images from the scanner manufacturers are shown on the left column. The data shown are: T1-weighted image, 3T ADC, and 64mT ADC (a, c, e respectively). The multiple resolutions and orientations are apparent. The same data are shown on the right after registration and interpolation to a shared reference frame (b, d, f respectively). Ventricle boundaries are shown in red. Note that this segmentation is performed originally on the 3 T T1-weighted image. After alignment, all segmentation information can be superimposed on all scans.

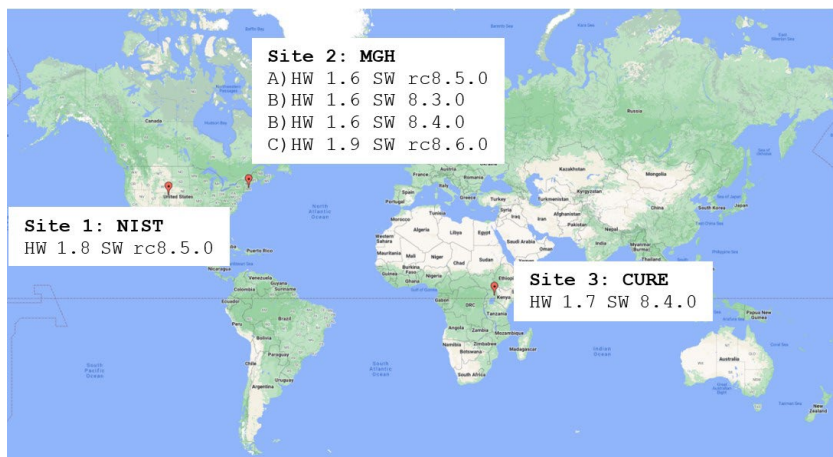


Figure 57. Data acquisition sites for geometric deformation analysis.

these models consisted of hundreds of scans of the Diffusion Phantom. For labels we used either voxel-based estimates of ADC obtained by standard, nonlinear regression analysis, or we restricted quantitative focus to the regions of interest within the image containing the polymer solutions with known, SI-traceable diffusivities. In the latter case, we also experimented with including the rest of the image as unlabeled data using a semi-supervised training protocol. The results of this study are

currently being analyzed for accuracy and generalizability. A paper is being prepared which we plan to submit for publication in FY 2024.

In addition, this past fiscal year we made first steps to extend this ML-based capability to measure ADC in the human brain. By design, the NIST Diffusion Phantom is very structured geometrically; material properties are piecewise homogenous and isotropic; and, to within a relatively high tolerance, the constituent diffusivities consist of six discrete values within the continuous scale of physical diffusivity. While such characteristics are common for calibration structures, it is also clear that human brain tissue is different in every regard. It follows that a very valid concern regarding our existing ML models is that any brain scan shown to these models for inference would effectively be well-outside the training distribution. Thus, a new training database is required.

Ideally this database would consist of paired brain scans conducted on both high- and low-field scanners. Furthermore, diverse scan contrasts, for example T1-weighted and diffusion-weighted, accompanied by tissue segmentation information would add immense value for the MRI research community investigating low-field applications. To the best of our knowledge, no such database currently exists.

In early FY 2023 we recruited 20 healthy participants to undergo volumetric MRI brain scans. Access to a 3 T system (MAGNETOM Prisma, VE11 software, Siemens Healthcare, Germany) was provided under a contract with the Psychology Department, University of Colorado at Boulder. Low-field scans were performed at NIST Boulder using a 64 mT system (Hyperfine Swoop 1.7, Guilford, CT) purchased by our research team with funds from an award under the NIST Use-Inspired AI Program. For all participants, the 3 T data collection consists of a single, high-resolution T1-weighted scan, and four diffusion-

weighted scans acquired with different b-value weightings. The 64 mT data collection consisted of six diffusion-weighted scans in which gradient pulses were applied sequentially along three orthogonal axes with two b-values for each direction. The three-axis scan set will allow for some estimation of diffusion anisotropy which is being investigated elsewhere as an indicator for stroke [3]. The resulting dataset consists of thousands of files occupying over 10 gigabytes of disk space.

While taking such a large collection of scans already requires substantial effort and coordination, this initial data acquisition is only the first step; significant post-processing is required. The data files from the MRI vendors are saved in variations of the DICOM standard. While this format is common in the medical community and readers are available in most programming languages, the DICOM standard is so vast and flexible that proprietary differences between vendor implementations can complicate intercomparison. Therefore, our first post-processing step entailed repackaging all vendor data into consistent data structures and writing these to files using the Hierarchical Data Format version 5 (HDF5). Next, the T1-weighted scans were run through state-of-the-art brain segmentation software to identify 33 tissue types for each participant [7]. The diffusion-weighted images were processed by NIST to estimate the apparent diffusion coefficients [2]. These ADC measurements may be compared to vendor-provided analysis of the same. Finally, intercomparison requires that all data be spatially co-registered. There are two frames of reference corresponding to the two scanners. Additionally, for the 3T data, while patients were stationary between scans, images were nevertheless acquired at different resolutions and orientations within the high-field frame due to the two scan protocols (T1-weighted and diffusion-weighted). Existing registration tools yielded mixed results for our data. Thus, we developed special-purpose interpolation and registration codes to accomplish these tasks.

Sample images from the database are shown in Figure 56. The initial data—T1-weighted and ADC acquired on the 3 T system, and ADC acquire on the 64 mT system—are shown on the left. Several points are notable. Firstly, the original images are not aligned with one another. Furthermore, the higher resolution and lower noise of the 3 T in comparison to the 64 mT system are clearly visible. The low contrast and resolution of the latter complicate registration algorithms; identification of brain tissues (i.e., segmentation) is currently not possible using existing tools for this task. These same scans after registration are shown on the right side of the figure. The 64 mT image is left untouched as interpolation of these images would propagate their noise. The 3 T scans are aligned to the 64 mT reference frame and interpolated to a 2x up sampling of the low-field grid in the scan plane. Finally, segmentation information that was determined from the 3 T T1-weighted scan can now

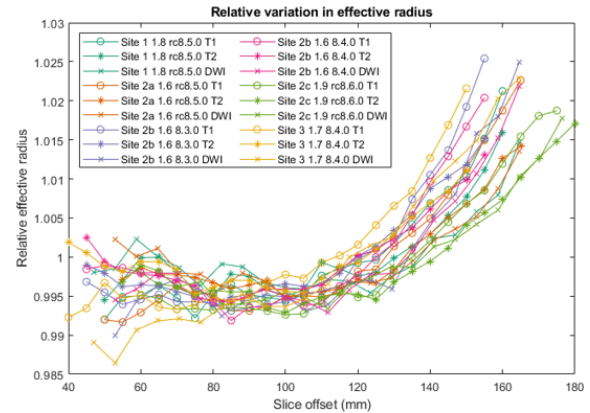


Figure 58. Variation of effective radius as a function of offset of slice from isocenter. This data includes different sites, different hardware versions, different software versions, and different sequences.

be used to demarcate brain tissues in the 64 mT ADC data.

In early FY 2024 we will continue to refine our analysis procedures and validate the database. Once completed, we look forward to publishing our results and making the database available to the MRI research community as a NIST data release. Current attempts to compare low-field MRI with its high-field counterpart use *ad hoc* techniques to generate “synthetic” low-field scans. The NIST Dual-Field MRI Database will provide a rich dataset that can be used to validate these techniques. For our purposes, we intend to develop novel augmentation techniques to extend the database and thereby generate training data to continue our research in ML-based analysis for low-field MRI.

Geometric Distortion and Low-Field MRI. In addition to the creation of the new database described above, in FY 2023 we initiated a new project to characterize geometric distortion induced by the current models of 64 mT scanners.

As mentioned in the introduction, low-field MRI is a radical departure from the current medical MRI paradigm in that it is mobile, and significantly less expensive to acquire and maintain. This technology is very attractive for medically underserved communities, and specifically in developing regions of the world. In the first quarter of FY 2023 we initiated a new collaboration with research teams from Massachusetts General Hospital (MGH), the Yale University School of Medicine, and the Children’s Hospital of Uganda in Mbale, Uganda (CURE). As documented in an article recently appearing in *Nature*, the team in Uganda is investigating the possibility of using low-field MRI to monitor pediatric hydrocephalus [8]. Hydrocephalus is a condition in which cerebrospinal fluid (CSF) accumulates in the brain, causing a build-up of pressure which, if not treated, can lead to mental impairment and sometimes

death. Diagnosis and treatment use brain imaging to determine the volume and location of excess CSF. The treatment plan and, if needed, surgical plan, require accurate volume measurements. For this reason, it is critical to characterize geometric distortions that may be introduced by the scanner. In FY 2023 we made initial steps toward this goal.

Working with collaborators, images of a cylindrical phantom were acquired using 64 mT scanners at three research sites: MGH, CURE, and NIST Boulder. Combined, the dataset consists of images from five different scanners and four software versions as indicated in the map shown in Figure 57. The analysis software was designed by the NIST team. First, pixels demarcating the perimeter of the phantom were determined using edge-detection and thresholding. Next, non-linear regression codes were used to identify the planar ellipse that results in the closest fit to these pixels. The elliptical parameters provide information on the “global” aspects of geometric distortion, for example: the area of the cylindrical cross section; its eccentricity, which provides a measure of elongation of one axis with respect to another; and the rotation of the principal axes. A plot of these parameters as a function of slice number provides a measure of scanner-induced distortion due to non-uniformities of magnetic fields throughout the bore.

One such plot is shown in Figure 58. Here we plot the effective radius defined as $r_{eff} = \sqrt{ab}$ where a and b are the lengths of the semimajor and semiminor axes in mm determined by the elliptical regression. In the plot we normalize by the radius of the phantom as specified by the manufacturer, $r_{cyl} = 55.5$ mm, resulting in a measure of relative error. The plot shows this quantity as a function of distance from the scanner isocenter for all scanners and a variety of scan types—T1, T2, and diffusion weighted. We observe a clear trend showing an increase in the size of the phantom as measured by the MRI as scan plane moves away from the isocenter. The maximum distortion across all the data is $\approx 3\%$, which in turn, would result in an area distortion of approximately 6% . This can be considered relatively stable. From conversations with the manufacturer, we have been told that considerable effort on their side has been made to correct for scanner-dependent distortions using proprietary software tools. Our measurements can be used to provide independent, quantitative assessments of such claims. The results of this work were presented by a NIST team member (SO) at the International Society of Magnetic Resonance Medicine in June 2023 [9].

In FY 2024 we will consider expanding upon this project. The cylindrical phantom used for the present study was provided by the vendor. It does not fill the entire operational field of view, nor does it have regular internal structures. Thus, our analysis to date is restricted to the perimeter of the phantom which results in

“global” information on geometric distortion (and incompletely global due to the phantom’s limited size.) One consideration for the future is to prototype a new reference phantom specially designed to characterize local distortion as a vector field sampled throughout a more complete volume within the scanner’s field of view. We hope to report on this in the future.

- [1] M. Figini, H. Lin, G. Ogbale, *et. al.* Image Quality Transfer Enhances the Contrast and Resolution of Low-Field MRI in African Paediatric Epilepsy Patients. arXiv (2020). URL: <https://arxiv.org/abs/2003.07216>
- [2] A. Dienstfrey, Z. Gimbutas, A. Peskin, *et. al.* Artificial Intelligence for Low-Field Magnetic Resonance Imaging. In *Applied and Computational Mathematics Division: Summary of Activities for Fiscal Year 2022* (ed. R. Boisvert), NIST Internal Report 8466, (2023), 54-57. DOI: [10.6028/NIST.IR.8466](https://doi.org/10.6028/NIST.IR.8466)
- [3] M. D. Budde and N. P. Skinner. Diffusion MRI in Acute Nervous System Injury. *Journal of Magnetic Resonance* **292** (2018), 137-148. DOI: [10.1016/j.jmr.2018.04.016](https://doi.org/10.1016/j.jmr.2018.04.016)
- [4] *Diffusion Standard Model 128 Product Manual*. Caliber MRI, Boulder, CO. URL: <https://qmri.com/>
- [5] S. E. Russek. *NIST/NIBIB Medical Imaging Phantom Lending Library*. NIST Public Data Repository, 2021. DOI: [10.18434/mds2-2366](https://doi.org/10.18434/mds2-2366)
- [6] M. A. Boss, K. E. Keenan, K. F. Stupic, *et. al.* Magnetic Resonance Imaging Biomarker Calibration Service: NMR Measurement of Isotropic Water Diffusion Coefficient. NIST Special Publication 250-100, 2023. DOI: [10.6028/NIST.SP.250-100](https://doi.org/10.6028/NIST.SP.250-100)
- [7] B. Billot, D. N. Greve, O. Puonti, *et. al.* SynthSeg: Segmentation of Brain MRI Scans of any Contrast and Resolution Without Retraining. *Medical Image Analysis* **86** (2023), 102789. DOI: [10.1016/j.media.2023.102789](https://doi.org/10.1016/j.media.2023.102789)
- [8] A. Webb and J. Obungoloch. Five Steps to Make MRI Scanners More Affordable to the World. *Nature* **615** (2023), 391-393. DOI: [10.1038/d41586-023-00759-x](https://doi.org/10.1038/d41586-023-00759-x)
- [9] S. E. Ogier, A. Sorby-Adams, K. V. Jordanova, *et. al.* “Multi-Continent Analysis of Geometric Distortion in Low-Field MRI.” International Society for Magnetic Resonance in Medicine Annual Meeting, London, 2023.

Time-dependent Multiclass Antibody Kinetics

Prajakta Bedekar
Rayanne Luke
Anthony Kearsley

The world’s response to the severe acute respiratory syndrome coronavirus 2 (SARS-CoV-2) pandemic raised questions about antibody kinetics, pushing them to the forefront of scientific research, especially in the context of public health and serosurveillance. Comprehensive study of such questions remains valuable as the

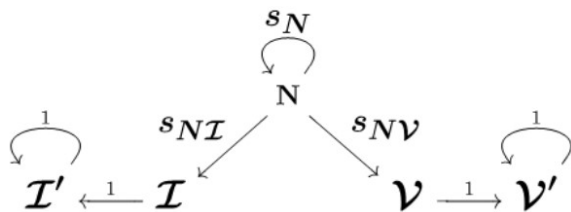


Figure 59. Graph describing the allowable movements between states. Here, N is naive, I is newly infected, I' is previously infected, V is newly vaccinated, and V' is previously vaccinated. Double subscripts on s denote the transition probability from the first state to the second.

lessons learnt from this pandemic can help us tackle future emergent diseases.

In our group's previous work, [1], we developed a new fundamental mathematical framework built on optimal decision theory that leveraged seroprevalence to classify samples into immune-naïve or previously infected. Then we extended this framework to accommodate multiple classes such as immune-naïve, infected, and vaccinated [2]. In parallel, we extended the binary framework to the time-dependent setting [3]. The latter work highlighted the interesting observation that an antibody measurement can be viewed as a convolution of the personal antibody response with the absolute timeline of the pandemic as measured by the incidence rates.

This framework provides valuable insights but can become unwieldy in a multiclass time-dependent setting. Personal immune responses to infection and vaccination may differ from each other, and their incidence rates will also be different in the absolute timeline. Furthermore, as a disease becomes endemic, personal trajectories of immune events for individuals can become longer and more intricate. Considering reinfection, revaccination, and cross effects is crucial. How these effects combine is an area of active theoretical and experimental research, as they can influence policy pertaining to timing of vaccination and booster inoculations.

To generalize the framework to enumerate different personal trajectories, we developed an improved framework using time-inhomogeneous Markov chains. We model the probability of transition from one state to another using incidence rates of infection and vaccination, then use the personal response models and the transition matrix to describe the total probability of obtaining an antibody measurement.

Work is ongoing on a steppingstone to the modeling of a more general real-life scenario. We assume that individuals may become either infected or vaccinated and then remain in that state. This emulates the time frame around January 2021, when very few people were infected or vaccinated more than once. We outline the probabilistic model as an extension of previous work, and then prove that using time-inhomogeneous Markov

chains (Figure 59) provides an equivalent approach. We use synthetic data for SARS-CoV-2 to demonstrate the equivalence numerically.

- [1] P. N. Patrone and A. J. Kearsley. Classification Under Uncertainty: Data Analysis for Diagnostic Antibody Testing. *Mathematical Medicine and Biology: A Journal of the IMA* **38**:3 (2021), 396–416. DOI: [10.1093/imammb/dqab007](https://doi.org/10.1093/imammb/dqab007)
- [2] R. A. Luke, A. J. Kearsley, and P. N. Patrone. Optimal Classification and Generalized Prevalence Estimates for Diagnostic Settings With More Than Two Classes. *Mathematical Biosciences* **358** (2023): 108982. DOI: [10.1016/j.mbs.2023.108982](https://doi.org/10.1016/j.mbs.2023.108982)
- [3] P. Bedekar, A. J. Kearsley, and P. N. Patrone. Prevalence Estimation and Optimal Classification Methods To Account For Time Dependence In Antibody Levels. *Journal of Theoretical Biology* **559** (2023): 111375. DOI: [10.1016/j.jtbi.2022.111375](https://doi.org/10.1016/j.jtbi.2022.111375)

Topological Data Analysis of the NIST Monoclonal Antibody (NISTmAb)

Melinda Kleczynski

Christina Bergonzo (NIST MML)

Anthony Kearsley

Many new medical treatments utilize monoclonal antibodies, a class of artificially produced antibodies. To inform analysis methods for large proteins including monoclonal antibodies, NIST provides the NISTmAb as a reference material [1]. NIST researchers have worked to provide information about this benchmark molecule's structure and composition; see, for example, [2].

Antibodies are dynamic objects, with a range of possible conformations. A single structure is not sufficient to characterize an antibody. Rather, a complete description would quantify the variability in its structure. Potential configurations can be explored using molecular dynamics simulations; see, for example, [3]. These simulations produce different arrangements of atoms in the antibody. Some of these arrangements are visually different. Mathematical analysis allows us to quantify differences in structure rather than relying on qualitative determinations.

We are exploring different organizations of atoms using techniques from topological data analysis (TDA). TDA is a relatively new field which generates features orthogonal to those produced by classical analysis methods. Traditional network analysis represents objects as nodes and connections between pairs of objects as edges. TDA extends this framework by allowing connections between arbitrary numbers of objects in a generalization of a network called a simplicial complex.

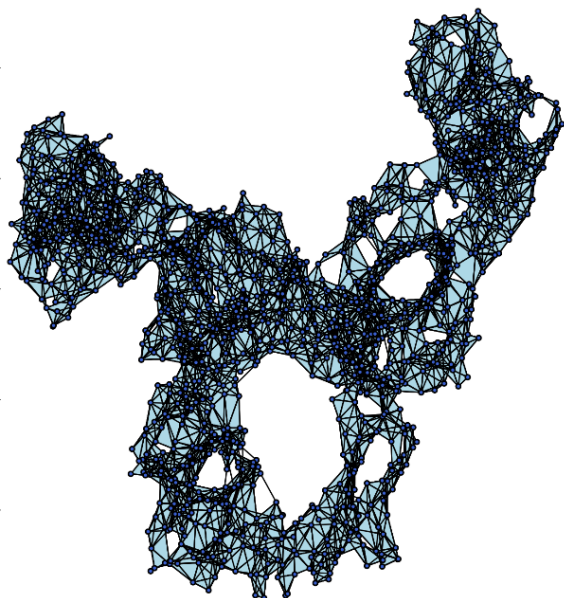


Figure 60. The NISTmAb represented as a simplicial complex.

See Figure 60 for a simplicial complex representation of the NISTmAb.

Criteria for constructing simplicial complexes ensure that their structural features can be detected using tools from linear algebra. Therefore, once the appropriate simplicial complexes are defined, their subsequent quantification is automated and efficient. Additionally, TDA reveals hierarchical structure and requires few parameter choices.

Using these techniques, we can measure a range of features in an antibody. This allows for classification of structures which emerge across different portions of molecular dynamics simulations. It also provides a tool for comparing different types of antibodies. Our preliminary analysis has already shown variability within a single molecule, as well as distinctions between different molecules.

We have documented a consistent topological feature associated with the global structure of the antibody. There are also intermittent features associated with movement of the different sections of the antibody relative to each other. Local topological features provide information about the location of secondary protein structures such as variable loops and β -sheets.

Our next step is to provide more interpretable explanations for topological features in molecular dynamics simulations. We will also work to quantify the variation in topological features associated with flexible components such as variable loops. We expect this work to result in a better understanding of the NISTmAb as well as guidelines for other researchers interested in topological feature extraction from molecular datasets.

[1] National Institute of Standards and Technology (NIST). NIST Monoclonal Antibody Reference Material 8671,

2023. Accessed 10/31/2023. URL: <https://www.nist.gov/programs-projects/nist-monoclonal-antibody-reference-material-8671>

[2] C. Bergonzo and D. T. Gallagher. Atomic Model Structure of the NIST Monoclonal Antibody (NISTmAb) Reference Material, 2021.

Impact of the Exposure Time and Distance Thresholds on the Performance of Automatic Contact Tracing

Brian Cloteaux
Vladimir Marbukh
Kamran Sayrafian

Automatic exposure notification apps operate based on guidelines that specify distance and time thresholds to measure the occurrence of contacts with infected individuals. In the United States 2 m/15 min thresholds are used to determine exposures due to a close contact. In this project, we analyze the performance of automatic exposure notification with Bluetooth-based proximity detection by investigating the impact of different distance and time thresholds as shown in Figure 61.

To the best of our knowledge, there are no comprehensive studies in the literature on the impact of these thresholds. Varying these thresholds effectively changes the size of the exposure zone and that will impact the number of individuals who could be identified as exposed. For example, a larger exposure zone potentially covers more people who could be in the vicinity of an infected person. This leads to a higher number of exposure notifications from the contact tracing app. However, the number of people who are really exposed to the infective dose does not necessarily increase. Assuming that all individuals who receive an exposure notification through the contact tracing app are required to isolate or quarantine for sufficient amount of time, this will then lead to higher number of *unnecessary quarantines*. These quarantines will incur economic costs for the individuals and society. On the other hand, larger exposure zone means smaller safe zone. This automatically reduces the chance of potentially exposed people who were undetected by the app. Since there is a probability that a percentage of these people are indeed exposed and possibly infected, larger exposure zone could help to limit *undetected infections* and avoid further retransmission of the virus throughout the society, especially during a high pandemic period.

Assume that the probability of infection ($P_{infect}(i, t)$) for individual i at time t based on his accumulative exposure by time t can be expressed by the following equation:

$$P_{infect}(i, t) = \text{Min} \left(\frac{1}{1 + \left(\frac{Exp_i(t)}{K - Exp_i(t)} \right)^{-\lambda}}, L \right) \quad (1)$$

where $K > 0$ is the duration of exposure that results in infection with certainty, $Exp_i(t)$ is the total time of exposure experienced by individual i up to time t , $\lambda > 0$ is a parameter that controls sensitivity of the infection probability versus exposure time, and $L < 1$ denotes the maximum probability of infection due to any amount of exposure. Using the above simplifying approximation for the probability of infection, we provide a mathematical framework to investigate the impact of these thresholds on the performance of the contact tracing system.

We consider the number of unnecessary quarantines and the undetected infections as metrics for the system's performance. This study is done through an agent-based simulation platform which emulates automatic exposure notification with Bluetooth-based proximity detection. The platform allows for a comprehensive analysis with several user-controlled parameters that can specify different scenarios. The results presented here consider a population of 135 agents moving within an area of size $162 \text{ m} \times 35 \text{ m}$ for 8 hours (i.e., typical length of a work-day). These numbers are chosen based on a standard laboratory building inside the campus area of the National Institute of Standards & Technology where the authors work. The number of infected individuals at the beginning of the simulation is set at 2% of the population. In addition, the probability of two agents starting a conversation once they are within one meter distance of each other is assumed to be 0.01 with an average conversation length of 3 min [1, 2]. Figure 62 shows an example of the results for various time threshold $T \in \{2, 3, 4, \dots, 23\}$ min while $D=2$. Curve fitting with quadratic function has been used to obtain the solid curves representing the data points obtained through simulations. Also, a confidence interval of one standard deviation has been considered for the results presented in this section.

For a given distance threshold D , the average number of unnecessary quarantines is a decreasing function of T while at the same time, the average number of undetected infections is an increasing function of T . Increasing the time threshold T will decrease the size of the exposure zone. A smaller exposure zone means a tighter constraint on exposure identification which in turn leads to a lower number of exposure detections. However, the percentage of infections among the exposed individuals will be higher due to the higher average exposure time experienced by those individuals. This directly results in a lower number of unnecessary quarantines or isolations. On the other hand, a smaller exposure zone means a larger safe zone which translates to higher average exposure time for the individuals inside this larger zone (equivalent to higher probability of

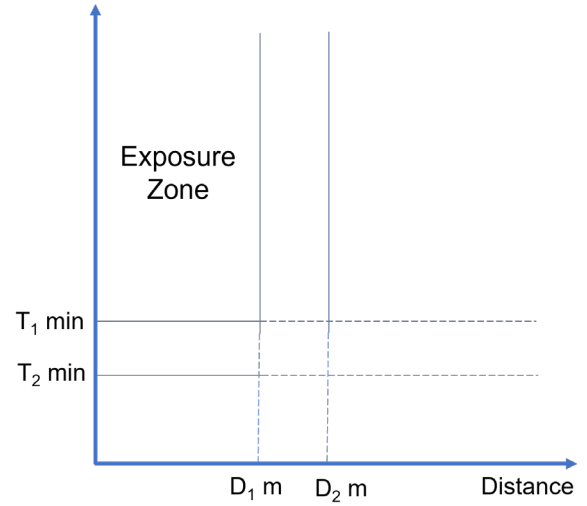


Figure 61. Varying exposure zone by changing exposure time and distance thresholds.

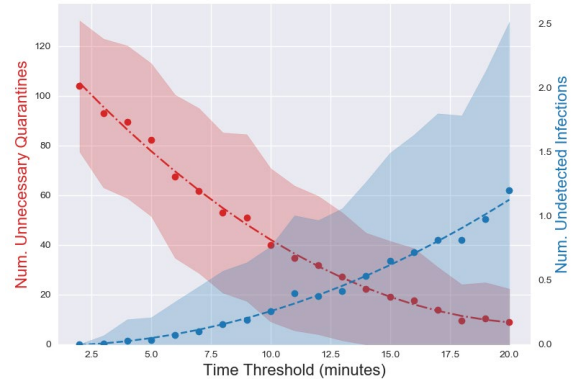


Figure 62. Number of unnecessary quarantines and undetected infections for various time thresholds ($K=5400$ s, $L=0.9$).

infections for those individuals). This results in a higher number of potentially infected people that are unidentified or undetected by the automatic contact tracing app.

The results of this project show an inherent trade-off between the performance metrics of the automatic exposure notification system. Using proper cost models, it would be possible to optimize the exposure notification system based on a variety of parameters such as environment, transmissibility of the virus, status of the pandemic, and general health or immunity level of the individual using the system. The authors plan to continue this research and further investigate this trade-off. Further details and results can be found in [3].

- [1] K. Sayrafian, B. Cloteaux, and V. Marbukh, "On the Performance of Automatic Exposure Determination Using Bluetooth-based Proximity Estimation." IEEE International Conference on Communications (ICC 2022), Seoul, South Korea, May 16-20, 2022.
- [2] K. Sayrafian, B. Cloteaux, and V. Marbukh, "Impact of Using Soft Exposure Thresholds in Automatic Contact Tracing." IEEE International Conference on E-health

Networking, Application & Services (IEEE HEALTHCOM 2022), Genoa, Italy, Oct. 17-19, 2022.

- [3] B. Cloteaux, V. Marbukh, and K. Sayrafian, "Impact of the Exposure Time and Distance Thresholds on the Performance of Automatic Contact Tracing," IoT-Health Workshop, IEEE International Conference on Communication Applications (IEEE ICC 2023), Rome, Italy, June 1, 2023.

Wireless Channel Characterization for UWB Communication in Capsule Endoscopy

Katjana Ladic

Kamran Sayrafian

Dina Šimunić (University of Zagreb, Croatia)

Kamya Y. Yazdandoost (KDDI Research Inc., Japan)

The emergence of high-resolution miniature video cameras along with other microsensor technology have increased the data rate and power consumption requirements for the next generation of capsule endoscopes. These requirements along with other features have made the Ultra-Wideband (UWB) technology an attractive candidate for wireless communication with the capsule endoscope. Our objective in this research is to obtain a statistical pathloss model that effectively captures the impact of transmitter antenna orientation as well as various body tissues as the capsule moves along its natural path inside the small intestine [1].

To obtain this model, we have developed a 3D immersive platform including a detailed computational human body and gastrointestinal tract models that allow for an in-depth study of the wireless propagation channel between a capsule and on-body receivers [2]. See Figure 63. Using the immersive platform, we have also developed an innovative method that enables judicious placement of the capsule along its natural trajectory inside the small intestine. This methodology allows us to obtain sufficient number of sample measurement points with a balanced transmitter-receiver distance distribution while covering the entire small intestine.

Define $PL(\mathbf{d}, \mathbf{f})$ to be the pathloss in dB between the capsule antenna and an on-body receiver at distance $\mathbf{d} \geq \mathbf{d}_0$ and frequency $\mathbf{f} \in [3.1, 4.1]$ GHz. Given the data from the selected measurement scenarios, the following log-distance statistical pathloss model is used to represent the capsule endoscope propagation channel:

$$PL(d, f) = PL(d_0, f) + 10n(f) \log_{10} \left(\frac{d}{d_0} \right) + S(f) \quad d \geq d_0 \quad (1)$$

where d_0 is the reference distance (chosen to be 50 mm), $n(f)$ is the pathloss exponent at frequency f and $S(f)$ is the fading component at frequency f , modeling the deviation from the mean value due to different body

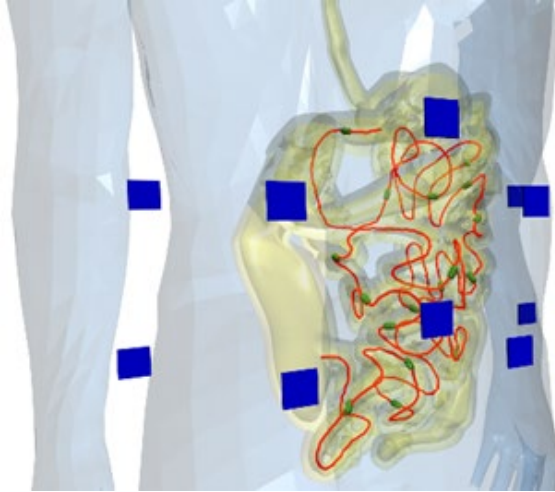


Figure 63. Locations of the on-body receivers (blue squares) and the centerline passing through the small intestine (red line).

tissues in the propagation path of the transmitted signal (e.g., bone, muscle, fat, etc.), receiver and transmitter positions and orientations and their antenna gains in different directions. We have shown that a normal distribution with zero mean and standard deviation $\sigma_s(f)$ (i.e., $N(0, \sigma_s(f))$) can be used to model the $S(f)$ component in the pathloss model (1). The pathloss exponent $n(f)$ heavily depends on the environment through which the RF signal is propagating. In free space, this exponent is two regardless of the frequency. However, since the human body is an extremely lossy environment, a higher value for this exponent is normally expected for propagation from wireless implants and ingestible electronics.

Figure 64 shows the scatter plot of the pathloss for the measurement scenarios (i.e., 200 propagation channels resulting from 20 selected capsule positions and 10 on-body receivers) as a function of transmitter-receiver distance at 3.6 GHz frequency. The candidate capsule locations inside the small intestine covers a range of 5 cm to 25 cm distances from the on-body receivers. The solid line in red is obtained by using the least squares linear regression and minimizing the root mean square deviation of sample pathloss data points. It represents the mean value of the pathloss samples in the scatter plot.

Table 4. Mean values of the parameters of the capsule pathloss model over 3.1 GHz to 4.1 GHz.

$\overline{PL}(d_0)$ (dB)	\bar{n}	$\bar{\sigma}_s$ (dB)
51.9	8.14	18.19

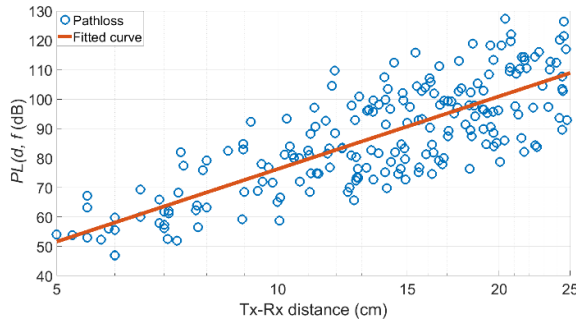


Figure 64. Scatter plot of the pathloss for the measured scenarios and the regression line at 3.6 GHz.

Parameters of the pathloss model in (1) can be obtained through numerical analysis at any frequency $f \in [3.1 \text{ } 4.1]$ GHz. The mean value of these parameters ($\overline{PL}(d_0)$, \bar{n} , $\bar{\sigma}_s$) over the frequency range 3.1 GHz to 4.1 GHz are provided in Table 4.

To the best of our knowledge, this is the first study that comprehensively captures the entire length of the small intestine while considering realistic positions for a capsule along its natural trajectory to conduct virtual measurements. The pathloss information obtained in this study can provide a more accurate link budget and better understanding of the feasible communication range as the capsule traverses the small intestine. This knowledge can also assist in identifying the minimum number and optimal placements of on-body receivers to ensure reliable signal reception from the capsule regardless of its position inside the GI tract. The statistical pathloss model obtained in this research has been contributed to the IEEE 802.15 Task Group 6ma as part of the standard channel model for the capsule endoscopy use-case. This task group is currently working on the revision of the IEEE 802.15.6-2012 standard for wireless body area networks. Further details and results can be found in [3].

- [1] K. Sayrafian, W. B. Yang, J. Hagedorn, J. Terrill, and K. Y. Yazdandoost. A Statistical Path Loss Model for Medical Implant Communication Channels. In *IEEE 20th International Symposium on Personal, Indoor and Mobile Radio Communications*, Tokyo, Japan, 2009, 2995-2999
- [2] K. Sayrafian, J. Hagedorn, W. -B. Yang, and J. Terrill. A Virtual Reality Platform to Study RF Propagation in Body Area Networks. In *IEEE 3rd International Conference on Cognitive Infocommunications (CogInfoCom)*, Kosice, Slovakia, 2012, 709-713.
- [3] K. Ladic, K. Sayrafian, D. Šimunić, and K. Y. Yazdandoost. Wireless Channel Characterization for UWB Communication in Capsule Endoscopy. *IEEE Access* **11** (2023), 95858-95873.

A Preliminary Study on Propagation Channels for Brain Telemetry Using a Flexible Wearable Antenna

Kamran Sayrafian

Mariella Särestöniemi (University of Oulu, Finland)

Marko Sonkki (Ericsson, Germany)

Jari Iinatti (University of Oulu, Finland)

Flexible electronics are envisioned to play a major role in future wearable medical devices. An important component of this technology is flexible antennas. In this project, a preliminary study of on-body and off-body propagation channels in Body Area Networks (BAN) using a small Ultra-Wide Band (UWB) flexible wearable antenna has been done. The on-body measurements include propagation channels between two wearable devices placed on the head and various locations on the arm (i.e., shoulder to wrist). The off-body measurements cover propagation channels between a head-mounted device and an external device placed at various distances from the body. The wearable devices in these measurements use a small flexible antenna that can easily conform to the surface of the body [1]. The measurements are conducted to better understand and characterize the wireless communication channels in applications such as brain monitoring or brain computer interface (BCI) [2].

The measurements were carried out in an anechoic chamber as well as a small laboratory room. A volunteer¹⁵ with the height of 160 cm participated in the experiments. The measurements were conducted using a Vector Network Analyzer (VNA) with IF (Intermediate Frequency) bandwidth of 100 kHz and a sweeping time of 200 ms. The VNA is calibrated to eliminate the cable loss. For off-body channel measurements, the flexible on-body antenna is placed on the side of the volunteer's head (just above the left ear) and secured using a flexible band. At this position, the on-body antenna is about 155 cm from the ground. The external antenna is mounted on a pole at the height of 160 cm from the ground and distance d ($10 \text{ cm} < d < 130 \text{ cm}$) from the volunteer's head. An example of the forward transmission coefficient (S_{21}) and Channel Impulse Response (CIR) at distances of 0.5 m and 1 m are shown in Figure 66. These measurements were conducted in a small laboratory environment.

Preliminary on-body measurements show promising results with the flexible antenna, even for the channel with the longest distance between the two antennas (i.e., the head-wrist channel). However, more in-depth evaluations with a larger number of volunteers with different body shapes and sizes will be necessary.

¹⁵ The experiments were conducted at the University of Oulu with University of Oulu Ethics Committee approval 10/2022 and ITL-2022-0350 at NIST.

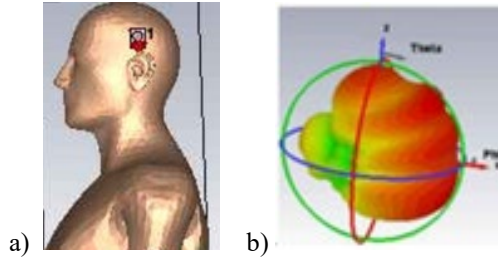


Figure 65. a) flexible antenna with the body model. b) 3D radiation patterns of the flexible antenna at: 2.45 GHz.

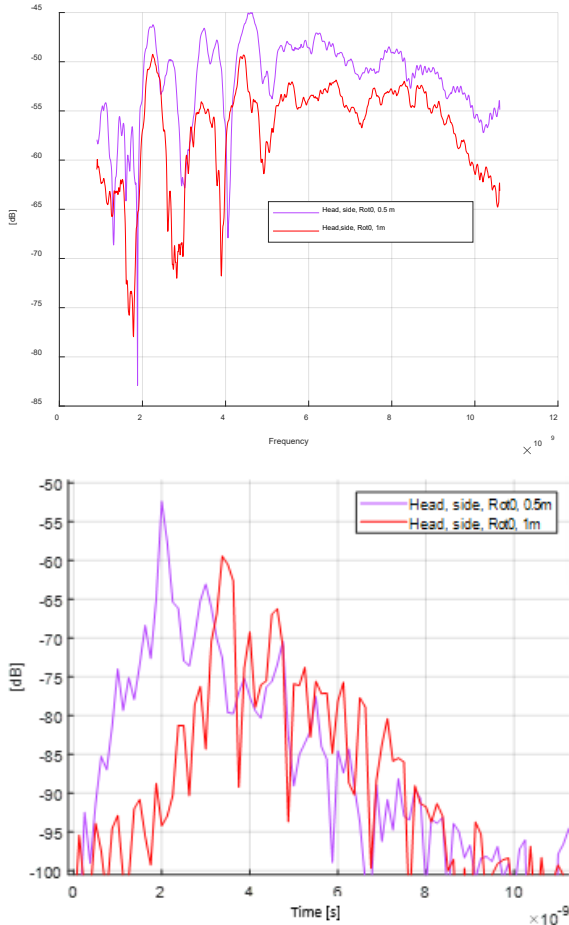


Figure 66. Off-body channel measurements with the flexible antenna. Top: Forward transmission coefficient (S_{21}). Bottom: Channel impulse response.

In addition, since the flexible antenna used in this study is linearly polarized, the impact of hand movements and rotations should also be studied. These evaluations will be part of our future research in this area.

More detailed comparisons between channel measurements conducted in an anechoic chamber and small laboratory are also needed to better identify the impact of the environment on the channel response. This is especially important for the off-body channel where other objects in the environment cause reflections and scattering of the transmitted signal. We also plan to conduct

more extensive measurements in different environments and antenna types and body locations. Those measurements will provide the necessary information to obtain a statistical channel model for a wireless BCI use case. Further details and results can be found in [3].

- [1] M. Särestöniemi M, Sonkki M, Myllymäki S, and Pomalaza-Raez. Wearable Flexible Antenna for UWB On-Body and Implant Communications. *Telecom 2:3* (2021), 285-301.
- [2] M. Särestöniemi, C. Pomalaza-Raez C., K. Sayrafian, T. Myllylä, and J. Iinatti. A Preliminary Study of RF Propagation for High Data Rate Brain Telemetry. In *Smart IoT and Big Data for Intelligent Health Management*, Lecture Notes of the Institute for Computer Sciences, Social Informatics and Telecommunications Engineering **420** (2021).
- [3] M. Särestöniemi, K. Sayrafian, M. Sonkki, and J. Iinatti. A Preliminary Study of On/Off-Body Propagation Channels for Brain Telemetry Using a Flexible Wearable Antenna. In *17th IEEE International Symposium on Medical Information and Communication Technology*, (IEEE ISMICT 2023), Lincoln, NE, May 10-12, 2023.

Adaptive Maximization of the Harvested Power for Wearable or Implantable Sensors

Kamran Sayrafian

Masoud Roudneshin (Concordia University, Canada)

Amir Aghdam (Concordia University, Canada)

Miniaturized wearable or implantable medical sensors (or actuators) are important components of the Internet of Things (IoT) in healthcare applications. However, their limited source of power is becoming a bottleneck for pervasive use of these devices, especially as their functionality increases. Kinetic-based micro-energy harvesters can generate power through natural human body motion. Therefore, they can be an attractive solution to supplement the source of power in medical wearables or implants.

The architecture based on the Coulomb Force Parametric Generator (CFPG) is the most viable micro-harvester solution for generating power from human motion. It has been shown that adaptive optimization of the electrostatic force in the CFPG architecture can lead to maximization of the harvested power [1, 2, 3]. In this project, we propose three methods to adaptively estimate the desirable electrostatic force in a CFPG using the input acceleration waveform, namely, linear estimation, multi-armed bandit, and a min-max-based approach (see Figure 67).

We evaluate the performance of the proposed adaptive approaches for a combination of different human activities over a long period of time. An acceleration

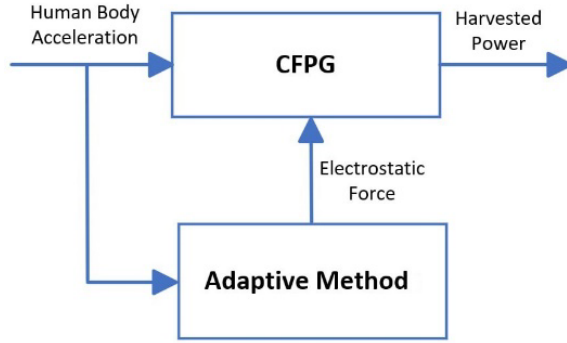


Figure 67. Schematic diagram of a CFPG using adaptive electrostatic force.

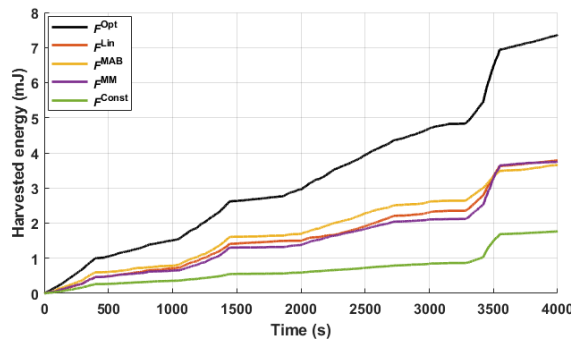


Figure 68. Comparison of the harvested energy using the proposed adaptive methodologies for a 4000 s acceleration waveform.

waveform with a duration of 4000 s is produced by concatenating acceleration data from various individual activities such as walking, jogging, sit-ups, roping, weight exercises and general random movements of the hand and shoulder¹⁶. Figure 68 displays the harvested energy as a result of using adaptive electrostatic force based on linear estimation (F^{Lin}), multi-armed bandit (F^{MAB}), and a min-max-based (F^{MM}) methodologies on the collected acceleration waveform. For comparison, the average harvested energy using three different constant holding forces (F^{Const}) is also shown in Figure 68. Considering the CFPG parameter values as well as the discrete decision set and adaptation interval constraints, the upper bound on the extracted energy (achievable through offline optimization, (F^{Opt})) is also plotted.

As observed, among the adaptive approaches, the min-max algorithm performs best, with over 10 % more extracted energy compared to the linear estimator. The improvement is due to the fact that this algorithm considers the asymmetry of the acceleration waveform for selecting the proper electrostatic holding force. The min-max adaptive methodology on average generates more than 100 % more energy compared to the case when a constant holding force is used. This is a promising gain,

especially for low-power wearable (or implantable) medical sensors or actuators.

The exact performance of the proposed methodologies depends on the nature of the acceleration waveform. However, in almost all practical scenarios and on average, there is a noticeable improvement in the harvested kinetic power from the human body motion compared to the case when a constant electrostatic force is used. The additional harvested power could supply the required resource to run a low-complexity adaptive algorithm as part of the CFPG architecture. Considering its computational complexity and performance with our acceleration dataset, the linear estimator is the best candidate among the studied methodologies. Knowledge of the exact location of the medical sensor on or inside the body could provide more specific information about the characteristics of the acceleration waveform that an embedded micro-harvester would experience. This information can help to further optimize the adaptive approach with the proper choice of its parameters. Further details can be found in [4].

- [1] M. Roudneshin, K. Sayrafian, and A. G. Aghdam. A Machine Learning Approach to the Estimation of Near-Optimal Electrostatic Force in Micro Energy-Harvesters. In *Proceedings of the IEEE International Conference on Wireless for Space and Extreme Environments (WiSEE)*, 2019.
- [2] M. Roudneshin, K. Sayrafian, and A. G. Aghdam. Adaptive Estimation of Near-Optimal Electrostatic Force in Micro Energy-Harvesters. In *Proceedings of the IEEE International Conference on Control Technology and Applications (CCTA)*, 2020.
- [3] M. Roudneshin, K. Sayrafian, and A. G. Aghdam. Maximizing Harvested Energy in Coulomb Force Parametric Generators. In *Proceedings of the American Control Conference (ACC)*, June 2022.
- [4] M. Roudneshin, K. Sayrafian, and A. Aghdam. Adaptive Maximization of the Harvested Power for Wearable or Implantable Sensors with Coulomb Force Parametric Generators. *IEEE Internet of Things* **10**:19 (2023), 16793-16803.

¹⁶ The experiments were conducted at Concordia University with research ethics approval numbers 30013664 at Concordia University and ITL-2021-0273 at NIST.

A Low Complexity Power Maximization Strategy for Coulomb Force Parametric Generators

Kamran Sayrafian

Hamid Mahboubi (Concordia University, Canada)

Amir Aghdam (Concordia University, Canada)

Limited source of power is one of the major challenges in developing miniaturized medical wearable or implantable sensors with more functionality. One possible solution is energy harvesting, the process of capturing and storing energy from external sources or the ambient environment. Kinetic-based micro energy-harvesting is a promising technology that could prolong the lifetime of batteries in small wearable or implantable devices [1, 2]. In this project, we analyze the dependency of the output power on the electrostatic force in such a micro-harvester architecture using a mathematical model of a Coulomb-force parametric generator. Then, we propose a low complexity strategy to adaptively change the electrostatic force in order to maximize the harvested power.

Aside from an exhaustive search, identifying a methodology that can determine the optimal value of this force is quite challenging. However, using observations with simple acceleration waveforms, such as step function and square wave, we can propose a very low-complexity methodology that can provide an approximate value for the electrostatic force. Figure 69 demonstrates a sample acceleration waveform and its approximation with a sequence of weighted step functions. Knowing the optimal solution for a step function acceleration, the optimal value for the electrostatic force for a general acceleration waveform can also be estimated.

Figure 70 displays the harvested energy using our proposed adaptive electrostatic force strategy, along with the optimal constant force (F_{opt}^c) and constant forces $F^c=0.5$ mN, $F^c=1.5$ mN. As observed, the harvested energy with the acceleration data from the chest after 100 s is 652.0 μ J, 263.7 μ J, 211.8 μ J and 141.2 μ J under the adaptive strategy, optimal constant electrostatic force, and constant forces $F^c=0.5$ mN and 1.5 mN, respectively. This indicates 147 %, 207 %, and 362 % increases in the harvested energy using our proposed adaptive strategy compared to the harvested energy using an optimal constant force, constant forces $F^c=0.5$ mN and 1.5 mN, respectively. These results indicate a noticeable gain in the harvested energy from the kinetic motion of the human body using our proposed low complexity adaptive strategy.

Simulation results for different human activities or sensor placement also confirm the noticeable increase in the harvested power that can be achieved using this strategy. Other sophisticated adaptive schemes that may lead to higher output power have also been proposed for

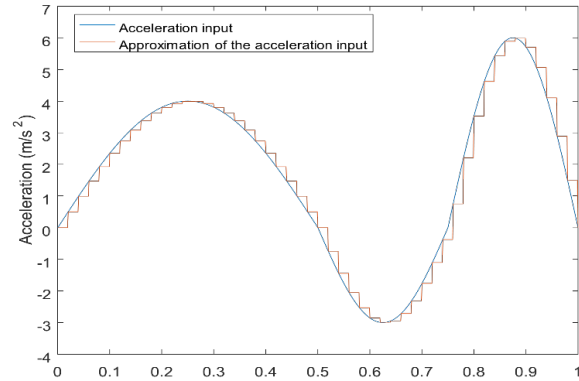


Figure 69. Sample acceleration waveform and its approximation.

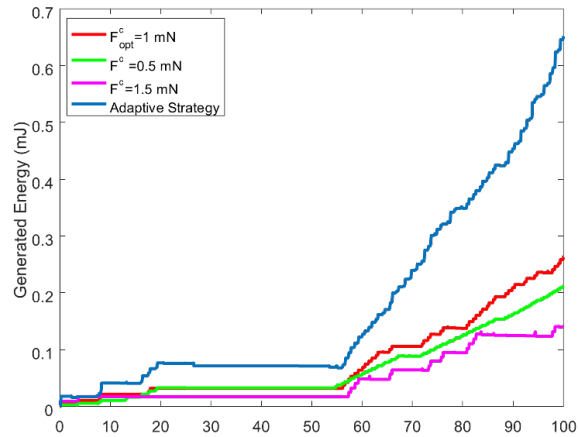


Figure 70. Harvested energy under the adaptive holding force strategy, optimal constant electrostatic force, $F^c = 0.5$ mN and $F^c = 1.5$ mN with the acceleration data from the chest.

this purpose [3]. However, the complexity of those schemes is extremely important as this additional adaptive module in the CFPG architecture would itself require power to operate. This required power reduces the overall achievable gain in the harvested power compared to the case with a constant electrostatic force. Although the computational complexity of the adaptive electrostatic force strategy proposed here is relatively low, further research to estimate its required power for a given adaptation interval is needed. In this project, a fixed adaptation interval has been assumed to simplify the general optimization problem. It is conceivable that joint electrostatic force and adaptation interval optimization could result in higher gains. Further details and results of this project can be found in [4].

- [1] D. Budic, D. Šimunic, and K. Sayrafian. Kinetic-based Micro Energy Harvesting for Wearable Sensors. In *Proceedings of the 6th IEEE International Conference on Cognitive Infocommunications (CogInfoCom)*, 2015, 505–509.
- [2] M. Dadfarnia, K. Sayrafian, P. Mitcheson, and J. S. Baras. Maximizing Output Power of a CFPG Micro Energy-Harvester for Wearable Medical Sensors. In *Proceedings of the 4th International Conference on*

Wireless Mobile Communication and Healthcare (MOBIHEALTH), 2014, 218–221.

- [3] M. Roudneshin, K. Sayrafian, and A. Aghdam. Adaptive Maximization of the Harvested Power for Wearable or Implantable Sensors with Coulomb Force Parametric Generators. *IEEE Internet of Things* **10**:19 (2023), 16793-16803.
- [4] H. Mahboubi, K. Sayrafian, and A. Aghdam. A Low Complexity Power Maximization Strategy for Coulomb Force Parametric Generators. *IEEE Access* **11** (2023), 42881-42884.

Modeling for Biological Field Effect Transistor Experiments

Ryan M. Evans

Seulki Cho (NIST PML)

Arvind Balijepalli (NIST PML)

Anthony Kearsley

Biological field effect transistors (Bio-FETs) are modern bioelectronics instruments offering novel biomarker measurements. In contrast with traditional measurement techniques that require specialized facilities and expensive equipment, Bio-FETs offer rapid, accurate and low-cost measurements. Since these instruments are hand-

$$C(x, 0, t) = C_i(x, 0, t) - \frac{Da\sqrt{D}l_s}{\sqrt{\pi}} \left\{ \int_{-1/2}^{1/2} \int_0^t \frac{1}{\sqrt{\tau}} \theta_3 \left(0, e^{-\epsilon^2/l_s^2 D \tau} \right) \frac{\partial B}{\partial \tau} (v, t - \tau) d\tau dv + 2 \sum_{n=1}^{\infty} \int_{-1/2}^{1/2} \int_0^t \frac{e^{-\lambda_n D \tau}}{\sqrt{\tau}} \theta_3 \left(0, e^{-\epsilon^2/l_s^2 D \tau} \right) \frac{\partial B}{\partial \tau} (v, t - \tau) d\tau \cos \left(\sqrt{\lambda_n} (v + 1/2l_s) \right) dv \cdot \cos \left(\sqrt{\lambda_n} (x + 1/2l_s) \right) \right\},$$

held and portable, they promise to yield wider accessibility to critical medical diagnostic tests. During a typical experiment, a chemical reactant bath is injected into a solution-well that contains a buffer fluid. These chemical reactants diffuse through the solution-well and bind with chemical reactants confined to a thin layer known as the biochemical gate on the sensor surface. This produces a time-series signal that can be used to analyze the chemical reaction of interest. See Figure 71 for an experimental Bio-FET signal.

Since estimating parameters associated with these experiments like kinetic coefficients can help us identify biomarkers, accurate mathematical models for these experiments are desired. Previous mathematical models have either not accounted for the time dependent nature of Bio-FET experiments [1–3] or have not included physically relevant transport processes [4–5]. A model recently published by Evans, Kearsley, and Balijepalli is the first dynamic model for Bio-FET experiments that

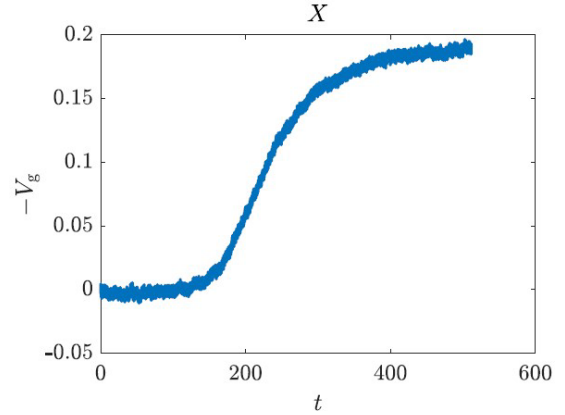


Figure 71. Experimental Bio-FET signal. The horizontal axis represents time in seconds, and the vertical axis represents voltage that is measured as a result of surface binding.

accounts for physically relevant transport effects, and it has been shown that this model compares favorably with experimental data [6].

The nonlinear integrodifferential equation (IDE) presented in [6] takes the form:

$$\frac{\partial B}{\partial t} = (1 - B)C(x, 0, t) - KB,$$

where

$\theta_3(\cdot, \cdot)$ is a third-order theta function [7, Eq. 20.2.3], $C_i(x, 0, t)$ satisfies the Neumann Problem on a rectangle with homogeneous boundary conditions and is a compactly supported Gaussian $f(x, y)$ at the initial time $t = 0$, and $B(x, t) = 0$. In [6] Evans and coworkers developed a method of lines (MOL) approximation to this equation that achieves an order of three-halves in time and second in space, the former of which comes from the singularity. After regularizing the singularity by using the definition of $\theta_3(\cdot, \cdot)$ and adding and subtracting

$$\frac{\partial B}{\partial \tau} (v, t)$$

from the first integrand, an expansion of the form

$$B(x, t) \approx \sum_{i=1}^N \phi_i(x) h_i(t)$$

was developed and substituted into the equation. In the above expansion the $\phi_i(x)$ are locally defined quadratics and the $h_i(t)$ are time-dependent functions that are determined by evaluating each side of the resulting equation at the center of each of the N hat functions, yielding a set of N ordinary differential equations. These equations are solved by with a semi-implicit discretization and the approximation

$$h_i'(t_m) \approx \frac{\Delta h_i^{(m)}}{\Delta t},$$

which yields a linear system that we can use to solve for $\Delta h_i^{(m)}$ and used to update h_i via the formula

$$h_i^{(m+1)} = h_i^{(m)} + \Delta h_i^{(m)}$$

for each i . We are currently developing a new numerical approximation to this system based on radial basis functions (RBF), which are known to have excellent interpolation properties. In particular, our RBF approximation centers around the expansion:

$$B(x, t) \approx \sum_{j=1}^M \sum_{i=1}^N w_{ij} \Phi_{ij}(x, t; z).$$

The weights w_{ij} are constant; there are many choices for the RBFs $\Phi_{ij}(x, t)$, we chose Gaussians

$$\Phi_{ij} = e^{-z[(x-x_i)^2+(t-t_j)^2]}.$$

The parameter z controls the Gaussians width. Substituting this RBF expansion into our IDE and evaluating at each of the nodes (x_i, t_j) gives a nonlinear system for the weights w_{ij} . A key advantage of this method is that, since the Gaussian is a known separable function of x and t , the singularity can be regularized with a substitution. It is expected that a numerical solution of the nonlinear algebraic can be rapidly achieved with Anderson acceleration [8]. It is expected that our RBF approximation will be even faster and more accurate

than the MOL approximation, giving even more rapid and precise simulations of Bio-FETs.

- [1] S. Baumgartner, M. Vasicek, A. Bulyha, N. Tassotti, and C. Heitzinger. Analysis of Field-Effect Biosensors Using Self-Consistent 3D Drift-Diffusion and Monte-Carlo Simulations. *Procedia Engineering* **25** (2011), 407-410.
- [2] C. Heitzinger, N. J. Mauser, and C. Ringhofer. Multiscale Modeling of Planar and Nanowire Field-Effect Biosensors. *SIAM Journal on Applied Mathematics* **70:5** (2010), 1634-1654.
- [3] D. Landheer, G. Aers, W. R. McKinnon, M. J. Deen, and J. C. Ranuarez. Model for the Field Effect from Layers of Biological Macromolecules on the Gates of Metal-Oxide-Semiconductor Transistors. *Journal of Applied Physics* **98:4** (2005), 044701.
- [4] X. Duan, Y. Li, N. K. Rajan, D. A. Routenberg, Y. Modis, and M. A. Reed. Quantification of The Affinities and Kinetics of Protein Interactions Using Silicon Nanowire Biosensors. *Nature Nanotechnology* **7:6** (2012), 401-407.
- [5] G. Tulzer, S. Baumgartner, E. Brunet, G. C. Mutinati, S. Steinhauer, A. Kck, P. E. Barbano, and C. Heitzinger. Kinetic Parameter Estimation and Fluctuation Analysis of CO at SNO₂ Single Nanowires. *Nanotechnology* **24:31** (2013), 315501.
- [6] R. M. Evans, A. Balijepalli, and A. J. Kearsley. Transport Phenomena in Biological Field Effect Transistors. *SIAM Journal on Applied Mathematics* **80:6** (2020), 2586-2607.
- [7] F. W. J. Olver, A. B. Olde Daalhuis, D. W. Lozier, B. I. Schneider, R. F. Boisvert, C. W. Clark, B. R. Miller, B. V. Saunders, H. S. Cohl, and M. A. McClain, eds. *NIST Digital Library of Mathematical Functions*. <http://dlmf.nist.gov/>, Release 1.1.8 of 2022-12-15.
- [8] Alex Toth and C. T. Kelley. Convergence Analysis for Anderson Acceleration. *SIAM Journal on Numerical Analysis* **53:2** (2015), 805-819.
- [9] R. M. Evans and A. J. Kearsley. Theta Functions and Mellin Asymptotics in Modeling Biological Field Effect Transistor Experiments. In review.
- [10] L. A. Melara, R. M. Evans, S. Cho, A. Balijepalli, and A. J. Kearsley. Optimal Bandwidth Selection in Stochastic Regression of Bio-FET Measurements. In review.

Materials Modeling

Mathematical modeling, computational simulation, and data analytics are key enablers of emerging manufacturing technologies. The Materials Genome Initiative (MGI), an interagency program with the goal of significantly reducing the time from discovery to commercial deployment of new materials using modeling, simulation, and informatics, is a case in point. To support the NIST role in the MGI, we develop and assess modeling and simulation techniques and tools, with emphasis on uncertainty quantification, and collaborate with other NIST Laboratories in their efforts to develop the measurement science infrastructure needed by the materials science and engineering community.

OOF: Finite Element Analysis of Material Microstructures

Stephen A. Langer

Günay Doğan

Andrew C.E. Reid (NIST MML)

Shahriyar Keshavarz (NIST MML)

<http://www.ctcms.nist.gov/oof/>

The OOF Project, a collaboration between ACMD and MML, is developing software tools for analyzing real material microstructure. The microstructure of a material is the (usually) complex ensemble of polycrystalline grains, second phases, cracks, pores, and other features occurring on length scales large compared to atomic sizes. The goal of OOF is to use data from a micrograph of a real or simulated material to compute its macroscopic behavior via finite element analysis.

The OOF user loads images into the program, assigns material properties to the features of the image, generates a finite element mesh that matches the geometry of the features, chooses which physical properties to solve for, and performs virtual experiments to determine the effect of the microstructural geometry on the material. OOF is intended to be a general tool, applicable to a wide variety of microstructures in a wide variety of physical situations. OOF2 and OOF3D are used by educators and researchers in industry, academia, and government labs worldwide.

There are two versions of OOF, OOF2 and OOF3D, each freely available on the OOF website. OOF2 starts with two dimensional images of microstructures and solves associated two-dimensional differential equations, assuming that the material being simulated is either a thin freely suspended film or a slice from a larger volume that is unvarying in the third dimension (generalizations of plane stress and plane strain, respectively). OOF3D starts with three dimensional images and solves equations in three dimensions. Development this year continued on multiple fronts.

In FY 2023 A. Reid and S. Keshavarz advanced the crystal-plasticity effort significantly, through the introduction of a new version of the test code which was better-aligned with the OOF architecture, but small and

simple enough for more robust experimentation. A version of this code is now able to run the power-law crystal plastic constitutive rule on a test mesh for as high a load and as many iterations as we have tried, including beyond the domain of validity of the model itself. The final task is to integrate this functionality back in to the actual OOF code base.

Image processing and image segmentation are the crucial first steps to an OOF analysis. In order to generate a mesh that conforms to the geometry of the microstructure, the user first needs to segment the image, namely identify, and mark the regions corresponding to the different phases or materials in the image. For better segmentation, the user usually needs to transform the image or enhance it with various image processing algorithms, e.g., image denoising, contrast enhancement. To provide this functionality, OOF has been relying on ImageMagick, a widely used image processing package, along with custom functions implemented by the OOF team.

In recent years, versatile image processing packages have emerged in the Python data analysis ecosystem. These provide diverse functionality to help process images and to analyze their contents. One of these packages is scikit-image, built by a community of researchers. It is open source and freely available. It is a good fit for OOF as it is written purely in Python (also used by OOF), and it is easy to download and install. G. Doğan and S. Langer began work to replace ImageMagick with scikit-image in OOF2 this year. This will make installation and maintenance easier and will provide better functionality and performance in practice. In FY 2024, we will focus on incorporating image segmentation functions from scikit-image, along with the functionality developed by G. Dogan and collaborators (described in the section *Computational Tools for Image and Shape Analysis* on page 17). We also expect that moving to a more Pythonic image processing infrastructure for OOF will make it easier to incorporate machine learning based image analysis functionality in the near future.

S. Langer completed upgrading OOF2 to use modern versions of the major external code libraries that it relies upon. OOF2 version 2.3, which was released in September, uses Python 3 (3.8 through 3.12) instead of

the obsolete and deprecated Python 2.7 required by previous versions. He is currently updating the OOF2 manual. In the process of updating and documenting the code, many bugs and other deficiencies were discovered and fixed.

The new versions of OOF2 and OOFCanvas, the library it uses for graphical displays, are available as source code from the OOF2 website. They can also be used downloaded and installed on Macintosh computers via MacPorts¹⁷ or run directly on the NSF nanoHUB facility¹⁸. At nanoHUB, OOF2 was used 4 300 times in FY23, and has been run 69 000 times since the first version was installed there in December 2007.

Mathematics of Uncertainty in Engineering Reliability

Jeffrey T. Fong

Pedro V. Marcal (MPACT Corp.)

Marvin Cohn (Intertek)

N. Alan Heckert (NIST ITL)

To ensure the safe operation of an engineering structure or system, be it a chemical processing plant, a nuclear power plant, a jet airliner, or a steel bridge, engineers need to first design, manufacture, assemble and install, test in laboratories and in the field, and operate with continuous monitoring and scheduled maintenance for all necessary components and connections that are required to make a system work as a whole without failure. Engineers need to estimate the reliability of all such components and connections and construct a fault tree to evaluate the system reliability of the whole structure or system.

Two basic categories of problems of uncertainty come up that require independent modeling approach, namely, (I) Uncertainty in loads, and (II) Uncertainty in material properties. In this project, we first address Category (I) by decomposing complex history of loads into a series of elemental fatigue (cyclic load at a fixed amplitude and frequency) and creep (constant load for a fixed time). We then address Category (II) by conducting fatigue life cycle tests and creep rupture time tests, with uncracked and cracked specimens for all elemental fatigue and creep cycles identified in the decomposed load series. Using a linear least-squares fit model for each elemental fatigue or creep test data set, we estimate the Category (II) uncertainty at the laboratory specimen-size scale.

To address the additional uncertainty due to a change of scale from specimen-size to the full-size component, we use the statistical theory of tolerance intervals, a modeling assumption, and a nonlinear least-

squares fit algorithm to obtain a formula for the minimum life (minL) of the full-size structure or component as a function of failure probability upper bound (FPUB). An inversion of the formula yields a FPUB vs. minL curve for each elemental fatigue or creep load history.

Using a second modeling assumption that FPUB is a measure of fatigue or creep damage and is an intrinsic property of the material with minL as its age marker that is load history-dependent, we then can construct the damage (FPUB) vs. load-specific-age (minL) curve for any complex load history by piecing together the series of elemental fatigue and creep loads using their individual damage vs. age curves, where the age parameter acts like an internal clock that is load-history dependent.

With this mathematical model based on experimental data, we have solved the Category (II) uncertainty problem for a general class of load histories involving fatigue, creep, and fatigue-creep interactions, thus paving the way to securing an estimate of the general reliability problem involving both Category (I) load and Category (II) material property uncertainties when the uncertainty in the operating load history is defined.

A Multi-Scale Creep, Fatigue, and Creep-Fatigue Interaction Model for Estimating Reliability of Steel Components at Elevated Temperatures. The American Society of Mechanical Engineers (ASME) Boiler and Pressure Vessel Code (BPVC) Committee has recently developed a new Section XI (Nuclear Components Inspection) Division 2 Code named *Reliability and Integrity Management (RIM)*. RIM incorporates a new concept known as “System-Based Code (SBC)” originally proposed by Asada and his colleagues (2001-2004), where an integrated approach from design to service inspection is introduced using

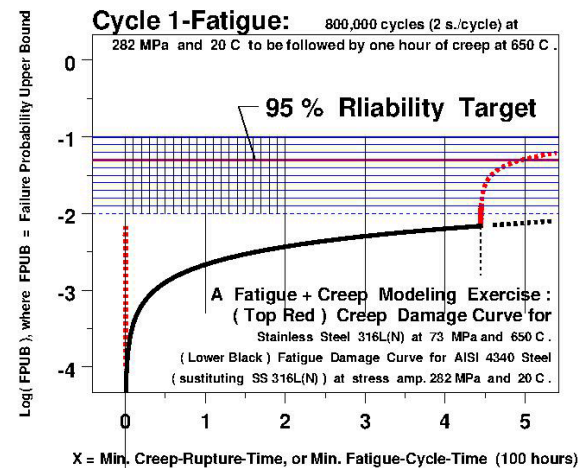


Figure 72. This plot completes the construction of the Fatigue-Creep Failure probability upper bound curve for the example.

¹⁷ <https://ports.macports.org/port/oof2/>

¹⁸ <https://nanohub.org/resources/oof2>

three new types of statistical quantities: (1) *system reliability index*, or *system co-reliability target* for any system consisting of structures and components, (2) *structural co-reliability*, for any structure, and (3) *component co-reliability* for any component, where co-reliability is defined as *1-reliability* and is equal to failure probability.

In a recent paper published in the *International Journal of Pressure Vessels and Piping* [4], Fong, Heckert, Filliben, and Freiman developed a new theory of fatigue and creep rupture life modeling for metal alloys at room and elevated temperatures such that the failure probability upper bound (FPUB) of a smooth component can be estimated from fatigue life and creep rupture time test data with simple loading histories. In this paper, we extend the theory to include a methodology to estimate not only the failure probability upper bound, but also the damage state of metal alloy components undergoing creep and fatigue with creep-fatigue interactions. To illustrate our methodology, we present numerical examples based on high temperature creep rupture time test data of stainless steel 316L(N) and room temperature fatigue life test data of AISI 4340 aircraft-quality steel. The significance and limitations of this new damage-state-based approach to modeling creep and fatigue reliability of steel components at elevated temperatures are presented and discussed.

As an example, we consider fatigue-creep cycling of a pseudo-material. To construct the FPUB curve for a different cycle, we begin with *Cycle 1-Fatigue*, i.e., fatigue at 282 MPa and 20 C for 444 hours, to be followed by one hour of creep at 73 MPa in 650 C. The results of the construction of the Fatigue-Creep FPUB curve are given in Figure 72.

- [1] *ASME Boiler and Pressure Vessel Code, Section XI, Division 2 - Requirements for Reliability and Integrity Management (RIM)*. Program for Nuclear Power Plants. American Society of Mechanical Engineers, 2021.
- [2] Y. Asada, M. Tashimo, and M. Ueta. System Based Code -Basic Structure. In *Proceedings of the 10th International Conference on Nuclear Engineering (ICONE-10)*, Arlington, VA, April 14- 18, 2002, Paper No. ICONE10-22731.
- [3] K. Kurisaka, R. Nakai, T. Asayama, and S. Takaya. Development of System Based Code (1) Reliability Target Derivation of Structures and Components. *Journal of Power and Energy Systems* **5**:1 (2011) 19-32.
- [4] J. T. Fong, N. A. Heckert, J. J. Filliben, and S. W. Freiman. A Multi-Scale Failure-Probability-based Fatigue or Creep Rupture Life Model for Metal Alloys. *International Journal of Pressure Vessels and Piping* **173** (2019), 79-93. DOI: [10.1016/j.ijpvp.2019.04.003](https://doi.org/10.1016/j.ijpvp.2019.04.003)
- [5] N. E. Dowling. *Mechanical Behavior of Materials*. 2nd edition, Prentice-Hall, 1999.
- [6] K. Wasmer. *Prediction of Creep Crack Growth in a Range of Steels*. Ph.D. thesis, Imperial College, London, U.K., 2003.
- [7] J. T. Fong, N. A. Heckert, J. J. Filliben, and S. W. Freiman. A Co-Reliability-Target-based Fatigue Failure Probability Model for Implementing the New ASME Boiler & Pressure Vessel Section XI Division 2 Reliability and Integrity Management Code: A Technical Brief. In *Proceedings of the ASME 2019 Pressure Vessel and Piping Division Conference*, July 14-19, 2019, San Antonio, TX, PVP2019-93508.
- [8] J. T. Fong, P. V. Marcal, R. Rainsberger, N. A. Heckert, J. J. Filliben, S. R. Doctor, and N. A. Finney. A Multiscale Failure-Probability-and-NDE-Based Fatigue Life Model for Estimating Component Co-Reliability of Uncracked and Cracked Pipes. In *Proceedings of the 2021 ASME Pressure Vessels & Piping Division Conference*, July 12-16, 2021, Virtual, Paper No. PVP2021-62169.
- [9] P. R. Nelson, M. Coffin, and K.A.F. Copeland. *Introductory Statistics for Engineering Experimentation*. Elsevier, 2006.
- [10] W. Q. Meeker, G. J. Hahn, and L. A. Escobar. *Statistical Intervals: A Guide for Practitioners and Researchers*. 2nd edition, Wiley, 2017.
- [11] N. R. Draper and H. Smith. *Applied Regression Analysis*. Chapters 1-3, pp. 1-103, and Chapter 10, pp. 263-304, Wiley, 1966.
- [12] M. G. Natrella. *Experimental Statistics*. National Bureau of Standards. Handbook 91 (August 1, 1963, reprinted with corrections October 1966), pages 1-14, 1-15, 2-13 to 2-15, Tables A-6 and A-7.
- [13] J. T. Fong, N. A. Heckert, J. J. Filliben, P. V. Marcal, and R. Rainsberger. Uncertainty of FEM Solutions Using a Nonlinear Least Squares Fit Method and a Design of Experiments Approach. In *Proceedings of the COMSOL Users' Conference*, Boston, MA, October 7-9, 2015.
- [14] J. T. Fong, N. A. Heckert, J. J. Filliben, P. V. Marcal, R. Rainsberger, and L. Ma. Uncertainty Quantification of Stresses in a Cracked Pipe Elbow Weldment Using a Logistic Function Fit, a Nonlinear Least Squares Algorithm, and a Super-parametric Method. *Procedia Engineering* **130** (2015), 135-149.
- [15] J. J. Filliben, and N. A. Heckert. *Dataplot: A Statistical Data Analysis Software System*. NIST, Gaithersburg, MD 20899, 2002.
- [16] N. A. Heckert and J. J. Filliben. *DATAPLOT Reference Manual, Volume I: Commands*. NIST Handbook 148, NIST, June 2003.
- [17] N. A. Heckert and J. J. Filliben. *Dataplot Reference Manual, Volume 2: Let Subcommands and Library Functions*. NIST Handbook 148, NIST, June 2003.
- [18] C. Forbes, M. Evans, N. Hastings, and B. Peacock. *Statistical Distributions*. 4th edition, Wiley, 2011.
- [19] P. F. Verhulst. Recherches Mathematiques sur la Loi d'Accroissement de la Population [Mathematical Researches into the Law of Population Growth Increase]. 1845, re-published in *Nouveaux Memoires de l'Academie Royale des Sciences et Belles-Lettres de Bruxelles* **18** (2013), 1-42.
- [20] C. Croarkin, W. Guthrie, N. A. Heckert, J. J. Filliben, P. Tobias, J. Prins, C. Zey, B. Hembree, and Trutna, eds. *NIST/SEMATECH e-Handbook of Statistical Methods*. URL: <http://www.itl.nist.gov/div898/handbook/>

Micromagnetic Modeling

Michael Donahue

Donald Porter

Mark-Alexander Henn

Robert McMichael (NIST PML)

Cindi Dennis (NIST MML)

<http://math.nist.gov/oommf/>

Advances in magnetic devices such as field sensors, spin torque oscillators, magnetic nonvolatile memory (MRAM), and thermal sensors are dependent on an understanding of magnetization processes in magnetic materials at the nanometer level. Micromagnetics, a mathematical model used to simulate magnetic behavior, is needed to interpret measurements at this scale. ACMMD is working with industrial and academic partners, as well as with colleagues in the NIST MML and PML, to improve the state-of-the-art in micromagnetic modeling.

We have developed a public domain computer code for performing computational micromagnetics, the Object-Oriented Micromagnetic Modeling Framework (OOMMF). OOMMF serves as an open, well-documented environment in which algorithms can be evaluated on benchmark problems. OOMMF has a modular structure that allows independent developers to contribute extensions that add to its basic functionality. OOMMF also provides a fully functional micromagnetic modeling system, handling three-dimensional problems, with extensible input and output mechanisms. From October 2022 through December 2023, the software was downloaded more than 5200 times by more than 3300 distinct client machines. The software is also available to the public via GitHub¹⁹ and nanoHUB²⁰. There are 202 known peer-reviewed journal articles published since from October 2022 to December 2023 that acknowledge the use of OOMMF. Total OOMMF citations now number 3674. OOMMF has become an invaluable tool in the magnetics research community.

Developments in the last year include:

- Released version 2.1a0 of OOMMF.²¹
 - Supports time-varying magnetization magnitudes.
 - Script-controlled simulation outputs for increased flexibility
 - New tools for processing simulation results.
 - Improved robustness of operations.
 - Continued maintenance of platform support and compatibility with Tcl/Tk.
- Released contributed OOMMF extension oommf-mel, computing magnetoelastic effects.²²

In addition to the continuing development of OOMMF, the project also does collaborative research using OOMMF. M. Donahue and M.-A. Henn are team members on the nanothermometry project Thermal MagIC.²³ Work for the Thermal MagIC project included the improvement of the image reconstruction in MPI by utilizing harmonic data and modeling particle relaxation, quantifying possible trade-offs between speed and accuracy by varying the sampling frequency, and further development of an algorithm that will be able to determine particle concentration and temperature simultaneously. Several recent publications report on this research [1-5]. Related work on antiferromagnetic modeling with University of Colorado graduate student Mingyu Hu (and advisor Mark Hofer) produced another paper [6] and a conference presentation [7].

M. Donahue is beginning a new CHIPS-funded project, “Metrology for Integration of New Magnetic Materials,” in partnership with Jim Booth, Pavel Kabos, and Ron Goldfarb. M. Donahue also served as the External Examiner on the Ph.D. Thesis Committee for Martin Lang at the University of Southampton (England).

- [1] T. Q. Bui, M.-A. Henn, W. L. Tew, M. A. Catterton, and S. I. Woods. Harmonic Dependence of Thermal Magnetic Particle Imaging. *Scientific Reports* **13** 15762 (2023). DOI: [10.1038/s41598-023-42620-1](https://doi.org/10.1038/s41598-023-42620-1)
- [2] K. N. Quelhas, M.-A. Henn, R. C. Farias, W. L. Tew, and S. I. Woods. Parallel MPI Image Reconstructions in GPU using CUDA. *International Journal on Magnetic Particle Imaging* **9**:1 (2023). DOI: [10.18416/IJMPI.2023.2303043](https://doi.org/10.18416/IJMPI.2023.2303043)
- [3] M.-A. Henn, K. N. Quelhas, and S. I. Woods. Investigating the Influence of Sampling Frequency on X-Space MPI Image Reconstructions. *International Journal on Magnetic Particle Imaging* **9**:1 (2023). DOI: [10.18416/IJMPI.2023.2303042](https://doi.org/10.18416/IJMPI.2023.2303042)
- [4] M.-A. Henn, T. Q. Bui, and S. I. Woods. Investigating the Harmonic Dependence of MPI Resolution. *International Journal on Magnetic Particle Imaging* **9**:1 (2023). DOI: [10.18416/IJMPI.2023.2303059](https://doi.org/10.18416/IJMPI.2023.2303059)
- [5] M.-A. Henn, K. N. Quelhas, T. Q. Bui, S. I. Woods, Improving Model-based MPI Image Reconstructions: Baseline Recovery, Receive Coil Sensitivity, Relaxation and Uncertainty Estimation. *International Journal on Magnetic Particle Imaging* **8**:1 (2022). DOI: [10.18416/IJMPI.2022.2208001](https://doi.org/10.18416/IJMPI.2022.2208001)
- [6] M. Hu, M. A. Hofer, and M. J. Donahue. Energetics of Phase Transitions in Homogeneous Antiferromagnets. *Applied Physics Letters* **123** (2023), 062401. DOI: [10.1063/5.0147368](https://doi.org/10.1063/5.0147368)
- [7] M. J. Donahue. “Energetics of Spin-flop and Spin-flip Transitions in Homogeneous Antiferromagnets.” Magnetism and Magnetic Materials 2022 Conference (MMM2022).

¹⁹ <https://github.com/fangohr/oommf>

²⁰ <https://nanohub.org/resources/oommf>

²¹ <https://math.nist.gov/oommf/software-21.html>

²² <https://github.com/yuyahagi/oommf-mel>

²³ <https://www.nist.gov/programs-projects/thermal-magic-si-traceable-method-3d-thermal-magnetic-imaging-and-control>

High Performance Computing and Visualization

Computational capability continues to advance rapidly, enabling modeling and simulation to be done with greatly increased fidelity. Doing so often requires computing resources well beyond what is available on the desktop. Developing software that makes effective use of such high-performance computing platforms remains very challenging, requiring expertise that application scientists rarely have. We maintain such expertise for application to NIST problems. Such computations, as well as modern experiments, typically produce large volumes of data, which cannot be readily comprehended. We are developing the infrastructure necessary for advanced interactive, quantitative visualization and analysis of scientific data, including the use of 3D immersive environments, and applying the resulting tools to NIST problems.

High Precision Calculations of Fundamental Properties of Few-Electron Atomic Systems

James Sims

Maria Ruiz (University of Erlangen, Germany)

Bholanath Padhy (Khallikote College, India)

<https://www.nist.gov/itl/math/computation-atomic-properties-hy-ci-method>

NIST has long been involved in supplying critically evaluated data on atomic and molecular properties such as the atomic properties of the elements contained in the Periodic Table and vibrational and electronic energy level data for neutral and ionic molecules contained in the NIST Chemistry WebBook. Fundamental to this work is the ability to predict, theoretically, a property more precisely than even the best experiments. It is our goal to be able to accomplish this for few-electron atomic systems.

While impressive advances have been made over the years in the study of atomic structure in both experiment and theory, the scarcity of information on atomic energy levels is acute, especially for highly ionized atoms. The availability of high precision results tails off as the state of ionization increases, not to mention higher angular momentum states. In addition, atomic anions have more diffuse electronic distributions, representing more challenging computational targets than the corresponding ground states.

In the past two decades, there have been breathtaking improvements in computer hardware and innovations in mathematical formulations and algorithms, leading to “virtual experiments” becoming a more and more cost effective and reliable way to investigate chemical and physical phenomena. Our contribution in this arena has been undertaking the theoretical development of our hybrid Hylleraas-CI (Hy-CI) wave function method to bring sub-chemical precision to atomic systems with more than two electrons.

Hy-CI has from its inception been an attempt to extend the success of the Hylleraas (Hy) method to

systems with more than three electrons, and hence is an attempt to solve not just the three-body problem but the more general N-body problem [1]. Fundamental to the method is the restriction of one r_{ij} per configuration state function (CSF). (For atomic systems with greater than four electrons, all relatively precise calculations nowadays adopt the Hy-CI methodology of one r_{ij} term per CSF.) In the case of three electron lithium systems, we have computed four excited states of the lithium atom to two orders of magnitude greater than has ever been done before [2]. At the four-electron level, to get truly precise chemical properties like familiar chemical electron affinities and ionization energies, it is important to get close to the nanohartree level we achieved for the three-electron atom, a significantly more difficult problem for four electrons than for three. By investigating more flexible atomic orbital basis sets and better configuration state function filtering techniques to control expansion lengths, we have been able to successfully tackle the four-electron case.

Progress to date has included computing the non-relativistic ground state energy of not only beryllium, but also many members of its isoelectronic sequence to eight significant digit precision. With the results from our calculations and a least-squares fit of the calculated energies, we have been able to compute the entire beryllium ground state isoelectronic sequence for $Z = 4$ through $Z = 113$ [3]. Li^- (with $Z=3$), nominally the first member of this series, has a decidedly different electronic structure and was not included in those calculations and subsequent discussions, but that omission has been corrected and we have subsequently carried out a large, comparable calculation for the Li^- ground state [4].

The first member of the Be isoelectronic ground state sequence, the negative Li^- ion, is also a four-electron system in which correlation plays a very important part in the binding. However due to the reduced nuclear charge, it is a more diffuse system in which one of its outer two L shell electrons moves at a greater distance from the nucleus than the other; hence its nodal structure is different from that of a coupled L shell with an identical pair of electrons. The ground state of the singlet S

state of Li⁻ is the same type of problem as the first excited state of Be; it is like Be(2s3s), not Be(2s2s). Completing this calculation has provided the necessary insight to enable the calculation of the Be first excited state of singlet S symmetry, Be(2s3s), to an order of magnitude better than previous calculations. Armed with this result, we have been able to continue this level of precision to the Be(2s4s) excited state and have calculated the higher, more diffuse Be(2s5s) through Be(2s7s) states as well, and in the process have demonstrated that Hy-CI can calculate the higher, more diffuse Rydberg states with more complicated nodal structures to the same level of precision as the less excited states [5].

While our work has demonstrated the efficacy of Hy-CI as a solution to the N-body problem for four or more electrons, this work has also shown the presence of a “double cusp” $r_{12}r_{34}$ term type slow convergence problem at the nanohartree precision level which is ultimately built into Hy-CI for four or more electrons. We have investigated a generalization of the Hy-CI method to an exponentially correlated Hy-CI (E-Hy-CI) method in which the single r_{ij} of an Hy-CI wave function is generalized to a form which pairs an exponential r_{ij} factor with linear r_{ij} , producing a correlation factor which has the right behavior in the vicinity of the r_{ij} cusp, and also as r_{ij} goes to infinity. While this was proposed in 2012 and there have been several papers on E-Hy-CI integrals, there were no computational tests until our calculations. Not only has the E-Hy part (the part that differs from conventional Hy-CI) been tested, but E-Hy-CI calculations have been done for spherically symmetrical and non-symmetrical orbitals as well.

The purpose of this research has been to determine how effective exponential correlation factors can be. By comparing convergence of the E-Hy-CI wave function expansion to that of the Hy-CI wave function without exponential factors, both convergence acceleration and an improvement in the precision for the same basis are demonstrated. This makes the application of the E-Hy-CI method to systems with $N > 4$, for which this formalism with at most a single exponentially correlated and linear r_{ij} factor leads to solvable integrals, very promising. The ground 1 singlet S state non-relativistic energy of He is computed to be -2.9037 2437 7034 1195 9831 1084 hartrees (Ha) for the best expansion [6].

We followed the success on the ground state of the He atom with calculations on the ground 1 singlet S and the 2 singlet S through 6 singlet S excited S states of the Li⁺ ion with the same technique, with results comparable to the He atom. This demonstrates the utility of the Hy-CI approach for not only ground but also excited states of S symmetry as well [7]. For a review of high precision studies of both Hy-CI and E-Hy-CI studies of atomic and molecular properties, see [8].

Our interest here is not just the wave functions and energies computed variationally with them, but also ultimately in the computation of atomic properties which the wave functions enable. When the energies are so phenomenally accurate, why not use the wave functions produced to determine important fundamental properties as well? Which brought us to the subject of the third paper in the E-Hy-CI series, computing oscillator strengths for the resonance transition of the helium isoelectronic sequence. To do that, we needed not just wave functions (and energies) for states of ¹S symmetry, but wave functions for states of ¹P symmetry as well.

In contrast to the closed shell $1s^2$ ¹S states, the ¹P states are open shell $1s2p$ ¹P states with the two electrons having different symmetries. The two different orbital exponent basis sets for ¹P are chosen to be representative of the two different electrons; in this case pairing an exponential r_{ij} factor with linear r_{ij} may have an enhanced role to play in providing the right behavior in the vicinity of the r_{ij} cusp and also the right behavior as r_{ij} goes to infinity. This resulted in E-Hy-CI wave functions for both the ¹S and ¹P lowest energy states for the Helium isoelectronic sequence first row (through the O⁺⁶ ion) which were accurate to 16-20 decimal places and for the ¹P states, the energies were the best ever computed.

The high-precision wave functions were used to compute oscillator strengths (also known as f values and transition probabilities) along with rigorous quantum mechanical upper and lower bounds in order to assess the quality of physical properties computed with these high precision wave functions. Interpolation techniques were used to carry out a graphical study of the oscillator strengths for $1s^2$ ¹S to $1s2p$ ¹P He isoelectronic sequence with rigorous non-relativistic quantum mechanical upper and lower bounds of (0.001 to 0.003) percent and probable precision less than or equal to 0.0000003, the best precision ever achieved. The significance of this work was recognized by the journal *Atoms* making this paper the cover story for the July 2023 issue [9].

Work is presently in progress (at the suggestion of Eli Pollak of the Weizmann Institute of Science, Israel) to compute lower bounds to energies. These are traditionally done by computing matrix elements of the square of the Hamiltonian (H^2), which present formidable mathematical difficulties when dealing with wave functions which have both exponential and linear r_{ij} terms. The Pollak-Martinazzo lower-bound theory [10] is intended to obviate this difficulty by computing variances using only data from the Hamiltonian matrix. However, it turns out that the quality of the ground state lower bound strongly depends not just on the ground state but also on the first excited state (and, to a lesser extent on higher states). Consequently, we intend to use E-Hy-CI wave functions to calculate the five lowest ¹S states of He I all in one wave function and the five lowest ¹P states of He I all in one wave function.

These wave functions will be used to calculate lower bounds to the energies both by calculating matrix elements of H^2 and by using the Pollak-Martinazzo lower-bound theory; they will also be used to calculate oscillator strengths, including upper and lower bounds, for the 25 lines arising from allowed transitions among these five 1S and five 1P states. The results of this study will be not only an assessment of the lower bound results but also oscillator strengths for the $n\ ^1S \rightarrow m\ ^1P$ transitions ($n = 1$ to 5 , $m = 2$ to 6) with rigorous upper and lower bounds.

- [1] J. S. Sims and S. A. Hagstrom. Combined Configuration Interaction – Hylleraas Type Wave Function Study of the Ground State of the Beryllium Atom. *Physical Review A* **4:3** (1971), 908. DOI: [10.1103/PhysRevA.4.908](https://doi.org/10.1103/PhysRevA.4.908)
- [2] J. S. Sims and S. A. Hagstrom. Hylleraas-Configuration Interaction Study of the $2\ ^2S$ Ground State of Neutral Lithium and the First Five Excited 2S States. *Physical Review A* **80** (2009), 052507. DOI: [10.1103/PhysRevA.80.052507](https://doi.org/10.1103/PhysRevA.80.052507)
- [3] J. S. Sims and S. A. Hagstrom. Hylleraas-Configuration Interaction Nonrelativistic Energies for the 1S Ground States of the Beryllium Isoelectronic Series up Through $Z = 113$. *Journal of Chemical Physics* **140** (2014), 224312. DOI: [10.1063/1.4881639](https://doi.org/10.1063/1.4881639)
- [4] J. S. Sims. Hylleraas-Configuration Interaction Study of the 1S Ground State of the Negative Li Ion. *Journal of Physics B: Atomic, Molecular and Optical Physics* **50** (2017), 245003. DOI: [10.1088/1361-6455/aa961e](https://doi.org/10.1088/1361-6455/aa961e)
- [5] J. S. Sims. Hylleraas-Configuration Interaction (Hy-CI) Non-Relativistic Energies for the $3\ ^1S$, $4\ ^1S$, $5\ ^1S$, $6\ ^1S$ and $7\ ^1S$ States of the Beryllium Atom. *Journal of Research of the National Institute of Standards and Technology* **125** (2020), 125006. DOI: [10.6028/jres.125.00625.006](https://doi.org/10.6028/jres.125.00625.006)
- [6] J. S. Sims, B. Padhy and M. B. Ruiz. Exponentially Correlated Hylleraas-Configuration Interaction (E-Hy-CI) Non-Relativistic Energy of the $1\ ^1S$ Ground State of the Helium Atom. *International Journal of Quantum Chemistry* **121:4** (2020), e26470. DOI: [10.1002/qua.26470](https://doi.org/10.1002/qua.26470)
- [7] J. S. Sims, B. Padhy, and M. B. Ruiz. Exponentially Correlated Hylleraas-Configuration Interaction (E-Hy-CI) Studies of Atomic Systems. II. Non-relativistic Energies of the $1\ ^1S$ through $6\ ^1S$ States of the Li^+ Ion. *International Journal of Quantum Chemistry* **122:1** (2021), e26823. DOI: [10.1002/qua.26823](https://doi.org/10.1002/qua.26823)
- [8] M. B. Ruiz, J. S. Sims, and B. Padhy. High-precision Hy-CI and E-Hy-CI Studies of Atomic and Molecular Properties. *Advances in Quantum Chemistry* **83** (2021), 171-208. DOI: [10.1016/bs.aiq.2021.05.010](https://doi.org/10.1016/bs.aiq.2021.05.010)
- [9] J. S. Sims, B. Padhy, and M. B. Ruiz. Exponentially Correlated Hylleraas-Configuration Interaction (E-Hy-CI) Studies of Atomic Systems. III. Upper and Lower Bounds to He-Sequence Oscillator Strengths for the Resonance $1\ ^1S \rightarrow 2\ ^1P$ Transition. *Atoms* **11:7** (2023), 107. DOI: [10.3390/atoms11070107](https://doi.org/10.3390/atoms11070107)
- [10] E. Pollak and R. Marinazzo. Lower Bounds for Coulombic Systems. *Journal of Chemical Theory and Computation* **17:3** (2021), 1535-1547. DOI: [10.1021/acs.jctc.0c01301](https://doi.org/10.1021/acs.jctc.0c01301)

Simulation of Dense Suspensions: Cementitious Materials

William George
 Nicos Martys (NIST EL)
 Jeffery Bullard (Texas A&M University)
 William Sherman
 Simon Su
 Steven Satterfield
 Judith Terrill
 Luke Haranick

A suspension is a collection of solid inclusions embedded in a fluid matrix. Suspensions play an important role in a wide variety of applications including paints, cement-based materials, slurries, and drilling fluids. Understanding the flow properties of a suspension is necessary in many such applications. However, measuring and predicting flow properties of suspensions remains challenging.

Suspensions can be quite complex, as the suspended inclusions may have a wide range of shapes and a broad size distribution. Further complicating matters is that different matrix fluids may have quite disparate flow behavior. While the simplest type of matrix fluid is Newtonian, where the local stress is proportional to the shear rate, the matrix fluid can also be non-Newtonian, exhibiting complex behavior including shear thinning (viscosity decreases with shear rate), shear thickening (viscosity increases with shear rate), viscoelasticity (exhibiting both viscous and elastic properties), or even have a time dependent viscosity (thixotropic).

The dense suspension simulation code, QDPD (a Dissipative Particle Dynamics code which uses Quaternions to track the tumbling of the suspended inclusions), that we have developed is generic in that it can be applied not only to cement, mortar, and concrete, but also to any dense suspension of interest including pharmaceuticals such as suspensions of monoclonal antibodies or industrial suspensions such as paints and drilling fluids. Although some modification to the code may be needed in each case, QDPD is fully parameterized to handle a wide range of dense suspensions from rocks suspended in a mortar to proteins suspended in a fluid.

Our focus this year has been on studying the rheological properties of cementitious materials which contain suspended fibers, such as Ultra High Performance Concrete (UHPC). These materials are of great interest because of their increased compressive and flexural strength as well as improved toughness and durability.

This work is part of a U.S. Army Corps of Engineers project in collaboration with Professor Jeffrey Bullard of the Department of Materials Science and Engineering at Texas A&M University, and Nicos Martys

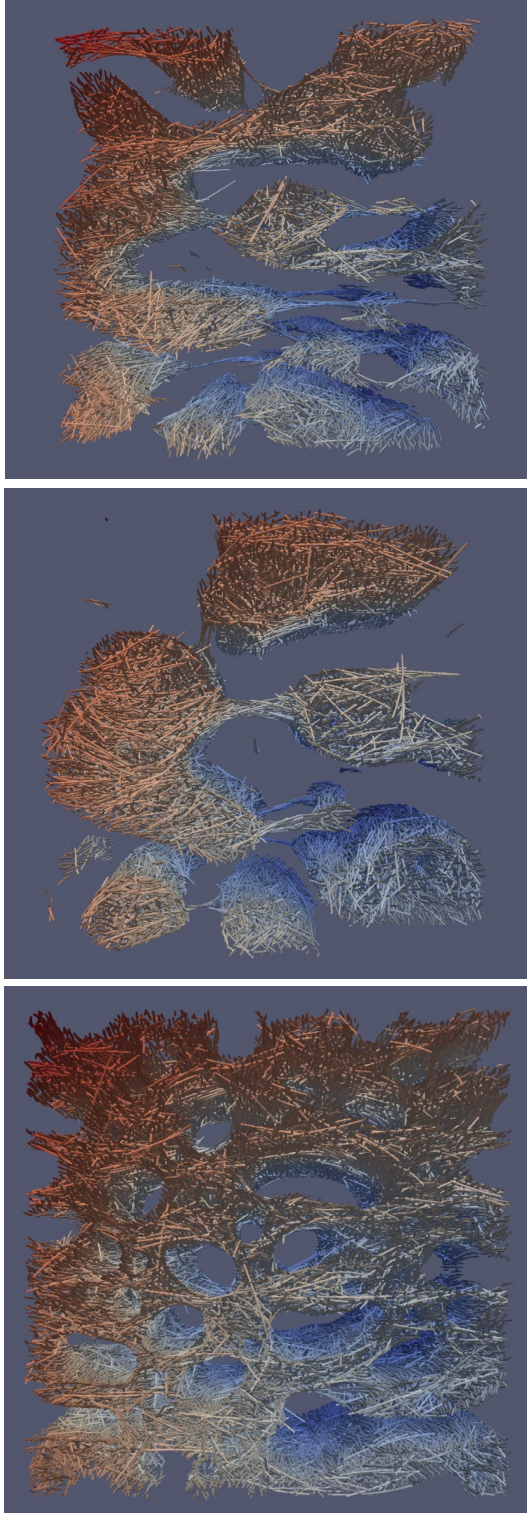


Figure 73. *Top:* Late stage phase separation of non-wetting fibers. The volume fraction of fibers is 10 %. Color indicates the velocity of the particles in the material. *Middle:* Same non-wetting fiber simulation as above, but after it was further strained. *Bottom:* Later stage phase separation of non-wetting fibers that are very stiff. The volume fraction of fibers in this system is 20 %. Note that at late stages there is the development of tube like structures built of fibers. Color indicates the velocity of the particles in the material.

of NIST EL. In order to simulate the specific UHPC materials of interest to the U.S. Army Corps of Engineers, we have enhanced the capabilities of QDPD to simulate both suspended flexible fibers (with stretching, bending, and twisting) and “stiff” steel fibers (no stretching, bending or twisting).

For this study, we are modeling the flow of such fibers in a Newtonian fluid and also in a non-Newtonian shear thinning paste that is similar to materials that are used in UHPC. The computational approach is based on a Smooth Particle Hydrodynamics (SPH) model that has been modified to account for the presence of fibers. We are investigating the influence of the wetting properties of the fibers in the fluid medium as well as the effect of stiff angular steel fibers, straight steel fibers, and flexible fibers. When the fibers are non-wetting, they tend to phase separate from the fluid as it is not energetically favorable to be in contact with the fluid. Wetting fibers do not exhibit this phase separation behavior. Images from several of these simulations showing phase separation are shown in Figure 73.

In the last year we have simulated more than 100 different systems of suspended fibers with varying properties, such as volume fraction of fibers, fiber wetting properties, fiber stiffness, and shearing velocity. Although we have begun the analysis of these results, this project is still in its early stage. Initial results have been presented [1]. We expect to analyze and report our complete results within the year.

Associated with this research, with the help of Luke Hawranick, a 2023 SURF (NIST Summer Undergraduate Research Fellowship) participant, we investigated some performance aspects of the QDPD code, specifically focusing on the inter-process communication used in this highly parallel program. One promising result from this investigation is the possibility of improving the performance of QDPD by re-ordering some of its operations in order to overlap inter-process communication with computations.

This year we have also started a related project to study the hydration of cement, using the NIST developed simulation code HydratiCA. This project is also in collaboration with Professor Jeffery Bullard and will be primarily performed by Luke Haranick, as a NIST Pathways intern from the University of West Virginia.

- [1] J. Bullard, N. Martys, and W. George. “Rheology of High Performance Cement-Based Materials for Use in Additive Manufacturing.” 8th Pacific Rim Conference on Rheology, University of British Columbia, Point Grey Campus, May 15-19, 2023.

Immersive Visualization for the Design of a Wearable Wireless Monitoring System

Simon Su

William Sherman

Judith Terrill

Kamran Sayrafian

Katjana Ladic (University of Zagreb, Croatia)

The NIST ITL Building the Future Program project, *A Wireless Wearable Technology to Detect Accumulation of Fluid in the Lungs*, strives to develop a wearable monitoring device for the detection and monitoring of pulmonary edema (i.e., fluid buildup in the lungs). The system works by placing small wearable antennas on the chest and back and monitoring signals in the MedRadio frequency band exchanged between them. To study this, a methodology has been developed to use a human body model to computationally emulate human lungs with various levels of fluid in the alveoli. Recently, the model has been enhanced to include dynamic breathing. Immersive visualization is being used to analyze simulation data from this model.

In a dynamic breathing simulation, every time step has a different grid illustrating the continually changing positions of organs in the body. Using immersive visualization, we can visualize the scanned data of the entire breathing process overlaid with the computationally generated data. Leveraging our work in transitioning to open-source visualization software (ParaView), and animation enhancement in ParaView, we are able to visualize the data life-sized and in real-time in our CAVE-format immersive visualization system. As described below, our effort to enhance ParaView with immersive capabilities enables us to move from desktop

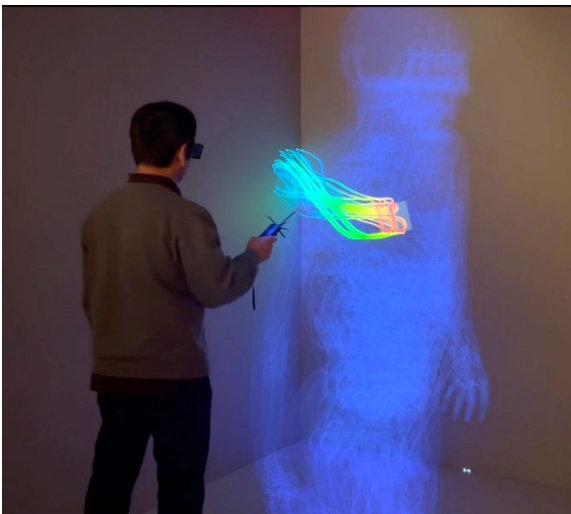


Figure 74. High resolution streamlines of RF energy data rendered in NIST CAVE

visualization directly to immersive displays without requiring custom development of an immersive visualization application.

Figure 74 shows an immersive visualization of streamlines of RF energy obtained from a computational simulation overlaid on scanned data from a human body for comparison. By building upon our new workflow model that makes use of the immersive features of the ParaView tool – an ongoing collaboration between NIST and Kitware – we are also able to concentrate our efforts in this project directly on how best to display the data in life-sized model and in real-time to simulate an actual human breathing process.

- [1] S. Su, I. Lopez-Coto, W. R. Sherman, K. Sayrafian, and J. Terrill. Immersive ParaView: An Immersive Scientific Workflow for the Advancement of Measurement Science. In *2022 IEEE International Symposium on Mixed and Augmented Reality Adjunct (ISMAR-Adjunct)*, Singapore, 2022, 139-145. DOI: [10.1109/ISMAR-Adjunct57072.2022.00034](https://doi.org/10.1109/ISMAR-Adjunct57072.2022.00034)
- [2] S. Su. “Future XR Technologies, Wearable Devices, and Content Authoring Tools for Immersive Collaborative Learning.” Panel at The Learning Multiverse: Immersive Technologies (IM-TECH) in Training and Education, George Mason University, September 7, 2023.

Visualization of Greenhouse Gas Emissions

William Sherman

Simon Su

Judith Terrill

James Whetstone (NIST SPO)

Israel Lopez Coto (NIST SPO)

Anna Karion (NIST SPO)

Kimberly Mueller (NIST SPO)

The NIST Greenhouse Gas (GHG) Measurements Program develops advanced tools and standards for accurately measuring GHG emissions so industries and governments will have the information they need to manage emissions effectively. ACMD’s High-Performance Computing and Visualization Group (HPCVG) is collaborating with James Whetstone, Leader of NIST’s Greenhouse Gas Measurements Program and his team of climate and weather simulation researchers to produce interactive visualizations of their data.

One of our goals in HPCVG is to reduce the turnaround time of immersive visualization development. In our latest work, we used the data from the Greenhouse Gas Measurements Program to demonstrate the enhancement of volume rendering in an immersive environment. Volume rendering is a challenge for the CAVE-style visualization rendering but is worth pursuing as it provides a more comprehensible visualization

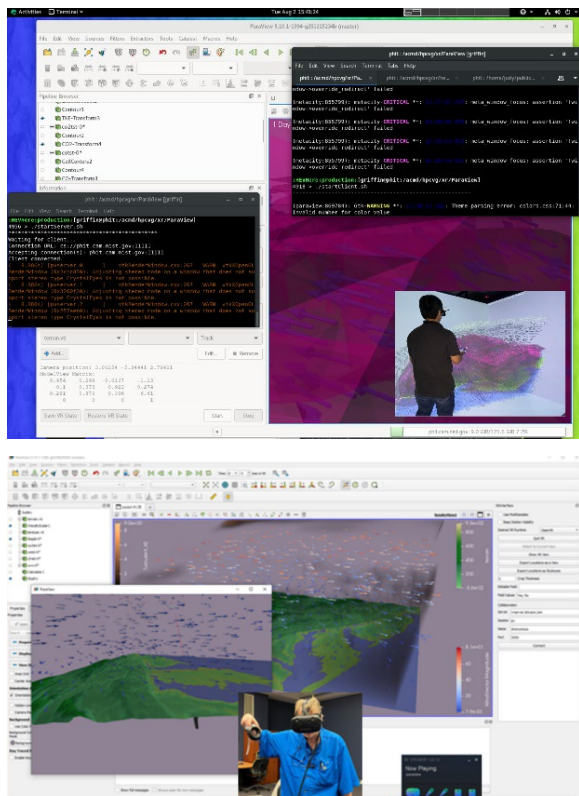


Figure 75. Visualizing GHG data in the NIST CAVE.

as compared with isosurface visualization to show the concentration of various chemical mixtures in the atmosphere. Also, for this project, time sequential volume rendering of simulation data for this program is important, and rendering time varying data in the ParaView CAVE interface works fine, though not as well through the head-mounted display (HMD) interface. Presently, volume rendering capability is available in the XR Interface plugin (for HMDs), and time sequential visualization of volume data works well in the CAVE. Our current effort is in making both visualization requirements work in both modalities.

In addition to enhancing visualization capability in an immersive environment, we are continuing our effort in the development of a native data loader for the data generated by the GHG Measurement Program. The native file loader in ParaView will complete our effort to streamline the development of a streamlined immersive visualization development.

Because the climate data has these challenges in visualizing the data, it serves as a good testbed for our software development collaboration with Kitware. Negotiations on a new Kitware collaboration slowed progress during the last year, but as of November 2023, our collaboration has been renewed, and work continues.

The interesting nature of the climate data also has served as a good case for demonstrating our efforts on

enhancing the immersive interface capabilities of ParaView, and thus has been shown at conferences such as Supercomputing 2023, International Symposium on Visual Computing (ISVC) 2023, and the 2023 DoE Computer Graphics Forum.

Transition to Open Source Visualization Software

*William George
Terence Griffin
Sandy Ressler
Steven Satterfield
William Sherman
Simon Su
Judith Terrill
Cory Quammen (Kitware)
Scott Wittenburg (Kitware)*

As part of our research on immersive measurements and analysis, the ACMD High Performance Computing and Visualization Group (HPCVG) operates a fully immersive visualization environment (IVE) and has developed high end visualization (HEV) software to run it. We started developing this software for our IVE more than two decades ago. During this time, we have upgraded and rewritten this software as our understanding of scientific visualization in an IVE developed and as outside innovations in hardware appeared. However, there were many limitations to our software. For example, it could only run on one specially configured operating system, and it had not kept up with recent advances in hardware visualization capabilities. Internally this software uses a scene-graph-based framework.

Our IVE is on a critical path for the success of collaborations with several NIST research groups and is used at every stage of these collaborations. These projects are diverse and span applications from nanotechnology to medical to materials, and often contribute to standard reference data and materials. For example, the IVE was essential in the success of NIST's development of standard reference materials (SRMs) for the measurement of the flow of cement paste, mortar, and concrete.

To take advantage of recent advances in visualization hardware, we are moving our IVE to ParaView, a fully open-source software environment. The ParaView software system is complex. Internally it uses a pipelined and proxy-based framework. The software consists of a Qt interface, which uses over 2000 VTK C++ classes to produce visualizations. It runs in an IVE as well as on Windows, Mac OS X, Linux, SGI, IBM Blue Gene, Cray and various Unix workstations, clusters, and supercomputers. It supports rendering shaders. It has a new real-time path-tracing back end using NVIDIA



Figure 76. Bill Sherman of ACMD speaks at SIGGRAPH.

RTX technology. Thus, ParaView extends the environments that the HPCVG HEV can work in, as well as provides access to real time ray tracing and global illumination made possible with the new GPUs. Access to high-end GPU rendering will continue to grow as ParaView adopts the ANARI rendering standard from the Khronos Group.

This year one contract with Kitware to work with us to develop needed extensions to ParaView was completed and a new one started. Specifically, we worked on the VR CAVE Interaction plugin, the 3D coordinate system, head tracking, and documentation. In the coming year we will work on the ParaView Desktop, CAVE Interaction Plugin, and XR Interface Plugins Collaboration mode. We will document the CAVE Interaction and XRInterface ParaView plugins. In addition, we will enhance the ability to read object representations in glTF (an emerging standard for models) and enhance the usability features of the existing “Macro” feature of ParaView.

Additional open-source software that we explore as part of an expanded suite of available tools for immersive visualization include the ANARI advanced rendering SDK, the VMD molecular visualization tool, and the Vrui suite of immersive visualization tools.

- [1] W. Sherman. “Immersive Visualization with the ParaView Open Source Tool.” Free and Open Source Software for XR (FOSS-XR) Minneapolis, MN, October 6, 2022.
- [2] S. Su. “High Performance Computing and Visualization Group at NIST.” Pitch Your Lab, IEEE International Symposium on Mixed and Augmented Reality (ISMAR), Singapore, October 20, 2022.
- [3] S. Su, W. Sherman, I. Lopez Coto, K. Sayrafian, and J. Terrill. “Immersive ParaView: An Immersive Scientific Workflow for the Advancement of Measurement Science.” IEEE International Symposium on Mixed and Augmented Reality (ISMAR), Workshop on Visual Analytics in Immersive Environments (VAinIE), Singapore, October 21, 2022.
- [4] W. S. Wittenberg. “Immersive ParaView and VTK.” DoE Computer Graphics Forum, Idaho Falls, ID, April 26, 2023.

- [5] W. Sherman. “Immersive Visualization with the ParaView Open Source Tool.” , Immersive Visualization BOF, SIGGRAPH '23 Los Angeles, CA, August 6, 2023.
- [6] W. Sherman. “Advances to the ParaView Immersive Interface.” Campus Alliance for Advanced Visualization (CAAV) Conference, Muncie, IN, October 25, 2023.
- [7] W. Sherman and S. Su. “Immersive Visualization with the ParaView Open Source Tool: A Tutorial.” International Symposium on Visual Computing (ISVC) 2023 conference, South Tahoe, NV, October 16, 2023.

Development of Visualization Infrastructure to Support Future Collaborations in a Hybrid Data Analysis Environment

Simon Su
William Sherman
Judith Terrill

This NIST ITL Building the Future project strives to develop a heterogeneous collaborative 3D visualization capability in ParaView. The development of the collaborative visualization capability was preceded with a code restructuring of related ParaView classes providing the collaborative visualization functionality. This will allow for easier implementation of the collaborative functionality across different ParaView visualization modalities.

Collaborative immersive visualization will play a crucial role in the visual analytics of computationally generated data of simulation experiments, in a hybrid working environment. Navigating the challenges of hybrid work will require a different type of infrastructure to support open and regular communications among geographically dispersed team members. Remote colleagues can use either a laptop computer, a desktop computer, a consumer grade head mount display system, or a CAVE-like immersive visualization system to perform collaborative visualization of the 3D scientific data.

Figure 77 shows a collaborative immersive visualization session between three collaborators. Presently, only ParaView users using head mounted display are supported. We are working on broadening collaborative visualization support to work across all ParaView visualization modalities, which includes addressing the challenges of user interaction with heterogeneous visualization systems.

This work builds on a core framework created for HMD users of ParaView, and we are reviewing the protocol used for collaboration to ensure it will accommodate all different interface modalities. The protocol will be expanded, as needed, to address these needs.

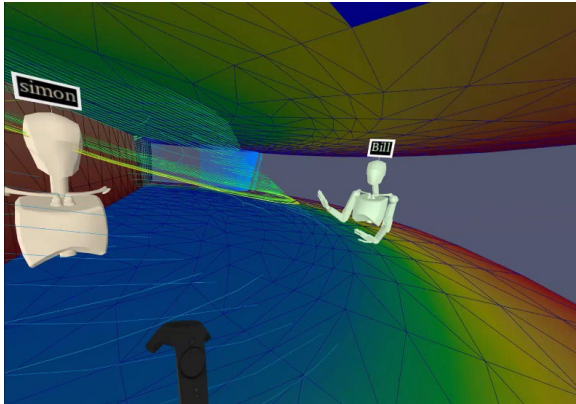


Figure 77. A researcher's avatar points to data of interest inside a collaborative 3D visualization.

- [1] W. Sherman. "Immersive Visualization with the ParaView Open Source Tool." FOSS-XR 2022, Minneapolis, MN, October 6, 2022.
- [2] S. Su, W. Sherman, I. Lopez Coto, K. Sayrafian, and J. Terrill. "Immersive ParaView: An Immersive Scientific Workflow for the Advancement of Measurement Science." IEEE ISMAR 2022 Workshop on Visual Analytics in Immersive Environments (VAinIE), Singapore, October 21, 2022.
- [3] W. Sherman, S. Su. Immersive Visualization with the ParaView Open Source Tool. NIST ACMD Seminar, Boulder Colorado, November 13, 2023.

Standards in Visualization

William Sherman
Sandy Ressler
Simon Su
Judith Terrill

ACMD staff participate in working groups of The Khronos Group related to immersive interfaces (OpenXR), advanced rendering (ANARI), and 3D Formats. As members of these working groups, we participate in weekly meetings, and raise issues and offer solutions to help advance the progress of those standards.

This past year the ANARI specification 1.0 was approved by the Khronos Board of Directors, and the OpenXR 1.1 specification is nearing approval. We also participated in two sub-groups within the OpenXR working group: namely, the OpenXR tutorial development committee, and the Monado open-source development committee.

As part of our commitment to advancing standards in immersive technologies and advanced rendering, we also worked on software that adheres to these standards. We worked with Kitware Inc. to ensure that their VTK and ParaView products both make use of the OpenXR

standard, and we performed tests to confirm the operation, and to suggest further improvements. Likewise, we worked with Kitware to add ANARI's rendering SDK as part of the VTK platform. We conducted tests that combined the ANARI and OpenXR standards using VTK and can confirm that these standards work well together. Development will continue on the ParaView project to incorporate ANARI as one of its rendering options. Separately, we continue to develop and test example programs that enable ANARI rendering in the NIST CAVE visualization system through the FreeVR open-source tool.

The 3D Formats Group is responsible for the continued evolution of glTF, a 3D graphics format becoming the "jpeg of 3D." The 3D Formats Group is actively involved in a variety of extensions to glTF. Primarily concerned with achieving high quality and high performance, taking advantage of GPU hardware is a signature overarching goal of the group. glTF is becoming more popular as a representation of 3D objects. Our participation ensures that it is aligned to our, and the public's needs, and keeps us on the leading edge of 3D format developments. glTF is now a formal ISO standard [1].

The NIST ACMD HPCVG team has also worked to promote these standards. Sherman presented the ANARI 1.0 specification at the Khronos BOF at the SIGGRAPH conference on computer graphics and interaction; see Figure 76. We presented the proposed standard at the annual DoE Computer Graphics Forum (DOE-CGF). We also promoted the use of tools that make use of these standards through a tutorial presented at the International Symposium on Visual Computing.

We recently expanded our participation in formal standards development. We were responsible for arranging for NIST membership in the Metaverse Standards Forum (MSF). The MSF has only existed for about two years yet already has approximately 2400 institutional members. Although not a formal standards development organization (SDO), the MSF is playing a key role in ensuring that many institutions involved with the actual standards development of the metaverse, talk to each other in a productive manner. We actively participate in the 3D Asset Interoperability Group.

We were invited to join (and now participate in) the IEEE Metaverse initiative steering committee. In addition to glTF, the Universal Scene Description (USD) format is also experiencing significant growth. USD has been selected by Nvidia, Apple and Adobe as the main file format for the "metaverse." The MSF is expending significant effort to ensure a high degree of interoperability between glTF and USD. USD is being developed under the auspices of the OUSD (Open USD) organization part of the ASWF (Academy Software Foundation) which is part of the Linux Foundation. USD is under the care of an organization with a history of

successful ISO standards development, and we continue to advocate for high degrees of interoperability.

- [1] *ISO/IEC 12113:2022, Information Technology, Runtime 3D Asset Delivery Format, Khronos glTF™ 2.0.*
- [2] S. Su. “Future XR Technologies, Wearable Devices, and Content Authoring Tools for Immersive Collaborative Learning.” Panel at The Learning Multiverse: Immersive Technologies (IM-TECH) in Training and Education, George Mason University, September 7, 2023.
- [3] W. Sherman and J. Amstutz. “An Overview of ANARI 1.0: The Industry’s First Open Standard, Cross-platform 3D Rendering Engine API.” SIGGRAPH 2023, Khronos Developer-Day BOF, August 9, 2023. URL: <https://www.youtube.com/watch?v=PAJYWvRdgaU>
- [4] W. Sherman. “Portable and Scalable 3D Rendering using ANARI.” DoE Computer Graphics Forum 2023, Idaho Falls, ID, April 26, 2023.
- [5] W. Sherman and S. Su. “Immersive Visualization with the ParaView Open-Source Tool: A Tutorial.” International Symposium on Visual Computing (ISVC), South Tahoe, NV, October 16, 2023.
- [6] S. Ressler. “Virtual Reality the Metaverse and All that Reality Stuff.” USPTO Patent Examiner Training, online, May 9, 2023. URL: <https://slides.com/d/xYgnkEk/live>

WebXR Graphics and Standards

Sandy Ressler

Nicos Martys (NIST EL)

Robert Ehrenreich (US Holocaust Memorial Museum)

Abigail Zola (US Holocaust Memorial Museum/Rhode Island School of Design)

“XR” has evolved to become a term that covers VR (virtual reality), AR (augmented reality) and MR (mixed reality). “WebXR” is a version of XR that is intimately connected to the Web. You go to a web page, click on the appropriate link and you become immersed into the application. You remain in the browser, but you are interacting with the application while wearing a headset that presents stereo imagery. Interaction is usually accomplished via specialized controllers, rather than the keyboard. The ability to use web pages with XR content with or without VR hardware makes these pages more widely useful as they do not depend on what is still exotic hardware. Simply put, 3D content that utilizes XR standards can be made useful whether or not you have immersive hardware.

In the case of AR, you remain in the real world because you still see the real world, with the graphics as an overlay. A current common method of using AR is via a mobile phone which uses its camera to capture the real

environment and overlays graphics on it. A compelling example is holding your phone up to a photo in a museum and the application presents more information about the contents of the photo.²⁴

3D Object Input and Capture. Viewing a 3D object on a web site first requires a representation of the object itself. Historically we have obtained these either from CAD systems or from visualization data. Missing from that set of objects are representations of “real” objects, artifacts that actually exist in real life. Photogrammetry hardware is becoming widely available. Your smartphone can take high quality images and some phones have LIDAR hardware as well to capture 3D point cloud data. As hardware for capturing the shape and texture of real objects has plummeted, 3D object capture is becoming democratized.

There is a desire to scan items such as museum artifacts, or simply physical objects that are of interest. Allowing curators or the general public to view and manipulate objects that are too precious to handle, or inaccessible, in real life is an important benefit to the creation and access of objects in our virtual world. The goal of this aspect of our WebXR project is to codify standards, processes, and techniques to enable dissemination of priceless artifacts more widely and to add information about these objects not easily seen via 2D representations. These types of capture processes fall into the domain of photogrammetry, and photometry. These are not new domains. Museums and forensic experts have been active in these domains for many years. We are beginning to assemble a working group of experts and end users to make NIST contributions in the context of web accessible objects and interactions with those objects. We’ve continued to hold meetings with staff of the United States Holocaust Memorial Museum as well as forensics experts at NIST.

In addition to scanned objects, we can also provide help with CAD-based models. We have begun working with a student at the United States Holocaust Memorial Museum who is investigating the reconstruction of a wartime hospital in Lodz Poland. The student has, by hand, reconstructed a version of the hospital. We have taken the data and converted it into a web accessible interactive 3D object that can be inspected from any point of view.²⁵ See Figure 78.

Web3D Visualization. Working with Nick Martys of NIST’s EL, we have begun visualizing data from a simulation of mortar. The data is the output of a large supercomputer-based simulation. We convert the data, in CSV format, into an interactive 3D dataset suitable for display in a web page. One of the key advantages of

²⁴ See, for example, <https://venturebeat.com/mobile/holocaust-memorial-museum-uses-augmented-reality-to-make-history-visceral/>

²⁵ <https://sketchfab.com/3d-models/lodz-hospital-mat-6c29374a832a4f6bb226a94283dbd034>



Figure 78. Reconstruction of wartime Lodz Poland hospital (Abigail Zola) as interactive 3D object.

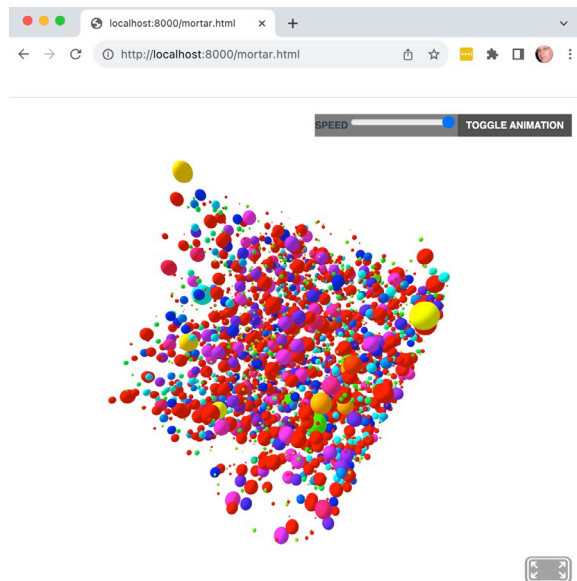


Figure 79. Web-based visualization of mortar simulation.

this is the ability to use common web interaction techniques such as sliders, buttons and so on just like a regular web page. These controls allow the user to adjust the speed of rotation or toggle the animation. In addition, if run on a computer with hardware supporting a head mounted display, the same web page can display 3D stereo immersive versions of the data. Figure 79 shows the web page. The goal is to allow the material scientist to interact and gain insight with simulation data quickly on their desktop computer using only a web browser.

3D Standards Participation. We have expanded our participation in formal standards development. At our lead, NIST has joined the Metaverse Standards Forum (MSF). The MSF has only existed for about two years

yet already has approximately 2400 institutional members. Although not a formal standards development organization, the MSF is playing a key role to ensure that many institutions involved with the actual standards development of the metaverse, talk to each other in a productive manner. We actively participate in the MSF's 3D Asset Interoperability Group.

We are also involved with standards efforts run by the Khronos Group. The Khronos Group is an industry-led consortium, and the participants are a highly skilled collection of technologists focused on real world practical problems. Their 3D Formats Group is responsible for the continued evolution of glTF, a 3D graphics format which is becoming the "jpeg of 3D." They are actively involved in a variety of extensions to glTF. Primarily concerned with achieving high quality and high performance, taking advantage of GPU hardware is a signature overarching goal of the group. glTF is becoming more popular as a representation of 3D objects. Our participation ensures that it is aligned to our, and the public's needs, and keeps us on the leading edge of 3D format developments. glTF is now a formal ISO standard [1].

In addition to glTF, the Universal Scene Description (USD) format is also experiencing significant growth. USD has been selected by Nvidia, Apple and Adobe as the main file format for the "metaverse." The MSF is expending significant effort to ensure a high degree of interoperability between glTF and USD. USD is being developed under the auspices of the OUSD (Open USD) organization, part of the ASWF (Academy Software Foundation), which is part of the Linux Foundation. USD is thus under the care of an organization with a history of successful ISO standards development. We continue to advocate for high degrees of interoperability.

- [1] *ISO/IEC 12113:2022 Information technology, Runtime 3D asset delivery format, Khronos glTF™ 2.0.* International Standards Organization and International Electrotechnical Commission, 2022. URL: <https://www.iso.org/standard/83990.html>

Towards Robust Autotuning of Noisy Quantum Dot Devices

Justyna P. Zwolak
Jacob M. Taylor (NIST PML)
Florian Luthi (Intel Corporation)
Mick Ramsey (Intel Corporation)
Joshua Ziegler (Intel Corporation)

Small device footprint and the possibility of operation at few-Kelvin temperatures make gate-defined quantum dots (QDs) an appealing candidate for a quantum computing platform. However, near-term devices possess a

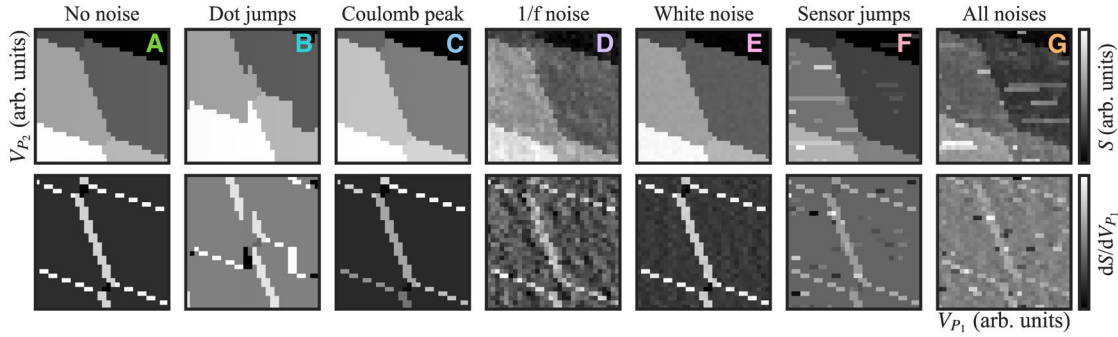


Figure 80. Various types of noise added to a simulated charge stability diagram for a QD device in a “double QD” state, with electrons trapped in two potential wells. The bright lines in the bottom row indicate a change of electron occupation in the device. All noise magnitudes are the same as for the best accuracy quoted except for dot jumps and Coulomb peak which have increased effect for visibility. Adapted from [2].

range of possible imperfections that need to be accounted for during tuning and operation of QD devices. These minor inconsistencies inherent to the fabrication process make a deterministic tuning of QD devices impossible. While some recent progress has been made towards automating elements of this process [1], a large part of the QDs initialization is still performed mostly manually through heuristic calibration.

The best strategies for automating initialization rely on supervised machine learning (ML) methods. ML algorithms enable autonomous identification of the state of the QD device as parameters are tuned. However, training such ML models requires large amounts of data with labeled device states. There are two paradigms for preparing datasets for training, each having its own advantages and limitations. The first is to use manually labeled experimental data. Unfortunately, human labeling is laborious, not very reliable, and not scalable, especially as gate-defined QD devices change or grow in qubit numbers and complexity. The other paradigm relies on simulated data that incorporate various types of realistic, physical noise.

An idealized noiseless charge stability diagram shows lines when an electron is added to the device’s trapping potential landscape overlaid on a uniform background, as shown in Figure 80A. Depending on the type of added noise, the appearance of simulated data changes as shown in Figure 80B-F. Using a set of 542 manually labeled experimental scans for testing, we found an about 46 % accuracy improvement in ML model’s performance, from 48.7(5.5) % for a simplistic model trained on noiseless simulated data to 95.0(9) %, when the model is trained on simulated data with all relevant noises added [2]. The best performance was achieved when sensor jumps, pink (1/f) noise, and white noise were varied together to yield a varied signal-to-noise ratio in the training dataset.

The noisy simulator allowed us also to develop a data quality control (DQC) module [2]. The utility of the DQC module was confirmed by showing a correlation between the accuracy of the state classifiers and the assessed quality. Specifically, for experimental data

assessed as “high quality” the state classifier has 96.4(9) % accuracy, for data assessed as “moderate quality” it has 91.9(2.1) % accuracy, and for “low quality” data the state classifier has 69.3(5.6) % accuracy, see Figure 81. This validates the ML DQC module as a tool to filter data that might lead to poor performance of an ML state classifier and, consequently, the tuner failure.

Another difficult to assess tuning failure mode is related to formation of the so-called *spurious* (or *unintended*) QDs that may form in small potential wells due to interface defects, surface roughness, or strain within the device. Spurious QD are highly undesirable since they may interfere with the QDs intended for use as qubits and cannot themselves be used as qubits. To avoid device tuning failure, spurious QDs must be identified when present and avoided. Visually, spurious QDs are recognized in large 2D scans as charge transitions with slopes diverging from a monotonic trend. As we show in [3], spurious dots can be identified automatically as transition lines with anomalous capacitive couplings relative to the transitions around them.

Figure 82(a) shows two charge stability diagrams: one capturing properly formed QD (left panel) and one capturing spurious QD (right panel). The small 2D regions in the plunger-plunger space, highlighted in these scans with the black boxes, are typical for topology setting algorithms [1]. In both cases, they are classified by a state classifier model as double QD state – a success from ML perspective. However, when looked at within a slightly larger voltage range, it is clear that in the latter case, the small scan captures an anti-crossing with a spurious QD, which for practical tuning purposes is a failure.

Our algorithm combines a pixel classifier, used to extract the high-level features from experimental data, as shown in Figure 82(b), with traditional fitting used to extract the slopes of the consecutive charge transitions which are manifestations of the capacitive coupling between the QDs, see Figure 82(c). For properly formed QD, as shown in the left panel in Figure 82(a), the magnitude of the capacitive coupling is expected to increase

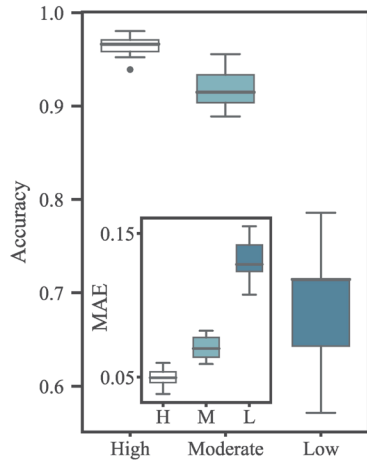


Figure 81. Box plots of model accuracy for each assigned quality class for the experimental data. Inset: box plots of the mean absolute error (MAE) for each quality class. Adapted from [2].

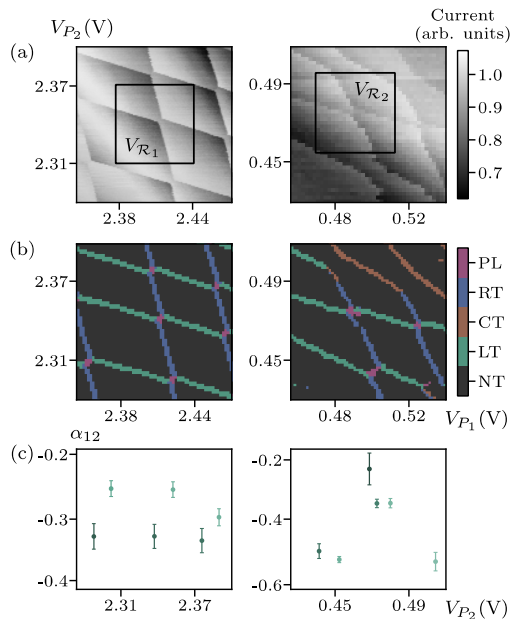


Figure 82. Spurious dot detections. (a) Two charge stability diagrams: one capturing properly formed QD (left) and one capturing spurious QD (right). The black boxes highlight small 2D scans typical of the auto-tuning approaches [1]. (b) Pixel classification results for charge stability diagrams shown in (a). (c) Plots of fitting results used to determine whether a spurious QD is present. Adapted from [3].

monotonically while the spacing between consecutive transition lines decreases as a charge is added, as shown in the left panel in Figure 82(c). The different shades of green are used to depict separate groups of transitions, i.e., transitions captured between the blue RT lines. On the contrary, a spurious QD, as shown in the right panel in Figure 82(a), can manifest itself by a non-monotonic behavior of the capacitive coupling between transitions. This is depicted graphically by either the most left or the center point (or group of points) not following the expected decreasing trend in the right panel in Figure

82(c). In practical applications, the automated detection of spurious QD fits nicely within the autotuning paradigm.

With these tools, we expand the applicability of ML-based autotuning strategies to non-ideal devices by making the ML models more robust against potential failure modes. This is especially important when considering future, large-scale QD devices. More broadly, we show that making simulated data more physical can greatly improve the efficacy of ML models when deployed in a real lab environment, which may be a useful insight for other experiments combining ML and physics.

- [1] J. P. Zwolak and J. M. Taylor. Colloquium: Advances in Automation of Quantum Dot Devices Control. *Reviews of Modern Physics* **95** (2023), 011006.
- [2] J. Ziegler, T. McJunkin, E. S. Joseph, S. S. Kalantre, B. Harpt, D. E. Savage, M. G. Lagally, M. A. Eriksson, J. M. Taylor, and J. P. Zwolak. Toward Robust Autotuning of Noisy Quantum Dot Devices. *Physical Review Applied* **17** (2022), 024069.
- [3] J. Ziegler, F. Luthi, M. Ramsey, F. Borjans, G. Zheng, J. P. Zwolak. Automated Extraction of Capacitive Coupling for Quantum Dot Systems. *Physical Review Applied* **19** (2023), 054077.

Tuning Arrays with Rays: Physics-informed Tuning of Quantum Dot Charge States

Justyna P. Zwolak
 Florian Luthi (Intel Corporation)
 Mick Ramsey (Intel Corporation)
 Joshua Ziegler (Intel Corporation)

Gate-defined quantum dots (QDs), formed by trapping electrons using finely calibrated electric gates, are a promising quantum computing platform. Unfortunately, working with single electrons means that the operating regime strongly depends on nanoscale details (e.g., material impurities and fabrication defects) that are difficult to control across devices. For QD devices to scale effectively, this operating regime must be identified using automated methods. There have been several recent demonstrations of automation of QD tuning, yet these approaches have only taken limited advantage of the designed effect of the electric gates on the device state [1]. Recently, we have developed an intuitive, reliable, and data-efficient modular autotuning procedure for automated global state and charge tuning in a framework termed physics-informed tuning (PIT) [2], depicted in Figure 83.

In QD devices with the overlapping gates architecture—the type of device we have mostly been focusing on—there are two types of electric gates used to control

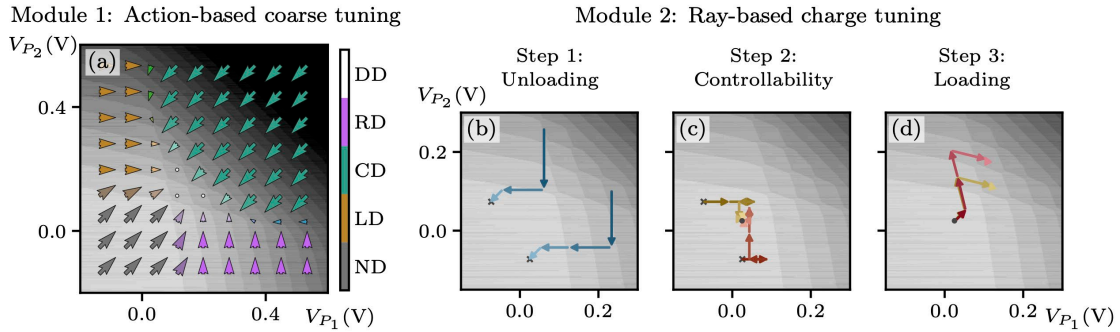


Figure 83. The flow of the physics-informed tuning (PIT) algorithm visualized using a simulated double-QD device. (a) The action-based coarse tuning module combines ML state predictions with the overall QD state topology to navigate the plunger-plunger gate space. The orientation and size of the arrows overlaying the scan correspond to the suggested gate voltage adjustment direction and magnitude, respectively. The expected outcome for the coarse-tuning module is a gate voltage configuration defining a double-QD state. (b)-(d) The ray-based charge tuning module. The charge tuning process involves three steps: (b) unloading the double QD of all electrons using the physical gates space with the termination point marked with an x ; (c) tuning to a region near the first charge transitions for both QDs (marked with a dot) and determining virtual gates; (d) loading the desired number of electrons on each QD using the virtual gate space. Panels (b)-(d) show charge tuning paths for two sample points, with the magnitude of the arrows representing the size of the consecutive steps and the color lightness indicating the progress of the unloading process. Reproduced from [2].

the flow of electrons. The plunger gates serve to create potential wells that can hold electrons. The barrier gates prevent the flow of electrons between trapping potentials or into the leads. Together, these gates serve to create an electrical potential landscape in which electrons can be trapped and manipulated. Typically, in heuristic tuning procedures, coarse voltage values for barriers and plungers that cut off electron flow are identified during the so-called “cold-start” stage [1]. These voltages are then used as a starting point for scanning pairs of plungers over a large range of voltages to identify the target regime where single electrons are trapped in each potential well.

In our previous work, we have tackled tuning of pairs of gates using algorithms that seek to maximize a fitness function designed to quantify the difference between the target and the captured state of the device. However, the optimization algorithms we relied on did not consider information about the pre-existing relationship between the states which led to repeated failures for tuning initialized far from the target area in voltage space [3, 4]. The several algorithms for navigating to specific charge states that have been demonstrated recently also show unsatisfactory performance [5-7].

To improve the effectiveness and efficiency of automatically setting the device topology as well as tuning to a desired charge configuration, PIT leverages the intended effect of each gate on the overall QD device state. In principle, changing voltages on a particular plunger gate should lead to a change of the electron occupation only in the corresponding potential well. We show that such targeted control (made possible by the virtue of virtual gates) combined with the knowledge of the expected device topology (i.e., relative position of states in the plunger-plunger space) and a machine learning (ML) model trained to identify the captured state of the

QD device, enable meaningful, efficient, and direct navigation to a target region in voltage space over a large range of voltages.

The first module of PIT, shown in Figure 83(a), is an *action-based tuning* algorithm that combines a ML classifier with physics knowledge to navigate to a target global state. The module is quite robust against noise, with an overall performance of 94.6(2.9) % when using ray-based measurements and 98.9(2.1) % when tuning with small two-dimensional (2D) scans for tuning to a double-QD (DD) state. When tested off-line using experimentally acquired large 2D scans, the success rate for the action-based coarse tuning is 97.1(3.5) % for a set consisting of seven scans from the QFlow 2.0 dataset [8] (exp-1) 92.5(6.5) % for a set consisting of 16 scans acquired using two double-QD configurations on two different three-QD $\text{Si}_x/\text{SiGe}_{1-x}$ devices fabricated on an industrial 300 mm process line (exp-2), see Figure 84.

Since local device measurements only contain information about changes in the electron occupation of each potential well, navigation to a specific charge occupation requires a more nuanced approach. We tackle this problem by following the typical procedure of first emptying a QD device of electrons and then loading a desired number back into each potential well. To achieve this most reliably, prior to the reloading stage, we calibrate the capacitive coupling of each gate to the potential wells using a virtualization method that combines ML with traditional fitting to derive the orthogonalization matrix [9]. The charge tuning module uses a series of one-dimensional (1D) measurements and a conventional peak finding algorithms to detect transitions in the 1D scans as electrons are loaded off and back onto each potential well. It proceeds in three steps to tune to a target charge state by first emptying the QDs of charge, followed by calibrating capacitive couplings

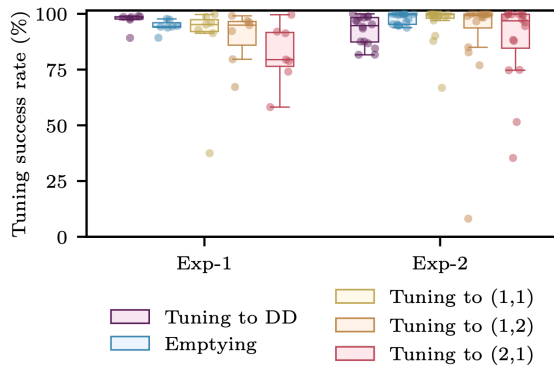


Figure 84. A box plot showing the off-line performance of the individual components of PIT with three target charge-state configurations. The central lines indicate medians for each test and the central box represents 50 % of the data. The whiskers extend to either the extreme values or 1.5x the interquartile range, whichever is closer to the median. The individual points on top of each box plot show the success rates for each device. Reproduced from [2].

and then navigating to the target charge state, see Figure 83(b-d). Tests of the charge tuning algorithm on simulated data show a success rate of 95.5(5.4) % for navigating from any point within the double QD region (the outcome of the action-based tuning step) to the single-electron regime in moderately noisy simulated scans, and is only slightly worse for off-line experimental tests, with an average of 89.7(17.4) % (median 97.5 %), see Figure 84.

In all tests, PIT terminates at most two transitions away from the target state. The main factor affecting the charge tuning success rates is either missing a transition or identifying noise as transitions when loading charges. One way to overcome this limitation is to develop a DQC module for the ray-based measurements analogous to the one used for the 2D scans during coarse tuning. Another way to boost the performance is to implement a “repeated measurement with voting” strategy.

PIT combines modern computer vision, ML, and data processing techniques with human heuristics to provide an intuitive, efficient, and reliable tool for QD device calibration. Moreover, the significantly reduced 1D data acquisition requirements combined with simplified data analysis techniques make PIT well suited for implementation with dedicated hardware closely integrated with the QD chip. It is thus a major step toward fully automated and scalable tuning of QD devices, a prerequisite to use QD-based quantum computers.

- [1] J. P. Zwolak and J. M. Taylor. *Colloquium: Advances in Automation of Quantum Dot Devices Control*. *Reviews of Modern Physics* **95** (2023), 011006.
- [2] J. Ziegler, F. Luthi, M. Ramsey, F. Borjans, G. Zheng, J. P. Zwolak. Tuning Arrays with Rays: Physics-informed Tuning of Quantum Dot Charge States. *Physical Review Applied* **20** (2023), 034067.
- [3] J. P. Zwolak, T. McJunkin, S. S. Kalantre, J. P. Dodson, E. R. MacQuarrie, D. E. Savage, M. G. Lagally, S. N.

Coppersmith, M. A. Eriksson, and J. M. Taylor. Autotuning of Double-Dot Devices In Situ with Machine Learning. *Physical Review Applied* **13** (2020), 034075.

- [4] J. P. Zwolak, T. McJunkin, S. S. Kalantre, S. F. Neyens, E. R. MacQuarrie, M. A. Eriksson, and J. M. Taylor. Ray-Based Framework for State Identification in Quantum Dot Devices. *PRX Quantum* **2** (2021), 020335.
- [5] R. Durrer, B. Kratochwil, J.V. Koski, A.J. Landig, C. Reichl, W. Wegscheider, T. Ihn, and E. Greplva. Automated Tuning of Double Quantum Dots into Specific Charge States Using Neural Networks. *Physical Review Applied* **13** (2020), 054019.
- [6] S. Czischek, V. Yon, M. Genest, M. Roux, S. Rochette, J. Camirand Lemyre, M. Moras, M. Pioro-Ladrière, D. Drouin, Y. Beilliard, and R. Melko. Miniaturizing Neural Networks for Charge State Autotuning in Quantum Dots. *Machine Learning: Science and Technology* **3** (2021), 015001.
- [7] M. Lapointe-Major, O. Germain, J. Camirand Lemyre, D. Lachance-Quirion, S. Rochette, F. Camirand Lemyre, and M. Pioro-Ladrière. Algorithm for Automated Tuning of a Quantum Dot into the Single-electron Regime. *Physical Review B* **102** (2020), 085301.
- [8] J. P. Zwolak, J. Ziegler, S. S. Kalantre, and J. M. Taylor. QFlow 2.0: Quantum dot data for machine learning, NIST, 2022. DOI: [10.18434/T4/1423788](https://doi.org/10.18434/T4/1423788)
- [9] J. Ziegler, F. Luthi, M. Ramsey, F. Borjans, G. Zheng, and J. P. Zwolak. Automated Extraction of Capacitive Coupling for Quantum Dot Systems. *Physical Review Applied* **19** (2023), 054077.

Principled State Identification for Quantum Dot Data

Justyna P. Zwolak

Brian J. Weber (*Intelligent Geometries, LLC*)

Confining electrons in arrays of semiconductor nanostructures, called quantum dots (QDs), is a promising approach to quantum computing. Due to the ease of control of the relevant parameters, fast measurement of the spin and charge states, relatively long coherence times, and their potential for scalability, QDs are gaining popularity as building blocks for solid-state quantum devices. However, the relevant parameter space scales exponentially with QD number (dimensionality), making heuristic control unfeasible. In semiconductor quantum computing, devices now have tens of individual electrostatic and dynamical gate voltages that must be carefully set to isolate the system to the single electron regime and to realize good qubit performance.

There has been recent work using machine learning (ML) techniques as part of the automation process [1]. However, training ML models requires large amounts of labeled data indicating the true state of the device for a given voltage range. So far, ML efforts for QDs rely on

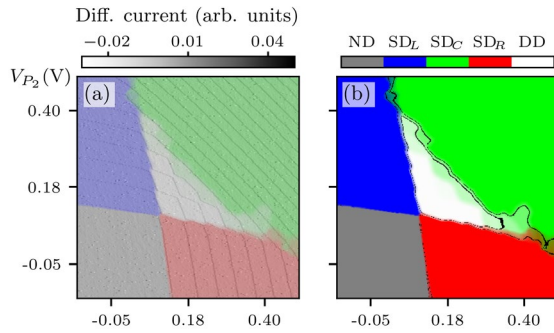


Figure 86. (a) A probabilistic domain decomposition for a sample noisy simulated device overlaying the charge sensor data. (b) Regions with confidence in the dominant label of at least 70%. Reproduced from [5].

datasets that come either from simulations (and thus may lack some important features representing real-world noise and imperfections) or are labeled manually (and thus are subject to qualitative or erroneous classification). Automatic labeling will streamline creation of large, accurate datasets for purposes of ML training. The ML approach also currently lacks explainable and interpretable features for reliable diagnostics. It is thus desirable to have a simplified and theoretically justified automated protocol for labelling experimental data.

The configuration space of a QD array supports irregular polytope tiling of the space, with each polytope indicating a distinct quantum state (e.g., a left or right single QD for a double QD device). The polytope shapes provide information about electron behavior within the discrete states they represent. Polytopes with similar characteristics will cluster together, allowing the subdivision of configuration space into distinct *domains* where the system exhibits a consistent behavior.

Our work is aimed at creating automatic procedures for identifying this domain decomposition and, if possible, automatically characterizing individual polytopes within each domain. The project currently focuses on the case of double QD devices, where the polygonal tessellation is readily understandable. In the past, we have successfully implemented the ray-based domain classification (RBC) schema, the theory behind which was developed in an earlier series of papers from our group [2, 3]. Building on this previous success, we are now developing RBC-based domain decomposition methods for experimentally acquired large two-dimensional (2D) charge stability diagrams of double QD devices; see the left panel in Figure 86 for an example of such measurement. In this approach, we create a selection of *observation points* (OPs) using a simple centralization

technique. From each OP we create a *fingerprint*, which is a list of distances along a set of evenly spaced rays from the OP to the nearest transition boundary along that ray. From each fingerprint we create a polygon model, an idealized representation of the charge region the OP lies within.

From theory, we know these polygons should cluster together by type into well-defined domains—hexagons, colored white in the left panel in Figure 86, should represent double-QD states. However, due to inherent noisiness in the measurements, many of these idealized models can be wrong. This means we cannot create a domain decomposition by individually classifying each polygon.

To overcome such limitations and facilitate the systematic processing of large volumes of experimentally acquired 2D charge stability diagrams, we have been developing tools for automated and unbiased analysis and labeling – *the QD auto-annotator* – that will streamline the creation of the QD data database for purposes of ML. The QD auto-annotator is a noise-robust automatic procedure for domain decomposition and characterization of individual polytopes within each domain. It leverages statistical methods for groupings of systematically similar polygons to create the desired domain divisions and the principles of geometry to produce state labels for simulated and experimental double-QD charge stability diagrams. The exact locations where one domain transitions to another are also statistically determined. This is the reason for the “fuzziness” along domain boundaries in the right panel in Figure 86. Moreover, each point receives a probability of being in each of the five domains, which allows for definition of label confidence.

The fingerprinting method, developed in dimension two, is well suited to higher dimensional generalizations, where no serious theoretical barrier exists to using our methods of model-building followed by statistical grouping. Technical hurdles exist in the form of understanding details of high-dimensional geometry, such as ray placement and polytope recognition. Preliminary work on this in the form of creating ray-placement estimates and rough polytope classifications has been completed [2, 4].

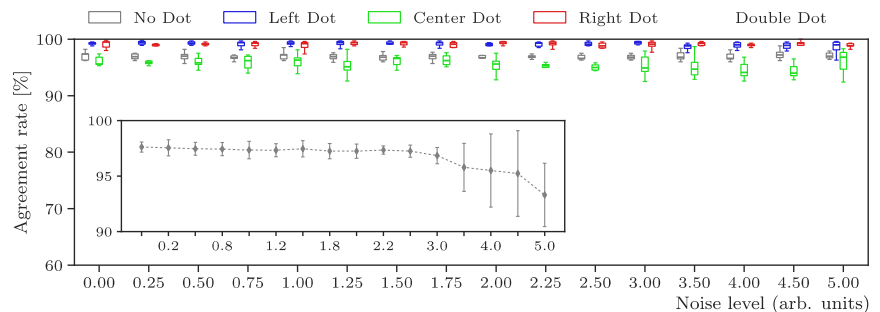


Figure 85. The performance of the QD auto-annotator on a per-domain basis for different noise levels for the 7 simulated devices. The inset shows an overall performance across all domains and all devices for each noise level. Reproduced from [5].

An important aspect of developing automated data labeling software is determining the robustness of the method across various noise regimes. Using the ground truth labels assigned at a pixel level during simulations and the QD auto-annotator labels we can quantify both the overall per-device agreement between labels as well as the per-class performance [5]. We observe an overall state assignment agreement at around 97 % when averaged over all devices for noise levels up to 3.00; see the inset in Figure 85. Once the noise level surpasses 3.00, the agreement deteriorates slightly to 95.6(3.3) % at noise level 4.00 and 93.3(2.8) % at noise level 5.00. On a per-domain level the performance is defined as the proportion of correct pixel assignments to the total number of pixels in each of the five domain regions, as determined by the ground truth labels. Figure 85 shows the performance of the QD auto-annotator on a per-domain basis for each noise level for the simulated devices we considered. The ND, SD_L, and SD_R state identifications remain almost perfectly robust up to the highest considered noise level. The center dot (CD) state shows a slight decay in performance at higher noise levels (at around noise level 3.00).

However, no substitute exists for real-world data. Although our methods work against the simulated datasets, relatively few experimental datasets are available. A major project goal is to collect datasets from many research teams around the world to establish a repository of datasets along with standardized labeling created using our methods hosted at data.nist.gov. Such a standardized repository of labelled data is consistent with the mission of NIST and would be of high value to the scientific community.

Another focus of future work is generalizing our methods to higher dimensions, with an aim of creating autotuning strategies for more than two QD at a time. Although theoretically straightforward, new challenges are expected related to high run-time expense and sparsity of available data. Theoretical understanding of higher-dimensional geometry will be a crucial component of this work.

- [1] J. P. Zwolak and J. M. Taylor. *Colloquium: Advances in Automation of Quantum Dot Devices Control*. *Reviews of Modern Physics* **95** (2023), 011006.
- [2] J. P. Zwolak, S. S. Kalantre, T. McJunkin, B. J. Weber, and J. M. Taylor. Ray-based Classification Framework for High-Dimensional Data. In *Third Workshop on Machine Learning and the Physical Sciences (MLAPS @ NeurIPS 2020)*, Vancouver, Canada, December 11, 2020.
- [3] J. P. Zwolak, T. McJunkin, S. S. Kalantre, S. F. Neyens, E. R. MacQuarrie, M. A. Eriksson, and J. M. Taylor. Ray-based Framework for State Identification in Quantum Dot Devices. *PRX Quantum* **2:2** (2021), 020335.
- [4] B. J. Weber, S. S. Kalantre, T. McJunkin, J. M. Taylor, and J. P. Zwolak. Theoretical Bounds on Data Requirements for the Ray-based Classification. *SN Computer Science* **3:1** (2022), 57.

- [5] B. Weber and J. P. Zwolak. QDA²: A Principled Approach to Automatically Annotating Charge Stability Diagrams. arXiv:2312.11206, 2023.

Optimizing High-Fidelity Readout Using Reinforcement Learning Methods

Justyna P. Zwolak

Harry S. Chalfin (University of Maryland)

M. D. Stewart, Jr. (NIST PML)

Michael Gullans (NIST PML)

Quantum dot (QD) devices are a promising candidate to realize quantum computing platforms. In our work, we focus on silicon spin qubit systems, in which individual electrons can be isolated, manipulated, and measured in a spin readout process [1, 2]. The goal of this project is to develop software tools for automated tuning of high-fidelity readout and control of silicon spin qubits.

While we focus on the well-established case of the Elzerman readout [3], the resulting optimization blueprint will be easily adaptable to other measurement schemes. The Elzerman spin readout relies on coupling of the spin state of a charge state to a current state. The presence or absence of a current signal can then be interpreted as a spin-up or spin-down measurement. However, as the readout becomes noisier, the corresponding fidelity begins to degrade. The chief aim of our work is redesigning the control circuit board to maximize the measurement fidelity. This requires us to also develop an efficient method to distinguish signal from noise in the readout phase. At present, we use a max-point method, predicting a spin-up electron if the maximum current signal during the readout phase is greater than a certain threshold and value, and predicting spin-down otherwise. In later phases of this project, we will incorporate machine-learning (ML) methods and physics-informed heuristics to build a model for automated readout analysis.

To redesign the circuit board, we use reinforcement learning (RL) methods. In the RL paradigm, the algorithm (called an *agent*) is learning the properties of a dynamical system (called an *environment*) by interacting with it through a series of *actions* and *rewards* that depend on the *state* of the environment changed in response to a given action. Our goal is to build a RL environment to study how the noise parameters caused by the control circuit affect the readout fidelity. Intuitively, one expects that fidelity is maximized when all noise parameters are minimized. However, in practice, it is not possible to fully eliminate the noise. Moreover, the hardware noise contribution at the individual circuit component-level to the overall fidelity as well as the correlation between the noise coming from the various

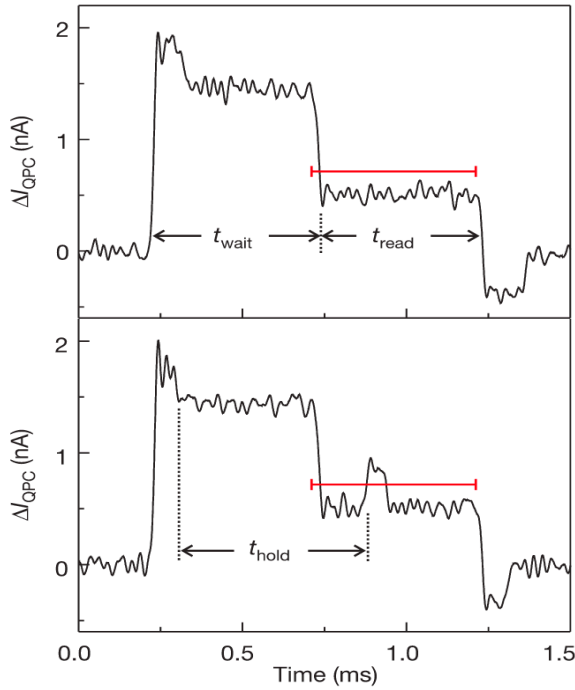


Figure 87. Sample spin readout signals for spin-down (above) and spin-up (below). The measurement depends on whether the current signal crosses a certain threshold value during the readout phase. Reproduced from [2].

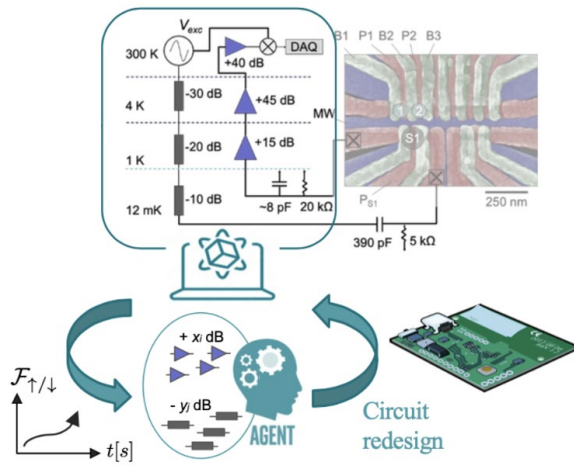


Figure 88. In the proposed framework, an AI agent proposes adjustments to the simulated circuit board and receives feedback based on the fidelity. By iteratively interacting with the, the agent learns how to optimize the circuit design.

components is yet to be quantified. Even the characterization of noise for the circuit components at cryogenic temperatures is an ongoing effort. Ultimately, we want to treat the circuit board setup as a RL environment, with states being defined as possible arrangements of the components and rearrangements defining unique actions; see Figure 88. The agent’s decision-making algorithm will then be tasked with determining the ideal

rearrangement of circuit components to maximizes the fidelity.

Currently, we focus on simulated current signals with controllable effects of Gaussian and $1/f$ noise. In our case, the environment is a two-dimensional (2D) lattice grid with coordinates defined by the Gaussian and $1/f$ noise parameters, the actions are adjustments of the noise levels, and the states are the resulting fidelities. The agent is a decision-making algorithm, guided by a neural network. Over the course of the training process, the agent learns by gradual adjustments to the weights and biases of the neural network. There are five possible actions: take one step in any of the four cardinal directions (corresponding to increasing or decreasing one of the two noises at the time) or “stand still.” Actions that would take the agent off the lattice are explicitly not allowed.

The model undergoes many training episodes, each of which begins with the agent in a random state in the environment and progresses by selecting actions at each time step according to rules that balance exploration of the environment with exploitation of the knowledge already gained. At the conclusion of each episode, the software simulates a large sample size of current signals with noise values determined by the final state. The fidelity of this sample is then calculated, and the agent earns a reward calculated through a monotonically increasing function of the fidelity. By giving the agent a reward only at the final step of each episode, the algorithm learns to prioritize long-term reward over short-term gains. Before the next training episode begins, the weights and biases of the neural network are gradually adjusted based on the newly updated memory of experiences. The neural network works by intaking the 2D coordinates of a state and outputting a score for each of the five actions, with the highest score corresponding to the model’s predicted best action for that state.

Over the course of many training episodes, the agent gradually learns the ideal strategy. An action map showing an example of a learned strategy is depicted in Figure 89. In this case, the best identified strategy is to move either leftward (blue arrow) or downward (purple arrow) at every lattice point, until it reaches the bottom left corner, where it should stand still (red dot). This comes as no surprise, as it is the fastest and simplest way to reach the ideal state, in which both noise values are minimized.

To confirm that the learned strategy is successful we run simulations to measure the fidelity at each point on the grid. Figure 90 shows the resulting 2D heatmap. In the simple example we consider, it is possible to generate a full heatmap indicating the fidelity throughout the entire parameter space. However, in a general case, when the number of circuit components increases from 50 to 100, such exploration is not feasible.

The purpose of this exercise is to build a software foundation for solving increasingly more complicated

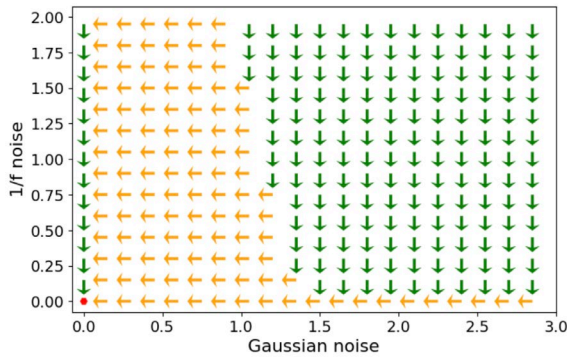


Figure 89. RL action map. At each step, the trained model recommends moving either leftward or downward until the agent reaches the desired state in the bottom left corner, where both noise parameters are set to 0.

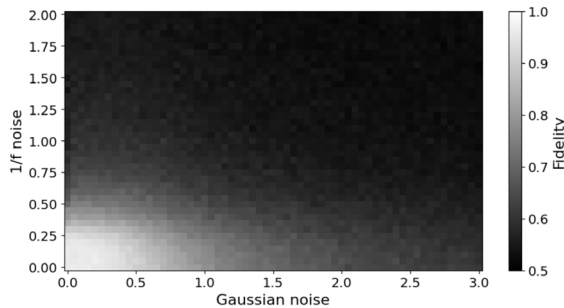


Figure 90. 2D fidelity heatmap. As expected, the fidelity is closest to 1.0 when both noise parameters are close to 0.

simulated readout problems using RL in which the ideal fidelity-maximizing strategy is neither obvious nor practically solvable for researchers. Recently we have begun collaboration with the group led by Prof. Anthony Sigillito from the University of Pennsylvania to develop a realistic simulation of the circuit board that accounts for all relevant noise types at the level of individual components. Moving forward, we will generalize this RL model to gradually more complex simulated readout problems which will increasingly resemble the physical circuit board responsible for executing the readout process.

- [1] J. P. Zwolak and J. M. Taylor. *Colloquium: Advances in Automation of Quantum Dot Devices Control. Reviews of Modern Physics* **95** (2023), 011006.
- [2] A.R. Mills, C.R. Guinn, M.M. Feldman, A.J. Sigillito, M.J. Gullans, M.T. Rakher, J. Kerckhoff, C.A.C. Jackson, and J. R. Petta. High-fidelity State Preparation, Quantum Control, and Readout of an Isotopically Enriched Silicon Spin Qubit. *Physical Review Applied* **18** (2022).
- [3] J. M. Elzerman, R. Hanson, L. H. W. Van Beveren, B. Witkamp, L. M. K. Vandersypen, and L. P. Kouwenhoven. Single-shot Read-out of an Individual Electron Spin in a Quantum Dot. *Nature* **430** (2004), 431.

Data Generation for Machine-Learning Classification of Quantum Dot Devices

Donovan Buterakos (University of Maryland)

Justyna P. Zwolak

Jacob Taylor (NIST PML)

Quantum dot (QD) qubits are one of the most promising candidate platforms for realizing scalable quantum information technologies, due to their long coherence times, small physical size, and their integration with the current semiconductor industry. However, progress has been slow due in part to the difficulty and complexity of tuning quantum dot devices. To date, tuning procedures have involved making many measurements, manually assessing the measured data, adjusting experimental device parameters in response, and repeating this process until the device is in its proper regime of operation. This process is time-consuming, becoming exponentially more difficult with each additional quantum dot added to the device. Thus, finding and automating a scalable tuning procedure is essential to creating industrial devices [1].

In 2020, we have proposed using machine-learning (ML) classification algorithms as a way to quickly analyze measured data and determine regimes of operation without the need of manual inspection [2]. More recently, by using a clever method of measuring data along so-called *rays* (a collection of evenly distributed one-dimensional (1D) sweeps) expanding outward from a central point, we have drastically reduced the number of measurements required to do so [3]. We have had success using these methods to classify data from experimental double-dot systems [4] and are currently expanding these techniques to larger devices.

Training ML models require large amounts of labeled data; however, experimental data is expensive and time-consuming to measure, and in addition, data labeling must be done manually. Thus, instead of using experimental data for training the model, we use a physical simulation of the device to create training data. This gives us two advantages. Firstly, data can be generated much more easily using a simulation than by using experimental devices. Secondly, having access to all the parameters of the simulation allows the data to be procedurally labeled, eliminating the need for manual data labeling. Using simulated data to train the ML model raises the concern that the simulation may not precisely reflect the reality of experimental devices. However, for DD devices, ML models trained on simulated data performed exceptionally well when benchmarked against experimental data [4].

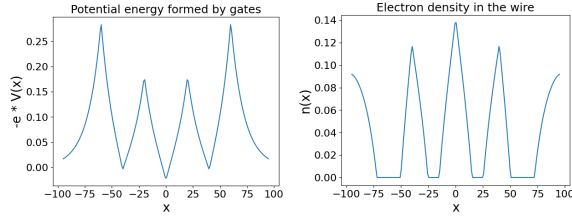


Figure 91. (Left) The potential energy $V(x)$ induced by electrostatic gates is input into the Thomas-Fermi calculation. (Right) The resulting electron density $n(x)$ is found by solving Eqn. (1) and (2).

Our simulation relies on a self-consistent Thomas-Fermi calculation [5] to solve the set of coupled integral equations for the electron density $n(x)$ of a (1D) nanowire

$$n(x) = \int_{-eV_{TF}(x)}^{\infty} \frac{g_0}{1+e^{\beta(\epsilon-E_F)}} d\epsilon \quad (1)$$

$$V_{TF}(x) = V(x) - \int n(x')K(x-x')dx' \quad (2)$$

where $V(x)$ is the potential induced by the electrostatic gates, $K(\Delta x)$ is the Coulomb potential, and $V_{TF}(x)$ is the so-called Thomas-Fermi potential, which is the total potential after including a correction from the electron density itself. After the electron density $n(x)$ is calculated (see Figure 91), we can determine the preferred number of electrons that inhabit each QD, which is roughly proportional to the area under $n(x)$.

The voltages of the plunger gates on each of the QDs are varied and the Thomas-Fermi calculation is repeated for each new set of voltages. The total charge on the device is then calculated, and the points are classified into one of 13 classes based on whether each QD is

empty, filled, or if two or more QDs have merged together, see Figure 92.

For training the ML model, points are uniformly selected from within the three-dimensional (3D) parameter space, and rays are extended outwards from each central point in multiple directions. For each point, the distance to the nearest transition line in each direction is recorded, along with the state of the central point. By averaging the inverse distance to the transition $\langle 1/\text{distance} \rangle$, we can quantify the defining features (so-called *fingerprints*) of each class. We plot fingerprints of the 13 classes in Figure 93. Crucially, fingerprints have distinct enough features from each other that a ML model can learn to distinguish between them.

We are currently using the data we generated to train deep neural network classifiers. Preliminary results tested against simulated data indicate that it is possible to train a model to characterize over 95 % of data points correctly. This can likely be improved with ongoing work.

The ability to procedurally classify the current operating regime of experimental devices can potentially save large amounts of time and expense when tuning the devices. Machine-learning classification is a substantial step towards fully automating the tuning process, which is essential for building scalable devices going forward.

- [1] J. P. Zwolak, J. M. Taylor, *et al.* Data Needs and Challenges of Quantum Dot Devices Automation: Workshop Report. arXiv:2312.14322, 2023.

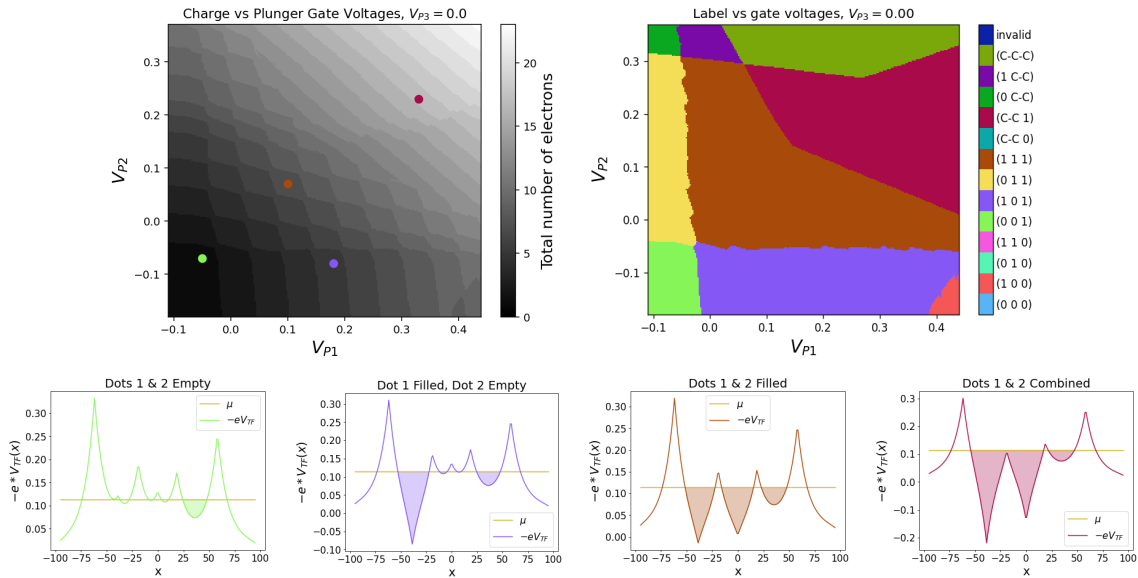


Figure 92. (Top Left) Charge stability diagram plotting the total charge on the device versus the plunger gate voltages on the first two QDs. The third plunger gate voltage is held constant, so this plot is a 2D slice of the full 3D space. (Top Right) State labels of the device for the same parameter space plotted on the left. There are 13 possible states, corresponding to whether each dot is empty (0), filled (1), or if multiple QDs are combined (C). (Bottom) Thomas Fermi potential $V_{TF}(x)$ for four different points marked on the top-left plot. They depict how QDs 1 and 2 can be empty, filled, or combined, corresponding to the state labels above.

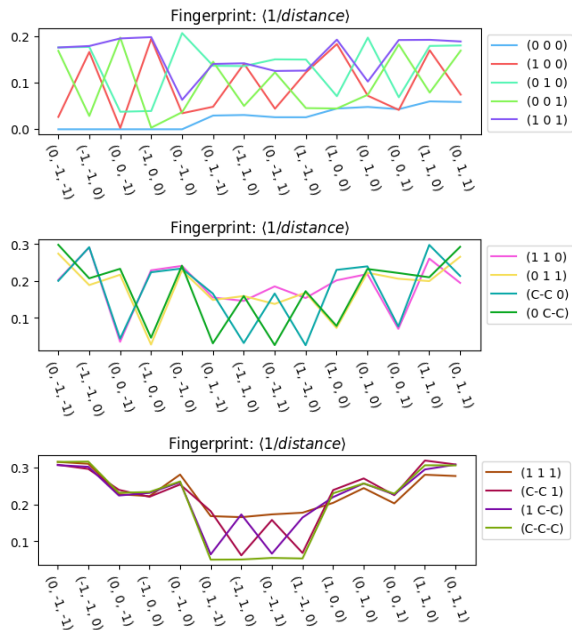


Figure 93. Fingerprints of the 13 classes, created by averaging $(1/\text{distance})$ over all points in a class.

- [2] J. P. Zwolak, T. McJunkin, *et al.* Autotuning of Double-Dot Devices in Situ with Machine Learning. *Physical Review Applied* **13** (2020), 034075.
- [3] J. P. Zwolak, T. McJunkin, S. S. Kalantre, S. F. Neyens, E. R. MacQuarrie, M. A. Eriksson, and J. M. Taylor. Ray-Based Framework for State Identification in Quantum Dot Devices. *PRX Quantum* **2** (2021), 020335.
- [4] J. Ziegler, F. Luthi, M. Ramsey, F. Borjans, G. Zheng, J. P. Zwolak. Tuning Arrays with Rays: Physics-Informed Tuning of Quantum Dot Charge States. *Physical Review Applied* **20** (2023), 034067.
- [5] J. P. Zwolak, S. S. Kalantre, X. Wu, S. Ragole, and J. M. Taylor. QFlow Lite Dataset: A Machine-learning Approach to the Charge States in Quantum Dot Experiments. *PLoS ONE* **13** (2018), e0205844.

Towards Robust Bootstrapping of Quantum Dot Devices

Justyna P. Zwolak

Danielle J. Middlebrooks

Anton Zubchenko (University of Copenhagen)

Torbjørn Raasø Rasmussen (Univ. of Copenhagen)

Anasua Chatterjee (University of Copenhagen)

Quantum computing is a type of computation whose operations can harness the phenomena of quantum mechanics performed on quantum computers. Most models of quantum computation are based on the quantum bit, or *qubit*, which is analogous to the bit in classical computation. One qubit realization is through

quantum dots (QDs). The tuning and management of QD qubits is a large and complex task. To properly form QDs, electrons have to be finely confined in a 3D space. This is achieved through tuning metallic gate electrodes producing electric fields that repel or attract electrons, see Figure 94. Tuning is typically done by human operators and requires hours of work. The more QDs (and gates) one tries to tune, the harder it is to tune them all simultaneously to get qubits that work together properly.

The tuning process is an essential yet repetitive step for initialization of QD-based qubits [1]. This process of tuning an unknown QD device can be divided into a sequence of distinct phases: bootstrapping, coarse tuning, charge state tuning, and fine tuning. Depending on the setup, an additional establishing controllability phase may be carried out after the charge state tuning phase to enable targeted gate control. In this work, we are focusing on the bootstrapping and coarse tuning steps specifically aimed at double QD (DQD) devices with charge sensing capabilities. DQDs host the singlet-triplet realization of qubits, which are currently being investigated as a possible quantum computing platform.

The tools used for automated tuning schemes vary from simple fittings to heuristic algorithms to traditional computer vision techniques. A host of machine learning (ML)-based techniques have also been utilized. Most of the tuning efforts are focused on the more advanced phases of tuning, assuming that the device is already pre-tuned, with a properly calibrated charge sensor, and that the safety regimes for all gates are already known. However, the initial bootstrapping phase of tuning is still nearly always done heuristically, requiring a highly trained researcher to be responsible for the subsequent decisions on how to adjust the relevant parameters.

We are currently developing an automated routine to bridge the gap between the initial device cool-down and a voltage configuration in which other, previously developed automation schemes can take over for a multiple QD device. One important step of the initial bootstrapping phase is to check which gates are functioning properly and which gates are not. To test this, decreasing voltage is applied to each gate, with the aim of confining the electron path and eventually cutting it off entirely, and current is measured through the device. By examining the plots of the voltage against the measured current, human experts determine whether the gate is working. We expect the plots to have a sigmoidal shape showing features related to the depletion of electrons under the metallic gate and in its vicinity. Instead of relying on human expertise for these decisions, we automate this process by applying a fitting procedure and extracting relevant features for classification and relevant voltages for subsequent tuning.

After learning gate-specific parameters, such as voltages at which current saturates and pinches off, the tuning routine proceeds to form a sensor dot that will serve as a detector of the electron transitions taking

place between the pair of quantum dots used to form a qubit. In general, forming a sensor dot is a time-consuming and labor-intensive task as it requires taking a multitude of two-dimensional scans and identification of the Coulomb blockade region by a trained specialist. Automation facilitates the ray-based detection of the oscillatory behavior, a critical aspect of the Coulomb blockade, thus significantly reducing the task's time complexity [2]. Automation provides an opportunity to quickly diagnose issues with the device, as well as fast retuning of the sensor. The formation of a high-quality sensor is a task of paramount importance for quantum computation, as it is essential for a fast qubit readout.

Recently, we have changed the measurement scheme to reflectometry (rf)-based charge sensing that allows the algorithm to see the very first electrons of each quantum dot, something that is typically not possible in current measurements. With the sensor in place, the protocol uses a neural network in conjunction with the previously mentioned gate-specific parameters to establish a double quantum dot region. This is achieved by algorithmic control of the plunger gates of each dot to adjust electron occupancy, as well as calibration of the barrier gate to regulate tunneling between the dots.

The result of this autotuning procedure provides a sufficient starting point for the wide-ranging set of tasks for control of QD qubits. With this approach, we can expand the applicability of automated tuning schemes to non-ideal devices by requiring little predetermined assumptions on the device. This is especially important when considering future, large-scale QD devices.

- [1] J. P. Zwolak and J. M. Taylor. *Colloquium: Advances in Automation of Quantum Dot Devices Control*. *Reviews of Modern Physics* **95** (2023), 011006.
- [2] J. P. Zwolak, T. McJunkin, S. S. Kalantre, S. F. Neyens, E. R. MacQuarrie, M. A. Eriksson, and J. M. Taylor. *Ray-Based Framework for State Identification in Quantum Dot Devices*. *PRX Quantum* **2** (2021), 020335.

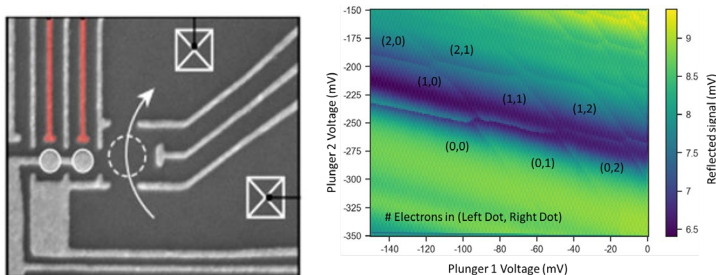


Figure 94. Device layout (left) and the double quantum dot (DQD) regime (right). The dashed circle represents the region where the sensor dot is formed. Due to its capacitive coupling to the double dot region (marked by two solid line circles), charge sensing can be performed by measuring current or reflected off the sensor dot rf-signal supplied at resonant frequency via the ohmics (represented by crossed squares). The plunger (colored) gates are used to control the quantity of electrons localized in the DQD.

FrEQuENT: A Framework Encoding for Quantum Dot Electronically Navigated Tuning

Justyna P. Zwolak

Danielle Middlebrooks

Daniel Schug (University of Maryland)

Tyler J. Kovach (University of Wisconsin-Madison)

Jared Benson (University of Wisconsin-Madison)

Patrick J. Walsh (University of Wisconsin-Madison)

Mark A. Eriksson (University of Wisconsin-Madison)

Different promising platforms have been developed to devise scalable qubits for quantum computing, each with corresponding advantages and disadvantages [1]. We focus on gate-defined quantum dots (QDs) with the overlapping gates architecture. One of the big challenges of this platform is the complexity required to control devices: there are many gates that need to be precisely configured. The SEM image in the bottom panel in Figure 95 demonstrates the problem. This quad-QD device has 29 connections for an up to 4-qubit architecture. This problem is not new, and many community members have been actively researching ways to automate various tasks relating to tune-up [2, 3]. In addition, a more global issue for almost all physical qubit platforms is connecting the abstract qubit to physical experimental devices losslessly at scale while removing scientists from the control loop [4].

We are currently developing intuitive, modular autotuning software for automating everything between a new QD device and abstract qubits in a framework deemed FrEQuENT [5]. The abstraction levels of the FrEQuENT software are depicted in Figure 95. Designed with scaling in mind, a single config sets up the entire software for an arbitrarily sized device.

Traditionally, scientists operate QD devices under manual control, a type of control that is inefficient in timeliness and scalability. We seek to change this. Manual control typically consists of a scientist sweeping the voltage applied on a gate to the connected sample, collecting the measured current data, and analyzing the data to extract parameters of interest. Usually, many sweeps are required, so there is a layer of abstraction between the scientists and the device to speed the process up. The abstraction we use here is the open-source QCoDeS.²⁶ Encapsulating all the scientists' functionality is our configurable Data Workers level, which replaces the need for traditional scientists to do the data handling and analysis for us.

²⁶ <https://github.com/QCoDeS/Qcodes>

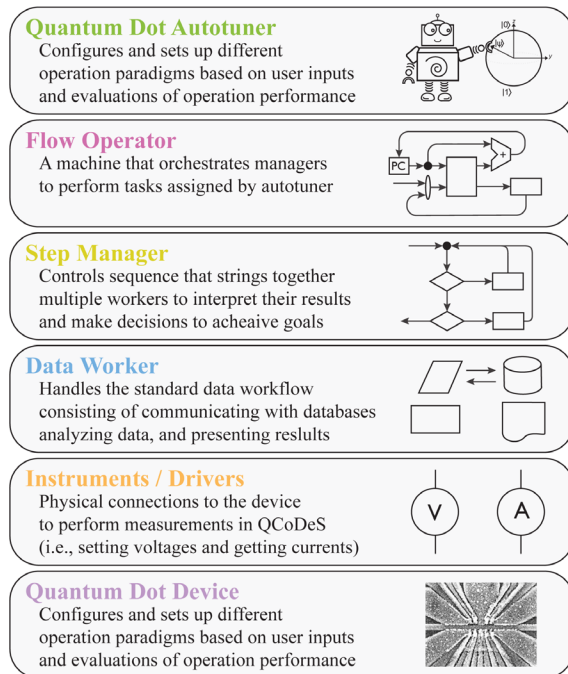


Figure 95. The abstraction levels of the FrEquENT software visualized as a top-down stack built on top of an experimental device. Cartoons are included at each abstraction level to indicate what behaviors are expected at each stage of the software. The SEM in the Quantum Dot Device section is of a quad-QD device with two charge sensors placed for readout above the main channel. This serves as an example as to what types of devices the software is being implemented for.

Following this is a decision on what to do next. Here, scientists check whether the measurement makes sense. If it does not make sense, they might decide to “tweak” a variable and try again, or they might quit and restart a particular measurement. If the measurement makes sense, maybe there is a closely related follow-up measurement to get to a parameter range of interest that should be measured next. Our Step Managers replace this functionality, as they are fully configurable to interact with Data Workers to achieve the scientific goal.

In practice, the entire measurement process is never straightforward in this fashion. Scientists sometimes need to reproduce previous measurements if they expect the device may have some changed characteristics. As a result, they loop back and recollect the missing data, repeating steps as needed. The design of our Flow Operators handles these operations as they can orchestrate the Step Managers and automatically loop back, recollecting missing data.

Finally, the highest level of abstraction allows to string together the high-level, complex sequences of instructions from the user to Flow Operators to autonomously drive the QD devices from start to finish. In the time frame of scientists, this would encompass weeks to months of work.

FrEquENT allows scientists to spend time where most needed, setting up devices with minimal involvement. It links between scientists and the bare metal QD gates to act as a tool, probing qubits and other abstract concepts. Once complete, this framework could extend beyond the bounds of traditional software and be reimplemented in hardware to reduce latency or placed on-chip to aid with scalable control. Because of this, its development leads towards fully automatic, scalable tuning of QD devices.

- [1] S. Resch, U. R. Karpuzcu. Quantum Computing: An Overview Across the System Stack. arXiv:1905.07240v3, 2019.
- [2] J. P. Zwolak and J. M. Taylor. *Colloquium: Advances in Automation of Quantum Dot Devices Control. Reviews of Modern Physics* **95** (2023), 011006.
- [3] J. P. Zwolak, T. McJunkin, S. S. Kalantre, J. P. Dodson, E. R. MacQuarrie, D. E. Savage, M. G. Lagally, S. N. Coppersmith, M. A. Eriksson, and J. M. Taylor. Autotuning of Double-Dot Devices In Situ with Machine Learning. *Physical Review Applied* **13** (2020), 034075.
- [4] L. M. K. Vandersypen, H. Bluhm, J. S. Clarke, *et al.* Interfacing Spin Qubits in Quantum Dots and Donors—Hot, Dense, and Coherent. *npj Quantum Information* **3** (2017), 34.
- [5] T. J. Kovach, D. Schug, M. A. Wolfe, P. Walsh, J. Benson, D. Middlebrooks, M. A. Eriksson, and J. P. Zwolak. FrEquENT: A Framework Encoding for Quantum Dot Electronically Navigated Tuning. In Preparation.

Machine Learning Applications in Laser Cooling and Trapping Atoms

Michael Doris (University of Maryland)

Justyna P. Zwolak

Ian Spielman (NIST PML)

Successful trapping and cooling of atoms requires the coordination of many pieces of equipment which must follow a specific sequence of events. A typical laser cooling and trapping sequence could be described by hundreds of parameters, which can make optimization attempts challenging and time-consuming. Even these parameters are constrained by the human-defined stages defining an experimental sequence; this strongly constrains the possible search space for optimization. Although many of these stages are guided by physical models, some of these require repeated trial and error and previous experience to find an optimum setup. A proposed solution to this is the use of machine learning (ML) to produce a compressed representation of experimental sequences that directly forms the parameter space to be optimized.

Currently, we are using neural networks (NN) to learn a representation of a typical cold atom sequence

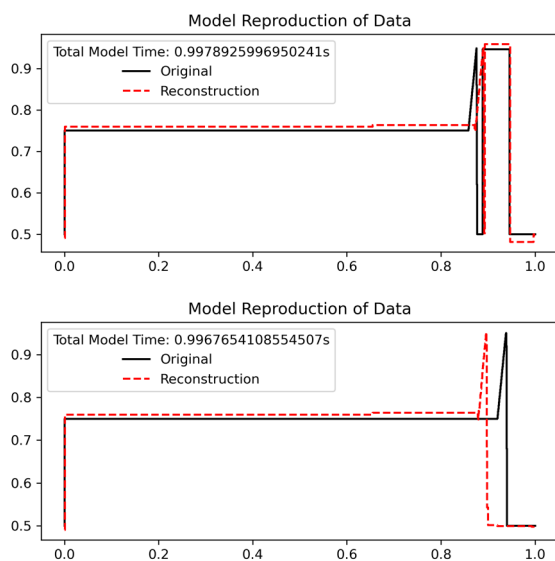


Figure 96. Output from the Transformer model of two command signals. The model can create variable length sequences that are easily converted into data the control software understands. The model gets close to the actual output voltages, but still occasionally commands inputs shifted in time. With further training the model could be taught to get the timing of its entries more correct.

and produce a latent space whose dimensionality is reduced. This is done by collecting the command signals sent to the devices that take part in a laser cooling and trapping sequence and training an ML model to reproduce them. Once a compressed representation is obtained, this space can be modified to produce slightly altered signals, which can be sent to our control software Labscript [1]. A basic interface has been written to integrate these models into Labscript and enable external optimizers to modify the compressed representation produced by these models. A typical optimization run would then involve capturing the command data from the equipment via Labscript after an experimental shot is completed, encoding this into a compressed representation, feeding this into an optimizer which will modify this latent space, decoding this space back into a valid control signal, and sending it back to Labscript to be used for the next experimental shot sequence. This would be repeated, and the optimizer would check for improvement in whatever metric was chosen.

So far, several ML model architectures and data processing techniques have been tested to reproduce a single command signal whose latent space can be modified and sent to Labscript. Initially, the most successful model was a fully connected encoder-decoder network with the data processed such that the original commands were interpolated into a continuous signal scaled between 0 and 1. This resulted in reproductions that followed the correct behavior but included noise in the output. More recently, we have successfully used a customized transformer architecture [2] and created a network that used the experiment shot data directly with

no interpolation. This model produced well-behaved latent spaces, which resulted in signal commands with less noise, but occasionally issued them shifted in time.

Now that we have models that can learn and reproduce single device signals, we are moving forward with model designs that will learn from all command signals in a single experimental shot sequence and reproduce multiple signals at once. These networks will produce our desired outcome, a compressed representation of entire shot sequences that result in trapped and cooled clouds of atoms, that external algorithms can use to optimize an experiment. Further integration into the Labscript Suite will also follow to streamline and automate the process.

- [1] P. T. Starkey, C. J. Billington, S. P. Johnstone, M. Jasperse, K. Helmerson, L. D. Turner, and R. P. Anderson. A Scripted Control System for Autonomous Hardware Timed Experiments. *Review of Scientific Instruments* **84** (2013), 085111.
- [2] A. Vaswani, N. Shazeer, N. Parmar, J. Uszkoreit, L. Jones, A. N. Gomez, L. Kaiser, and I. Polosukhin. Attention is All You Need. *Advances in Neural Information Processing Systems (NeurIPS)* **30** (2017).

Predicting the Temperature of an Atomic Cloud Using Machine Learning

Guilherme de Sousa (University of Maryland)
 Brady Egleston (University of Maryland)
 Justyna P. Zwolak
 Ian Spielman (NIST PML)

In the past decade, we witnessed the rapid growth of the machine learning (ML) community and its applications. Nowadays, there are numerous uses of ML algorithms and examples in day-to-day life and sciences.

Our work focuses on using ML models to learn the physical parameters of cold atom experiments: the cloud temperature and the number of atoms in the cloud. To estimate the temperature of the cloud, one typically makes a destructive measurement: the trapped atoms are released from the trap and imaged after a period of free expansion, giving access to the velocity distribution. It is desirable to obtain temperature without disturbing the atomic ensemble. Therefore, our goal is to estimate the temperature and atom number using only non-invasive fluorescence images. As a proof of concept, we trained several ML models with differing levels of complexity to predict the temperature and number of atoms using two fluorescence images taken at the same time in two different orientations (imaging the xy plane and yz plane).

The three ML models we consider are (1) a linear model, (2) a fully connected neural network (FNN)

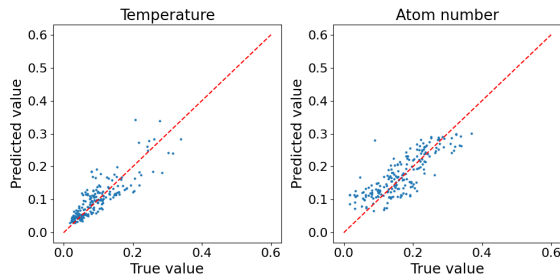


Figure 97. Preliminary results for predicting temperature and number of atoms using the CNN model. The axes are scaled to be normalized between zero and one, and the red dotted line represents the perfect prediction.

model, and (3) a convolution neural network (CNN) model. The simplest linear model is both the most straightforward to implement and the least precise. The FNN can learn the non-linear correlations when the dataset has enough spatial correlation between the fluorescence images. The more complex CNN model builds in translational invariance, which is desirable since the locations of the cloud in the image vary between measurements. The CNN is most accurate at predicting the temperature and number of atoms accurately as it learns how to measure size, position, orientation, and intensity and correlate those with the physical parameters. The typical error we observed with all models is 13 % to 20 %. The error of the CNN ranges from 4 % to 15 % for temperature and 16 % to 18 % for atom number depending on the specific dataset, see Figure 97.

ML models that rely only on non-invasive measurements can be implemented as part of experiments, allowing us to estimate parameters of interest (here, atom temperature and numbers) in real time and use that information to guide the evolution of the experiment. One immediate application of the ML models of this work is to use fluorescence images of the cloud to estimate temperature and check if the cooling techniques are being used efficiently during the evolution. An ML model can apply real-time feedback in the experiment. Using fast and non-invasive measurements, like the fluorescence image, one can estimate physical parameters that can be used to decide which next step to apply or correct and stabilize the system around a particular state. The typical evaluation time for all models is 0.03 ms to 0.07 ms, which is fast enough within the experimental timescale. A manuscript reporting this work is currently being prepared.

The final result of this project will deploy modern and state-of-the-art ML models and tools to speed up and increase the accuracy of cold atom experiments. Studying quantum phenomena in cold atom systems can also benefit from ML techniques, designed to learn complex patterns from output signals and images. Further

questions to be answered include an in-depth investigation of the prediction accuracy of the models for different stages of the BEC formation.

- [1] S. Das Sarma, D.L. Deng, and L.M. Duan. Machine Learning Meets Quantum Physics. *Physics Today* **72** (2019), 48–54.
- [2] A. L. Migdall, J. V. Prodan, W. D. Phillips, T. H. Bergeman, and H. J. Metcalf. First Observation of Magnetically Trapped Neutral Atoms. *Physical Review Letters* **54** (1985), 2596–2599.
- [3] S. Guo, A. R. Fritsch, C. Greenberg, I. B. Spielman, and J. P. Zwolak. Machine-learning Enhanced Dark Soliton Detection in Bose–Einstein Condensates. *Machine Learning: Science and Technology* **2** (2021), 035020.

Quantum Information

An emerging discipline at the intersection of physics and computer science, quantum information science is likely to revolutionize 21st century science and technology in the same way that lasers, electronics, and computers did in the 20th century. By encoding information into quantum states of matter, one can, in theory, enable phenomenal increases in information storage and processing capability. At the same time, such computers would threaten the public-key infrastructure that secures all of electronic commerce. Although many of the necessary physical manipulations of quantum states have been demonstrated experimentally, scaling these up to enable fully capable quantum computers remains a grand challenge. We engage in (a) theoretical studies to understand the power of quantum computing, (b) collaborative efforts with the multi-laboratory experimental quantum science program at NIST to characterize and benchmark specific physical realizations of quantum information processing, and (c) demonstration and assessment of technologies for quantum communication.

Quantum Information Science

Shawn Geller

Scott Glancy

Emanuel Knill

Alex Kwiatkowski

Tasshi Dennis (NIST PML)

Konrad Lehnert (NIST PML)

Sae Woo Nam (NIST PML)

Arik Agavayan (University of Colorado)

Akira Kyle (University of Colorado)

Curtis Rau (University of Colorado)

Akshay Seshadri (University of Colorado)

Lynden K. Shalm (University of Colorado)

Mohammad Alhejji (University of New Mexico)

Lucas Kocia (Sandia National Laboratory)

James R. van Meter (HRL Laboratories, Palo Alto)

Ezad Shojaee (IonQ)

Yanbao Zhang (Oak Ridge National Lab)

Quantum information science covers a broad range of research that involves the use of quantum physics to gain advantages for computation, communication and measurement. The advantages are based on a logical treatment of quantum systems to optimize their control and measurement. For this purpose, the quantum systems are often expressed in terms of elementary subsystems such as quantum bits (qubits) generalizing the familiar classical computational bits, and quantum modes (qumodes) that abstract quantum harmonic oscillators. These subsystems are then manipulated with quantum gates and related elementary and local control operations that generalize classical Boolean logic gates. One of the most visible results of this treatment is the development of simple few-qubit quantum computers by numerous institutions and companies, some of which are already available for testing on the internet.

Here we highlight some of ACMD's research on fundamental aspects of quantum information science. These include basic studies of

- quantum transduction for quantum networking,
- development of a broadband generalization of pulsed homodyne quadrature measurements,
- studies of rigorous confidence intervals for quantum measurements, and
- basic research on the ability of gravitational perturbation to create squeezed states of the electromagnetic field.

Quantum Transduction. Quantum communication between different quantum computers is best implemented with quantum information carried by optical photons. However, most quantum computers use stationary qubits and qumodes that do not readily exchange information with optical photons. As a result it is required to transduce the quantum computer's native quantum information to optical photons. ACMD researchers are participating in research on transducing quantum information between superconducting qubits and qumodes at microwave frequencies to optical photons. In this research the transduction requires an intermediary, such as a micromechanical system or a quantum dot (QD) coupled to a surface-acoustic-wave (SAW) cavity.

Previously, ACMD research delimited the tolerable loss and added noise for transduction with Gaussian processing [1]. Theoretical investigation of NIST's QD/SAW system revealed that one of the strategies considered for using this system would fail to produce usable entanglement, a prerequisite for transduction. However, a short-pulse strategy can produce entanglement at relevant rates with system parameters thought to be achievable in the near future. Current research involves optimizing short pulse strategies and interpreting results from experiments to characterize the quantum performance of the QD/SAW system.

Broadband Pulsed Quadrature Measurements. Conventional methods for measuring quadratures of the electromagnetic field use methods and detectors whose bandwidth is limited to a fraction of the center frequency of the quadrature. ACMD researchers are investigating

how to overcome this bandwidth limitation when measuring specific quadratures of octave-spanning pulses in the presence of an octave-spanning background. They realized that it is possible to replace the photon detectors or counters in conventional pulsed homodyne measurements of quadratures with calorimeters, such as those developed at NIST. Calorimeters can have high energy-efficiency over a broad band of frequencies. ACMD researchers determined how to shape the needed local oscillator (LO) and interpret the calorimeter readings to measure broadband quadratures. The measurement approaches an ideal quadrature measurement in the limit of large amplitude of the LO.

Recently, ACMD researchers developed the needed theory for determining the difference between the ideal quadrature measurement and the implemented one depending on the amplitude and the optical signal, finding readily evaluable bounds in terms of energy-related quantities of the optical signal being measured.

Confidence Intervals. For most quantum measurement scenarios, it is difficult to obtain guaranteed confidence intervals on quantities of interest, particularly when the significance levels needed are extremely high, such as when certifying the performance of quantum randomness generation. ACMD researchers have developed a powerful and flexible strategy for obtaining such confidence intervals even when the data is neither identically nor independently distributed [2]. They have further developed the theory and protocols by introducing estimation factors. Estimation factors broadly unify the previous approaches, and progress has been made in determining how to optimize estimation factors for estimating general functions of the mean of a multidimensional random variable.

Gravitational Squeezing. It is well known that free fields propagating on a gravitational background become “squeezed,” which means that the vacuum of the free field is not preserved, and energy density can become non-zero. To good approximation, the electromagnetic field behaves as a free field in the absence of charges. Since squeezing is an important and valuable resource for quantum information, ACMD researchers became interested in the question of when and how squeezing could be generated by local changes to the gravitational background. As expected, the effect is small. Nevertheless, as a toy example, they are quantitatively investigating the effect of a temporary, periodic in time and translation invariant change on the vacuum of the field. They have explicitly shown that such changes generically lead to exponential growth of the energy density and quantified the asymptotic growth. Work is ongoing to compare this to related analysis in the literature.

[1] A. Kwiatkowski, E. Shojaei, S. Agrawal, A. Kyle, C. L. Rau, S. Glancy, and E. Knill. Constraints on Gaussian Error Channels and Measurements for Quantum

Communication. *Physical Review A* **107** (2023), 042604. DOI: [10.1103/PhysRevA.107.042604](https://doi.org/10.1103/PhysRevA.107.042604)

[2] E. Knill, Y. Zhang, and P. Bierhorst. Generation of Quantum Randomness by Probability Estimation with Classical Side Information. *Physical Review Research* **2** (2020), 033465. DOI: [10.1103/PhysRevResearch.2.033465](https://doi.org/10.1103/PhysRevResearch.2.033465)

Quantum Characterization Theory and Applications

Victor V. Albert

Shawn Geller

Thomas Gerrits

Scott Glancy

Emanuel Knill

Alex Kwiatkowski

Yi-Kai Liu

Adam D. Brandt (NIST PML)

Alejandra L. Collopy (NIST PML)

Michael J. Gullans (NIST PML)

Adam M. Kaufman (NIST PML)

Dietrich Leibfried (NIST PML)

Daniel Slichter (NIST PML)

Jacob M. Taylor (NIST PML)

Andrew Wilson (NIST PML)

Arik Avagyan (University of Colorado)

Christaina M. Bowers (University of Colorado)

Daniel C. Cole (University of Colorado)

Riley Dawkins (Louisiana State University)

William J. Eckner (University of Colorado)

Stephen D. Erickson (University of Colorado)

Demetry Farfurnik (University of Maryland)

Srilekha Gandhari (University of Maryland)

Mohammad Hafezi (University of Maryland)

Pan-Yu Hou (University of Colorado)

Kaixin Huang (University of Maryland)

Hannah Knaack (University of Colorado)

Nathan Schine (University of Colorado)

Alireza Seif (University of Maryland)

Laurent J. Stephenson (University of Colorado)

Hilma Vasconcelos (Federal University of Ceará)

Jenny J. Wu (University of Colorado)

Aaron W. Young (University of Colorado)

Giorgio Zarantonello (University of Colorado)

Many emerging technologies already exploit or will exploit quantum mechanical effects to enhance metrology, computation, and communication. Developing these technologies requires improved methods to characterize the performance of quantum devices. This characterization requires solving statistical problems such as estimating an underlying quantum state, measurement, or process by using a collection of measurements made on the quantum system. Alternatively, one may also want to estimate figures-of-merit such as fidelity, error

rates, entanglement measures, or success measures for particular tasks. Accurate quantum characterization allows experimentalists and engineers to answer questions like “What is happening in my quantum experiment?” or “How well will my system perform some quantum information protocol?” and to characterize uncertainty in that answer.

Randomized benchmarking is a very popular method to measure the error rates of quantum logic gates. Sequences of random logic gates are applied, and one observes how the probability of obtaining the correct output qubit state decreases with increasing sequence length. ACMD researchers have studied how to choose the sequence lengths so that one can obtain the most precise estimate of the individual gate error rate in a limited wall clock time. They have also studied how randomizing every sequence produces more accurate error rate estimates than repeating the same random sequence. ACMD researchers collaborated with the NIST Ion Storage Group to demonstrate the improvements to randomized benchmarking with a trapped-ion qubit [1].

Solid-state qubits often suffer from noise that contains non-Markovian effects, which can be characterized using noise spectroscopy. ACMD researchers are developing random pulse sequences that can reveal different properties of the noise, compared to deterministic pulse sequences. These random pulse sequences can be used for real-time monitoring of the total noise strength, compressed sensing of sparse noise spectra, and parametric fitting of effective models of the environment. ACMD researchers have obtained several theoretical results and carried out numerical simulations for a quantum dot system, showing the feasibility of this approach [2].

To characterize nonlinear interactions between photons, such as those being developed for photon logic gates, ACMD researchers have developed a generalization of traditional homodyne detection. Traditional homodyne detection requires a strong reference beam and can only estimate the state in the mode matching the reference beam, but our generalization can use a weak reference beam (as required for some integrated circuit designs) and can learn about correlations between the signal mode and photons in nearby modes [3]. ACMD and PML researchers are designing an experiment to demonstrate this technique.

ACMD researchers have applied shadow tomography [4] to obtain new rigorous guarantees on well-established tomographic protocols for continuous-variable (CV) systems, such as optical fields or trapped ion motion. Shadow tomography is a novel randomized tomographic framework that is based on approximating a quantum state by succinct “snapshots” or “shadows” that can be easily extracted and stored on a classical computer. The framework comes with rigorously proven guarantees on the minimum number of such shadows required to achieve high accuracy with high probability.

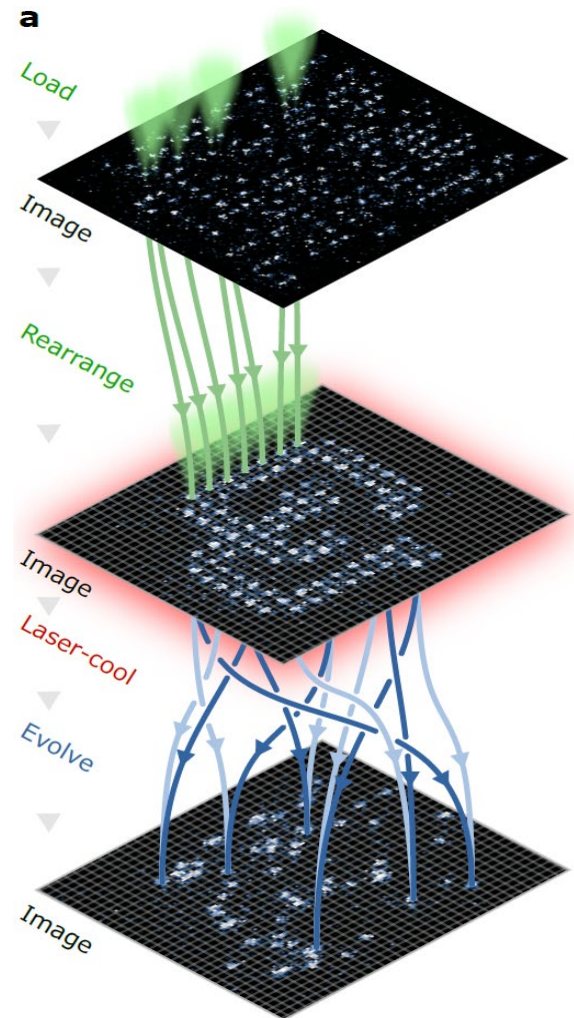


Figure 98. *Assembling Strontium atoms in an optical lattice boson sampler. States containing up to 180 atoms are prepared and measured on-demand in an optical lattice (grey grid) via site- and atom-resolved imaging (pictured images are single-shot experimental data), parallelized rearrangement with optical tweezers (green cones and trajectories), and high-fidelity laser cooling. The evolution of these atoms in the lattice is described by factorially many (in particle number) different interfering multiparticle trajectories (light and dark blue lines show two possible interfering trajectories for a subset of atoms but are for illustration purposes only).*

While this framework was originally designed for intrinsically multi-qubit systems, we show that certain experimentally relevant CV protocols, such as homodyne and photon-number-resolving tomography, can also be viewed through the lens of this framework. This yields useful guarantees that dictate how many measurement rounds of a protocol are required to reach a desired accuracy of state estimation. The required number of rounds for a multimode CV system scales polynomially with both the number of CV modes and the maximum occupation (e.g., photon) number of each mode. ACMD researchers have benchmarked their bounds against numerical simulation and experimental data from a

previous NIST optical homodyne experiment [5]. Details can be found in the preprint [6].

A basic resource state for continuous-variable quantum information processing is a low-temperature squeezed state. Such states are often prepared in optical modes or in the motion of trapped ions. ACMD researchers have developed a method to estimate the amount of squeezing, temperature, and other parameters of a multi-mode squeezed state from measurements of the number of photons or phonons in the state [7, 8]. They have applied this method to ion motion and temperature in past experiments where the ions were previously assumed to have temperature 0 K. They are designing a new trapped-ion experiment to demonstrate this method.

Some protocols for quantum information processing with trapped ions involve encoding and manipulating information using the ions' motion. Important goals are to transfer quanta from one oscillation mode to another and to show entanglement between oscillation modes. These capabilities were recently demonstrated at NIST with a three-ion, Beryllium-Magnesium-Beryllium crystal. ACMD researchers showed that the fidelity of the “beam splitter” operation that transfers quanta from one mode to another was at least 97.9 % with 84 % confidence. [9]

Researchers at JILA have an optical lattice atom trap, which consists of a lattice of cells, each of which may contain some number of Strontium atoms. See Figure 98. Single atoms can be loaded into any subset of the cells and allowed to hop from cell to cell as time evolves. If all atoms are indistinguishable, they behave as non-interacting bosons. Such “boson samplers” have computational powers beyond those of classical computers. ACMD researchers have characterized the performance of JILA's atomic boson sampler with up to 180 atoms distributed among ≈ 1000 cells. The atoms have indistinguishability of 99.5 %, and their behavior shows critical features of boson samplers [10].

- [1] A. Kwiatkowski, L. J. Stephenson, H. M. Knaack, A. L. Collopy, C. M. Bowers, D. Leibfried, D. H. Slichter, S. Glancy, E. Knill. Optimized Experiment Design and Analysis for Fully Randomized Benchmarking. Preprint: [arXiv:2312.15836](https://arxiv.org/abs/2312.15836)
- [2] K. Huang, A. Seif, D. Farfurnik, M. Hafezi and Y.-K. Liu. Random Pulse Sequences for Qubit Noise Spectroscopy. Preprint: [arXiv:2303.00909](https://arxiv.org/abs/2303.00909)
- [3] A. Avagyan, E. Knill, S. Glancy, and H. Vasconcelos. State Tomography with Photon Counting after a Beam Splitter. In preparation.
- [4] H.-Y. Huang, R. Kueng, and J. Preskill. Predicting Many Properties of a Quantum System from Very Few Measurements. *Nature Physics* **16** (2020), 1050. DOI: [10.1038/s41567-020-0932-7](https://doi.org/10.1038/s41567-020-0932-7)
- [5] T. Gerrits, S. Glancy, T. S. Clement, B. Calkins, A. E. Lita, A. J. Miller, A. L. Migdall, S. W. Nam, R. P. Mirin,

and E. Knill. Generation of Optical Coherent-state Superpositions by Number-resolved Photon Subtraction from the Squeezed Vacuum. *Physical Review A* **82** (2010), 031802. DOI: [10.1103/PhysRevA.82.031802](https://doi.org/10.1103/PhysRevA.82.031802)

- [6] S. Gandhari, V. V. Albert, T. Gerrits, J. M. Taylor, and M. J. Gullans. Precision Bounds on Continuous-Variable State Tomography using Classical Shadows. Preprint, [arXiv:2211.05149](https://arxiv.org/abs/2211.05149)
- [7] I. Bezerra, H. Vasconcelos, and S. Glancy. Quadrature Squeezing and Temperature Estimation from the Fock Distribution. *Quantum Information Processing* **21** (2022), 365. DOI: [10.1007/s11128-022-03677-5](https://doi.org/10.1007/s11128-022-03677-5)
- [8] A. Avagyan, E. Knill, and S. Glancy. Multi-Mode Gaussian State Analysis with Photon Counting. *Journal of Physics B: Atomic, Molecular and Optical Physics* **56** (2023), 145501. DOI: [10.1088/1361-6455/ace175](https://doi.org/10.1088/1361-6455/ace175)
- [9] P.-Y. Hou, J. J. Wu, S. D. Erickson, D. C. Cole, G. Zaran-tonello, A. D. Brandt, S. Geller, A. Kwiatkowski, S. Glancy, E. Knill, A. C. Wilson, D. H. Slichter, D. Leibfried. Coherent coupling and non-destructive measurement of trapped-ion mechanical oscillators. Preprint: [arXiv:2308.05158](https://arxiv.org/abs/2308.05158)
- [10] Aaron W. Young, Shawn Geller, William J. Eckner, Nathan Schine, Scott Glancy, Emanuel Knill, Adam M. Kaufman. An Atomic Boson Sampler. Preprint: [arXiv:2307.06936](https://arxiv.org/abs/2307.06936)

Tests of Quantum Computational Advantage

Yi-Kai Liu

Alexey Gorshkov (NIST PML)

Lucas T. Brady (NASA Ames Research Center)

Jacob Bringewatt (University of Maryland)

Andrew Childs (University of Maryland)

Dhruv Devulapalli (University of Maryland)

Luis Pedro Garcia-Pintos (University of Maryland)

Dominik Hangleiter (University of Maryland)

Alicia Kollar (University of Maryland)

Zhenning Liu (University of Maryland)

In recent years, there has been rapid progress in the development of experimental quantum information processors, leading to the first demonstrations of “quantum computational advantage,” where a quantum device solves a computational problem that would be difficult or intractable on a classical computer. However, these experimental quantum devices have significant limitations: they suffer from noise and errors, and they do not have enough qubits to perform fault-tolerant quantum computation. Such devices are sometimes called *noisy intermediate-scale quantum* (NISQ) devices.

Quantum computational advantage using NISQ devices can be difficult to study, because it is sometimes unclear whether a NISQ device has actually solved a hard computational problem correctly, due to the effects

of noise in the NISQ device, and the difficulty of reproducing the results using a classical computer. This has motivated the development of new methods for testing or verifying NISQ devices.

An interesting class of NISQ devices are so-called *analog* quantum devices, which can have large numbers of qubits, but have fewer degrees of control, compared to *digital* quantum computers. Analog quantum devices are easier to build than digital quantum computers, and they may be able to solve useful problems by performing adiabatic optimization, quantum annealing, and analog quantum simulation. But they cannot perform universal quantum computation or run quantum algorithms that are described by quantum circuits. They also cannot implement many of the methods that are used to verify the operation of digital quantum computers.

We are investigating two approaches to testing quantum computational advantage in analog quantum devices. One uses quantum speed limits, which upper-bound the speed at which a quantum system can evolve, in terms of mathematical properties of the Hamiltonian and the quantum state of the system [1]. These speed limits can potentially be used to rule out the possibility of a quantum computational advantage, when performing quantum annealing. Here the speed limits provide a converse to the adiabatic theorem: they say that the algorithm must fail if one runs it too fast. In addition, these speed limits can potentially be used for benchmarking analog quantum simulators, and for detecting the presence of noise and decoherence in these devices. This is because loss of coherence makes it harder for a system to perform a fast unitary time-evolution.

In our second approach, we consider a class of quantum computations that involve time evolution with a Hamiltonian consisting of Pauli $ZZ + Z$ terms, and measurements in the Pauli X basis. This class of quantum computations serves as the basis for several proposed experiments (put forward by other authors) to demonstrate quantum computational supremacy on analog quantum simulators. We develop a novel technique for verifying these kinds of experiments, by using a globally accessible control qubit to prepare the Feynman-Kitaev history state for this time evolution operator [2]. This allows efficient verification of the time-evolved state, and it produces a rigorous lower bound on the fidelity. This method has strengths and weaknesses: it only requires a constant number of samples, but it also requires trusted measurements.

- [1] L. P. García-Pintos, L. T. Brady, J. Bringewatt and Y.-K. Liu. Lower Bounds on Quantum Annealing Times. *Physical Review Letters* **130** (2023), 140601. DOI: [10.1103/PhysRevLett.130.140601](https://doi.org/10.1103/PhysRevLett.130.140601)
- [2] Z. Liu, D. Devulapalli, D. Hangleiter, Y.-K. Liu, A. Kollár, A. Gorshkov and A. Childs. Efficiently Verifiable Quantum Advantage on Near-Term Analog Quantum Simulators. In preparation.

Time-energy Uncertainty Relation for Noisy Quantum Metrology

Victor V. Albert

Jens Eisert (Freie Universität Berlin)

Philippe Faist (Freie Universität Berlin)

John Preskill (Caltech)

Joseph M. Renes (ETH Zurich)

Mischa P. Woods (ETH Zurich)

Quantum mechanics places fundamental limits on how well we can measure a physical quantity when using a quantum system as a probe. The most famous tradeoff is the Heisenberg uncertainty relation between the precision with which one can measure an object's position and momentum. The more precise the measurement of one of these "conjugate" variables, the less information one is able to extract about the other.

Another tradeoff often encountered in quantum error correction is the tradeoff between the effect of an observer and the uncontrolled environment on a quantum system. Typically, the less information the environment is able to extract from a quantum system, the more will be preserved for a later observer. One can think of the environment as a malevolent observer, whose clandestine probing of the system obscures the useful quantum information stored within the system. In this work [1], we introduce and study a fundamental trade-off which relates the amount by which noise reduces the accuracy of a quantum clock to the amount of information about the energy of the clock that leaks to the environment.

Specifically, we consider an idealized scenario in which a party, Alice, prepares an initial pure state of the clock, allows the clock to evolve for a time that is not precisely known, and then transmits the clock through a noisy channel to a party Bob. Meanwhile, the environment (Eve) receives any information about the clock that is lost during transmission. We prove that Bob's loss of quantum Fisher information about the elapsed time is equal to Eve's gain of quantum Fisher information about a complementary energy parameter. We also prove a similar, but more general, trade-off that applies when Bob and Eve wish to estimate the values of parameters associated with two non-commuting observables. We derive the necessary and sufficient conditions for the accuracy of the clock to be unaffected by the noise, which form a subset of the Knill-Laflamme error-correction conditions.

A state and its local time-evolution direction, if they satisfy these conditions, form a metrological error-correcting code. We provide a scheme to construct metrological codes in the stabilizer formalism. We show that there are metrological codes that cannot be written as a quantum error-correcting code in which the Hamiltonian acts as a logical operator, potentially offering new

schemes for constructing states that do not lose any sensitivity upon application of a noisy channel.

- [1] P. Faist, M. P. Woods, V. V. Albert, J. M. Renes, J. Eisert, and J. Preskill. Time-energy Uncertainty Relation for Noisy Quantum Metrology. *PRX Quantum* **4** (2023), 040336. DOI: [10.1103/PRXQuantum.4.040336](https://doi.org/10.1103/PRXQuantum.4.040336)

Taxonomy of Classical and Quantum Error-correcting Codes

Victor V. Albert

Philippe Faist (Freie Universität Berlin)

Michael L. Liu (Amherst College)

Nathanan Tantivasadakarn (Caltech)

Classical and quantum error correction lies at the intersection of computer science, engineering, physics, and mathematics. Classical coding theory has been around for over 70 years, yielding an enormous literature collection. Quantum error correction is more recent but arguably more diverse, encompassing subfields from solid-state physics to complexity theory. Collecting and accurately synthesizing such a hyper-field is as formidable as it is useful.

We have created and actively maintain the Error Correction Zoo²⁷ to categorize and organize known classical and quantum error-correction schemes. The work involved is taxonomic, i.e., collecting and processing literature as well as developing a classification scheme for the thousands of available classical and quantum error-correcting codes. This year, the zoo’s website enjoyed approximately 500 unique visitors per day, and there have been 92 external contributors so far.

Code entries form the primary content of the zoo. An entry can be a specific instance of a well-known code or a large family of codes, depending on community interest. The idea is to have a dedicated up-to-date webpage for each family, collecting original work, related protocols, and real-world implementations. Codes are organized into kingdoms by alphabet (or Hilbert space structure in the quantum case), with “parent” and “cousin” fields listing notable relations and connections. At the time of writing, there are 641 entries, split roughly even between classical and quantum error-correction codes.

This summer, three undergraduate students contributed to the zoo through the REU-CAAR program at the University of Maryland College Park. Discussing the state of the art of the field led one of the students to start a collaboration and complete a manuscript on previously overlooked properties of an important class of codes called subsystem CSS codes [1].

- [1] M. L. Liu, N. Tantivasadakarn, and V. V. Albert. Subsystem CSS Codes, a Tighter Stabilizer-to-CSS Mapping, and Goursat’s Lemma. Preprint [arXiv:2311.18003](https://arxiv.org/abs/2311.18003)

Bounds on Autonomous Quantum Error Correction

Victor V. Albert

Alexey V. Gorshkov (NIST PML)

Simon Lieu (Amazon AWS)

Yu-Jie Liu (Technical University of Munich)

Oles Shtanko (IBM)

Error correction is necessary to develop useful quantum computers and to communicate quantum information in robust fashion. Typically, one or more rounds of “active” error detection and correction are done in a discrete or stroboscopic fashion. The alternative approach of continuous or “passive” error correction [1] allows such rounds to be applied in continuous and autonomous fashion. Autonomous error correction is possible by carefully engineering the environment underlying a target quantum system.

Despite being relevant to several experimental platforms, not much is known about the true power of the autonomous approach. For a large class of many-body quantum codes, we show [2] that, to achieve error suppression comparable to conventional error correction, autonomous decoders generally require correction rates that grow with code size. For codes with a threshold, we show that it is possible to achieve faster-than-polynomial decay of the logical error rate with code size by using super-logarithmic scaling of the correction rate.

- [1] C. Ahn, A. C. Doherty, and A. J. Landahl. Continuous Quantum Error Correction via Quantum Feedback Control. *Physical Review A* **65** (2002), 042301.
- [2] O. Shtanko, Y.-J. Liu, S. Lieu, A. V. Gorshkov, and V. V. Albert. Bounds on Autonomous Quantum Error Correction. Preprint: [arXiv:2308.16233](https://arxiv.org/abs/2308.16233)

²⁷ <https://errorcorrectionzoo.org>

Realizing Phases of Quantum Matter with a Generalized Stabilizer Formalism

Victor V. Albert

David Aasen (Microsoft & UC Santa Barbara)

Jason Alicea (Caltech)

Christopher Feichsin (University of Maryland)

Wenjie Ji (UC Santa Barbara)

John Preskill (Caltech)

Nathanan Tantivasadakarn (Caltech)

Wenqing Xu (University of Maryland)

The Pauli stabilizer formalism [1] is the gold standard for defining and characterizing quantum error correcting codes, preparing entangled many-body states, understanding quantum circuits, and defining microscopic models that realize exotic and useful quantum phases of matter. While there has been progress in expanding the range of possible quantum phases realizable via this formalism, a broad swath of other phases remains unobtainable via a Pauli stabilizer description. As a result, such phases are very difficult to work with at the level of lattice models and, consequently, also out of range of most of today's digital quantum devices. Realizing such phases would bring us closer to fully topological quantum computation, which, in contrast to the many other available blueprints for a quantum computer, holds the promise of computation in an inherently robust fashion.

We attempt to bring exotic non-Pauli-stabilizer phases closer to realization by generalizing the Pauli stabilizer formalism. Our generalization is applicable to systems comprised of qudits valued in finite groups G , which, most famously, realize non-abelian gauge theories as well as quantum-double topological order — the first known model capable of fault-tolerant topological quantum computation with anyons. We construct and analyze two models defined on such spaces which are computationally powerful and conceptually rich: gapped edges of the quantum double [2] and the generalized cluster state [3].

We derive a standalone Ising-like model for a general quantum double edge and show that this model is a generalized version of a previously studied model called the flux ladder [4]. Armed with this model, we map out a web of connections for quantum double models, generalizing the existing web for the Kitaev surface code, the current primary blueprint for a quantum computer. We develop Jordan-Wigner-like mode operators that are directly related to anyonic ribbon operators of the quantum double model. We obtain a continuum description of the general flux ladder and recast a particular case in terms of fermions with the help of non-Abelian bosonization. We make connections to established electronic

systems, brightening the prospects of eventual realization of exotic quantum-double topological phases.

We also study the generalized cluster state on a group-valued Hilbert space [5], showing that it realizes symmetry-protected topological (SPT) order protected by a fusion category symmetry. We identify several signatures of SPT order: gapped edge modes, algebraic structure under stacking, and topological response. Each of these sections serves as a stage for developing tools for applying the generalized stabilizer formalism to the study of microscopic models. We also discuss the implementation of measurement-based quantum computation (MBQC) using the generalized cluster state, generalizing the MBQC formalism to qudits valued in non-Abelian groups.

- [1] D. Gottesman. Spin Chains, Stabilizer Codes and Quantum Error Correction. Preprint: [arXiv:quant-ph/9705052](https://arxiv.org/abs/quant-ph/9705052)
- [2] V. V. Albert, D. Aasen, W. Xu, W. Ji, J. Alicea, and J. Preskill. Spin Chains, Defects, and Quantum Wires for the Quantum-Double Edge. Preprint: [arXiv:2111.12096](https://arxiv.org/abs/2111.12096)
- [3] C. Feichsin, N. Tantivasadakarn, and V. V. Albert. Non-invertible Symmetry-protected Topological Order in a Group-based Cluster State. Preprint: [arXiv:2312.09272](https://arxiv.org/abs/2312.09272)
- [4] M. I. K. Munk, A. Rasmussen, and M. Burrelo. Dyonic Zero-energy Modes. *Physical Review B* **98** (2018), 245135. DOI: [10.1103/PhysRevB.98.245135](https://doi.org/10.1103/PhysRevB.98.245135)
- [5] C. G. Brell. Generalized Cluster States Based on Finite Groups. *New J. Phys.* **17** (2015), 023029. DOI: [10.1088/1367-2630/17/2/023029](https://doi.org/10.1088/1367-2630/17/2/023029)

New Frontiers in Molecular Quantum Information Processing

Victor V. Albert

Wesley C. Campbell (UCLA)

Eric R. Hudson (UCLA)

Eric Kubischta (University of Maryland)

Mikhail Lemeshko (IST Austria)

The size of a quantum system's state space provides a fundamental upper bound to the system's memory and processing capacity. Many of today's state-of-the-art quantum devices are built out of single atoms, whose state space consists of electronic and nuclear-spin degrees of freedom. Molecular systems offer additional continuous degrees of freedom corresponding to molecular rotations and vibrations.

Molecular state space was assumed to be mostly uncontrollable because of the inability to isolate a single molecular species in aggregate experiments. However, working off past successes in trapping single atomic ions (in part, spearheaded by NIST), experimental attempts at isolating and trapping single molecules are well under way [3].

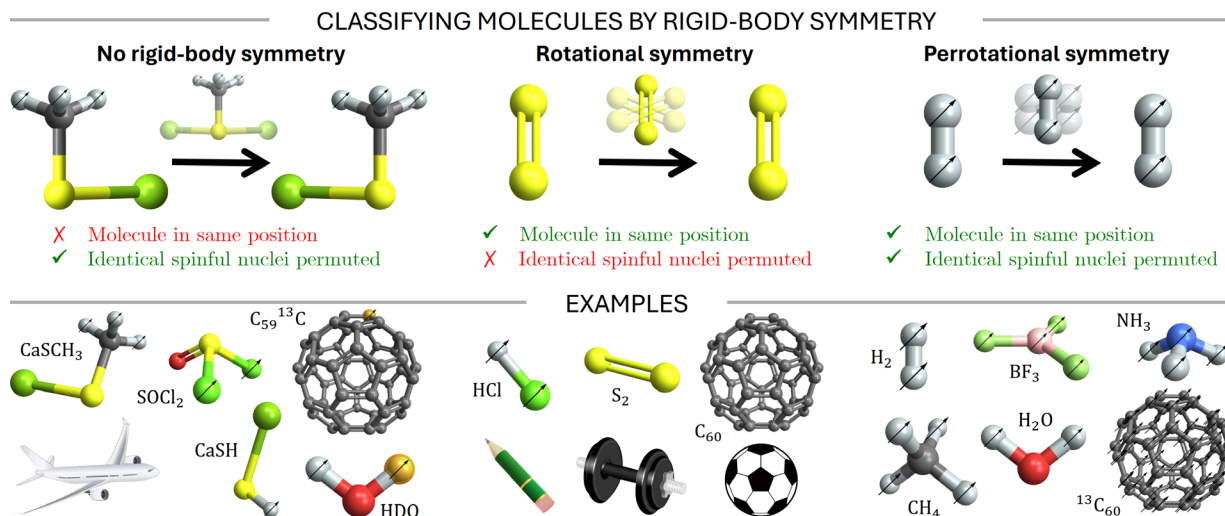


Figure 99. Rigid bodies can be characterized by their behavior under orientation-preserving rotations. Orientations, or angular positions, of asymmetric molecules are the same as those of any rigid body (e.g., an airplane) whose center of mass is fixed. While every rotation moves an asymmetric molecule to a different position, rotationally symmetric molecules remain in the same position under some rotations. Such molecules can have nonzero nuclear spin (marked by “¹³”), but any rotations that permute identical spinful nuclei must also rotate the rest of the molecule into a different position. Molecule-frame rotations that permute spinful nuclei and do leave the rest of the molecule invariant have to produce the molecule’s nuclear-spin statistics. We call any molecule admitting such permutation-rotations a “perrotationally symmetric” molecule. The rotational state space of such molecules has no macroscopic analogue and exhibits several interesting and potential useful features. All molecules were drawn in Mathematica 13 [6]. The following public-domain photos from freesvg.org are pictured: [dumbbell](#), [round pencil](#), [plane](#), and [soccer ball](#).

The theory of molecular state spaces, developed well before the end of the last century, has also been tailored mostly to aggregate molecular systems [4]. As experimental control of molecules improves and various quantum applications come to focus, it is important that the conventional theory is (1) re-tuned to model single trapped molecules and (2) re-examined considering several decades of development in quantum information science and technology.

We formulate a phase space for rotational and nuclear-spin states of arbitrary rigid closed-shell molecules. Taking in molecular geometry and nuclear-spin data, our framework yields admissible position and momentum states, inter-convertible via a generalized Fourier transform. We classify molecules into three types — asymmetric, rotationally symmetric, and perrotationally symmetric—with the last type having no macroscopic analogue due to nuclear-spin statistics constraints.

We identify two predominant features of perrotationally symmetric state spaces that are Hamiltonian-independent and induced solely by symmetry and spin statistics. First, many molecular species are intrinsically rotation-spin entangled in a way that cannot be broken without transitioning to another species. Second, adiabatic changes in orientation realize naturally robust operations in the form of an Abelian or even non-Abelian monodromy, akin to what is achieved by braiding anyonic quasiparticles or realizing fault-tolerant quantum gates.

In collaboration with an external team of experimentalists, we also develop tunable error-correcting

codes that are more practical than previous molecular encodings, require lower average energy, can directly protect against photonic processes up to arbitrary order, and are applicable to a broader set of atomic and molecular systems [5].

- [1] V. V. Albert, J. P. Covey, and J. Preskill. Robust Encoding of a Qubit in a Molecule. *Physical Review X* **10** (2020), 031050. DOI: [10.1103/PhysRevX.10.031050](https://doi.org/10.1103/PhysRevX.10.031050)
- [2] D. DeMille, J. M. Doyle, A. O. Sushkov. Probing the Frontiers of Particle Physics with Tabletop-scale Experiments. *Science* **357** (2017), 6355. DOI: [10.1126/science.aal3003](https://doi.org/10.1126/science.aal3003)
- [3] B. L. Augenbraun, J. M. Doyle, T. Zelevinsky, and I. Kozyryev. Molecular Asymmetry and Optical Cycling: Laser Cooling Asymmetric Top Molecules. *Physical Review X* **10** (2020), 031022. DOI: [10.1103/PhysRevX.10.031022](https://doi.org/10.1103/PhysRevX.10.031022)
- [4] P. R. Bunker and P. Jensen. *Molecular Symmetry and Spectroscopy*. 2nd ed., 2006.
- [5] S. P. Jain, E. R. Hudson, W. C. Campbell, and V. V. Albert. *Æ Codes*. Preprint: [arXiv:2311.12324](https://arxiv.org/abs/2311.12324)
- [6] Wolfram Research Inc., *Mathematica*, Version 13.0 (2023), Champaign, IL.

Quantum Algorithms and the Power of Forgetting

Matthew Coudron

Andrew M. Childs (University of Maryland)

Amin Shiraz Gilani (University of Maryland)

In 2003, Childs et al. [1] proved that there exists a polynomial time quantum algorithm, in particular a quantum walk algorithm, which solves a computational problem known as the Welded Tree Oracle Problem exponentially faster than is possible classically. It was later shown, in [2], that the Welded Tree Oracle Problem was fundamentally different than any previously defined oracle problem, in that it requires polynomially large quantum depth to solve. In fact, this property even separates the Welded Tree Oracle Problem from the quantum factoring algorithm, which can be parallelized to require just logarithmic quantum depth. This makes the Welded Tree Problem an intriguing object of study when searching for novel quantum properties of algorithms. Our ongoing project, [3], has achieved progress toward resolving a remarkable open question, originally alluded to in [1]. To state the open question, we first need to give a more detailed description of the Welded Tree Oracle Problem.

The Welded Tree Oracle Problem is a computational problem concerning a graph consisting of two binary trees of height n , joined together at their leaves by a random cycle. Figure 100 provides an example of such a graph, for $n=4$.

Each vertex of the graph is assigned a unique, random bit-string label of length $2n$. The root vertex of the left binary tree is called the ENTRANCE, and the root vertex of the right binary tree is called the EXIT. The input to the Welded Tree Oracle Problem is not a complete description of the graph, but rather an “Oracle” black-box function, which, when queried at label of any vertex in the graph, outputs the bit-string labels of its nearest neighbors. In other words, if we think of the Welded Tree graph as a maze, in which each vertex is a room and each edge is a hallway, then the oracle simply tells us which rooms neighbor the room that we are currently in, without revealing any global structure of the graph. The computational goal in the Welded Tree Oracle Problem is, given the oracle function for the graph, and the label of the ENTRANCE vertex, to find the label of the EXIT vertex using as few queries to the oracle as possible. The original result of [1] is that a quantum computer, which can query the oracle in superposition, can solve this problem in polynomially many queries (and with a polynomial time quantum algorithm), whereas an algorithm that only makes classical queries probably requires exponentially many queries to find the EXIT.

Note that the classical hardness result makes some intuitive sense because the Welded Tree Graph has 2^{n+2}

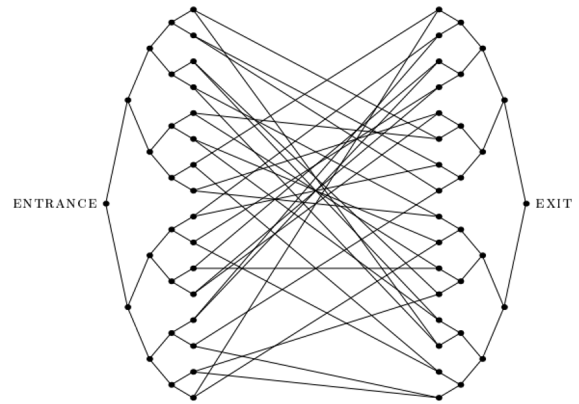


Figure 100. A welded tree graph for $n=4$.

vertices total, a number which is exponential in the height, n , of the binary trees, and in the number of bits of the bit string labels. Furthermore, the cycle in the middle is random, so one would expect that a classical algorithm might “get lost” in this maze while searching for the EXIT.

A famous open question, first discussed in [1], is whether or not there exists a polynomial time quantum algorithm which can find a *path* of vertices from ENTRANCE to EXIT in the Welded Tree Oracle Problem. Standard classical intuition would suggest that, since there is an efficient algorithm which can find the EXIT starting from the ENTRANCE, there must also be an algorithm which can find a path from ENTRANCE to EXIT. However, the algorithm which efficiently finds the EXIT starting from the ENTRANCE is a quantum algorithm and not clearly subject to classical intuition. In fact, surprisingly, and for the first time, we have partial evidence that, in the quantum world, this path-finding problem may actually be computationally hard. In particular, we are able to show that perhaps the most natural class of quantum algorithms for ENTRANCE-EXIT path finding, which we call “rooted algorithms,” probably cannot find a path from ENTRANCE to EXIT in fewer than exponentially many quantum queries. Informally, “rooted algorithms” are those quantum algorithms for pathfinding which maintain, at every point in the superposition and every step of the algorithm, a memory of at least one path from their current position in the Welded Tree graph, back to the ENTRANCE vertex. Not only is this class the most natural first attempt at a quantum path-finding algorithm, but it is hard to imagine what possible benefit an algorithm could gain from not being rooted, and “forgetting” its way back to the ENTRANCE. It would seem odd to take a such a non-rooted approach given that the entire goal of the algorithm is to output a path from ENTRANCE to EXIT in the end. Our no-go result for rooted algorithms shows that, bizarrely, while a quantum algorithm can find its way from ENTRANCE to

EXIT in the Welded Tree Oracle Problem, in order to do so it must necessarily “forget where it started.”

At the technical level our result is interesting in that it employs a novel technique we call a “transcript simulation” in order to prove that rooted algorithms cannot have constructive or destructive interference that exceed classical algorithms by more than a polynomial amount. This can then be combined with a new style of classical hardness result, which we also devised, in order to show that rooted quantum algorithms are no more capable of finding the EXIT than classical algorithms. The intuition behind this approach is that the need of rooted algorithms to constantly maintain knowledge of a path from their current position in the graph back to the ENTRANCE actually destroys the constructive and destructive interference that made the original EXIT-finding algorithm of [1] work. The interference is destroyed because storing a path back to the ENTRANCE forces a separation between different branches of the superposition. Our paper, [3], was published in the proceedings of the 2023 Innovations in Theoretical Computer Science (ITCS) conference and has been accepted for presentation at the 2023 Theory of Quantum Computing, Communications, and Cryptography (TQC) conference. We believe that, with more work, we will eventually be able to prove that there is no polynomial time quantum algorithm of any sort (not just “rooted” algorithms) which can find a path from ENTRANCE to EXIT in the Welded Tree Graph with better than exponentially small probability. Such a result would be a resolution of a long-standing open problem in the field.

- [1] A. M. Childs, R. Cleve, E. Deotto, E. Farhi, S. Gutmann, and D. A. Spielman. Exponential Algorithmic Speedup by a Quantum Walk. In *Proceedings of the 35th Annual ACM Symposium on Theory of Computing*, June 9-11, 2003, San Diego, CA, 59–68. DOI: [10.1145/780542.780552](https://doi.org/10.1145/780542.780552)
- [2] M. Coudron and S. Menda. Computations with Greater Quantum Depth are Strictly More Powerful (Relative to an Oracle). In *Proceedings of the 52nd Annual ACM SIGACT Symposium on Theory of Computing*, 2022. DOI: [10.1145/3357713.3384269](https://doi.org/10.1145/3357713.3384269)
- [3] A. M. Childs, M. Coudron, and A. S. Gilani. Quantum Algorithms and the Power of Forgetting. In *14th Innovations in Theoretical Computer Science Conference (ITCS 2023)* (Y. Tauman Kalai, ed.), Leibniz International Proceedings in Informatics (LIPIcs) **251**, Schloss Dagstuhl–Leibniz-Zentrum für Informatik, 2023, 37:1-37:22. DOI: [10.4230/LIPIcs.ITCS.2023.37](https://doi.org/10.4230/LIPIcs.ITCS.2023.37)

Quantum Depth in the Random Oracle Model

Matthew Coudron

Atul Singh Arora (Caltech)

Andrea Coladangelo (U. of California, Berkeley)

Alexandru Gheorghiu (ETH Zurich)

Uttam Singh (Polish Academy of Sciences)

Hendrik Waldner (Max Planck Institute)

The circuit depth required to perform a quantum or classical computation, which is defined as the minimal number of layers of basic computational gates required to perform the whole computation, has direct relevance to our ability to perform the computation on near term quantum hardware or on a parallel computing architecture, as well as many other applications. Within quantum computing, purely classical operations are considered relatively “cheap” to implement, whereas coherent quantum gate operations are relatively “expensive.” Consequently, the model which most aptly captures the power of low-depth quantum circuits in the context of near term quantum computing is that of hybrid quantum circuits formed by the composition of low-depth quantum circuits, interleaved with much higher-depth classical circuits. This notion of interleaving low-depth quantum circuits with high depth classical circuits has no analogous counterpart in the study of circuit depth in classical computer science. It turns out that this novel composition has a number of nuances and subtleties that defy previously known mathematical techniques for studying circuit depth, and yet, are relevant to the most famous quantum computations known to date.

The intriguing and subtle nature of these hybrid quantum circuits is best highlighted by two well-known open problems posed in 2005. In the first, [1], Richard Jozsa conjectured that all polynomial size quantum computations, regardless of depth, can be efficiently simulated by hybrid quantum-classical circuits which only employ logarithmic depth quantum circuits, as in Figure 102. In the second, [2], Scott Aaronson’s 9th semi-grand challenge in quantum computation asks for a proof of a statement that is technically incomparable to [1], but morally opposite: That there exists a computational problem that can be efficiently solved by polynomial size quantum computations but cannot be efficiently solved by hybrid quantum-classical circuits shown in Figure 101. Despite their intriguing nature, and their fundamental importance to our understanding of quantum computation, these two problems remained open for 17 years. Our work [5] gives the first solution to the open problems due to Jozsa and Aaronson [1, 2], resolving Aaronson’s conjecture in the affirmative, and Jozsa’s conjecture in the negative. Our main result is to construct a computational problem, instantiated using a

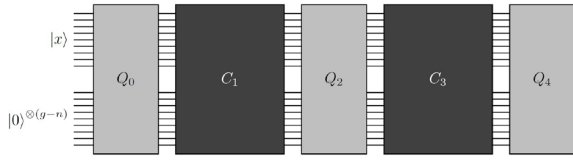


Figure 101. Q boxes are quantum circuits of depth $\log(n)$. C boxes are classical circuits of depth polynomial in n .

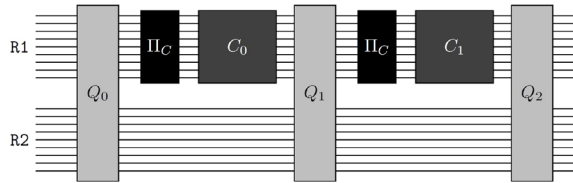


Figure 102. Q boxes are quantum circuits of depth 1. C boxes are classical circuits of depth polynomial in n . π boxes are measurements in the standard basis.

cryptographic hash function, for which there is a polynomial time quantum algorithm, but for which there provably does not exist an algorithm of the form shown in Figure 101 or Figure 102 that can solve the problem with better than exponentially small probability.

More specifically, our main contribution is to exhibit the first *cryptographically instantiable* computational problem which provably separates polynomial depth quantum computations from the computations of the forms shown in either Figure 101 or Figure 102. Regular oracle separations between these types of computations were established in 2020 [3, 4], but it is not clear that those oracle separations are cryptographically instantiable. Our strategy was to prove a new oracle separation based on a special type of oracle called a Random Oracle. The significance of a Random Oracle separation, in this context, is that there exists a non-oracular instantiation of the same problem in which the random oracle is replaced by a cryptographic hash function, which is indistinguishable from a random oracle under a widely known cryptographic assumption. This satisfies Aaronson’s stipulation that the computational problem must be concretely instantiable (it must be possible to write the problem statement down on paper), rather than a “black box” oracle separation, in order to resolve his 9th semi-grand challenge in quantum computing [2].

The computational problem that we construct is produced by recursively composing a new type of “proof of quantumness,” such as the version pioneered by Yamakawa and Zhandry [6]. Concretely, our problem asks: Given a particular type of error correcting code C on $\{0,1\}^{n-m}$ specified by its generator matrix, and a hash function H mapping $\{0,1\}^n \rightarrow \{0,1\}$ which is specified as the composition of d separately provided hash functions, FIND a bit string in $x \in \{0,1\}^{n-m}$ which lies in the error correcting code C , and has the property that all m length n substrings of x are mapped to 0 by the

hash function H . The polynomial time quantum algorithm to solve this search problem utilizes the quantum Fourier transform. At the level of techniques, the key contribution that we make is to prove that, because the hash function H is defined as a composition of d separately provided hash functions, no quantum algorithm of depth less than d should make essentially “any progress” towards finding the answer. Since efficient classical query algorithms also cannot make progress toward solving the problem, setting d to be greater than the depth of the quantum circuits in Figure 101 (for example), will then resolve Aaronson’s 9th semi-grand challenge in quantum computing [2]. Proving all of this, despite the nuances of the hybrid quantum-classical model, is quite involved. It required importing exponential hiding techniques, and other techniques used [3, 4], as well as developing a new technique which we call “shadow oracles.” We also explore a variety of other ways to compose quantum and classical circuits beyond Figure 101 and Figure 102 and show that our techniques yield results about those new classes as well.

- [1] R. Jozsa. An Introduction to Measurement Based Quantum Computation. In *Quantum Information Processing* (D. G. Angelakis, et al., eds.), IOS Press, 2006, 137-158.
- [2] S. Aaronson. Ten Semi-Grand Challenges for Quantum Computing Theory. 2005. URL: <https://www.scott-aaronson.com/writings/qchallenge.html>
- [3] M. Coudron and S. Menda. Computations with Greater Quantum Depth Are Strictly More Powerful (Relative to an Oracle). In *Proceedings of the 52nd Annual ACM SIGACT Symposium on Theory of Computing*, 2020, 889–901. DOI: [10.1145/3357713.3384269](https://doi.org/10.1145/3357713.3384269)
- [4] N.-H. Chia, K.-M. Chung and C.-Y. Lai. On the Need for Large Quantum Depth. In *Proceedings of the 52nd Annual ACM SIGACT Symposium on Theory of Computing*, 2020. 902–915. DOI: [10.1145/3357713.3384291](https://doi.org/10.1145/3357713.3384291)
- [5] A. S. Arora, A. Coladangelo, M. Coudron, A. Gheorghiu, U. Singh, and H. Waldner. Quantum Depth in the Random Oracle Model. In *Proceedings of the 55th Annual ACM Symposium on Theory of Computing (STOC 2023)*, 2023, 1111–1124. DOI: [10.1145/3564246.3585153](https://doi.org/10.1145/3564246.3585153)
- [6] T. Yamakawa and M. Zhandry. Verifiable Quantum Advantage without Structure. Preprint arXiv:2204.02063 URL: <http://arxiv.org/abs/2204.02063>

Local Hamiltonians with No Low-Energy Stabilizer States

Matthew Coudron

Nolan J. Coble (University of Maryland)

Jon Nelson (University of Maryland)

Seyed Sajjad Nezhadi (University of Maryland)

The recently-defined No Low-energy Sampleable States (NLSS) conjecture of Gharibian and Le Gall [1] posits the existence of a family of local Hamiltonians where all

quantum states of low-enough constant energy do not have succinct representations allowing perfect sampling access. States that can be prepared using only Clifford gates (i.e., stabilizer states) are an example of sampleable states, so the NLSS conjecture implies the existence of local Hamiltonians whose low-energy space contains no stabilizer states. In our work, [3], we take a step towards the NLSS conjecture by constructing families of Hamiltonians that exhibit this requisite “no low-energy stabilizer states” property.

Our construction works via a simple alteration to local Hamiltonians corresponding to CSS codes. Our method can also be applied to the recent No Low-energy Trivial States (NLTS) Hamiltonians of Anshu, Breuckmann, and Nirkhe [2], resulting in a family of local Hamiltonians whose low-energy space contains neither stabilizer states nor trivial states. We hope that our techniques will eventually be helpful for constructing Hamiltonians which simultaneously satisfy NLSS and NLTS.

To understand the motivation behind our work it is important to take a step back and note that each of the conjectures in this particular branch of Hamiltonian complexity, including the NLTS conjecture, the NLSS conjecture, and many others, are all attempts to gain insight into a very widely known open problem in the field called the Quantum Probabilistically Checkable Proof (PCP) conjecture. Classical Probabilistically Checkable Proofs (PCPs) are considered to be one of the crowning achievements of modern theoretical computer science and have numerous emerging applications, from cryptography (SNARKS) to hardness of approximation results. The Quantum PCP conjecture, if resolved, could have analogous applications to quantum computing, and would also have implications for the possibility of experimentally producing entangled quantum states that remain coherent at high temperatures, among other things. The Quantum PCP conjecture itself is a complexity theoretic claim about a computational problem involved in simulating quantum mechanical systems which are governed by a Hamiltonian. Briefly put, the Quantum PCP conjecture postulates that it is QMA-hard (a computational hardness notion involving complexity classes) to approximate the ground state energy of a local Hamiltonian to within a constant. This simple statement, if proven, could have all the widespread implications discussed above, and the proof techniques would likely be valuable in and of themselves. However, a pre-requisite to proving that any problem is QMA-hard is to first prove that it cannot be solved in the smaller complexity class Non-Deterministic Polynomial Time (NP). This pre-requisite is the motivator for the NLTS conjecture, the NLSS conjecture, and for our own work. If the NLTS conjecture had been false, the ground state energy problem for local Hamiltonians would have been contained in NP. If the NLSS conjecture is false then the

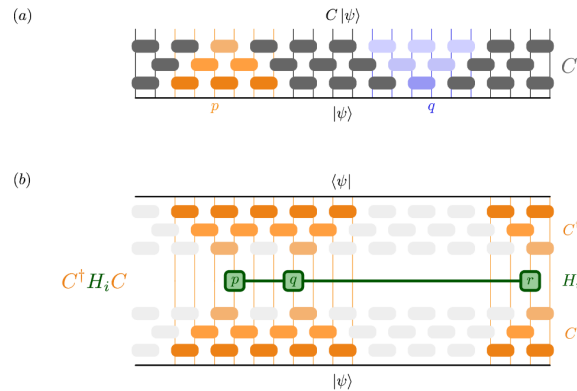


Figure 103. Conjugation method for modifying local Hamiltonians. See text for discussion.

problem would be contained in a complexity class called MA, which is much smaller than QMA.

Our result is a necessary pre-requisite of the NLSS conjectures, addressing the following important issue: The NLTS conjecture, while now proven, has only been proven with Hamiltonians whose ground state energy problem is clearly contained in MA because the ground states are stabilizer states and therefore efficiently sampleable (the exact reasoning behind all of these connections is non-trivial and is laid out in [1], where the NLSS conjecture was first stated).

At the level of techniques, we contribute a conceptually simple new procedure in which we begin with a regular local Hamiltonian and modify it by conjugating it (multiplying on either side) by low depth quantum circuit as shown in Figure 103. Part (a) of Figure 103 illustrates a generic low-depth quantum circuit C , comprised of a constant number of layers of quantum gates. Part (b) of Figure 103 illustrates what happens when a local Hamiltonian term H_i is conjugated by the low-depth quantum circuit C . A local Hamiltonian which is conjugated by a constant depth quantum circuit remains a local Hamiltonian since its Hamiltonian properties are preserved by the unitarity of the quantum circuit, and its locality is only increased by the spread of the “light cones” within the circuit C which originate from one particular Hamiltonian term (these are the gates colored orange in part (b) of Figure 103). Since C is constant depth, the increase in the locality of the Hamiltonian is merely constant. In [3] we are able to show, through a series of combinatorial arguments that, if we take the local Hamiltonian from known constructions of quantum Low Density Parity Check (LDPC) error correcting codes and conjugate those Hamiltonians by a $\pi/8$ rotation on every qubit (which is a low depth circuit), then no stabilizer state can have low energy relative to the resulting Hamiltonian. Since the resulting Hamiltonian must still be local, by the above argument and Figure 103, the desired result follows. We are hopeful that

these techniques will prove useful in further extending known NLTS results to more general settings.

- [1] S. Gharibian and F. Le Gall. Dequantizing the Quantum Singular Value Transformation: Hardness and Applications to Quantum Chemistry and the Quantum PCP Conjecture. In *Proceedings of the 54th Annual ACM SIGACT Symposium on Theory of Computing*, June 2022, 19–32. DOI: [10.1145/3519935.351999](https://doi.org/10.1145/3519935.351999)
- [2] A. Anshu, N. Breuckmann, and C. Nirkhe. NLTS Hamiltonians from Good Quantum Codes. June 2022, preprint arXiv:2206.13228. URL: <http://arxiv.org/abs/2206.13228>
- [3] N. J. Coble, M. Coudron, J. Nelson, and S. Sajjad Nezhadi. Local Hamiltonians with No Low-Energy Stabilizer States. In *18th Conference on the Theory of Quantum Computation, Communication and Cryptography (TQC 2023)*. Leibniz International Proceedings in Informatics (LIPIcs) 266 (2023), 14:1-14:21. DOI: [10.4230/LIPIcs.TQC.2023.14](https://doi.org/10.4230/LIPIcs.TQC.2023.14)

Post-Quantum Cryptography

Yi-Kai Liu

Gorjan Alagic (NIST ITL)

Maxime Bros (NIST ITL)

Lily Chen (NIST ITL)

David Cooper (NIST ITL)

Quynh Dang (NIST ITL)

Thinh Dang (NIST ITL)

John Kelsey (NIST ITL)

Jacob Lichtinger (NIST ITL)

Carl Miller (NIST ITL)

Dustin Moody (NIST ITL)

Rene Peralta (NIST ITL)

Ray Perlner (NIST ITL)

Angela Robinson (NIST ITL)

Hamilton Silberg (NIST ITL)

Daniel Smith-Tone (NIST ITL)

Noah Waller (NIST ITL)

Since 2016, NIST has been leading an open, competition-like process to develop standards for post-quantum cryptography (PQC). The goal is to standardize new schemes for public-key encryption, key establishment, and digital signatures, in order to replace existing schemes that would be vulnerable to cryptanalysis using quantum computers, such as RSA, Diffie-Hellman, and elliptic curve cryptosystems. These new post-quantum cryptosystems will be crucial for secure web browsing, digital certificates, and secure software updates, and many other applications. While large quantum computers have not yet been built, NIST believes it is prudent to prepare for that possibility, in order to provide long-term security for sensitive information that may remain sensitive for many years into the future.

In August 2023, NIST posted the initial public drafts of three Federal Information Processing Standards (FIPS), for public review:

- FIPS 203, Module-Lattice-Based Key-Encapsulation Mechanism Standard
- FIPS 204, Module-Lattice-Based Digital Signature Standard
- FIPS 205, Stateless Hash-Based Digital Signature Standard

These draft standards were derived from three post-quantum cryptosystems (CRYSTALS-Kyber, CRYSTALS-Dilithium and SPHINCS+) that were selected by NIST for standardization in 2022. Currently, NIST is reviewing the public comments on these draft standards. NIST expects to publish final versions of these standards in 2024. In addition, NIST is in the process of drafting FIPS 206, FFT-Over-NTRU-Lattice-Based Digital Signature Standard, which is based on a fourth cryptosystem (Falcon) that was selected by NIST for standardization in 2022.

At the same time, NIST is continuing its evaluation process, and may select additional cryptosystems for standardization in the future, in order to mitigate the risk of unexpected advances in cryptanalysis, and to support use-cases that require cryptosystems with special properties. For this purpose, NIST chose four key establishment algorithms (BIKE, Classic McEliece, HQC and SIKE) for a fourth round of evaluation, which began in 2022 and is ongoing. NIST also issued a new call for submissions in 2022, for additional signature schemes. These submissions were due in June 2023, and are currently undergoing evaluation by NIST and the cryptography community. Additional information is available on the NIST PQC web page²⁸.

To engage with the post-quantum cryptography community and other stakeholders, NIST has been organizing a series of virtual seminars on recent developments in PQC and is planning to hold its Fifth PQC Standardization Conference on April 10-12, 2024, in Rockville, Maryland (in-person). NIST is also working with industry on PQC migration issues, through the National Cybersecurity Center of Excellence (NCCoE).

To support these activities, NIST also carries out independent analysis and research on post-quantum cryptography [1, 2], as well as related topics such as quantum algorithms [3]. Finally, through the Joint Center for Quantum Information Computer Science (QuICS), NIST helped host the PQCrypto 2023, the 14th International Workshop on Post-Quantum Cryptography, on August 16-18, 2023, in College Park, Maryland [4].

- [1] R. A. Perlner, J. Kelsey, and D. A. Cooper. Breaking Category Five SPHINCS+ with SHA-256. In *Proceedings of*

²⁸ <https://csrc.nist.gov/Projects/post-quantum-cryptography>

- PQCrypto 2022, Lecture Notes in Computer Science* **13512** (2022) 501-522. DOI: [10.1007/978-3-031-17234-2_23](https://doi.org/10.1007/978-3-031-17234-2_23)
- [2] J. Kelsey A. Jackson, C. A. Miller, and D. Wang. Evaluating the Security of CRYSTALS-Dilithium in the Quantum Random Oracle Model. Preprint: [arXiv:2312.16619](https://arxiv.org/abs/2312.16619)
- [3] Y.-K. Liu. An Uncertainty Principle for the Curvelet Transform, and the Infeasibility of Quantum Algorithms for Finding Short Lattice Vectors. Preprint: [arXiv:2310.03735](https://arxiv.org/abs/2310.03735)
- [4] T. Johansson, D. Smith-Tone (eds.). *Proceedings of PQCrypto 2023, Lecture Notes in Computer Science* 14154 (2023). DOI: [10.1007/978-3-031-40003-2](https://doi.org/10.1007/978-3-031-40003-2)

Modern Quantum Tools for Bosonic Systems

Victor V. Albert

Ivan A Burenkov (NIST PML)

Michael J. Gullans (NIST PML)

Sergey V. Polyakov (NIST PML)

Alexander Barg (University of Maryland)

Eric Culf (University of Ottawa)

Joseph T. Iosue (University of Maryland)

Shubham P. Jain (University of Maryland)

En-Juo Kuo (University of Maryland)

Kunal Sharma (IBM)

Thomas Vidick (Weizmann Institute of Science)

Yixu Wang (University of Maryland)

Yijia Xu (University of Maryland)

Utilization of the features of quantum mechanics promises to eventually increase our understanding of chemical processes, communicate securely, and accurately measure signals. However, most quantum protocols are focused on the abstract qubit (i.e., discrete-variable or DV) systems, and many of them cannot be readily available to bosonic or continuous-variable (CV) systems — optical fibers, free-space communication, microwave and optical cavities, motional degrees of freedom of atoms and ions, and mechanical resonators — without substantial reformulation.

For example, quantum tomography is a field concerned with characterizing quantum systems, an important task whose completion is necessary for realizing most of the aforementioned long-term goals. However, tomography of quantum many-body systems is plagued with the “exponential wall” — the fact that complete characterization of a state or operation on a many-qubit quantum system requires either a computation time or a memory size that scales exponentially with the number of qubits. An active area of research is thus devoted to developing efficient protocols for such tasks. A recent breakthrough result called shadow tomography has substantially simplified the task of approximating

quantum systems [1]. However, it is unclear how to develop similar important tools in CV systems because qubit shadows revolved around the notion of state designs, which have not, up to now, existed in the CV world.

For another example, fiber-based and free-space communication are described by CV systems, so development of secure CV protocols is critical to realizing quantum communication in the real world. However, there is a tradeoff between provable security and ease of use, as some of the simplest CV protocols are not device independent, i.e., such protocols cannot be securely implemented without additional knowledge that the devices involved are also secure.

Members of Victor’s group, along with collaborators at NIST and around the world, are spearheading a new research direction to extend state-of-the-art qubit-based tomographic, error-correction, and cryptographic quantum protocols to CV systems in the following ways.

- Theory of quantum codes defined on quantum systems parameterized by spheres [2], encapsulating several physically relevant quantum coding schemes for CV, spin, and molecular systems. The framework of quantum spherical codes provides a quantum analogue to the classical spherical codes, a subfield of coding theory that has been around since Shannon. This framework has direct applications to near-term experimental CV proposals, and we anticipate that this work will pave the way for many novel, well-protected, and experimentally feasible logical qubits. We are also in the process of adapting this framework to gain insight into how quantum mechanics can be used to better transmit classical information.
- Homological error-correcting codes and oscillators and rotors [3]. Conventional CV systems are characterized by linear position and momentum and are not thought to exhibit the unique topology of angular (a.k.a. rotor) quantum systems that are parameterized by periodic variables. Our work shows that a mapping of an angular system into a CV system can be used to develop CV codes previously available only to rotor systems. We also identify the (Clifford) group structure of rotor operations and show that analogous operations for conventional CV systems are available under the mapping.
- Theory of appropriately defined CV state designs, and their applications to design-based CV shadow tomography [4]. These results are the first to extend the notion of a design (a.k.a. quadrature or summation rule) to infinite-dimensional spaces and are expected to have other applications to state distinction, randomized benchmarking, entanglement detection, fidelity estimation, cryptography, sensing, fundamental physics, and error correction.

- [One-sided device-independent cryptographic protocol utilizing squeezed states](#) whose proof of security is based on a CV extension of DV monogamy-of-entanglement games [5]. This work establishes this well-known protocol as the first one-sided device-independent CV protocol, to the authors' knowledge.
 - [Unified decoding framework](#) for concatenated DV and CV error-correcting codes [6].
 - [Review of bosonic coding](#) [7] for computer scientists and others outside of physics.
- [1] H.-Y. Huang, R. Kueng, and J. Preskill. Predicting Many Properties of a Quantum System from Very Few Measurements. *Nature Physics* **16** (2020), 1050. DOI: [10.1038/s41567-020-0932-7](https://doi.org/10.1038/s41567-020-0932-7).
 - [2] S. P. Jain, J. T. Iosue, A. Barg, and V. V. Albert. Quantum Spherical Codes. Preprint: [arXiv:2302.11593](https://arxiv.org/abs/2302.11593)
 - [3] Y. Xu, Y. Wang, and V. V. Albert. Clifford Operations and Homological Codes for Rotors and Oscillators. Preprint: [arXiv:2311.07679](https://arxiv.org/abs/2311.07679)
 - [4] J. Iosue, K. Sharma, M. Gullans, and V. Albert. Continuous-variable Quantum State Designs: Theory and Applications. *Physical Review X* **14** (2023), 011013. DOI: [10.1103/PhysRevX.14.011013](https://doi.org/10.1103/PhysRevX.14.011013)
 - [5] E. Culf, T. Vidick, and V. V. Albert. Group Coset Monogamy Games and an Application to Device-independent Continuous-variable QKD. Preprint: [arXiv:2212.03935](https://arxiv.org/abs/2212.03935)
 - [6] Y. Xu, Y. Wang, E.-J. Kuo, and V. V. Albert. Qubit-Oscillator Concatenated Codes: Decoding Formalism and Code Comparison. *PRX Quantum* **4** (2023), 020342. DOI: [10.1103/PRXQuantum.4.020342](https://doi.org/10.1103/PRXQuantum.4.020342)
 - [7] V. V. Albert. Bosonic Coding: Introduction and Use Cases. Preprint: [arXiv:2211.05714](https://arxiv.org/abs/2211.05714)

Single Photon Sources and Detectors Dictionary

Thomas Gerrits
 Oliver Slattery
 Paulina Kuo
 Alan Migdall (NIST PML)
 Sergey Polyakov (NIST PML)
 Josh Bienfang (NIST PML)

In collaboration with researchers from PML, we developed and published a dictionary that defines terms and metrics relevant to the characterization of single-photon detectors and sources, with the goal of promoting better understanding and communication, and providing a useful reference for the quantum and single-photon communities [1].

Our goal is to develop a common language to promote clarity and understanding and to facilitate the development of single-photon quantum technologies.

Clear definitions can accelerate technology development and device interoperability, and a common language allows commercial devices to be compared directly against each other and therefore helps users to evaluate the device performance.

We sought to build on existing publications, to be independent of any application, and to develop non-exclusionary definitions based on fundamental processes that would remain relevant even in the context of potential future, unknown technologies. In pursuit of consensus, we edited and revised a first draft according to feedback from a wide variety of experts in the field. With the published version of this document, we now seek feedback from the larger single-photon community. We expect this dictionary to be a living document that can be updated and expanded, with updates occurring annually.

- [1] J. C. Bienfang, T. Gerrits, P. S. Kuo, A. Migdall, S.V. Polyakov, and O. Slattery. Single-Photon Sources and Detectors Dictionary. NIST IR 8486, National Institute of Standards and Technology, 2023. DOI: [10.6028/NIST.IR.8486](https://doi.org/10.6028/NIST.IR.8486)

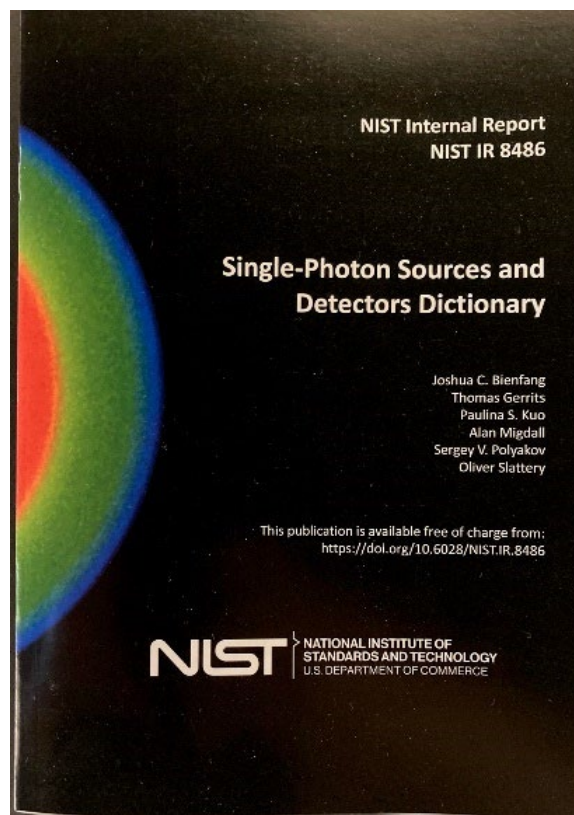


Figure 104. Single-Photon Sources and Detectors Dictionary

Network Synchronized Source of Indistinguishable Photons for Quantum Networking

Nijil Lal

Paulina Kuo

Thomas Gerrits

Oliver Slattery

Ya-Shian Li-Baboud (NIST ITL)

Jabir MV (NIST CTL)

Ivan Burenkov (NIST PML)

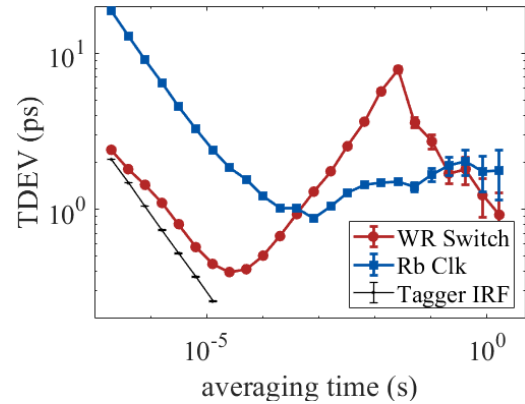
Sergey Polyakov (NIST PML)

Scalable quantum networks require source synchronization at the picosecond-level. In addition, quantum interference is crucial for the realization of many quantum network protocols such as entanglement swapping and teleportation. A network compatible source should thus meet the design constraints, that are: picosecond-level jitter, single spatial and temporal-bandwidth mode, pulse duration of at least 10 ps, telecom C-band wavelength, as well as to provide a high single-photon rate.

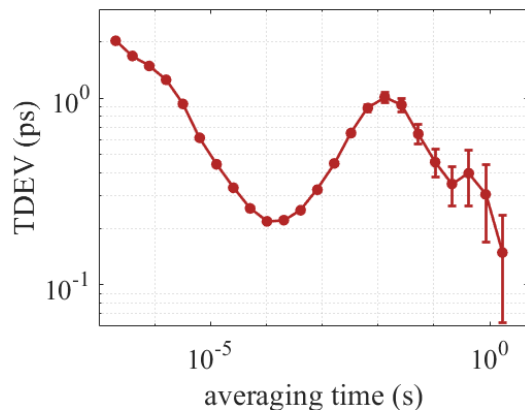
In collaboration with ITL, PML and CTL, we have built and characterized a network source of indistinguishable photons that provides transform-limited heralded single photons at the telecom C-band, shows high indistinguishability and is successfully synchronized to a network clock. Using a volume Bragg grating (VBG) of 0.1 nm bandwidth in the output of a parametric down-conversion process, we obtain photons in nearly single time-bandwidth mode. This yields indistinguishable photons of ≈ 35 ps pulse duration that are sufficiently larger than the expected single photon jitter in the system. Time deviation (TDEV) measurements corresponding to the synchronization of our source using different clock recovery systems show sub-10 picosecond-level jitter for longer averaging times (Figure 105a).

For the network clock distributed by a White Rabbit (WR) Precision Time Protocol (WR-PTP) [1, 2], which has now been standardized as part of the high-accuracy precision time protocol (HA-PTP), our source shows sub-picosecond jitter levels for shorter time scales. We have also verified pico-second level jitter for the synchronization of two network clocks, distributed by two WRs separated by an 88 km fiber spool (Figure 105b).

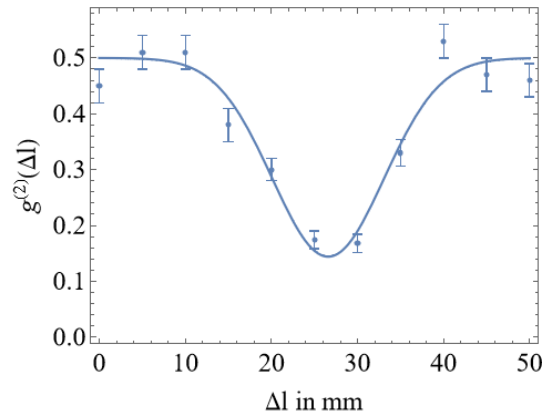
Double-heralded Hong-Ou-Mandel (HOM) interference [3] between heralded single photons generated in two independent down-conversion events in our source (separated by 112.5 ns) show high indistinguishability (Figure 105c). The estimation for an upper limit for the system jitter from this quantum measurement independently verify the range of single photon source jitter calculated through TDEV analysis of pump synchronization.



(a)



(b)



(c)

Figure 105. (a) TDEV of the source timing jitter when synchronized to a Rb-Clock (blue squares) and a network clock distributed by a low jitter WR (red circles). Black curve is the baseline defined by the time tagger instrument response function. (b) TDEV for the synchronization of two network clocks (a WR timeTransmitter & a WR timeReceiver) separated by an 88 km fiber spool. (c) Hong-Ou-Mandel dip showing the quantum interference between heralded single photons generated in independent down-conversion events.

Ongoing work includes developing an identical source at the University of Maryland which will be used to demonstrate precise time transfer and synchronization between sources of indistinguishable photons located at independent network nodes. This would further demonstrate that the source may serve as a scalable modular unit in a multi-node, long distance quantum network infrastructure.

- [1] I. A. Burenkov, A. Semionov, Hala, T. Gerrits, A. Rahmouni, D.J. Anand, Y.S. Li-Baboud, O. Slattery, A. Battou, and S.V. Polyakov. Synchronization and Coexistence in Quantum Networks. *Optics Express* **31**:7 (2023),11431-11446.
- [2] IEEE Standard for a Precision Clock Synchronization Protocol for Networked Measurement and Control Systems. 263 IEEE Std 1588-2019 (Revision IEEE Std 1588-2008), 2020.
- [3] S. V. Polyakov, A. Muller, E. B. Flagg, A. Ling, N. Borjemscaia, E. Van Keuren, A. Migdall, and G. S. Solomon. Coalescence of Single Photons Emitted by Disparate Single-Photon Sources: The Example of InAs Quantum Dots and Parametric Down-conversion Sources. *Physical Review Letters* **107** (2011), 157402.

Polarization Stabilization for Quantum Networks

Yicheng Shi
Thomas Gerrits
Oliver Slattery

In fiber-based quantum networks, reliable transmission of polarization encoded photons remains a challenging task. Due to the fiber routing geometry, the presence of birefringence in combination with changes to the fiber environment, the polarization states of propagating photons are randomly changed overtime, as shown in Figure 106. To ensure continuous operation of a quantum network, a stabilization scheme is required to actively compensate for this change in polarization.

We have developed a prototype to perform polarization stabilization at the single-photon level, which minimizes optical crosstalk between the quantum and classical channels. Our device achieves stabilization by injecting a polarization reference signal that coexists with quantum network photons. Polarization of the reference light is modulated and measured synchronously across the fiber to generate an error signal, which is in turn used to set a polarization controller to compensate for the fiber-induced polarization change [1].

We tested the performance of our prototype device over a 6 km fiber spool in our laboratory. The fiber spool is heated-up and cooled-down between 15°C and 30°C inside an incubator to emulate temperature changes of a

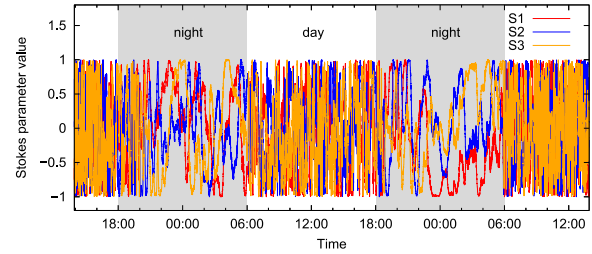


Figure 106. Survey of polarization stability over a 128 km fiber loop-back between NIST and the University of Maryland. Polarized laser light is injected into the fiber loop and its polarization is monitored over 2 days.

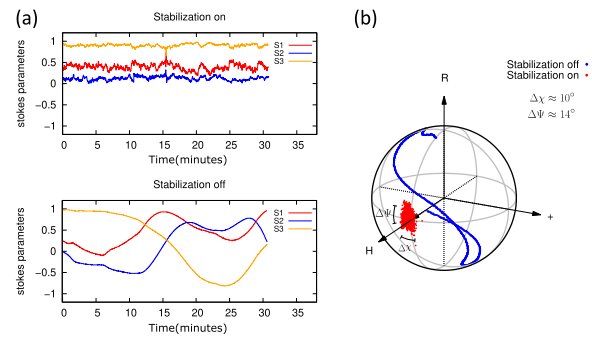


Figure 107. (a) Stokes parameters of probe light sent across a 6 km fiber spool with (top) and without (polarization stabilization). (b) Polarization state of probe light displayed as points on the Poincaré sphere.

deployed fiber. Our device achieves initial fiber stabilization within 30 seconds and runs continuously in the background. While the stabilization scheme is running, the transmitted polarization state remains stable against the changing temperature as shown in Figure 107(a). The uncertainty of the output polarization state is $\pm 5^\circ/\pm 7^\circ$ in azimuth/elevation angle as displayed by the red datapoints in Figure 107(b), which yields a fidelity above 98%. This is in stark contrast to the polarization changes induced when our stabilization scheme is not running, as shown in the lower graph in Figure 107(a) and the blue datapoints in Figure 107(b).

In its current stage, our device is capable of stabilizing fibers that are fluctuating over a time scale of tens of minutes, which is sufficient for most buried telecom fibers. With further development, we aim to increase the feedback bandwidth and allow our device to stabilize more rapid fiber changes that happens on the scale of seconds, which is observed on fibers that are aerial based. We expect such a polarization stabilization scheme to be implemented between various fiber links to support the stable operation of the DC-QNet.

- [1] Y. Shi, T. Gerrits, and O. Slattery. Towards Continuous Fiber Birefringence Compensation with Single-Photon-Level Light. In *CLEO 2023 Technical Digest Series*, Optica Publishing Group, 2023, paper JTh2A.24.

Deployed Metropolitan-Scale Precision Time Synchronization for Quantum Networking

Thomas Gerrits
 Anouar Rahmouni
 Paulina Kuo
 Yicheng Shi
 Oliver Slattery
 Ya-Shian Li-Baboud (NIST ITL)
 Ishaan Bhardvaj (NIST ITL)
 Ivan Burenkov (NIST PML)
 Abdella Battou (NIST CTL)
 Mheni Merzouki (NIST CTL)
 Wayne McKenzie (LTS)
 Mark Morris (LTS)
 Gerry Baumgartner (LTS)
 Anne Marie Richards (LTS)
 Shirali Patel (LTS)
 Millicent Ayako (LTS)
 Bruce Crabill (MAX)

Precision time synchronization between quantum nodes is required to support quantum state distribution at practical rates and distances [1]. Requirements depend on the qubit and quantum network protocol implementation and can range from sub-nanosecond to sub-10 picosecond synchronization for entanglement distribution, entanglement swapping and quantum teleportation [1, 4]. Precision time synchronization enables quantum-augmented protocols such as position verification that combines classical bits and qubits along with precise time of flight information [2].

NIST (ITL, CTL, PML), the Laboratory of Telecommunications Sciences (LTS), and Mid-Atlantic Crossroads designed, established, and characterized several architectures to evaluate the feasibility of using the commercially available White Rabbit Precision Time Protocol (WR-PTP) [3] for precision time synchronization between quantum nodes in the Washington Metropolitan Quantum Network Research Consortium (DC-QNet). A bi-directional 64 km link and a 128 km loopback link resulted in Maximum Time Interval Errors below 100 ps and 200 ps, respectively, over five days as shown in Figure 108. (a) *Maximum time interval error (MTIE)* and (b) *time deviation (TDEV)*. [4]. Where the fiber temperature remains relatively stable, sub-10 ps synchronization precision has been observed in the laboratory.

WR-PTP is an Ethernet-based protocol for optical two-way time transfer (O-TWTFT), which has now evolved to become the IEEE 1588 High-Accuracy PTP profile [5]. The availability of commercial off-the-shelf components that are interoperable with existing telecommunications infrastructure enables rapid

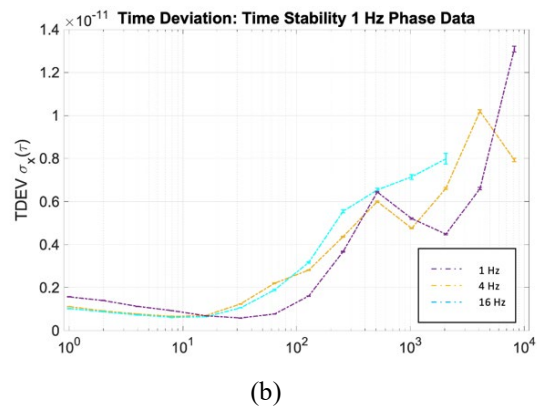
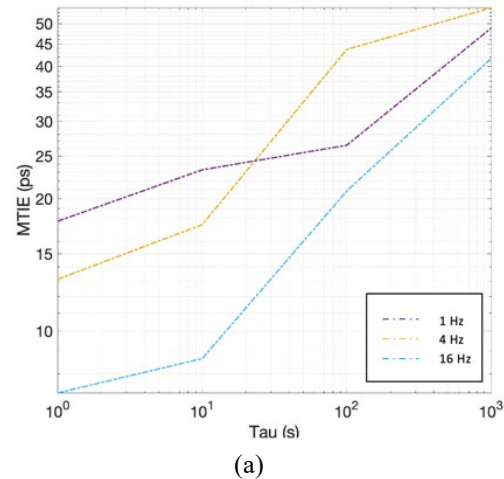


Figure 108. (a) *Maximum time interval error (MTIE)* and (b) *time deviation (TDEV)*.

deployment in quantum research networks. Additionally, the feasibility of coexistence among classical optical communications for time distribution, along with single-photon level entangled quantum state distribution, could provide the practical benefit of being able to estimate the path delay in-situ and provide active delay compensation for realizing quantum interference between remote sources.

O-TWTFT methods rely on the symmetric path delay or a calibrated coefficient to compensate for path delay asymmetry. In deployed optical fibers, chromatic dispersion, changes in fiber length, and polarization dependent losses due to environmental conditions can change the group delay and the optical pulse characteristics at the receiver. In situations where the environment has a large effect on deployed fibers, such as aerial fiber, variations can degrade the accuracy of the path delay compensation necessary for picosecond level time transfer.

This study provides a characterization of deployed fiber between two remote locations of DC-QNet and three potential methods to measure, estimate, or predict in-situ transit time or clock offsets based on chromatic dispersion or polarization drift. Chromatic dispersion

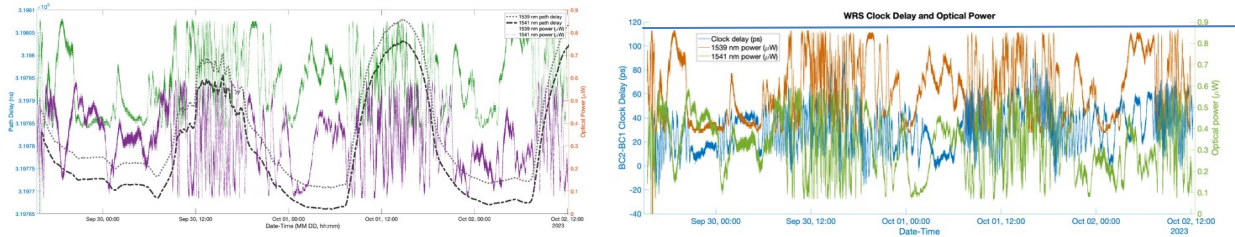


Figure 109. (left) Path transit time and optical power. (right) Clock delay and optical power on both links.

and polarization stability were measured to understand their impacts on differential group delays and clock synchronization precision towards active compensation. One way delay measurements from one link in a fiber pair showed similar changes in path delay variation as the other link and has the potential to be used to estimate the path delay between links. Finally, the third method is to replace the measurements with interpretable machine learning techniques to predict the transit time variation and clock offsets based on changes in the environmental parameters.

- [1] I. A. Burenkov, A. Semionov, T. Gerrits, A. Rahmouni, D.J. Anand, Y.S. Li-Baboud, O. Slattery, A. Battou, and S.V. Polyakov. Synchronization and Coexistence in Quantum Networks. *Optics Express* **31**:7 (2023), 11431–11446.
- [2] A. Bluhm, M. Christandl, and F. Spielman. A Single-Qubit Position Verification Protocol That Is Secure Against Multi-Qubit Attacks. *Nature Physics* **18** (2022), 623–626.
- [3] E. Cota, M. Lipiński, T. Włostowski, E van der Bij, and J Serrano. White Rabbit Specification: Draft for Comments, July 2011, v2.0.
- [4] T. Gerrits, I. A. Burenkov, Y. S. Li-Baboud, A. Rahmouni, D. J. Anand, O. Slattery, A. Battou, and S. V. Polyakov. White Rabbit-assisted Quantum Network Node Synchronization with Quantum Channel Coexistence. In *CLEO: QELS Fundamental Science, 2022*, FM1C-2.
- [5] W. McKenzie, Y.S. Li-Baboud, M. Morris, G. Baumgartner, A. Rahmouni, P. Kuo, O. Slattery, B. Crabill, M. Merzouki, A. Battou, and T. Gerrits. Sub-200 ps Quantum Network Node Synchronization Over a 128 km Link White Rabbit Architecture. In *CLEO: Fundamental Science, 2023*, FF3A-3).
- [6] IEEE Standard for a Precision Clock Synchronization Protocol for Networked Measurement and Control Systems. IEEE Standard 1588-2019 (Revision of IEEE Standard 1588-2008) June 16, 2020. DOI: [10.1109/IEEESTD.2020.9120376](https://doi.org/10.1109/IEEESTD.2020.9120376)

Quantum Network and Component Metrology

Thomas Gerrits
 Oliver Slattery
 Anouar Rahmouni
 Yicheng Shi
 Jaden He
 Pranish Shrestha
 Sonja Hakala
 Scott Glancy
 Manny Knill
 Riley Dawkins
 Paulina Kuo
 Lijun Ma
 Xiao Tang
 Nijil Lal
 Ya-Shian Li-Baboud (NIST ITL)
 Abdella Battou (NIST CTL)
 Amar Abane (NIST CTL)
 Abderrahim Amlou (NIST CTL)
 Lydia Ait Oucheggou (NIST CTL)
 Mheni Merzouki (NIST CTL)
 Jabir Marakkarakath Vadakkepurayil (NIST CTL)
 Alan Migdall (NIST PML)
 Sergey Polyakov (NIST PML)
 Josh Bienfang (NIST PML)
 Ivan Burenkov (NIST PML)
 Ping-Shine Shaw (NIST PML)
 Hristina Georgieva (PTB Germany)

The Quantum Network and Component Metrology Project focuses on the characterization of quantum network links, components, and protocols. Measurement protocols and deployable tools are developed in our lab and used within our NIST Gaithersburg quantum network testbed (NG-QNet) and the regional quantum network called the DC-QNet. We collaborate with researchers across different NIST units (PML, ITL and CTL) as well as with researchers from other government agencies and industry. The project tackles measurement challenges for single-photon devices and components, and therefore works closely with companies within the Quantum Economic Development Consortium (QED-C) on component characterization and solving measurement

challenges [1]. Last year's highlights include: Demonstration of coexistence between quantum entanglement and classical signals; Fiber polarization stabilization at the single-photon level (see page 131); Progress towards the establishment of a quantum network metrology node at the University of Maryland (UMD); Publication of a Single Photon Source and Detector dictionary to provide clarity in language (see page 129); Setup of infrastructure to measure optical fiber connector losses with less than 1 % uncertainties; bilateral comparison of single-photon detector calibration capabilities between NIST and PTB, and nascent efforts to develop infrastructure for continuous variable quantum states of light network metrology.

UMD Quantum Network Metrology Node. In classical optical communication, improved metrology has ensured the success of each new generation of systems. Quantum networks are much more complex than classical networks and will require novel and innovative metrology to succeed. We are leading the development of quantum network metrology protocols and are collaborating with researchers at the NIST/UMD Joint Quantum Institute (Alan Migdall) and share a lab space at the University of Maryland at College Park that is connected to the NIST campus via a 62 km quantum network fiber link. The lab serves as a quantum network beacon of well-characterized quantum signals and as the first deployed NIST metrology node for the DC-QNet and NIST testbeds. The location also serves as workforce development for students and is an accessible hotspot for collaborators within the DC-QNet. The node currently consists of a single-photon source, polarization entanglement analyzers, time-taggers and synchronization equipment as shown in Figure 110. Over the next year, we plan to deploy beacon signal sources that will serve to encode metrology signals into weak laser pulses to be detected at a user receiver station within the quantum network. This will serve the DC-QNet with well-characterized and known states of light for the verification and operation of fiber links.

Fiber Connector Loss Measurements. Quantum networks will require low-loss components to preserve the quantum state they are carrying. The ultimate loss within a quantum network should be dominated by unavoidable physical constraints, such as the optical fiber loss, and loss due to splicing or connecting fibers that is caused by mode-field diameter mismatches. The loss between components should not be dominated by mechanical inaccuracies of fiber mating connectors. The need for a low-loss, high-repeatability connector has recently been noted in a QED-C report on single-photon measurement infrastructure [1]. For example, fiber connector loss currently poses the largest uncertainty component for single-photon detector calibration [2]. While splicing the detector to the measurement apparatus will yield the lowest uncertainty, splicing detectors in flexible-grid



Figure 110. Deployed, rack-mounted quantum network node at the University of Maryland. (Photo by T. Gerrits, NIST)

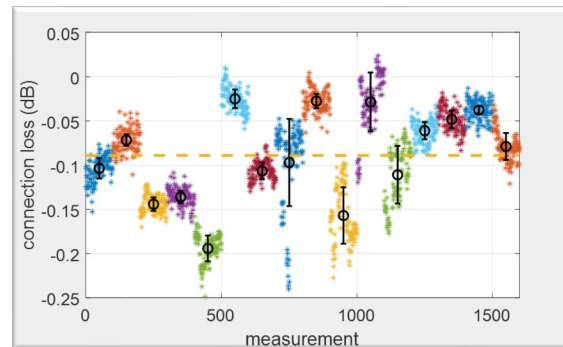


Figure 111. Loss evaluation of 16 random fiber connector combinations.

quantum networks is infeasible. To enable the development of a low-loss, high repeatability fiber connector, we are developing the measurement infrastructure and protocols to evaluate a fiber connector's loss and repeatability, a task we are tackling in collaboration with industry. Figure 111 shows the initial loss evaluation of 16 randomly selected fiber connectors. We are leveraging existing infrastructure (single-photon detector and single-photon-source characterization, existing quantum metrology lab infrastructure, and the NIST-Gaithersburg quantum network testbed) to develop the necessary tools and protocols [2-4] with an anticipated uncertainty below 1 %.

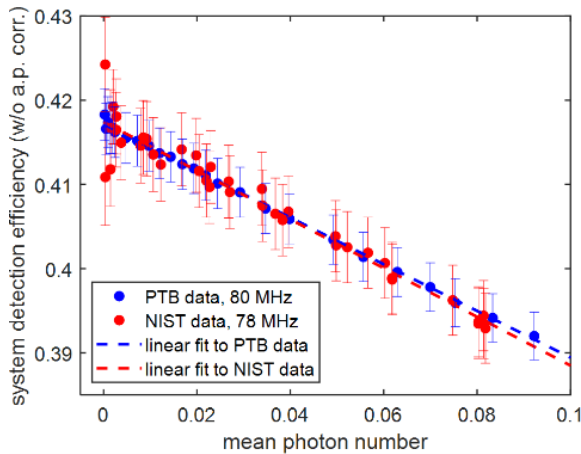


Figure 112. Measurement of single-photon detector efficiency vs. mean photon number input at a wavelength of 930 nm; blue: PTB data and fit; red: NIST data and fit.

Bilateral Comparison of Single-Photon Detector Calibration Capability. A baseline characterization tool for optical quantum components and quantum networks is the characterization and calibration of single-photon detectors. Methods for calibrating single-photon detectors are developed, used, and applied in various National Metrology Institutes (NMIs) and academia. Almost all methods rely on the precise knowledge of the input photon rate or mean photon number of the photon source used at the detector’s input plane. The most conventional method used at NMIs relies on a calibration chain that is tied and traced to the SI, while bridging the gap between microwatts and femtowatts of optical power. The calibration capability can be evaluated by comparing independent calibration chains within the community. We engaged with PTB in Germany and performed two independent measurements of a single-photon detector’s detection efficiency using the NIST Gaithersburg calibration chain and PTB calibration chain. Figure 112 shows the results of our bilateral comparison for a single-photon wavelength of 930 nm. We see excellent agreement between both measurements within each laboratory’s uncertainty estimates.

Continuous Variable Quantum Network Metrology. Exotic quantum states of light exploiting the continuous variable (CV) nature of light are an important tool for optical quantum information processing and form the basis of a compelling platform for quantum computing, now being pursued by the corporation Xanadu [5] and many academic research groups. In the long run, CV states may improve the performance of quantum networks, computers, and sensors as they allow a greater diversity of states than are available with only discrete variable protocols. Their development needs to be supported by advanced measurement techniques and technology to control, verify, and monitor the states and their correlations with each other and with extraneous

light. We are leveraging existing expertise and tools within ITL to begin the development a measurement infrastructure for CV states of light at telecom wavelengths around 1550 nm. We have established a partnership with Louisiana State University and are currently setting up a weak-field homodyne (WFH) detection system and plan to achieve first demonstrations by the end of this year. WFH detection is a measurement technique with a weak local oscillator (LO) reference light devised by members of the team [6, 7]. Besides eliminating crosstalk that a strong LO causes, WFH can also determine the characteristics of light in other modes and how this light is correlated with the mode of interest. It can distinguish between signal and noise photons. We plan to investigate the robustness of this technique in optical fibers that co-propagate a strong classical signal and will investigate the noise induced by the strong classical signal.

- [1] Single-photon Measurement Infrastructure for Quantum Applications (SPMIQA): Needs and Priorities. Quantum Economic Development Consortium (QED-C), 2022. URL: <https://quantumconsortium.org/single-photon-report>
- [2] T. Gerrits et al. Calibration of Free-space and Fiber-coupled Single-photon Detectors. *Metrologia* **57** (2020), 015002.
- [3] A. Rahmouni, T. Gerrits, A. Migdall, O. Slattery, P.-S. Shaw, J. P. Rice. A Self-Validated Detector for Characterization of Quantum Network Components. In *Conference on Lasers and Electro-Optics (CLEO)*, 2022, paper AW5P.6.
- [4] A. Rahmouni, S. Saha, O. Slattery, and T. Gerrits. Hyper-spectral Photon-counting Optical Time Domain Reflectometry. In *Proceedings of the SPIE* **12238** (2022), Quantum Communications and Quantum Imaging XX, paper 12238-7. DOI: 10.1117/12.2633451
- [5] J. M. Arrazola et al. Quantum Circuits with Many Photons on a Programmable Nanophotonic Chip. *Nature* **591** (2021), 54-60.
- [6] A. Avagyan et al. “State Tomography with Photon Counting After a Beam Splitter.” 22nd Annual SQuInT Workshop. Eugene, OR, February 8-10, 2020.
- [7] A. Avagyan, Quantum State Characterization Using Measurement Configurations Inspired by Homodyne Detection. Ph.D. Thesis, 2023. URL: <https://arxiv.org/abs/2305.19397>

Thin-film Lithium Niobate Integrated Photonics for Quantum Information Processing

Pavan Sessa Challa Kumar
Paulina Kuo
N. Klimov (NIST PML)

Performing quantum information processing using integrated optics is an attractive alternative to processing using free-space or bulk optics because integrated optics offers compact size and monolithic construction for high repeatability and phase stability. We have been exploring thin-film lithium niobate (TFLN) for integrated quantum photonics. TFLN offers multiple functionalities at the same time, including waveguiding, electro-optic modulation and optical frequency conversion (for quantum frequency conversion or entangled photon-pair generation) [1]. The initial step is to develop a process to fabricate low-loss waveguides in TFLN.

Using the NIST nanofabrication facility, we have performed a systematic study of argon-plasma dry etching of TFLN [2]. We have identified masking materials (see Figure 113). We have also optimized parameters for the dry etching to produce low-roughness waveguide sidewalls, which are needed to achieve low optical losses. Redeposited material forms during dry etching, so we have developed a wet-cleaning procedure to remove the redeposition. Scanning electronic microscope (SEM) images of the etching waveguides show highly promising results. We are developing a process to polish the waveguide end-facets for optical testing of the etched TFLN waveguides. Our goal is to develop a TFLN integrated-optics chip that can perform quantum measurements such as entanglement visibility or Bell-state measurements.

- [1] D. Zhu, et al. Integrated photonics on thin-film lithium niobate. *Advances in Optics and Photonics* **13** (2021), 242.
- [2] S. Challa, N. Klimov, and P. Kuo. "Argon-Plasma Dry Etch of sub-Micron Feature-Size Waveguides in Thin-Film Lithium Niobate." American Vacuum Science 69th International Symposium & Exhibition, Portland, Oregon, November 5-10, 2023.

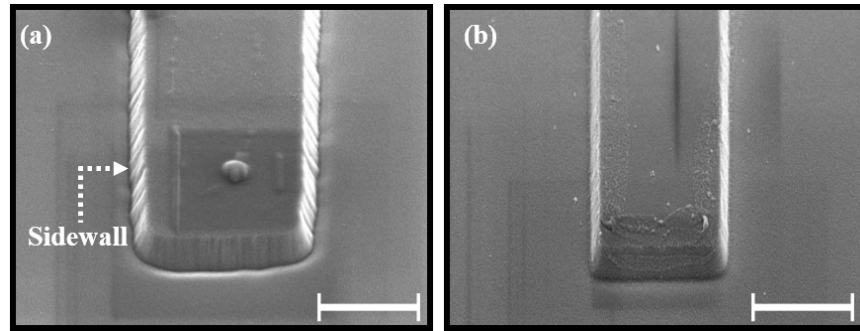


Figure 113. SEM images of etched TFLN waveguides using (a) photoresist soft mask and (b) Cr hard mask. The Cr mask produces smoother sidewalls. Some redeposited material is visible along the surfaces of the waveguides. Rectangular shadows are artifacts from the SEM imaging.

Frequency Translation for Quantum Networking

Paulina Kuo
Dileep Reddy (NIST PML)
Varun Verma (NIST PML)
Sae Woo Nam (NIST PML)
Andrius Zukauskas (Royal Inst. of Tech., Sweden)
Carlota Canalias (Royal Inst. of Tech., Sweden)

Quantum networks are collections of nodes and channels that distribute quantum information and perform quantum-enabled tasks such as entanglement distribution, quantum communications, and quantum computing. A common challenge in hybrid quantum networks (networks that involve diverse technologies such as spontaneous parametric downconversion (SPDC) photon-pair sources, quantum dots, or individual ions, as sketched in Figure 114 is to match the wavelengths and bandwidths of the photons that connect the nodes. Photon interference during a Bell state measurement requires that the two incoming photons are at the same wavelength. Bandwidth matching is critical when attempting to have a photon interact with a narrow atomic or ionic transition in a quantum memory or in an

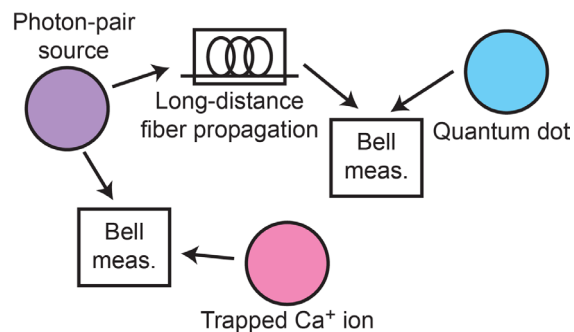


Figure 114. Conceptual sketch of a hybrid quantum network that has different nodes connected by photons that interfere at Bell state measurements.

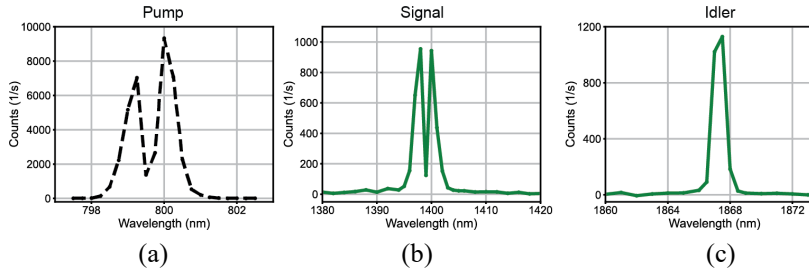


Figure 115. Spectra of the (a) pump, (b) signal and (c) idler, demonstrating transfer of the spectral features of the pump to the signal during BW SPDC.

optical cavity. If the bandwidth of the incident photon is too large, then the interaction efficiency is low and photon loss is incurred. Quantum frequency conversion [1] can be used to match the center wavelengths of the photons. Spectral filtering can be used to match bandwidths (at the expense of loss). We explore a new way to engineer the wavelength, bandwidth, and other spectral features of single photons: frequency translation using backward-wave spontaneous parametric downconversion (BW SPDC).

In BW SPDC, photon pairs are produced with the configuration such that the longest-wavelength photon (the idler) propagates in a direction opposite to the other photons (the pump and signal). The phasematching relationship for BW SPDC is unique and dictates that the idler is very narrowband and is nearly insensitive to pump-frequency tuning, which implies that any spectral modulation at the pump is transferred to the signal photons in a process called frequency translation. Using BW SPDC, spectrally engineered features at the pump can be frequency translated to the signal. By using the idler as a herald photon, this process can enable the production of spectrally engineered, heralded single photons, which are useful tools for quantum networks. We experimentally explore the process of frequency translation using BW SPDC.

In our experiment, we used a 500-nm period, periodically poled KTiOPO_4 (PPKTP) crystal to perform BW SPDC using 800 nm pump, 1400 nm signal and 1870 nm idler [2]. The pump was modulated by sending the 800-nm, 1-ps pulses through single-mode fiber that imparted self-phase modulation to the pump beam. We observed the SPDC output spectra using a grating monochromator and superconducting nanowire single-photon detectors. The recorded spectra are plotted in Figure 115. We observed a two-peak spectrum at the pump that is replicated at the signal near 1400 nm. Within the resolution of the monochromator, the idler is highly narrowband in spectrum. This method of producing spectrally shaped, heralded single photons at the signal wavelength is desirable compared to conventional filtering and spectral shaping of the signal photons because it avoids loss at the signal and idler, and maintains high pair-generation efficiency [2]. Another potential application for these spectrally shaped photons is their

use in all-optical quantum computing using frequency-bin qubits [3]. In the future, we plan more detailed studies of the spectral response of the BW SPDC to better understand the mechanism and limitations of BW SPDC frequency translation.

[1] P. Kumar, Quantum Frequency Conversion. *Optics Letters* **15**:24 (1990), 1476.

[2] P. S. Kuo, D. V. Reddy, V. Verma, S. W. Nam, A. Zulkas, and C.

Canalias, Photon-Pair Production and Frequency Translation Using Backward-Wave Spontaneous Parametric Downconversion. *Optica Quantum* **1**:2 (2023), 43. DOI: [10.1364/OPTICAQ.500021](https://doi.org/10.1364/OPTICAQ.500021)

[3] J. M. Lukens and P. Lougovski. Frequency-encoded Photonic Qubits for Scalable Quantum Information Processing. *Optica* **4**:1 (2017), 8.

SiC-based Integrated Quantum Device Efforts

Lijun Ma

Anouar Rahmouni

Oliver Slattery

Thomas Gerrits

Xiao Tang

Qing Li (CMU)

Lutong Cai (CMU)

Michael Spencer (Morgan State University)

Ali Adibi (Georgia Tech)

Silicon carbide (SiC) has emerged as a promising material for quantum information processing and quantum communication [1, 2]. As a third-generation wide-bandgap semiconductor material with various polytypes of crystal structure, SiC has many favorable properties for photonic and quantum applications. Because SiC device fabrication is compatible with the existing CMOS foundry, it enables quantum chips with a small footprint, reduced optical power budget, and affordable manufacturing cost.

We have worked with colleagues in Carnegie Mellon University (CMU) on the development and characterization of an entangled photon source based on a SiC micro-ring. The device is based on a 4H-silicon-carbide-on-insulator platform. A silicon dioxide (SiO_2) layer provides isolation from the silicon substrate, and a compact 36- μm -radius SiC micro-ring resonator is employed for the photon pair generation.

In FY 2022, we investigated the possibility of photon pair generation based on the spontaneous four-wave

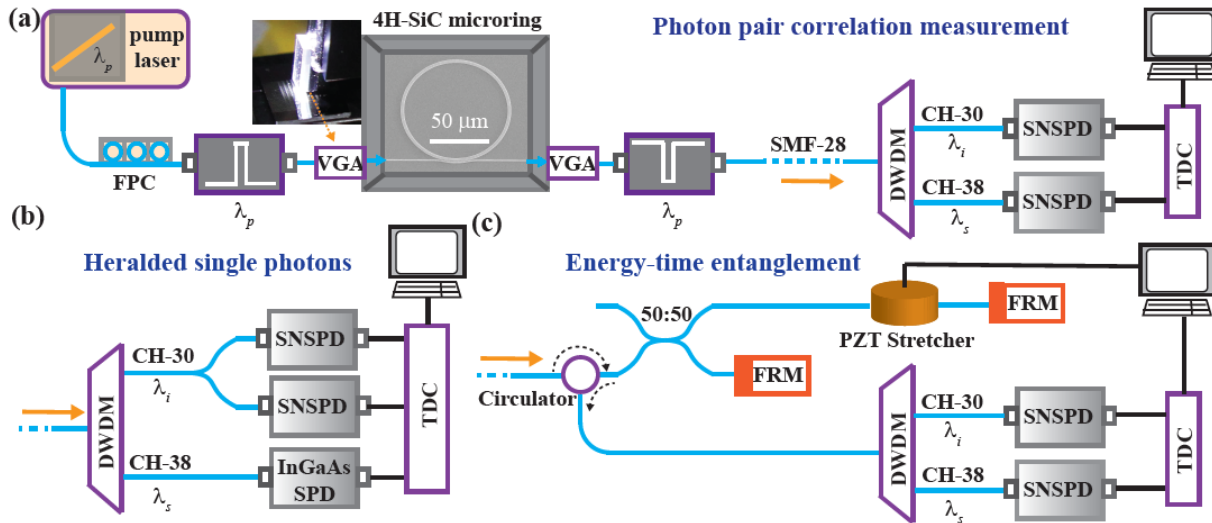


Figure 117. SiC entangled photon source and experimental set-up.

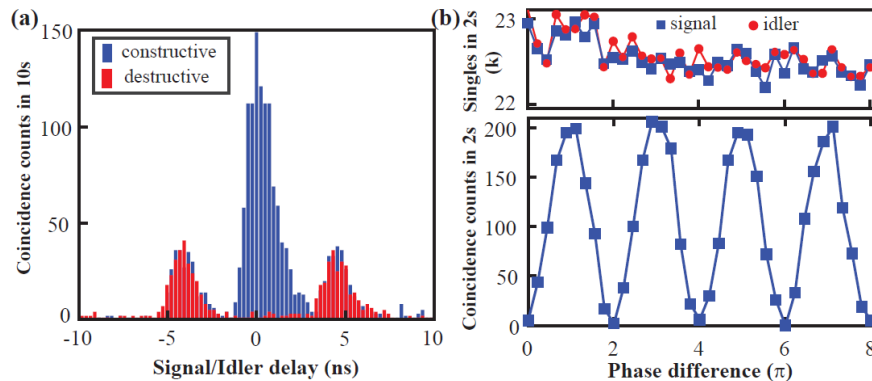


Figure 116. Time-energy entanglement measurement from SiC-based entangled photon source.

mixing (SFWM) process in a SiC micro-ring resonator and demonstrated single photon temporal coincidence in the platform. This was the first report of a single photon coincidence measurement from SFWM in any SiC platform. During this year, we further improved the quality of SiC devices as well as the source experimental setup, resulting in significantly better coincidence-to-accidental ratio (CAR) and the demonstration of a time-bin entanglement scheme with the highest ever reported visibility for any SiC platform.

Figure 117 summarizes the experimental setup for the device characterization. With the improvement of device and the experimental set-up, we realized on-resonance pair generation rates exceeding 1×10^6 counts/s for an on-chip power near 5 mW. The CAR was measured to be as high as 620 without any background which is a clear signature of correlated pair-detection events. We further created energy-time entanglement using a folded Franson interferometer. By varying the phase of the interferometer, the interference fringes of energy-time entangled photons can be produced as shown in Figure 116. The visibility is estimated to be larger than

99 % without background subtraction, which far exceeds the limit of theoretical requirement of $\frac{1}{\sqrt{2}} \approx 71\%$ to verify the entangled nature of produced photon pairs.

In addition to research on the entangled photon source, we also collaborated with CMU, Morgan State University (MSU) and Georgia Institute of Technology to investigate optically addressable spin qubits in SiC devices, particularly from Vanadium

doped SiC. The emission photon wavelengths in such devices are in telecom bands and is ideal as telecom compatible single photon emitters and quantum memories.

SiC is a third-generation semiconductor material and has emerged as an important platform in chips technology. This research has the potential to realize a multitude of key quantum communication building blocks on a single chip. With further research and improvement, it is possible for these devices to be deployed into our quantum network testbed effort at NIST, which would provide important proof-of-concept to industry.

- [1] A. Rahmouni, L. Ma, R. Wang, J. Li, X. Tang, T. Gerrits, Qing Li, and O. Slattery. Photon Pair Generation with Greater Than 600 Coincidence-to-Accidental Ratio in the 4H-SiC-on-Insulator Platform. *In Proceedings of Quantum 2.0*, Denver, June 2023. DOI: 10.1364/QUANTUM.2023.QM4A.2
- [2] A. Rahmouni, L. Ma, X. Tang, T. Gerrits, L. Cai, Q. Li, and O. Slattery. Towards Entangled Photon Pair Generation from a SiC-based Microring Resonator. In

Proceedings of the 2022 Conference of the Society of Photo-Optical Instrumentation Engineers (SPIE): Optics and Photonics, October 2022. DOI: 10.1117/12.2632597

- [3] A. Rahmouni, L. Ma, L. Cai, X. Tang, T. Gerrits, Q. Li and O. Slattery. “Microring-Based Photon Pair Sources in the 4H-SiC-on-Insulator Platform.” *Single Photon Workshop*, Seoul, Korea, October 31 - November 4, 2022.
- [4] L. Ma and O. Slattery. “SiC-Based Quantum Devices for Quantum Communication and Networks.”, *Conference on Quantum Information*, Seoul, Korea, July 2023.

Joint Center for Quantum Information and Computer Science

Victor Albert

Matthew Coudron

Yi-Kai Liu

Justyna Zwolak

Gorjan Alagic (NIST ITL)

Carl Miller (NIST ITL)

Alexey Gorshkov (NIST PML)

Michael Gullans (NIST PML)

Jacob Taylor (NIST PML)

Nicole Yunger Halpern (NIST PML)

Andrew Childs (University of Maryland)

<http://quics.umd.edu/>

Established in October 2014, the Joint Center for Quantum Information and Computer Science (QuICS) is a cooperative venture of NIST and the University of Maryland (UMD) to promote basic research in understanding how quantum systems can be effectively used to store, transport and process information. QuICS brings together researchers from the University of Maryland Institute for Advanced Computer Studies (UMIACS) and the UMD Department of Computer Science and Physics with NIST’s Information Technology and Physical Measurement Laboratories, together with postdocs, students, and a host of visiting scientists.

QuICS has quickly established itself as a premier center for research in quantum information science. Fourteen Fellows, five Affiliate Fellows, one Adjunct Fellow, 20 postdocs, and 67 graduate students are currently associated with the center. In CY 2023, seven QuICS students successfully defended their dissertations and were awarded Ph.D. degrees from UMD. Yi-Kai Liu of ACMD is Co-Director of the Center along with Andrew Childs of the UMD Computer Science Department.

This year, Zohreh Davoudi, an Associate Professor in the UMD Department of Physics, became a QuICS

Fellow. At QuICS she explores analog, digital, and hybrid approaches to simulating quantum field theories of nature with a range of quantum-simulating and quantum-computing platforms, from trapped-ions to solid-state systems.

The Center continues to be very productive. In CY 2023 some 70 research papers were produced by those associated with the center. Some 88 seminars by both internal and external speakers were held. Another measure of success is the strong presence of QuICS members on the program of the annual Quantum Information Processing Conference (QIP), the premier venue for theoretical research on quantum information processing, whose selection for talks is highly competitive. QuICS members presented six talks at QIP 2023, which was held in Ghent, Belgium in February. Five QuICS members were on the Program Committee for QIP 2023, making QuICS the most-represented institution on the committee.

In August, QuICS hosted a major quantum cryptography conference on the UMD campus. QCrypt 2023, the latest in a series of annual conferences on all aspects of quantum cryptography (previously organized by QuICS in 2016), was held in the Iribe Center from August 14-18.²⁹ This event brought together 220 researchers from 28 countries and featured opening remarks by UMD President Daryll Pines and NIST Associate Director for Laboratory Programs Charles Romine.

Finally, QuICS members received several awards this year. Highlights include the NIST Samuel Wesley Stratton Award, awarded to Alexey Gorshkov for significant research contributions that advance the mission of NIST, and the Mary Somerville Medal of the Institute of Physics and the 2023 PROSE Award from the American Association of Publishers awarded to Nicole Yunger Halpern for her popular science book *Quantum Steam-punk: The Physics of Yesterday’s Tomorrow*. [1]

- [1] Nicole Yunger Halpern. *Quantum Steam-punk: The Physics of Yesterday’s Tomorrow*. Johns Hopkins University Press, 2022.

²⁹ <https://2023.qcrypt.net/>

Foundations of Measurement Science for Information Systems

ITL assumes primary responsibility within NIST for the development of measurement science infrastructure and related standards for IT and its applications. ACMD develops the mathematical foundations for such work. This can be very challenging. For example, many large-scale information-centric systems can be characterized as an interconnection of many independently operating components (e.g., software systems, communication networks, the power grid, transportation systems, financial systems). A looming new example of importance to NIST is the Internet of Things. Exactly how the structure of such large-scale interconnected systems and the local dynamics of its components leads to system-level behavior is only weakly understood. This inability to predict the systemic risk inherent in system design leaves us open to unrealized potential to improve systems or to avoid potentially devastating failures. Characterizing complex systems and their security and reliability properties remains a challenging measurement science problem.

Algorithms for Identifying Important Network Nodes for Communication and Spread

Fern Y. Hunt

Roldan Pozo

The identification of nodes in a network that enable the fastest spread of information is an important, if not fundamental, problem in network control and design. It is applicable to the optimal placement of sensors, the design of secure networks, and the problem of control when network resources are limited. Our approach to this problem has its origins in models of opinion dynamics and the spread of innovation in social networks. The mode of communication between nodes is described by simple models of random or deterministic propagation of information from a node to its neighbors. During the past few years, we have made progress in understanding the structural requirements for sets of nodes for effective spread in networks and have developed scalable algorithms for constructing these sets in real world networks.

We consider a discrete time model of information spread (represented by a variable assigned to each node) in a network with a set of nodes V and a subset $A \subseteq V$ of k nodes representing leaders or stubborn agents that are initially assigned a single value. Propagation occurs by iterated averaging or diffusion defined by a stochastic matrix P . All node values will eventually converge to the single value at a speed determined by the sub-stochastic matrix $P|_A$, the matrix P restricted to the complement of A . An effective spreader in this situation is, then, a set of nodes for which convergence to this single value is fastest, i.e., the set A for which the Perron-Frobenius eigenvalue of $P|_A$ is largest. Using a classical result of Markov chain theory, the problem can be recast in terms of finding the set A of cardinality k that minimizes the mean first hitting time, i.e., the expected time a random walker reaches the target set A for the first time.

We first proposed a polynomial time algorithm for finding an approximation to the optimal set [1]. It is an

extension of the classic greedy algorithm; it begins with a class of optimal and near optimal starter sets of smaller cardinalities rather than the conventional choice of a best singleton set. An optimal spreader in our setting is defined in terms of a set function F where for a subset $A \subset V$, $F(A)$ is the sum of mean first arrival times to A by random walkers that start at nodes outside of A . Direct comparison of the algorithm results with the actual optimal solution and lower bounds on the performance ratio can be obtained because F is a supermodular set function [2]. However, for large complex networks commonly encountered in applications, another approach is needed.

We then developed a set of fast heuristics that work well on graphs with large hubs, a common feature of complex networks. When the desired set cardinality is k , subsets of hub vertices are rapidly screened to produce candidate sets. Each set consists of k nodes whose first (or higher order) neighborhoods have minimal overlap. After further screening, the offered approximation is selected by ranking the results of a Monte Carlo calculation of the optimal set F for each candidate. This process allows us to find near optimal and optimal spreaders in networks with millions of nodes and dozens of millions of edges in less than a few seconds on a typical laptop. After conducting tests on real world graphs from diverse application areas including molecular biology, traffic control, and social networks, we hypothesize that the method is most effective in terms of speed and quality of offered solutions when it is used on graphs with a large ratio of maximal degree to average degree.

Understanding that the resulting offered set was an approximate solution of a discrete stochastic optimization problem, we established sufficient conditions that imply that it is also an approximate solution of the original problem. The first step was to establish the accuracy of the Monte Carlo calculation of F . The fact that the first hitting time to a set A has a distribution with exponential tails means that a sample average of simulated hitting times produces a consistent estimate of F in the limit of large sample size i.e., number of simulations.

Establishing the degree of optimality of any offered solution is very difficult since supermodularity cannot

be used and the size of the graphs are so large. However, the methods we use make it possible to rapidly sample the distribution of possible F values. We suppose the screening and ranking procedures produce candidate sets with F values that rank in the highest percentile of a distribution of such values over all subsets of fixed cardinality. Independent repetition of the heuristic calculation enables us to produce an estimate of a fixed percentile value along with a confidence interval for that estimate. The latter follows from an application of Chebyshev's inequality. Note that the resulting interval contains both the offered solution value and the optimal value of the original problem. Even in the case of a large number of repetitions, this approach is promising because it takes very little time to perform a single execution. The results of our work are reported in [3].

We have also studied related models of information spread, such as the broadcast model (k -median problem) which seeks the minimal sum of distances, and epidemiological models (Susceptible-Infected-Recovered) that better represent the spread of infectious diseases on network topologies. We have studied and compared the efficacy of several heuristic algorithms used in the literature and have developed a different approach (minimizing overlapping neighborhoods) which aims to produce quality solutions at a fraction of the computational cost, making it appropriate for use on large networks. For example, we are able to process graphs of several million vertices with competitive solutions that run one to two orders of magnitude faster than previous methods. From previous analysis, we have focused on more than 16 000 experiments of network/algorithm/ k -value combinations and have created parallel OpenMP C++ applications for the evaluation of these models. This effort has yielded important insights on establishing best practices for approximating methods on real networks and providing efficient solution techniques to this challenging problem. A summary of these results is presented in [4].

- [1] F. Hunt. Using First Hitting Times to Maximize the Rate of Convergence to Consensus. Preprint, 2018. URL: [arXiv:1812.08881](https://arxiv.org/abs/1812.08881)
- [2] F. Hunt. An Algorithm for Identifying Optimal Spreaders in a Random Walk Model of Network Communication. *Journal of Research of the NIST* **121** (2016), 121008. DOI: [10.6028/jres.121.008](https://doi.org/10.6028/jres.121.008)
- [3] F. Hunt and R. Pozo, Fast Methods for Identifying Effective Spreaders in Real Network. *Journal of Research of the NIST* **125** (2020), 125036. DOI: [10.6028/jres.125.036](https://doi.org/10.6028/jres.125.036)
- [4] R. Pozo. Approximation of Algorithms for k -median Problems on Complex Networks: Theory and Practice. Preprint, 2023. DOI: [10.48550/arXiv.2312.07644](https://doi.org/10.48550/arXiv.2312.07644)

Towards Risk Evaluation and Mitigation in Networked Systems

Vladimir Marbukh

The first focus of our current research is mitigation of systemic risk in networked systems while retaining economic and convenience benefits of interconnectivity. The difficulty is that the same interconnectivity which makes possible information exchange, dynamic resource allocation, risk diversification, etc. also enables undesirable contagion due to cascading overload, computer virus propagation, etc. Systemic risk is often measured by the distance to the point of the undesirable transition in the space of exogenous parameters. However, this measure does not account for potential losses if such a transition occurs due to unavoidable uncertainties in these same exogenous parameters. Apparently, abrupt/discontinuous transitions carry higher risk than gradual/continuous ones. It has been shown in [1] on an example of Susceptible-Infected-Susceptible (SIS) infection that even in a case of gradual/continuous transition, a higher safety margin with respect to infection threshold may be associated with higher losses if this threshold is breached. In [2] the risk metric Viral Conductance (VC) is proposed, which accounts for both the safety margin and losses due to the possible breach of the infection threshold.

Due to the arbitrary nature of assumptions about the possibility and depth of this breach, in [3] we have proposed and discussed potential advantages of a systemic risk metric based on the notion of Entropic Value at Systemic Risk, which overcomes some limitations of VR. In the case of abrupt/discontinuous transitions, which are often associated with metastability, systemic risk metrics should also account for the system time horizon of interest. Since economic pressures drive system operations towards the stability boundary, the system operational equilibrium is likely to be metastable, and thus the systemic risk of transition to a systemically failed equilibrium depends on the likelihood that the system time horizon of interest exceeds the lifetime of the operational equilibrium.

The approximation of systemic risk due to possible transition to an undesirable metastable state that we proposed in [4], takes advantage of the time scale separation between "rare" system transitions between metastable states approximated by a two-state Markov process and "fast" convergence to the corresponding metastable equilibrium. Following the Landau theory of phase transitions, [4] describes these rare transitions between metastable equilibria by potential dynamics for the portion of failed/infected network nodes, which represent the order parameter in the Landau theory of phase transitions. The transition rates between metastable equilibria sharply decrease with increase in the height of

the “potential barrier” in the corresponding potential dynamics.

Our results [5-8] suggest a potential practical benefit of the proposed systemic risk quantification for risk aware system design and operation. In particular, [5-8] define and discuss a concept of a risk-adjusted operational region which reduces the conventional operational region by a system designer/operator risk-tolerance-dependent safety margin. This safety margin is non-existent for risk neutral decision makers and increases with a decrease in the risk tolerance. In the case of a discontinuous stability loss on the boundary of the operational region associated with metastability, the safety margin also depends on the relation of life expectancies of the metastable equilibria and the system time horizon.

Future research should address practicality of the proposed in [3-4] risk metric in application to systemic failures in various real-life large-scale interconnected infrastructures, e.g., power grids, distributed computing infrastructure, etc. This would require sufficiently “high resolution” analysis of systemic risk in a proximity of the boundary of the risk-adjusted operational region. A significant practical impact for controlling large-scale networked systems would have a possibility of systemic risk evaluation in real time. Our attempts [5-8] to move in this direction, may be a source of cautious optimism in the feasibility of this program.

The second focus area of our current research is evaluation/mitigation of adversarial risk in networked systems. The security metric we discuss in [9-10] combines the risks of known and unknown attacks, where inherent uncertainties of unknown attacks are addressed within framework of robust risk metrics. The proposed metric depends on the decision-maker risk tolerance and expectations of the attack severity. For the example of Moving Target Defense (MTD), we argue that the proposed risk metric may provide guidance not only for assessing zero-day security risks but also for risk mitigation. The risk minimization proposed in [9-10] interpolates between the Bayesian and game-theoretic frameworks depending on the decision-maker risk tolerance and the attack severity.

Future research should address practicality of the proposed metric by evaluating specific systems and risk mitigation techniques. We expect that the known computational advantages of entropic risk measures may ensure computational tractability of the proposed security risk metric for practical systems. On a more fundamental level, we are planning to develop adversarial risk metrics allowing for an intelligent attack, which is preceded by a reconnaissance phase to discover and then target system weak points. System defenders could use such metrics to effectively allocate limited defense resources between prevention of the information gathering during reconnaissance phase on the one hand and

hardening the system vulnerabilities on the other hand.

- [1] P. Van Mieghem. Epidemic Phase Transition of the SIS-type in Network. *Europhysics* **97** (2012), 48004.
- [2] R. E. Kooij, P. Schumm, C. Scoglio, and M. Youssef. A New Metric for Robustness with Respect to Virus Spread *Networking*, Lecture Note in Computer Science **5550** (2009), 562–572.
- [3] V. Marbukh. Towards Evaluation & Mitigation of the Entropic Value at Systemic Risk in Networked Systems. In *Book of Abstracts of the 12th International Conference on Complex Networks and their Applications*, Menton, France, November 28-30, 2023.
- [4] V. Marbukh. Systemic Risk of Discontinuous Failures in Large-Scale Networks within Time Horizon: Work in Progress. In *Book of Abstracts of the 12th International Conference on Complex Networks and their Applications*, Menton France, November 28-30, 2023.
- [5] V. Marbukh. Towards Evaluation/Mitigation Risk of Systemic Failures in a Recoverable Network with Redistributed Elastic Load. In *14th ACM/SPEC International Conference on Performance Engineering (ICPE 2023)*, Coimbra, Portugal, April 15-19, 2023.
- [6] V. Marbukh. “Network Resiliency to Systemic Failures within Time Horizon by Managing Robustness/Recoverability Capabilities: Work in Progress.” International School and Conference on Network Science 2023, (NetSci 2023), Vienna, Austria, July 10-14, 2023.
- [7] V. Marbukh. “Systemic Risk of Cascading Failures/Overloads in a Recoverable Network under Redistributed Elastic Load: Work in Progress.” International School and Conference on Network Science 2023, (NetSci 2023), Vienna, Austria, July 10-14, 2023.
- [8] V. Marbukh. On Potential Risks of “Natural” Hybrid Load Balancing in Large-Scale Clouds: Work in Progress. In *IEEE Consumer Communications & Networking Conference (IEEE CCNC 2023)*, Las Vegas, NV, January 8-11, 2023.
- [9] V. Marbukh. Towards Incorporating a Possibility of Zero-day Attacks into Security Risk Metrics: Work in Progress. In *IEEE Consumer Communications & Networking Conference (IEEE CCNC 2023)*, Las Vegas, NV, January 8-11, 2023.
- [10] V. Marbukh. Towards Security Metrics Combining Risks of Known and Zero-day Attacks: Work in Progress. In *IEEE/IFIP Network Operations and Management Symposium (NOMS 2023)*, Miami, FL, May 8–12, 2023.

Measurements of the Effects of Homophily on Epidemic Processes

Richard J. La

The spread of malware and viruses in computer networks and information systems, contagious diseases, rumors, and new product information is often modeled using epidemic processes on graphs. The graphs are

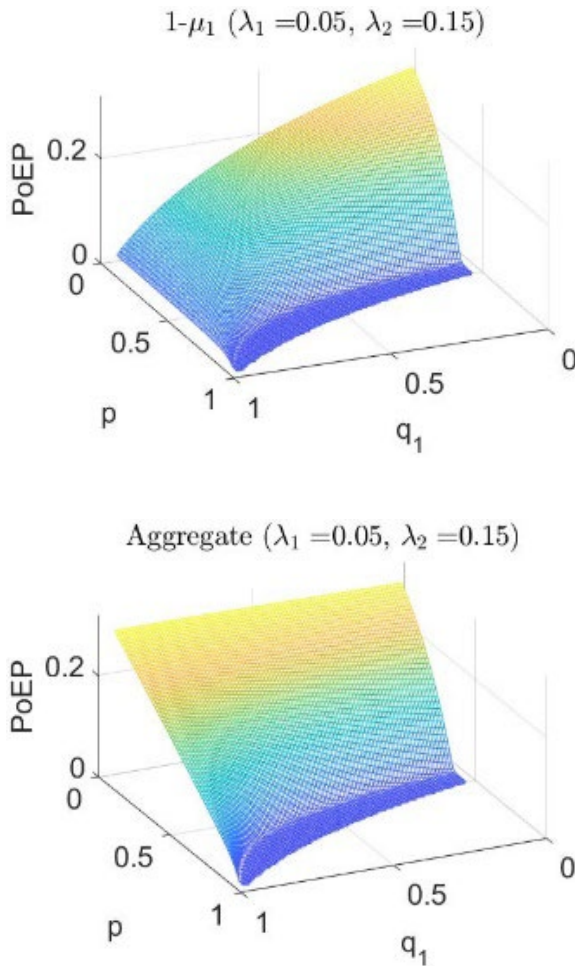


Figure 118. Plot of PoEPs as a function of the fraction of type 1 population (p) and the probability that a neighbor of a type 1 individual is of type 1 (q_1). When q_1 is greater than p , it indicates the presence of homophily. The parameter λ_i , $i = 1, 2$, is the probability that a type i individual will contract the disease when exposed. The top plot is the PoEPs of type 1 individuals, and the bottom plot is the weighted average PoEPs of both type 1 and type 2 individuals.

used to capture the connectivity between interacting systems or contacts between individuals. Studies have revealed that both engineered networks and natural networks display several interesting properties, such as the small world phenomenon, high transitivity (or clustering), and degree correlations. These properties influence how contagious diseases, information or viruses spread over networks. For this reason, it is important to understand how they affect the dynamics of epidemic processes on networks.

Another property that has been observed widely in social networks is homophily [1]. It refers to the observation that people tend to be friends with others who share common beliefs or similar background and is shown to have significant impact on our decisions. For example, a close circle of friends may have similar opinions about vaccines and the risks from an infectious disease. As a result, when one member of the circle is

antivaccine or does not believe in vaccines, other members may be less likely to get vaccinated (than the general public) and be more likely to contract the disease when exposed.

Despite its prevalence, the effect of homophily on epidemic processes is not well understood. The goal of the project is to investigate how homophily influences the spread of infectious diseases in a large population and quantify its impact using a suitable metric. Although our study is carried out in the context of a disease epidemic, our framework and results apply to other applications, including information or virus propagation in information networks and systems.

Consider a population consisting of two types of individuals, e.g., vaccinated vs. unvaccinated. Our proposed framework adopts the probability of experiencing an epidemic (PoEP) starting with a single infected individual at the beginning as our metric. Using the proposed framework and metric, we derived a set of conditions that can be obtained from the system parameters and determine how homophily changes the PoEPs [2]. Finally, we conducted numerical studies to validate our findings.

Figure 118 plots the PoEPs for an example scenario with two populations. When exposed, a type 1 individual contracts the disease with probability 0.05, while a type 2 individual gets infected with probability 0.15. We vary the fraction of type 1 individuals in the population (p) and the probability that a randomly chosen neighbor of a type 1 individual is also of type 1 (q_1). When $q_1 > p$, homophily is present in the population. The top plot shows the PoEPs for type 1 individuals that are less likely to contract the disease, and the bottom plot shows the average PoEPs for the entire population.

The top plot indicates that when p is small, homophily benefits type 1 individuals in that they are less likely to trigger an epidemic when they become infected. When homophily is present, one may suspect that this is intuitive since infected type 1 individuals may be less likely to spread the disease to neighbors because of the assumption that type 1 individuals contract the disease with lower probability. However, when p is large, somewhat surprisingly, the opposite is true. Furthermore, homophily tends to increase the average PoEPs for the population, which suggests that the homophily is harmful in that the population is more likely to suffer an epidemic when a new contagious disease emerges.

- [1] M. McPherson, L. Smith-Lovin, and J. M. Cook. Birds of a Feather: Homophily. *Annual Review of Sociology* 27 (2001), 415–444.
- [2] R. J. La. “Effects of Homophily in Epidemic Processes.” *12th International Conference on Complex Networks and Their Applications*, November 2023.

Determination and Measurements of Interference Between Network Slices in 5G/6G Networks

Richard J. La

Van Sy Mai (NIST CTL)

Tao Zhang (NIST CTL)

As diverse network applications and services demand widely varying service level requirements (SLRs), network slicing has gained growing interest. Network slicing is a network architecture in which a set of logical networks are supported on the same physical infrastructure and networks. The overall network slicing framework is shown in Figure 119. Each network slice (NS) is an end-to-end logical network tailored to support a specific set of SLRs. In principle, an NS is supposed to be isolated from other NSs so that it does not experience performance degradation when it shares (virtual) resources with other NSs, such as communication links, data buses, and virtual machines on which virtual network functions are run.

In practice, however, it has been observed that when multiple NSs share (virtual) resources, NSs are not isolated adequately and can affect the performance of other NSs [1, 2, 3]. This suggests that, in order to ensure that the SLRs of NSs are satisfied regardless of the activities of other NSs, it is crucial to identify any potential interference among existing NSs and take corrective actions when necessary. The overarching goal of this project is to design a suite of algorithms for (a) identifying groups of interfering NSs and (b) finding appropriate remedial actions to prevent violation of SLRs that could lead to unacceptable performance.

Our recent efforts focused on finding suitable metrics for measuring interference among NSs and based on the metrics, identifying the interference patterns among NSs based on network measurements, such as end-to-end packet delays and packet loss rates. Our proposed algorithm first identifies possible pairwise interference among NSs, which is represented by an interference graph, and lists all maximal cliques in the interference graph. Then, for each maximal clique in the interference graph, it clusters the network measurements collected from the NSs that belong to the clique and, for each cluster, acquires the NSs that oftentimes deviate from their normal behavior simultaneously.

In order for the proposed algorithm to work effectively, we need to determine for each maximal clique a suitable number of clusters of network measurements, which we analyze to uncover different groups of NSs that could potentially interfere with each other. To this end, we evaluate the quality of clusters for different numbers of clusters and choose an optimal number of clusters using different clustering evaluation criteria.

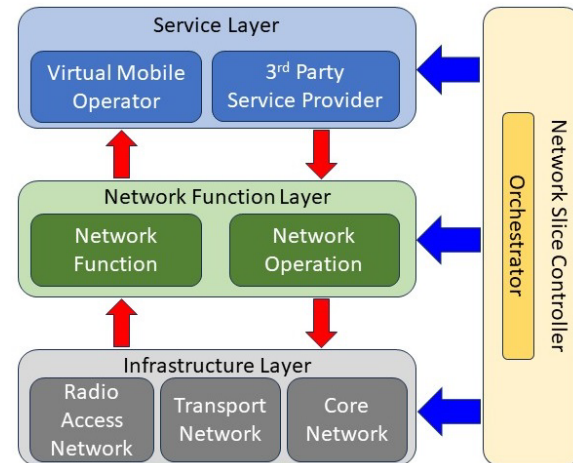


Figure 119. 5G network slicing framework.

Covariance based interference Graph

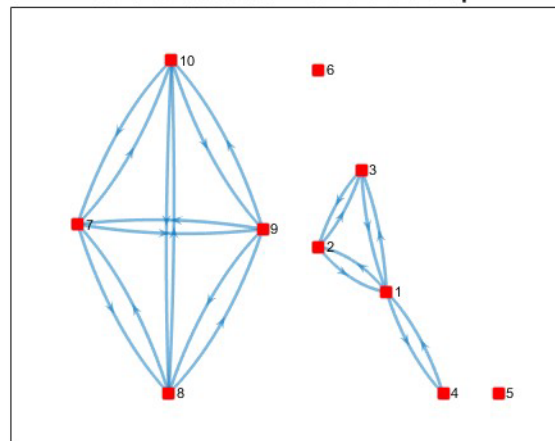


Figure 120. Plot of an interference graph that captures pairwise interference between network slices. The network slices are represented as red squares with the NS numbers next to them, and possible interference by an NS to another NS is indicated by a directed edge.

Figure 120 shows an interference graph constructed by our algorithm for a scenario with 10 NSs sharing six distinct resources. The graph is constructed from network measurements consisting of end-to-end delay measurements for the 10 NSs over 250 simulation epochs. There are three maximal cliques in the interference graph – $\{1, 4\}$, $\{1, 2, 3\}$, and $\{7, 8, 9, 10\}$. For each of these three maximal cliques, our proposed algorithm tries to identify all subsets of NSs that frequently experience abnormal behavior at the same time.

Our future efforts will focus on the following. First, the proposed algorithm can identify the sharing NSs for each resource that causes performance degradation in measurements. However, it suffers from false positives in that it also produces subsets of NSs as possible interfering NSs when they do not share resources together. We suspect that this is due to the clustering algorithm that is currently employed (which is either the k-means

clustering or the Gaussian mixture model clustering). We plan to refine our clustering algorithm to reduce the false positive rates of our algorithm.

Second, once our algorithm can identify the interference patterns reliably, we need to discover which NS(s) are responsible for causing performance degradation in the network measurements and, if appropriate, find a suitable action to be taken in a timely fashion. Such actions could include migration of flows or setting up new NS(s). Importantly, this needs to be performed without causing interference to other existing NSs with minimal impact.

- [1] S. Amri, H. Hamdi, and Z. Brahmi. Inter-VM Interference in Cloud Environments: A Survey. In *14th IEEE/ACS International Conference on Computer Systems and Applications*, October 2017.
- [2] W. Lin, C. Xiong, W. Wu, F. Shi, K. Li, and M. Xu. Performance Interference of Virtual Machines: A Survey. *ACM Computing Surveys* **55**:254 (2023), 1–37.
- [3] Q. Zhang, F. Liu, and C. Zeng. Adaptive Interference-Aware VNF Placement for Service-Customized 5G Network Slices. In *IEEE Conference on Computer Communications*, May 2019.

Towards Developing Carbon Aware Algorithms

Brian Cloteaux
Vladimir Marbukh

Our modern society has been, in large part, built upon communication and computing, which consume a sizable portion of produced energy. Energy generation and its uses have become interwoven into our society. Unfortunately, in recent years we have experienced the increasing negative ecological impact of carbon-based energy sources. Reducing this negative impact through wider use of green energy while still supporting the technological advances is becoming a paramount challenge of modern society.

A significant problem in reducing the use of carbon-based energy in highly distributed computations is the intermittency of green versus non-green energy sources due to variability of the external conditions such as wind velocities and the amount of sunlight [1]. Mitigating this problem can be approached by scheduling based on the amount of green energy available at different server centers and storing green energy for later use. Due to the complexity of the problem, simulations may play an important role in finding practical solutions.

Simulating Energy Usage for Job Replication. Resource usage versus performance trade-offs occur naturally in distributed algorithms. Distributing sub-calculations based on resource constraints (such as time or

attached peripherals) is a well-studied field. Our initial approach has been to introduce the additional constraint of carbon expenditure, and then study the trade-off between the time (both computation time and latency) and energy usage.

We are focusing on these trade-offs in the application of computational replication for mitigating intermittency [2]. Replication covers a set of strategies where jobs can be submitted to multiple servers at the same time for processing. By using replication, jobs can potentially benefit in two ways: first, protection against server crashing and slowdowns, and second, providing a quicker response time since the response time of the job is essentially dictated by the shortest server queue in which a replicated job is placed. Unfortunately, by allowing multiple copies of a job to start, we are obviously expending energy usage. We are interested in maintaining the advantages of job replication while mitigating the additional energy usage.

To study this trade-off, we have developed a simulation framework allowing us to examine the effects of various models and policies on the usage of sustainable energy for distributing jobs across different server farms [3, 4]. These models are built by combining features such as redundancy policies and server slowdown distributions [5, 6] with communication and server energy usage models [7].

Our simulation suite allows us to evaluate different scenarios for distributing replicated jobs under various energy policies. Some results produced by this software package for various scenarios are shown in Figure 121 and Figure 122. Figure 121 shows the trade-off curves between job latency and energy usage for various replication levels. In this figure Total Energy is the amount of energy available, while Run Time is the time to job completion. So, for example, if one has 750 joules of energy, 2 replicates is the best option, followed by 4, and then 1. As expected, higher level of replication becomes beneficial for reducing job latency with increase in the energy supply. Figure 122 shows the minimal achievable job latency with optimal redundancy level vs. energy expenditure. A point on this curve is deemed infeasible if no amount of replication can achieve a solution in the given time. This minimal achievable job latency curve also represents the Pareto optimal frontier separating feasible and infeasible regions in two-dimensional space of run time vs. energy expenditure. That is, the Pareto curve indicates the shortest time to solution for a given energy budget.

Current and Future Work. Currently, we are extending this work by developing cost-based algorithms for balancing energy usage with performance [8]. These mechanisms will allow for individual jobs to “purchase” job replication based on their resource needs and the current costs associated with individual servers. These costs could fluctuate based on the availability of energy supplies for the server. The aim of this line of research is to

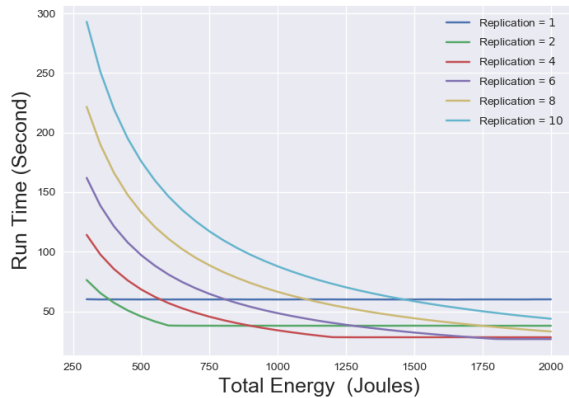


Figure 121. The tradeoff of energy use versus latency time for a cancel-on-completion redundancy policy [4, 6].

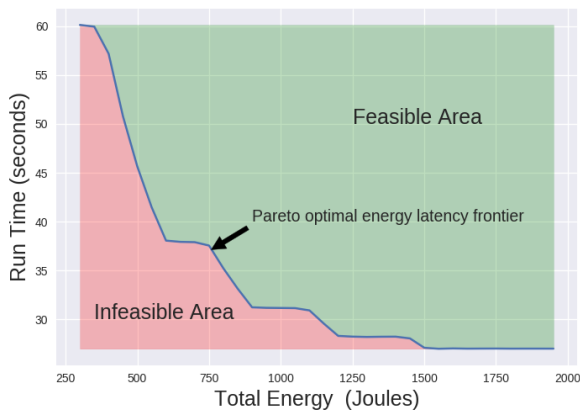


Figure 122. The feasible region for run time vs. energy expenditure.

develop non-centralized algorithms for balancing energy usage with latency [9].

- [1] A. Agarwal et al. Redesigning Data Centers for Renewable Energy. In *Proceedings of the Twentieth ACM Workshop on Hot Topics in Networks (HotNets '21)*, November 2021, 45–52. DOI: [10.1145/3484266.3487394](https://doi.org/10.1145/3484266.3487394)
- [2] G. Gowrisankaran, S. S. Reynolds, and M. Samano. Intermittency and the Value of Renewable Energy. *Journal of Political Economy* 124:4 (2016), 1187–1234. DOI: [10.1086/686733](https://doi.org/10.1086/686733)
- [3] V. Marbukh and B. Cloteaux. “Simulating Job Replication Versus Its Energy Usage.” Winter Simulation Conference, San Antonio, Texas, December 2023.
- [4] V. Marbukh and B. Cloteaux. “Towards Mitigating Intermittency of Renewable Energy Supply in Large-Scale Infrastructures with Job Replication.” Carbon Aware Networks Workshop, University of Oxford, UK, September 19, 2023.
- [5] K. Gardner, M. Harchol-Balter, A. Scheller-Wolf, M. Velednitsky, and S. Zbarsky. Redundancy-d: The Power of d Choices for Redundancy. *Operations Research* 65:4 (2017), 1078–1094 DOI: [10.1287/opre.2016.1582](https://doi.org/10.1287/opre.2016.1582)
- [6] K. Gardner, M. Harchol-Balter, A. Scheller-Wolf, and B. Van Houdt. A Better Model for Job Redundancy: Decoupling Server Slowdown and Job Size. *IEEE/ACM*

Transactions on Networking 25:6 (2017), 3353–3367. DOI: [10.1109/TNET.2017.2744607](https://doi.org/10.1109/TNET.2017.2744607)

- [7] D. Boru, D. Kliazovich, F. Granelli, P. Bouvry, and A. Y. Zomaya. Energy-efficient Data Replication in Cloud Computing Datacenters. *Cluster Computing* 18:1 (2015), 385–402. DOI: [10.1007/s10586-014-0404-x](https://doi.org/10.1007/s10586-014-0404-x)
- [8] D. P. Palomar and M. Chiang. A Tutorial on Decomposition Methods for Network Utility Maximization. *IEEE Journal on Selected Areas in Communications* 24:8 (2006), 1439–1451. DOI: [10.1109/JSAC.2006.879350](https://doi.org/10.1109/JSAC.2006.879350)
- [9] V. Marbukh and K. Mills. Demand Pricing & Resource Allocation in Market-Based Compute Grids: A Model and Initial Results. In *Seventh International Conference on Networking (ICN 2008)*, April 2008, 752–757. DOI: [10.1109/ICN.2008.36](https://doi.org/10.1109/ICN.2008.36)

Combinatorial Testing for Software Based Systems

Raghu N. Kacker

James F. Lawrence

D. Richard Kuhn (NIST ITL)

M. S. Raunak (NIST ITL)

Yu Lei (University of Texas at Arlington)

Dimitris E. Simos (SBA-Research, Austria)

Eric Wong (University of Texas at Dallas)

Itzel Dominguez-Mendoza (CENAM, Mexico)

<https://csrc.nist.gov/projects/automated-combinatorial-testing-for-software>

In 1997, the Mars Pathfinder began experiencing system resets at seemingly unpredictable times soon after it landed and began collecting data. Fortunately, engineers were able to deduce and correct the problem, which occurred only when (1) a particular type of data was being collected, and (2) intermediate priority tasks exceeded a certain load, resulting in a blocking condition that eventually triggered a reset. Situations of this type are known as interaction faults. Many real-time failures of software-based systems have been traced to such faults. These are often insidious in that they may remain hidden until the unfortunate combination is encountered during system operation.

Combinatorial testing (CT) is a versatile methodology for detecting interaction faults. CT began as pairwise (2-way) testing in which all pairs of the test values for all pairs of test factors are checked. Thus, pairwise testing can detect faults involving single factors or interactions between two factors. CT is based on an empirical observation, referred to as the interaction rule, that while the behavior of a software system may be affected by many factors, only a few are involved in any given failure. NIST investigations of failures in actual systems have shown that while most faults involved a single factor or interaction between two factors, some

faults involved three or more factors [1]. (A fault involving more than six factors has not yet been reported.) Thus, pairwise testing is useful, but it may not be adequate for detecting interaction faults involving more than two test factors.

More than a decade ago, NIST took the initiative to extend pairwise (2-way) CT to higher strength t-way CT for $t > 2$. NIST has helped make CT practical by developing research tools and techniques for generating combinatorial test suites. CT has now gained significant interest from the international software testing community. Many successful results from the use of CT in aerospace, automotive, and financial service industries, as well as defense, security, and electronic medical systems have since been reported.

A suite of test cases for combinatorial t -way testing includes (covers), at least once, all possible t -tuples of the test values for every set (combination) of t factors out of the complete set of all k factors that are tested ($k > t$). Use of mathematical objects called covering arrays makes it possible to check all t -tuples of the test values with a small number of test cases. Table 5 shows a covering array of 13 rows and 10 columns each having two possible values, 0 and 1. Columns correspond to the factors and the rows correspond to the test cases. The number of possible sets (combinations) of 3 out of 10 test factors is $\binom{10}{3} = \frac{10!}{(10-3)! 3!} = 120$. When each factor has two possible values, each set of 3 factors can have $2^3 = 8$ possible triples of test values ((0, 0, 0), (0, 0, 1), (0, 1, 0), (0, 1, 1), (1, 0, 0), (1, 0, 1), (1, 1, 0), (1, 1, 1)). So, the total number of possible triples of values for all 10 factors is $120 \times 8 = 960$. A test suite based on Table 5 includes (covers) at least once all 960 distinct triples of the test values of ten factors using just 13 tests.

In practice, one wants a minimal covering array, that is an array which covers all possible t -tuples of the test values for every set of t out of all k factors with the least number of rows (test cases). In practice, many factors have dependencies and constraints; hence not all combinations of the test values may be logically or physically valid. A combinatorial test suite must avoid such forbidden combinations. Generating minimal covering arrays that avoid forbidden combinations is a difficult computational problem [2]. A great deal of research has been done to develop mathematical and computational methods to generate minimal covering arrays of this type. NIST and its collaborators have developed several such algorithms.

NIST-Developed Tools. NIST has developed several research tools to make CT practical. ACTS (for Automated Combinatorial Testing for Software), which was developed in cooperation with the University of Texas at Arlington, includes several algorithms to generate high strength test suites for CT [3]. The ACTS algorithms are optimized to efficiently avoid forbidden combinations of test settings. More than 4775 users have

Table 5. A covering array of 13 rows includes all eight triplets (000, 001, 010, 011, 100, 101, 110, and 111) of the possible values (0 and 1) for every one of the 120 possible sets of 3 out of 10 test factors represented by the columns (for example, see colored entries)

Rows	Columns									
	1	2	3	4	5	6	7	8	9	10
1	0	0	0	0	0	0	0	0	0	0
2	1	1	1	1	1	1	1	1	1	1
3	1	1	1	0	1	0	0	0	0	1
4	1	0	1	1	0	1	0	1	0	0
5	1	0	0	0	1	1	1	0	0	0
6	0	1	1	0	0	1	0	0	1	0
7	0	0	1	0	1	0	1	1	1	0
8	1	1	0	1	0	0	1	0	1	0
9	0	0	0	1	1	1	0	0	1	1
10	0	0	1	1	0	0	1	0	0	1
11	0	1	0	1	1	0	0	1	0	0
12	1	0	0	0	0	0	0	1	1	1
13	0	1	0	0	0	1	1	1	0	1

downloaded executable versions of the ACTS algorithms from the NIST webpage for CT. (It is difficult to ascertain the number of users because some users have redistributed to others, and some are students who may have used it only once for a single project.)

A second research tool, CCM (for Combinatorial Coverage Measurement), developed jointly by NIST and a guest researcher from CENAM, the national metrology institute of Mexico, characterizes the incompleteness of a test suite that may not have been developed from a CT viewpoint. Basic combinatorial coverage measurements describe the incompleteness of a test suite relative to a test suite based on a covering array that includes all possible t -tuples of values for every t -factor combination for various values of t . The combinatorial deficiency of a test suite can be remedied by additional tests. Thus, CCM can help guide the expansion of a test suite to satisfy stated combinatorial requirements [4]. The latest version of CCM supports constraints which exclude forbidden combinations of values. A parallel processing version is also available.

Impact of NIST Research. NIST efforts have sparked a surge of research and application of combinatorial testing technology. A 2010 NIST Special Publication on CT was downloaded more than 30 000 times by the end of 2014 [5]. In 2013, we published a book with Chapman and Hall/CRC Press on this topic [6].

One of the first large-scale users that we worked with is a group at the U.S. Air Force Base in Eglin, Florida. The behavior of one of their systems depended on the sequential order of certain events. This led to the problem of testing sequences of events, which required development of new mathematical objects called sequence covering arrays [7, 8, 9]. Lockheed-Martin, a

large U.S. defense contractor, reported (based on eight projects) that use of CT reduced cost of testing by about 20 % with 20 % to 50 % improvement in test coverage [10]. CT methods are now being used in diverse areas such as financial services, automotive, automation, avionics, video coding standards, and for security testing. The NIST webpage for CT cites over forty application papers.

For testing a software-based system, no single approach is enough. Multiple approaches are generally needed at various stages of software development and installation. CT complements other approaches for testing, verification, and validation of software-based systems. CT is now included in software engineering courses taught in many universities. NIST efforts on technology transfer of CT tools and techniques received the 2009 Excellence in Technology Transfer Award from the Federal Laboratory Consortium-Mid Atlantic Region. A 2013 paper describing the ACTS research tool [3] received the Most Influential Paper of the Decade Award by the 2023 IEEE International Conference on Software, Testing, Verification and Validation (ICST) held in Dublin, Ireland, April 16-22, 2023.

CT has also gained significant interest from the research community. In 2012, NIST took the lead in organizing a workshop on CT³⁰ in conjunction with the 2012 IEEE International Conference on Software Testing, Verification, and Validation (ICST), a premier conference in this field. Since then, an International Workshop on Combinatorial Testing (IWCT) has become an annual event for sharing advancements in CT tools and techniques, as well as results from practical industrial use of CT. The twelfth such IWCT³¹ was held in Dublin, Ireland on April 16, 2021, in conjunction with ICST 2023³². Four of our team (Kacker, Kuhn, Lei, and Simos) were among the co-organizers. The IWCT 2023 received 13 submissions. The Program Committee accepted 11 papers. Four of the 11 papers were summaries of previously published journal papers.

Recent accomplishments. The following accomplishments occurred during this reporting period.

Measurement of the adequacy of a test suite with respect to the modeled test space [11]. The adequacy of a test suite is typically assessed with respect to a criterion such as requirements coverage or code coverage. This paper presents a metric for the adequacy of a test suite with respect to the modeled test space. A test suite that does not include at least all possible pairs (or triples) of test values is very likely inadequate because system failures may involve more than a single parameter.

MagicMirror: towards high coverage fuzzing of smart contracts [12]. A smart contract is often used to handle

financial transactions. Unlike traditional programs, contract codes cannot be changed after deployment. Thus, it is crucial to test smart contracts thoroughly before deployment. In this paper, we present a fuzzing approach to testing smart contracts. Our fuzzing approach utilizes constraint solving, selective state exploration, and combinatorial testing to improve code coverage. Constraint solving generates test inputs that meet preconditions in a smart contract. Selective state exploration allows different state-dependent behaviors to be exercised while alleviating the state explosion problem. Combinatorial testing is used to exercise parameter interactions in a systematic manner. We implemented our approach in a tool called MagicMirror and evaluated our approach using more than 2000 contracts. The experimental results show that MagicMirror effectively achieves high code coverage and detects vulnerabilities.

Synthetic data generation using combinatorial testing and variational autoencoder [13]. Data is a crucial component in machine learning. However, many datasets contain sensitive information such as personally identifiable health and financial data. Access to these datasets must be restricted to avoid potential security concerns. Synthetic data generation addresses this problem by generating artificial data that are similar to, and thus could be used in place of, the original real-world data. This research introduces a synthetic data generation approach called CT-VAE that uses Combinatorial Testing (CT) and Variational Autoencoder (VAE) technology. We first use VAE to learn the distribution of the real-world data and encode it in a latent, lower-dimensional space. Next, we use CT to sample the latent space by generating a t -way set of latent vectors, each of which represents a data point in the latent space. A synthetic dataset is generated from the t -way set by decoding each latent vector in the set. Our experimental evaluation suggests that machine learning models trained with synthetic datasets generated using our approach could achieve performance that is very similar to those trained with real-world datasets. Furthermore, our approach performs better than several state-of-the-art synthetic data generation approaches.

Ordered t -way combinations for testing state-based systems [14]. Fault detection often depends on the specific order of inputs that establish states which eventually lead to a failure. However, beyond basic structural coverage metrics, it is often difficult to determine if the code has been exercised sufficiently to ensure confidence in its functions. Measures are needed to ensure that relevant combinations of input values have been tested with adequate diversity of ordering to ensure correct operation. Combinatorial testing and combinatorial coverage

³⁰ <http://www.research.ibm.com/haifa/Workshops/ct2012/>

³¹ <https://conf.researchr.org/home/icst-2023/iwct-2023>

³² <https://conf.researchr.org/home/icst-2023>

measures have been applied to many types of applications but have some deficiencies for verifying and testing state-based systems where the response depends on both input values and the current system state. In such systems, internal states change as input values are processed. Examples include network protocols, which may be in listening, partial connection, full connection, disconnected, and other states depending on the values of packet fields and the order of packets received. This paper discusses definitions for ordered t -way combination arrays and proves results regarding the construction of adequate blocks of test inputs, including consecutive ordering of combinations and with interleaving allowed. The application of the results to verify and test state-based systems is also illustrated.

SmartExecutor: coverage-driven symbolic execution guided by a function dependency graph [15]. Symbolic execution of smart contracts suffers from sequence explosion. Some existing tools limit the sequence length, thus being unable to adequately evaluate some functions. In this paper, we propose a graph-guided symbolic execution that can target those harder-to-cover functions without constraining the sequence depth. The graph is based on data dependency. We design a two-phase execution process. The first phase can be used to identify the harder-to-cover functions while the second attempts to cover the identified functions. We have developed a tool called SmartExecutor and conducted an experimental evaluation on the SGuard dataset. The experimental results indicate that compared with a state-of-the-art symbolic execution tool Mythril, SmartExecutor achieves higher code coverage and detects more vulnerabilities with less time.

We are continuing research involving use of combinatorial methods for trust and assurance of machine learning models, autonomous systems, for model debugging, for security of smart contracts, cybersecurity, and risk factors identification. The research includes development of supporting tools.

- [1] D. R. Kuhn, D. R. Wallace, and A. M. Gallo, Jr. Software Fault Interactions, and Implications for Software Testing. *IEEE Transactions on Software Engineering* **30** (2004), 418-421. DOI: [10.1109/TSE.2004.24](https://doi.org/10.1109/TSE.2004.24)
- [2] L. Kampel and D. E. Simos. A Survey on the State of the Art of Complexity Problems for Covering Arrays. *Theoretical Computer Science* **800** (2019), 107-124. DOI: [10.1016/j.tcs.2019.10.019](https://doi.org/10.1016/j.tcs.2019.10.019)
- [3] L. Yu, Y. Lei, R. N. Kacker, and D. R. Kuhn. ACTS: A Combinatorial Test Generation Tool. In *Proceedings of the 2013 IEEE Sixth International Conference on Software Testing, Verification and Validation (ICST)*, Luxembourg, March 18-22, 2013, 370-375. DOI: [10.1109/ICST.2013.52](https://doi.org/10.1109/ICST.2013.52)
- [4] D. R. Kuhn, R. N. Kacker, and Y. Lei. Combinatorial Coverage as an Aspect of Test Quality. *CrossTalk: The Journal of Defense Software Engineering*, (March/April 2015), 19-23.
- [5] D. R. Kuhn, R. N. Kacker, and Y. Lei. Practical Combinatorial Testing. NIST Special Publication 800-142, October 2010. URL: <http://nvlpubs.nist.gov/nistpubs/Legacy/SP/nistspecialpublication800-142.pdf>
- [6] D. R. Kuhn, R. N. Kacker, and Y. Lei. *Introduction to Combinatorial Testing*. CRC Press, 2013.
- [7] D. R. Kuhn, J. M. Higdon, J. F. Lawrence, R. N. Kacker, and Y. Lei. Combinatorial Methods for Event Sequence Testing. In *Proceedings of the 5-th IEEE International Conference on Software Testing, Verification and Validation Workshops (ICSTW)*, Montreal, Quebec, Canada, April 17-21, 2012, 601-609. DOI: [10.1109/ICST.2012.147](https://doi.org/10.1109/ICST.2012.147)
- [8] D. R. Kuhn, J. M. Higdon, J. F. Lawrence, R. N. Kacker and Y. Lei. Efficient Methods for Interoperability Testing using Event Sequences. *CrossTalk: The Journal of Defense Software Engineering*, (July/August 2012), 15-18. <https://apps.dtic.mil/docs/citations/ADA566540>
- [9] Y. M. Chee, C. J. Colbourn, D. Horsley, and J. Zhou. Sequence Covering Arrays. *SIAM Journal of Discrete Mathematics*, **27** (2013), 1844-1861. DOI: [10.1137/120894099](https://doi.org/10.1137/120894099)
- [10] J. Hagar, D. R. Kuhn, R. N. Kacker, and T. Wissink. Introducing Combinatorial Testing in a Large Organization. *IEEE Computer* **48** (2015), 64-72. DOI: [10.1109/MC.2015.114](https://doi.org/10.1109/MC.2015.114)
- [11] R. N. Kacker, D. R. Kuhn, Y. Lei, and D. E. Simos. Measurement of the Adequacy of a Test Suite with Respect to the Modeled Test Space. *IEEE Software* **39** (Sept-Oct 2022), 62-67. DOI: [10.1109/MS.2021.3108060](https://doi.org/10.1109/MS.2021.3108060)
- [12] H. Feng, X. Ren, Q. Wei, Y. Lei, R. N. Kacker, D. R. Kuhn, and D. E. Simos. MagicMirror: Towards High-Coverage Fuzzing of Smart Contracts. In *Proceedings of the 2023 IEEE International Conference on Software, Testing, Verification and Validation (ICST)*, Dublin, Ireland, April 16-22, 2023, 141-152. DOI: [10.1109/ICST57152.2023.00022](https://doi.org/10.1109/ICST57152.2023.00022)
- [13] K. Khadka, J. Chandrasekaran, Y. Lei, R. N. Kacker, and D. R. Kuhn. Synthetic Data Generation Using Combinatorial Testing and Variational Autoencoder. In *Proceedings of the 2023 IEEE International Conference on Software Testing, Verification and Validation Workshops (ICSTW)*, Dublin, Ireland, April 16, 2023, 228-236. DOI: [10.1109/ICSTW58534.2023.00048](https://doi.org/10.1109/ICSTW58534.2023.00048)
- [14] D. R. Kuhn, M. S. Raunak, and R. N. Kacker. Ordered t -way Combinations for Testing State-based Systems. In *Proceedings of the 2023 IEEE International Conference on Software Testing, Verification and Validation Workshops (ICSTW)*, Dublin, Ireland, April 16, 2023, 246-254. DOI: [10.1109/ICSTW58534.2023.00050](https://doi.org/10.1109/ICSTW58534.2023.00050)
- [15] Q. Wei, F. Sikder, H. Feng, Y. Lei, R. N. Kacker, and D. R. Kuhn. SmartExecutor: Coverage-Driven Symbolic Execution Guided by a Function Dependency Graph. In *Proceedings of the 5th Conference on Blockchain Research & Applications for Innovative Networks and Services (BRAINS)*, Paris, France, October 11-13, 2023, 1-8. DOI: [10.1109/BRAINS59668.2023.10316942](https://doi.org/10.1109/BRAINS59668.2023.10316942)

Measurements of the Benefits of Incremental Server Learning in Federated Learning with Heterogeneous Datasets

Richard J. La
Van Sy Mai (NIST CTL)
Tao Zhang (NIST CTL)

With rapid advances in sensing technologies, in many applications a large amount of data is generated at many spatially distributed devices. Given the expected volume of data, it is often impractical to transfer all data to a server where centralized learning can be performed. In order to deal with this issue, various forms of distributed learning have been proposed.

Among such distributed learning approaches, Federated Learning (FL) has received much interest, in particular when the privacy of data is of concern [1]. In FL, a coordinating server (CS) maintains a global machine learning (ML) model that is communicated to (a subset of) clients at each round, which perform local learning using their own local datasets. Once they finish updating their local ML models, the updated models are forwarded to the CS, which then aggregates the forwarded models to update the global ML model. Since local datasets are only used to update the local ML models at the clients, no data is shared among the clients or with the CS, thereby addressing the issue of data privacy.

It has been demonstrated that FL can perform an ML task efficiently when the clients' datasets are homogeneous with similar distributions. However, when clients' datasets are heterogeneous and their distributions vary considerably, its performance can suffer significantly, leading to slow convergence or oscillations in the trained ML model. In order to address this issue, researchers proposed several different techniques, such as SCAFFOLD [2], FedDyn [3], and FedDC [4].

In some applications, it may be possible to collect a small dataset that can be used by the CS to perform its own learning to improve the overall learning process. The goal of this project is to examine the benefits of incremental server learning in FL both analytically and numerically. We proved that incremental learning by the CS based on even a very small dataset can help alleviate the client data distribution drifts and accelerate the learning when the current global ML is far from a (local) optimum, which is likely true at the beginning [5, 6]. Moreover, the improvement is shown to depend on the server dataset distribution and its variance, which decreases with the dataset size.

In addition, we implemented incremental server learning in conjunction with some of existing approaches, including SCAFFOLD, FedDyn, and FedDC. Figure 123 plots the test accuracy of a global ML model

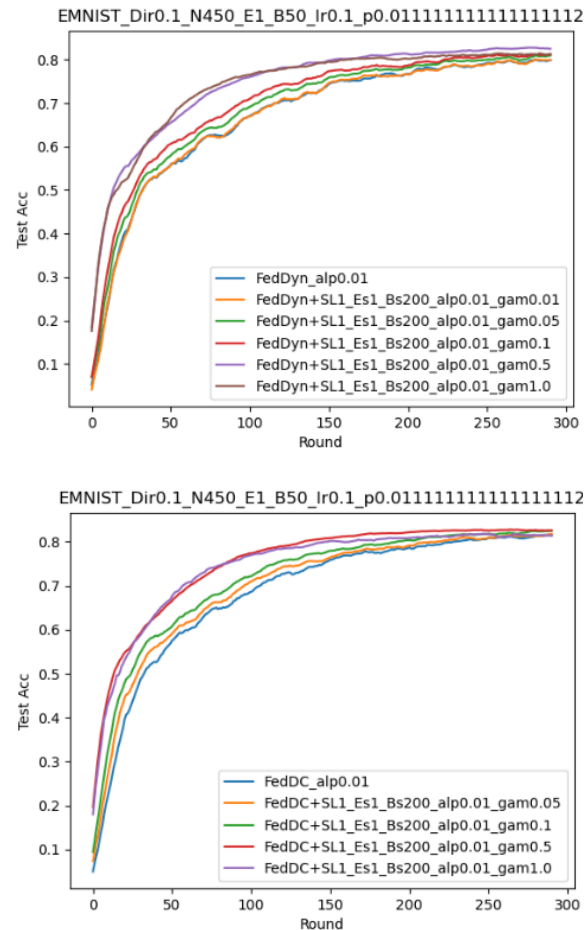


Figure 123. Plot of test accuracy for EMNIST dataset with varying server learning weights. (SL = Server Learning). The figures plot the accuracy as a function of the number of training rounds with different weights for the server learning (γ). Top figure is for FedDyn and FedDyn+SL, and bottom figure is for FedDC and FedDC+SL

(convolutional neural network) as a function of training round, which is obtained using the EMNIST dataset with 45 labels. In order to evaluate the benefits of incremental server learning, we ran the incremental server learning in conjunction with FedDyn and FedDC with varying weights to the server learning. The plots indicate that the incremental server learning provides considerable improvement in initial learning rates; FedDyn and FedDC require 120 to 140 training rounds to reach training accuracy of 70 percent. With the incremental server learning (with γ of 0.5), it only takes roughly 60 training rounds to reach 70 percent training accuracy.

- [1] B. McMahan, E. Moore, D. Ramage, S. Hampson, and B.A. y Arcas. Communication-efficient Learning of Deep Networks from Decentralized Data. In *20th International Conference on Artificial Intelligence and Statistics*, April 2017.
- [2] S. P. Karimireddy, S. Kale, M. Mohri, S. Reddi, S. Stich, and A. T. Suresh. SCAFFOLD: Stochastic Controlled

- Averaging for Federated Learning. In *37th International Conference on Machine Learning*, July 2020.
- [3] D. A. E. Acar, Y. Zha, R. M. Navarro, M. Mattina, P. N. Whatmough, and V. Saligrama. Federated Learning Based on Dynamic Regularization. In *38th International Conference on Machine Learning*, July 2021.
- [4] L. Gao, H. Fu, L. Li, Y. Chen, M. Xu, and C.-Z. Xu. FedDC: Federated Learning with Non-IID Data via Local Drift Decoupling and Correction. In *IEEE/CVF Conference on Computer Vision and Pattern*, June 2022.
- [5] V. S. Mai, R. J. La, T. Zhang, Y. Huang, and A. Battou. Federated Learning with Server Learning for Non-IID Data. In *57th Annual Conference on Information Sciences and Systems*, March 2023.
- [6] V. S. Mai, R. J. La, and T. Zhang. Federated Learning with Server Learning: Enhancing Performance for Non-IID Data. Preprint [arXiv:2210.02614](https://arxiv.org/abs/2210.02614), 2022.

Topological Analysis of Detector Ensembles for Cybersecurity Applications

Melinda Kleczynski
Alden Dima (NIST ITL)
Anthony Kearsley

Neural networks increasingly perform tasks such as traffic sign classification with real-world safety implications. Failures of these systems could cause harm to users or bystanders. Training these networks requires datasets which are frequently too large for manual quality control. This creates an opening for Trojan attacks which poison neural networks by tampering with the training data. For example, a manipulated training image may have a yellow square added to a stop sign together with an incorrect “speed limit sign” label (see Figure 124). If this neural network is deployed in an autonomous vehicle, then adding a sticky note to a stop sign may prevent the vehicle from recognizing the sign and stopping safely.

Trojan detectors attempt to identify compromised neural networks. Participants in the IARPA TrojAI Challenge [1] compete to create the best Trojan detector for clean and poisoned neural networks generated by NIST researchers. Each challenge round results in the submission of several different detectors. These detectors may employ a range of strategies for identifying compromised neural networks. An ensemble of multiple Trojan detectors can significantly improve performance

beyond that of any individual detector. We want to choose complementary sets of detectors so that the deficiencies of one detector are reinforced by the strengths of another. There is a need for optimal detector selection schemes which identify small groups of detectors which form high-performing ensembles.

Motivated by applications of topological data analysis to assessing sensor coverage [2], we are utilizing mathematical techniques to measure the topological diversity of detector ensembles. Topological data analysis doesn’t require a strict notion of distance, making these tools well-suited for quantifying abstract spaces of Trojan detectors. Preliminary results show that ensembles with higher topological diversity are more likely to outperform the average detector in the ensemble.

One of the challenges of working with the TrojAI detectors is that there is a mixture of output types. Some detectors only return two unique outputs, essentially acting as a binary classifier. Other detectors return numerical scores of neural networks. In our preliminary work, we applied a threshold to the outputs to obtain binary predictions from all classifiers. In our ongoing work, we will expand our pipeline to use numerical scores when they are available. We hypothesize that this added information will further improve the value of topological scores of detector ensembles.

- [1] National Institute of Standards and Technology (NIST). TrojAI. 2021. Accessed 11/8/2023. URL: <https://www.nist.gov/itl/ssd/trojai>
- [2] R. Ghrist and A. Muhammad. Coverage and Hole-detection in Sensor Networks via Homology. In *IPSN 2005. Fourth International Symposium on Information Processing in Sensor Networks*, 2005, 254–260.

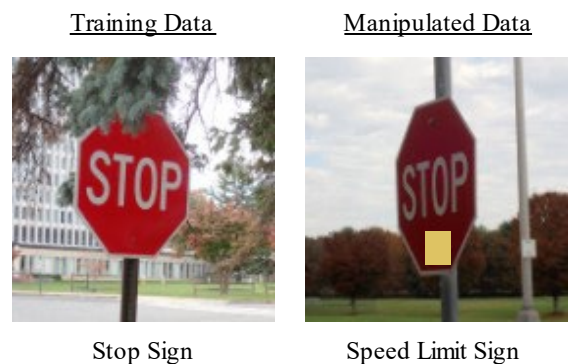


Figure 124. Illustration of manipulated training data.

Mathematical Knowledge Management

We work with researchers in academia and industry to develop technologies, tools, and standards for representation, exchange, and use of mathematical data. Of particular concern are semantic-based representations which can provide the basis for interoperability of mathematical information processing systems. We apply these representations to the development and dissemination of reference data for applied mathematics. The centerpiece of this effort is the Digital Library of Mathematical Functions, a freely available interactive and richly linked online resource, providing essential information on the properties of the special functions of applied mathematics, the foundation of mathematical modeling in all of science and engineering.

Digital Library of Mathematical Functions

Barry I. Schneider

Bruce R. Miller

Bonita V. Saunders

Howard S. Cohl

Ronald F. Boisvert

Charles W. Clark (NIST PML)

Adri B. Olde Daalhuis (University of Edinburgh, UK)

Gergő Nemes (Alfréd Rényi Institute of Mathematics, Hungary and Tokyo Metropolitan University, Japan)

Wolter Groenvelt (Delft University of Technology, the Netherlands)

Tom Koornwinder (Korteweg-de Vries Institute for Mathematics, the Netherlands)

Yuan Xu (University of Oregon)

Bill Reinhardt (University of Washington)

Daniel W. Lozier

<http://dlmf.nist.gov/>

Progress in science has often been catalyzed by advances in mathematics. More recently, developments in the physical sciences have influenced pure mathematics. This symbiotic relationship has been extremely beneficial to both fields. Mathematical developments have found numerous applications in practical problem-solving in all fields of science and engineering, while cutting-edge science has been a major driver of mathematical research. Often the mathematical objects at the intersection of mathematics and physical science are mathematical functions. Effective use of these tools requires ready access to their many properties, a need that was capably satisfied for more than 50 years by the *Handbook of Mathematical Functions with Formulas, Graphs, and Mathematical Tables*, which was published by the National Bureau of Standards (NBS) in 1964 [1].

The 21st century successor to the NBS Handbook, the freely accessible online Digital Library of Mathematical Functions (DLMF) together with the accompanying book, the *NIST Handbook of Mathematical Functions* [2], published by Cambridge University Press in 2010, are collectively referred to as the DLMF.

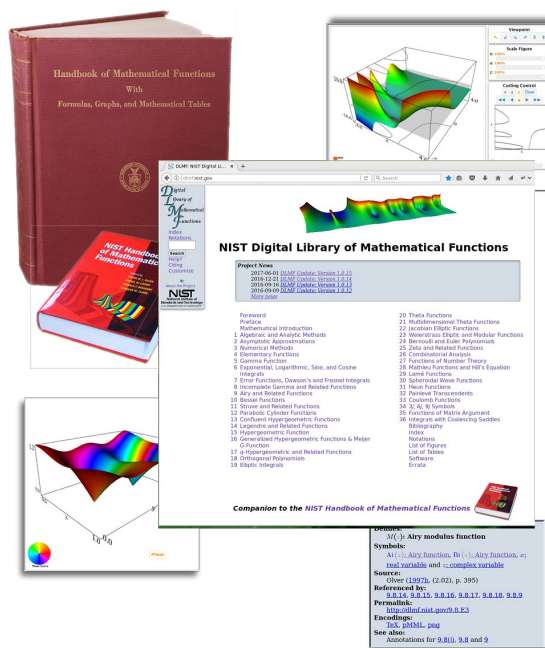


Figure 125. A visual history of the DLMF from its roots in the 1964 NBS Handbook to the graphical contents of the present DLMF.

The DLMF continues to serve as the gold standard reference for the properties of the special functions of applied mathematics.

The DLMF has considerably extended the scope of the original handbook as well as improving accessibility to the worldwide community of scientists and mathematicians. To cite a few examples, the new handbook contains more than twice as many formulas as the old one, coverage of more functions, in more detail, and an up-to-date list of references. The website covers everything in the handbook and much more: additional formulas and graphics, math-aware search, interactive zooming and rotation of 3D graphs, internal links to symbol definitions and cross-references, and external links to online references and sources of software.

While the original Handbook still receives an enormous number of citations, citations to the DLMF are steadily growing in relation to the original handbook. Google Scholar now reports more than 9,186 citations to

the DLMF, a roughly 12 % increase from 2022. During CY 2023, the DLMF website served about 5.1M pages to some 351 000 unique users.

Today's DLMF is the product of many years of effort by more than 50 contributors. Its initial release in 2010, however, was not the end of the project. Corrections to errors, clarifications, bibliographic updates, and addition of new material all need to be made on a continuing basis. And new chapters covering emerging subject areas need to be added to assure the continued vitality of the DLMF deep into the 21st century. Since October of 2022, there were six DLMF releases, 1.1.7 (2022-10-15), 1.1.8 (2022-12-15), 1.1.9 (2023-03-15), 1.1.10 (2023-06-15), 1.1.11 (2023-09-15), and 1.1.12 (2023-12-15) which kept us on our quarterly release schedule. In Release 1.1.0 (2020-12-15) we introduced the capability to create new chapters, sections, subsections, and equations using a decimal numbering scheme using “_” to delimit intermediate numbers for sections, equations, etc. Over the past 18 months, twenty-three new equations and one new subsection were introduced into the DLMF.

The updating of various DLMF chapters and the development of new ones continues. These include a new chapter on Several Variable Orthogonal Polynomials (SVOP) and substantial updates to the chapters on Orthogonal Polynomials (OP), Algebraic and Analytic Methods (AL) and Painlevé Transcendents (PT). Four authors and one validator have been carrying out this work. Drafts are now available for two of these chapters and are being externally reviewed. External validation of the chapters is following in much the same manner as the original DLMF. The OP and AL external validation was completed by Wolter Groenevelt in May 2022. The OP and AL internal validation was completed in October 2023 and the updated material was sent to Roderick Wong and Wolter Groenevelt for external final validation. It is expected that the full revision of the OP and AL chapters will be released in early 2024.

One of the design goals for the DLMF was that each formula would be connected to a proof in the literature. This data, visible as annotations on the website, provides either a proof for the formula, a reference to the proof for the formula or, for definitions, a reference which gives that definition. Unfortunately, this information had not previously been provided in all cases. Our work to systematically verify the completeness and traceability to published proofs for DLMF formulae at the equation level is well underway. This audit has been completed for Chapter 9 (Airy and Related Functions) and Chapter 25 (Zeta and Related Functions, with validation provided by Gergő Nemes) and is actively continuing for Chapters 1-5 and 22-30. Furthermore, inherited metadata at the subsection and section levels has been fully deployed.

The DLMF is now fully utilizing GitHub's capabilities for ongoing maintenance, as well as tracking

changes and enhancements. In particular, changes to the DLMF are now implemented via GitHub issues and targeted pull requests of GitHub branches, each of which are reviewed by other project members before merging with the master branch in full adoption. All changes are reviewed and discussed by the DLMF team at weekly DLMF meetings of the editorial staff prior to their appearance which occurs in quarterly DLMF revisions.

There have been notable additional advances during the current reporting period.

- We now use browser-native MathML rendering for mathematics, by default, in all browsers which support MathML.
- A significant number of mathematical formulas, errata and new mathematical information have been provided, many of which originated from the DLMF readership, validation staff, and contributors. Furthermore, mathematical constraints and symbols associated with equations and in the text, have been improved, clarified, corrected, or disambiguated.
- Proof sketches in Chapters 9, 25, and elsewhere are now carefully differentiated at the equation level, providing useful metadata for the origination of formulas.
- We have included enhanced coverage of the Lambert W -function which includes a precise description of the multi-valued description with indices for the separate branches. This includes the introduction of the Wright- ω function and the tree T -function.
- Improved notations and updated citations have been introduced.

- [1] M. Abramowitz and I. Stegun, eds. *Handbook of Mathematical Functions with Formulas, Graphs and Mathematical Tables*. Applied Mathematics Series 55, National Bureau of Standards, Washington, DC 1964.
- [2] F. Olver, D. Lozier, R. Boisvert and C. Clark, eds. *NIST Handbook of Mathematical Functions*. Cambridge University Press, 2010.

Visualization of Complex Functions Data

Bonita Saunders
Bruce Miller
Sandy Ressler
Brian Antonishek (NIST EL)
Qiming Wang (NIST retired)

Although the DLMF³³ provides definitions, recurrence relations, differential equations, asymptotic expansions, and other information crucial for understanding complex mathematical functions arising in application areas of the mathematical and physical sciences, interactive visualizations can provide additional clarity as indicated in Figure 126.

Ensuring the quality and accessibility of the DLMF's visualizations is our first priority, but addressing changes suggested by DLMF users, other members of the DLMF editorial staff, and chapter authors is also very important. For example, based on feedback received, modified and new figures related to the Lambert W -Function were added to Chapter 4 on Elementary Functions. In particular, notations for the principal and lower branch solutions were changed to coincide with conventions more commonly found in the literature. Another figure was added to show the function's mapping on five branches, or Riemann sheets. Hopefully, this work will eventually lead to the design of interactive 3D visualizations of Riemann surfaces. Additional figures are also under development for the chapter on Orthogonal Polynomials, which is undergoing extensive modifications in content.

We continue to look for opportunities to generalize our work to benefit the larger research community. Our current work on adaptive meshes to improve our underlying computational grids supports our design process, but it may also interest other researchers in the fields of mesh generation, optimization, approximation theory, or any area related to the design of curves and surfaces for mathematical or physical applications. To keep abreast of work in mesh generation we have become more involved with the International Meshing Roundtable (IMR) conferences which are now supported by SIAM. DLMF Graphics Editor B. Saunders attended SIAM IMR 2023 in Amsterdam, The Netherlands and was asked to serve on the organizing committee for the 2024 conference.

We note that our recent presentations [1-4] have shown that aspects of our work can be appreciated by both specialized and more general audiences. Some talks may not yield immediate collaborators but can still enhance the division's visibility and plant seeds for new connections.

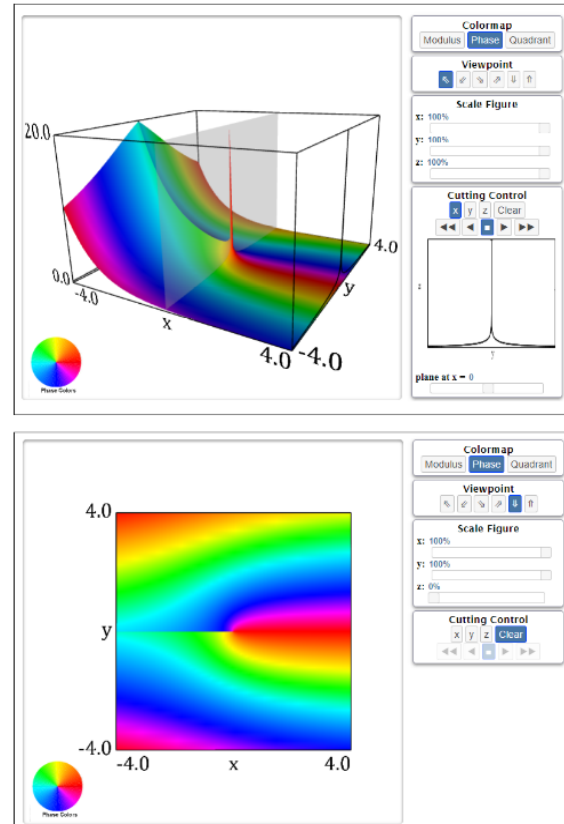


Figure 126. DLMF visualizations provide several options for exploring mathematical function surfaces. In the top figure, the modulus of the principal value of the exponential integral $E_1(x+iy)$ is shown with a phase color map, cutting plane and pop-up control window indicating convergence to ∞ at the origin. Other options allow users to change the color map, examine different viewpoints and scale the figure in various coordinate directions. In the bottom figure, the function's height is scaled down to create a density plot that reveals the cut along the negative real axis. DLMF Figure 6.3.3: <http://dlmf.nist.gov/6.3.F3>

As time permits, we also continue to explore opportunities to increase user visibility. Some DLMF chapters display chapter related thumbnail images on the title page. Creating a gallery of images for all chapters would add visual interest to the DLMF. Each image would link to a short descriptive sidebar that could include links to the chapter's application section or related function visualizations. New and updated DLMF chapters currently under development can provide a test bed for this work.

- [1] B. Saunders. "NIST Digital Library of Mathematical Functions." George Mason University Mathematics Students Visit, NIST, Gaithersburg, MD, August 2, 2023.
- [2] B. Saunders. "NIST Digital Library of Mathematical Functions: Updates and Related Work." Minisymposium on Software for Special Functions, SIAM Conference on

³³ <https://dlmf.nist.gov/>

Computational Science and Engineering (CSE23), Amsterdam, The Netherlands, February 26 - March 3, 2023.

- [3] B. Saunders. “Research in Computational and Applied Mathematics at NIST: NIST’s DLMF and More.” SIAM Student Chapter, Jaypee University of Information Technology, Solan, HP, India, January 11, 2023 (virtual).
- [4] B. Saunders. “Research in Computational and Applied Mathematics at the National Institute of Standards and Technology: NIST’s DLMF and More.” Applied Mathematics and Scientific Computing Seminar, Temple University, Philadelphia, PA, November 30, 2022.

DLMF Standard Reference Tables on Demand

Bonita Saunders

Bruce Miller

Marjorie McClain (Retired)

Annie Cuyt (University of Antwerp)

Stefan Becuwe (University of Antwerp)

Franky Backeljauw (University of Antwerp)

Sean Brooks (Coppin State University)

Ron Buckmire (Occidental College)

Rachel Vincent-Finley (Southern U. and A&M College)

Christopher Schanzle

<http://dlmftables.uantwerpen.be/>

Although reliable computing machines, computer algebra systems, and multiple precision computational packages have diminished the need for tables of reference values for computing function values by interpolation, mathematical and physical scientists, numerical analysts, and software developers still need a way to test software for computing mathematical functions. DLMF Standard Reference Tables on Demand (DLMF Tables) is a collaborative project between ACMD and the University of Antwerp Computational Mathematics Research Group (CMA) [1-5] to address this problem. The goal is to develop an online system where users can generate tables of special function values at user-specified precision with an error certification to test their own algorithms or confirm the accuracy of results from a commercial or publicly available package.

The DLMF Tables team has developed a beta site at the University of Antwerp, based on CMA’s MpIeee, a multiple precision IEEE 754/854 compliant C++ floating point arithmetic library. Ultimately, the goal is a permanent NIST location accessible from the NIST Digital Library of Mathematical Functions (DLMF). In 2020 three researchers were added to the DLMF Tables

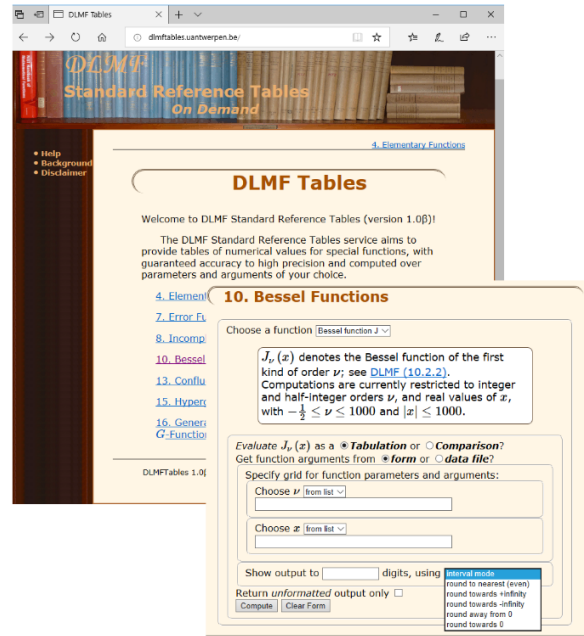


Figure 127. DLMF Tables generates tables of special function values at user specified precision. Users input real values and parameters where the function is to be evaluated. The user may request output in interval mode, where the output is shown as a table of intervals that bound the true results or may request output in one of several rounding modes. Users may also choose to compare their own table of values to the reference values generated by the system.

team through the inaugural ADJOINT Workshop³⁴ sponsored by the Mathematical Sciences Research Institute (MSRI) in Berkeley, California [6]. The group members, from various universities, were supported by MSRI through NSF, NSA, and Sloan grants³⁵ for more than a year. Post-workshop contact has continued with online meetings to discuss and verify applicable results from the literature, including Higham [7] and CMA [1-5]. The ADJOINT group’s work led to three invited talks at the 2021 Joint Mathematics Meetings [8] and two more talks at ADJOINT and AWM minisymposia at the 2022 Joint Mathematics Meetings [9,10]. Also, an update of the group’s work was presented at a MSRI reunion during the summer of 2022 [11].

Information on the DLMF Tables project was also presented at an invited talk on DLMF updates and related projects at a minisymposium on Software for Special Functions at the SIAM Conference on Computational Science and Engineering (CSE23) in Amsterdam, The Netherlands in March 2023. After the talk, B. Saunders met with Annie Cuyt, leader of U. Antwerp CMA, to discuss possible next steps. A paper co-authored by the ADJOINT group with members of the ACMD and U. Antwerp teams is under review [13].

³⁴ <https://www.msri.org/web/msri/scientific/adjoint>

³⁵ S. Brooks, R. Buckmire, and R. Vincent-Finley were supported in this work by National Science Foundation, Grant Nos. DMS-1915954 and DMS-2016406; National Security Agency, Grant No. H98230-20-

1-0015; and Sloan Foundation, Grant No. G-2020-12602 as participants in ADJOINT 2020 hosted by the Mathematical Sciences Research Institute in Berkeley, California.

ACMD has primarily been responsible for the front-end interface for DLMF Tables, while CMA designed and maintains the back-end computational engine built around the error analysis and MplEee library. The work with the ADJOINT group marks a significant step toward merging these capabilities so that CMA's function computation codes can be maintained and eventually, further developed here at NIST.

- [1] F. Backeljauw, S. Becuwe, A. Cuyt, J. Van Deun, and D. Lozier. Validated Evaluation of Special Mathematical Functions. *Science of Computer Programming* **10** (2013), 1016.
- [2] M. Colman, A. Cuyt, and J. Van Deun. Validated Computation of Certain Hypergeometric Functions. *ACM Transactions on Mathematical Software* **38**:2 (January 2012), 11.
- [3] F. Backeljauw. A Library for Radix-independent Multiprecision IEEE-compliant Floating-point Arithmetic. Technical Report 2009-01, Department of Mathematics and Computer Science, Universiteit Antwerpen, 2009.
- [4] A. Cuyt, V. B. Petersen, B. Verdonk, H. Waadeland, and W. B. Jones. *Handbook of Continued Fractions for Special Functions*. Springer, New York, 2008.
- [5] A. Cuyt, B. Verdonk, and H. Waadeland. Efficient and Reliable Multiprecision Implementation of Elementary and Special Functions. *SIAM Journal of Scientific Computing* **28** (2006), 1437-1462.
- [6] B. Saunders, S. Brooks, R. Buckmire, and R. Vincent-Finley. "Validated Numerical Computation of Mathematical Functions." African Diaspora Joint Mathematics Workshop (ADJOINT) 2020, Online, June 26, 2020.
- [7] N. Higham. *Accuracy and Stability of Numerical Algorithms*. Second edition. Society for Industrial and Applied Mathematics, Philadelphia, 2002.
- [8] B. Saunders, S. Brooks, R. Buckmire, and R. Vincent-Finley. "Validated Computation of Special Functions I: Overview, II: Error Analysis, III: DLMF Tables." ADJOINT Research Showcase, 2021 Joint Mathematics Meetings, Online, January 9, 2021.
- [9] B. Saunders, S. Brooks, R. Buckmire, and R. Vincent-Finley. "Rounding Error Analysis for Validated Computation of Special Functions." Special Session on the MSRI African Diaspora Joint Mathematics (ADJOINT) Workshop, I, Joint Mathematics Meetings, I, Online, April 6, 2022.
- [10] B. Saunders, S. Brooks, R. Buckmire, R. Vincent-Finley, F. Backeljauw, S. Becuwe, B. Miller, M. McClain, A. Cuyt, "Validated Computation of Special Mathematical Functions." AWM Special Session on Celebrating the Mathematical Contributions of the AWM, I, Joint Mathematics Meetings, Online, April 7, 2022.
- [11] R. Buckmire, B. Saunders, R. Vincent-Finley, S. Brooks, "Saunders ADJOINT Team Update on Validated Numerical Computations Research." ADJOINT Reunion Workshop, Online, July 1, 2022.
- [12] B. Saunders. "NIST Digital Library of Mathematical Functions: Updates and Related Work." Minisymposium on Software for Special Functions, SIAM Conference on

Computational Science and Engineering (CSE23), Amsterdam, The Netherlands, February 26 - March 3, 2023.

- [13] B. Saunders, S. Brooks, R. Vincent-Finley, R. Buckmire, F. Backeljauw, S. Becuwe, B. Miller, M. McClain, A. Cuyt. Validated Computation of Special Mathematical Functions. In review.

NIST Digital Repository of Mathematical Formulae

Howard S. Cohl

Bonita V. Saunders

Abdou Youssef

Moritz Schubotz

Andre Greiner-Petter (University of Wuppertal)

Miguel Lopez (University of Maryland)

Philipp Scharpf (University of Konstanz)

The NIST Digital Repository of Mathematical Formulae (DRMF) is an online compendium of formulae for orthogonal polynomials and special functions (OPSF) designed to a) facilitate interaction among a community of mathematicians and scientists interested in OPSF; b) be expandable, allowing the input of new formulae from the literature; c) provide information for related linked open data projects; d) represent the context-free full semantic information concerning individual formulas; e) have a user friendly, consistent, and hyperlinkable viewpoint and authoring perspective; f) contain easily searchable mathematics; and g) take advantage of modern MathML tools for easy-to-read, scalably rendered content-driven mathematics.

Our DRMF implementation, previously built using MediaWiki (the wiki software used by Wikipedia), is currently in migration to a different software platform, namely the platform used by the NIST Digital Library of Mathematical Functions (DLMF). See Figure 127 for the current draft of the DRMF home page, and Figure 128 for a sample DRMF formula page. The DRMF has been summarized in a series of papers [1-3]. A key asset in the development of DRMF context free semantic content is the utilization of a set of LaTeX macros and macro call functionality created by Bruce Miller (ACMD) to achieve the encapsulation of semantic information within the NIST Digital Library of Mathematical Functions (DLMF) [4]. These macros give us the capability to tie LaTeX commands in a mostly unambiguous way to mathematical functions defined in an OPSF context. There are currently 540 DLMF LaTeX macros, as well as an additional 156 which have been created specifically for the DRMF. Most if not all DLMF macros have at least one DLMF web page associated with them. One goal is to have definition pages for all additional DRMF macros. The use of DLMF and DRMF macros guarantees mathematical and structural consistency

DRMF

Index
Notations

Search
Help?
Citing
Customize

About the Project
NIST
National Institute of
Standards and Technology
U.S. Department of Commerce

**NIST Digital Repository of
Mathematical Formulae**

50 Koekoek, Lesky and
Swarttouw: Chapter 01

51 Koekoek, Lesky and
Swarttouw: Chapter 09

52 Koekoek, Lesky and
Swarttouw: Chapter 14

53 Continued Fractions for
Special Functions

54 eCF: Encoding Continued
Fraction Knowledge in
Computational Form
LABEL:ch:ZZ

© 2010-2018 NIST / Privacy Policy / Disclaimer / Feedback; Version 1.0.19; Release date 2018-06-22. If you have difficulties viewing this site, please consult our [Help](#) pages.
This is a **DRAFT** of DLMF (built by hcohl; 2018-08-29). It is not yet in final, validated form and is not suitable for citation.

Figure 128. Draft of the DRMF home page displaying the current table of contents.

throughout the DRMF. We refer to LaTeX source with incorporated DLMF and DRMF macros as semantic LaTeX.

DRMF formula seeding is currently focused on 1) Koekoek, Lesky, and Swarttouw (KLS) chapters 1 (Definitions and Miscellaneous Formulas), 9 (Hypergeometric Orthogonal Polynomials), and 14 (Basic Hypergeometric Orthogonal Polynomials [5]); 2) Koorwinder KLS addendum LaTeX data [5]; 3) Wolfram Computational Knowledge of Continued Fractions Project (eCF) [3]; 4) Continued Fractions for Special Function (CFSF) Maple dataset hosted by the University of Antwerp [3, 7]; 5) Bateman Manuscript Project (BMP) books [8]; and 6) Magnus, Oberhettinger, and Soni (MOS) books [3, 9]. For these seed projects, we are developing Python and Java software to incorporate DLMF and DRMF macros into the corresponding LaTeX source. Our coding efforts have also focused on extracting formula data from LaTeX source as well as generating DRMF semantic LaTeX. We have developed Java software for the seeding of the eCF and CFSF projects which involve conversion from Mathematica and Maple format to DLMF and DRMF macro incorporated semantic LaTeX [3].

In August 2014, the DRMF Project obtained permission and license to use BMP material as seed content for the DRMF from Adam Cochran, Associate General Counsel of Caltech. Caltech has loaned us copies of the BMP. In February 2018, we received permission and license to use the KLS and MOS material as seed content for the DRMF from Springer Nature. We plan on implementing the BMP and MOS datasets using mathematical optical character recognition software to obtain LaTeX source using software developed with MathType.

Current and future DRMF MediaWiki development projects include the production of formula output representations (such as semantic LaTeX, MathML, Mathematica, Maple, and Sage); incorporation of sophisticated DLMF and DRMF macro related formula

search; and the development of capabilities for user community formula input. In this vein, A. Youssef has written a grammar-based mathematical language processor (MLP) that uses JavaCC to parse mathematical LaTeX expressions [10]. Based on the MLP, A. Greiner-Petter has developed a Java tool referred to as LaCAS_t to convert mathematical LaTeX expressions, which contain DLMF and DRMF macros, to a given computer algebra system source format. This Java tool provides further information of the conversion about possible ambiguities and differences in definitions, domains and

branch cuts between the semantic LaTeX source and the CAS source. Furthermore, it is designed to be easily extendable to other computer algebra systems and currently supports Maple and Mathematica input sources. NIST ACMD SURF student Miguel Lopez worked on the project “Conversion of Mathematica source to LaTeX.” In [11] which focuses on LaCAS_t, we present a first comprehensive approach to verify a digital mathematical and two computer algebra systems with one another by converting mathematical expressions from one system to the other. This is accomplished by our development of LaCAS_t which translates formulae from the NIST Digital Library of Mathematical Functions to the computer algebra systems Maple and Mathematica. This tool will be actively used in DRMF.

In [12], we explore the future of digital mathematics libraries where semantic content is significantly enhanced. In [13], we conceive to generalize citation-based information retrieval methods as applied to mathematical concepts through machine learning-based approaches to the formula concept retrieval and formula concept discovery tasks.

The KLS datasets have been uploaded to our DLMF platform as well as the CFSF and eCF datasets. By working with Andrea Fisher-Scherer, Rights Administrator, Artists Rights Society, New York, NY, we have received permission from Foundation Vasarely, to use an image of one of Victor Vasarely's paintings as the DRMF logo; see Figure 127.

- [1] H. S. Cohl, M. A. McClain, B. V. Saunders, M. Schubotz and J. C. Williams. Digital Repository of Mathematical Formulae. *Lecture Notes in Artificial Intelligence* **8543** (2014), Proceedings of the Conferences on Intelligent Computer Mathematics 2014, Coimbra, Portugal, July 7-11, 2014, (S. M. Watt, J. H. Davenport, A. P. Sexton, P. Sojka, and J. Urban, eds.), Springer, 419-422.
- [2] H. S. Cohl, M. Schubotz, M. A. McClain, B. V. Saunders, Cherry Y. Zou, Azeem S. Mohammed, and Alex A. Danoff. Growing the Digital Repository of Mathematical

Formula Discussion Read View source View history Search DRMF

Formula:DLmf:25.5:E1

<< Reflection Formulas formula in Integral Representations Formula DLmf.25.5:E2 >>

$$\zeta(s) = \frac{1}{\Gamma(s)} \int_0^{\infty} \frac{x^{s-1}}{e^x - 1} dx$$

Contents [hide]

- 1 Constraint(s)
- 2 Proof
- 3 Symbols List
- 4 Bibliography
- 5 URL links

Constraint(s)

$\Re s > 1$

Proof

We ask users to provide proof(s), reference(s) to proof(s), or further clarification on the proof(s) in this space.

Symbols List

ζ : Riemann zeta function : <http://dlmf.nist.gov/25.2#E1>

Γ : Euler's gamma function : <http://dlmf.nist.gov/5.2#E1>

\int : Integral : <http://dlmf.nist.gov/1.4#iv>

e : the base of the natural logarithm : <http://dlmf.nist.gov/4.2.E11>

$d^n x$: differential : <http://dlmf.nist.gov/1.4#iv>

$\Re z$: real part : <http://dlmf.nist.gov/1.9#E2>

Bibliography

Equation (1), Section 25.5 of **DLMF**

URL links

We ask users to provide relevant URL links in this space.

Figure 129. Sample DRMF page, taken from the KLS Chapter 1 dataset.

- Formulae with Generic LaTeX Sources. *Lecture Notes in Artificial Intelligence* **9150** (2015), Proceedings of the Conference on Intelligent Computer Mathematics 2015, Washington DC, USA, July 13-17, 2015, (M. Kerber, J. Carette, C. Kaliszyk, F. Rabe, and V. Sorge, eds.), Springer, 280-287.
- [3] H. S. Cohl, M. Schubotz, A. Youssef, A. Greiner-Petter, J. Gerhard, B. V. Saunders, M. A. McClain, J. Bang, and K. Chen. Semantic Preserving Bijective Mappings of Mathematical Formulae between Word Processors and Computer Algebra Systems. *Lecture Notes in Computer Science* **10383** (2017), Proceedings of the Conference on Intelligent Computer Mathematics 2017, Edinburgh, Scotland, U.K., July 17-21, 2017, (H. Geuvers, M. England, O. Hasan, F. Rabe, O. Teschke, eds.), Springer, 115-131.
- [4] B. Miller. “Drafting DLMF Content Dictionaries.” OpenMath Workshop, 9th Conference on Intelligent Computer Mathematics, CICM 2016, Bialystok, Poland.
- [5] R. Koekoek, P. A. Lesky, and R. F. Swarttouw. *Hypergeometric Orthogonal Polynomials and their q -Analogues*. Springer Monographs in Mathematics, Springer-Verlag, Berlin, 2010.
- [6] T. H. Koornwinder. Additions to the Formula Lists in Hypergeometric Orthogonal Polynomials and their q -analogues by Koekoek, Lesky and Swarttouw. arXiv:1401.0815, June 2015.
- [7] A. Cuyt, V. Petersen, H. Waadeland, W. B. Jones, F. Backeljauw, C. Bonan-Hamada, and S. Becuwe. *Handbook of Continued Fractions for Special Functions*. Springer, New York, 2008.
- [8] A. Erdelyi, W. Magnus, F. Oberhettinger, and F. G. Tricomi. *Higher Transcendental Functions*. Vols. I, II, III, Robert E. Krieger Publishing Co., Melbourne, FL, 1981.
- [9] H. S. Cohl, A. Greiner-Petter, and M. Schubotz. Automated Symbolic and Numerical Testing of DLMF Formulae using Computer Algebra Systems. *Lecture Notes in Computer Science* **11006** (2018), Proceedings of the Conference on Intelligent Computer Mathematics 2018, Hagenberg, Austria, August 13-17, 2018, (F. Rabe, W. Farmer, G.O. Passmore, A. Youssef, eds.), Springer, 39-52.
- [10] A. Youssef. Part-of-Math Tagging and Applications. *Lecture Notes in Computer Science* **10383** (2017), Proceedings of the Conference on Intelligent Computer Mathematics 2017, Edinburgh, Scotland, U.K., July 17-21, 2017, (H. Geuvers, M. England, O. Hasan, F. Rabe, O. Teschke, eds.), Springer, 356-374.
- [11] A. Greiner-Petter, H. S. Cohl, A. Youssef, M. Schubotz, A. Trost, R. Dey, A. Aizawa, and B. Gipp. Comparative Verification of the Digital Library of Mathematical Functions and Computer Algebra Systems. *Lecture Notes in Computer Science* **13243** (2022), Tools and Algorithms for the Construction and Analysis of Systems (TACAS 2022), Held as Part of the European Joint Conferences on Theory and Practice of Software (ETAPS 2022), Springer, Cham, Eds. D. Fisman, G. Rosu, Munich, Germany, April 2-7, 2022, Springer, 87-105.
- [12] H. S. Cohl and M. Schubotz, The Digital Shadow of Mathematics and its Ramifications. *Jahrbuch über die Fortschritte der Mathematik*, to appear.
- [13] P. Scharpf, M. Schubotz, and H. S. Cohl, C. Breiteringer, B. Gipp. Discovery and Recognition of Formula Concepts using Machine Learning. *Scientometrics* **128** (2023), 4971-5025.

Accessible Scientific Document Corpora

Bruce Miller
 Deyan Ginev
 Tom Wiesing (University of Erlangen, Germany)

It’s nice when a plan comes together, especially when a confluence of developments brings success beyond expectations. Consider the situation with scientific documents. The needs of various interested parties—authors, publishers, vendors and of course a wide variety of readers—do not always harmonize, and the community is often considered too small for significant investment. Yet, recent initiatives to make research

more open and equitable show that the subject is important.³⁶

Authors of mathematics-heavy papers have tended to favor the TeX document system for its expressiveness, extensibility, and high-quality typesetting, with the usual product being in PDF format. On the other hand, readers are becoming more comfortable with web technologies which allow them to search for and read materials on a variety of devices from cell phones and tablets to desktop browsers. These web formats are not only more adaptable but can be more structured and generally have significantly better accessibility than the PDF format. Moreover, these formats are more amenable to search and other machine processing such as machine learning. Yet, converting from an older, programmable format such as TeX into modern web formats is challenging. And even full browser support for the web formats themselves, such as MathML, a special markup for mathematics, have been slow in coming.

When we began the Digital Library of Mathematical Functions (DLMF) project,³⁷ it was clear that our authoring needs required TeX, but it was equally clear that the final product should be available not only in print, but also on the web. The gap between those needs led us to develop LaTeXML: a tool for converting TeX documents into modern web formats including HTML and MathML.³⁸

The same need for expressiveness motivates most authors who submit preprints to the preprint archive, arXiv.org, operated by Cornell University. The arXiv contains over two million scientific preprints in TeX format and submissions continue to grow. The success of the DLMF project led us to consider the challenge: whether our tools could cope with the less disciplined markup of arXiv and yield a corpus of machine-readable STEM documents for research into search and machine-learning. An example [1] leverages the fact that TeX allows, but doesn't require, the use of semantic markup that explicitly indicates which parts of a document are definitions or theorems. We can use the instances of that markup as training data which allows the system to recognize the "signature" of definitions and theorems in other documents, even though no explicit markup had been used.

This side project eventually led to 75 % of the arXiv's corpus being converted without obvious error, and as much as 95 % being somewhat usable. Moreover, the resulting HTML documents, while not perfect, proved to be surprisingly readable. In HTML form, the documents are much more adaptable than the traditional PDF, being readable on tablets and cell phones, as well as in the usual desktop browsers. Even better, the format is more easily processed by assistive technologies such

as braille, and screen readers that read the contents aloud.

In the meantime, accessibility is an increasingly recognized concern³⁹, browser support for web standards such as MathML have improved, and users spend more time on cell phones than desktop computers. The W3C's Math Working Group is currently developing enhancements to MathML to further improve its accessibility. Recognizing these trends, and the relatively good quality of our conversions, the arXiv project has adopted LaTeXML for converting their preprints to HTML.⁴⁰ They are now making preprints available in HTML format, alongside the traditional PDF. Additionally, they have engaged the accessibility community to further improve the accessibility. These collaborations and cross-fertilization should ultimately improve the utility and accessibility of the scientific research literature, not to mention the original DLMF project.

[1] D. Ginev and B. R. Miller. Scientific Statement Classification over arXiv.org. arXiv:1908.10993.

Linear and Nonlinear Exploration of Rotating Self-Gravitating Inviscid Incompressible Fluid Ellipsoids

Howard S. Cohl

Stephen Sorokanich

Joel E. Tohline (Louisiana State University)

Evan Gawlik (University of Hawaii)

In the classic book by Nobel Laureate Subramanyan Chandrasekhar entitled *Ellipsoidal Figures of Equilibrium*, Chandrasekhar explores the classical study of rotating self-gravitating inviscid incompressible fluid ellipsoids [1]. This classic subject has been studied by great mathematicians such as Maclaurin, Jacobi, Meyer, Liouville, Dirichlet, Dedekind, Riemann, Poincaré, Cartan, Roche, Darwin (the fifth child of Charles Darwin) and Jeans. These fluid ellipsoids being incompressible, have constant density. The steady solution in the case of non-rotation is a sphere. When one introduces rotation, the steady solutions are rotating oblate spheroids. These are referred to as Maclaurin spheroids. It is known that as one increases the angular momentum in the Maclaurin spheroids, the figure becomes unstable to a shape changing instability and the equilibrium configuration becomes a tri-axial ellipsoid. In the case where the angular momentum vector is parallel to the vorticity, these are referred to as Riemann S-type ellipsoids [2].

³⁶ <https://open.science.gov/>

³⁷ <https://dlmf.nist.gov/>

³⁸ <https://dlmf.nist.gov/LaTeXML/>

³⁹ <https://www.w3.org/WAI/>

⁴⁰ <https://blog.arxiv.org/2023/12/21/accessibility-update-arxiv-now-offers-papers-in-html-format>

We have two concurrent research projects related to the evolution and instability of the ellipsoidal equilibrium figures:

- (i) *A numerical exploration of the linear stability of Riemann S-type ellipsoids.* The stability analysis proceeds from the linearized Euler equations for the self-gravitating system and maps the stability landscape with respect to the variables of the problem (major axes of the ellipsoid, angular velocity). We hope to resolve this stability diagram with higher order harmonics using the same technique, which was pioneered by Chandrasekhar's student, Norman Lebovitz in [3].
- (ii) *Investigation of three-dimensional nonlinear computational fluid dynamics solutions using finite element methods to simulate the nonlinear evolution of these unstable incompressible fluid ellipsoids.* This entails simulation of the incompressible Euler equations for rotating self-gravitating masses with particular focus on the evolution of the free-boundary, coupling finite element methods with level-set techniques.

The incompressible Euler equations are a coupled system of nonlinear partial differential equations in two unknowns, $\mathbf{u}(x, y, z, t)$ and $p(x, y, z, t)$, the velocity and pressure fields, which describe an idealized incompressible fluid with no viscous effects in an Eulerian frame of reference. The absence of the second-order spatial differential operator describing the kinematic viscosity from the momentum equation (which is present, e.g., in the incompressible Navier-Stokes equations), as well as the divergence-free incompressibility constraint on the velocity field, renders this system particularly difficult to simulate, due in part to the infinite speed of sound propagation which is a characteristic property of this system.

Numerical solution of the incompressible Euler system using many common methods (e.g., the Finite-Volume method) is rendered impossible, since a vanishing timestep would be required to capture such effects.⁴¹ It is nonetheless desirable to develop a robust tool to simulate the nonlinear development of instabilities for *incompressible* dynamics, since the incompressible, inviscid systems are amenable to quantitative stability analysis [4-7], over more realistic fluid systems. Reproducing the analytical stability results which exist for this system will be an important benchmarking tool for our numerics.

The above constraints have led us to adopt the finite element method (FEM) as our primary means of simulating the nonlinear evolution of an incompressible, inviscid fluid. A promising aspect of implementing the finite element method for the incompressible Euler equations will be the ability to couple a finite element

solver with a level-set method for the evolving boundary of a self-gravitating fluid (and the potential to solve for the dynamics of the surface without considering the dynamics of the volume). Resolving the topological transformation of the surface of a rapidly spinning incompressible ellipsoid is a long-standing open problem (dating at least back to Darwin). A prevailing hypothesis predicts the eventual fission of self-gravitating fluids into two teardrop-shaped objects in orbit around one another when the angular velocity of the parent body is high enough. This is believed to be the primary mechanism behind the formation of binary star systems [8]. FEMs are particularly well-suited for modeling the time evolution of surfaces and have been used to successfully model incompressible fluid systems.

With respect to the stability analysis of the Riemann ellipsoids, we are refining a numerical method first introduced by Lebovitz et. al. [5-7], and later developed extensively by Cohl [9]. The linear stability analysis of any dynamical system is based on the magnitude of the eigenvalues of the linearized system around a known stable solution. Starting from a linearization of the Euler equations around the known S-type ellipsoids, the resulting eigenvalue problem is truncated in the basis of ellipsoidal harmonics, allowing for the development of a numerical procedure for evaluating the stability of S-type ellipsoids to small perturbations. The form of Eulerian perturbation to the Newtonian gravitational potential, which is diagonal in the basis of ellipsoidal harmonics, allows for this truncation. We are particularly interested in the fine structure of the boundary of the region of stability as the major and semi-major axes of S-type solutions vary.

The ellipsoidal harmonics, like their cousins the spherical harmonics, are solutions to Laplace's equation in the ellipsoidal coordinate system. The properties of ellipsoidal harmonic functions are critical to the study of problems displaying triaxial symmetry, and their efficient numerical handling is an ongoing subject of research [10, 11]. A major component of this project will be the supplementation of the Digital Library of Mathematical Functions [12] with relevant information on the ellipsoidal harmonic functions collected while studying the gravitational equilibrium figures. This project also has a direct application to the study of astronomical and geophysical phenomena [13].

This nonlinear system has never been directly simulated; this is perhaps due to the complexities of incompressible, inviscid systems (such as infinite speed of sound) as well as the complicated free-boundary physics at play. While computationally challenging, direct simulation will allow us to consider the dynamics of arbitrary perturbations to the Riemann S-type ellipsoids. We are currently developing finite element code for this problem which uses the open source library FEniCS [14,

⁴¹ See Tohline, <https://tohline.education/SelfGravitatingFluids>

15], and a scheme which implicitly conserves volume, density, and energy. This scheme is based on the work of Evan Gawlik [16], with whom we are in correspondence.

There are significant hurdles in implementing the method of Gawlik et. al. [16] to the gravitational Euler system. We face the challenge of showing that this finite element scheme conserves the aforementioned quantities with moving boundary. Additionally, we would like to apply this method to 2D axisymmetric fluid configurations, which would allow us to reduce the dimensionality of the simulation. Writing out the Euler equations in cylindrical coordinates, however, changes the bilinear variational form involved in implementing the finite element method. It must therefore be verified a priori that energy, density, etc. are indeed conserved for the scheme in cylindrical coordinates.

Another technical challenge that has emerged in implementing this system is numerical error introduced via solving for the gravitational potential. It is most straightforward in a finite element simulation to solve Poisson's equation for the Newtonian gravitational potential with suitable boundary data given on the free surface of the fluid. For axisymmetric initial data (i.e., the Maclaurin spheroids), for example, the time evolution of the system preserves axisymmetry, and we specify the Dirichlet boundary data for Newtonian gravitational potential using a simplification of Green's function derived in [17]. This method is very sensitive to the finite element mesh at the surface of the fluid, since the integral kernel used in the evaluation retains a singularity.

In [18], we explore the properties of the implicitly defined bounding curves of the Riemann S-type ellipsoids which are referred to as the lower and upper self-adjoint sequences. These curves can be defined using Legendre incomplete elliptic integrals and as well other equivalent functions. We have been able to derive interesting properties of these curves, and as well their higher derivatives at important locations such as how they intersect the Maclaurin line at $b/a = 1$.

- [1] S. Chandrasekhar. *Ellipsoidal Figures of Equilibrium*. Dover Publications, New York, 1969.
- [2] B. Riemann. Ein Beitrag zu den Untersuchungen über die Bewegung eines flüssigen gleichartigen Ellipsoides. *Abhandlungen der Königlichen Gesellschaft der Wissenschaften zu Göttingen* **9**, 1860.
- [3] N. Lebovitz and A. Lifschitz. New Global Instabilities of the Riemann Ellipsoids. *The Astrophysical Journal* **458**:2 (1969), 699-713.
- [4] S. Chandrasekhar. The Equilibrium and the Stability of the Riemann Ellipsoids. I. *Astrophysical Journal* **142** (1965), 890-961.
- [5] N. R. Lebovitz. Lagrangian Perturbations of Riemann Ellipsoids. *Geophysical & Astrophysical Fluid Dynamics* **47** (1989), 225-236.
- [6] N. Lebovitz and A. Lifschitz. The Stability Equations for Rotating, Inviscid Fluids: Galerkin Methods And Orthogonal Bases. *Geophysical & Astrophysical Fluid Dynamics* **46**:4 (1989), 221-243.
- [7] N. Lebovitz and A. Lifschitz. Short-Wavelength Instabilities of Riemann Ellipsoids. *Philosophical Transactions of the Royal Society of London Series A* **354**:1709 (1996), 927-950.
- [8] J. E. Tohline. The Origin of Binary Stars. *Annual Reviews in Astronomy and Astrophysics* **40** (2002), 349-385.
- [9] H. S. Cohl, Linear Instability Analysis of the Ellipsoidal Figures of Equilibrium. Unpublished.
- [10] G. Dassios. Private communication.
- [11] G. Dassios. Ellipsoidal Harmonics: Theory and Applications. In *Encyclopedia of Mathematics and its Applications*, Cambridge University Press, Cambridge, 2012.
- [12] F. W. J. Olver, A. B. Olde Daalhuis, D. W. Lozier, B. I. Schneider, R. F. Boisvert, C. W. Clark, B. R. Miller, B. V. Saunders, H. S. Cohl, and M. A. McClain, eds. *NIST Digital Library of Mathematical Functions*. <http://dlmf.nist.gov/>, Release 1.1.12, December 15, 2023.
- [13] C. Hunter. On Secular Stability, Secular Instability, and Points of Bifurcation of Rotating Gaseous Masses. *Astrophysical Journal* **213** (1977), 497-517.
- [14] A. Logg, G. N. Wells, and J. Hake. DOLFIN: a C++/Python Finite Element Library. In *Automated Solution of Differential Equations by the Finite Element Method*. (A. Logg, K.-A. Mardal, and G. N. Wells, ed.), *Lecture Notes in Computational Science and Engineering* **84**, Chapter 10. Springer, (2012).
- [15] M. S. Alnaes, J. Blechta, J. Hake, A. Johansson, B. Kehlet, A. Logg, C. N. Richardson, J. Ring, M. E. Rognes, and G. N. Wells. The FEniCS Project Version 1.5. *Archive of Numerical Software* **3** (2015).
- [16] E. Gawlik and F. Gay-Balmaz. A Conservative Finite Element Method for the Incompressible Euler Equations with Variable Density. *Journal of Computational Physics* **412** (2020), 109439.
- [17] H. S. Cohl and J. E. Tohline. A Compact Cylindrical Green's Function Expansion for the Solution Of Potential Problems. *The Astrophysical Journal* **527** (1999), 86-101.
- [18] H. S. Cohl and S. Sorokanich. Elliptic Integral Study of Riemann S-Type Ellipsoid Lower and Upper Self-Adjoint Sequences. In preparation.

Fundamental Solutions and Formulas for Special Functions and Orthogonal Polynomials

Howard S. Cohl

Camilo Montoya

Lisa Ritter

Roberto S. Costas-Santos (U. Loyola Andalucia)

Hans Volkmer (U. of Wisconsin-Milwaukee)

Gestur Olafsson (Louisiana State University)

Mourad E. H. Ismail (U. of Central Florida)

Tom H. Koornwinder (Korteweg-de Vries Institute for Mathematics)

James Lawrence

Jessica E. Hirtenstein (University of California Davis)

Philbert R. Hwang (University of Maryland)

Tanay Wakhare (MIT)

The concept of a function expresses the idea that one quantity (the input) completely determines another quantity (the output). Our research concerns special functions and orthogonal polynomials. A special function is a function that has appeared in the mathematical sciences so often that it has been given a name. Green's functions (named after the British mathematician George Green, who first developed the concept in the 1830s) describe the influence of linear natural phenomena such as electromagnetism, gravity, heat and waves. For example, in electrostatics, a Green's function describes the influence of a point charge, called the source, over all of space. The inputs for fundamental solutions (Green's functions) are all of space (apart from a singular region), and the output is the "force" exerted from the point throughout space. Green's functions are fundamental to the study of inhomogeneous partial differential equations and are powerful in that they provide a mechanism for obtaining their solutions.

We investigate fundamental solutions of linear partial differential equations on highly symmetric Riemannian manifolds (harmonic, rank-one symmetric spaces) such as real, complex, quaternionic, and octonionic, hyperbolic, and projective spaces. Our recent focus has been on applications of fundamental solutions for linear elliptic partial differential operators on spaces of constant curvature. With Olafsson and Montoya (NIST/NRC postdoc), we investigate fundamental solutions of the Laplace-Beltrami operator on rank one symmetric spaces of compact and noncompact type [1, 2]. Cohl, Ritter (previous NIST/NRC postdoc), Hirtenstein (previous NIST SURF student), and Lawrence derived Gegenbauer expansions and addition theorems for binomial and logarithmic fundamental solutions of the polyharmonic operator in even-dimensional Euclidean space in Vilenkin polyspherical coordinates for powers of the Laplacian greater than or equal to the dimension divided by two [3].

With Volkmer, we continue our investigation of a fundamental solution expansions for Laplace's equation in the 17 conformally inequivalent coordinate systems which separate Laplace's equation. Recently, we have been investigating the rotationally invariant cyclidic coordinate systems of this type, namely flat-ring cyclide, bi-cyclide and disk cyclide coordinates. We have completed the investigation for bi-cyclide [4] coordinates.

In the following works, we expand on the properties of terminating and nonterminating generalized and basic hypergeometric functions to study themselves and their respective generalized and basic hypergeometric orthogonal polynomials (hereafter orthogonal polynomials) in the Askey and q -Askey schemes. By utilizing connection relations, we have computed generalizations of generalized and basic hypergeometric orthogonal polynomial generating functions as well as corresponding definite integrals using orthogonality.

With Costas-Santos, Hwang and Wakhare, our series-rearrangement technique is extended to generalizations of other generating functions for basic hypergeometric orthogonal polynomials in [5]. Here, we derive generalizations of generating functions for Askey-Wilson, q -ultraspherical/Rogers, q -Laguerre, and little q -Laguerre/Wall polynomials. We are also interested in the fundamental transformation, representation (symmetry) properties of the special functions and orthogonal polynomials which one often encounters in applied mathematics and mathematical physics.

With Costas-Santos, we examine the symmetric transformation and representation properties of the Askey-Wilson polynomials with a focus on the terminating very-well poised ${}_8W_7$ representations. We examine the representation relation to the order of the well-known symmetry group of the terminating ${}_4\phi_3$ Askey-Wilson representations given by the symmetric group S_6 with respect to their and transformation inversion symmetries [6]. We have also investigated the use of integral representations for nonterminating basic hypergeometric functions and orthogonal polynomials [7, 8].

With Costas-Santos, we developed a series of papers which describe transformation and representation theory of symmetric basic hypergeometric orthogonal polynomials, namely the Askey-Wilson polynomials (4 symmetric free parameters (sfp)) and its symmetric subfamilies, the continuous dual q -Hahn polynomials (3 sfp), the Al-Salam-Chihara polynomials (2 sfp), the continuous big q -Hermite polynomials and the continuous q -Hermite polynomials, and their q -inverse analogues [9]. Here we derive double product representations of nonterminating basic hypergeometric series using diagonalization, a method introduced by Theo William Chaundy in 1943. We also present some generating functions that arise from it in the q and q -inverse Askey schemes. Using this q -Chaundy theorem which expresses a product of two nonterminating basic hypergeometric series as a sum over a terminating basic

hypergeometric series, we study generating functions for the symmetric families of orthogonal polynomials in the q and q -inverse Askey scheme. By applying the q -Chaundy theorem to q -exponential generating functions due to Ismail, we are able to derive alternative expansions of these generating functions and from these, new terminating basic hypergeometric representations for the continuous q -Hermite and q -inverse Hermite polynomials are derived. These representations are connected by new quadratic transformations for the terminating basic hypergeometric series involved. We also exploit duality relations for continuous dual q -Hahn and continuous dual q -inverse Hahn with big q -Jacobi polynomials as well as duality relations for the Al-Salam-Chihara and the q -inverse Al-Salam-Chihara polynomials with the little q -Jacobi polynomials to derive new generating relations for the big and little q -Jacobi polynomials. Some limiting q to 1- cases are considered.

With Costas-Santos we studied the relation between the Ferrers function of the first kind and Gegenbauer polynomials to derive a collection of new formulas [10]. With Ritter, we derive 5-term contiguous relations for the linearization coefficients of generalized and basic hypergeometric orthogonal polynomials such as Laguerre, Gegenbauer, Hermite and Jacobi polynomials [11]. In [12], we are continuing this project with Jacobi functions of the first and second kind and their trigonometric limiting functions on the cut $(-1, 1)$. In [13], Cohl, with Costas-Santos, Durand, Montoya, and Olafsson computed double summation addition theorems for Jacobi functions of the second kind. In [14], Cohl and Costas-Santos derive orthogonality relations for the big -1 Jacobi polynomials for non-standard parameters. In [15], Cohl and Costas-Santos compute special values for the continuous q -Jacobi polynomials and then apply them to the Poisson kernel for continuous q -Jacobi polynomials to derive new generating functions and arbitrary argument transformation formulas.

Richard A. Askey passed away on October 9, 2019. Cohl, Ismail, and Wu have edited a memorial article for Dick Askey which was published in *The Notices of the American Mathematical Society* [16]. With 63 colleagues, Cohl and Ismail prepared a *Liber Amicorum for Dick Askey* which was presented to him and his family at an event held on September 4, 2019, in his hometown of Madison, Wisconsin. Cohl and Ismail have submitted an extended version of the *Liber Amicorum* composed of the remembrances of 83 of his colleagues which will be published online with *Celebratio Mathematica* [17]. Cohl, Alladi, Garvan, Ismail and Rosengren wrote the Preface for the Ramanujan Journal, Special Issues in Memory of Richard Askey [18].

Cohl remains editor or co-editor for a special issue on symmetry in special functions and orthogonal polynomials in the journal *Symmetry*; special volume dedicated to the legacy of Dick Askey for *The Ramanujan Journal*, OP-SF NET, SIAM Activity Group on

Orthogonal Polynomials and Special Functions; and *The Ramanujan Journal*.

- [1] H. S. Cohl, C. Montoya, and G. Olafsson. Fundamental Solutions for the Laplace-Beltrami Operator and its Eigenfunction Expansions in Complex Hyperbolic Geometry. In preparation.
- [2] H. S. Cohl, C. Montoya, and G. Olafsson. Fundamental Solutions for the Laplace-Beltrami Operator and its Eigenfunction Expansions in Complex Projective Geometry. In preparation.
- [3] H. S. Cohl, J. E. Hirtenstein, J. Lawrence, and L. Ritter. Gegenbauer Expansions and Addition Theorems for a Binomial and Logarithmic Fundamental Solution of the Even-Dimensional Euclidean Polyharmonic Equation. *Journal of Mathematical Analysis and Applications* **517**:2 (2023), 126576.
- [4] B. Alexander, H. S. Cohl, and H. Volkmer. Internal and External Harmonics in Bi-Cyclide Coordinates. *Journal of Physics A: Mathematical and Theoretical* **56** (2023), 325203.
- [5] H. S. Cohl, R. S. Costas-Santos, P. R. Hwang, and T. V. Wakhare. Generalizations of Generating Functions for Basic Hypergeometric Orthogonal Polynomials. *Open Journal of Mathematical Sciences* **6**:1 (2022) 248-261.
- [6] H. S. Cohl and R. S. Costas-Santos. Symmetry of Terminating Basic Hypergeometric Representations of the Askey-Wilson Polynomials. *Journal of Mathematical Analysis and Applications* **517**:1 (2023), 126583.
- [7] H. S. Cohl and R. S. Costas-Santos. Utility of Integral Representations for Basic Hypergeometric Functions and Orthogonal Polynomials. *The Ramanujan Journal, Special Issue in Memory of Richard Askey* **61**:2 (2023), 649-674.
- [8] H. S. Cohl and R. S. Costas-Santos. Nonterminating Transformations and Summations Associated with Some q -Mellin-Barnes Integrals. *Advances in Applied Mathematics* **147** (2023), 102517.
- [9] H. S. Cohl and R. S. Costas-Santos. A q -Chaundy Representation for the Product of Two Nonterminating Basic Hypergeometric Series and its Symmetric and Dual Relations. In preparation.
- [10] H. S. Cohl and R. S. Costas-Santos. On the Relation between Gegenbauer Polynomials and the Ferrers Function of the First Kind. *Analysis Mathematica* **48**:3 (2022), 695-716.
- [11] H. S. Cohl and L. Ritter. Two-dimensional Contiguous Relations for Linearization Coefficients of Orthogonal Polynomials in the Askey-scheme. *Integral Transforms and Special Functions* **34**:9 (2023), 635-658.
- [12] H. S. Cohl and R. S. Costas-Santos. Multi-integral Representations for Jacobi Functions of the First and Second Kind. *Arab Journal of Basic and Applied Sciences* **30**:1 (2023), 583-592.
- [13] H. S. Cohl, R. S. Costas-Santos, L. Durand, C. Montoya, and G. Olafsson. Double Summation Addition Theorems for Jacobi Functions of the First and Second Kind. In review.
- [14] H. S. Cohl and R. S. Costas-Santos. Orthogonality of the Big -1 Jacobi Polynomials for Non-standard Parameters.

- AMS Contemporary Mathematics Proceedings on Hypergeometric Functions, q -series and Applications*, to appear.
- [15] H. S. Cohl and R. S. Costas-Santos. Special Values for the Continuous q -Jacobi Polynomials with Applications to its Poisson Kernel. *Proceedings of the 16th International Symposium on Orthogonal Polynomials, Special Functions and Applications*, to appear.
- [16] M. E. H. Ismail, H. S. Cohl and H.-H. Wu, eds. The Legacy of Dick Askey (1933-2019). *Notices of the American Mathematical Society* **69**:1 (2022), 59-75.
- [17] H. S. Cohl and M. E. H. Ismail, eds. Richard Allen Askey Collection and Liber Amicorum: a Friendship Book for Dick Askey. *Celebratio Mathematica*, 2023.
- [18] K. Alladi, H. S. Cohl, F. G. Garvan, M. E. H. Ismail, and H. Rosengren. Preface. *The Ramanujan Journal, Special Issue in Memory of Richard Askey* **61** (2023), 1-16.

Outreach and Diversity

ACMD staff engage in a variety of efforts that serve to educate the general public about the work of the division and to encourage students to consider careers in science and engineering. We are also involved in internal efforts to improve diversity and inclusivity, which are important for both recruitment and retention of a high-performing workforce. Some of these efforts are described here.

Student Internships in ACMD

Ronald Boisvert

ACMD is committed to helping to prepare the next generation of scientific researchers by providing internships of various types to students at each of the graduate, undergraduate, and high school levels. The NIST programs used to enable such internships include the following:

- *Foreign Guest Researcher Program.* Provides stipends to support visits of guest researchers from foreign institutions for periods of a few weeks to several years.
- *Pathways Program.* Provides temporary Federal appointments to students, typically one to two years. Allows easy conversion to full-time permanent status. (Restricted to U.S. Citizens.)
- *Professional Research Experience Program (PREP)*⁴². A cooperative agreement with thirteen universities⁴³ that provides a mechanism for NIST to support internships for students from those institutions on the Gaithersburg campus throughout the year. A similar agreement with four universities⁴⁴ exists for the NIST Boulder Labs.
- *Student Volunteer Program.* A mechanism that provides unpaid internships for students.
- *Summer High School Internship (SHIP) Program*⁴⁵. SHIP uses the Student Volunteer Program to organize a competitive summer volunteer program for high school students.
- *Summer Undergraduate Research Fellowship (SURF) Program*⁴⁶. A competitive program providing undergraduates a 10-week research experience at NIST.

Funding for all of these programs comes from the Division hosting the student. The Pathways Program, the PREP Program, and the Foreign Guest Researcher Program can also be used to support postdoctoral researchers.

⁴² <https://www.nist.gov/iaao/academic-affairs-office/nist-professional-research-experience-program-prep>

⁴³ Georgetown University, George Washington University, Michigan Tech, Montgomery College, the University of Maryland College Park, and a consortium of Johns Hopkins University, Morgan State University, Bowie State University, the University of Maryland Eastern Shore, Coppin State University, Tuskegee University, North Carolina

In total, during the last 15 months, ACMD supported the work of 40 student interns, including 19 graduate students, 17 undergraduates, and four high school students. See Table 6 and Table 7 for a complete listing.

ACMD staff members are also active in the education of graduate students, serving both as Ph.D. advisers and as members of thesis committees. See page 199.

Network Analysis to Investigate Physics Programmatic Survey Results

Justyna P. Zwolak

Robert P. Dalka (University of Maryland)

Physics graduate studies are substantial efforts, on the part of individual students, departments, and institutions of higher education. Understanding the factors that lead to student success and attrition is crucial for improving these programs. In physics education research (PER), the various aspects of student experiences are often assessed via Likert-style surveys. In our previous work, we proposed the *Network Analysis for Likert-style Surveys* (NALS) approach to modeling and evaluating Likert-style survey results [1]. NALS was validated using the results from the Aspects of Student Experience Survey (ASES). ASES is an instrument designed to assess physics graduate student experiences of departmental support structures [2]. Our current work is building on this past project, leveraging NALS to provide a unique interpretation of responses to the ASES instrument for well-defined demographic groups.

NALS involves a series of steps necessary to generate a network from survey responses. These steps include: (a) creating a bipartite network of respondents

Agricultural and Technical University, and the State University of New York at Binghamton.

⁴⁴ Colorado School of Mines, the University of Colorado Boulder, the University of Colorado Denver, and New Mexico State University.

⁴⁵ <https://www.nist.gov/careers/student-opportunities/summer-high-school-intern-program>

⁴⁶ <https://www.nist.gov/surf>

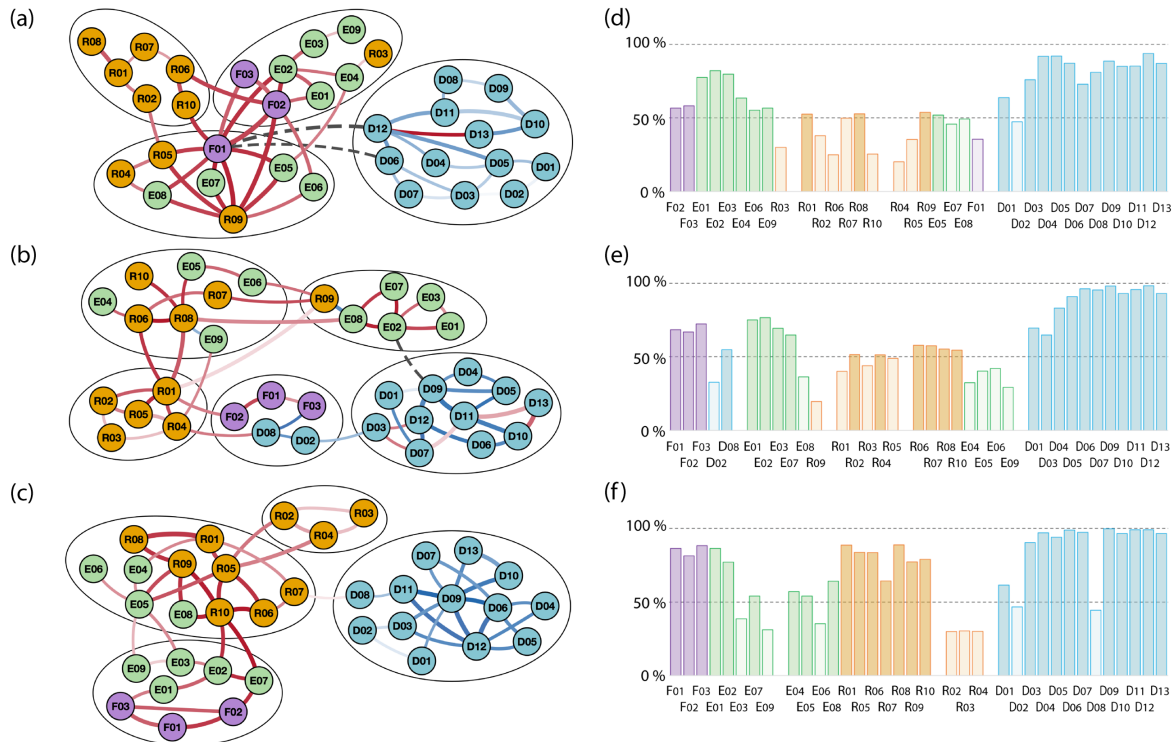


Figure 130. Plots and histograms for networks based on respondent's indicated funding source: (a) research, (b) non-research, and (c) mixed funding. Plots (d) – (f) show the corresponding bootstrapped frequency. In the network plots, the four original themes are highlighted with different colors. Positive temperature edges are indicated in red and negative temperature edges are indicated in blue. New clusters are indicated by the circled regions. Each histogram is grouped by the clusters in the respective network, with nodes not reaching 50% stability made transparent.

and response selections; (b) projecting the network onto response selections using the edge weights to indicate number of respondents selecting both responses; (c) building an item relation matrix for each possible item pair; (d) calculating a similarity value between items and recording the ratio of mutual agree to mutual disagree selections as temperature; and (e) determining the backbone of the resulting network through identifying the most significant edges.

In our previous work [1], we showed that by using NALS we can reliably identify clusters through modular analysis of the resulting network. We also demonstrated that there are important and meaningful differences between the NALS clusters and clusters found through a traditional survey validity method such as the principal component analysis (PCA). In using NALS, we can identify additional information that is not a result of running PCA. Our analysis found four modular communities within the ASES network: social and scholarly exploration (*E*), mentoring and research experience (*R*), professional and academic development (*D*), and financial support (*F*). While Mentoring and Research Experience and Financial Support had been previously identified through PCA, Social and Scholarly Exploration and Professional and Academic Development were unique to the NALS approach.

In our current work, we leverage NALS to provide a unique interpretation of responses to the ASES instrument for well-defined demographic groups. Each demographic split results in a distinct set of networks built only from the relevant responses. In addition to NALS, we also perform a stability analysis of the NA clusters to further confirm the validity of the observed themes. We chose to focus on four demographics for which the subgroups were well-defined and sufficiently large to apply the NALS methodology: the type of program in which students are enrolled (bridge and non-bridge), gender (women and men), the number of semesters since enrollment (less than five semesters and five or more semesters), and type of support available since enrollment (research, non-research, and mixed).

Our analysis reveals that for some demographic groups, NALS produces several new clusters that typically include nodes from multiple original clusters. However, some of the new clusters, especially the smaller ones, turn out to be unstable and tend to revert to the original *R*, *E*, *D*, and *F* clusters during bootstrapping tests. Overall, we find that a certain level of divergence from the full network persists in the demographic-based networks, indicating that there are aspects of experiences that are unique to specific demographic groups.

Figure 129 shows a comparison of the three networks generated based on financial support data. Out of the four original thematic clusters, the professional and academic development theme (cluster D) is most often recovered in the demographic-based networks. However, while in the network based on full ASES dataset the D nodes form a separate component connected exclusively through negative temperature similarity, in both research [Figure 129(b)] and non-research [Figure 129(b)] funding-based networks some D nodes are connected via positive temperature similarity. This indicates that students with exclusively research or non-research support experience some of the aspects of professional and academic development identified above. However, the significant prevalence of negative temperature edges for this theme suggests that the majority of students, regardless of their demographics, are not experiencing these supports within their department.

Looking at the types of connections that the D nodes have extending outside of that thematic cluster allows for additional interpretation. For example, in the research network, there are the two edges of dissimilarity connecting tuition (F_{01}) to both time management training and PI training (D_{06} and D_{12} , respectively). This means that while graduate students supported solely through research assistantships have their tuition fully supported (all other edges connecting this node within the network have a positive temperature) and may not worry about their financial stability in graduate school, they are not supported in advancing certain skills important for their academic careers.

The second theme persistent in all but one considered network is the financial support (cluster F). The three F nodes are almost always clustered together within the demographic-based networks; however, they often tend to get grouped into larger clusters with additional nodes from other themes, Figure 129 (b,c). The only network in which the F nodes are separated is the research network, shown in Figure 129(a), where the central position played by the tuition item (F_{01}) helps to mix around the clustering in the sampled networks. In fact, it is the only one in which an F node is most central in terms of both the local and global connectivity, as quantified by the closeness and betweenness centrality measures, with $C_D(F_{01}) = 11$ and $C_B(F_{01}) = 348$, respectively. Ref. [3] presents a detailed analysis of all 10 demographic-based networks.

Using the full ASES dataset, we have confirmed that the thematic clusters found through NALS are stable against small data perturbation which indicates that the themes are well suited to capture patterns in graduate students' experiences. Additionally, we have shown that for demographic-based networks, NALS can reveal certain unique features that shed light on the needs of particular demographic groups. More details about this work can be found in Ref. [3].

- [1] R.P. Dalka, D. Sachmpazidi, C. Henderson, and J.P. Zwolak. Network Analysis Approach to Likert-style Surveys. *Physical Review Physics Education Research* **18** (2002), 020113.
- [2] D. Sachmpazidi and C. Henderson. Departmental Support Structures for Physics Graduate Students: Development and Psychometric Evaluation of a Self-Report Instrument. *Physical Review Physics Education Research* **17** (2021), 010123.
- [3] R. P. Dalka and J. P. Zwolak. Network Analysis of Graduate Program Support Structures Through Experiences of Various Demographic Groups. arXiv: 2309.04637, 2023.

A Modular Analysis of Ego-driven Institutional Networks

Robert P. Dalka (University of Maryland)
Justyna P. Zwolak

Social network analysis (SNA) is a method for studying relationships within formal and informal groups of individuals, organizations, or even countries. When used to study institutional networks, it helps to explore the social ties within and between formal organizations to better understand phenomena such as knowledge and resource transfer, social influences within teams, or the effect of team building on the dynamics of an organization's social network. However, building social networks often requires personally identifiable information, which in certain organizations can be difficult or impossible to collect. To overcome this limitation, we proposed an alternative method for evaluating interconnectedness within or between organizations. The proposed institutional network analysis uses a projection of anonymous ego-centric data onto organizational units as a proxy to capture the organizational network structure, rather than individual employees [1].

The networks used in this study are built based on the NIST Interactions Survey data [2]. This dataset captures two distinct types of social interactions among NIST employees: their work-related collaborations and advice-seeking. The two resulting networks are expected to exhibit somewhat different structures: whereas collaborating on a project necessitates interaction with other employees to fulfill the organization's mission, not everyone seeks advice internally or in a systematic way. We build and analyze both networks to demonstrate and validate our approach.

Previously, we employed a modular analysis to determine whether the projected unit-based networks accurately reflect the network structure of the organizational units that comprise NIST. We find that the structure restored in the projected network closely resembles the NIST organizational structure for the collaboration network. The advice network has more variability in the communities identified as well as more

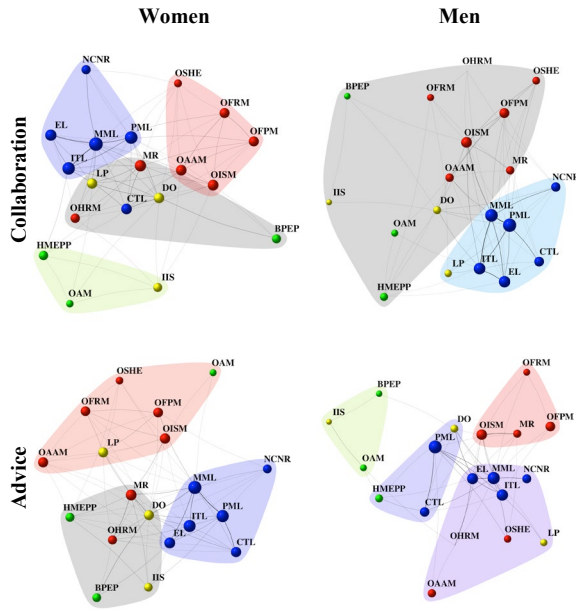


Figure 131. The communities identified within gendered networks. The gendered networks for both collaboration and advice; women collaboration (top left), men collaboration (top right), women advice (bottom left), and men advice (bottom right). The nodes are sized by the number of responses from each OU. Each OU (node) is labeled and colored by the organizational division to which it belongs, with OUs belonging to Laboratory Programs shown as blue nodes, Management Resources as red nodes, Innovation and Industry Services as green nodes, and OUs serving administrative functions shown as yellow nodes. The shaded regions indicate the identified communities.

intermixing between units. We also find that the community assignment for the advice network is less stable and more susceptible to sampling bias, as opposed to the collaboration network.

The first report based on the NIST Interactions Survey focused on comparison of work and advice ego-networks between different categories of demographics (e.g., gender, age group, duty station). Unsurprisingly, the study found the organizational unit (OU) affiliation to be the most important factor in shaping the work collaboration networks. Interestingly, in the advice networks, OU affiliation, gender, and age all played a role. While gender-based differences in ego networks were not observed in the work collaboration networks, some distinctions were found in the advice networks. In terms of age-dependencies, it was found that respondents in the 18 to 39 age range preferred older advice networks. The study in this report did not find any significant differences between minority and non-minority employees for either work collaboration or advice ego-networks.

Our current work focuses on the full inter-OU social networks established based on responses to the two NIST Interaction Survey questions. We study how strong the self-reported connections between OUs are

and how they differ between types of networks and respondent demographics. In doing so, we can investigate how the relationships, both collaboration and advice, map onto the structure of OU-level NIST network [3].

- [1] R. P. Dalka and J. P. Zwolak. Restoring the Structure: A Modular Analysis of Ego-driven Organizational Networks. arXiv:2201.01290, 2022.
- [2] L. Espinal, C. Young, and J. P. Zwolak. Mapping Employee Networks Through the NIST Interactions Survey. NISTIR 8375, June 2021. DOI: [10.6028/NIST.IR.8375](https://doi.org/10.6028/NIST.IR.8375)
- [3] R. P. Dalka and J. P. Zwolak. Organizational Network Analysis of NIST Inclusivity Network Data. In preparation.

Aspects of Postdoctoral Researcher Experience Scale Survey

Justyna P. Zwolak

Robert P. Dalka (University of Maryland)

High attrition rates in science, technology, engineering, and mathematics disciplines are an ongoing problem. Most studies to date have focused on undergraduate and graduate student attrition, with a particular emphasis on students' attributes, undergraduate preparation, and mentoring relationships. Systematic studies looking into the experiences of postdoctoral researchers are few and far between. One example is a recent post-COVID survey organized by *Nature* [1]. The responses to that survey uncovered a list of issues that postdoctoral researchers face: "high pressure, long hours, relatively low wages compared with those for analogous research positions outside academia, and pervasive job insecurity" [2]. Another example is a study that investigates challenges that female postdocs face in academia [3]. The study revealed that a sense of belonging, and the overall work environment are critical for female postdocs to overcome the decision to leave academia.

The goal of the Aspects of Postdoctoral Researcher Experience Scale Survey (APRES) study is to assess the experiences of postdoctoral researchers at NIST. This study will be used to inform what changes might be necessary to ensure that the time postdoctoral researchers spend at NIST prepares them well for the next steps on their career path.

The original "Aspects of Student Experience Scale" (ASES) survey was developed by researchers at Western Michigan University to study what factors foster a supportive environment for graduate students [4]. The questions included in ASES were developed based on prior literature and the American Physical Society Bridge Program (APSBP) recommendations, revised based on APSBP feedback, and subjected to psychometric evaluation. It has been demonstrated that ASES

meets the standard criteria for divergent validity, discriminant validity, and internal consistency. The APRES is a revised version of the ASES survey, modified to be relevant to NIST postdoctoral researchers. The revisions include replacing references to the “department” with “OU” or “division”, as appropriate, replacing “graduate student” with “postdoctoral researcher”, “courses” with “professional development”, etc. The resulting APRES was discussed with researchers having prior experience working with ASES. We have made every attempt to ensure the resulting APRES survey is as anonymous as possible, while still ensuring we are able to capture data that will enable us to tease out where we may have concerns about the postdoctoral researchers’ experiences at NIST.

This survey was administered in Fall 2023 to all Postdoctoral Researchers, including Federal and non-Federal employees, in the Information Technology Laboratory (ITL) at NIST. Non-Federal employees may include guest researchers, contractors, and other early-career researchers working at or for NIST. It is important to survey all postdoctoral researchers to ensure all viewpoints regarding experiences at NIST are considered and to capture an unbiased sample. For the purpose of this work, postdoctoral researchers are defined as early-career researchers no more than seven years from receiving their Ph.D. This includes NRC postdocs, federal term employees, and guest researchers (US citizens and foreign nationals) supported via the NIST PREP program or other agreements with external institutions.

The survey responses are currently being analyzed to identify common themes in responses. These themes may include postdoctoral researchers’ social and scholarly exploration support, mentoring and research experience, professional and academic development, and financial stability. The proposed analysis plan includes a quantitative summary for each question, with count per response for multiple-choice questions and mean response for scaled questions. Secondary analysis will include using the network analysis approach to Likert-style surveys (NALS) of the full response data [5]. We will be looking for areas where we need to improve postdoctoral researchers’ experiences at NIST. Finally, the results will be shared in a report (in preparation) to NIST leadership, staff, and the public. The results will be posted to NIST internal and external websites.

- [1] C. Woolston. Pandemic Darkens Postdocs’ Work and Career Hopes. *Nature* **585** (2020), 309-312.
- [2] C. Woolston. Postdocs Under Pressure: “Can I even do this any more?” *Nature* **587** (2020), 689-692.
- [3] R. Ysseldyk, K. H. Greenaway, E. Hassinger, S. Zutrauen, J. Lintz, and M. P. Bhatia. A Leak in the Academic Pipeline: Identity and Health Among Postdoctoral Women. *Frontiers in Psychology* **10** (2019), 1297.
- [4] D. Sachmpazidi and C. Henderson. Departmental Support Structures for Physics Graduate Students:

Development and Psychometric Evaluation of a Self-Report Instrument. *Physical Review Physics Education Research* **17** (2021), 010123.

- [5] R. P. Dalka, D. Sachmpazidi, C. Henderson, and J. P. Zwolak. Network Analysis Approach to Likert-Style Surveys. *Physical Review Physics Education Research* **18** (2022), 020113.

An Evaluation of the NIST Scientific Integrity Program

*Justyna P. Zwolak
Anne Andrews (NIST RPO)*

The National Institute of Standards and Technology (NIST) Scientific Integrity Program was formally established in policy in 2011. It is NIST’s policy to promote scientific integrity by creating a culture of personal and organizational responsibility where the practice and management of scientific research and its products are free from undue influences that are not essential to the practice of science, such as personal or social allegiances, beliefs, or interests. NIST’s dedication to scientific integrity is highlighted with this assertion on the internal website:

NIST is an organization with strong values, reflected both in our history and our current work. NIST leadership and staff will uphold these values to ensure a high-performing environment that is safe and respectful of all.

The annual evaluation of the NIST Scientific Integrity Program provides a summary of activities and updates about the program status for the period between 1 June 2022 and 30 September 2023.

A baseline evaluation of the program was conducted in May 2023 and included a survey of NIST staff. The purpose of the baseline evaluation was to get a sense of the current staff’s awareness before implementing planned updates. In addition, it served to identify areas where the program needs to focus or improve.

The survey, sent by email with an invitation from the NIST Associate Director for Laboratory Programs, was open to all staff. The survey remained open for three weeks, with a reminder sent one week before the closing date. Of 3416 Federal employees and 4646 Associates included in the NIST Federal Workforce database, 373 Federal and 33 non-Federal respondents completed the survey, resulting in 10.9 % and 0.7 % response rates, respectively. Since the participants were not required to answer any of the questions, a survey was considered completed whenever the participant selected the *Submit* button, regardless of how many questions were answered. All survey questions were answered by at least

97.5 % of respondents, while the demographic questions, included at the end of the survey, were responded to by at least 94.8 %.

The first two sets of survey questions pertained to the respondents' knowledge of the Scientific Integrity Policy (SIP) and the Research Conduct Policy (RCP) as well as their attitudes toward handling allegations related to scientific integrity and research misconduct. Figure 1, showing a comparison of responses to questions about the respondents' familiarity with SIP and RCP, indicates slightly more responses were aware of the RCP than of the SIP, at about 56 % vs. 50 %, respectively. A detailed analysis of all survey questions is presented in the NIST Special Publication [1].

In addition to answering survey questions, the respondents were given an opportunity to provide general comments and feedback about NIST's SIP and RCP. The most common theme in the open-ended questions was a request for more training about both policies. Respondents also asked for resources that would present these policies in a more accessible format, such as a course on the Commerce Learning Center or via iNET and should be included as part of the annual training requirements. A number of respondents expressed disappointment with how the ERB process is being handled, requesting authorship guidelines that would explain who should be included in publications.

The program evaluation highlighted several areas where the program could be improved, and more guidance would be helpful. The baseline assessment

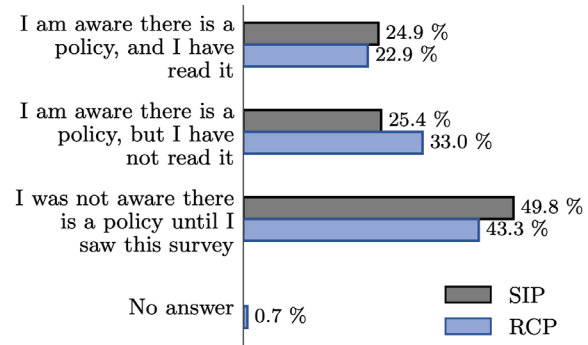


Figure 132. A comparison of responses to questions about the respondents' familiarity with the Scientific Integrity Policy (SIP) and the Research Conduct Policy (RCP).

validated our assumption that while staff believe scientific integrity is important at NIST, they are not familiar with our established program. The SIO will finalize the awareness training program and begin deployment in FY 2024. In addition, the NIST Scientific Integrity Officer (SIO) and SIP team will work with the Subcommittee for Scientific Integrity to develop an implementation and evaluation plan by the end of FY 2024. The full report is forthcoming [1].

- [1] A. Andrews and J. P. Zwolak. NIST Scientific Integrity Program: Annual Report. In preparation.

Table 6. Student interns in ACMD –High School and Undergraduate

Name	From	Program		Mentor	Topic
Blank, Eve	CalTech	U	SURF	Z. Grey	Geometric interpretations for imaging and shape analysis
Burbery, Peter	Marshall University	U	SURF	H. Cohl	Translation of Mathematica source to LaTeX
Cooksey, Isaac	U. of Maryland	U	DGR	A. Kearsley	Mathematical optimization
Hakala, Sonja	U. Maryland	U	PREP	T. Gerrits	Quantum network node metrology
Harvey, Katherine	Hillsdale College	U	SURF	R. Evans	Approximate solutions to a nonlinear model for biological field effect transistor experiments
Hawranick, Luke	West Virginia U.	U	PATH	W. George	Inter-node communication performance tuning
He, Dongxing	U. Maryland	U	PREP	T. Gerrits	Quantum network component metrology
Jia, Leon	U. California Berkeley	U	SURF	L. Ma	Characterization of quantum memories and SiC-based quantum devices
Ko, Morgan	U. Maryland	U	SURF	J. Terrill	Making 3D formats accessible for scientific data
Krepets, Mikhail	U. Maryland	U	SURF	M. Mascagni	Implementing walk-on-spheres using a GPU
Liu, Joseph	Montgomery College	U	PREP	S. Su	Extending ParaView software for immersive visualization applications
Raman, Akhil	Poolesville, HS	H	SHIP	S. Su	HMD immersive visualization with ParaView
Shaikh, Faadil Abdullah	U. Maryland	U	SURF	M. Mascagni	Solving exterior walk-on-spheres problems using the Kelvin transform
Shen, Angela	Montgomery Blair HS	H	SHIP	O. Slattery	Entanglement distribution simulation
Stone, Sarah	Montgomery Blair HS	H	SHIP	H. Cohl	Computationally generated mathematical n-ary tree art on smooth two-dimensional manifolds
Su, Ruisi	Carnegie Mellon U.	U	FGR	A. Kearsley	Detecting network anomalies
Szilagyi, Michael	George Mason U.	U	SURF	J. Terrill	Converting GLSL shaders to run in ParaView
Vazquez Correa, Joshua	Montgomery College	U	PREP	S. Su	Extending ParaView software for immersive visualization applications
Wolcott, Thomas	U. Maryland	U	SURF	B. Schneider	Developing a science gateway for atomic, molecular, and optical science
Xiao, Lilian	Poolesville HS	H	DGR	J. Terrill	Making 3D formats accessible for scientific data
Xiao, Vivian	U. Pennsylvania	U	DGR	A. Kearsley	Optimization in chemometrics

Legend

<i>G</i>	<i>Graduate Student</i>	<i>PREP</i>	<i>Professional Research Experience Program</i>
<i>U</i>	<i>Undergraduate</i>	<i>FGR</i>	<i>Foreign Guest Researcher</i>
<i>H</i>	<i>High School</i>	<i>DGR</i>	<i>Domestic Guest Researcher</i>
		<i>SHIP</i>	<i>Summer High School Internship Program</i>
		<i>SURF</i>	<i>Summer Undergraduate Research Fellowship</i>
		<i>PATH</i>	<i>Pathways Program</i>

Table 7. Student interns in ACMD – Graduate Students.

Name	From	Program	Mentor	Topic	
Agrawal, Sristy	U. Colorado Boulder	G	FGR	S. Glancy	Resource based quantum information theory
Alhejji, Mohamad	U. Colorado Boulder	G	PREP	E. Knill	Quantum randomness protocols
Avagyan, Arik	U. Colorado Boulder	G	PREP	E. Knill	Quantum information processing
Centner, Raymond	U. South Florida	G	NSF	H. Cohl	Special values and Poisson kernel for Askey-Wilson polynomials
Chalfin, Harry	U. of Maryland	G	DGR	J. Zwolak	Tuning high-fidelity operation of spin qubits
Dawkins, Riley	Louisiana State U.	G	DGR	T. Gerrits	Weak field homodyne detection
Fox, Matthew	U. Colorado Boulder	G	DGR	S. Glancy	Topics in theoretical quantum information science
Geller, Shawn	U. Colorado Boulder	G	PREP	E. Knill	Characterization of quantum state preparation and measurement errors
Hall, Carole	Stony Brook U.	G	DGR	G. Dogan	Measure of shape similarity and complexity
Kwiatkowski, Alexander	U. Colorado Boulder	G	PREP	E. Knill	Quantum networking
Ladic, Katjana	U. Zagreb, Croatia	G	FGR	K. Sayrafian	Ultra wideband channel characterization for ingestible microbots
Mazur, Marcel	U. Colorado Boulder	G	DGR	S. Glancy	Topics in theoretical quantum information science
Ornstein, Joel	U. Colorado Boulder	G	DGR	S. Glancy	Quantum information journal club
Park, Jiyoung	Texas A&M U.	G	NSF	G. Dogan	Machine learning approaches to image segmentation
Schneider, Ryan	U. C. San Diego	G	DGR	B. Schneider	Collocation methods to solve the electronic Schrödinger equation
Schreiber, Jeanie	George Mason U.	G	NSF	Z. Grey	Applications of differential geometry
Seshadri, Akshay	U. Colorado Boulder	G	PREP	E. Knill	Quantum measurement statistics
Shrestha, Pranish	Morgan State University	G	PREP	T. Gerrits	Optical fiber-link noise characterization
van de Poll, May An	U. Colorado Boulder	G	PREP	E. Knill	Analysis of quantum optical measurements

Legend

<i>G</i>	<i>Graduate Student</i>	<i>PREP</i>	<i>Professional Research Experience Program</i>
<i>U</i>	<i>Undergraduate</i>	<i>FGR</i>	<i>Foreign Guest Researcher</i>
<i>H</i>	<i>High School</i>	<i>DGR</i>	<i>Domestic Guest Researcher</i>
		<i>NSF</i>	<i>NSF Mathematical Sciences Graduate Internship Program</i>

Publications

Note: Names of (co-)authors with a Division affiliation during this reporting period are underlined.

Appeared

Refereed Journals

1. B. Alexander, H. Cohl, and H. Volkmer. Internal and External Harmonics in Bi-cyclide Coordinates. *Journal of Physics A: Mathematical and Theoretical*, **56** 325203 (2023). DOI: [10.48550/arXiv.2303.02235](https://doi.org/10.48550/arXiv.2303.02235)
2. K. Alladi, H. Cohl, F. Garvan, M. Ismail, and H. Rosengren. Preface to Special Issues in Memory of Richard Askey. *The Ramanujan Journal*, Special Issue in Memory of Richard Askey **61** (2023), 1-6. DOI: [10.1007/s11139-023-00732-2](https://doi.org/10.1007/s11139-023-00732-2)
3. E. Atindama, P. Lef, G. Doğan, and P. Athavale. Restoration of Noisy Orientation Maps from Electron Backscatter Diffraction Imaging. *Integrating Materials and Manufacturing Innovation* **12**:3 (2023), 251-266. DOI: [10.1007/s40192-023-00304-8](https://doi.org/10.1007/s40192-023-00304-8)
4. A. Avagyan, E. Knill, S. Glancy. Multi-Mode Gaussian State Analysis with Total-photon Counting. *Journal of Physics B*, **8** (2023), 14501. DOI: [10.1088/1361-6455/ace175](https://doi.org/10.1088/1361-6455/ace175)
5. P. Bedekar, A. Kearsley, and P. Patrone. Prevalence Estimation and Optimal Classification Methods to Account for Time Dependence in Antibody Levels. *Journal of Theoretical Biology* **559** (2023), 111375. DOI: [10.1016/j.jtbi.2022.111375](https://doi.org/10.1016/j.jtbi.2022.111375)
6. I. Bezerra, H. Vasconcelos, and S. Glancy. Quadrature Squeezing and Temperature Estimation from the Fock Distribution. *Quantum Information Processing* **21** (2022), 365. DOI: [10.1007/s11128-022-03677-5](https://doi.org/10.1007/s11128-022-03677-5)
7. I. Bray, X. Weber, D. Fursa, A. Kadryrov, B. Schneider, S. Pamidighantam, M. Cytowski, and A. Kheifets. Taking the Convergent Close-coupling Method Beyond Helium: The Utility of the Hartree-Fock Theory. *ATOMS* **10**:1 (2022), 22. DOI: [10.3390/atoms10010022](https://doi.org/10.3390/atoms10010022)
8. T. Bui, M.-A. Henn, W. Tew, M. Catterton, and S. Woods. Harmonic Dependence of Thermal Magnetic Particle Imaging. *Scientific Reports* **13** (2023), 15762. DOI: [10.1038/s41598-023-42620-1](https://doi.org/10.1038/s41598-023-42620-1)
9. I. Burenkov, A. Semionova, FNU Hala, T. Gerrits, A. Rahmouni, D. Anand, Y. Li-Baboud, O. Slattery, A. Battou, and S. Polyakov. Synchronization and Coexistence in Quantum Networks. *Optics Express* **31**:7 (2023), 11431-11446. DOI: [10.1364/OE.480486](https://doi.org/10.1364/OE.480486)
10. S. Chattopadhyay, C. Marante, B. Schneider, and L. Argenti. Two-photon Double Ionization with Finite Pulses: Application of the Virtual Sequential Model to Helium. *Physical Review A* **108** (2023), 013114. DOI: [10.1103/PhysRevA.108.013114](https://doi.org/10.1103/PhysRevA.108.013114)
11. H. Cohl, R. Costas-Santos, P. Hwang, and T. Wakhare. Generalizations of Generating Functions for Basic Hypergeometric Orthogonal Polynomials. *Open Journal of Mathematical Sciences* **6**:1 (2022), 248-261. DOI: [10.48550/arXiv.1411.1371](https://doi.org/10.48550/arXiv.1411.1371)
12. H. Cohl and R. Costas-Santos. Symmetry of Terminating Basic Hypergeometric Series Representations of the Askey-Wilson Polynomials. *Journal of Mathematical Analysis and Applications* **517**:1 (2023), 126583. DOI: [10.1016/j.jmaa.2022.126583](https://doi.org/10.1016/j.jmaa.2022.126583)
13. H. Cohl, J. Hirtenstein, J. Lawrence, and L. Ritter. Gegenbauer Expansions and Addition Theorems for a Binomial and Logarithmic Fundamental Solution of the even-dimensional Euclidean polyharmonic Equation. *Journal of Mathematical Analysis and Applications* **517**:2 (2023), 126576. DOI: [10.1016/j.jmaa.2022.126576](https://doi.org/10.1016/j.jmaa.2022.126576)
14. H. Cohl and R. Costas-Santos. Nonterminating Transformations and Summations Associated with some q -Mellin-Barnes Integrals. *Advances in Applied Analysis* **147** (2023), 102517. DOI: [10.1016/j.aam.2023.102517](https://doi.org/10.1016/j.aam.2023.102517)
15. H. Cohl and R. Costas-Santos. Utility of Integral Representations for Basic Hypergeometric Functions and Orthogonal Polynomials. *The Ramanujan Journal*, Special Issue in Memory of Richard Askey, **61**:2 (2023), 649-674. DOI: [10.1007/s11139-021-00509-5](https://doi.org/10.1007/s11139-021-00509-5)
16. H. Cohl and L. Ritter. Two-dimensional Contiguous Relations for the Linearization Coefficients of Classical Orthogonal Polynomials. *Integral Transforms and Special Functions* **34**:9 (2023), 635-658. DOI: [10.1080/10652469.2023.2180502](https://doi.org/10.1080/10652469.2023.2180502)
17. H. Cohl and R. Costas-Santos. Multi-integral Representations for Jacobi Functions of the First and Second Kind. *Arab Journal of Basic and Applied Sciences*, **30**:1 (2023), 583-592. DOI: [10.1080/25765299.2023.2268911](https://doi.org/10.1080/25765299.2023.2268911)
18. C. Couteau, S. Barz, T. Durt, T. Gerrits, J. Huwer, R. Prevedel, J. Rarity, A. Shields, and G. Weihs. Applications of Single Photons in Quantum Metrology, Biology and the Foundations of Quantum Physics. *Nature Reviews Physics* **5** (2023), 354. DOI: [10.1038/s42254-023-00583-2](https://doi.org/10.1038/s42254-023-00583-2)
19. R. DeJaco, J. Majikes, J. Little, and A. Kearsley. Binding, Brightness, or Noise? Extracting Temperature-dependent Properties of Dye Bound to DNA.

- Biophysical Journal* **122** (2023),1364-1375. DOI: [10.1016/j.bpj.2023.03.002](https://doi.org/10.1016/j.bpj.2023.03.002)
20. R. DeJaco, M. Roberts, E. Romsos, P. Vallone, A. Kearsley, Reducing Bias and Quantifying Uncertainty in Fluorescence Produced by PCR. *Bulletin of Mathematical Biology* **85** (2023), 83. DOI: [10.1007/s11538-023-01182-z](https://doi.org/10.1007/s11538-023-01182-z)
 21. O. Doronina, Z. Grey, and A. Glaws. G2Aero: A Python Package for Separable Shape Tensors. *Journal of Open Source Software*. **8**:89 (2023), 5408. DOI: [10.21105/joss.05408](https://doi.org/10.21105/joss.05408)
 22. P. Faist, M. Woods, V. Albert, J. Renes, J. Eisert, and J. Preskill. Time-energy Uncertainty Relation for Noisy Quantum Metrology. *PRX Quantum* **4** (2023), 040336. DOI: [10.1103/PRXQuantum.4.040336](https://doi.org/10.1103/PRXQuantum.4.040336)
 23. S. Freiman, J. Fong, and N. Heckert. New Statistical Methodology for Assessing Mechanical Survivability of Brittle Materials. *Journal of Strength, Fracture, and Complexity* **16** (2023), 1-15. DOI: [10.3233/SFC-221504](https://doi.org/10.3233/SFC-221504)
 24. A. R. Fritsch, S. Guo, S. M. Koh, I. B. Spielman, and J. P. Zwolak. Dark Solitons in Bose-Einstein Condensates: A Dataset for Many-body Physics Research. *Machine Learning: Science and Technology* **3**:4 (2022), 047001. DOI: [10.1088/2632-2153/ac9454](https://doi.org/10.1088/2632-2153/ac9454)
 25. L. García-Pintos, L. Brady, J. Bringewatt, and Y.-K. Liu. Lower Bounds on Quantum Annealing Times. *Physical Review Letters* **130** (2023), 140601. DOI: [10.1103/PhysRevLett.130.140601](https://doi.org/10.1103/PhysRevLett.130.140601)
 26. Z. Grey, O. Doronina, and A. Glaws. Separable Shape Tensors for Aerodynamic Design. *Journal of Computational Design and Engineering* **10**:1 (2023), 468-487. DOI: [10.1093/jcde/qwac140](https://doi.org/10.1093/jcde/qwac140)
 27. Z. Guo, Z. Liu, G. Barbastathis, Q. Zhang, M. Glinzky, B. Alpert, and Z. Levine. Noise-Resilient Deep Learning for Integrated Circuit Tomography. *Optics Express* **31**:10 (2023), 15355. DOI: [10.1364/OE.486213](https://doi.org/10.1364/OE.486213)
 28. K. Hamilton, K. Bartschat, N. Douguet, S. Pamidighantam, and B. Schneider. Simulation For All: The Atomic, Molecular, and Optical Science Gateway. *Computing in Science and Engineering* **25**:68 (2023), 68-72. DOI: [10.1109/MCSE.2023.3312888](https://doi.org/10.1109/MCSE.2023.3312888)
 29. M.-A. Henn, K. Quelhas, and S. Woods. Investigating the Influence of Sampling Frequency on X-Space MPI Image Reconstructions. *International Journal on Magnetic Particle Imaging* **9**:1 (2023). DOI: [10.18416/IJMPI.2023.2303042](https://doi.org/10.18416/IJMPI.2023.2303042)
 30. M.-A. Henn, T. Bui, and S. Woods. Investigating the Harmonic Dependence of MPI Resolution. *International Journal on Magnetic Particle Imaging* **9**:1 (2023). DOI: [10.18416/IJMPI.2023.2303059](https://doi.org/10.18416/IJMPI.2023.2303059)
 31. M. Hu, M. Hofer, and M. Donahue. Energetics of Phase Transitions in Homogeneous Antiferromagnets. *Applied Physics Letters* **123** (2023), 062401. DOI: [10.1063/5.0147368](https://doi.org/10.1063/5.0147368)
 32. J. Iosue, K. Sharma, M. Gullans, and V. Albert. Continuous-variable Quantum State Designs: Theory and Applications. *Physical Review X* **14** (2023), 011013. DOI: [10.1103/PhysRevX.14.011013](https://doi.org/10.1103/PhysRevX.14.011013)
 33. P. Kuo, D. Reddy, V. Verma, S. Nam, A. Zukauskas, and C. Canalias. Photon-pair Production and Frequency Translation Using Backward-wave Spontaneous Parametric Down Conversion. *Optica Quantum* **1**:2 (2023), 43. DOI: [10.1364/OPTICAQ.500021](https://doi.org/10.1364/OPTICAQ.500021)
 34. A. Kwiatkowski, E. Shojaee, S. Agrawal, A. Kyle, C. Rau, S. Glancy, and E. Knill. Constraints on Gaussian Error Channels and Measurements for Quantum Communication. *Physical Review A* **107** (2023), 042604. DOI: [10.1103/PhysRevA.107.042604](https://doi.org/10.1103/PhysRevA.107.042604)
 35. A. Kyle, C. Rau, W. Warfield, A. Kwiatkowski, J. D. Teufel, K. Lehnert, and T. Dennis. Optically Distributing Remote Two-node Microwave Entanglement Using Doubly Parametric Quantum Transducers. *Physical Review Applied* **20** (2023), 014005. DOI: [10.1103/PhysRevApplied.20.014005](https://doi.org/10.1103/PhysRevApplied.20.014005)
 36. K. Ladic, K. Sayrafian, D. Simunic, and K. Yazdandoost. Wireless Channel Characterization for UWB Communication in Capsule Endoscopy. *IEEE Access* **11** (August 2023), 95858 – 95873. DOI: [10.1109/ACCESS.2023.3310216](https://doi.org/10.1109/ACCESS.2023.3310216)
 37. Z. Levine, B. Alpert, A. Dagel, J. Fowler, E. Jimenez, N. Nakamura, D. Swetz, P. Szypryt, K. Thompson, and J. Ullom. A Tabletop X-Ray Tomography Instrument for Nanometer-Scale Imaging. *Microsystems & Nanoengineering* **9**:47 (2023), 47. DOI: [10.1038/s41378-023-00510-6](https://doi.org/10.1038/s41378-023-00510-6)
 38. R. Luke, A. Kearsley, N. Pisanic, Y. Manabe, D. Thomas, C. Heaney, and P. Patrone. Modeling in Higher Dimensions to Improve Diagnostic Testing Accuracy: Theory and Examples for Multiplex Saliva-Based SARS-CoV-2 Assays. *PLOS One*, **18**:3 (2023), e0280823. DOI: [10.1371/journal.pone.0280823](https://doi.org/10.1371/journal.pone.0280823)
 39. R. Luke, A. Kearsley, and P. Patrone. Optimal Multiclass Classification and Generalized Prevalence Estimates for Diagnostic Settings with More Than Two Classes. *Mathematical Biosciences* **358** (2023), 108982. DOI: [10.1016/j.mbs.2023.108982](https://doi.org/10.1016/j.mbs.2023.108982)
 40. H. Mahboubi, K. Sayrafian, and A. Aghdam. A Low Complexity Power Maximization Strategy for Coulomb Force Parametric Generators, *IEEE Access* **11** (May 2023), 42881–42894. DOI: [10.1109/ACCESS.2023.3260106](https://doi.org/10.1109/ACCESS.2023.3260106)

41. A. McCaughan, B. Oripov, N. Ganesh, S. Nam, A. Dienstfrey, S. Buckley. Multiplexed Gradient Descent: Fast Online Training of Modern Datasets on Hardware Neural Networks Without Backpropagation. *APL Machine Learning* **1**:2 (2023), 026118. DOI: [10.1063/5.0157645](https://doi.org/10.1063/5.0157645)
42. A. Moorthy, A. Kearsley, W. Mallard, W. Wallace, and S. Stein. Inferring the Nominal Molecular Mass of an Analyte from its Electron Ionization Mass Spectrum. *Analytical Chemistry* **95**:35 (2023), 13132–13139. DOI: [10.1021/acs.analchem.3c01815](https://doi.org/10.1021/acs.analchem.3c01815)
43. A. Moorthy, E. Erisman, A. Kearsley, Y. Liang, E. Sisco, and W. Wallace. On the Challenge of Unambiguous Identification of Fentanyl Analogs: Exploring Measurement Diversity using Standard Reference Mass Spectral Libraries. *Journal of Forensic Sciences* **68**:5 (2023), 1494-1503. DOI: [10.1111/1556-4029.15322](https://doi.org/10.1111/1556-4029.15322)
44. K. Quelhas, M.-A. Henn, R. Farias, W. Tew, and S. Woods. Parallel MPI Image Reconstructions in GPU using CUDA. *International Journal on Magnetic Particle Imaging* **9**:1 (2023). DOI: [10.18416/IJMPI.2023.2303043](https://doi.org/10.18416/IJMPI.2023.2303043)
45. J. Randazzo, C. Marante, S. Chattopadhyay, B. Schneider, J. Olsen, and L. Argenti. ASTRA: a Transition-Density-Matrix Approach to Molecular Ionization. *Physical Review Research* **5** (2023), 043125. DOI: [10.1103/PhysRevResearch.5.043115](https://doi.org/10.1103/PhysRevResearch.5.043115)
46. M. Roudneshin, K. Sayrafian, and A. Aghdam. Adaptive Maximization of the Harvested Power for Wearable or Implantable Sensors with Coulomb Force Parametric Generators. *IEEE Internet of Things Journal* **10**:19 (April 2023), 16793–16803. DOI: [10.1109/JIOT.2023.3269953](https://doi.org/10.1109/JIOT.2023.3269953)
47. L. Scarlett, M. Zammit, I. Bray, B. Schneider, and D. Fursa. Convergent Close Coupling Calculations of Electron Scattering on HeH⁺. *Physical Review A* **106** (2022), 042818. DOI: [10.1103/PhysRevA.106.042818](https://doi.org/10.1103/PhysRevA.106.042818)
48. L. Scarlett, E. Jong, S. Odellia, M. Zammit, Y. Ralchenko, B. Schneider, I. Bray, and D. Fursa. Complete Collision Data Set for Electrons Scattering on Molecular Hydrogen and its Isotopologues: IV. Vibrationally-Resolved Ionization of the Ground and Excited Electronic States. *Atomic Data and Nuclear Data Tables* **151** (2023), 01573. DOI: [10.1016/j.adt.2023.101573](https://doi.org/10.1016/j.adt.2023.101573)
49. P. Scharpf, M. Schubotz, C. Breitingner, H. Cohl, and B. Gipp. Discovery and Recognition of Formula Concepts using Machine Learning. *Scientometrics* **128** (2023), 4971-5025. DOI: [10.48550/arXiv.2303.01994](https://doi.org/10.48550/arXiv.2303.01994)
50. B. Schneider, K. Hamilton, and K. Bartschat. Generalizations of the R-Matrix Method to the Treatment of the Interaction of Short Pulse Electromagnetic Radiation with Atoms. *ATOMS* **10**:3 (2022), 23. DOI: [10.3390/atoms10010026](https://doi.org/10.3390/atoms10010026)
51. R. Schneider, H. Gharibnejed, and B. Schneider. ITVOLT: An Iterative Solver for the Time-Dependent Schrödinger Equation. *Computer Physics Communications* **291** (2023), 108780. DOI: [10.1016/j.cpc.2023.108780](https://doi.org/10.1016/j.cpc.2023.108780)
52. J. Sims, B. Padhy, and M. Ruiz. Exponentially Correlated Hylleraas-Configuration-Interaction Studies of Atomic Systems. III. Upper and Lower Bounds to He-Sequence Oscillator Strengths for the Resonance singlet S – singlet P Transition. *Atoms* **11**:7 (2023), 107. DOI: [10.3390/atoms11070107](https://doi.org/10.3390/atoms11070107)
53. A. Singor, J. Savage, I. Bray, B. Schneider, and D. Fursa. Continuum Solutions to the Two-Center Coulomb Problem in Prolate Spheroidal Coordinates. *Computer Physics Communications* **282** (2023), 108514. DOI: [10.1016/j.cpc.2022.108514](https://doi.org/10.1016/j.cpc.2022.108514)
54. S. Sorokanich. Beyond Mean Field: Condensate Coupled with Pair Excitations. *Journal of Mathematical Physics* **64**:8 (2023), 081904. DOI: [10.1063/5.0125971](https://doi.org/10.1063/5.0125971)
55. L. Wang, P. Patrone, A. Kearsley, J. Izac, A. Gaigalas, J. Prostko, H. Kwon, W. Tang, M. Kosikova, H. Xie, L. Tian, E. Elsheikh, E. Kwee, T. Kemp, S. Jochum, N. Thornburg, L. McDonald, A. Gundlapalli, and S. Lin-Gibson. Monoclonal Antibodies as SARS-CoV-2 Serology Standards: Experimental Validation and Broader Implications for Correlates of Protection. *International Journal of Molecular Sciences* **24**:21 (2023), 15705. DOI: [10.3390/ijms242115705](https://doi.org/10.3390/ijms242115705)
56. Y. Xu, Y. Wang, E.-J. Kuo, and V. Albert. Qubit-Oscillator Concatenated Codes: Decoding Formalism and Code Comparison. *PRX Quantum* **4** (2023), 020342. DOI: [10.1103/PRXQuantum.4.020342](https://doi.org/10.1103/PRXQuantum.4.020342)
57. O. Yousuf, I. Hossen, M. Daniels, M. Lueker-Boden, and A. Dienstfrey. Device Modeling Bias in ReRAM-Based Neural Network Simulations. *IEEE Journal on Emerging and Selected Topics in Circuits and Systems* **13**:1 (2023), 042318. DOI: [10.1109/JETCAS.2023.3238295](https://doi.org/10.1109/JETCAS.2023.3238295)
58. H. Zhao, G. Bryant, W. Griffin, J. Terrill and J. Chen. Evaluating Glyph Design for Showing Large-Magnitude-Range Quantum Spins. *IEEE Transactions on Visualization and Computer Graphics* **28** (December 2022). DOI: [10.1109/TVCG.2022.3232591](https://doi.org/10.1109/TVCG.2022.3232591)
59. J. Ziegler, F. Luthi, M. Ramsey, F. Borjans, G. Zheng, and J. Zwolak. Tuning Arrays with Rays: Physics-informed Tuning of Quantum Dot Charge

- States. *Physical Review Applied* **20**:3 (2023), 034067. DOI: [10.1103/PhysRevApplied.20.034067](https://doi.org/10.1103/PhysRevApplied.20.034067)
60. J. Ziegler, F. Luthi, M. Ramsey, F. Borjans, G. Zheng, and J. Zwolak. Automated Extraction of Capacitive Coupling for Quantum Dot Systems. *Physical Review Applied* **19**:5 (2023), 054077. DOI: [10.1103/PhysRevApplied.19.054077](https://doi.org/10.1103/PhysRevApplied.19.054077)
 61. J. Zwolak and J. Taylor. Colloquium: Advances in Automation of Quantum Dot Devices Control. *Reviews of Modern Physics* **95**:1 (2023), 011006. DOI: [10.1103/RevModPhys.95.011006](https://doi.org/10.1103/RevModPhys.95.011006)
- ### In Conference Proceedings
1. A. Arora, A. Coladangelo, M. Coudron, A. Gheorghiu, U. Singh, and H. Waldner. Quantum Depth in the Random Oracle Model. In *Proceedings of the 55th Annual ACM Symposium on Theory of Computing (STOC 2023)*. Orlando, FL, June 20-23, 2023, 1111–1124. DOI: [10.1145/3564246.3585153](https://doi.org/10.1145/3564246.3585153)
 2. B. Barnes and M.-A. Henn. Addressing Misclassification Costs in Machine Learning Through Asymmetric Loss Functions. In *SPIE 12496 Metrology, Inspection, and Process Control XXXVII, 124961C*, San Jose, California, February 26-March 2, 2023. DOI: [10.1117/12.2662027](https://doi.org/10.1117/12.2662027)
 3. J. Bienfang, T. Gerrits, P. Kuo, A. Migdall, S. Polyakov, and O. Slattery. A Single-Photon Dictionary to Support the Emerging Quantum Industry. *Technical Digest Series of Optica, CLEO: Applications and Technology 2023*, San Jose, California, May 7-12, 2023. DOI: [10.1364/CLEO_AT.2023.AM4N.7](https://doi.org/10.1364/CLEO_AT.2023.AM4N.7)
 4. I. Burenkov, A. Semionova, Hala, T. Gerrits, A. Rahmouni, D. Anand, Y. Li-Baboud, O. Slattery, A. Battou, and S. Polyakov. Fundamental Coexistence Limit of Quantum States with White Rabbit Synchronization in Quantum Networks. In *Technical Digest Series of Optica, CLEO: Applications and Technology 2023*, San Jose, CA, US, May 2023, FM1A.4. DOI: [10.1364/CLEO_FS.2023.FM1A.4](https://doi.org/10.1364/CLEO_FS.2023.FM1A.4)
 5. I. Burenkov, A. Semionova, T. Gerrits, A. Rahmouni, D. Anand, Y. Li-Baboud, O. Slattery, A. Battou, and S. Polyakov. Coexistence of 100 Wave-Multiplexed Quantum Channels with Classical Synchronization. In *SPIE Photonics West Proceedings Volume PC12446, Quantum Computing, Communication, and Simulation III*, San Francisco, CA, March 2023. DOI: [10.1117/12.2648488](https://doi.org/10.1117/12.2648488)
 6. A. Childs, M. Coudron, and A. Gilani. Quantum Algorithms and the Power of Forgetting. In *14th Innovations in Theoretical Computer Science Conference, Leibniz International Series in Informatics* **251** (2023), 37. DOI: [10.4230/LIPIcs.ITCS.2023.37](https://doi.org/10.4230/LIPIcs.ITCS.2023.37)
 7. B. Cloteaux, V. Marbukh, and K. Sayrafian. Impact of the Exposure Time and Distance Thresholds on the Performance of Automatic Contact Tracing. In *2023 IEEE International Conference on Communications Workshops (ICC Workshops)*, Rome, Italy, June 1, 2023, 1701-1706. DOI: [10.1109/ICCWorkshops57953.2023.10283674](https://doi.org/10.1109/ICCWorkshops57953.2023.10283674)
 8. N. Coble, M. Coudron, J. Nelson, and S. Nezhadi. Local Hamiltonians with No Low-Energy Stabilizer States. In *18th Conference on the Theory of Quantum Computation, Communication and Cryptography, Leibniz International Series in Informatics* **266** (2023), 14. DOI: [10.4230/LIPIcs.TQC.2023.14](https://doi.org/10.4230/LIPIcs.TQC.2023.14)
 9. J. Fong, N. Heckert, P. Marcal, and M. Cohn. A Failure-Probability and Damage-state-based Fatigue and Creep Model in Thermal Fatigue. In *2023 ASME Pressure Vessels & Piping Division Conference*, Atlanta, GA, July 16-21, 2023. DOI: [10.1115/PVP2023-106831](https://doi.org/10.1115/PVP2023-106831)
 10. J. Fong, N. Finney, Jr., S. Doctor, and N. Heckert. A Quantitative Relationship Between the Pod Qualification of an Inspector and the Estimated Upper Bound Failure Probability of a Fatigue-loaded Uncracked Component When the Inspector Found No Crack. In *2023 ASME 50th Annual Review of Progress in Quantitative Nondestructive Evaluation Conference*, Austin, TX, July 24-27, 2023. DOI: [10.1115/QNDE2023-108683](https://doi.org/10.1115/QNDE2023-108683)
 11. H. Feng, X. Ren, Q. Wei, Y. Lei, R. Kacker, D. Kuhn, and D. Simos. MagicMirror: Towards High-Coverage Fuzzing of Smart Contracts. In *Proceedings of the 2023 IEEE International Conference on Software, Testing, Verification and Validation (ICST 2024)*, Dublin, Ireland, April 16-22, 2023, 141-152. DOI: [10.1109/ICST57152.2023.00022](https://doi.org/10.1109/ICST57152.2023.00022)
 12. B. Garn, D. Schreiber, D. Simos, D. Kuhn, J. Voas, and R. Kacker. Summary of Combinatorial Methods for Testing Internet of Things Smart Home Systems. In *Proceedings of the 2023 IEEE International Conference on Software, Testing, Verification and Validation Workshops (ICSTW)* Dublin, Ireland, April 16-22, 2023, 266-267. DOI: [10.1109/ICSTW58534.2023.00054](https://doi.org/10.1109/ICSTW58534.2023.00054)
 13. S. Jabbireddy, S. Li, X. Meng, J. E. Terrill, A. Varshney, T. Hoelt, W. Aigner, and B. Wang. Accelerated Volume Rendering with Volume Guided Neural Denoising. In *Proceedings of the EUROVIS 25th EuroGraphics Conference on Visualization*, Leipzig, Germany, June 12-16, 2023. DOI: [10.2312/evs.20231042](https://doi.org/10.2312/evs.20231042)
 14. R. Kacker. What Did the Current SI Do to the Uncertainties in Measurement of Defining Constants? In *Proceedings of the 2023 Conference: Sensor and*

- Measurement Science International* (SMSI 2023), Nuremberg, Germany, May 8-11, 2023. DOI: [10.5162/SMSI2023/A7.1](https://doi.org/10.5162/SMSI2023/A7.1)
15. K. Khadka, J. Chandrasekaran, Y. Lei, R. Kacker, and D. Kuhn. Synthetic Data Generation Using Combinatorial Testing and Variational Autoencoder. In *Proceedings of the 2023 IEEE International Conference on Software, Testing, Verification and Validation Workshops (ICSTW)* Dublin, Ireland, April 16-22, 2023, 228-236. DOI: [10.1109/ICSTW58534.2023.00048](https://doi.org/10.1109/ICSTW58534.2023.00048)
 16. P. Kuo. Observation of Backward-Wave Spontaneous Parametric Downconversion in Sub- μm PPKTP. *Technical Digest Series of Optica, Frontiers in Optics + Laser Science 2022*, Rochester, New York, October 17-20, 2022. DOI: [10.1364/FIO.2022.FM5B.7](https://doi.org/10.1364/FIO.2022.FM5B.7)
 17. P. Kuo, D. Reddy, V. Verma, S. Nam, A. Zukauskas, and C. Canalias. Frequency Translation Using Backward-Wave Spontaneous Parametric Downconversion. *Technical Digest Series of Optica, CLEO: Science and Innovations 2023*, San Jose, California, May 7-12, 2023. DOI: [10.1364/CLEO_SI.2023.SW4G.5](https://doi.org/10.1364/CLEO_SI.2023.SW4G.5)
 18. D. Kuhn, M. Raunak, and R. Kacker. Ordered t-way Combinations for Testing State-based Systems. In *Proceedings of the 2023 IEEE International Conference on Software, Testing, Verification and Validation Workshops (ICSTW)* Dublin, Ireland, April 16-22, 2023, 246-254. DOI: [10.1109/ICSTW58534.2023.00050](https://doi.org/10.1109/ICSTW58534.2023.00050)
 19. N. Lal, I. Burenkov, Y. Li-Baboud, P. Kuo, T. Gerrits, O. Slattery and S. Polyakov. Towards a Scalable Network Source of Single Photons. In *Proceedings of the SPIE PC12446, Quantum Computing, Communication, and Simulation III*, SPIE Quantum West, San Francisco, CA, March 2023. DOI: [10.1117/12.2650314](https://doi.org/10.1117/12.2650314)
 20. L. Ma and L. Ding. Hybrid Quantum Edge Computing Network. In *Proceedings of the 2022 Conference of the Society of Photo-Optical Instrumentation Engineers (SPIE): Optics and Photonics, Quantum Communications and Quantum Imaging XX 122380*, San Diego, CA, October 2022. DOI: [10.1117/12.2633020](https://doi.org/10.1117/12.2633020)
 21. H. Mahboubi, K. Sayrafian, and A. Aghdam. Adaptive Maximization of Harvested Kinetic Energy for Small Wearable Medical Sensors. *IEEE International Conference on Communication Applications (IEEE ICC 2023)*, Rome, Italy, May 29-31, 2023. DOI: [10.1109/ICC45041.2023.10279411](https://doi.org/10.1109/ICC45041.2023.10279411)
 22. V. Mai and R. La. Investments in Robustness of Complex Systems: Algorithm Design. In *Proceedings of the 11th International Conference on Complex Networks & Their Applications (Complex Networks 2022)*, Palermo, Italy, November 8-10, 2022. DOI: [10.1007/978-3-031-21131-7_32](https://doi.org/10.1007/978-3-031-21131-7_32)
 23. V. Mai, R. La, and A. Battou. Optimal Cybersecurity Investments Using SIS Model: Weakly Connected Networks. In *Proceedings of the 2022 IEEE Global Communications Conference (Globecom'20)*, Hybrid (Rio de Janeiro, Brazil), December 4-8, 2022. DOI: [10.1109/GLOBECOM48099.2022.10001358](https://doi.org/10.1109/GLOBECOM48099.2022.10001358)
 24. V.-S. Mai, R. La, T. Zhang, Y. Huang, and A. Battou. Federated Learning with Server Learning for Non-IID Data. In *Proceedings of the 57th Annual Conference on Information Sciences and Systems (CISS)*, Baltimore, MD, March 22-24, 2023. DOI: [10.1109/CISS56502.2023.10089643](https://doi.org/10.1109/CISS56502.2023.10089643)
 25. W. McKenzie, Y. Li-Baboud, M. Morris, G. Baumgartner, A. Rahmouni, P. Kuo, O. Slattery, B. Crabill, M. Merzouki, A. Battou, and T. Gerrits. Sub-200 ps Quantum Network Node Synchronization over a 128 km Link White Rabbit Architecture. *Technical Digest Series of Optica, CLEO: Fundamental Science 2023*, San Jose, California, May 7-12, 2023. DOI: [CLEO_FS.2023.FF3A.3](https://doi.org/10.1364/CLEO_FS.2023.FF3A.3)
 26. S. Pamidighantam, D. De Silva, M. Christie, S. Mhatre, A. Scrinzi, and B. Schneider. Advanced Application User Interfaces for Time-Dependent Recursive Indexing (tRecX) Code: from Design to Production Deployment. *PEARC '23: Practice and Experience in Advanced Research Computing*. 2023, 237-241. DOI: [10.1145/3569951.3597569](https://doi.org/10.1145/3569951.3597569)
 27. A. Rahmouni, P. Kuo, Y. Shi, M. Jabir, N. Lal, I. Burenkov, Y. Li-Baboud, M. Merzouki, A. Battou, S. Polyakov, O. Slattery, and T. Gerrits. Experimental Demonstration of Local Area Entanglement Distribution between two Distant Nodes, Coexisting with Classical Synchronization. *Technical Digest Series of Optica, CLEO: Fundamental Science 2023*, San Jose, California, May 7-12, 2023. DOI: [CLEO_FS.2023.FF3A.4](https://doi.org/10.1364/CLEO_FS.2023.FF3A.4)
 28. A. Rahmouni, L. Ma, R. Wang, J. Li, X. Tang, T. Gerrits, Qing Li, O. Slattery. Photon Pair Generation with Greater Than 600 Coincidence-to-Accidental Ratio in the 4H-SiC-on-Insulator Platform. In *Proceedings of Quantum 2.0*, Denver, CO, June 2023. DOI: [10.1364/QUANTUM.2023.QM4A.2](https://doi.org/10.1364/QUANTUM.2023.QM4A.2)
 29. A. Rahmouni, L. Ma, X. Tang, T. Gerrits, L. Cai, Q. Li, and O. Slattery. Towards Entangled Photon Pair Generation from a SiC-based Microring Resonator. In *Proceedings of the 2022 Conference of the Society of Photo-Optical Instrumentation Engineers (SPIE): Optics and Photonics*, San Diego, CA, October 2022. DOI: [10.1117/12.2632597](https://doi.org/10.1117/12.2632597)

30. [A. Rahmouni](#), [S. Saha](#), [O. Slattery](#), and [T. Gerrits](#). Hyperspectral Photon-Counting Optical Time Domain Reflectometry. In *Proceedings of the 2022 Conference of the Society of Photo-Optical Instrumentation Engineers (SPIE): Optics and Photonics*, October 2022. DOI: [10.1117/12.2633451](https://doi.org/10.1117/12.2633451)
31. M. Roudneshin, [K. Sayrafian](#), and A. Aghdam. An Asymmetric Adaptive Approach to Enhance Output Power in Kinetic-Based Microgenerators. *IEEE Sensors 2022*, Dallas, TX, Oct. 30-Nov. 2, 2022. DOI: [10.1109/SENSOR52175.2022.9967112](https://doi.org/10.1109/SENSOR52175.2022.9967112)
32. M. Särestöniemi, [K. Sayrafian](#), M. Sonkki, and J. Iinatti. A Preliminary Study of On/Off-Body Propagation Channels for Brain Telemetry Using a Flexible Wearable Antenna. *17th IEEE International Symposium on Medical Information and Communication technology (IEEE ISMICT 2023)*, Lincoln, NE, May 10-12, 2023. DOI: [10.1109/ISMICT58261.2023.10152221](https://doi.org/10.1109/ISMICT58261.2023.10152221)
33. [K. Sayrafian](#), [B. Cloteaux](#), and [V. Marbukh](#). Impact of Using Soft Exposure Thresholds in Automatic Contact Tracing. In *2022 IEEE International Conference on E-health Networking, Application & Services (HealthCom)*, Genoa, Italy, October 17-19 2022. DOI: [10.1109/HealthCom54947.2022.9982790](https://doi.org/10.1109/HealthCom54947.2022.9982790)
34. D. Schug, S. Yerramreddy, R. Caruana, C. Greenberg, and [J. P. Zwolak](#). Extending Explainable Boosting Machines to Scientific Image Data. In: *Proceedings of the Machine Learning and the Physical Sciences Workshop*, (NeurIPS 2023), New Orleans, LA, USA [December 15, 2023] (2023).
35. [Y. Shi](#), [T. Gerrits](#), and [O. Slattery](#). Towards Continuous Fiber Birefringence Compensation with Single-Photon-Level Light, In *Proceedings of CLEO*, San Jose, CA, May 2023. DOI: [10.1364/CLEO_AT.2023.JTh2A.24](https://doi.org/10.1364/CLEO_AT.2023.JTh2A.24)
36. [O. Slattery](#) and A. Black. Experimental Ambitions for a DC-Area Quantum Network Testbed, In *Proceedings of the GOMACTech-2023 Conference*, March 2023.
37. [S. Su](#), I. Lopez-Coto, [W. Sherman](#), [K. Sayrafian](#), and [J. Terrill](#). Immersive ParaView: An Immersive Scientific Workflow for the Advancement of Measurement Science. In *21st IEEE International Symposium on Mixed and Augmented Reality (IEEE ISMAR)*, Singapore, October 17-21, 2022. DOI: [10.1109/ISMAR-Adjunct57072.2022.00034](https://doi.org/10.1109/ISMAR-Adjunct57072.2022.00034)
38. D. Suchetan, S. Tan, S. Smith, S. Choi and [M. Coudron](#). Approximating Output Probabilities of Shallow Quantum Circuits which are Geometrically-local in any Fixed Dimension. In *17th Conference on the Theory of Quantum Computation, Communication and Cryptography Leibniz International Series in Informatics 9* (2022), 1-17. DOI: [10.4230/LIPIcs.TQC.2022.9](https://doi.org/10.4230/LIPIcs.TQC.2022.9)
39. Q. Wei, F. Sikder, H. Feng, Y. Lei, [R. Kacker](#), and D. Kuhn. SmartExecutor: Coverage-Driven Symbolic Execution Guided by a Function Dependency Graph. In *Proceedings of the 2023 IEEE Conference on Blockchain Research & Applications for Innovative Networks and Services (BRAINS)*, Paris, France, October 11-13, 2023. DOI: [10.1109/BRAINS59668.2023.10316942](https://doi.org/10.1109/BRAINS59668.2023.10316942)

Technical Reports

1. J. Bienfang, [T. Gerrits](#), [P. Kuo](#), A. Migdall, S. Polyakov, and [O. Slattery](#). Single-Photon Sources and Detectors Dictionary. NIST IR 8486, September 2023. DOI: [10.6028/NIST.IR.8486](https://doi.org/10.6028/NIST.IR.8486)
2. [J. Bernal](#) and [J. Lawrence](#). Partial Elastic Shape Registration of 3D Surfaces Using Dynamic Programming. NIST Technical Note 2274, November 2023. DOI: [10.6028/NIST.TN.2274](https://doi.org/10.6028/NIST.TN.2274)
3. R. Boisvert (ed.). Applied and Computational Mathematics Division: Summary of Activities for Fiscal Year 2022. NIST IR 8466, May 2023. DOI: [10.6028/NIST.IR.8466](https://doi.org/10.6028/NIST.IR.8466)
4. N. Coble, [M. Coudron](#), J. Nelson, and S. Nezhadi. Hamiltonians Whose Low-energy States Require $\Omega(n)$ T gates. URL: <https://arxiv.org/abs/2310.01347>
5. K. E. Sharpless, R. L. Avila, [R. F. Boisvert](#), A. K. Dohne, J. Fowler, R. B. Glenn, G. Greene, R. Hanisch, A. Medina-Smith, A. Munter, J. Petrusky, Y. Ralchenko, C. D. Rowland, J. A. St Pierre, A. Wunderlich, and J. Zhang. The NIST Plan for Providing Public Access to Results of Federally Funded Research. NISTIR 8084e2023, October 2023. DOI: [10.6028/NIST.IR.8084e2023](https://doi.org/10.6028/NIST.IR.8084e2023)

Other Publications

1. [H. Cohl](#) and M. Ismail (eds.). Liber Amicorum, a Friendship Book for Dick Askey. *Celebratio Mathematica*. URL: https://celebratio.org/Askey_RA/cover/888/

Blog Posts

1. [P. Bedekar](#), [A. Kearsley](#), and [P. Patrone](#). Optimal Time-dependent Prevalence Estimation and Classification. *SIAM News Blog*, February 15, 2023. <https://sinews.siam.org/Details-Page/optimal-time-dependent-prevalence-estimation-and-classification-1>
2. [R. DeJaco](#). Measuring the Accuracy of PCR Tests Can Improve Health Care Beyond COVID-19. *NIST Taking Measure Blog*, September 13, 2023. URL: <https://www.nist.gov/blogs/taking-measure/measuring-accuracy-pcr-tests-can-improve-health-care-beyond-covid-19>

3. S. Ressler. Under Pressure: Blaise Pascal, the Barometer and Bike Tires. *NIST Taking Measure Blog*, June 14, 2023. URL: <https://www.nist.gov/blogs/taking-measure/under-pressure-blaise-pascal-barometer-and-bike-tires>
4. S. Ressler. What's in a Name? The Tesla. *NIST Taking Measure Blog*, July 10, 2023. URL: <https://www.nist.gov/blogs/taking-measure/whats-name-tesla>
5. J. Zwolak. Ada Lovelace: The World's First Computer Programmer Who Predicted Artificial Intelligence. *NIST Taking Measure Blog*, March 22, 2023. URL: <https://www.nist.gov/blogs/taking-measure/ada-lovelace-worlds-first-computer-programmer-who-predicted-artificial>

Accepted

1. D. Anderson, D. Brager, and A. Kearsley. Spatially Dependent Model for Rods and Cones in the Retina. *Journal of Theoretical Biology*.
2. A. Carasso. Data Assimilation in 2D Hyperbolic/Parabolic Systems Using a Stabilized Explicit Finite Difference Scheme Run Backward in Time. *Applied Mathematics in Science and Engineering* **32**:1 (2024), 2282641. DOI: [10.1080/27690911.2023.2282641](https://doi.org/10.1080/27690911.2023.2282641)
3. J. Chandrasekaran, E. Lanus, T. Cody, L. Freeman, R. Kacker, M. Raunak, and D. Kuhn. Leveraging Combinatorial Coverage in ML Product Lifecycle. *IEEE Computer*.
4. B. Cloteaux. Graphic Approximation of Integer Sequences. In *53rd Southeastern International Conference on Combinatorics, Graph Theory & Computing*, Boca Raton, FL, 2022.
5. H. Cohl and M. Schubotz. The Digital Shadow of Mathematics and its Ramifications. *Jahrbuch über die Fortschritte der Mathematik*.
6. H. Cohl and R. Costas-Santos. Special Values of the Continuous q -Jacobi Polynomials. *Proceedings of 16th International Symposium on Orthogonal Polynomials, Special Functions and Applications*.
7. H. Cohl and R. Costas-Santos. Orthogonality of the Big -1 Jacobi Polynomials for Non-standard Parameters. *Hypergeometric Functions, q -series and Generalizations, AMS Contemporary Mathematics*.
8. R. F. DeJaco and A. J. Kearsley. Understanding Fast Adsorption in Single-Solute Breakthrough Curves. *Communications in Nonlinear Science and Numerical Simulation*.
9. L. Devroye and J. Nolan. Random Variate Generation for the First Hit of the Symmetric Stable Process in \mathbb{R}^d . *Journal of Statistical Theory and Practice*.
10. R. La. Effects of Homophily in Epidemic Processes. In *Proceedings of the 12th International Conference on Complex Networks and Their Applications (Complex Networks 2023)*, Menton, France, November 28-30, 2023.
11. V.-S. Mai, R. La, T. Zhang, and A. Battou. Distributed Optimization with Global Constraints Using Noisy Measurements. *IEEE Transactions on Automatic Control*. DOI: [10.1109/TAC.2023.3277312](https://doi.org/10.1109/TAC.2023.3277312)
12. V. Marbukh and B. Cloteaux. Simulating Job Replication Versus Its Energy Usage. In *2023 Winter Simulation Conference*, San Antonio, TX, 2023.
13. J. Nolan, D. Audus, and J. Douglas. Computation of Riesz α -capacity C_α of general sets in \mathbb{R}^d using Stable Random Walks. *SIAM Journal on Applied Mathematics*.
14. P. Patrone and A. Kearsley. Minimizing Uncertainty in Prevalence Estimates. *Statistics and Probability Letters* **205** (2024), 109946. DOI: [10.1016/j.spl.2023.109946](https://doi.org/10.1016/j.spl.2023.109946)
15. P. Patrone, M. DiSalvo, A. Kearsley, G. McFadden, and G. Cooksey. Reproducibility in Cytometry: Signals Analysis and its Connection to Uncertainty Quantification. *PLOS One*.
16. R. Pozo. Approximation Algorithms for k-median Problems on Complex Networks: Theory and Practice. In *Complex Networks & Their Applications XII, Proceedings of the Twelfth International Conference on Complex Networks and Their Applications*.
17. J. Wu and R. Kacker. Data Dependence and Significance Testing in a Three-Distribution ROC Analysis of Speaker Recognition Evaluation. *IEEE Transactions on Audio, Speech, and Language Processing*.

In Review

1. F. Abel, E. De Lima Correa, T. Bui, A. Biacchi, M. Donahue, S. Woods, A. Hight Walker, and C. Dennis. Synthesis and Size Dependence of Strongly Interacting Ferrite Nano-Objects: Implications for Magnetic Particle Imaging and Spatially Resolved Thermometry.
2. V. Albert. Bosonic Coding: Introduction and Use Cases.
3. V. Albert, D. Aasen, W. Xu, W. Ji, J. Alicea, and J. Preskill. Spin Chains, Defects, and Quantum Wires for the Quantum-Double Edge.

4. [M. Alhejji](#) and [E. Knill](#). Towards a Resolution of the Spin Alignment Problem.
5. [B. Cloteaux](#). ReFeRS: A Lightweight Framework for Reproducible Simulation Research.
6. [B. Cloteaux](#). A Note on the Minimal Hamming Distance to a Graphic Sequence.
7. [H. Cohl](#), [R. Costas-Santos](#), [L. Durand](#), [C. Montoya](#), and [G. Ólafsson](#). Double Summation Addition Theorems for Jacobi Functions of the First and Second Kind.
8. [E. Culf](#), [T. Vidick](#), [V. Albert](#). Group Coset Monogamy Games and an Application to Device-Independent Continuous-variable QKD.
9. [R. P. Dalka](#) and [J. P. Zwolak](#). Network Analysis of Graduate Program Support Structures Through Experiences of Various Demographic Groups.
10. [R. P. Dalka](#) and [J. P. Zwolak](#). Restoring the Structure: A Modular Analysis of Ego-Driven Organizational Networks.
11. [N. Drachman](#), [P. Patrone](#), and [G. Cooksey](#). Dynamics of Optofluidic Flow Measurements.
12. [J. Fong](#), [S. Freiman](#), and [N. Heckert](#). An Error-analysis-based Multi-scale Reliability Model for Predicting the Minimum Time-to-failure of Brittle Components with Environment-Assisted Crack Growth.
13. [S. Gandhari](#), [V. Albert](#), [T. Gerrits](#), [J. Taylor](#), and [M. Gullans](#). Continuous-Variable Shadow Tomography.
14. [S. Jain](#), [E. Hudson](#), [W. Campbell](#), and [V. Albert](#). \mathbb{A} Codes.
15. [S. Jain](#), [J. Iosue](#), [A. Barg](#), and [V. Albert](#). Quantum Spherical Codes.
16. [A. Kearsley](#), [R. Evans](#), and [B. Saunders](#). Theta Functions and Mellin Asymptotics in Modeling Biological Field Effect Transistor Experiments.
17. [A. Kwiatkowski](#), [E. Shojaei](#), [S. Agrawal](#), [A. Kyle](#), [C. Rau](#), [S. Glancy](#), and [E. Knill](#). Constraints on Gaussian Error Channels and Measurements for Quantum Communication.
18. [M. Liu](#), [N. Tantivasadakarn](#), and [V. Albert](#). Subsystem CSS Codes, a Tighter Stabilizer-to-CSS Mapping, and Goursat's Lemma.
19. [Y.-K. Liu](#). Uncertainty Relations for the Curvelet Transform, and the Infeasibility of Quantum Algorithms for Lattice Problems.
20. [V.-S. Mai](#), [R. La](#), and [T. Zhang](#). Analysis of Enhanced Federated Learning on Non-IID Data with Server Learning.
21. [D. McGlynn](#), [J. Eveleth](#), [N. Andriamaharavo](#), and [A. Kearsley](#). Improved Discrimination of Mass Spectral Isomers using the High Dimensional Consensus Mass Spectral Similarity Algorithm.
22. [L. Melara](#), [R. Evans](#), [S. Cho](#), [A. Balijepalli](#), and [A. Kearsley](#). Optimal Bandwidth Selection in Stochastic Regression of Bio-FET Measurements.
23. [N. Nakamura](#), [P. Szypryt](#), [A. Dagel](#), [B. Alpert](#), [D. Bennett](#), [W. Doriese](#), [M. Durkin](#), [J. Fowler](#), [D. Fox](#), [J. Gard](#), [R. Goodner](#), [J. Harris](#), [G. Hilton](#), [E. Jimenez](#), [B. Kernen](#), [K. Larson](#), [Z. Levine](#), [D. McArthur](#), [K. Morgan](#), [G. O'Neil](#), [C. Pappas](#), [C. Reintsema](#), [D. Schmidt](#), [P. Schulz](#), [K. Thompson](#), [J. Ullom](#), [L. Vale](#), [C. Vaughan](#), [C. Walker](#), [J. Weber](#), [J. Wheeler](#), and [D. Swetz](#). A Tabletop X-Ray Tomography Instrument for Nanometer-Scale Imaging: Integration of a Scanning Electron Microscope with a Transition-Edge Sensor Spectrometer. arXiv:2212.10591.
24. [P. Patrone](#), [L. Wang](#), [S. Lin-Gibson](#), and [A. Kearsley](#). Uncertainty Quantification of Antibody Measurements: Physical Principles and Implications for Standardization.
25. [B.V. Saunders](#), [S. Brooks](#), [R. Buckmire](#), [R.E. Vincent-Finley](#), [F. Backeljauw](#), [S. Becuwe](#), [B. Miller](#), [M. McClain](#), [A. Cuyt](#). Validated Computation of Special Mathematical Functions.
26. [C. Qu](#), [B. Schneider](#), [A. Kearsley](#), [W. Keyrouz](#), and [T. Allison](#). Prediction of Mass Spectra via Molecular Structure Based Machine Learning.
27. [C. Qu](#), [B. Schneider](#), [A. Kearsley](#), [W. Keyrouz](#), and [T. Allison](#). Applying Graph Neural Network Models to Molecular Property Prediction.
28. [K. Quelhas](#), [M.-A. Henn](#), [R. Farias](#), [W. Tew](#), and [S. Woods](#). GPU-Accelerated Parallel Image Reconstruction Strategies for Magnetic Particle Imaging.
29. [K. Quelhas](#), [M.-A. Henn](#), [R. Farias](#), [W. Tew](#), and [S. Woods](#). Parallel 3D Temperature Image Reconstruction Using Multi-Color Magnetic Particle Imaging (MPI).
30. [A. Rahmouni](#), [R. Wang](#), [J. Li](#), [X. Tang](#), [T. Gerrits](#), [O. Slattery](#), [Q. Li](#), [L. Ma](#). Entangled Photon Pair Generation in an Integrated Silicon Carbide Platform.
31. [S. Shree](#), [Y. Lei](#), [R. Kacker](#), and [D. Kuhn](#). Proxima: Influence Analysis using Proxy Model.
32. [S. Shree](#), [Y. Lei](#), [R. Kacker](#), and [D. Kuhn](#). The Effect of Model Compression on Influence Analysis.
33. [O. Shtanko](#), [Y.-J. Liu](#), [S. Lieu](#), [A. Gorshkov](#), and [V. Albert](#). Bounds on Autonomous Quantum Error Correction.

34. [S. Sorokanich](#). Excitation Spectrum for the Lee-Huang-Yang Model for Bose Gas in a Periodic Box.
35. B. Weber and [J. P. Zwolak](#). QDA²: A Principled Approach to Automatically Annotating Charge Stability Diagrams.
36. Q. Wei, F. Sikder, H. Feng, Y. Lei, [R. Kacker](#), and D. Kuhn. SmartExecutor: Coverage-Driven Symbolic Execution Guided via State Prioritization and Function Selection.
37. Y. Xu, Y. Wang, and [V. Albert](#). Clifford Operations and Homological Codes for Rotors and Oscillators.
38. A. Young, [S. Geller](#), W. Eckner, N. Schine, [S. Glancy](#), [E. Knill](#), and A. Kaufman. An Atomic Boson Sampler.
39. [J. Zwolak](#), J. Taylor, R. Andrews, J. Benson, G. Bryant, D. Buterakos, A. Chatterjee, S. Das Sarma, M. Eriksson, E. Greplova, M. Gullans, F. Hader, T. Kovach, P. Mundada, M. Ramsey, T. Rasmussen, B. Severin, A. Sigillito, B. Undseth, and [B. Weber](#). Data Needs and Challenges of Quantum Dot Devices Automation: Workshop Report.

Patents

1. A. Balijepalli, J. Majikes, A. Kanwal, P. Vallone, K. Kiesler, E. Romsos, and [A. Kearsley](#). US Department of Commerce, assignee. Agile Nucleic Acid Sensor and Measuring a Biomarker. Patent Application US 17/845,682. October 13, 2022.
2. S. Buckley, A. McCaughan, [A. Dienstfrey](#), S. Nam. System and Method for Parameter Multiplexed Gradient Descent. Provisional Patent Application, NIST Docket 22-051US1, July 19, 2023.
3. G. Cooksey, [A. Kearsley](#), and [P. Patrone](#). Multiplexed Amplitude Modulation Photometer and Performing Multiplexed Amplitude Modulation Photometry. Provisional Patent Application 20210055201.
4. G. Cooksey, [A. Kearsley](#), and [P. Patrone](#). Serial Flow Cytometer. Provisional Patent Application 20210302300.
5. [A. Kearsley](#), [P. Patrone](#), E. Romsos, and P. Vallone. System and Method for Data Analysis in Quantitative PCR Measurements. Provisional Patent Application 20210395807.
6. [K. Sayrafian](#). Lung Fluid Monitor and Monitoring Fluid Level in a Lung. Patent Application Serial Number PCT/US22/48217, October 28, 2022.

ACMD in the News

1. [The FedTech Startup Studio's Real-World Approach Advances Technology Transfer](#). NIST News Update, March 22, 2023.
2. [Spotlight: The Runaway Hit for Software Testing](#). NIST News Update, June 30, 2023.
3. [A Summer of Science: NIST Interns' Stories of Their Time in the Lab](#). NIST Taking Measure Blog, August 2, 2023.
4. Ben Brubaker. [To Move Fast, Quantum Maze Solvers Must Forget the Past](#). Quanta Magazine, July 20, 2023.

Presentations

Note: When multiple presenters are listed, names of co-presenters with an ACMD affiliation during this reporting period are underlined.

Invited Talks

1. V. Albert. "Quantum Spherical Codes." Frontiers in Quantum Information and Technology Seminar, Midwest Quantum Collaboratory, Online, Ann Arbor, MI, November 16, 2023.
2. V. Albert. "Quantum Spherical Codes." 6th International Conference on Quantum Error Correction, (QEC2023), Sydney, Australia, November 2, 2023.
3. V. Albert. "Phases of Quantum Matter from a Computer-science Perspective." Machine Learning for Materials Research 2023, University of Maryland, College Park, MD, August 11, 2023.
4. V. Albert. "Phases of Quantum Matter from a Computer-science Perspective." 127th Qiskit Quantum Information Science Seminar, Online, June 30, 2023.
5. V. Albert. "Bosonic Coding and Quantum Spherical Codes." Virginia Tech Quantum Information Science Workshop for Early Career Researchers (VTQ-QIS), Arlington, VA, June 29, 2023.
6. V. Albert. "Quantum Spherical Codes." Boulder Boulder Quantum Workshop (BBQ2023), Boulder, CO, June 20, 2023.
7. V. Albert. "Quantum Error Correction." InQubator for Quantum Simulation Seminar, University of Washington, Seattle, Washington, May 24, 2023.
8. V. Albert. "Something for Everybody: Modern Quantum Tools for Bosonic Systems." Centre for Quantum Information and Quantum Control

- (CQIQC) Seminar, University of Toronto, Toronto, Canada, April 28, 2023.
9. V. Albert. “Quantum Spherical Codes.” International Molecule-type Workshop: Quantum Error Correction, Kyoto, Japan, March 27, 2023.
 10. V. Albert. “Quantum Phases of Matter from a Computer Science Perspective.” Focus Week: Quantum Many Body Systems and Quantum Information, Research Program on Quantum Information, Instituto de Ciencias Matematicas, Madrid, Spain, March 16, 2023.
 11. V. Albert. “Quantum Toolbox for Molecular State Spaces.” Symposium Quantum Optics and Quantum Information with Rigid Rotors (SAMOP 2023), German Physical Society (DPG) Spring Meeting, Hannover, Germany, March 10, 2023.
 12. V. Albert. “Spin Chains, Defects, and Quantum Wires for the Quantum-Double Edge.” Special Condensed Matter Seminar, Tel Aviv University, Tel Aviv, Israel, February 26, 2023.
 13. V. Albert. “Modern Quantum Tools for Bosonic Systems.” QuICS Stakeholder Day, University of Maryland, College Park, MD, February 15, 2023.
 14. V. Albert. “Bosonic Codes.” ML4Q Concept Seminar, University of Cologne, Cologne, Germany, January 26, 2023.
 15. V. Albert. “Overview of the Error-correction Zoo.” TIM/Lockheed Martin Quantum Meeting, University of Maryland College Park, College Park, MD, January 23, 2023.
 16. V. Albert. “Quantum Error Correction: Pedagogical Overview and Applications.” Physics Colloquium, University of South Florida, Tampa, FL, January 20, 2023.
 17. V. Albert. “Spin Chains, Defects, and Quantum Wires for the Quantum-Double Edge.” Condensed Matter Theory Center (CMTC) JLDS Seminar, University of Maryland, College Park, MD, November 1, 2022.
 18. A. Battou, A. Abane, T. Gerrits, S. Polyakov, L. Ait-Oucheggou, Z. Maasaoui, B. Decina and G. Borsuk. “Multiverse: Quantum Optical Network Management.” GOMACTech 2023, San Diego, CA, March 20-23, 2023.
 19. P. Bedekar, I. Timofeyev, and M. Perepelitsa. “Mathematical Models of Self-Organized Patterning of Stem Cells.” PDE Seminar, Ohio State University, Columbus, Ohio, April 25, 2023.
 20. P. Bedekar. “Case Study 3: Separating Uncertainties Through Modeling and Inference.” Cyto 2023, Montreal, Canada, May 2023.
 21. P. Bedekar, A. Kearsley, and P. Patrone. “Case Studies in Modeling and Optimization for Diagnostics.” 10th International Congress on Industrial and Applied Mathematics (ICIAM), Waseda University, Tokyo, Japan, August 22, 2023.
 22. P. Bedekar, I. Timofeyev, and M. Perepelitsa. “Mathematical Models of Self-Organized Patterning of Stem Cells.” Association for Women in Mathematics Research Symposium, Atlanta, Georgia, October 1, 2023.
 23. P. Bedekar, A. Kearsley, and P. Patrone. “Optimal Time-Dependent Classification for Diagnostic Testing.” Postdoctoral Seminar, Johns Hopkins University, Baltimore, Maryland, November 16, 2023.
 24. B. Cloteaux. “Bluetooth-based Automatic Contact Tracing Systems,” Computer Science Seminar, Old Dominion University, Norfolk, VA, April 21, 2023.
 25. H. Cohl. “Symmetric and Nonsymmetric Representations for Poisson Kernels of Askey-Wilson Polynomials.” Ibero-American Network of Researchers in Orthogonal Polynomials, Functional Equations and Applications (RIPOEFA) Seminar, Online, October 28, 2022.
 26. G. Cooksey, P. Patrone, M. DiSalvo, M. Catterton, and P. Bedekar. “Uncertainty Quantification in Cytometry.” 90 Minute Tutorial, Cyto 2023, Montreal, Quebec, May 20, 2023.
 27. R. DeJaco, M. Roberts, E. Romsos, P. Vallone, and A. Kearsley. “Reducing Bias and Quantifying Uncertainty in Fluorescence Produced by PCR.” Post Doctoral Applied Mathematics and Statistics Seminar, Johns Hopkins University, Baltimore, MD October 13, 2022.
 28. R. DeJaco and A. Kearsley. “Formation of Traveling Waves in Single-Solute Chromatography.” Partial Differential Equations (PDE) Seminar Series, Ohio State University, Columbus, OH, November 8, 2022.
 29. G. Doğan. “Shapes and Geometries in Image Analysis.” Applied Math Seminar, Clarkson University, Potsdam, NY, October 17, 2022.
 30. G. Doğan. “Efficient Algorithms to Compute Elastic Shape Distances between Closed Curves.” HK-SIAM Biennial Conference, Hong Kong, August 28 - September 1, 2023.

31. J. Fong. "What is ASME BPVC Section V (NDE) Article 14 and Why it Needs to be Revised?" ASME Boiler and Pressure Vessel Code Sec. XI Division 2 Working Group, Monitoring and Nondestructive Examination (MANDE) Committee Meeting, Pittsburgh, PA, November 6, 2022.
32. J. Fong. "What is ASME BPVC Section V (NDE) Article 14 and Why it Needs to be Revised?" ASME Boiler and Pressure Vessel Code Sec. V Subgroup General Requirements Committee Meeting, Pittsburgh, PA, November 9, 2022.
33. J. Fong. "A Relation Between the State of Integrity of a Component and the POD Qualification of an NDE Examiner When No Crack Was Found and the Examiner's POD was < 100 %." French Atomic Energy Commission (CEA) Saclay Research Laboratory, Gil-sur-Yvette, Paris, France, June 19, 2023.
34. J. Fong, "A Multi-Scale Creep, Fatigue, and Creep-Fatigue Interaction Model for Estimating Reliability of Steel Components at Elevated Temperatures." French Atomic Energy Commission (CEA) Saclay Research Laboratory, Gil-sur-Yvette, Paris, France, June 20, 2023.
35. T. Gerrits. "Photon-number Resolving Transition Edge Sensors for QIP." Applications of Superconducting Electronics and Detectors Workshop, Jefferson Lab, Newport News, VA, Online, November 28 - December 1, 2022.
36. T. Gerrits. "Quantum Network Metrology." Quantum Economic Development Consortium (QED-C) Marketplace Webinar, February 2023.
37. T. Gerrits. "Quantum Network Metrology." SPIE Photonics West, San Francisco, CA, January 28 - February 2, 2023.
38. T. Gerrits. "Quantum Network and Component Metrology." Photonics North, Montreal, Canada, June 12-15, 2023.
39. T. Gerrits, A. Battou. "Quantum Network and Component Metrology." Advanced Communications Technology Working Group Seminar, April 2023.
40. S. Glancy. "How to Believe Quantum Bayesianism and Many Worlds." Quantum Information and Probability: From Foundations to Engineering, Linnaeus University, Växjö, Sweden, June 13-16, 2023.
41. Z. Grey. "Separable Shape Tensors: Generative Modeling of Discrete Planar Curves." Colorado School of Mines, Kernel Club, Golden, CO, February 15, 2023.
42. Z. Grey. "Separable Shape Tensors: Generative Modeling of Discrete Planar Curves." DOE/NREL AI for Wind Energy Workshop, Boulder, CO, June 27, 2023.
43. Z. Grey. "Separable Shape Tensors with Aerodynamic Applications." 17th U.S. National Congress on Computational Mechanics, Albuquerque, NM, July 24, 2023.
44. F. Hunt, "A Markov Chain Approach to Finding Effective Spreaders in a Network." Mathematical Association of America (MAA) MathFest, Tampa, FL, August 3, 2023.
45. A. Kearsley. "Optimization and Math Modelling in COVID19 Data Analysis." Special Session in Modeling and Analysis in Analytical Chemistry, VI International Conference on Applied Mathematics, Modeling and Computational Science (AMMCS), Waterloo, Ontario, Canada, August 14-18, 2023.
46. A. Kearsley. "Mathematical Modelling and the Fentanyl Epidemic." Undergraduate Seminar, Shippensburg University, Shippensburg PA, October 23, 2023.
47. M. Kleczynski and C. Giusti. "Topological Data Analysis of Long-Term Plant-Pollinator Data." Special Session on Discrete, Algebraic, and Topological Methods in Mathematical Biology, American Mathematical Society Fall Central Sectional Meeting, Creighton University, Omaha, NE, October 7, 2023.
48. M. Kleczynski. "Topological Data Analysis of Coordinate-Based and Interaction-Based Datasets." Mathematics and Statistics Colloquium, American University, Washington, DC, October 31, 2023.
49. A. Kwiatkowski. "Optimized Experiment Design and Analysis for Fully Randomized Benchmarking." RQS-QuICS Special Seminar, University of Maryland, College Park, MD, November 9, 2023.
50. A. Kwiatkowski. "Optimized Experiment Design and Analysis for Fully Randomized Benchmarking." Quantum Systems Accelerator (QSA) Trapped Ion Topical Group Seminar, October 16, 2023.
51. R. La, "Enhanced Federated Learning with Server Learning: Benefits and Limitations." 9th IEEE World Forum on the Internet of Things (IoT), Hybrid (Aveiro, Portugal), October 25, 2023.
52. R. Luke. "Optimal Multiclass Classification and Prevalence Estimation with Applications to SARS-CoV-2 Antibody Assays." Biomathematics Seminar, Virginia Commonwealth University, Richmond, VA, September 22, 2023.

53. R. Luke. "Optimal Multiclass Classification and Prevalence Estimation with Applications to SARS-CoV-2 Antibody Assays." Infectious Disease Dynamics Seminar, Johns Hopkins School of Public Health, Baltimore, MD, June 22, 2023.
54. R. Luke. "Optimal Multiclass Classification and Prevalence Estimation with Applications to SARS-CoV-2 Antibody Assays." Applied Mathematics, Statistics, and Data Science Master's Seminar, Johns Hopkins University, Baltimore, MD, March 14, 2023.
55. R. Luke. "Improving SARS-CoV-2 Diagnostic Testing Accuracy using Higher Dimensional Probability Models." Mathematical Modeling Seminar, Rochester Institute of Technology, Rochester, NY, October 4, 2022.
56. R. Luke. "Improving SARS-CoV-2 Diagnostic Testing Accuracy using Higher Dimensional Probability Models." Shippensburg University, Mathematics Department Seminar, Shippensburg, PA, October 6, 2022.
57. L. Ma and O. Slattery. "SiC-Based Quantum Devices for Quantum Communication and Networks." Conference on Quantum Information, Seoul, Korea, July 2023.
58. D. Middlebrooks and J. Zwolak. "Cold-Start Tuning." Seminar, University of Copenhagen, Copenhagen, Denmark, December 8, 2022.
59. S. Ressler. "Virtual Reality the Metaverse and All that Reality Stuff." USPTO Patent Examiner Training, Online, May 9, 2023.
60. B. Saunders. "Research in Computational and Applied Mathematics at the National Institute of Standards and Technology: NIST's DLMF and More." Applied Mathematics and Scientific Computing Seminar, Temple University, Philadelphia, PA, November 30, 2022.
61. B. Saunders. "NIST Digital Library of Mathematical Functions: Updates and Related Work", Minisymposium on Software for Special Functions, SIAM Conference on Computational Science and Engineering (CSE23), Amsterdam, The Netherlands, February 26 - March 3, 2023.
62. B. Saunders. "Research in Computational and Applied Mathematics at NIST: NIST's DLMF and More." SIAM Student Chapter, Jaypee University of Information Technology, Solan, HP, India, January 11, 2023 (virtual).
63. B. Saunders. "Computational and Applied Mathematics at NIST." 2023 American Mathematical Society Mini-conference on Education: Enhancing Grad Programs in the Math Sciences for Student Success, Washington, D.C., September 28, 2023.
64. K. Sayrafian. "A Wireless Wearable System to Monitor Levels of Fluids in the Lungs." 2nd NIST Technology Showcase, Online, March 13, 2023.
65. K. Sayrafian. "New Frontiers in eHealth: Challenges, Opportunities, and Future Perspectives." IEEE International Conference on E-health Networking, Applications and Services, Genoa, Italy, Oct. 18, 2022.
66. K. Sayrafian. "Standardization Landscape for 6G *in vivo* Milli/micro/nano-Robotic Services." IEEE Conference on Standards for Communications and Networking, Munich, Germany, 6–8 Nov. 8, 2023.
67. D. Schug, S. Yerramreddy, R. Caruana, C. Greenberg, and J. Zwolak. "Extending Explainable Boosting Machines to Scientific Image Data." 17th U.S. National Congress on Computational Mechanics, Albuquerque, NM, July 23-27, 2023.
68. W. Sherman. "Scientific Visualization in VR." Guest Lecture, Course CSCI-5619 (Virtual Reality and 3D-User Interaction), University of Minnesota, Minneapolis Minnesota, October 5, 2022.
69. O. Slattery, L. Ma, A. Rahmouni, X. Tang, T. Gerits, Q. Li and M. Spencer. "Quantum Communication and Networking Project – Silicon Carbide in Quantum Communication." 7th International Conference on Electronic Materials and Nanotechnology for the Green Environment, Jeju, Korea, November 6-9, 2022.
70. O. Slattery and A. Black. "Experimental Ambitions for a DC-Area Quantum Network Testbed." GOMACTech 2023, San Diego, CA, US, March 20-23, 2023.
71. S. Sorokanich. "Gravitational Equilibrium Figures: Then and Now." Mathematics Seminar, University of Scranton, Scranton, PA, October 24, 2023.
72. S. Su. "Future XR Technologies, Wearable Devices, and Content Authoring Tools for Immersive Collaborative Learning." The Learning Multiverse: Immersive Technologies (IM-TECH) in Training and Education, George Mason University, September 7, 2023.
73. B. Weber and J. Zwolak. "Automatic Labeling of Domains in Experimental Data Scans." Workshop on Advances in Automation of Quantum Dot Device Control, Gaithersburg, MD, July 19-20, 2023.
74. J. Zwolak. "Tuning Quantum Dot Arrays with Rays." Center for Emergent Matter Science, RIKEN, Tokyo, Japan, November 8, 2023.

75. J. Zwolak. "Extending Explainable Boosting Machines to Scientific Image Data." Machine Learning for Materials Research Bootcamp and Workshop, University of Maryland, College Park, MD, August 11, 2023.
76. J. Zwolak. "Network Analysis for Likert-style Surveys." Discipline-Based Education Research (DBER) Seminar, Florida International University, Online, April 12, 2023.
77. J. Zwolak. "Students Experiences in a Classroom: The Social Network Perspective." The Discipline-Based Science Education Research Center (dB-SERC) Seminar, University of Pittsburgh, Virtual, February 6, 2023.
78. J. Zwolak. "Tuning Quantum Dot Arrays with Rays." QuTech Seminar, Delft University of Technology, Delft, Netherlands, December 6, 2022.
79. J. Zwolak. "Mathematical and Computational Science Research at NIST." Seminar, Drexel University, Philadelphia, PA, November 7, 2022.
- Use in Additive Manufacturing." 8th Pacific Rim Conference on Rheology, University of British Columbia, Point Grey Campus, May 15-19, 2023.
8. I. Burenkov, A. Semionova, T. Gerrits, A. Rahmouni, D. Aanand, Y. Li-Baboud, O. Slattery, A. Battou and S. Polyakov. "Coexistence of 100 Wave-Multiplexed Quantum Channels with Classical Synchronization." SPIE Photonics West, San Francisco, CA, January 28 - February 2, 2023.
9. I. Burenkov, A. Semionova, Hala, T. Gerrits, A. Rahmouni, D. Anand, Y. Li-Baboud, O. Slattery, A. Battou, and S. Polyakov. "Fundamental Coexistence Limit of Quantum States with White Rabbit Synchronization in Quantum Networks." CLEO May 2023, San Jose, CA, US, May 7-12, 2023.
10. S. Challa, N. Klimov, and P. Kuo. "Argon-Plasma Dry Etch of sub-Micron Feature-Size Waveguides in Thing-Film Lithium Niobate." American Vacuum Society 69th International Symposium and Exhibition, Portland, OR, November 5-10, 2023.
11. S. Chattopadhyay, C. Marante Valdes, J. Olsen, B. Schneider, and L. Argenti. "A Finite-pulse Virtual-sequential Model for the Two-photon Double Ionization of Ne and Ar." APS Division of Atomic, Molecular and Optical Physics Annual Meeting, Spokane, WA, June 5-9, 2023.

Conference Presentations

1. D. Anderson. "Spatially Dependent Model for Rods and Cones in the Retina." Joint Mathematics Meeting, Boston, MA, January 6, 2023.
2. B. Barnes and M.-A. Henn. "Addressing Misclassification Costs in Machine Learning Through Asymmetric Loss Functions." SPIE Advanced Lithography + Patterning 2023, San Jose, California, March 1, 2023.
3. P. Bedekar, P. Patrone, M. DiSalvo, M. Catterton, and G. Cooksey. "Uncertainty Quantification for Fluorescence Intensity Measurements." Cyto 2023, Montreal, Canada. May 2023.
4. J. Bienfang, T. Gerrits, P. Kuo, A. Migdall, S. Polyakov, and O. Slattery. "Dictionary of Single-photon Terms to Support the Emerging Quantum Industry." SPIE Quantum West, San Francisco, CA, January 28 – February 2, 2023.
5. J. Bienfang, T. Gerrits, P. Kuo, A. Migdall, S. Polyakov, and O. Slattery. "A Single-Photon Dictionary to Support the Emerging Quantum Industry." CLEO 2023, San Jose, CA, May 7–12, 2023.
6. J. Bienfang, T. Gerrits, P. Kuo, O. Slattery, S. Polyakov and A. Migdall. "A Dictionary of Single-Photon Terms to Support the Emerging Quantum Industry." Single Photon Workshop, Seoul, Korea, October 31 - November 4, 2022.
7. J. Bullard, N. Martys, and W. George. "Rheology of High Performance Cement-Based Materials for
12. H. Cohl. "Representations and Special Values for Nonsymmetric and Symmetric Poisson Kernels of the Askey-Wilson Polynomials." Fall Western Sectional Meeting, American Mathematical Society, University of Utah, Salt Lake City, UT, October 22, 2022.
13. H. Cohl. "Double Summation Addition Theorems for Jacobi Functions of the First and Second Kind." Spring Eastern Virtual Sectional Meeting, American Mathematical Society, Online, April 1, 2023.
14. E. Culf, T. Vidick, and V. Albert. "Group Coset Monogamy Games and an Application to Device-independent Continuous-variable QKD." 13th Annual Conference on Quantum Cryptography (QCrypt), University of Maryland College Park, College Park, MD, August 18, 2023.
15. R. DeJaco and A. Kearsley. "Understanding the Break-through Curve When Adsorption is Fast." American Institute of Chemical Engineers Annual Meeting, Phoenix, AZ, November 15, 2022.
16. R. DeJaco, M. Roberts, E. Romsos, P. Vallone, and A. J. Kearsley. "Reducing Bias and Quantifying Uncertainty in Fluorescence Produced by PCR." Society for Mathematical Biology, Columbus, OH, July 17, 2023.

17. R. DeJaco, M. J. Roberts, E. L. Romsos, P. M. Val-lone, A. J. Kearsley. “Reducing Bias and Quantifying Uncertainty in Fluorescence Produced by PCR.” American Institute of Chemical Engineers Annual Meeting, Orlando, FL, November 8th, 2023.
18. G. Doğan. “An Algorithm to Mesh 2d Regions in Segmented Images.” SIAM Conference on Computational Science and Engineering, Amsterdam, Netherlands, February 26 - March 3, 2023.
19. G. Doğan. “Efficient Algorithms to Compute Elastic Shape Distances between Closed Curves.” International Congress on Industrial and Applied Mathematics (ICIAM), Tokyo, Japan, August 20-25, 2023.
20. M. Donahue. “Energetics of Spin-Flop and Spin-Flip Transitions in Homogeneous Antiferromagnets.” Magnetism and Magnetic Materials 2022 Conference, Minneapolis, MN, October 31 – November 4, 2022.
21. R. Evans, A. Balijepalli, and A. Kearsley. “A Mathematical Model for Biological Field Effect Transistors.” Fall Eastern Sectional Meeting 2022, American Mathematical Society, Amherst, MA, October 1, 2022.
22. J. Fong. “A Verified and Validated Finite Element Solution of a Nano-Calibration Problem in Near-Field Scanning Microwave Microscopy.” NANOTECH Conference, Paris, France, June 28, 2023.
23. J. Fong. “A Failure-Probability and Damage State Based Fatigue and Creep Model for Estimating Reliability of Stainless Steel 316L(N) Components in Thermal Fatigue.” ASME Pressure Vessel and Piping (PVP) Conference, Atlanta, GA, July 18, 2023.
24. J. Fong, “A Multi-Scale Creep, Fatigue, and Creep-Fatigue Interaction Model for Estimating Reliability of Steel Components at Elevated Temperatures.” ASME Pressure Vessel and Piping (PVP) Conference, Atlanta, GA, July 18, 2023.
25. J. Fong, “A Quantitative Relationship Between the Pod Qualification of an Inspector and the Estimated Upper Bound Failure Probability of a Fatigue-loaded Uncracked Component when the Inspector Found no Crack.” 2023 Quantitative Nondestructive Evaluation (NDE) Conference, Austin, TX, July 24, 2023.
26. S. Geller, A. Young, S. Glancy, and E. Knill. “Robust Estimators of Multiparticle Indistinguishability.” American Physical Society Division of Atomic, Molecular and Optical Physics (DAMOP) Meeting, Spokane, WA, June 9, 2023.
27. Z. Gimbutas. “Quadratures for Edge and Corner Discretization Schemes in Three Dimensions.” SIAM Conference on Computational Science and Engineering (CSE23), Amsterdam, The Netherlands, March 1, 2023.
28. J. Iosue, K. Sharma, M. Gullans, and V. Albert. “Continuous-variable Quantum State Designs: Theory and Applications.” 2023 Quantum Information Processing Conference (QIP2023), University of Ghent, Ghent, Belgium, February 7, 2023.
29. L. Jia. “The Role of Monolayer Viscosity in Langmuir Film Hole Closure Dynamics.” 76th Annual Meeting of the American Physical Society Division of Fluid Dynamics, Washington, DC, November 19-21, 2023.
30. G. Kavuri, J. Palfree, Y. Zhang, J. Bienfang, M. Mitchell, M. Mazurek, M. Stevens, E. Knill, R. Mirin, S. Nam, and L. Shalm. “Serving Verifiable, Device-independent Randomness to the Public.” CLEO: Applications and Technology, May 7-12, 2023.
31. P. Kuo. “Observation of Backward-Wave Spontaneous Parametric Downconversion in Sub- μm PPKTP.” Frontiers in Optics + Laser Science, Hybrid, Rochester, NY, October 17–20, 2022.
32. P. Kuo. “Frequency Translation Using Backward-Wave Spontaneous Parametric Downconversion.” CLEO 2023, San Jose, CA, May 7–12, 2023.
33. A. Kwiatkowski. “Optimized Experiment Design and Analysis for Fully Randomized Benchmarking.” Assessing Performance of Quantum Computers, Estes Park, Colorado, October 2-5, 2023.
34. A. Kwiatkowski. “Optimized Experiment Design and Analysis for Fully Randomized Benchmarking.” Southwest Quantum Information and Technology Workshop, Albuquerque, New Mexico, October 26-28, 2023.
35. A. Kwiatkowski. “Protocols for Optical-microwave Quantum Transduction with Quantum Dots and Surface-acoustic-wave Cavities.” Annual Meeting of the American Physical Society (APS) Division of Atomic, Molecular, and Optical Physics (DAMOP), Spokane, WA, June 5-9, 2023.
36. R. La. “Investments in Robustness of Complex Systems: Algorithm Design.” 11th International Conference on Complex Networks and Their Applications (Complex Networks 2022), Palermo, Italy, November 8-10, 2023.

37. R. La. “Federated Learning with Server Learning for Non-IID Data.” 57th Annual Conference on Information Sciences and Systems (CISS), Baltimore, MD, March 22-24, 2023.
38. R. La. “Effects of Homophily in Epidemic Processes.” 12th International Conference on Complex Networks and Their Applications (Complex Networks 2023), Menton, France, November 28-30, 2023.
39. N. Lal, I. Burenkov, Y.-S. Li-Baboud, P. Kuo, T. Gerrits, O. Slattery, and S. V. Polyakov. “Towards a Scalable Network Source of Single Photons.” SPIE Quantum West, San Francisco, CA, January 28 – February 2, 2023.
40. R. Luke. “Multiclass Classification and Prevalence Estimation with Applications to SARS-CoV-2 Antibody Assays.” Joint Mathematics Meetings, Boston, MA, January 4-7, 2023.
41. R. Luke. “Multiclass Classification and Prevalence Estimation with Applications to SARS-CoV-2 Antibody Assays.” Southeastern-Atlantic Regional Conference on Differential Equations, North Carolina State University, Raleigh, NC, November 12-13, 2022.
42. C. Marante Valdes, F. Faria, J. Randazzo, B. Schneider, J. Olsen, and L. Argenti. “ASTRA: a Scalable Wave-function Approach to the Photoionization of Polyatomic Molecules.” American Physical Society (APS) Division of Atomic, Molecular and Optical Physics (DAMOP) Annual Meeting, Spokane, WA, June 5-9, 2023.
43. V. Marbukh. “Towards Security Metrics Combining Risks of Known and Zero-day Attacks: Work in Progress.” IEEE/IFIP Network Operations and Management Symposium (NOMS 2023), Miami, FL, May 8-12, 2023.
44. W. McKenzie, Y. Li-Baboud, M. Morris, G. Baumgartner, A. Rahmouni, P. Kuo, O. Slattery, B. Crabill, M. Merzouki, A. Battou, and T. Gerrits. “Sub-200 ps Quantum Network Node Synchronization over a 128 km Link White Rabbit Architecture.” CLEO 2023, San Jose, CA, May 7–12, 2023.
45. D. Middlebrooks and J. Zwolak. “Towards Robust Automation of Quantum Dot Bootstrapping.” American Physical Society (APS) March Meeting, Las Vegas, NV, March 5-10, 2023.
46. J. Nolan. “Simulating Entering and Exiting Balls by an Isotropic Stable Process.” International Conference on Statistical Distributions and Applications (ICOSDA), Huntington, WV, October 15, 2022.



Figure 133. ACMD had good representation at the Joint Math Meetings held in January 2023. From left to right: Nadejda Veselinova Drenska (JHU), Danielle Middlebrooks, Ryan Schneider, Ryan Evans, Rayanne Luke, Prajakta Bedekar. (Photo courtesy of A. J. Kearsley)

47. J. Nolan. “Riesz Capacity via Hitting Distributions for Stable Processes.” Workshop in Honor of Richard Davis, Columbia University, New York, NY, January 21, 2023.
48. J. Nolan. “Random Walks and Capacity.” American University Colloquium, Washington, DC, February 21, 2023.
49. J. Nolan. “Simulating Entering and Exiting Balls by an Isotropic Stable Process.” University of Nevada, Reno, Online, April 14, 2023.
50. J. Nolan. “Riesz Capacity for Multi-dimensional Sets.” Conference on Extreme Value Analysis, Bocconi University, Milan, Italy, June 27, 2023.
51. C. Ochoa, J. Freericks, J. Zwolak, and L. Doughty. “Investigating Students’ Fluency with Quantum Ideas in the Context of Interaction-Free Experiments.” American Physical Society (APS) March Meeting, Las Vegas, NV, March 5-10, 2023.
52. P. Patrone. “Uncertainty Quantification of Signals Analysis for Cytometry: Multiplets, Tracking, and Gating.” Cyto 2023, Montreal, Quebec, May 20-24, 2023.
53. A. Rahmouni, P. Kuo, Y. Shi, M. Jabir, N. Lal, I. A. Burenkov, Y. Li-Baboud, M. Merzouki, A. Battou, S. Polyakov, O. Slattery, and T. Gerrits. “Experimental Demonstration of Local Area Entanglement Distribution Between Two Distant Nodes, Coexisting with Classical Synchronization.” CLEO 2023, San Jose, CA, May 7–12, 2023.
54. A. Rahmouni, L. Ma, R. Wang, J. Li, X. Tang, T. Gerrits, Q. Li, O. Slattery. “Photon Pair Generation with Greater than 600 Coincidence-to-Accidental Ratio in the 4H-SiC-on-Insulator Platform.” Quantum 2.0, Denver, CO, June 19-22, 2023.
55. A. Rahmouni, L. Ma, L. Cai, X. Tang, T. Gerrits, Q. Li and O. Slattery. “Microring-Based Photon

- Pair Sources in the 4H-SiC-on-Insulator Platform.” Single Photon Workshop, Seoul, Korea, October 31 - November 4, 2022.
56. M. Ramsey, F. Luthi, R. Savytsky, S. Bojarski, and J. Zwolak. “Maximum Entropy for Fine-Tuning Quantum Dot Arrays.” American Physical Society (APS) March Meeting, Las Vegas, NV, March 20-22, 2023.
 57. L. Ritter, A. Fritsch, I. Spielman, and J. Zwolak. “Autonomous Analysis of Excitations in Bose-Einstein Condensates.” American Physical Society (APS) March Meeting, Las Vegas, NV, March 20-22, 2023.
 58. K. Sayrafian. “Impact of Using Soft Exposure Thresholds in Automatic Contact Tracing.” IEEE International Conference on E-health Networking, Application & Services, Genoa, Italy, Oct. 17-19, 2022.
 59. K. Sayrafian. “Impact of the Exposure Time and Distance Thresholds on the Performance of Automatic Contact Tracing.” IoT-Health workshop at IEEE International Conference on Communication Applications, Rome, Italy, June 1, 2023.
 60. R. Schneider, B. Schneider, and H. Gharibnejad. “ITVOLT: An Iterative Solver for the Time-Dependent Schrödinger Equation.” American Physical Society (APS) Division of Atomic, Molecular and Optical Physics (DAMOP) Annual Meeting, Spokane, WA, June 5-9, 2023.
 61. W. Sherman. “Advances to the ParaView Immersive Interface.” Campus Alliance for Advanced Visualization (CAAV) Conference, Ball State University, Muncie, IN, October 25, 2023.
 62. W. Sherman and S. Su. Immersive Visualization with the ParaView Open Source Tool: A Tutorial.” International Symposium on Visual Computing (ISVC), Lake Tahoe, NV, October 16, 2023.
 63. W. Sherman and J. Amstutz. “An Overview of ANARI 1.0: The Industry’s First Open Standard, Cross-platform 3D Rendering Engine API.” Khronos Developer Day Birds of a Feather (BOF) Session, SIGGRAPH Conference, Los Angeles, CA, August 9, 2023.
 64. W. Sherman. “Immersive Visualization with the ParaView Open Source Tool” Immersive Visualization Birds of a Feather (BOF) Session, SIGGRAPH Conference, Los Angeles, CA, August 6, 2023.
 65. W. Sherman. “Portable and Scalable 3D Rendering using ANAR.” DoE Computer Graphics Forum, Idaho Falls, ID, April 26, 2023.
 66. W. Sherman. “Immersive Visualization Laboratories: Motivations and Intentions of the Workshop, Workshop on Immersive Visualization Laboratories - Past, Present and Future.” IEEE VR (Virtual Reality) Conference, Hybrid, Shanghai, China, March 26, 2023.
 67. W. Sherman. “Immersive Visualization with the ParaView Open Source Tool.” FOSS-XR, Minneapolis, MN, October 6, 2022.
 68. A. Shen, Y. Shi and O. Slattery. “Simulating a Polarization Entanglement Distribution Experiment with Practical Issues.” QCrypt, College Park, MD, August 14-18, 2023.
 69. S. Su, W. Sherman, I. Lopez Coto, K. Sayrafian, and J. Terrill. “Immersive ParaView: An Immersive Scientific Workflow for the Advancement of Measurement Science.” IEEE ISMAR Workshop on Visual Analytics in Immersive Environments (VAinIE), Singapore, October 21, 2022.
 70. S. Su. “High Performance Computing and Visualization Group at NIST.” Pitch Your Lab, IEEE International Symposium on Mixed and Augmented Reality (ISMAR), Singapore, Singapore, October 20, 2022.
 71. A. Young, S. Geller, W. Eckner, N. Schine, N. Opong, A. Cao, S. Glancy, E. Knill, and A. Kaufman. “Tweezer-programmable Hubbard Models and Boson Sampling.” 54th Annual Meeting of the American Physical Society (APS) Division of Atomic, Molecular and Optical Physics (DAMOP), Spokane, WA, June 7, 2023.
 72. A. Young, S. Geller, W. Eckner, N. Schine, S. Glancy, E. Knill, and A. Kaufman. “An Atomic Boson Sampler.” Southwest Quantum Information Technology Workshop, Albuquerque, NM, October 27, 2023.
 73. J. Ziegler, F. Luthi, M. Ramsey, F. Borjans, G. Zheng, and J. Zwolak. “A Data-efficient Quantum Dot Charge Tuning Framework.” Silicon Quantum Electronics Workshop, Orford, Quebec, Canada, October 3-5, 2022.
 74. J. Zwolak and J. Ziegler. “Autonomous Identification of Quantum Dot Device Failure Modes.” Silicon Quantum Electronics Workshop, Orford, Quebec, Canada (October 3-5, 2022).

Poster Presentations

1. A. Abane, D. Anand, A. Amlou, L. Ait Ouheggou, Y. Li-Baboud, A. Battou, J. Bienfang, I. Burenkov, Hala, P. Kuo, A. Migdall, S. Polyakov, A. Rahmouni, D. Reddy, P. Shaw, O. Slattery,

- and T. Gerrits. “Optical Quantum Network Metrology.” Single Photon Workshop, Seoul, Korea, October 31 - November 4, 2022.
2. V. Albert. “Error-correction Zoo.” 2023 Quantum Information Processing Conference (QIP2023), University of Ghent, Ghent, Belgium, February 7, 2023.
 3. P. Bedekar, A. Kearsley, and P. Patrone. “Prevalence Estimation and Optimal Classification Methods to Account for Time Dependence in Antibody Levels.” Johns Hopkins University Department of Medicine, Whiting School of Engineering Research Retreat, Baltimore, Maryland, February 17, 2023.
 4. P. Bedekar, A. Kearsley, and P. Patrone. “Prevalence Estimation and Optimal Classification Methods to Account for Time Dependence in Antibody Levels.” SeroNet Investigators Meeting, Bethesda, Maryland, March 22, 2023.
 5. H. Chalfin, T. Boykin II, M.D. Stewart, Jr., M. Gullans, and J. Zwolak. “Optimizing High-Fidelity Readout Circuit Using Reinforcement Learning Methods.” Workshop on Advances in Automation of Quantum Dot Device Control, Gaithersburg, MD (July 19-20, 2023).
 6. H. Chalfin, T. Boykin, M. Stewart, M. Gullans, and J. Zwolak. “Towards Automated Tuning of High-Fidelity Readout and Gate Control for Silicon Spin Qubits.” QuICS Stakeholder’s Day, February 15, 2023.
 7. R. DeJaco, M. J. Roberts, E. L. Romsos, P. M. Valone, and A. J. Kearsley. “Reducing Bias and Quantifying Uncertainty in Fluorescence Produced by PCR.” Society of Industrial and Applied Mathematics Washington-Baltimore Section Fall Meeting, Arlington, VA, November 4th, 2022.
 8. R. DeJaco, J. M. Majikes, J. A. Liddle, and A. J. Kearsley. “Extracting Thermodynamic and Fluorescent Properties of Intercalating Dyes from Temperature-programmed PCR Measurements with Modeling and Optimization.” American Institute of Chemical Engineering Annual Meeting, Phoenix, AZ, November 15th, 2022.
 9. R. DeJaco, W. S. McGivern, J. A. Manion, D. Siderius, H. G. Nguyen, and A. J. Kearsley. “Inferring Diffusion Coefficients from Break-through-Curve Measurements Under Uncertainty.” American Institute of Chemical Engineers Annual Meeting, Orlando, FL, November 7th, 2023.
 10. G. Doğan. “Scikit-Shape: Python Toolbox for Shape and Image Analysis.” SIAM Conference on Computational Science and Engineering, Amsterdam, Netherlands, February 26 - March 3, 2023.
 11. M. Doris, G. De Sousa, D. D’Amato, I. B. Spielman, and J. Zwolak. “Machine Learning Applications in Laser Cooling and Trapping Atoms.” Humboldt Kolleg: Synthetic Quantum Matter, Vilnius, Lithuania, July 2-6, 2023.
 12. S. Geller, A. Young, S. Glancy, and E. Knill. “Robust Estimators of Multiparticle Indistinguishability.” Southwest Quantum Information Technology Workshop, Albuquerque, NM, October 26, 2023.
 13. S. Geller, A. Young, S. Glancy, and E. Knill. “Robust Estimators of Multiparticle Indistinguishability.” Assessing the Performance of Quantum Computers Workshop, Estes Park, CO, October 2, 2023.
 14. H. Georgieva, T. Gerrits, H. Hofer, A. Rahmouni, O. Slattery, M. López, J. Bienfang, A. Migdall, and S. Kück. “Comparison of the Detection Efficiency Calibration of a Single-Photon Avalanche Detector between NIST and PTB.” Teddington, UK, September 2023.
 15. S. Glancy. “How to Believe Quantum Bayesianism and Many Worlds.” Southwest Quantum Information Technology Workshop, University of New Mexico, Albuquerque, NM, October 26-28, 2023.
 16. K. Hamilton, K. Bartschat, I. Bray, A. Brown, N. Douguet, C. Fischer, J. Vasquez, J. Gorfinkiel, R. Lucchese, F. Martín, S. Pamidighantam, B. Schneider, and A. Scrinzi. The Science Gateway for Atomic, Molecular, and Optical Science (AMOS), American Physical Society (APS) Division of Atomic, Molecular and Optical Physics (DAMOP) Annual Meeting, Spokane, WA, June 5-9, 2023.
 17. M.-A. Henn, K. Quelhas, and S. Woods. Investigating the Influence of Sampling Frequency on X-Space MPI Image Reconstructions. International Workshop on Magnetic Particle Imaging, Aachen, Germany, March 23, 2023
 18. M.-A. Henn, T. Bui, and S. Woods. Investigating the Harmonic Dependence of MPI Resolution. International Workshop on Magnetic Particle Imaging, Aachen, Germany, March 23, 2023
 19. T. Kovach, M. Wolfe, P. Marciniak, P. Walsh, E. Joseph, B. Coe, J. Reily, A. Rogers, J. Benson, D. Middlebrooks, D. Schug, G. Bernhardt, J. Zwolak, M. Eriksson. “Quantum Dot Device Screening at 1.2K.” Silicon Quantum Electronics Workshop 2023, Kyoto, Japan, October 31 -November 2, 2023.

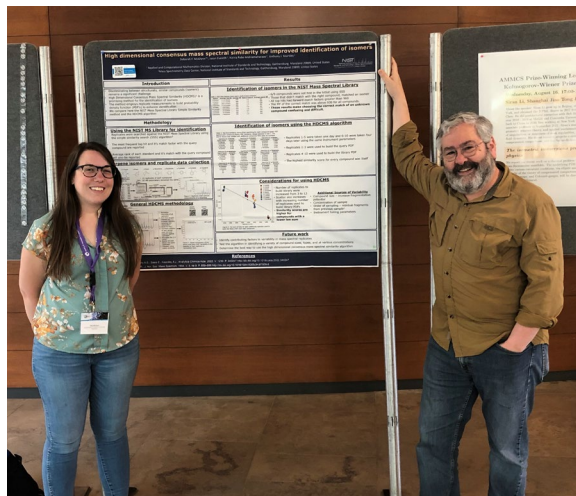


Figure 134. Deborah McGlynn and mentor Anthony Kearsley at the VI International Applied Mathematics, Modeling and Computational Science, Waterloo, Canada. McGlynn won the Best Poster Award there. (Photo courtesy of A. J. Kearsley)

20. A. Kwiatkowski. “Choosing Sequence Lengths for Single-shot-randomized Clifford Benchmarking.” Southwest Quantum Information Technology Workshop, Berkeley, CA, October 21, 2022.
21. R. Luke. “Multiclass Classification and Prevalence Estimation with Applications to SARS-CoV-2 Antibody Assays.” SeroNet Investigators Meeting, National Institutes of Health, Bethesda, MD, March 22, 2023.
22. R. Luke. “Multiclass Classification and Prevalence Estimation with Applications to SARS-CoV-2 Antibody Assays.” Department of Medicine and Whiting School of Engineering Research Retreat, Johns Hopkins University, Baltimore, MD, February 17, 2023.
23. R. Luke. “Multiclass Classification and Prevalence Estimation with Applications to SARS-CoV-2 Antibody Assays.” Society for Industrial and Applied Mathematics DC/Baltimore Sectional Meeting, Arlington, VA, November 4, 2022.
24. C. Marante, J. Randazzo, B. Schneider, J. Olsen, and L. Argenti. Photoionization of Polyatomic Molecules with ASTRA: a Scalable Wave-function Approach. XXXIII International Conference on Photonic, Electron and Atomic Collisions, Ottawa, Canada, July 25-August 1, 2023.
25. D. Middlebrooks, L. Lausen, T. Rasmussen, A. Chatterjee, and J. Zwolak. “Towards Robust Automation of Quantum Dot Device Control.” Workshop on Advances in Automation of Quantum Dot Device Control, Gaithersburg, MD, July 19-20, 2023.
26. V. Marbukh and B. Cloteaux. “Simulating Job Replication Versus Its Energy Usage.” 2023 Winter Simulation Conference, San Antonio, TX, December 10, 2023.
27. D. McGlynn. “High Dimensional Consensus Mass Spectral Similarity for Improved Discrimination of Mass Spectral Isomers.” 72nd American Society of Mass Spectrometry (ASMS) Conference on Mass Spectrometry and Allied Topics, Houston, TX, June 2023.
28. D. McGlynn. “Classification of Complex Mass Spectral Datasets using Spectral and Retention Similarities.” Gordon Research Conference on Atmospheric Chemistry, Newry, ME, July 2023.
29. D. McGlynn “Improved Discrimination of Mass Spectral Isomers using the High Dimensional Consensus Mass Spectral Similarity Algorithm.” VI International Applied Mathematics, Modeling and Computational Science, Waterloo, Ontario, Canada, August 2023.
30. A. Moorthy E. Erisman, A. Kearsley, Y. Liang, E. Sisco, and W. Wallace. “Characterizing the Likelihood of Misidentifying Fentanyl Analogs using the NIST23 EI-MS Library.” American Society of Mass Spectrometry (ASMS) Annual Meeting, Houston, Texas, June 4-8, 2023.
31. J. Nolan. “Stable Motion and Riesz Capacity.” Stochastic Processes and Applications 2023, University of Lisbon, Portugal, July 25, 2023.
32. S. Ogier, A. Sorby-Adams, K. Jordanova, A. Dienstfrey, Z. Gimbutas, J. Guo, J. Kirsch, S. Schiff, R. Mulondo, J. Obungoloch, M. Poorman, J. Pitts, W. Kimberly, and K. Keenan. “Multi-Continent Analysis of Geometric Distortion in Low-Field MRI.” International Society for Magnetic Resonance in Medicine Annual Meeting 2023 (ISMRM2023), Toronto, ON, Canada, June 8, 2023.
33. P. Patrone, L. Wang, S. Lin-Gibson, and A. Kearsley. “Physical Principles of Uncertainty Quantification for Serology: Implications for Standardization and Correlates of Protection.” SeroNet Investigators Meeting, Bethesda, MD, March 21-23, 2023.
34. A. Rahmouni, T. Gerrits, A. Migdall, O. Slattery, P. Shaw and J. Rice. “A Low-Cost Optical Trap Detector for Characterization of Quantum Network Components.” Single Photon Workshop, Seoul, Korea, October 31 - November 4, 2022.
35. K. Quelhas, M.-A. Henn, R. Farias, W. Tew, and S. Woods. “Parallel MPI Image Reconstructions in GPU using CUDA.” International Workshop on

- Magnetic Particle Imaging, Aachen, Germany, March 23, 2023.
36. [D. Schug](#), [S. Yerramreddy](#), [R. Caruana](#), [C. Greenberg](#), and [J. Zwolak](#). “Extending Explainable Boosting Machines to Scientific Image Data.” Workshop on Machine Learning and the Physical Sciences, Annual Conference on Neural Information Processing Systems, New Orleans, LA, December 3, 2023.
 37. [Y. Shi](#), [T. Gerrits](#), and [O. Slattery](#), “Towards Continuous Fiber Birefringence Compensation with Single-Photon-Level Light.” 2023 Conference on Lasers and Electro Optics (CLEO), San José, CA, US, May 7-12, 2023.
 38. [Y. Shi](#), [T. Gerrits](#), and [O. Slattery](#), “Continuous Fiber Polarization Stabilization with Single-Photon-Level Light.” QCRYPT 2023, College Park, MD, August 14 - 18, 2023.
 39. [A. Short](#), [C. Marante](#), [J. Randazzo](#), [B. Schneider](#), [J. Olsen](#), and [L. Argenti](#). Correlation Effects in O₂ Attosecond Transient Absorption. Division of Atomic, Molecular and Optical Physics Annual Meeting, Spokane, WA, June 5-9, 2023.
 40. [O. Slattery](#), [T. Gerrits](#), [S. Polyakov](#), [J. Bienfang](#), [L. Ma](#), [Y. Li-Baboud](#), and [A. Battou](#). “Overview of the Washington Metropolitan Quantum Network Research Consortium (DC-QNet).” NATO Science and Technology Organization (STO) Research Symposium on Quantum Network Technology for Defense and Security, Amsterdam, October 3 - 4, 2023.
 41. [Y. Zhang](#), [A. Seshadri](#), and [E. Knill](#). “Confidence-interval Construction with Non-i.i.d. Spot-checking Trials and Its Application in Quantum Information.” Quantum 2.0, Denver, CO, June 18-22, 2023.
 42. [J. Zwolak](#), [B. Weber](#), [F. Luthi](#), and [F. Borjans](#). “Principled Approach to Automatically Annotating Experimental Data.” Silicon Quantum Electronics Workshop 2023, Kyoto, Japan, October 31 -November 2, 2023.
3. [V. Albert](#). “[Quantum Quartered](#).” Computerphile YouTube Channel (Sean Riley, producer), June 8, 2023.

Web Services

Note: ACMD provides a variety of information and services on its website. Below is a list of major services provided that are currently under active maintenance. If there are a group of authors, ACMD staff names are underlined.

1. [Atomic, Molecular and Optical Sciences Gateway](#): a portal for research and education in atomic, molecular and optical science.
2. [Digital Library of Mathematical Functions](#): a repository of information on the special functions of applied mathematics.
3. [Digital Repository of Mathematical Formulae](#): a repository of information on special function and orthogonal polynomial formulae.
4. [DLMF Standard Reference Tables on Demand](#): an online software testing service providing tables of values for special functions, with guaranteed accuracy to high precision.
5. [Error-correction Zoo](#): a repository of information about classical and quantum error-correcting codes.
6. [muMAG](#): a collection of micromagnetic reference problems and submitted solutions.

Software Released

Note: ACMD distributes a large number of software packages that have been developed in the course of its work. Listed below are particular packages which have seen new releases during the reporting period.

Multimedia

1. [V. Albert](#). “[Quantum: Current State 2023](#).” Computerphile YouTube Channel (Sean Riley, producer), June 15, 2023.
 2. [V. Albert](#). “[Quantum Computing in Reality: Beyond the Hype](#).” Computerphile YouTube Channel (Sean Riley, producer), June 12, 2023.
1. [ACTS](#): Advanced Combinatorial Testing System. Basic Version. [R. Kuhn](#), [R. Kacker](#), and [M. S. Raunak](#).
 2. [G2Aero](#): A Python Package for Separable Shape Tensors. Version 1.0.0. [O. Doronina](#), [A. Glaws](#), [R. King](#), [G. Vijayakumar](#), and [Z. Grey](#).
 3. [Itcl](#): C++ Inspired Object Oriented Commands for Tcl. Version 4.2.3 (11/22/2022). [D. G. Porter](#).
 4. [LaTeXML](#): A LaTeX to XML, HTML, MathML+ Converter: Version 0.8.7 (12/16/2022). [B. Miller](#).
 5. [OOF2](#): Two-Dimensional Analysis of Materials with Complex Microstructures. Versions 2.3.1

- (9/20/23) and 2.3.2 (12/4/23). [S. Langer](#), A. Reid, [G. Doğan](#), and S. Keshavarz.
6. [OOFCanvas](#): A Graphics Library for use in OOF2 and Elsewhere. Version 1.1.1 (9/20/23). [S. A. Langer](#) and A. C. E. Reid.
 7. [OOMMF](#): The Object Oriented MicroMagnetic Framework. Version 2.1a0 (9/27/2023). [M. J. Donahue](#) and [D. G. Porter](#).
 8. [ParaView CAVE Interaction Plugin and XR Interface](#). ParaView Version 5.12.0. [W. Sherman](#), [S. Su](#), [S. Wittenburg](#), [S. Satterfield](#), [T. Griffin](#), and [J. E. Terrill](#).
 9. [Scikit-shape](#): Python Package for Shape and Image Analysis. Version 0.4 (9/12/23). [G. Doğan](#).
 10. [Tcl/Tk](#): Extensible Scripting Language and GUI Toolkit. Version 8.6.13 (11/22/2022). [D. Porter](#).
 11. [TDBC](#): Database Connection Commands for Tcl. Version 1.1.5 (11/22/2022). [D. G. Porter](#).
 12. [Thread](#): Thread Management Commands for Tcl. Version 2.8.8 (11/22/2022). [D. G. Porter](#).
 13. [VEMOS](#): Visual Explorer for Metrics of Similarity, Version 1.2 (9/30/23), [G. Doğan](#).
1. Melinda Kleczynski (University of Delaware). [Using Topological Data Analysis to Reveal the Structure of Ecological Systems](#). October 4, 2022.
 2. Gabriel D. Chaves-O'Flynn (Polish Academy of Sciences). [Thermally Activated Transitions Between Micromagnetic States](#). October 14, 2022.
 3. Tim Kelley (North Carolina State University). [Anderson Acceleration: Convergence Theory and Numerical Experience](#). October 18, 2022.
 4. Eleni Adam (Old Dominion University). [NPGREAT: Assembling the Human Telomeres and Subtelomeres with the Use of Ultralong Nanopore and Linked-Read Datasets](#). November 1, 2022.
 5. Ioannis Sakiotis (Old Dominion University). [PAGANI and m-Cubes: Parallel Adaptive GPU Algorithms for Numerical Integration](#). November 15, 2022.
 6. Lap-Fai Yu (George Mason University). [Creating the Extended Reality of the Future with Artificial Intelligence and Computational Design](#). November 30, 2022.
 7. Maryam Yashtini (Georgetown University). [Counting Objects By Diffused Index: Geometry-Free and Training-Free Approach](#). December 13, 2022.
 8. Samy Wu Fung (Colorado School of Mines). [Using Hamilton Jacobi PDEs in Optimization](#). January 24, 2023.
 9. Navid Mohammad Mirzaei (University of Massachusetts Amherst). [Spatial Heterogeneity in the Tumor Microenvironment: The Impact of Immune Cells](#). February 3, 2023.
 10. John Evans (University of Colorado – Boulder). [Isogeometric Analysis: Fundamentals, Challenges, and Current Research Thrusts](#). February 7, 2023.
 11. Leroy Jia (Flatiron Institute). [Membrane Mechanics Meet Minimal Manifolds](#). February 15, 2023.
 12. Mikhail Belkin (University of California - San Diego). [From Classical Statistics to Modern Deep Learning](#). February 21, 2023.
 13. Howard Heaton (Edge & Node / Typal Research LLC). [Explainable Models via Data-Driven Optimization](#). March 7, 2023.
 14. Andreas Mang (University of Houston). [CLAIRE: Scalable Multi-GPU Algorithms for Diffeomorphic Image Registration in 3D](#). March 23, 2023.
 15. Maryam Alsolami (Florida State University). [Various Approximate Methods to Measure the Uniformity Of Quasirandom Sequences](#). April 4, 2023.

Data Released

1. Software and data associated with the article titled, “Binding, Brightness, or Noise? Extracting Temperature-dependent Properties of Dye Bound to DNA.” Version v3.0.0 (03/15/2023). [R. F. DeJaco](#). DOI: [10.18434/mds2-2762](#)
2. Software and Data associated with “Reducing Bias and Quantifying Uncertainty in Fluorescence Produced by PCR.” Version v0.9.1 (03/30/23). [R. F. DeJaco](#). DOI: [10.18434/mds2-2910](#)
3. Software and Data Associated with “Understanding Fast Adsorption in Single-Solute Breakthrough Curves.” Version v0.0 (10/30/23). [R. F. DeJaco](#). DOI: [10.18434/mds2-3103](#)

Conferences, Minisymposia, Lecture Series, Courses

ACMD Seminar Series

Stephen Langer served as Chair of the ACMD Seminar Series. There were 28 talks presented during this period; talks are listed chronologically.

16. Pratyush Tiwary (University of Maryland). [Artificial Chemical Intelligence: AI for Chemistry and Chemistry for AI](#). April 19, 2023.
 17. Nicolas Charon (Johns Hopkins University). [Geometric Data Analysis: A Riemannian Perspective](#). May 2, 2023.
 18. Julia Seilert (Technische Universität Berlin). [\(Re\)Engineering Functional Fat Phases For Spreads And Chocolates Manufacturing](#). May 9, 2023.
 19. Yukun Yue (Carnegie Mellon University). [On Convergence Analysis of an IEQ-Based Numerical Scheme for Hydrodynamical Q-Tensor Model](#). May 16, 2023.
 20. Eric Shirley (NIST Sensor Science Division). [Practical Diffraction Corrections in Radiometry using Special Functions and the DLME](#). June 27, 2023.
 21. Andrew White (Rolls-Royce Corporation). [Uncertainty Aggregation Through Model Development and Assessment Towards Prediction](#). July 11, 2023.
 22. Jeongsu Kyeong (Temple University). [The Neumann Problem for the bi-Laplacian in Infinite Sectors](#). August 22, 2023.
 23. Anne Talkington (University of Virginia). [Systems Modeling for Effective Therapeutic Intervention in the Tumor Microenvironment](#). September 19, 2023.
 24. Andrew Rukhin (NIST Statistical Engineering Division). [Parity Based Statistics, Extreme Value Theory and the Bible of Mathematics](#). October 17, 2023.
 25. Wonjun Lee (University of Minnesota). [Monotone Generative Modeling via a Gromov-Monge Embedding](#). October 31, 2023.
 26. William Sherman (NIST ACMD). [Immersive Para-View](#). November 13, 2023.
 27. Brennan Sprinkle (Colorado School of Mines). [The Countscope: Measuring Self and Collective Diffusion with Fancy Counting](#). November 28, 2023.
 28. Jennifer Wei (OpenFold). [Applications in Machine Learning for Structure Elucidation](#). December 12, 2023.
- Non-Equilibrium Quantum Dynamics, University of Colorado, Boulder, CO, July 17 - 21, 2023.
3. V. Albert. "Modern Quantum Coding Theory with Four Qubits." Three lectures. The 3rd Condensed Matter Summer School: Dynamics and Quantum Information in Many-body Systems, University of Minnesota, Minneapolis, MN, June 12 - 21, 2023.
 4. V. Albert. "Quantum STEM." Classroom lecture. Quantum To Go program, Online, Harper College, Palatine, IL, April 18, 2023.
 5. V. Albert. "Bosonic Coding: Introduction and Use Cases." Three lectures. Quantum Winter School: Challenges and Advances in Quantum Computing, Technion University, Haifa, Israel, February 26 - March 2, 2023.

Conference Organization

Leadership

1. P. Kuo. Subcommittee Chair: FS 3: Quantum Photonics. Conference on Lasers and Electro-optics, San Jose, CA, May 7-12, 2023.
2. Y.-K. Liu. General Chair. 14th International Conference on Post-Quantum Cryptography. College Park, MD, August 16-18, 2023.
3. K. Sayrafian. Lead Organizer and Co-Chair: 5th International IoT-Health Workshop. IEEE International Conference on Communications. Rome, Italy, June 1, 2023.
4. K. Sayrafian. Co-Chair: Industry Panel. IEEE Global Communications Conference, Kuala Lumpur, Malaysia, December 4-8, 2023.
5. W. Sherman. Co-organizer. Workshop on Immersive Visualization Laboratories - Past, Present and Future, IEEE VR (Virtual Reality) Conference, Hybrid, Shanghai, China, March 26, 2023.
6. O. Slattery. Co-Chair. QCRYPT 2023, College Park, MD. August 14 -18, 2023.
7. S. Su. Co-organizer. Workshop on Immersive Visualization Laboratories - Past, Present and Future, IEEE VR (Virtual Reality) Conference, Hybrid, Shanghai, China, March 26, 2023.
8. J. Zwolak. Co-organizer. Workshop on Advances in Automation of Quantum Dot Devices Control, Rockville, MD, July 19-20, 2023.

Committee Membership

1. V. Albert. "Boot Camp: Modern Quantum Coding Theory with Four Qubits." 2023 Quantum World Congress, Tysons, VA, September 26, 2023.
2. V. Albert. "Modern Quantum Coding Theory with Four Qubits." Four lectures. Boulder School 2023: International Conference on Quantum Information Processing (QIP), Taipei, Taiwan, January 13-19, 2024.

2. H. Cohl. Steering Committee. Orthogonal Polynomials and Special Functions Conference Series.
3. T. Gerrits. Scientific Committee. Single Photon Workshop (SPW) Series.
4. T. Gerrits. Program Committee: Quantum Information, Communications and Sensing. CLEO Europe/EQEC, Munich, Germany, June 26-30, 2023.
5. T. Gerrits. Program Committee. SPIE Quantum Technologies, Strasbourg, France. April 8-10, 2024.
6. S. Glancy. Organizing Committee. Southwest Quantum Information Technology Workshop, Albuquerque, NM, October 26-28, 2023.
7. S. Glancy. Organizing Committee. Quantum Information and Probability: from Foundations to Engineering, Växjö, Sweden, June 13-16, 2023.
8. R. Kacker. Steering Committee and Program Committee. International Workshop on Combinatorial Testing, International Conference on Software, Testing, Verification and Validation (ICST 2024), Dublin, Ireland, April 16-22, 2023.
9. P. Kuo. Program Committee: Quantum Computing, Communication, and Simulation III. SPIE Photonics West, San Francisco, CA, January 28 – February 2, 2023.
10. R. La. Technical Program Committee. IEEE International Conference on Computer Communications (INFOCOM 23), New York, NY, May 17-20, 2023.
11. R. La. Technical Program Committee. IEEE International Conference on Computer Communications (INFOCOM 24). Vancouver, Canada, May 20-23, 2024.
12. R. La. Technical Program Committee. International Conference on Complex Networks and Their Applications (Complex Networks 23), Menton, France, November 28-30, 2023.
13. N. Lal. Local Organizing Committee. QCRYPT 2023, College Park, MD. August 14-18, 2023.
14. L. Ma. Local Organizing Committee. QCRYPT 2023, College Park, MD. August 14-18, 2023.
15. B. Saunders. Member, Organizing Committee, SIAM International Meshing Roundtable 2024, Baltimore, MD.
16. W. Sherman. Executive Board. Community Alliance for Advanced Visualization (CAAV) Series.
17. O. Slattery. Program Committee: Quantum Communications and Imaging XII. SPIE Optics and Photonics, San Diego, August 2023.
18. O. Slattery, Local Organizing Committee. QCRYPT 2023, College Park, MD. August 14-18, 2023.
19. O. Slattery. Steering Committee. Workshop for Quantum Repeaters and Networks (WQRN) Series.
20. O. Slattery. Program Committee. Workshop for Quantum Repeaters and Networks (WQRN), Montreux, Switzerland, September 11-13, 2024.
21. S. Su. Program Committee. IEEE Conference on Virtual Reality and 3D User Interfaces (IEEE VR), Shanghai, China, March 25-29, 2023.
22. S. Su. Program Board. 15th International Conference on Virtual, Augmented and Mixed Reality, HCI International, Copenhagen, Denmark, July 23-28, 2023.

Session Organization

1. P. Bedekar. Co-Organizer, Special Session: Early Career Researchers in Mathematical Biology and Differential Equations. Association for Women in Mathematics (AWM) Research Symposium, Atlanta, Georgia, October 1-2, 2023.
2. H. Cohl. Co-Organizer, Special Session: Hypergeometric Functions and q -series. Fall Western Sectional Meeting of the American Mathematical Society, University of Utah, Salt Lake City, Utah, October 22-23, 2022.
3. H. Cohl. Co-Organizer, Special Session: Hypergeometric Functions, q -series and Generalizations. Spring Eastern Virtual Sectional Meeting of the American Mathematical Society, April 1-2, 2023.
4. G. Doğan. Co-Organizer: Minisymposium 01136, Advances in Variational Models and PDEs for Images. International Congress on Industrial and Applied Mathematics (ICIAM), Tokyo, Japan, August 20-25, 2023.
5. A. Kearsley. Co-organizer: Minisymposium 00794, Mathematical Modelling and Disease, International Congress on Industrial and Applied Mathematics (ICIAM), Tokyo, Japan, August 20-25, 2023.
6. K. Sayrafian. Co-Organizer and Co-Chair: Measurement & Modelling of Radio Waves Propagation for Indoor Communication. URSI General Assembly and Scientific Symposium, Sapporo, Japan, August 19-26, 2023.

- W. Sherman. Co-Organizer: Birds of a Feather on Immersive Visualization. SIGGRAPH '23, Los Angeles, CA, August 6, 2023.

Other Professional Activities

Internal

- R. Boisvert. Coordinator. ITL Quantum Information Program.
- R. Boisvert. Member. NIST Research Computing Advisory Committee.
- R. Boisvert. Member. NIST Open Access to Research (OAR) Committee.
- T. Burns. Co-Director. ITL Summer Undergraduate Research Fellowship (SURF) Program.
- B. Cloteaux. Member. Washington Editorial Review Board.
- T. Gerrits. Organizer. Quantum Optics Seminar Series.
- Z. Gimbutas. Member. ITL Awards Committee.
- S. Glancy. Member. ITL Diversity Committee.
- Z. Grey. Organizer. ACMD Seminar Series.
- R. Kacker. Member. ITL Diversity Committee.
- P. Kuo. Member. NIST Diversity, Equity, Inclusion and Accessibility (DEIA) Implementation Team.
- P. Kuo. Member. ITL Space Task Force.
- L. Ma. Organizer. Quantum Repeater Journal Club
- D. Porter. Member. ITL Awards Committee
- B. Schneider. Chair. High Performance Computing Working Group, NIST Research Computing Advisory Committee.
- O. Slattery. Laser Safety Representative. ITL Safety Committee.
- O. Slattery. Member. ITL Space Task Force.
- O. Slattery. ITL Representative. NIST Laser Safety Committee.
- S. Sorokanich. Judge. Summer High School Internship (SHIP) Program Poster Session, August 9, 2023.
- J. Zwolak. ITL Representative. NIST DEIA Council.

External

Editorial

- R. Boisvert. Associate Editor. *ACM Transactions on Mathematical Software*.
- H. Cohl. Co-Editor: Special Issues in Memory of Richard A. Askey. *The Ramanujan Journal*.
- H. Cohl. Co-Editor. *OP-SF NET*, SIAM Activity Group on Orthogonal Polynomials and Special Functions.
- H. Cohl. Editor, *The Ramanujan Journal*.
- H. Cohl. Co-Editor: Richard A. Askey Volume. Springer Nature.
- H. Cohl. Co-Editor: Series on Hypergeometric Functions, q-series, Generalizations and Applications, AMS Contemporary Mathematics Proceedings.
- T. Gerrits. Associate Editor, *Optics Express*.
- Z. Gimbutas. Member, Editorial Board. *Advances in Computational Mathematics*.
- S. Glancy. Associate Editor. *Quantum Information Processing*.
- R. La. Associate Editor. *IEEE/ACM Transactions on Networking*.
- Bonita Saunders. Associate Editor, *MAA Mathematics Magazine*.
- B. Saunders. Webmaster/SIAM Engage Moderator, SIAM Activity Group on Orthogonal Polynomials and Special Functions (SIAG/OPSF).
- K. Sayrafian. Associate Editor. *International Journal of Wireless Information Networks*.
- B. Schneider. Associate Editor in Chief. *IEEE Computing in Science and Engineering*.
- B. Schneider. Specialist Editor. *Computational Physics Communications*.
- S. Su. Associate Editor. *PRESENCE: Virtual and Augmented Reality*.

Boards and Committees

- R. Boisvert. Member. International Federation of Information Processing Working Group 2.5 (Numerical Software).
- R. Boisvert. Member. Reproducibility Badging and Definitions Working Group, National Information Standards Organization (NISO).

3. R. Boisvert. NIST Representative. National Science and Technology Council (NSTC) Subcommittee on Future Advanced Computing Ecosystem (FACE).
4. B. Cloteaux. Member, Advisory Board. Department of Computer Science, New Mexico State University.
5. A. Dienstfrey. Vice-Chair. International Federation of Information Processing Working Group 2.5 (Numerical Software).
6. J. T. Fong. Member. American Society of Mechanical Engineers (ASME) Boiler and Pressure Vessel Code Committee.
7. T. Gerrits. NIST Representative. DC-QNet Science and Technology Advisory Committee.
8. F. Hunt. Member, Science Policy Committee. American Mathematical Society.
9. P. Kuo. Member, DC-QNet Interfaces Specifications Working Group.
10. L. Ma. Co-principal Investigator. Center for Quantum Error Correction, Joint Korea-US Quantum Research Center.
11. L. Ma. Member. ISO/TC229 (Nanotechnology Standards Development), WG2 on the Standard ISO/TS 80004-12 (Nanotechnologies Vocabulary Part 12: Quantum Phenomena in Nanotechnology).
12. D. Porter. Member Tc1 Core Team.
13. S. Ressler. Member. Immersive Web Working Group, World Wide Web Consortium (W3C).
14. S. Ressler. NIST Representative. W3C Advisory Committee.
15. S. Ressler. NIST Representative. Khronos Group.
16. S. Ressler. Member. 3D Formats Working Group, Khronos Group.
17. S. Ressler. Member. Working Groups, Metaverse Standards Forum.
18. S. Ressler. Member, Steering Committee. IEEE Metaverse Initiative.
19. B. Saunders. Member, Board of Trustees. Society for Industrial and Applied Mathematics (SIAM).
20. B. Saunders. Member, SIAM Systems Oversight Committee.
21. B. Saunders. Member, SIAM Human Resources Committee.
22. B. Saunders. Chair, AWM-MAA Falconer Lecture Nominating Committee.
23. B. Saunders. Member, Washington Academy of Sciences Awards Review Panel.
24. B. Saunders. Member, Advisory Board, DoD Center of Excellence on Advanced Electro-Photonics with Two-Dimensional Materials, Morgan State University, Baltimore, MD
25. K. Sayrafian. Voting Member. IEEE802.15 Task Group 6ma (Body Area Networks).
26. K. Sayrafian. Member. IEEE P2731 Standard Working Group (Unified Terminology for Brain-Computer Interfaces).
27. K. Sayrafian. Core Member. COST CA20120: Intelligence-Enabling Radio Communications for Seamless Inclusive Interactions.
28. K. Sayrafian. Member. Digital Health Research and Development Interagency Working Group.
29. K. Sayrafian. Co-Chair, Vertical Track 1: Health and Well-Being. COST CA20120: Intelligence-Enabling Radio Communications for Seamless Inclusive Interactions.
30. B. Schneider. NIST Representative. High End Computing (HEC) Interagency Working Group, Networking and Information Technology Research and Development (NITRD) Program.
31. W. Sherman. Member. OpenXR Working Group, Khronos Group.
32. W. Sherman. Member. ANARI Working Group, Khronos Group.
33. O. Slattery. Co-Chair. Interagency Working Group on Quantum Networks (QN-IWG), Office of Science and Technology Policy (OSTP).
34. O. Slattery. Co-Chair. DC-QNet Experiments Working Group.
35. S. Su. Member. 3D Formats Working Group, Khronos Group.
36. S. Su. Member. OpenXR Working Group, Khronos Group.
37. S. Su. Member. ANARI Working Group, Khronos Group.
38. J. Zwolak. Member. Survey Interagency Working Group. OSTP Subcommittee on Scientific Integrity.

Adjunct Academic Appointments

1. V. Albert. Adjunct Assistant Professor. Department of Physics, University of Maryland, College Park, MD.

2. V. Albert. Affiliated Faculty Member. Applied Mathematics & Statistics, and Scientific Computation (AMSC) Program, University of Maryland, College Park, MD.
3. M. Coudron. Adjunct Assistant Professor. Department of Computer Science, University of Maryland, College Park, MD.
4. S. Glancy. Lecturer. Department of Physics, Colorado University, Boulder, CO.
5. E. Knill. Lecturer. Department of Physics, Colorado University, Boulder, CO.
6. E. Knill. Fellow. Center for Theory of Quantum Matter, Department of Physics, Colorado University, Boulder, CO.
7. P. Kuo. Adjunct Associate Professor. Department of Physics, University of Maryland, College Park, MD.
8. Y. Liu. Co-Director. Joint Center for Quantum Information and Computer Science (QuICS), University of Maryland, College Park, MD.
9. Y. Liu. Adjunct Associate Professor. Department of Computer Science, University of Maryland, College Park, MD.
10. K. Sayrafian. Affiliate Associate Professor. Electrical & Computer Engineering Department, Concordia University, Montreal Canada.
11. W. Sherman. Adjunct Faculty. Luddy School of Informatics, Computing, and Engineering, Indiana University, Bloomington, IN.
12. S. Su. Adjunct I. Media Arts and Technologies, Department, Montgomery College, Rockville, MD.
13. J. Zwolak. Adjunct Assistant Professor, Department of Physics, University of Maryland, College Park, MD.
6. H. Cohl. Member, Ph.D. Thesis Committee. The George Washington University: Fatimah Alshamari.
7. M. Donahue. Member, Ph.D. Thesis Committee. University of Southampton, Southampton, UK: M. Lang.
8. Z. Gimbutas. Member, Ph.D. Thesis Committee. Department of Mathematics, Southern Methodist University: A. Slobodkins.
9. S. Glancy. Member, Ph.D. Thesis Committee. University of Colorado, Boulder: C. Rao.
10. S. Glancy. Ph.D. Co-Advisor. University of Colorado, Boulder: A. Avagyan.
11. Y.-K. Liu. Member, Ph.D. Thesis Committee. University of Maryland, College Park: N. Rodrigues.
12. Y.-K. Liu. Member, Ph.D. Thesis Committee. University of Maryland, College Park: D. Wang.
13. B. Miller, Member, Ph.D. Thesis Committee. University of Erlangen, Germany: D. Ginev
14. K. Sayrafian. Ph.D. Co-Advisor. University of Zagreb, Croatia: K. Ladic.
15. S. Su. Member, Ph.D. Thesis Committee. Tallinn University of Technology: K. Kullman.
16. J. Zwolak. Ph.D. Co-Advisor. University of Maryland: R. P. Dalka.
17. J. Zwolak. Ph.D. Co-Advisor. University of Maryland: University of Maryland: H. C. Chalfin.

Community Outreach

Thesis Direction

1. V. Albert. Ph.D. Advisor. University of Maryland: S. Jain.
2. V. Albert. Ph.D. Advisor. University of Maryland: E. Kubischta.
3. V. Albert. Ph.D. Advisor. University of Maryland: Y. Xu.
4. V. Albert. Ph.D. Co-Advisor. University of Maryland: J. Kunjummen.
5. V. Albert. Ph.D. Co-Advisor. University of Maryland: J. Iosue.
1. V. Albert. Undergraduate Advisor, University of Maryland.
2. P. Bedekar. Speaker. Association for Women in Mathematics Graduate Chapter, Johns Hopkins University, October 30, 2023.
3. R. Boisvert. "Opportunities at NIST." Institute for Robust Quantum Simulation Annual Workshop, University of Maryland, College Park, MD, June 21, 2023.
4. R. F. Boisvert. "Opportunities at NIST." Computer and Computational Sciences Research Day, University of Maryland, College Park, MD, August 24, 2023.
5. B. Cloteaux. Panelist, Hour of Code, Online, Southern New Hampshire University, December 4, 2023.
6. G. Doğan. Organizer. Odyssey of the Mind Program, Cabin John Middle School, Potomac, MD, October 2022 - March 2023.

7. G. Doğan. Organizer. Coding Club, Cabin John Middle School, Potomac, MD, March - June 2023.
8. F. Hunt. Interviewed at “Meet a Mathematician,” National Museum of Mathematics, New York, NY, October 30, 2023.
9. B. Saunders. SIAM Visiting Lecturer.
10. J. Zwolak. Tutor. Mary of Nazareth Catholic School.
11. J. Zwolak. Student Outreach. Drexel University, November 7, 2022.

Awards and Recognition

External

1. S. Challa. American Vacuum Society Nanoscale Science and Technology Division Early Career Award. November 2023.
2. R. Kacker, R. Kuhn and Y. Lei. Most Influential Paper of the Decade Award. IEEE International Conference on Software, Testing, Verification and Validation (ICST), Dublin, Ireland, April 16-22, 2023. For the 2013 paper “ACTS: A Combinatorial Test Generation Tool.” (Joint award)
3. D. McGlynn. Best Poster Award. VI International Applied Mathematics, Modeling and Computational Science, Waterloo, Canada, August 2023.
4. D. Middlebrooks. MGB-SIAM Early Career (MSEC) Fellowship.
5. O. Slattery. DC-QNet Exceptional Leadership Award. For “Serving as DC-QNet Execution Manager of DARPA Seed Study on a Quantum Augmented Classical Testbed,” September 12, 2023.
6. O. Slattery, T. Gerrits, Y. Li-Baboud, S. Polyakov, J. Bienfang, P. Kuo, A. Battou, and K. Srinivasan. DC-QNet Outstanding Contribution Award. For “Implementing the DARPA QuANET Feasibility Study”.

Internal

1. S. Geller. ITL Associates Reflection Award. For contributions to the DOC Gold Medal (below). August 8, 2023.
2. T. Gerrits, T. Jimenez, M. Stevens, and C. Camp. Department of Commerce Bronze Medal. For “Work on two-photon absorption with entangled light.”
3. J. Teufel, J. Aumentado, K. Cicak, R. Simmonds, S. Glancy, and E. Knill. Department of Commerce

Gold Medal. For “pioneering experimental techniques to generate and precisely measure the quantum entanglement of two macroscopic mechanical resonators.” January 2023.

4. A. Kwiatkowski. ITL Associates Reflection Award. For contributions to the DOC Gold Medal (above). August 8, 2023.
5. G. McFadden. NIST Portrait Gallery of Distinguished Scientists, Engineers and Administrators. October 2022.
6. A. Rahmouni. ITL Outstanding Associate Award. For “excellence in experimental research on quantum devices and systems aligned to the nist quantum program and metrology mission.” August 8, 2023.
7. B. Schneider and W. Keyrouz. ITL Outstanding Collaboration Award. For “a collaborative, NIST-wide effort to develop and document a coherent vision for research computing at NIST.” August 8, 2023

Funding Received

During FY 2023 ACMD’s yearly allocation of base funding from the NIST Information Technology Laboratory was supplemented with funding from a variety of internal and external competitions. Such funding represented 26 % of the Division’s FY 2023 budget. Below we list the major sources of such funding.

Note: For joint projects, names of ACMD participants are underlined.

External

1. T. Gerrits, L. Ma, O. Slattery, Z. Levine. Free-Space Memory-Based High-Rate Single Photon Source. Air Force Research Laboratory.
2. R. King, Z. Grey, A. Doostan, and G. Geraci. DOE/WETO A14 Wind Program. US Department of Energy.
3. O. Slattery, T. Gerrits, S. Polyakov, A. Battou, J. Bienfang, Y. Li-Baboud, P. Kuo, L. Ma, and K. Srinivasan. Seed Study on Quantum Augmented Classical Networks. DARPA.

Internal

1. B. Alpert, et al. Ture Becquerel: A New Paradigm for 21st Century Radioactivity Measurements. NIST Innovations in Measurement Science.

2. B. Cloteaux and V. Marbukh. Towards Developing Carbon Efficient Algorithms. 2023 ITL Building the Future Program.
3. M. Coudron. Verification of protein Structure Prediction Algorithms. 2023 ITL Building the Future Program.
4. A. Dienstfrey, Z. Gimbutas, et al. AI for Low-field MRI. NIST AI Initiative.
5. A. Dienstfrey. Neuromorphic Computing. NIST AI Initiative.
6. M. Donahue, et al. Thermal MagIC: An SI-traceable Method for 3D Thermal Magnetic Imaging and Control. NIST Innovations in Measurement Science.
7. G. Doğan. Better Deep Learning by Incorporating Expectations. 2023 ITL Building the Future Program.
8. R. Evans, A. Kearsley, A. Balijepalli, S. Cho, and C. Schanzle. Modeling, UQ, and Calibration for Bio-FETs. 2023 ITL Building the Future Program.
9. A. Kearsley and D. Anderson. Investigation of Full Cooling/Warming Cycle in Cryobiology. 2023 ITL Building the Future Program.
10. A. Kearsley and C. Schanzle. Compound Identification Algorithms for the DART-MS Library. 2023 ITL Building the Future Program.
11. T. Gerrits, S. Glancy, E. Knill, A. Avagyan, and M. A. van de Poll. Metrology for Continuous Variable Quantum Computing and Networking. 2023 ITL Building the Future Program.
12. T. Gerrits. Quantum Network and Component Metrology in Support of NIST's Quantum Networking, the DC-QNet, the Quantum Industry and the QED-C. NIST Quantum Initiative.
13. T. Gerrits and A. Migdall. Procurement and Verification of Low-Loss Optical Fiber Connectors in Support of Quantum Industry. NIST Quantum Initiative.
14. E. Knill, et al. Establishing the Science and Technology of Networks for Superconducting Quantum Computers. NIST Innovations in Measurement Science.
15. D. Leibfried, A. Wilson, E. Knill, and S. Glancy. A Practical Quantum Repeater Unit. NIST Quantum Network Grand Challenge.
16. Y.-K. Liu. Cryptographic Tests of Quantumness. 2023 ITL Building the Future Program.
17. L. Ma, O. Slattery, T. Gerrits, X. Tang, and A. Rahmouni. Integrated Entangled Photon Source Based on Silicon Carbide Devices. 2023 ITL Building the Future Program.
18. P. Patrone, A. Kearsley, G. McFadden, G. Cooksey, S. Sakar, L. Wang. NIST in a Drop: Revolutionizing Measurements of Single-cell Kinetics. NIST Innovations in Measurement Science.
19. P. Patrone, A. Kearsley, P. Bedekar, and R. Luke. Advanced Analysis and Uncertainty Quantification for Diagnostic Testing II. 2023 ITL Building the Future Program.
20. K. Sayrafian. A Wireless Wearable Technology to Detect Accumulation of Fluid in the Lungs – Part II. 2023 ITL Building the Future Program.
21. O. Slattery, A. Battou, and N. Zimmerman. for Quantum Network Testbeds on NIST Campus and on DC-QNet. NIST Quantum Network Grand Challenge.
22. O. Slattery. Novel Bell State Analyzer for WDM-compatible Entanglement Swapping and Teleportation. NIST Quantum Initiative.
23. S. Su, W. Sherman, and K. Sayrafian. Development of Visualization Infrastructure to Support Future Collaboration in a Hybrid Data Analysis Environment. 2023 ITL Building the Future Program.
24. J. Zwolak, C. Greenberg, and J. Ziegler. Explainable Boosting Machines for Image Data. 2023 ITL Building the Future Program.

Grants Funded

ACMD awards a small amount of funding through the NIST Grants Program for projects that make direct contributions to its research programs. During FY 2023 the following cooperative agreements were active.

1. Boğaziçi University: *Design of a Subcutaneous Implant Antenna for Brain Computer Interface*. PI: Sema Dumanli Oktar
2. George Washington University: *Algorithmic Development for Hardware AI Coprocessors*. PI: Gina Adam
3. Louisiana State University: *Metrology for Continuous variable Quantum Computing and Networking*. PI: Omar S. Magana-Loaiza
4. Purdue University: *Effective Range of Fluid-mediated Particle-particle Interactions in an Optical Flow Meter*. PI: Kaitlyn Hood.
5. Theiss Research: *Exploiting Alternate Computing Technologies*. PI: Alan Mink.
6. University of Edinburgh: *Applicable Resurgence and Uniform Asymptotics*. PI: Adri Olde-Daalhuis.

7. University of Maryland: *Joint Center for Quantum Information and Computer Science (QuICS)*. PI: Andrew Childs.
8. University of Minnesota: *NIST-IMA Postdoctoral Fellowship in Analysis of Machine Learning*. PI: Daniel Spirn.
9. University of Texas at Arlington: *Explaining and Debugging Machine Learning Models by Neighborhood Exploration*. PI: Yu Lei.

External Contacts

ACMD staff members interact with a wide variety of organizations in the course of their work. Examples of these follow.

Industrial Labs

Amazon AWS
 Boeing Company
 Computational Physics, Inc.
 Corning
 Diamond USA
 Ericsson (Germany)
 Fraunhofer IGD (Germany)
 GE Global Research Center
 HRL Laboratories
 IBM
 Intel Corporation
 Intelligent Geometries, LLC
 Intertek
 IonQ
 Jix Reality Ltd.
 KDDI Research Inc. (Japan)
 Ki3Photonics
 Kitware
 Lumos NanoLabs
 Max Planck Institute (Germany)
 Microsoft Research
 MPACT, Inc.
 NTT Corporation (Japan)
 Photon Spot Inc.
 Prorenata Labs
 Quantinuum
 Quantum Opus
 Qunnect
 Roche, Regeneron, Abbott Labs
 SRI
 Varjo
 Xanadu Quantum Technologies, Inc.

Government/Non-profit Organizations

American Society of Mechanical Engineers
 Argonne National Laboratory
 Army Research Laboratory

Center for Disease Control
 Consejo Nacional de Investigaciones Científicas y Técnicas (Argentina)
 Defense Advanced Research Projects Agency
 El Centro Nacional de Metrología – CENAM (Mexico)
 ETH Zurich (Switzerland)
 Federal Communications Commission
 Flatiron Institute
 Food and Drug Administration
 IEEE Computer Society
 IEEE Metaverse Initiative Steering Committee
 Institute of Science and Technology Austria
 Jet Propulsion Laboratory
 Johns Hopkins University Applied Physics Laboratory
 Khronos Group
 Korteweg-de Vries Inst. for Mathematics (Netherlands)
 Korean Institute of Science and Technology (S. Korea)
 Laboratory for Telecommunication Sciences
 Lawrence Berkeley National Laboratory
 Leibniz Supercomputing Center
 Metaverse Standards Forum
 Mid-Atlantic Crossroads (MAX)
 NASA Ames Research Center
 NASA Goddard Space Flight Center
 National Archives and Records Administration
 National Institute of Biomedical Imaging and Bioengineering
 National Institutes of Health
 National Physical Laboratory (UK)
 National Research Council (Canada)
 National Security Agency
 National Science Foundation
 National Renewable Energy Laboratory (NREL)
 Naval Research Laboratory
 Oak Ridge National Laboratory
 OpenMath Society
 Pacific Northwest National Laboratory
 Physikalisch-Technische Bundesanstalt (Germany)
 Polish Academy of Sciences
 Poolesville High School
 Quantum Economic Development Consortium
 Royal Institute of Technology (Sweden)
 Sandia National Laboratories
 SBA Research (Austria)
 Simons Laufer Mathematical Sciences Institute
 US Army Corps of Engineers
 US Department of Energy
 US Holocaust Memorial Museum
 US Naval Observatory
 US Office of Naval Research (USNO)
 Washington Metro Quantum Network Research Consortium
 World Wide Web Consortium

Universities

Aarhus University (Denmark)

Alfréd Rényi Institute of Mathematics (Hungary)
American University
Beihang University (China)
Beijing Institute of Technology (China)
Bogazici University (Turkey)
Brown University
CalTech
Carnegie Mellon University
China University of Petroleum (China)
Clarkson University
Clemson University
Colorado School of Mines
Columbia University
Concordia University (Canada)
Coppin State University
Cornell University
Courant Institute of Mathematical Sciences
Curtin University (Australia)
Dalian University of Science and Tech (China)
Delft University of Technology (Netherlands)
Drake University
Drexel University
East China U. of Science and Tech (China)
European University Cyprus (Cyprus)
Federal University of Ceará (Brazil)
Flatiron Institute
Florida State University
Freie Universität Berlin (Germany)
Friedrich-Alexander-University (Germany)
Gdansk University of Technology (Poland)
George Mason University
Georgia Tech
Harvard University
Imperial College London (UK)
Indian Institute of Technology (India)
Indiana University
Jacobs University Bremen (Germany)
Johns Hopkins University
Kennesaw State University
Khallikote College (India)
Koç University (Turkey)
Louisiana State University
Loyola University Andalucia (Spain)
Massachusetts Institute of Technology (MIT)
Morgan State University
National University of Singapore (Singapore)
New York University
Northwestern University
Occidental College
Open University (UK)
Oregon State University
Old Dominion University
Polytechnic University of Valencia (Spain)
Portland State University
Rhode Island School of Design
Rice University
Royal Institute of Technology (Sweden)
Shandong University (China)
Southern Methodist University
Southern New Hampshire University
Southern University and A&M College
Stanford University
Stony Brook University
Tallinn University of Technology (Estonia)
Technical University of Denmark (Denmark)
Technische Universität München
Temple University
Texas A&M University
Tokyo Metropolitan University (Japan)
Tokyo University of Science (Japan)
Tsinghua University (China)
Tufts University
University of Antwerp (Belgium)
Universidad Autónoma de Madrid (Spain)
University of Belfast (UK)
University of British Columbia (Canada)
University of California, Berkeley
University of California, Davis
University of California, Los Angeles
University of California, Santa Barbara
University of Central Florida
University of Chicago
University of Colorado, Boulder
University of Colorado, Denver
University of Copenhagen (Denmark)
University of the District of Columbia
University of Edinburgh (UK)
University of Erlangen (Germany)
University of Hawaii
University of Houston
University of Illinois, Urbana-Champaign
University of Konstanz (Germany)
University of Limerick (Ireland)
University of Lisbon (Portugal)
University of Manchester (UK)
University of Maryland, Baltimore County
University of Maryland, College Park
University of Massachusetts
University of Michigan
University of New Mexico
University of Oregon
University of Oulu (Finland)
University of Ottawa (Canada)
University of Pennsylvania
University of Saskatchewan (Canada)
University of Scranton
University of Sheffield (UK)
University of Southampton (UK)
University of Southern California
University of South Carolina
University of Strathclyde (UK)
University of Texas at Arlington
University of Texas at Dallas
University of Washington

University of Wisconsin, Madison
University of Wuppertal (Germany)
University of Zagreb (Croatia)
Virginia Commonwealth University
Virginia Polytechnic Institute
Weizmann Institute of Science (Israel)
Worcester Polytechnic University
Yale University

Staff

ACMD consists of full-time permanent Federal staff located at NIST laboratories in Gaithersburg, MD and Boulder, CO. This full-time staff is supplemented with a variety of special appointments. The following list reflects all non-student appointments held during any portion of the reporting period (October 2022 – December 2023). Students and interns are listed on pages 171 and 172.

* Denotes staff at NIST Boulder.

† Denotes part-time Federal staff.

Division Staff

Ronald Boisvert, *Chief*, Ph.D. (Computer Science), Purdue University, 1979

*Elsie (Meliza) Lane, *Administrative Assistant*

Lochi Orr, *Administrative Assistant*, A.A. (Criminal Justice), Grantham University, 2009

†Alfred Carasso, Ph.D. (Mathematics), University of Wisconsin, 1968

Roldan Pozo, Ph.D. (Computer Science), University of Colorado at Boulder, 1991

Kamran Sayrafian, Ph.D. (Electrical and Computer Engineering), University of Maryland, 1999

Christopher Schanzle, B.S. (Computer Science), University of Maryland Baltimore County, 1989

Mathematical Analysis and Modeling Group

Timothy Burns, *Leader*, Ph.D. (Mathematics), University of New Mexico, 1977

*Bradley Alpert, Ph.D. (Computer Science), Yale University, 1990

*Andrew Dienstfrey, Ph.D. (Mathematics), New York University, 1998

Ryan Evans, Ph.D. (Applied Mathematics), University of Delaware, 2016

†Jeffrey Fong, Ph. D. (Applied Mechanics and Mathematics), Stanford University, 1966

*Zydrunas Gimbutas, Ph.D. (Applied Mathematics), Yale University, 1999

*Zachary Grey, Ph.D. (Computational and Applied Mathematics), Colorado School of Mines, 2019

Leroy Jia, Ph.D. (Applied Mathematics), Brown University, 2018

Raghu Kacker, Ph.D. (Statistics), Iowa State University, 1979

Anthony Kearsley, Ph.D. (Computational and Applied Mathematics), Rice University, 1996

Danielle Middlebrooks, Ph.D. (Applied Mathematics, Statistics and Scientific Computing), University of Maryland, 2020

Paul Patrone, Ph.D. (Physics), University of Maryland, 2013

NRC Postdoctoral Associates

Robert DeJaco, Ph.D. (Chemical Engineering), University of Minnesota, 2020

Melinda Kleczynski, Ph.D. (Applied Mathematics), University of Delaware, 2023

Rayanne Luke, Ph.D. (Applied Mathematics), University of Delaware, 2021

Deborah McGlynn, Ph.D. (Civil and Environmental Engineering), Virginia Tech, 2022

Anne Talkington, Ph.D. (Computational Biology), University of North Carolina, 2021

Faculty Appointee (Name, Degree / Home Institution)

Daniel Anderson, Ph.D. / George Mason University

Michael Mascagni, Ph.D. / Florida State University

John Nolan, Ph.D. / American University

Florian Potra, Ph.D. / University of Maryland Baltimore County

Guest Researchers (Name, Degree / Home Institution)

Prajakta Bedekar, Ph.D. / Johns Hopkins University

Kaitlyn Hood, Ph.D. / Purdue University

Fern Hunt, Ph.D. / NIST Scientist Emeritus

Amudhan Krishnaswamy Usha, Ph.D. / Chakra Consulting Inc.

Yu (Jeff) Lei, Ph.D. / University of Texas at Arlington
 Geoffrey McFadden, Ph.D. / NIST Scientist Emeritus
 Matthew Roberts, Ph.D. / Institute for Defense Analysis
 Dimitrios Simos, Ph.D. / SBA Research, Austria
 Stephen Tennyson, B.S. / University of Maryland

Mathematical Software Group

Bonita Saunders, *Leader*, Ph.D. (Mathematics), Old Dominion University, 1985
 Javier Bernal, Ph.D. (Mathematics), Catholic University, 1980
 Howard Cohl, Ph.D. (Mathematics), University of Auckland, 2010
 Günay Doğan, Ph.D. (Applied Mathematics and Scientific Computing), University of Maryland, 2006
 Michael Donahue, Ph.D. (Mathematics), Ohio State University, 1991
 Stephen Langer, Ph.D. (Physics), Cornell University, 1989
 Bruce Miller, Ph.D. (Physics), University of Texas at Austin, 1983
 Donald Porter, D.Sc. (Electrical Engineering), Washington University, 1996
 Barry Schneider, Ph.D. (Physics), University of Chicago, 1969

NRC Postdoctoral Associates

William Earwood, Ph.D. (Chemistry), University of Mississippi, 2022
 Camilo Montoya, Ph.D. (Mathematics), Florida International University, 2022
 Lisa Ritter, Ph.D. (Mathematics), University of Hawai'i at Mānoa, 2021
 Stephen Sorokanich, Ph.D. (Mathematics), University of Maryland, College Park, 2022

Faculty Appointees (Name, Degree / Home Institution)

Abdou Youssef, Ph.D. / George Washington University

Guest Researchers (Name, Degree / Home Institution)

Luca Argenti, Ph.D. / University of Central Florida
 Joel Bowman, Ph.D. / Emory University
 Nicolas Douguet, Ph.D. / Kennesaw State University
 Heman Gharibnejad, Ph.D. / Computational Physics Inc.
 Mark Alexander Henn, Ph.D. / University of Maryland
 Daniel Lozier, Ph.D. / NIST, Retired
 Carlos Antonio Marante Valdes, Ph.D. / University of Central Florida
 Adri Olde Daalhuis, Ph.D. / University of Edinburgh
 Jeppe Olsen, Ph.D. / Aarhus University, Denmark
 Chen Qu, Ph.D. / GBS Dakota IT, LLC
 Moritz Schubotz, Ph.D. / University of Karlsruhe, Germany

Computing and Communications Theory Group

Ronald Boisvert, *Acting Leader*, Ph.D. (Computer Science), Purdue University, 1979
 Victor Albert, Ph.D. (Physics), Yale University, 2017
 Brian Cloteaux, Ph.D. (Computer Science), New Mexico State University, 2007
 Matthew Coudron, Ph.D. (Computer Science), Massachusetts Institute of Technology, 2017
 *Shawn Geller, M.S. (Physics), University of Colorado, 2021
 Thomas Gerrits, Ph.D. (Physics), Radboud University Nijmegen, 2004
 *Scott Glancy, Ph.D. (Physics), University of Notre Dame, 2003
 *Emanuel Knill, *NIST Fellow*, Ph.D. (Mathematics), University of Colorado at Boulder, 1991
 Paulina Kuo, Ph.D. (Physics), Stanford University, 2008
 *Alexander Kwiatkowski, M.S. (Applied and Engineering Physics), Stanford University, 2017
 Yi-Kai Liu, Ph.D. (Computer Science), University of California, San Diego, 2007
 Lijun Ma, Ph.D. (Precision Instruments and Machinery), Tsinghua University, 2001

Vladimir Marbukh, Ph.D. (Mathematics) Leningrad Polytechnic University, 1986
 Oliver Slattery, *Project Leader*, Ph.D. (Physics), University of Limerick, 2015

Faculty Appointees (Name, Degree / Home Institution)

James Lawrence, Ph.D. / George Mason University
 Richard La, Ph.D. / University of Maryland
 Debasis Mitra, Ph.D. / Columbia University

Guest Researchers (Name, Degree / Home Institution)

Mehdi Alasti, Ph.D. / GBS Dakota IT
 Isabel Beichl, Ph.D. / NIST, Retired
 Sesha Challa / Pusan National University (India)
 Nijil Lal Cheriya Koyyottummal, Ph.D. / University of Napoli Federico II
 Shon Cook, B.S. / SRI International
 Joseph Christesen, Ph.D. / SRI International
 Hristina Georgieva, Ph.D. / Physikalisch-Technische Bundesanstalt (PTB)
 Assane Gueye, Ph.D. / Prometheus Computing
 Navin Lingaraju, Ph.D. / University of Maryland, College Park
 *Karl Mayer, Ph.D. / Honeywell
 Alan Mink, Ph.D. / Theiss Research
 Anouar Rahmouni, Ph.D. / Moroccan Foundation for Advanced Sci., Innovation and Research
 Samprity Saha, Ph.D. / Virginia Commonwealth University
 Yicheng Shi, Ph.D. / National University of Singapore
 *Ezad Shojaee, Ph.D. / University of Colorado
 Francis Sullivan, Ph.D. / IDA Center for Computing Sciences
 Xiao Tang, Ph.D. / NIST Retired
 *James Van Meter, Ph.D. / HRL Laboratories

High Performance Computing and Visualization Group

Judith Terrill, *Leader*, Ph.D. (Information Technology), George Mason University, 1998
 William George, Ph.D. (Computer/Computational Science), Clemson University, 1995
 Terence Griffin, B.S. (Mathematics), St. Mary's College of Maryland, 1987
 Sandy Ressler, M.F.A. (Visual Arts), Rutgers University, 1980
 William Sherman, M.S. (Computer Science), University of Illinois, 1989
 Simon Su, Ph.D. (Computer Science), University of Houston, 2001
 Justyna Zwolak, Ph.D. (Physics), Nicolaus Copernicus University, Poland, 2011

Guest Researchers (Name, Degree / Home Institution)

Donovan Buterakos, Ph.D. / University of Maryland
 John Hagedorn, M.S. / Chakra Consulting
 Steven Satterfield, M.S. / NIST Retired
 James Sims, Ph.D. / NIST (retired)
 Brian Weber, Ph.D. / Shanghai Institute of Technical Physics

Glossary of Acronyms

1D	one-dimensional
2D	two-dimensional
3D	three-dimensional
ACCESS	NSF Advanced Cyberinfrastructure Coordination Ecosystem
ACM	Association for Computing Machinery
ACMD	NIST/ITL Applied and Computational Mathematics Division
ACTS	Advanced Combinatorial Testing System (software)
ADC	apparent diffusion coefficient
AI	artificial intelligence
AL	Analytic Methods (DLMF chapter)
AMOS	atomic molecular and optical science
AMS	American Mathematical Society
ANARI	Analytic Rendering Interface for Data Visualization
APRES	Aspects of Postdoctoral Researcher Experience Scale Survey
APS	American Physical Society
APSBP	American Physical Society Bridge Program
AR	augmented reality
arXiv	preprint archive at https://arxiv.org/
ASES	Aspects of Student Experience Survey
ASME	American Society of Mechanical Engineers
ASMS	American Society of Mass Spectrometry
ASTRA	Attosecond TRAnitions (software)
ASWF	Academy Software Foundation
ATI	above threshold ionization
AVS	American Vacuum Society
AWM	Association for Women in Mathematics
AWS	Amazon Web Services
BAN	body area network
BCI	brain-computer interface
BEC	Bose-Einstein Condensate
BDD	bounded distance decoding
Bio-FET	biological field effect transistor
BMP	Bateman Manuscript Project
BPVC	Boiler and Pressure Vessel Code
Bq	becquerel: absolute activity of radionuclide mixtures
BW	backward wave
CAD	computer aided design
Caltech	California Institute of Technology
CAP	complex absorbing potential
CAR	coincidence-to-accidental
CAS	computer algebra system
CAVE	CAVE Automatic Virtual Environment
CC	close coupling
CCD	charge-coupled device
CCM	Combinatorial Coverage Measurement (software)
CENAM	Center for Metrology of Mexico
CERN	European Organization for Nuclear Research
CHIPS	Creating Helpful Incentives to Produce Semiconductors (Federal program)
CI	configuration interaction
CIR	channel impulse response
CICM	Conference on Intelligent Computer Mathematics
CFPG	Coulomb force parametric generator
CFSF	Continued Fractions for Special Functions
CLEO	Conference on Lasers and Electro-Optics

CMOS	complementary metal-oxide semiconductor
CMU	Carnegie Mellon University
CNN	convolutional neural network
COVID	coronavirus disease
CS	coordinating server
CSF	configuration state function
CSF	cerebrospinal fluid
CSS	quantum error correcting code named after Calderbank, Shor, and Steane
CSV	comma separated values (format)
CT	computed tomography
CT	combinatorial testing
CTL	NIST Communications Technology Laboratory
CURE	Children's Hospital of Uganda
CV	continuous (quantum) variables
CY	calendar year
DARPA	Defense Advanced Research Projects Agency
DC-QNet	DC area Quantum Network testbed
DGR	NIST Domestic Guest Researcher
DHS	US Department of Homeland Security
DICOM	international standard to transmit, store, and process medical imaging information
DLMF	Digital Library of Mathematical Functions
DNA	deoxyribonucleic acid
DNN	deep neural network
DOC	US Department of Commerce
DOD	US Department of Defense
DOE	US Department of Energy
DOI	digital object identifier
DQC	data quality control
DQD	double quantum dot
DRMF	Digital Repository of Mathematical Formulae
DV	discrete (quantum) variable
EBSD	electron backscatter diffraction
eCF	Wolfram Computational Knowledge of Continued Fractions Project
EBM	explainable boosting machine
E-Health	electronic health care
E-Hy-CI	exponentially correlated Hy-CI
EI-MS	electron ionization mass spectrometer
EL	NIST Engineering Laboratory
EPA	Environmental Protection Agency
EPA	entangled photon analyzer
EPS	entangled photon source
ERB	NIST Editorial Review Board
ESBD	electron back-scatter diffraction
FEM	finite element method
FFT	fast Fourier transform
FGR	NIST Foreign Guest Researcher Program
FL	federated learning
FNN	fully connected neural network
FPUB	failure probability upper bound
FY	fiscal year
GAMS	generalized additive models
GC-EI-MS	gas chromatography coupled electron-ionization mass spectroscopy
GDS	Graphic Design System (file format for electronic design automation)
GHG	greenhouse gas
glTF	standard file format for three-dimensional scenes and models
GMSE	NIST Graduate Measurement Science and Engineering internship program
GNN	graph neural network

GPU	graphical processing unit
Grad-CAM	gradient-weighted class activation mapping
GTO	Gaussian-type orbital
GUI	graphical user interface
GWT	Gabor wavelet transform
HA-PTP	high accuracy precision time protocol
HDC	high-dimensional consensus
HDC-MLE	HDC maximum likelihood
HDCMS	HDC mass spectral
HEC	High End Computing
HEV	high end visualization
HHG	high harmonic generation
HHS	US Department of Health and Human Services
HIM	helium ion microscope
HMD	head-mounted display
HOM	Hong-Ou-Mandel interference
HPCVG	ACMD High Performance Computing and Visualization Group
HSS	hybrid similarity search
HTML	hypertext markup language
Hy	Hylleraas
Hy-CI	Hylleraas-Configuration Interaction technique
IARPA	Intelligence Advanced Research Projects Agency
IC	integrated circuit
ICC	IEEE International Conference on Communications
ICIAM	International Congress on Industrial and Applied Mathematics
ICST	International Conference of Software Testing
IDE	integrodifferential equation
IEEE	Institute of Electronics and Electrical Engineers
IF	intermediate frequency
IFIP	International Federation for Information Processing
IMS	NIST Innovations in Measurement Science (internal funding program)
iNET	NIST internal web site
IoT	Internet of things
IR	infrared
IS	photoreceptor inner segment
ISO	International Standards Organization
ISTA	Institute of Science and Technology Austria
IT	information technology
ITL	NIST Information Technology Laboratory
ITVOLT	ITerative VOLTerra propagator (software)
IVE	immersive visualization environment
IWCT	International Workshop on Combinatorial Testing
JHU	Johns Hopkins University
KLS	Koekoek, Lesky and Swarttouw
KS	Kolmogorov-Smirnoff
LaCAST	Java tool to convert math expressions from LaTeX to computer algebra systems
LaTeX	a math-oriented text processing system
LaTeXML	a LaTeX to Math ML converter
LBNL	Lawrence Berkeley National Laboratory
LDPC	low-density parity checks
LIDAR	light detection and ranging
LO	local oscillator
LWE	learning with errors
MAA	Mathematical Association of America
MathML	Mathematical Markup Language (W3C standard)
MBQC	measurement-based quantum computation
MGB	Mathematically Gifted and Black

MGH	Massachusetts General Hospital
MGI	Materials Genome Initiative
minL	minimum life
MIT	Massachusetts Institute of Technology
ML	machine learning
MLP	mathematical language processing
MML	NIST Material Measurement Laboratory
MOL	method of lines
MOS	Magnus, Oberhettinger, and Soni
MRAM	magneto-resistive random-access memory
MRI	magnetic resonance imaging
MS	mass spectrometry
MSF	Metaverse Standards Forum
MSGI	NSF Mathematical Sciences Graduate Internship program
MTD	moving target defense
MW	molecular weight
NALS	network analysis for Likert-style surveys
nanoHUB	Web portal for nanotechnology research at https://nanohub.org/
NBS	National Bureau of Standards (former name of NIST)
NDE	non-destructive evaluation
NG-QNET	NIST Gaithersburg Quantum Network
NISQ	noisy intermediate-scale quantum
NIST	National Institute of Standards and Technology
NISTIR	NIST Internal Report
NISTmAb	NIST monoclonal antibody reference material
NITRD	Networking and Information Technology Research and Development
NLSS	no low-energy sampleable states
NLTS	no low-energy trivial states
NMI	National Metrology Institute
NN	neural network
NRC	National Research Council
NREL	National Renewable Energy Laboratory
NS	network slice
NSF	National Science Foundation
ODE	ordinary differential equation
OOF	Object-Oriented Finite Elements (software)
OOF3D	3D version of OOF
OOMMF	Object-Oriented Micromagnetic Modeling Framework (software)
OP	orthogonal polynomials
OpenXR	Open Extended Reality
OPSF	orthogonal polynomials and special functions
OS	photoreceptor outer segments
OSTP	White House Office of Science and Technology Policy
O-TWTFT	optical two-way time transfer
OU	NIST organizational unit
OUSD	Open USD
PAML	physics-assisted machine learning
PCA	principal component analysis
PCP	probabilistically checkable proof
PDE	partial differential equation
PDF	probability density function
PET	positron emission tomography
PI	principal investigator
PIT	physics-informed tuning
PML	NIST Physical Measurement Laboratory
PoEP	probability of experiencing a pandemic
PPKTP	periodically poled KTiOPO ₄

PQC	post-quantum cryptography
PREP	NIST Professional Research Education Program
PT	Painlevé transcendents (DLMF chapter)
PTB	Physikalisch-Technische Bundesanstalt (German metrology institute)
QED-C	Quantum Economic Development Consortium
QCrypt	annual conference on quantum cryptography
QD	quantum dot
QDPD	Quaternion-based Dissipative Particle Dynamics simulation code
QIP	Quantum Information Processing (conference)
QKD	quantum key distribution
QMA	Quantum Merlin-Arthur complexity class
QNGC	Quantum Networks Grand Challenge (internal NIST funding program)
QuANET	DARPA Quantum Augmented Network program
QuICS	UMD-NIST Joint Center for Quantum Information and Computer Science
RAVEN	IARPA Rapid Analysis of Various Emerging Nanoelectronics program
RCP	Research Conduct Policy
RBF	radial basis function
REU	Research Experience for Undergraduates
REU-CAAR	REU Combinatorics, Algorithms, and AI for Real Problems program (UMD)
RF	radio frequency
RGB	red-green-blue color system
RI	retention index
RIM	reliability and integrity management
RL	reinforcement learning
RPA	random phase approximation
RPE	retinal pigment epithelium
RPO	Research Protections Office
RSA	Rivest-Shamir-Adelman public key cryptographic algorithm
SARS	severe acute respiratory syndrome
SARS-CoV-2	the virus that causes the respiratory disease COVID-19
SAW	surface acoustic wave
SDK	software development kit
SEM	scanning electron microscopy
SFWM	spontaneous four wave mixing
SHIP	Summer High School Internship Program
SI	International System of Units
SIO	Scientific Integrity Officer
SIP	Scientific Integrity Policy
SIAM	Society for Industrial and Applied Mathematics
SiC	silicon carbide
SIGGRAPH	ACM Special Interest Group on Graphics
SIS	susceptible-infected-susceptible
SLR	service-level requirement
SNA	social network analysis
SNSPD	superconducting nanowire single-photon detectors
SPDC	spontaneous parametric down conversion
SPH	smooth particle hydrodynamics
SPIE	International Society for Optical Engineering
SPO	NIST Special Programs Office
SPT	symmetry-protected topological order
SRM	standard reference material
STEM	science, technology, engineering, and mathematics
SURF	NIST Student Undergraduate Research Fellowship program
SVOP	several variable orthogonal polynomials (DLMF chapter)
SVP	shortest vector problem
SVP	NIST Student Volunteer Program
TDA	topological data analysis

TDEV	time deviation
TDM	transition density matrix
TDMCC	transition density matrix, close coupling
TDSE	time domain Schrodinger equation
TEM	transmission electron microscope
TES	transition edge sensor
TFLN	thin-film lithium niobate
TOMCAT	TOmographic Microscopy and Coherent rAdiology experimentTs
TSQNT	Time-Synchronized Quantum Network Testbed
TV	total variation
UC	University of California
UCLA	University of California Los Angeles
UHPC	ultra-high-performance concrete
UK	United Kingdom
UMD	University of Maryland
UMIACS	University of Maryland Institute for Advanced Computer Studies
UQ	uncertainty quantification
URL	universal resource locator
URSI	International Union of Radio Science
USD	Universal Scene Description
UWB	ultra-wideband
VAE	variational auto-encoder
VAMAS	Versailles Project on Advance Materials and Standards
VBG	volume Bragg grating
VC	viral conductance
VEMOS	Visual Explorer for Metric of Similarity (software)
VNA	vector network analyzer
VR	virtual reality
VTK	visualization software library
W3C	World Wide Web Consortium
WFH	weak-field homodyne
WIOB	walk-in-out-balls algorithm
WR	White Rabbit
WR-PTP	White Rabbit precision time protocol
XR	extended reality
XSEDE	NSF eXtreme Science and Engineering Discovery Environment
ZE	Zeta and related functions (DLMF chapter)
ZP	NIST scientific professional pay band